STATIC LOAD TESTING OF A DAMAGED, CONTINUOUS

PRESTRESSED CONCRETE BRIDGE

Except where reference is made to the work of others, the work described in this thesis is my own or was done in collaboration with my advisory committee. This thesis does not include proprietary or classified information.

_____

William Ernest Fason

Certificate of Approval:

| | |
|---|---|
| _____ | _____ |
| Anton K. Schindler<br>Gottlieb Associate Professor<br>Civil Engineering | Robert W. Barnes, Chair<br>James J. Mallett Associate Professor<br>Civil Engineering |
| _____ | _____ |
| Mary L. Hughes<br>Instructor<br>Civil Engineering | George T. Flowers<br>Dean<br>Graduate School |

# STATIC LOAD TESTING OF A DAMAGED, CONTINUOUS PRESTRESSED CONCRETE BRIDGE

William Ernest Fason

A Thesis

Submitted to the

Graduate Faculty of

Auburn University

in Partial Fulfillment of the

Requirements for the

Degree of

Master of Science

Auburn, Alabama
May 9, 2009

STATIC LOAD TESTING OF A DAMAGED, CONTINUOUS

PRESTRESSED CONCRETE BRIDGE

William Ernest Fason

Permission is granted to Auburn University to make copies of this thesis at its discretion, upon the request of individuals or institutions and at their expense. The author reserves all publication rights.

_____
Signature of Author

_____
Date of Graduation

THESIS ABSTRACT

STATIC LOAD TESTING OF A DAMAGED, CONTINUOUS

PRESTRESSED CONCRETE BRIDGE

William E Fason

Master of Science, May 9, 2009
(B.S., Auburn University, 2003)

318 Typed Pages

Directed by Robert W. Barnes

Shortly after the completion of interstate highway I-565 in Huntsville, Alabama, cracks were discovered in the continuous end of many of the prestressed concrete bulb-tee girders. Alabama Department of Transportation (ALDOT) employees determined that differential temperature gradients across the depth of the members were the likely cause. ALDOT personnel, along with Auburn University personnel, performed additional research to verify the causes of the cracking and to investigate possible repair methods. It was concluded that the temperature gradients were the cause of the cracking, and a fiber-reinforced polymer (FRP) repair was designed. Load tests before and after

the FRP repair were recommended to determine the effectiveness of the repair. A finite-element model (FEM) analysis was conducted as well to verify the behavior of the bridge and to determine the possible effects of the repair.

The current state of the bridge was observed and recorded, and a pre-repair load test was conducted in order to provide a baseline to which the post repair load test results could be compared. A comparison between the two will provide a method of determining the effectiveness of the repair. The load test was focused on two girders that exhibited typical cracking behavior. The girders were tested with concrete surface strain gages, deflectometers, and crack opening devices. The pre-repair load test results showed that the bridge is acting in either a partially continuous or fully continuous manner.

An additional goal of the test was to determine the effectiveness of superpositioning in bridge girders. It was determined that superpositioning was effective for large scale bridge behavior measurements such as deflections, but was not applicable for more localized measurements like strains and crack openings.

A follow-up load test will be required to determine the effectiveness of the FRP repair. The results can be compared to the FEM results in order to verify the FEM predictions.

Style manual used The Chicago Manual of Style

Computer software used Microsoft Word, Microsoft Excel

TABLE OF CONTENTS

LIST OF TABLES

LIST OF FIGURES

# CHAPTER 1

# INTRODUCTION

## 1.1 PROJECT OVERVIEW

Shortly after the completion of interstate highway I-565 in Huntsville, Alabama, cracks were discovered in the continuous end of many of the prestressed concrete bulb-tee girders. After a second inspection revealed more serious cracking, the Alabama Department of Transportation (ALDOT) began to monitor these bridges more closely. Efforts were made to alleviate the problem, and studies were undertaken to determine the cause of the cracking. False supports were designed and placed under the bridge to prevent a bridge collapse in the event of a girder failing.

Temperature gradients across the cross section of the bulb-tee girders were determined to be the cause of the cracks (Gao 2003). Reinforcement details in the girder ends contributed to the severity of this cracking (Gao 2003). Later, an externally bonded fiber-reinforced polymer (FRP) repair was developed to bring the girders back to their required strength. A pre-repair and post-repair load test were recommended to determine the effectiveness of the repair.

This thesis describes the pre-repair static load tests. In the test, bridge girders were instrumented, and data were collected while ALDOT load trucks were positioned in predetermined locations along the bridge surface. The results of the tests were recorded, and the measured bridge response was examined to gain insight into the structural

behavior of the system. Conclusions about the behavior of the bridge are reported, and ideas are introduced about the possible variation of bridge behavior with temperature.

Finally, a portion of the load test was focused on using the principle of superposition to determine whether the existing bridge superstructure is behaving as a linear-elastic system under service-level loads.

## 1.2 NEED FOR RESEARCH

It is much more efficient to provide an in-place repair for cracked girders than to completely shut down or reroute interstate highway traffic to rebuild a bridge. An effective in-place repair is needed for these bridge girders. The pre-repair load test and a post-repair load test are required to determine the effectiveness of the FRP repair. The pre-repair load test results provide a baseline for which the post-repair load test results can be compared. The pre-repair load test will also provide information to better understand the current bridge behavior.

## 1.3 OBJECTIVES

The objective of the research described in this thesis is to perform the pre-repair static load test required to determine the effectiveness of the FRP repair and analyze the results. The pre-repair test will provide a baseline to which the post-repair test can be compared. The test data is also analyzed to determine both the behavior of the cracked girders and the effectiveness of superposition.

## 1.4 THESIS ORGANIZATION

Chapter 2 provides background information and a summary of the previous research conducted on the bridge girders. Chapter 3 provides a detailed examination of the pre-repair bridge conditions. Chapter 4 details the instrumentation of the bridge girders for

testing. Chapter 5 provides an explanation the load testing procedure. The test results and a discussion of those results are included in Chapter 6. Chapter 7 contains a summary of the research and conclusions. Chapter 8 includes recommendations regarding the post-repair test as well as possible future research.

# CHAPTER 2

# BACKGROUND AND RESEARCH

Interstate I-565 in downtown Huntsville was constructed in a five-part project. The project consisted of 2.45 miles of elevated highway and cost the state of Alabama $91,045,779. Construction started January 29, 1988 and was completed March 27, 1991 (ALDOT 1994d). Bridges were constructed using either steel or prestressed concrete girders, both having a cast-in-place concrete deck. Bridges were also constructed as either simply supported or continuous structures. Two-, three-, and four-span continuous girders were used.

## 2.1 UNEXPECTED CRACKING OF PRESTRESSED CONCRETE GIRDERS

A routine bridge inspection in 1992 revealed hairline cracks in the continuous ends of many of the prestressed bulb-tee girders. During March and April of 1994, about eighteen months after the initial bridge inspection, another bridge inspection revealed much more serious cracking. Inspections revealed that the previous hairline cracks had propagated and widened up to 0.25 inches. As seen in Figure 2-1, cracks were primarily located near the continuous end of prestressed concrete bulb-tee girders made continuous for live loads. Cracks started at the bottom of the girders and propagated through the bottom flange and into the web. With cracking starting at the bottom of the girder, positive moment is the likely cause of cracking. The cracked prestressed girders types were either Bulb-Tee 54 (BT-54) or Bulb-Tee 63 (BT-63), each being 54-inches deep or

63-inches deep, respectively. Typical AASHTO I-shaped prestressed girders exhibited no cracking. Cracks in the face of the continuity diaphragms were also located during the second inspection, as indicated in Figure 2-2. ALDOT personnel thought that the diaphragm cracks were caused by the girders pulling away from the continuity diaphragm.

**Figure 2-1:** Cracks in Continuous Ends of Girders (Barnes 2007)

After the second inspection had alerted ALDOT officials to the problem, a survey was taken to assess the cracking in all of the Huntsville I-565 prestressed girders. Approximately 3 percent of continuous prestressed girders contained cracks (ALDOT 1994c). Only bulb-tee girders were cracked. No standard AASHTO I-girders exhibited cracking. Cracks in the continuity diaphragm faces were also more prevalent in bents supporting bulb-tee girders. Eighty-five percent of the bents had end cracks in the

continuity diaphragm (ALDOT 1994c). An example of this cracking may be seen in Figure 2-3. From Table 2-1 below, it can clearly be seen that the bulb-tee girders, especially BT-54 girders, experienced significantly more problems than the uncracked AASHTO girders.


**Figure 2-2:** Cracks in Continuity Diaphragm

After realizing the severity of the cracking, ALDOT personnel quickly took action to rectify the situation. False supports, as seen in Figure 2-4, were installed under all cracked girders to prevent a possible collapse. False supports were installed within 10 feet of the bents. The top of the false supports were placed approximately 1 inch from the bottom of the girder and bearing pads were attached atop the false supports between them and the girder as seen in Figure 2-5. The gap allowed for day to day movements of the bridge due to traffic and thermal loads.

**Figure 2-3:** End Cracks in the Continuity Diaphragm

**Table 2-1:** Summary of Cracking in Prestressed Concrete Girders Made Continuous

(Swenson 2003)

| | BT-54 Girders | | BT-63 Girders | | AASHTO Types I, III, IV Girders | |
|---|---|---|---|---|---|---|
| | No. of Girders | No. of Cracked Girders | No. of Girders | No. of Cracked Girders | No. of Girders | No. of Cracked Girders |
| Mainline | 732 | 33 | 656 | 9 | 72 | 0 |
| Ramp | 560 | 24 | 140 | 8 | 174 | 0 |
| Total | 1292 | 57 | 796 | 17 | 246 | 0 |

**Figure 2-4:** False Supports

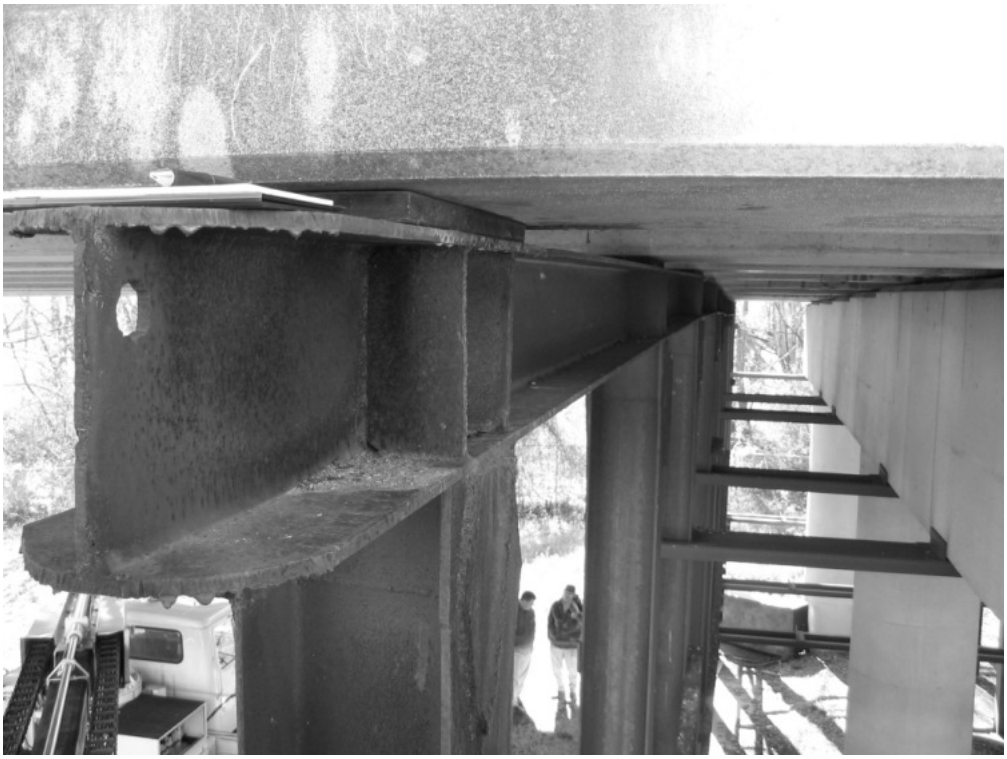

**Figure 2-5:** Bearing Pad Between Top of False Support and Bottom of Bulb-Tee Girder

Epoxy was also injected into the cracks located near the ends of the prestressed girders when the cracks were wide open, as seen in Figure 2-6. The epoxy was used to attempt to seal existing cracks, as well as to prevent future growth of the cracks. However, new cracks often formed near the epoxy-injected cracks, and many epoxy-injected cracks reopened. Examples of this can be seen throughout these bridges.


**Figure 2-6:** Epoxy-Injected Cracks

Once precautions had been taken to prevent the failure of the bridges, ALDOT personnel tested the bridge to find the cause of the cracking in the prestressed bulb-tee girders. In order to determine the cause, bridges were instrumented to determine the effects of wind, traffic, and thermal loadings. Shortly thereafter, it was obvious that neither wind nor traffic loadings were responsible for the damage. However, a large temperature gradient existing across the depth of the bridge cross section caused

unexpected stresses and upward deflections. The thermal differences between the bridge deck and girders ultimately caused the cracking throughout the prestressed girder ends. As discussed in the next section, research conducted by the Auburn University Highway Research Center supported this conclusion.

## 2.2 EARLIER RESEARCH ON HUNTSVILLE I-565 CRACKED GIRDERS

Engineers representing the Auburn University Highway Research Center, working alongside ALDOT engineers, have researched causes for cracking in the bridge girders, strength deficiencies caused by the cracking, and the feasibility of a fiber-reinforced polymer (FRP) strengthening system for the bridge.

### 2.2.1 CAUSES FOR CRACKING

Ningyu Gao (2003) of Auburn University researched the I-565 girders in search of a cause for the extensive cracking. Gao analyzed an interior girder line of a typical two-span continuous structure considering time-dependent and temperature-dependent effects, as well as the effects caused by the construction sequence. A step-by-step, finite time interval analysis was used to calculate stresses in the girder, deck slab, and continuity diaphragm. The analysis first calculated the time-dependent stresses caused by the prestress force and dead loads. Secondly, a nonlinear temperature distribution analysis was conducted to calculate the temperature-dependent stresses that would result from temperature profiles actually measured in the girders. Finally, stresses caused by thermal effects were superimposed onto the stresses caused by time-dependent effects in order to determine the stresses caused by the combination of the two.

#### 2.2.1.1 Nonlinear Temperature Distributions

As mentioned earlier, cracking was caused by large positive moments near the continuous ends of the girders. "Positive moment over the pier in precast prestressed bridges made continuous may come from the following ways: time-dependent effects, temperature effects, construction timing and sequence" (Gao 2003). In order to determine the probable cause for the extreme positive moments that caused cracking, each possibility was investigated. Gao (2003) found that construction timing and sequence had "little effect on the girder performance as long as there are only a few days difference between the deck and diaphragm casting times". Gao also determined that the time-dependent effects of creep due to the prestress force and shrinkage could cause cracking in the restrained girder ends, but "this cracking would be unlikely to occur until the bridge was at least 10 years old". Because of the cracking at earlier ages, it is not likely that time-dependent effects are the primary cause of cracking in the girders.

Temperature gradients across the composite sections were determined to be the primary cause of cracking. Temperature data were recorded by ALDOT personnel at several different times, and the data collected by ALDOT personnel at 14:15:35 on May 19, 1994 was found to be the worst-case of the collected data. The nonlinear temperature distribution analysis was based on these data. As the recorded temperature data came from only a couple of days in the course of one year, there is a very low probability that the recorded temperature distribution was the worst that the bridge had experienced in its lifetime. When the temperature data were collected, the measured ambient temperature was only 18.2° C (64.8° F). During an extreme summer day ambient temperatures may reach 38° C (100° F), possibly causing a more extreme temperature difference between

the bridge deck and girders. In the recorded data, bridge deck temperatures were much higher than temperatures throughout the girders. The non-uniform temperature distribution caused the bridge to deflect upward, an occurrence known as "sun cambering". While girder sections near midspan move upward, girder sections near the continuity diaphragm were restrained from rotating or deflecting by the continuity between spans. Large positive restraint moments developed near the supports. The positive moments in the cross sections near the support caused very large tensile stresses in the bottom flange of the prestressed concrete girders. In the case of the I-565 bridges, many of the tensile stresses were large enough to cause cracking. The cracks caused by positive moments began in the girder's bottom flange and extended into the web. A few of the cracks have propagated enough to approach the upper flange of the girders. Gao found that temperature-dependent effects caused cracking much earlier than time-dependent effects, probably soon after continuity was established. Gao (2003) concluded that the nonlinear temperature distribution throughout the bridge superstructure was the primary cause for the severe cracking in the prestressed bulb-tee girders.

#### 2.2.1.2 Locations of cracks

After researching the cause, it is not surprising that the prestressed girders cracked, but the locations of the cracking are different than one might think. Positive moments should be the highest near the continuity diaphragm, and therefore, one would expect the cracking to occur at the end of the girder or possibly at the interface between the girder and the continuity diaphragm. Cracking in the I-565 girders normally starts a few feet from the girder ends.

Two precast prestressed girders are made continuous by connecting them in such a way that the connection is rigid, being able to carry both positive and negative moment. The negative moment reinforcement is placed in the cast-in-place concrete deck. The positive moment reinforcement is placed into the precast girders before the concrete is poured. The reinforcement is extended out of the girder ends. Once in place, the positive moment steel extends into the spaced use for the continuity diaphragm, then the continuity diaphragm is cast, encasing the positive moment reinforcement. As seen in Figure 2-7, the positive moment reinforcement in the continuity diaphragm allows the two girders and the continuity diaphragm to act rigidly together, providing the desired continuity. The positive moment reinforcement extends 40.5 inches into the girder, measured from the continuous end. The primary problem with this location is that it closely aligns with the first debonding point of ten prestressed strands, 48 inches from the continuous end of the girder. A significant stress concentration is caused by the short distance between these two points. "Furthermore, temperature-induced stresses were so large near this region that the risk of actual peak stress shifting to these cutoff and debonding points was very high" (Gao 2003). From Gao's work, it can be concluded that the tensile stresses caused by thermal gradients were high enough to cause cracking. Once the stresses reached a high level, the cracking occurred a few feet from the girder end because of the stress concentrations caused by the reinforcement cutoffs and debonding.

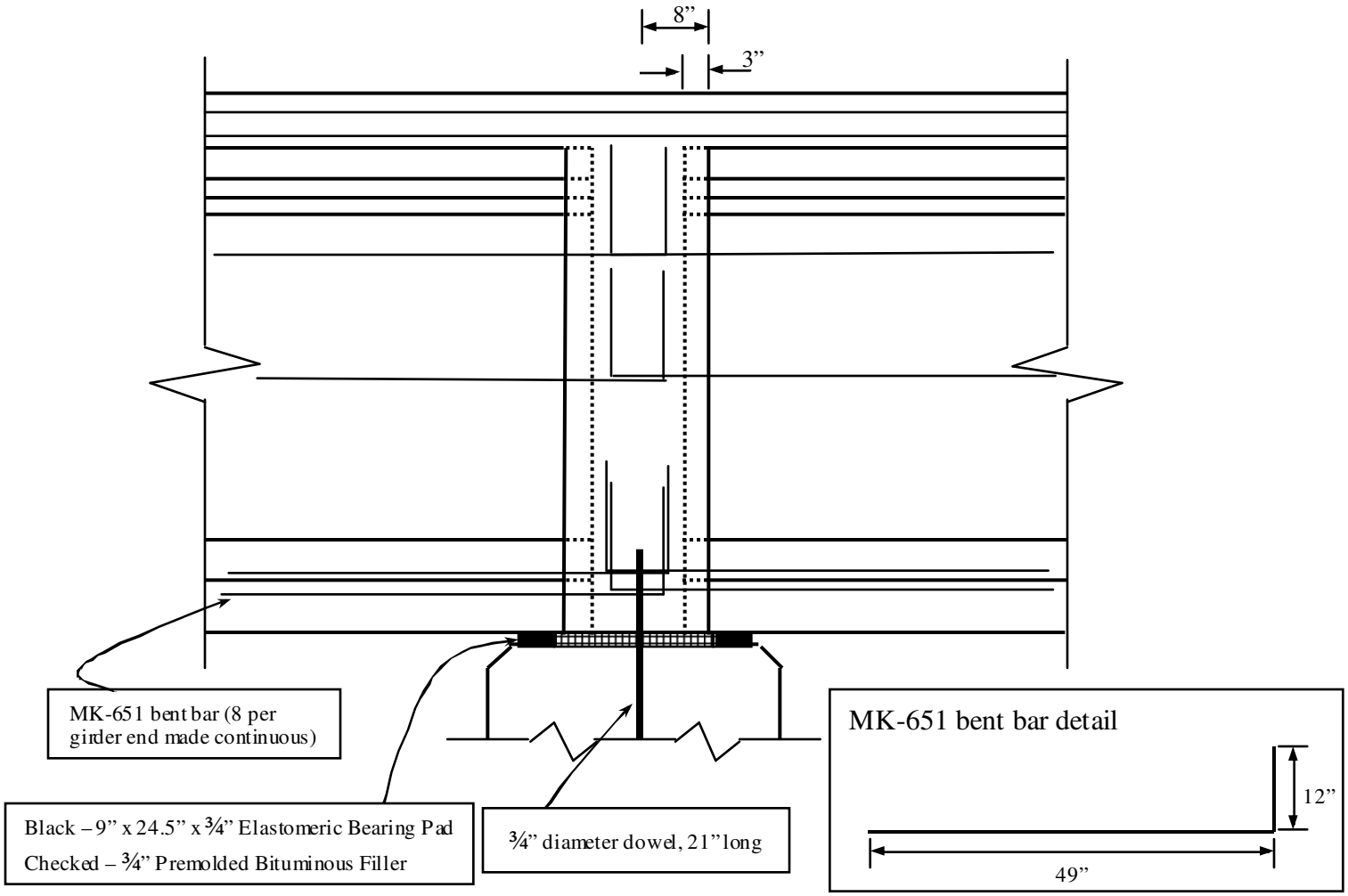


**Figure 2-7:** Detail of Continuity Diaphragm at Interior Support (Swenson 2003a)

### 2.2.2 RESULTS OF CRACKING

The number and size of the cracks led to serious concerns about the integrity of the bridge structures. The primary concern for these girders is the manner in which the cracking in the anchorage zone of the prestressed tendons has affected the effective prestress force near the continuous girder ends. If the effective prestress force is significantly reduced, as suspected, shear and flexural capacities may be severely reduced.

Cracking in the anchorage zones of a prestressed tendon can cause anchorage failures for the tendon. Slipping of the prestressed tendons is the most common type of failure. Normally, tendon yielding is not possible, because there is not enough bonded length for the strands to develop fully on both sides of the cracks. Swenson (2003a) calculated the development length of a 0.5-in. (12.7-mm) special prestressing tendon to be 80 inches by AASHTO LRFD Bridge Design Specifications. Based on the measured crack widths and that the location of the cracks were well within this development length, Swenson (2003a) concluded that the prestressing strands have slipped as a result of the cracks in the girder end and that it is appropriate and conservative to assume that all of the prestressing force in the strands has been lost between the cracks and the girder end.

Loss of effective prestress has serious consequences on the strength of the girders. If the effective prestressing force is lost, any benefits due to the pre-compression of the concrete in this region of the girder have also been lost. If the pre-compression was necessary to achieve the design strength, the girder may now have insufficient capacity, especially in shear. Pre-compression of the concrete through prestressing allows the concrete itself to resist more shear force (i.e., more shear force is required to cause

principle tensile stresses to reach cracking stress levels when the concrete is pre-compressed). Shear resistance in a prestressed concrete beam is usually considered as the sum of the shear resistance of the concrete itself and the shear resistance provided by the steel stirrups. Shear resistance is comprised of both a horizontal tension tie and vertical compression component. Concrete is very weak in tension, and steel reinforcement is required to provide the horizontal tension tie in shear resistance. Compression is resisted by the concrete, and the tension ties are provided by the stirrups and the longitudinal reinforcement in the bottom flange of the girder, either prestressed or non-prestressed reinforcement. Therefore, both stirrups and longitudinal reinforcement are required to achieve proper shear capacity. If the prestressing tendons have slipped in the I-565 girders, and there is no adequately developed longitudinal reinforcement in the bottom flange to carry the tensile forces formed there, the girders may not be able to carry the shear forces for which they were designed. Considering the possible effects of the girder cracking, the girders were analyzed more thoroughly to find all possible strength deficiencies.

### 2.2.3 Analysis of Cracked Girders

Swenson (2003a) used three different analytical methods in determining if there are strength deficiencies in the prestressed bulb-tee girders. Elastic structural analysis was used to develop factored ultimate shear and moment envelopes for both interior and exterior girders. A sectional model was then used to calculate shear and moment capacities of a typical cracked girder. The calculated capacities were compared to the factored ultimate shear and moment envelopes to determine the location and size of strength deficiencies. Finally, a strut-and-tie analysis was used to determine the forces in

the prestressed tendons and FRP. Once the required force in the FRP was determined, a repair technique could be selected.

#### 2.2.3.1 Possible Types of Behavior

The I-565 spans in question contain two-span continuous girders with severe cracking near the continuous ends. In Swenson's (2003a) analysis of the I-565 girders, three possible behaviors of the girders were explored: two-span continuous behavior (as designed), two independent simply-supported (SS) spans, and girders acting continuous over the supports with an internal hinge at the cracked cross sections. Each of these behaviors was investigated for strength deficiencies.

#### 2.2.3.2 Analysis Results

"The results of the analytical procedures revealed that only one of three types of behavior considered in the analysis of the cracked bulb-tee girders is acceptable under factored ultimate loads: two-span continuous behavior" (Swenson 2003a). Shear capacity is sufficient if the bridge behaves in accordance with the two-span continuous model. Swenson (2003a) determined that there was a slight deficiency in negative moment capacity over the support if the girders are acting completely two-span continuous. It is possible for a plastic hinge to form over supports under AASHTO LRFD factored design loads, leading the girders to act as simply supported (SS) girders. Also, there is not adequate tensile capacity in the longitudinal tension reinforcement over a short distance near the support in the simply supported girder end. There has been no cracking at these ends. Therefore, this is not thought to be a problem. Positive moment capacity is adequate for this model.

The second model examined consisted of girders acting continuously with an internal hinge at the cracked cross section. Flexural capacity of this model was sufficient. Because shear demands were much greater in the SS model, they were not analyzed for this model.

The SS model exhibited more strength deficiencies than the other two models. In order for complete simply supported behavior to occur, continuity over the support must be completely lost. If this is the case, both interior and exterior girders lack proper positive moment capacity. "The deficiency of positive moment capacity is the result of the loss of effective prestressing force in the tendons caused by the large cracks in the continuous end of the girder" (Swenson 2003a). The shear capacity of both the interior and exterior girders was deemed to be insufficient because of a deficiency in the longitudinal tensile reinforcement on the flexural tension side of the member.

### 2.2.4 FIBER REINFORCED POLYMER REPAIR

FRP reinforcement has been used effectively for strengthening of reinforced concrete structures. However, it has not been used to repair girders with the strength deficiencies seen in the I-565 bridge girders. Flexural strengthening and column wrapping are the most common types of FRP retrofits, while shear strengthening makes up a very small percentage. Swenson (2003a) developed a method to repair the girders by wrapping the bottom flange of the girders with FRP. To be conservative, FRP strengthening was designed based on the worst-case effects of completely simply supported spans. He determined that the "most efficient way to provide anchorage is through the bond between the FRP reinforcement and the concrete surface" (Swenson 2003a). Mechanical anchorage of the FRP was not feasible.

During analysis, Swenson (2003a) found that "the critical load cases for the simply supported girder will control the required tensile capacity of the external FRP reinforcement". The FRP reinforcement has very high tensile strength. By bonding FRP to the bottom flange of the girder, it compensates for the slipped prestressed strands to provide the necessary longitudinal tensile capacity in the bottom flange of the girder near the girder ends. If attached and bonded properly, the FRP would "increase the tensile capacity of the longitudinal reinforcement at the cracked end of the girder, increase the design shear capacity of strengthened cross sections, and ensure that factored ultimate shear forces can be transferred" by the girders (Swenson 2003a). The FRP will allow the existing shear reinforcement to become effective by providing the necessary tension tie between stirrups. Thermal-induced cracking (if it continues to occur) will be shifted to more desirable locations outside the span of the girder (behind the bearing).

The FRP repair proposed by Swenson (2003a) consists of 4 plies of uniaxial FRP, Tyfo SCH-41 composite, with the primary fibers running parallel to the longitudinal axis of the girders. The FRP plies are wrapped around the bottom flange of the girder and start at the face of the continuity diaphragm. The bottom ply runs 120 inches toward the center of the girders, and each subsequent layer ends 6 inches before the previous layer. Anchorage of FRP is very critical for this application. Therefore, special consideration must be taken around bearing pads in order for the FRP to have the proper bonding length to provide necessary strength at critical sections. The FRP placement scheme can be seen in Figures 2-8 and 2-9.

### 2.2.5 FINITE-ELEMENT ANALYSIS

Shapiro (2007) created finite-element models of the bridge to provide a basis with which to compare the bridge load test results. The various models created were "designed to simulate the current behavior of the bridge and to predict the change in behavior due to the repair work." Shapiro concluded that the bridge was behaving as if there were hinges at the cracked sections and that the FRP repair would essentially return the bridge to fully continuous behavior. Shapiro also concluded that eight strain gages should be relocated from near the top of the web to the FRP reinforcement on the bottom flange for post-repair testing.

Shapiro's initial set of models consisted of three different models. The first model was an uncracked model. The second model had the cracks modeled as "seams", which separated adjacent elements and allowed the affected elements to act independently of each other. This allowed the cracks to open, but would also allow the cracks to close without transferring compressive stresses. The "seams" allowed the cracked element surfaces to overlap each other, meaning that compression could not be transferred across the "seam" in this model even if the loads caused the cracks to close. Shapiro justified this assumption by theorizing that the initial crack widths are larger than the crack closings seen in her finite-element analysis, and therefore compression can not be carried across the crack. Shapiro's third model was a modification of the second model. The cracks were modeled in the same manner, but longitudinal reinforcement was added and assumed to be developed on either side of the crack. Under most loadings the reinforcement was seen to be in compression at the crack locations. Shapiro concluded that the results from the pre-repair load test matched the third model the best, and

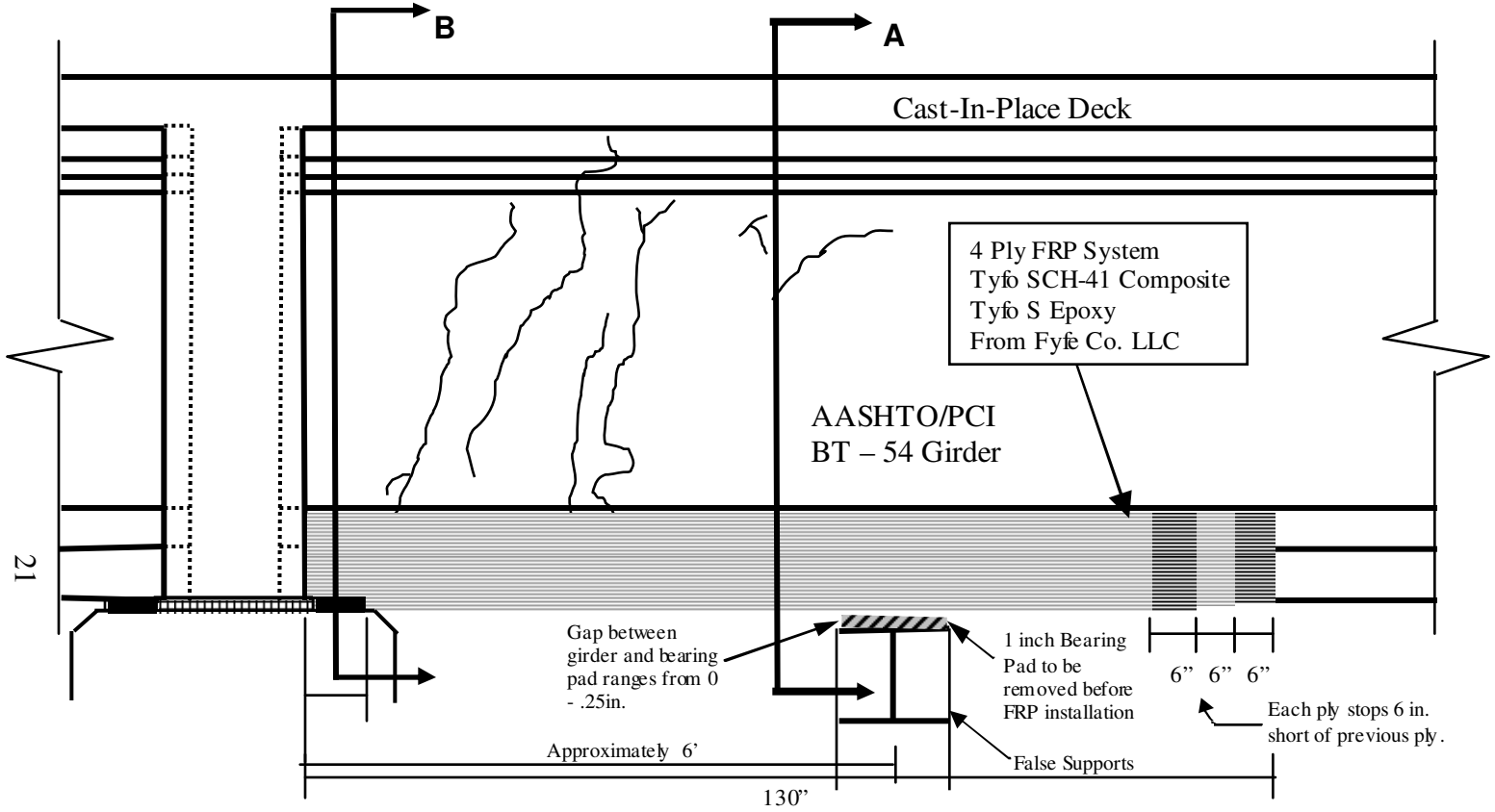


**Figure 2-8:** Elevation drawing of proposed FRP Repair (Swenson 2003a)

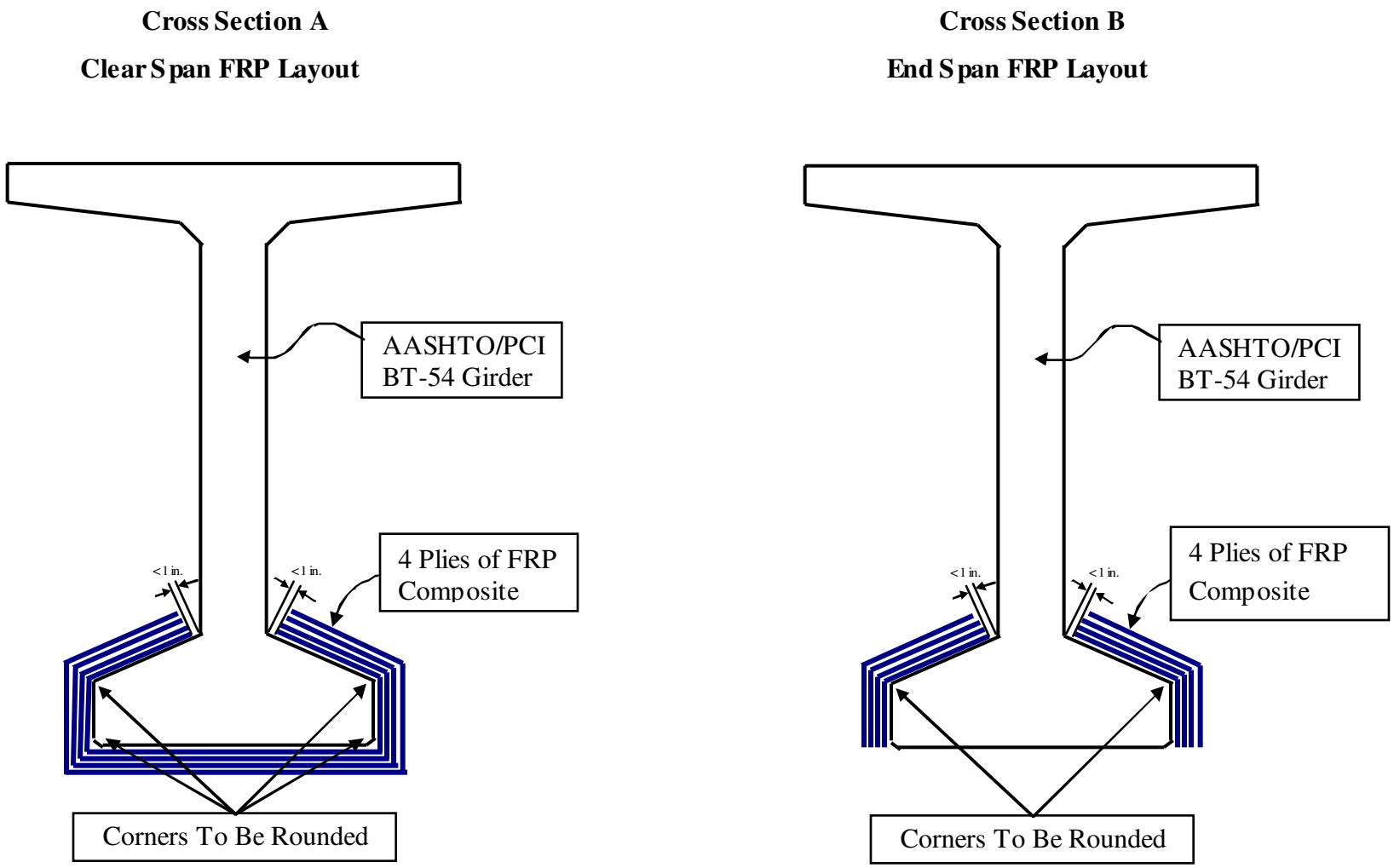


**Figure 2-9:** FRP Layout - Cross Section A and B Profile (Swenson 2003a)

concluded that the bridge was currently behaving as a continuous beam with hinges at the cracked sections, and the prestressing strands were acting as effective reinforcement under the service-level test loads.

After selecting a proper base model to match the current behavior of the bridge, Shapiro added FRP reinforcement to the model in accordance with the design proposed by Swenson, and re-analyzed it. Based on the results, it was concluded that the FRP returned the bridge to nearly continuous behavior. The analysis results showed that the FRP was acting in compression, potentially proving that Swenson's analysis, which predicted high tensile strains in the FRP, may be overly conservative. Shapiro did not attempt to analyze the enhanced strength of the bridge due to the FRP repair; she only worked to provide the predicted behavior change of the bridge that should be anticipated in post-repair testing.

## 2.3 BRIDGE SPANS TO BE TESTED

Gao's and Swenson's research included analyses of Northbound Spans 4 and 5 of the I-565 bridge girders. Later it was decided that the actual repair should take place on Northbound Spans 10 and 11. The horizontal curvature and individual span lengths of the girders vary slightly between these two continuous units. Girders in all four spans contain identical reinforcement. Also, all four spans contain identical design material properties of the concrete and steel (Swenson 2003b).

### 2.3.1 DESCRIPTION OF BRIDGE LAYOUT

Northbound Spans 10 and 11 are joined at Bent 11 to form a two-span continuous structure. Both spans have a length of 101.40 ft and zero horizontal curvature. Each girder has a length of 99.42 ft and a clear span length of 98.50 ft (Swenson 2003a). Each

span has nine prestressed concrete bulb-tee 54 (BT-54) girders spaced eight feet apart center to center. Figure 2-10 shows a typical cross section of a BT54 girder and Figure 2-11 shows a typical cross sectional view of the bridge. Each prestressed girder is reinforced identically and contains both draped and debonded prestressing strands. The deck is 70.75-ft wide and 6.5-in. thick. The 28-day compressive strength of the deck is 4000 psi, and only Grade 40 mild steel reinforcement with an elastic modulus of 29,000 ksi is used in the deck (Swenson 2003b). A continuity diaphragm was used to establish continuity between spans. A portion of the deck was cast at the same time as the continuity diaphragm to further enhance the continuity. Figures 2-12 through 2-19 contain various views showing the prestressed tendon layout, vertical shear reinforcement, reinforcement in the continuity diaphragm, and longitudinal mild steel reinforcement in the deck. Appendix A provides a plan layout for the two-span continuous bridge tested.

## 2.4 CURRENT RESEARCH

Personnel at Auburn University are currently researching the benefits of an actual FRP installation. To determine the benefits of the FRP application several steps were proposed. Initially, a review of the current status of the girder ends and bent to which the FRP shall be applied was conducted. Secondly, the bridge was load tested before repair. Next, the FRP is applied, and finally, a bridge load test must be conducted after the FRP is applied. This report will detail the first two steps of this process: the review of the current bridge status and the details for the load test before FRP is applied.

### 2.4.1 CURRENT BRIDGE STATUS – BENT 11

Before FRP repair or the pre-FRP application load test could begin, a survey of the current bridge status was completed. The purpose of the survey was to inspect the actual bridge girders to be tested and to identify any additional problems that may be encountered during the load test or FRP application. A more thorough description of this survey is contained in Chapter 3.

### 2.4.2 PRE-FRP APPLICATION LOAD TEST

The pre-FRP application load test had two goals. The first goal was to determine how the bridge is behaving. The second goal was to provide a baseline to which later tests could be compared. Swenson (2003a) noted that "[l]oad testing of the structure would be helpful in determining the behavior of the structure under service level loads but may not provide any other useful information".

## 2.5 FUTURE RESEARCH

Following the pre-FRP application load test, the final two steps will carried out: FRP application and the post-FRP application load test. The final load test will help to determine the actual benefits of FRP when compared to the unstrengthened load test.

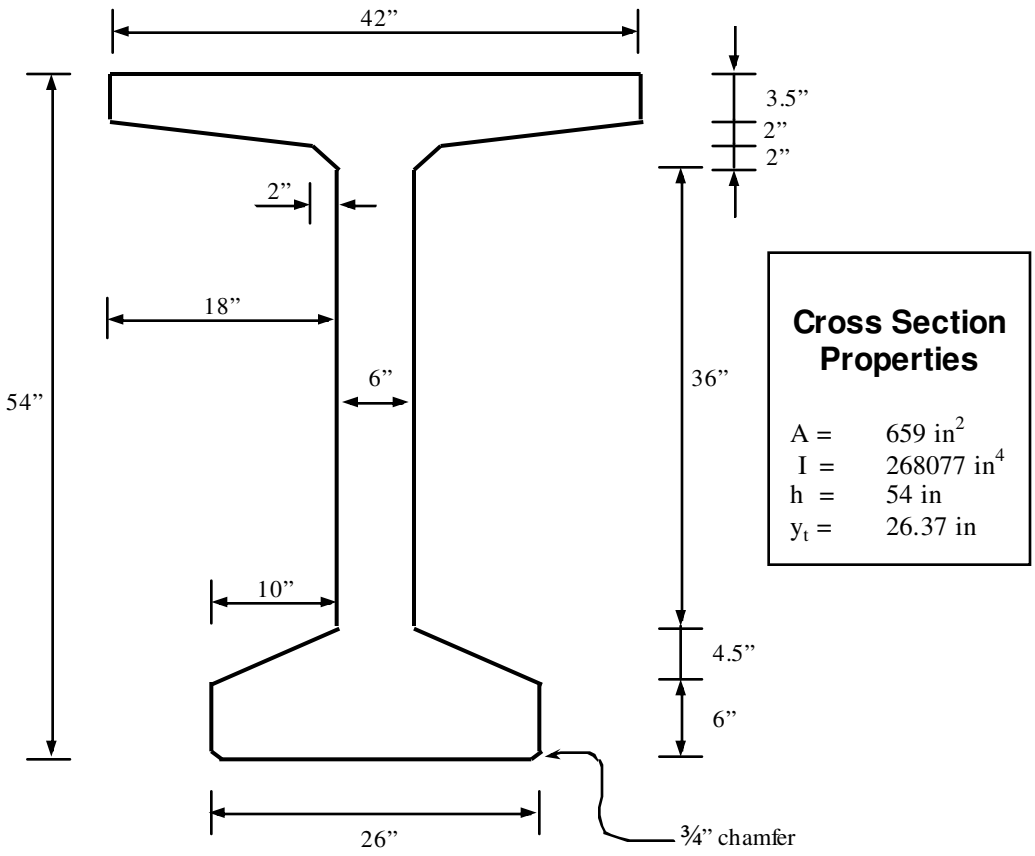


**Figure 2-10:** Cross Section of a Typical BT54 Girder (Swenson 2003a)

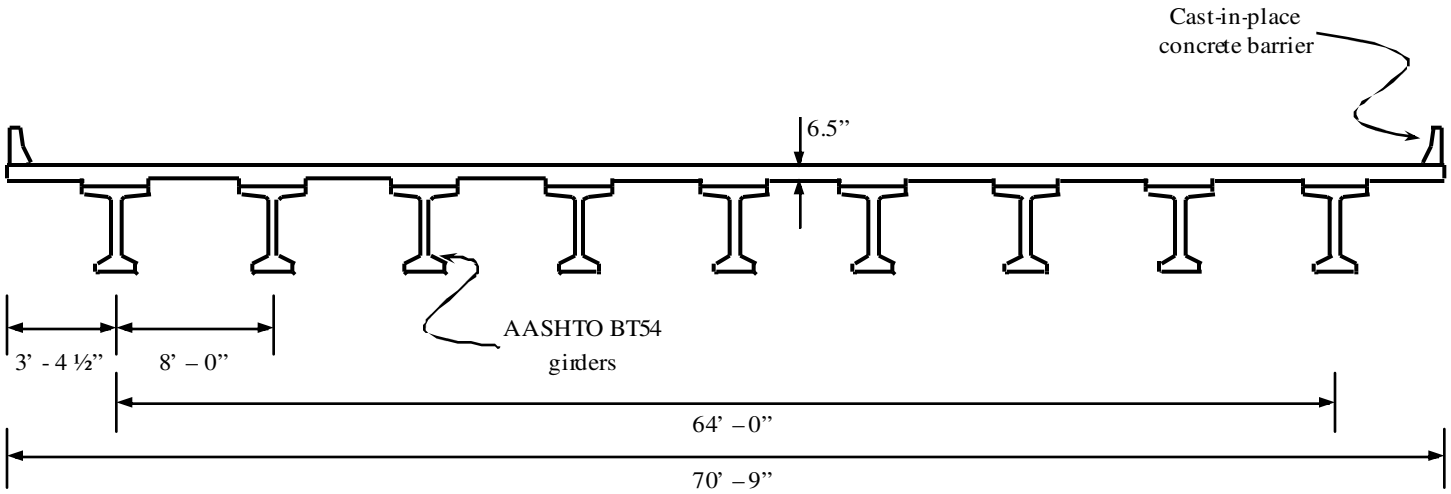


**Figure 2-11:** Cross Section of a Typical Critical Span (Swenson 2003a)

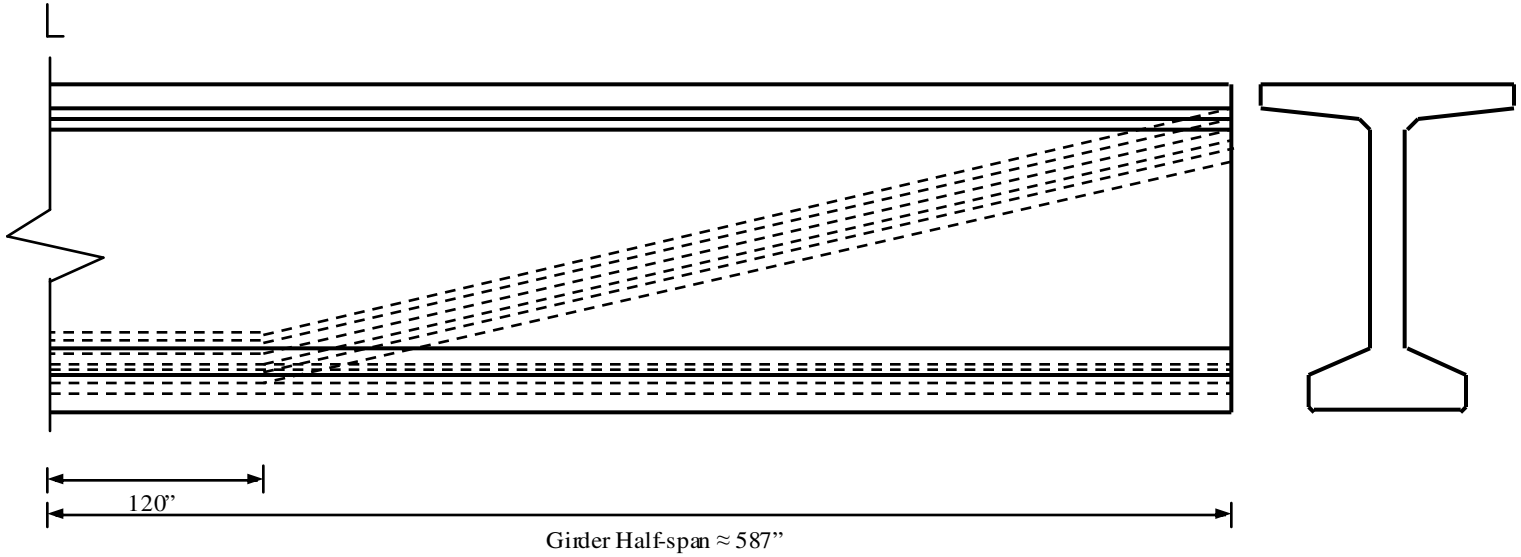


**Figure 2-12:** Longitudinal Profile of Prestressing Tendons (Swenson 2003a)

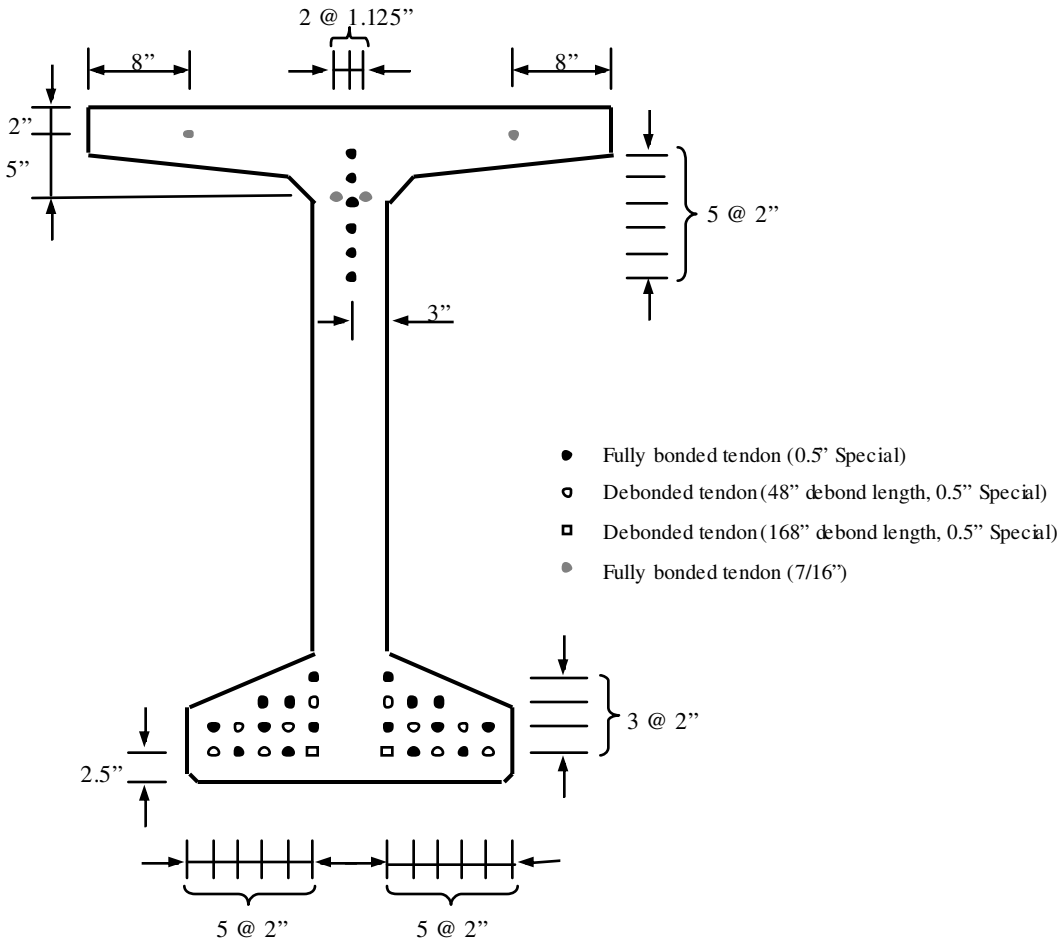


**Figure 2-13:** Cross-sectional Prestressing Tendon Profile at Girder End (Swenson 2003a)

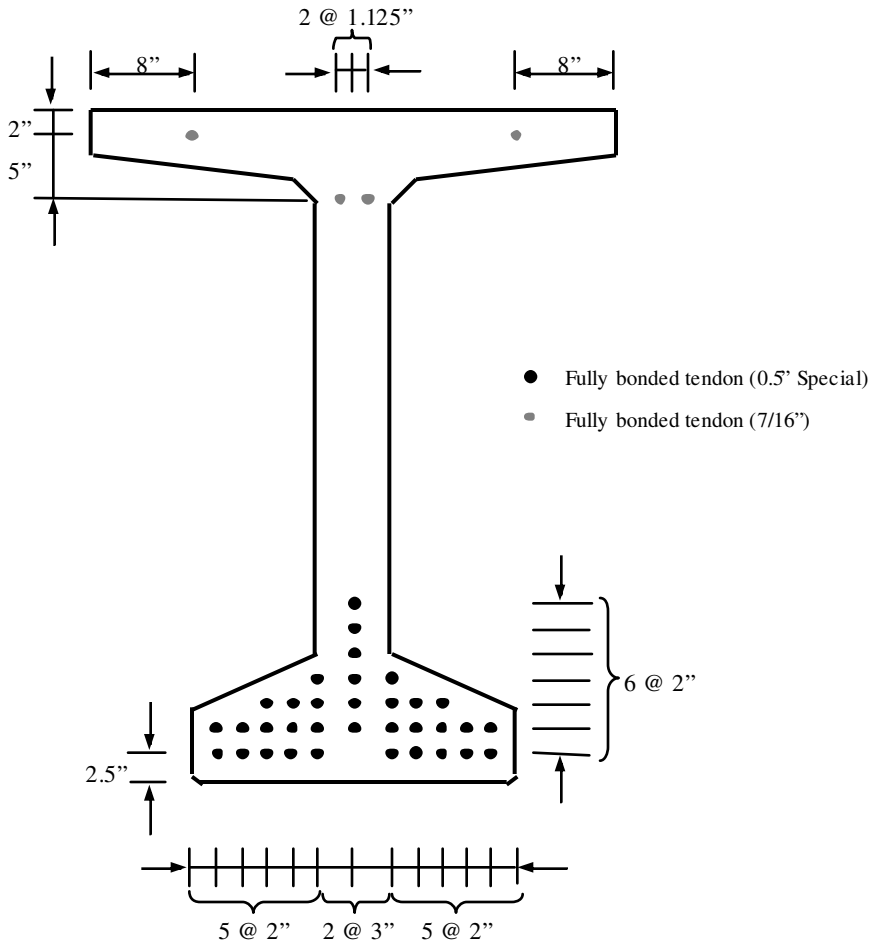


**Figure 2-14:** Cross-sectional Prestressing Tendon Profile at Midspan (Swenson 2003a)

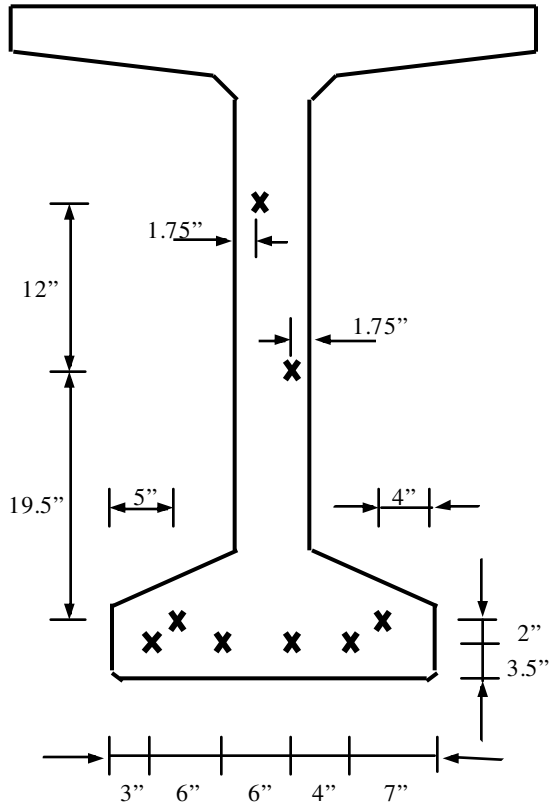


**Figure 2-15:** Location of Mild Steel Bend Bars (Swenson 2003a)

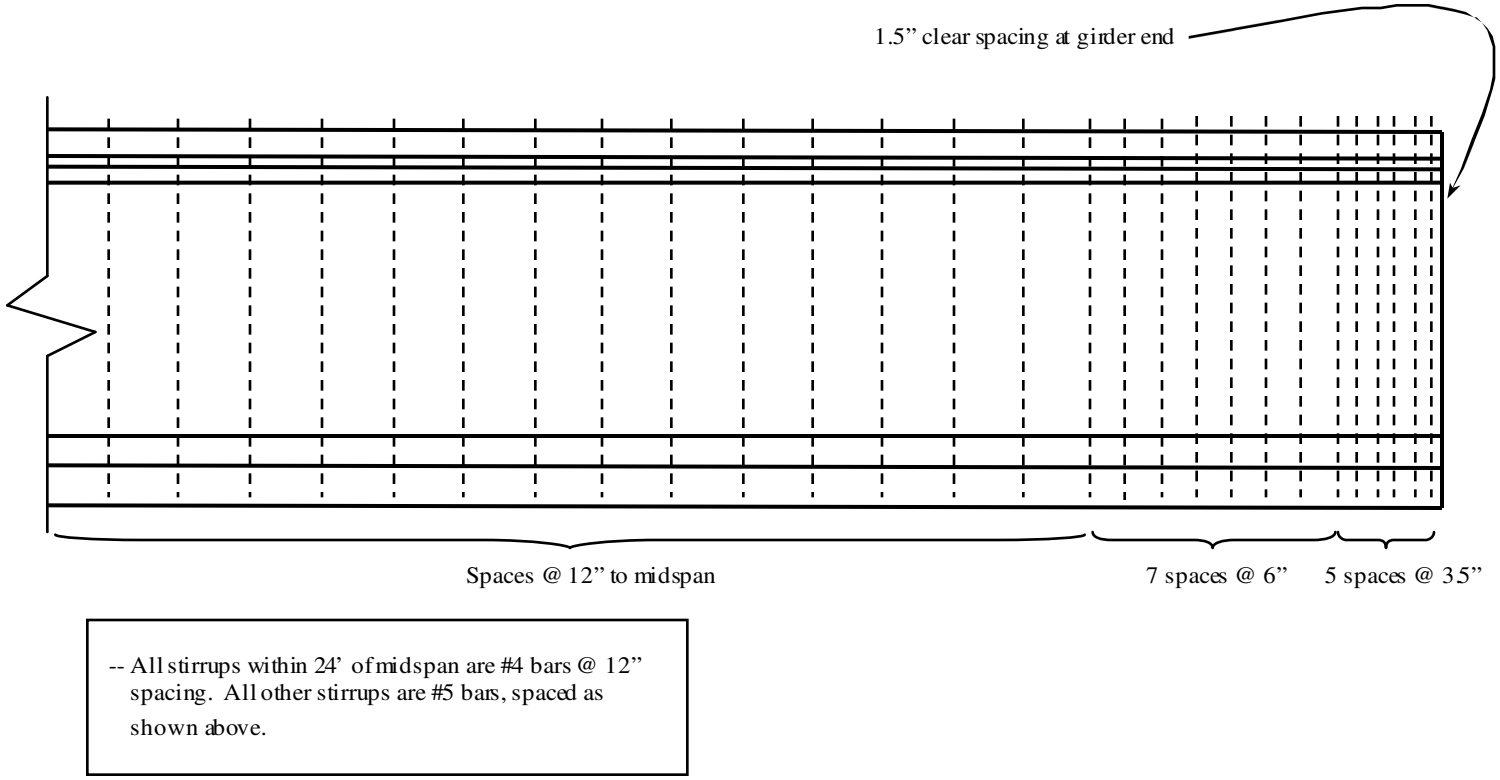


**Figure 2-16:** Location of Vertical Shear Reinforcement in a Typical BT54 Girder (Swenson 2003a)

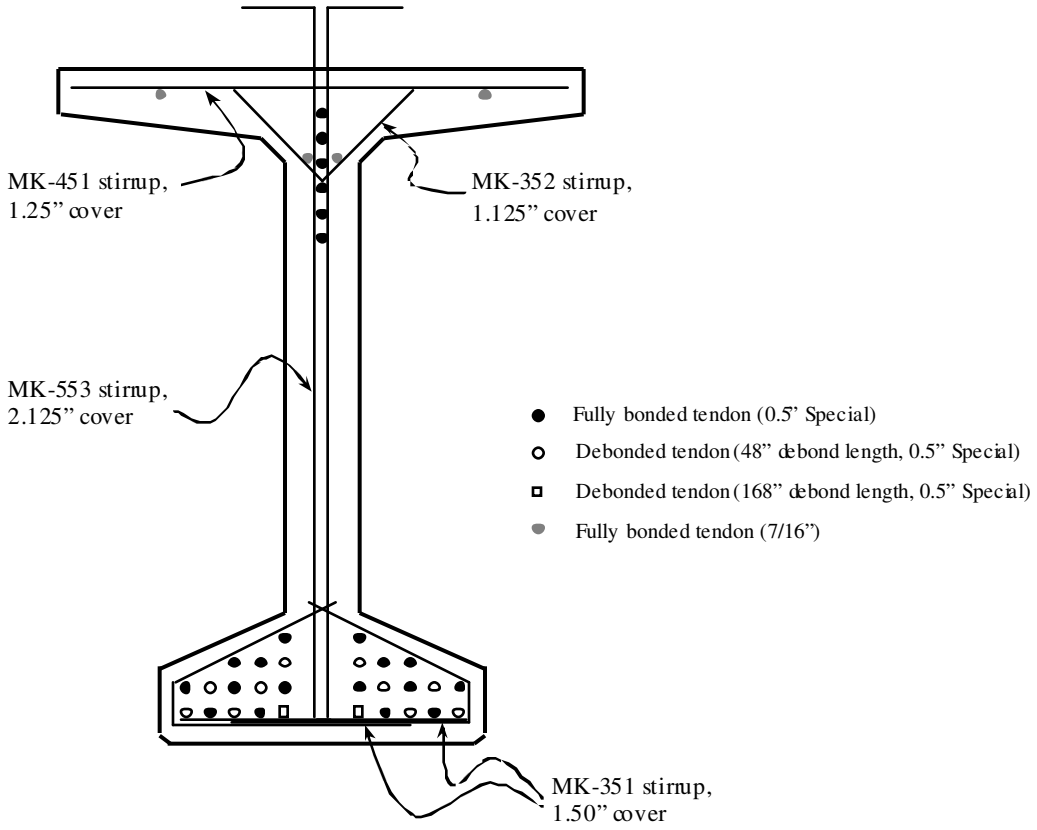


**Figure 2-17:** Cross-sectional Configuration of the Vertical Shear Reinforcement at the Girder End (Swenson 2003a)

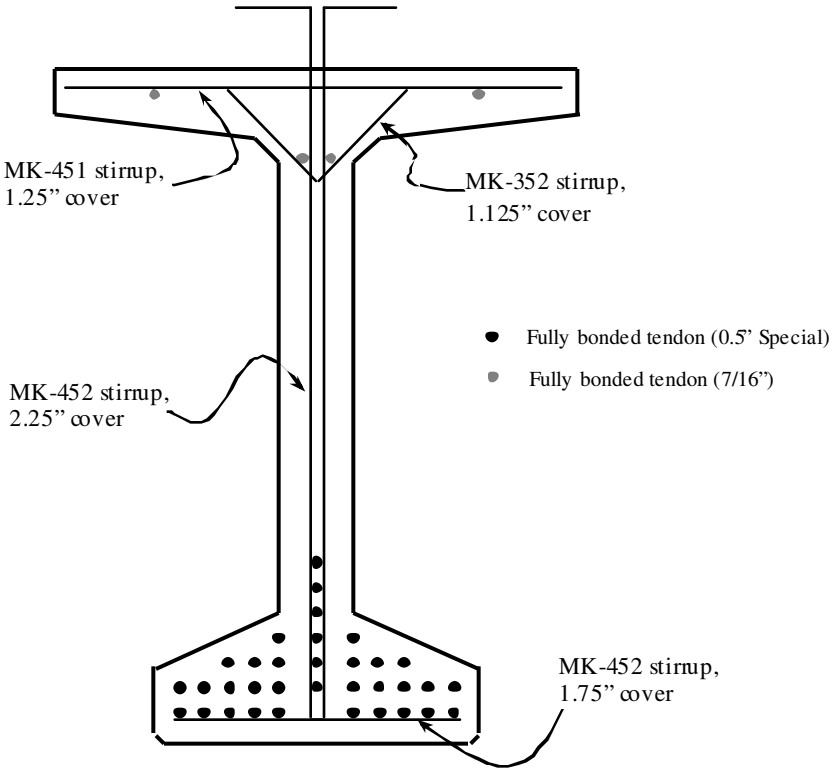


**Figure 2-18:** Cross-sectional Configuration of the Vertical Shear Reinforcement at Midspan (Swenson 2003a)

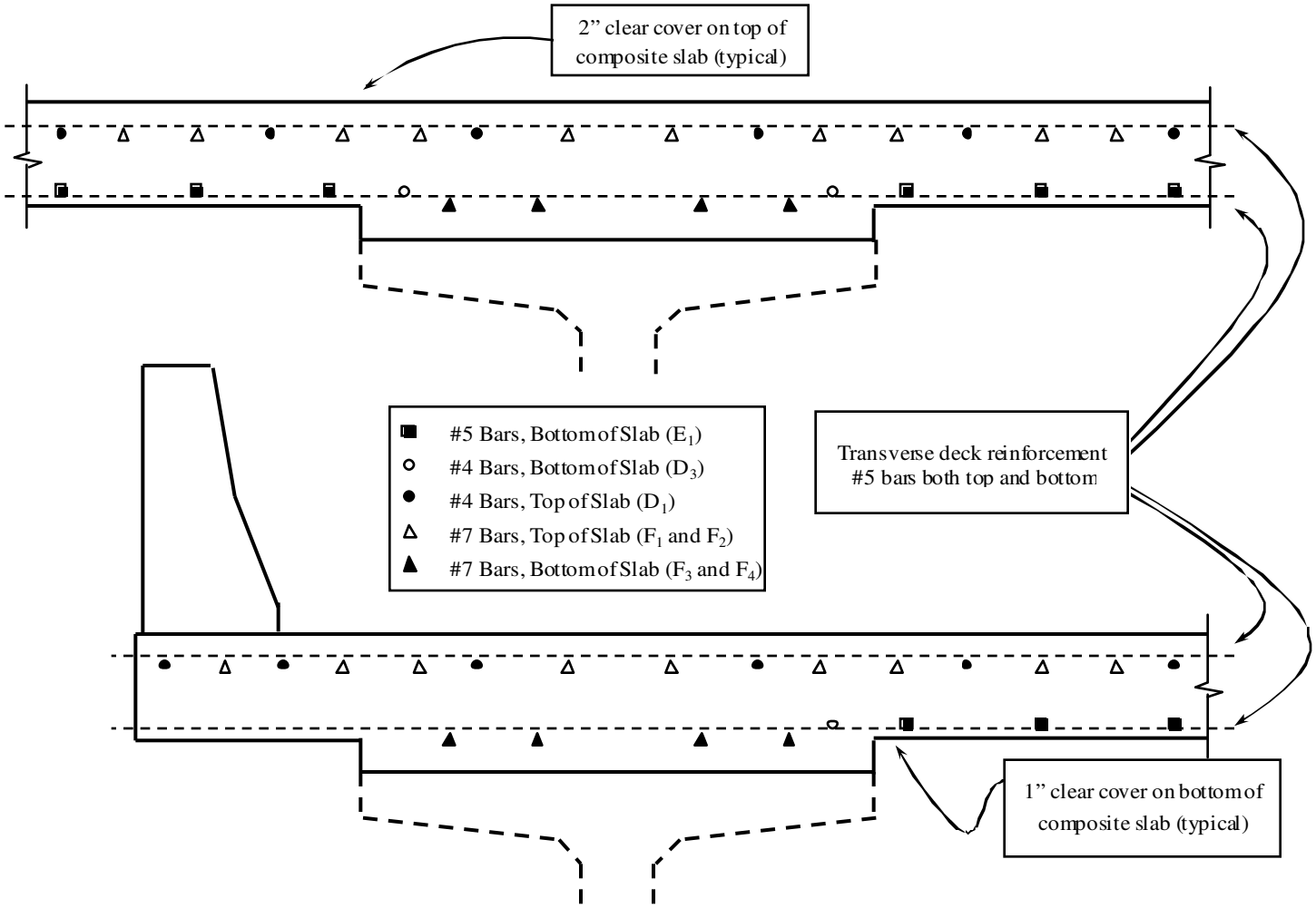


**Figure 2-19:** Longitudinal Mild Steel Reinforcement in the Deck Slab (Swenson 2003a)

# CHAPTER 3

# PRE-REPAIR BRIDGE CONDITIONS

On April 2, 2004, a team from the Auburn University Highway Research Center traveled to Huntsville to assess the condition of girders supported by Bent 11 connecting Northbound Spans 10 and 11 of I-565. The team consisted of Dr. Robert Barnes, Dr. Anton Schindler, Jiangong Xu, and Bill Fason. The inspection lasted approximately four hours, from 8:30 am until 12:30 pm. The weather was clear and cool, with temperatures starting at around 40° F and reaching approximately 55° F by the end of the inspection.

The team, assisted by employees from the Alabama Department of Transportation (ALDOT), used lift trucks to visually inspect each of the nine girder lines supported by Bent 11. Pictures were taken of each face of the eighteen girder ends, and existing cracks were noted. Figures 3-1 and 3-2 show both the bent and girder ends supported by the bent. The goal was to determine the existing conditions of the prestressed concrete girders in order to anticipate any problems that could arise during the pre-repair load test or during the placement of the Fiber Reinforced Polymer (FRP) repair.

## 3.1 FALSE SUPPORTS AND BEARING PADS

After the girders were examined, several items of concern arose. They ranged from cracking and surface preparation to difficulty of FRP installation. The most obvious problem was the location of the existing false supports and their proximity to the girders. The initial (post-cracking) design called for the false supports, which are located

approximately six feet from the bent, to be placed one inch below the girder soffits. The one-inch gap was to be partially filled with an elastomeric bearing pad as shown in Figure 3-3. On inspection, it was obvious that the gap between some of the girders and the false supports had been reduced. As depicted in Figure 3-4, a few girders appeared as though they were actually resting on the bearing pads. The small gap or lack thereof caused several concerns. One was whether the girders were depending on the false support for adequate strength. From initial inspection, this was not thought to be the case. The second concern was how to remove the bearing pad if it is being compressed. One final concern was the difficulty of placing the FRP with only ¾" to 1" of clearance between false supports and girders. This issue must be addressed by the FRP installer.

**Figure 3-1:** Bent 11 South View

**Figure 3-2:** Bent 11 North View

**Figure 3-3:** Proper Space Between Girder and False Support

**Figure 3-4:** Girder Resting on Bearing Pad

### 3.2 SURFACE PREPARATION FOR FRP APPLICATION

Another major problem is the general item of surface preparation. The ACI Guide for the Design and Construction of Externally Bonded FRP Systems for Strengthening Concrete Structures (ACI 440.2R-02) states that "Surface preparation for bond-critical applications should be in accordance with recommendations of ACI 546R and ICRI 03730." Several areas of concern arose here. A typical FRP manufacturer (Fyfe Co. 2004) specifies that the chamfered corners of the girders must be rounded to a radius of 1 inch. Rounding the corners will "prevent stress concentrations in the FRP system and voids between the FRP system and the concrete" (ACI 440.2R-02). Each of the bottom corners of the BT-54 girders must be rounded as shown in Figure 3-5.

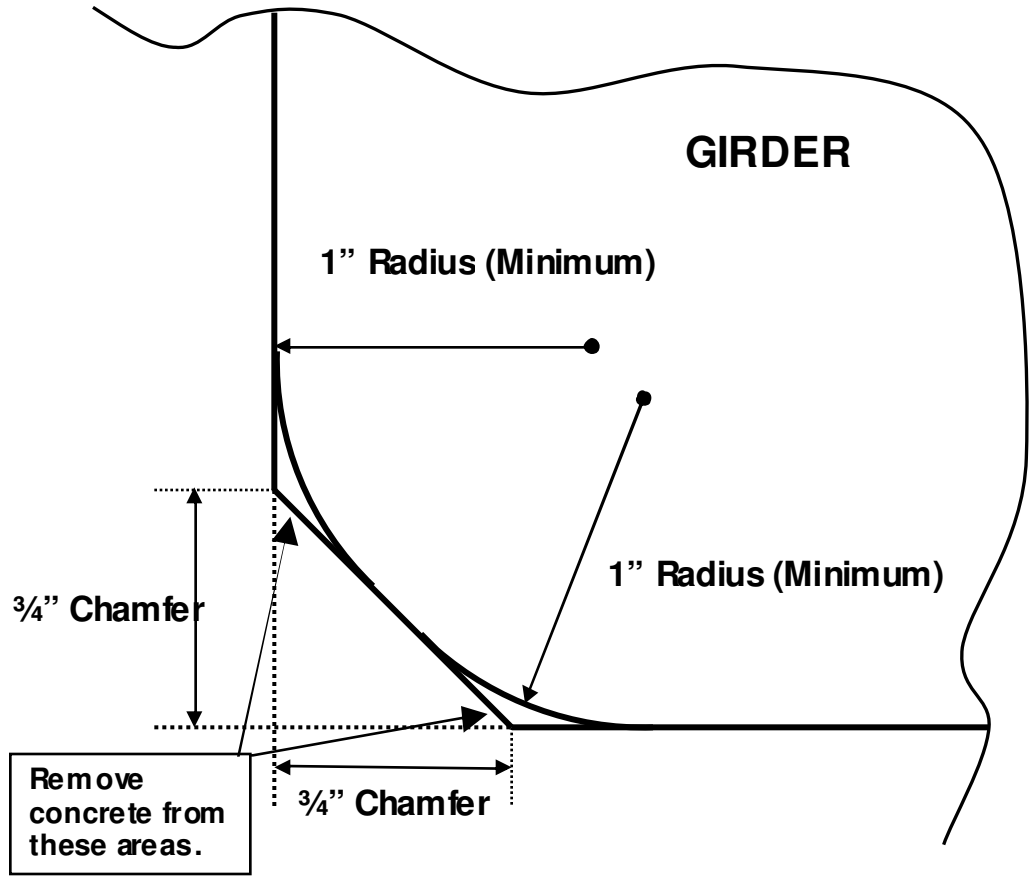


**Figure 3-5:** Proper Rounding of ¾" Chamfered Corners of Girders

"Surface preparation can be accomplished using abrasive or water-blasting techniques. All laitance, dust, dirt, oil, curing compound, existing coatings, and any other matter that could interfere with the bond of the FRP system to the concrete should be removed" (ACI 440.2R-02). The primary material that must be removed from the surface of the girders prior to FRP installation is the excess epoxy and sealant that was previously used to inject into large cracks. Examples of the epoxy remaining on the surface can be seen in Figure 3-6. "Bug holes and other small surface voids should be completely exposed during surface profiling. After the profiling operations are complete, the surface should be cleaned and protected before FRP installation so that no materials that can interfere with bond are redeposited on the surface" (ACI 440.2R-02). Any bug

holes and voids, as seen in Figure 3-7, remaining after the surface profiling should be filled with epoxy putty. "For surfaces that do not allow complete encasement with the composite system, surfaces shall be prepared for bonding by means of abrasive blasting or grinding to achieve a 1/16" minimum amplitude. All contact surfaces shall then be cleaned by hand or compressed air" (Fyfe 2004).

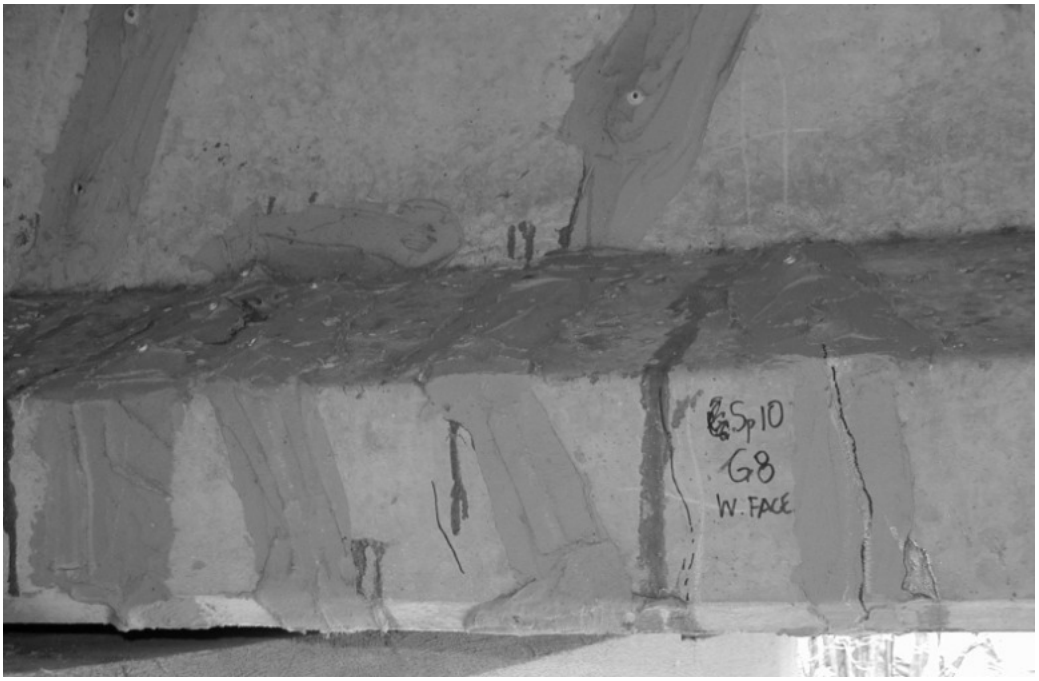


**Figure 3-6:** Epoxy Sealant to be Removed from Girders Prior to FRP Installation.

### 3.3 FRP INSTALLATION AT GIRDER SUPPORT

The proposed design for the external FRP strengthening system can be found in Section 8.3 of Swenson's thesis (2003a). Design sketches for the FRP system were presented earlier in Chapter 2 of this thesis. The FRP must be installed around the bearing pad on Bent 11. The limited amount of space between the girders and the false support could possibly present difficulties during FRP installation.

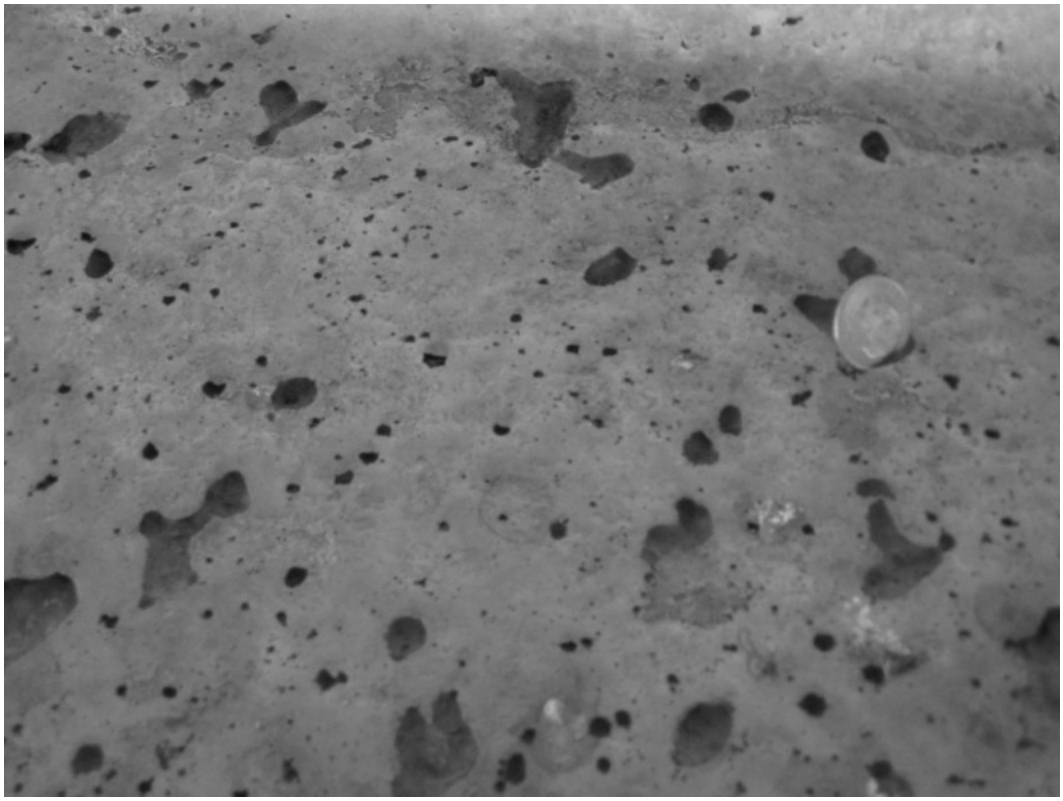

**Figure 3-7:** Bug Holes to be Filled with Epoxy Putty (Dime for Size Reference)

### 3.4 OVERVIEW OF CURRENT CONDITIONS

During the investigation of Bent 11, several different types of cracks were encountered in both the girder ends and in the continuity diaphragm. The first type was large cracks that had previously been injected with an epoxy in order to seal the crack and in an attempt to prevent additional movement of the crack that might damage the reinforcement. These cracks were the most obvious and were located on most girders. The epoxy remaining on the surface must be removed before FRP installation.

There were also many cracks present that had not yet been repaired with epoxy. There were even a few cracks that cracked through or immediately adjacent to the epoxy since the initial cracking was repaired. These unsealed cracks are the ones that cause the most concern for the bridge, because they indicate that the bridge has cracked further

since the repair. Figure 3-8 shows all three types of cracks: the older cracks sealed with epoxy, unsealed cracks marked with a black marker, and a sealed crack that has reopened marked with a black marker on top of the epoxy.

It is stated in ACI 440 that, "Some FRP manufacturers have reported that the movement of cracks 0.010 in. (0.3 mm) and wider can affect the performance of the externally bonded FRP system through delamination or fiber crushing" (ACI 440). Therefore, ACI 440 suggests that "cracks wider than 0.010 in. (0.3 mm) should be pressure injected with epoxy in accordance with ACI 224.1R." During the inspection of the bridge, no existing cracks were found that measured larger than 0.01 in. No additional epoxy injection will be necessary prior to FRP installation.

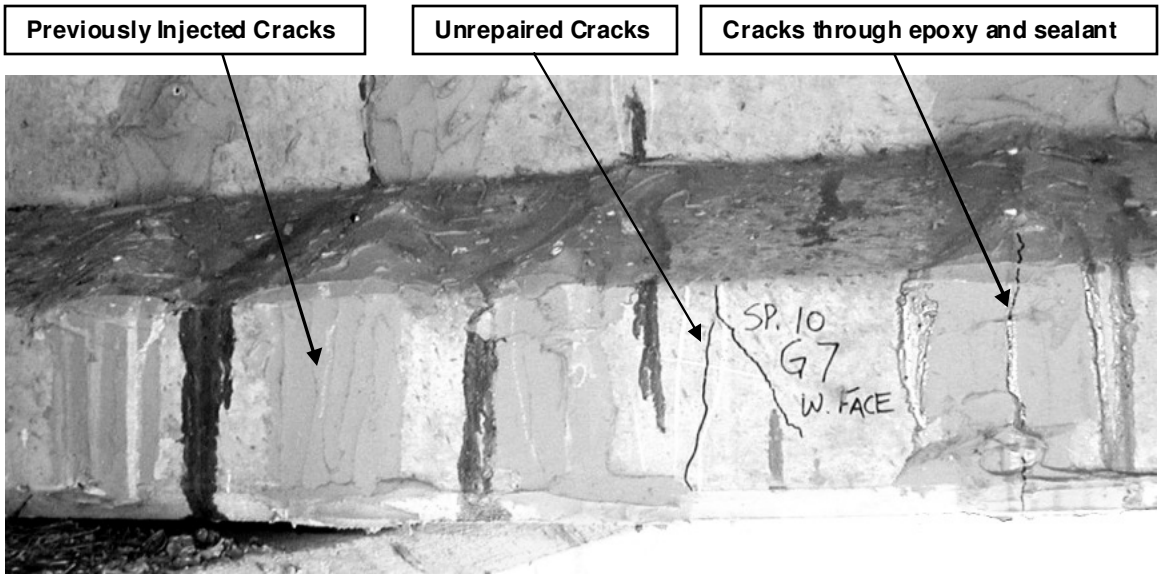


**Figure 3-8:** Types of Cracking

## 3.5 CRACK LOCATIONS AND SUMMARY—GIRDER BY GIRDER

Figure 3-9 shows the basic layout and orientation of the girder lines and bents for I-565 Spans 10 and 11. The area that was inspected is also shown. The continuity diaphragm connects girders from Span 10 with those from Span 11. Tables 3-1 and 3-2 provide a summary of the existing conditions.

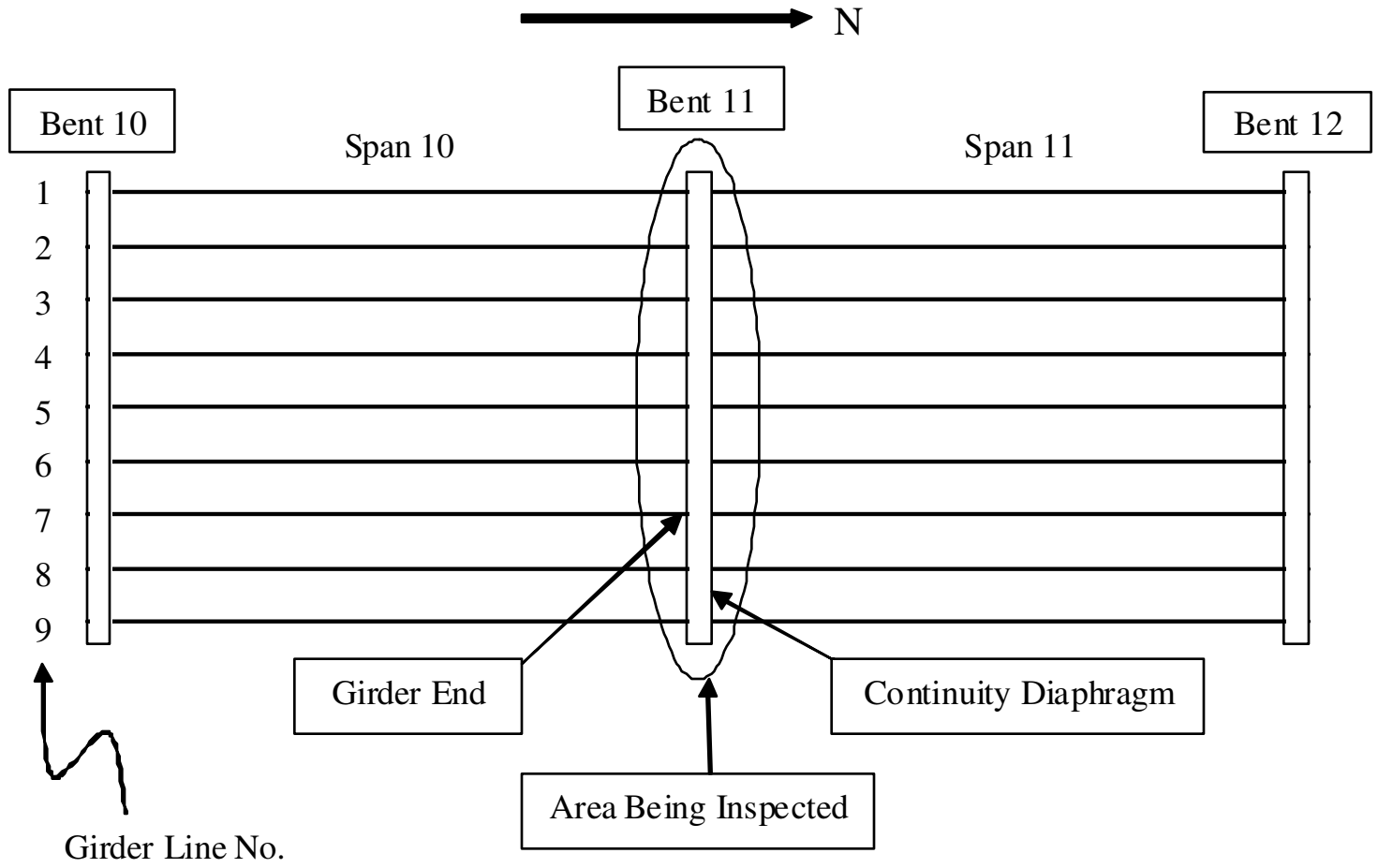


**Figure 3-9:** Girder Line Numbering Layout

**Table 3-1:** Summary of Existing Conditions - Span 10

| | Span 10 | | | | |
|---|---|---|---|---|---|
| | Existing Conditions | | | | |
| | **View** | **Unsealed Cracks** | **Sealed Cracks** | **Minimum Support Clearance (in.)** | **Notes** |
| **Girder 1** | West | Present | None | 1 1/8 | |
| | East | Present | None | | |
| **Continuity Diaphragm** | Cracking and Spalling | | | | |
| **Girder 2** | West | None | None | 1 1/4 | Almost Completely separated from Continuity Diaphragm. |
| | East | None | None | | |
| **Continuity Diaphragm** | Cracking and Spalling | | | | |
| **Girder 3** | West | None | Present | 1 1/8 | Previous Cracks have been sealed. Small unsealed cracks in the Bottom Flange of Bulb-Tee |
| | East | Present | Present | | |
| **Continuity Diaphragm** | Cracking and Small amounts of Spalling | | | | |
| **Girder 4** | West | None | Present | 1 1/4 | |
| | East | Present | Present | | |
| **Continuity Diaphragm** | Cracking, Spalling, Cores going behind Girder 4 and Saw Cut going behind Girder 5 | | | | |
| **Girder 5** | West | None | Present | 1 1/8 | |
| | East | None | Present | | |
| **Continuity Diaphragm** | Cracking | | | | |
| **Girder 6** | West | Present | Present | 1 | |
| | East | Present | Present | | |
| **Continuity Diaphragm** | Minimal Cracking and Spalling, Shrinkage Crack | | | | |
| **Girder 7** | West | Present | Present | On Bearing Pad around 7/8" | New Cracks through Sealed Cracks. Crack Widths around 0.005 inches. |
| | East | Present | Present | | |
| **Continuity Diaphragm** | Shrinkage Crack | | | | |
| **Girder 8** | West | Present | Present | 1 | New Cracks through Sealed Cracks. Crack Widths around 0.005 inches. |
| | East | Present | Present | | |
| **Continuity Diaphragm** | Shrinkage Crack and Minimal Spalling | | | | |
| **Girder 9** | West | Present | None | | |
| | East | Present | None | | |

**Table 3-2:** Summary of Existing Conditions - Span 11

| | Span 11 | | | | |
|---|---|---|---|---|---|
| | Existing Conditions | | | | |
| | **View** | **Unsealed Cracks** | **Sealed Cracks** | **Minimum Support Clearance (in.)** | **Notes** |
| **Girder 1** | West | None | Present | On Bearing Pad | Bolts on Outside Face of Girder, Probably for Restraint |
| | East | Present | None | | |
| **Continuity Diaphragm** | None | | | | |
| **Girder 2** | West | None | None | 1 1/8 | Large Cracks around Continuity Diaphagm, Girder interface on opposing face |
| | East | None | None | | |
| **Continuity Diaphragm** | None | | | | |
| **Girder 3** | West | None | Present | On Bearing Pad | |
| | East | None | Present | | |
| **Continuity Diaphragm** | Cracking, Spalling, and Holes Drilled Behind Girder 4 | | | | |
| **Girder 4** | West | None | Present | On Bearing Pad | |
| | East | None | Present | | |
| **Continuity Diaphragm** | None | | | | |
| **Girder 5** | West | None | Present | On Bearing Pad | |
| | East | None | Present | | |
| **Continuity Diaphragm** | Cracking, Spalling, Holes Drilled Behind Girder 5, and Rebar showing beside Girder 6 | | | | |
| **Girder 6** | West | None | Present | 1 1/8 | |
| | East | None | Present | | |
| **Continuity Diaphragm** | Severe Crack beside Girder 6, and Shrinkage Crack | | | | |
| **Girder 7** | West | Present | Present | On Bearing Pad | Large Number of Cracks |
| | East | Present | Present | | |
| **Continuity Diaphragm** | Minimal Cracking | | | | |
| **Girder 8** | West | Present | Present | On Bearing Pad | Large Number of Cracks |
| | East | Present | Present | | |
| **Continuity Diaphragm** | Minimal Cracking | | | | |
| **Girder 9** | West | Present | Present | On Bearing Pad around 1" | |
| | East | None | Present | | |

### 3.5.1 GIRDER LINE 1

Girder Line 1 exhibits both sealed and unsealed cracks as depicted in Figure 3-10. The only notable feature unique to this girder line is a bolt located near the connection with the continuity diaphragm on the west side of Span 11. This bolt will probably need to be removed before FRP installation.

### 3.5.2 GIRDER LINE 2

As can be seen in Figure 3-11, Girder Line 2 exhibits no substantial cracking on the girder face. It must be noted that on the Span 10 side, the girder has almost completely separated from the continuity diaphragm. The continuity diaphragm has large cracks and spalled areas near the girder interface. Girder Line 2 is unique in that it does not have serious cracking on the girder faces.

### 3.5.3 GIRDER LINE 3

As can be seen in Figure 3-12, Girder Line 3 exhibits primarily cracks that have been previously sealed. The Span 10 side, west view, has a small unsealed crack in the bottom flange.

### 3.5.4 GIRDER LINE 4

As can be seen in Figure 3-13, Girder Line 4 has a large number of sealed cracks, while only a couple of small unsealed cracks are present on the Span 10 side, west view.

### 3.5.5 GIRDER LINE 5

As can be seen in Figure 3-14, Girder Line 5 exhibits large sealed cracks.

### 3.5.6 GIRDER LINE 6

As can be seen in Figure 3-15, Girder Line 6 exhibits mainly large sealed cracks. A few unsealed cracks are present at the bottom of the Span 10 side.

### 3.5.7 GIRDER LINE 7

As can be seen in Figure 3-16, Girder Line 7 exhibits a large number of both sealed and unsealed cracks. The number of new unsealed cracks is unique to Girder Lines 7 and 8. Span 11 has unsealed cracks paralleling sealed cracks and running nearly the entire depth of the beam. Span 10 has shorter unsealed cracks that remain in the bottom flange, as well as sealed cracks that have recracked through the epoxy.

### 3.5.8 GIRDER LINE 8

As can be seen in Figure 3-17, Girder Line 8 exhibits cracking very similar to Girder Line 7. There are large sealed cracks. Span 11 has long unsealed cracks, while Span 10 has shorter unsealed cracks with one previously sealed crack that had cracked again.

### 3.5.9 GIRDER LINE 9

As can be seen in Figure 3-18, Girder Line 9 exhibits sealed cracks on Span 11 and unsealed cracks on Span 10. Span 11 also has a few small unsealed cracks.

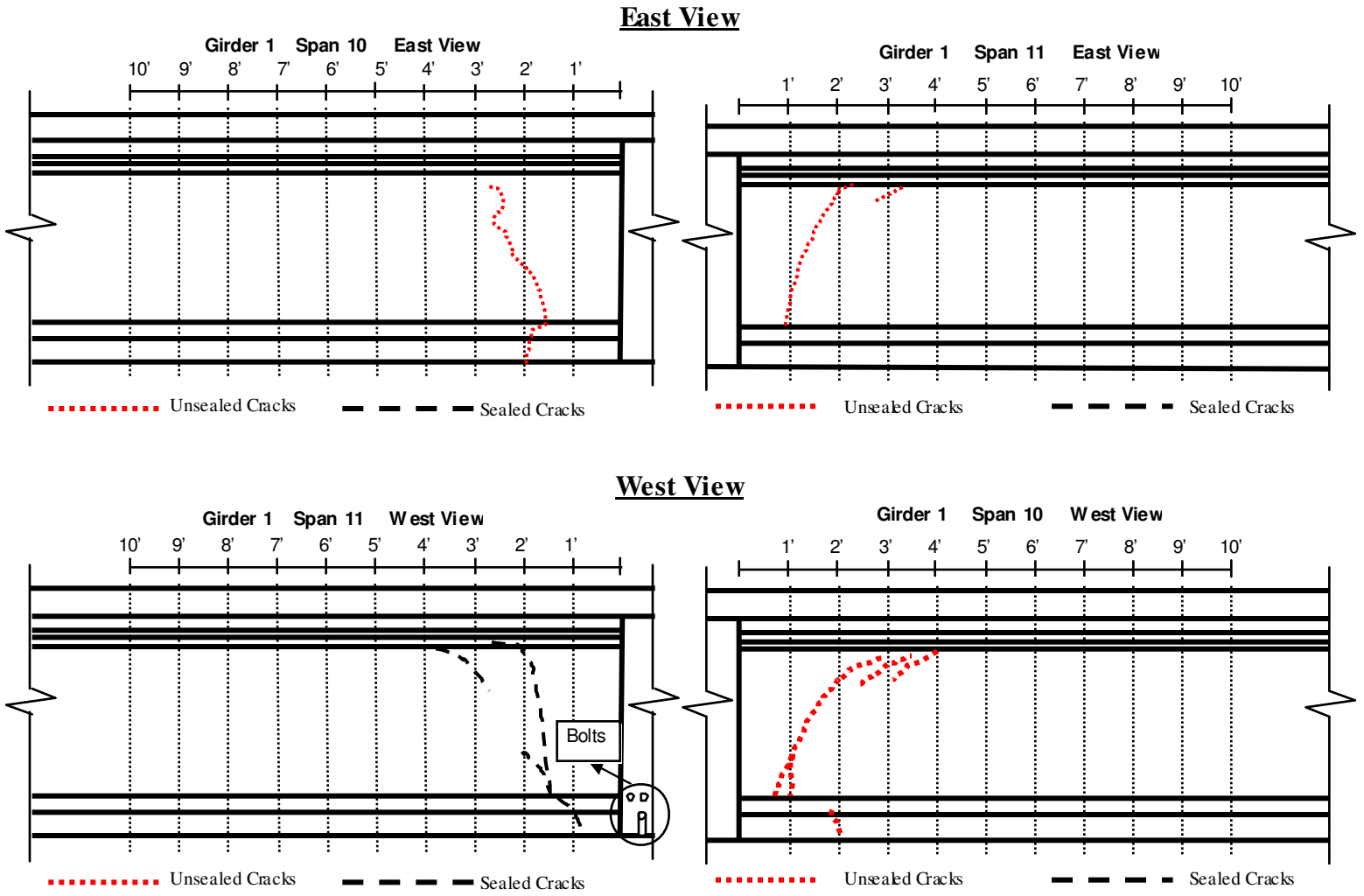


**Figure 3-10:** Girder Line 1 Cracking

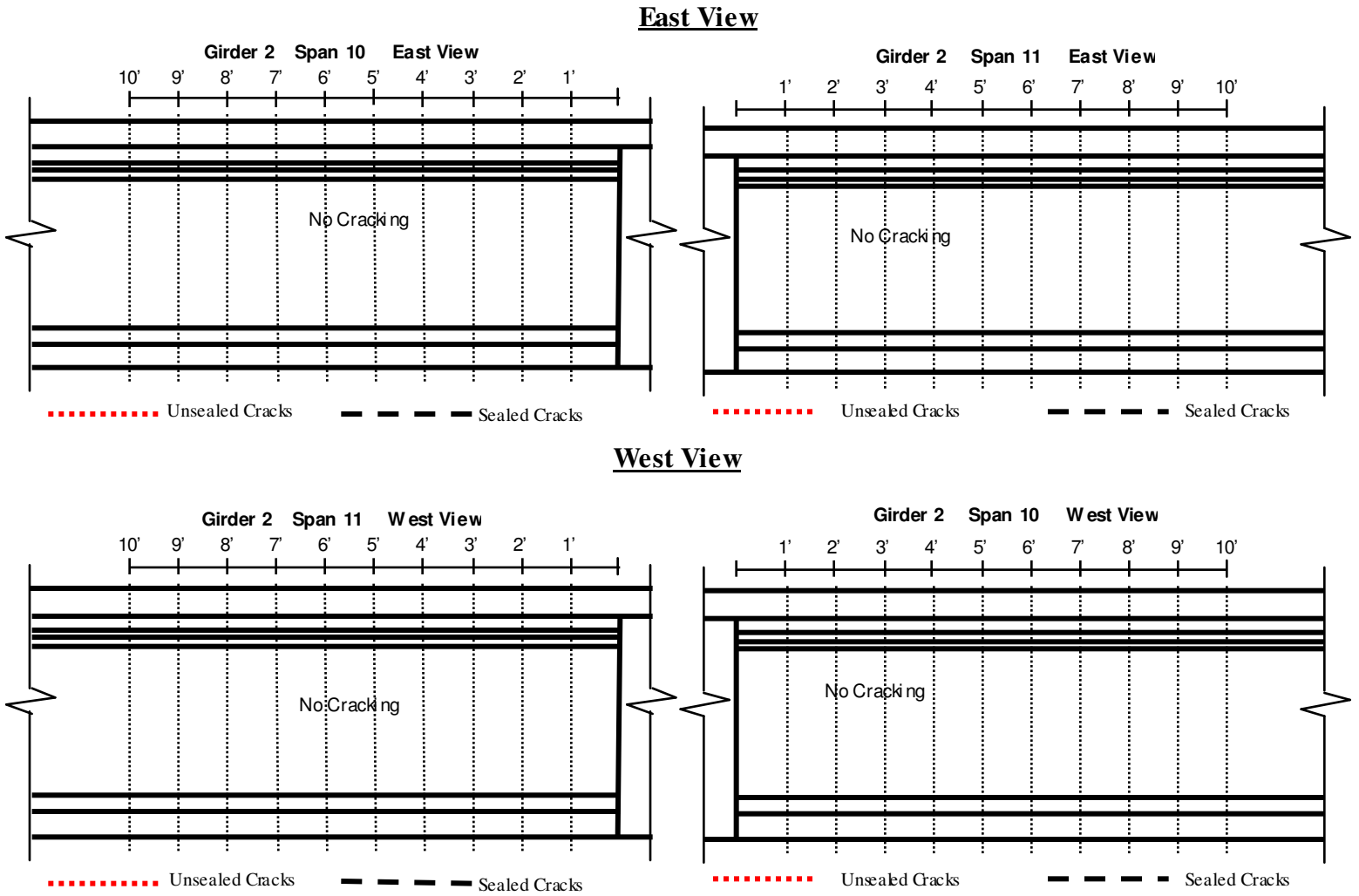


**Figure 3-11:** Girder Line 2 Cracking

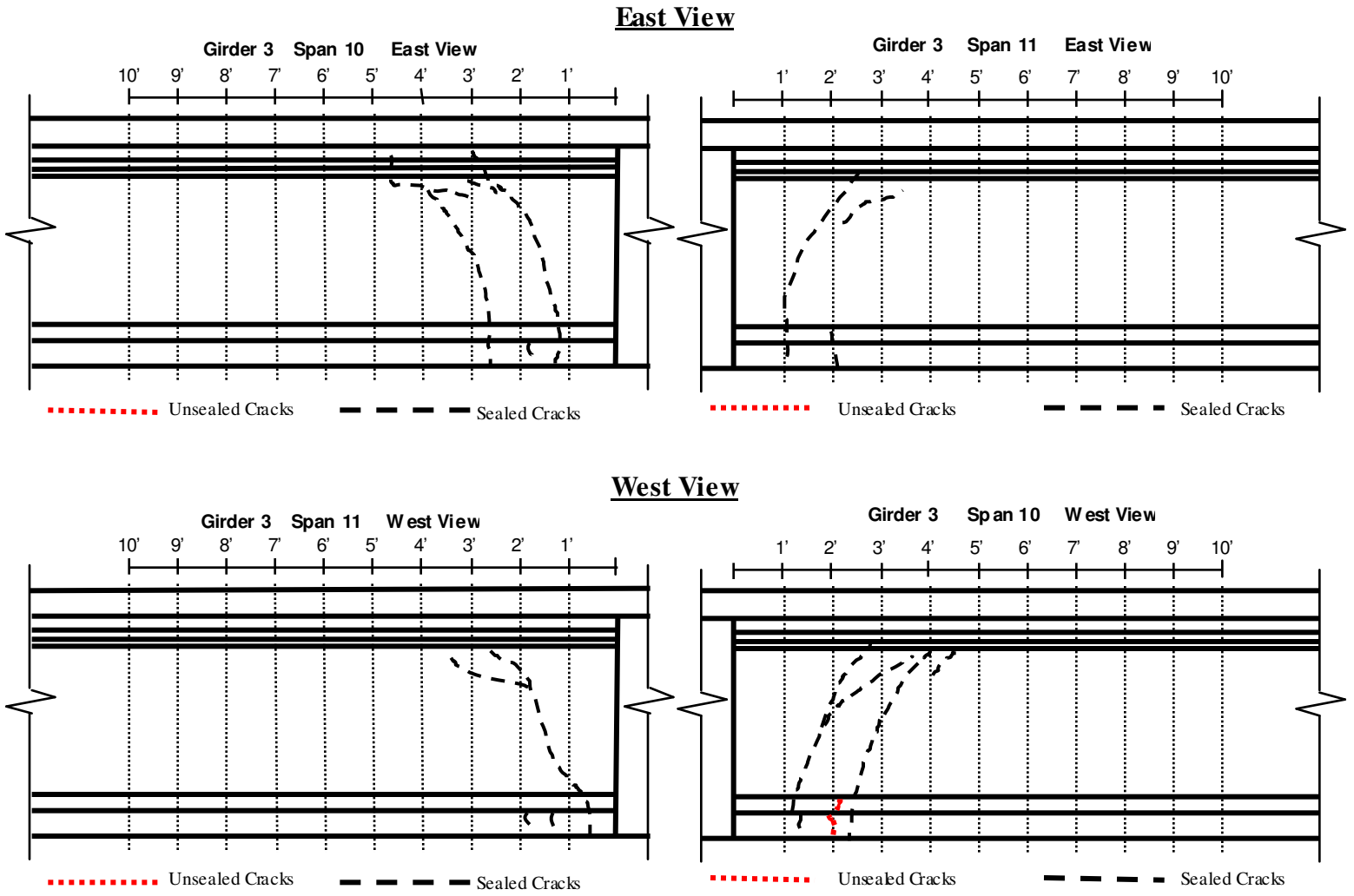


**Figure 3-12:** Girder Line 3 Cracking

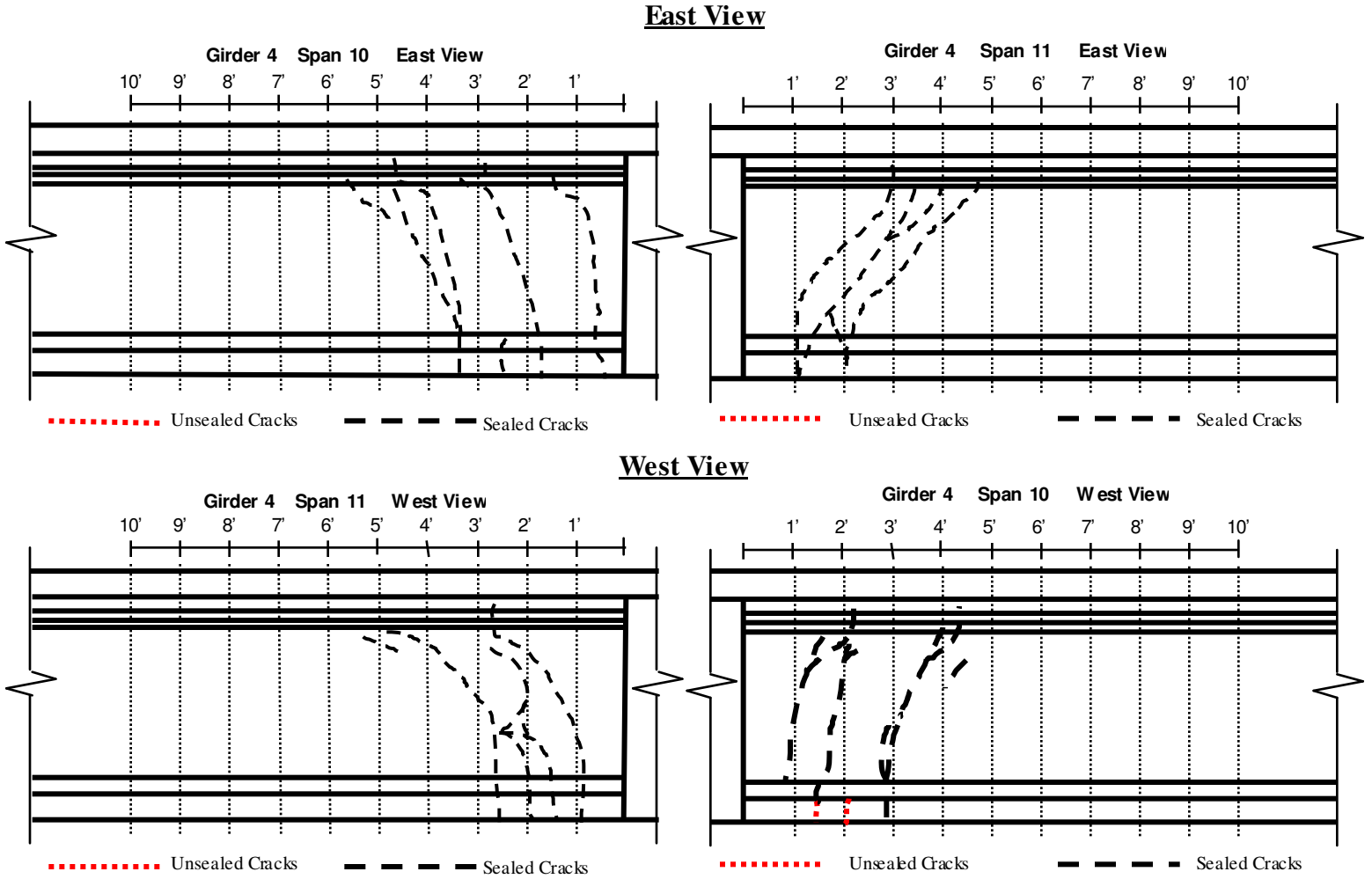


**Figure 3-13:** Girder Line 4 Cracking

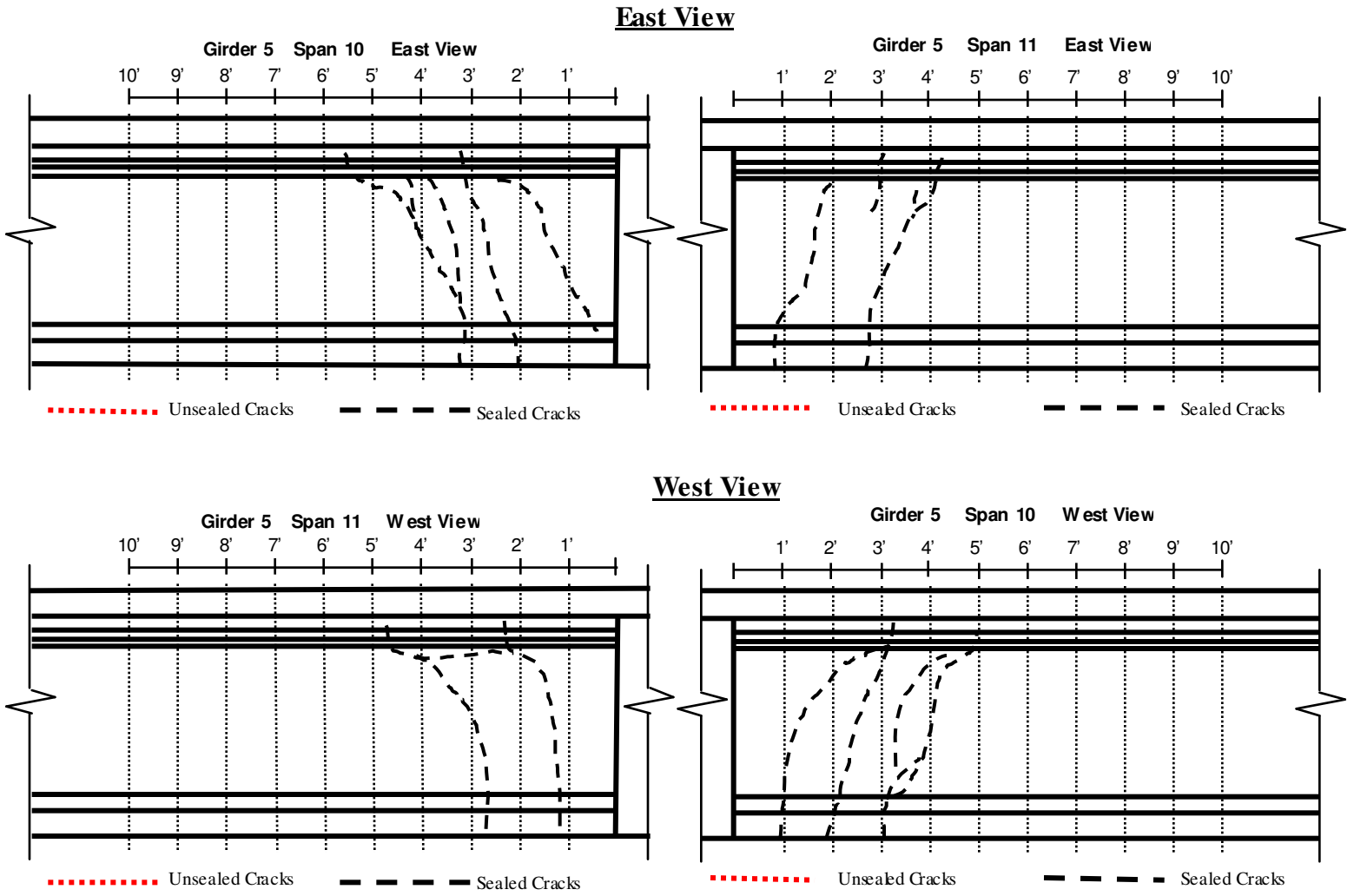


**Figure 3-14:** Girder Line 5 Cracking

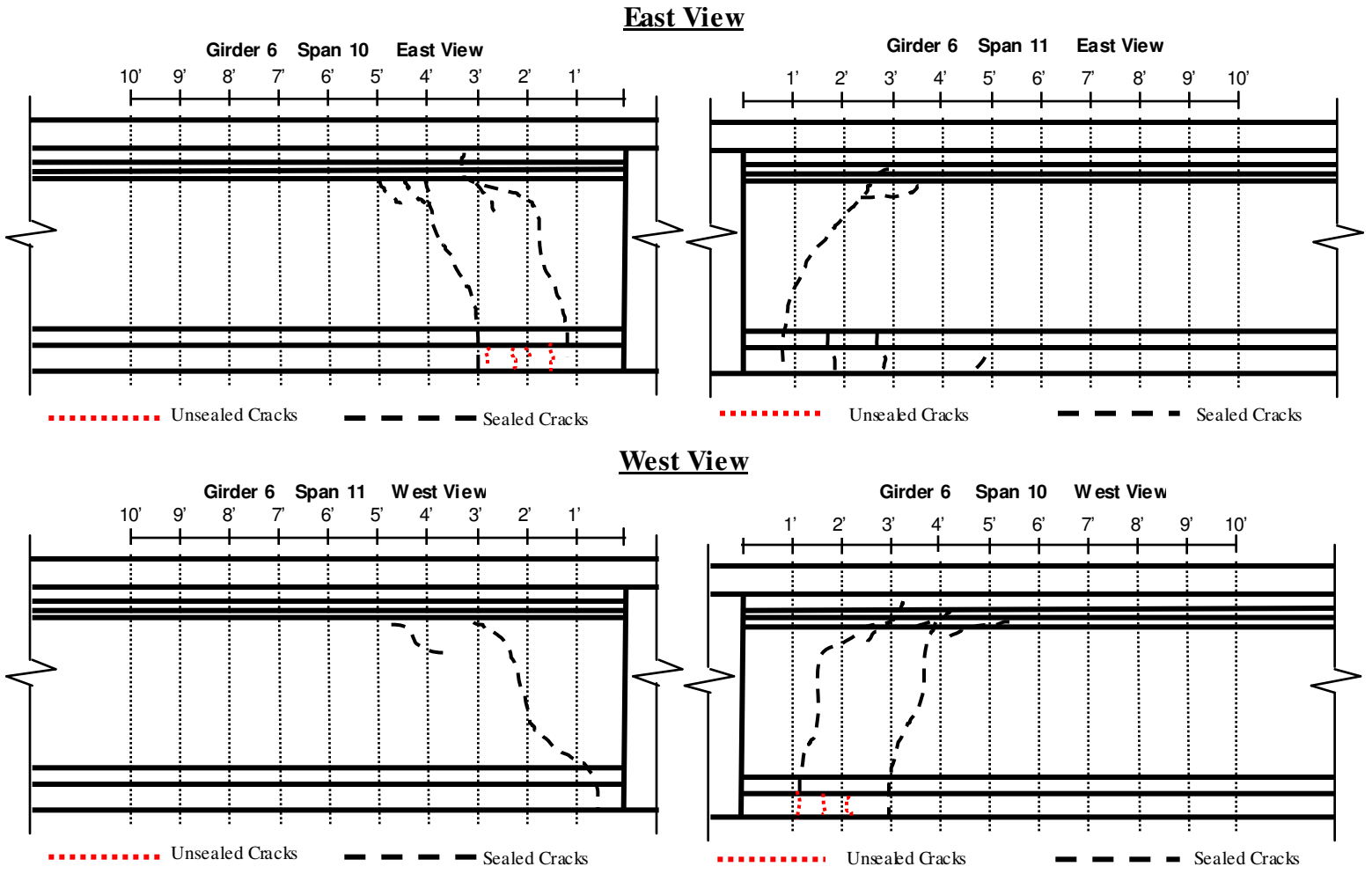


**Figure 3-15:** Girder Line 6 Cracking

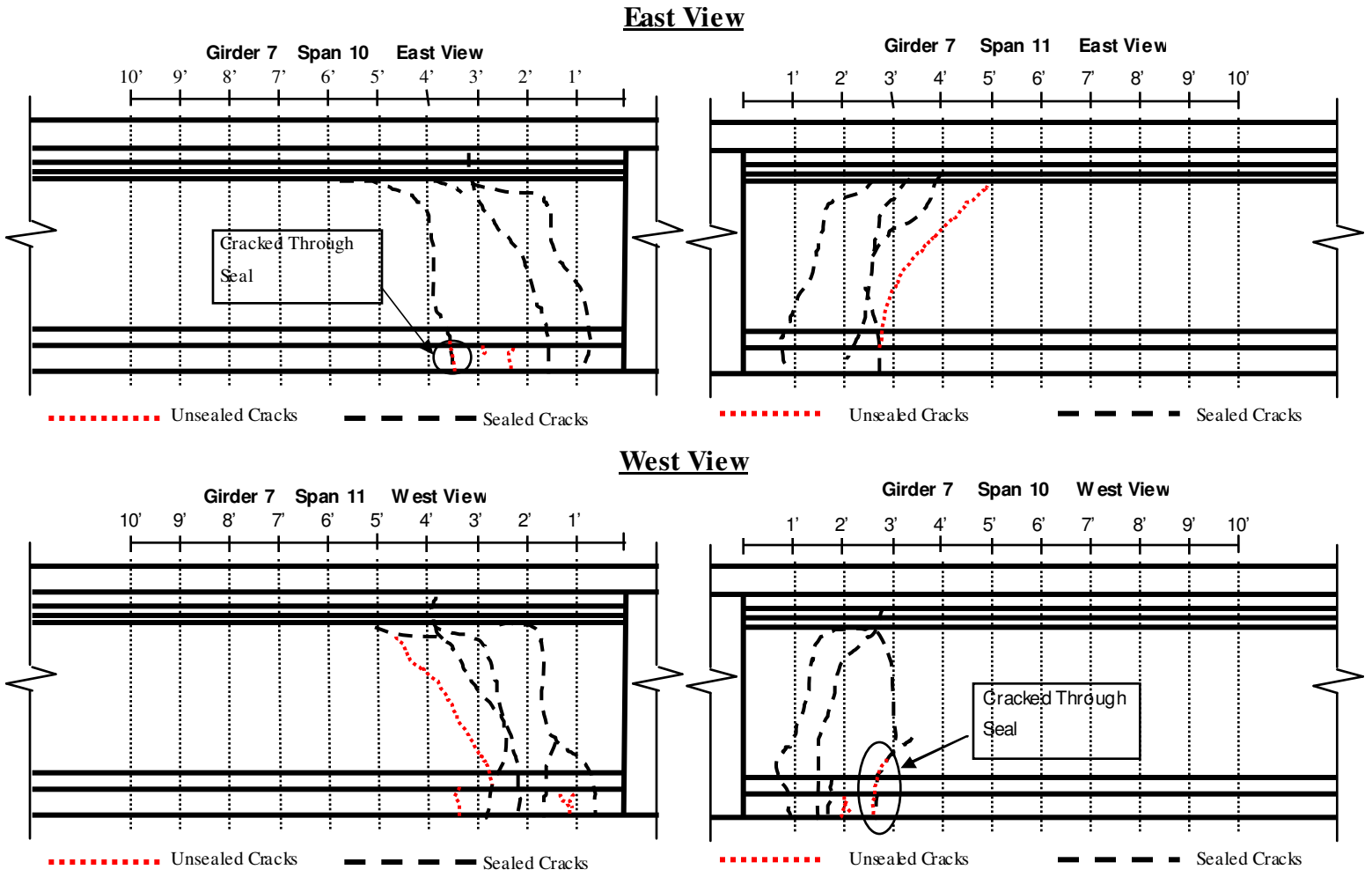


**Figure 3-16:** Girder Line 7 Cracking

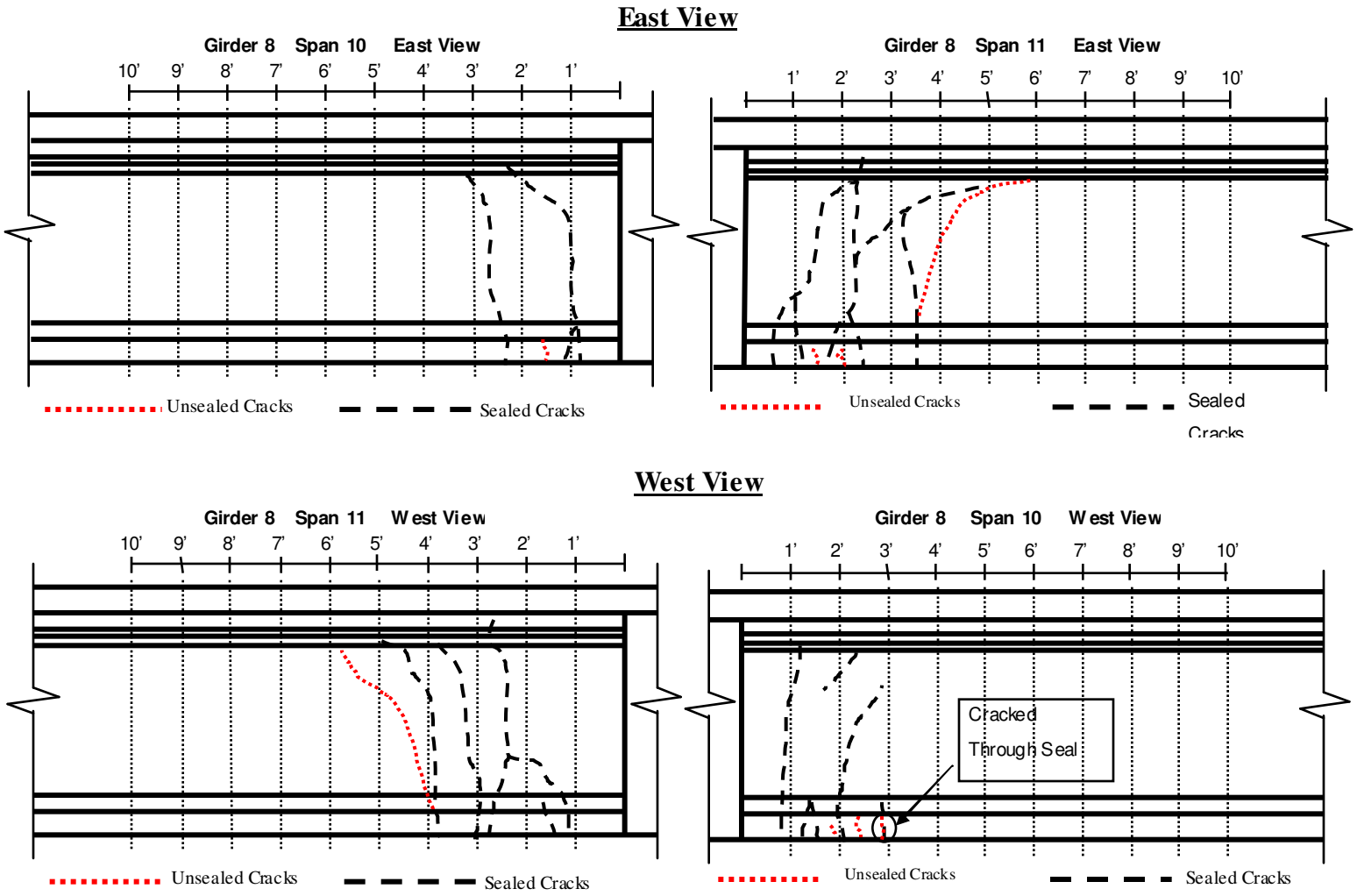


**Figure 3-17:** Girder Line 8 Cracking

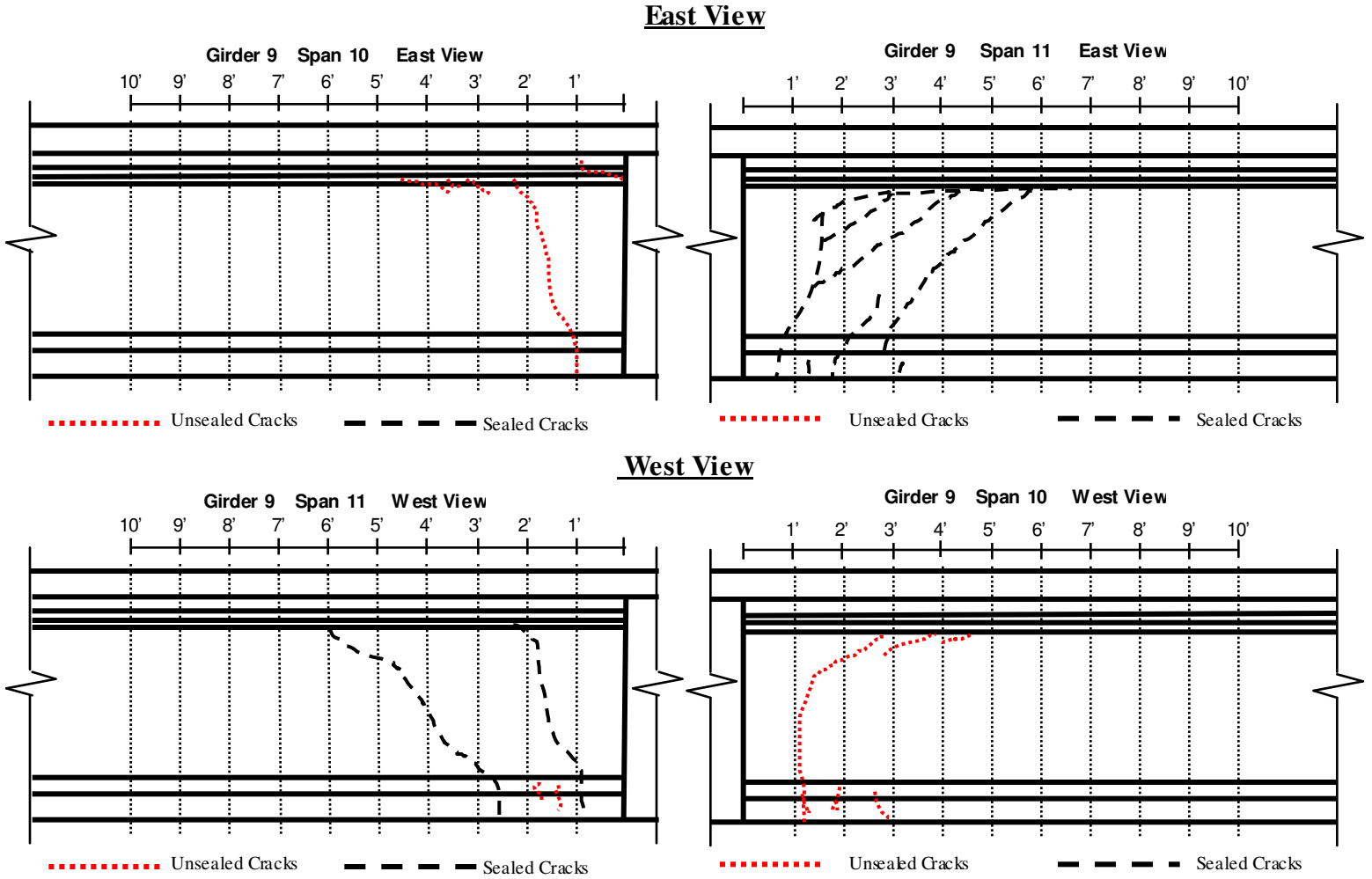


**Figure 3-18:** Girder Line 9 Cracking

## 3.6 CRACK LOCATIONS AND SUMMARY—CONTINUITY DIAPHRAGM

### 3.6.1 BETWEEN GIRDER LINES 1 AND 2

As can be seen in Figure 3-19, large cracks and spalled areas are located on the south side of the continuity diaphragm between these girder lines. There is not much cracking on the north side.

### 3.6.2 BETWEEN GIRDER LINES 2 AND 3

As can be seen in Figure 3-20, cracking and spalled areas are primarily located on the south side. There is not much cracking on the north side.

### 3.6.3 BETWEEN GIRDER LINES 3 AND 4

As can be seen in Figure 3-21, the south side primarily exhibited cracks with a few small spalled areas. The north side has large spalled areas as well as several drilled cores from an earlier abandoned attempt to release the girder continuity at the diaphragm.

### 3.6.4 BETWEEN GIRDER LINES 4 AND 5

As can be seen in Figure 3-22, the south side has cracks, spalled areas, cores, and a saw cut. There is not much cracking on the north side.

### 3.6.5 BETWEEN GIRDER LINES 5 AND 6

As can be seen in Figure 3-23, the south side has only cracks. The north side has cracks, spalled areas with exposed reinforcing bars, and drilled cores.

### 3.6.6 BETWEEN GIRDER LINES 6 AND 7

As can be seen in Figure 3-24, the south side has cracking with one small spalled area. The north side has mainly cracking with one rather large crack.

### 3.6.7 BETWEEN GIRDER LINES 7 AND 8

As can be seen in Figure 3-25, both sides have only small cracks.

### 3.6.8 BETWEEN GIRDER LINES 8 AND 9

As can be seen in Figure 3-26, the south side has both cracking and spalling. The north side has only a small amount of cracking.

## 3.7 SUMMARY OF EXISTING CONDITIONS

All girders have significant cracking within the girder end regions with the exception of Girder Line 2. None of the unsealed cracks measured as large as 0.01 in. Therefore, none of the unsealed cracks need to be epoxy injected, and no special attention should be given to the handling of the unsealed cracks. Before the FRP can be installed properly, the concrete surfaces must be carefully prepared, removing all debris, epoxy on the surface, and any other substances that may impede bonding between the concrete and FRP. It was decided that the repair contractor would bear responsibility for removal of bearing pads above the false supports.

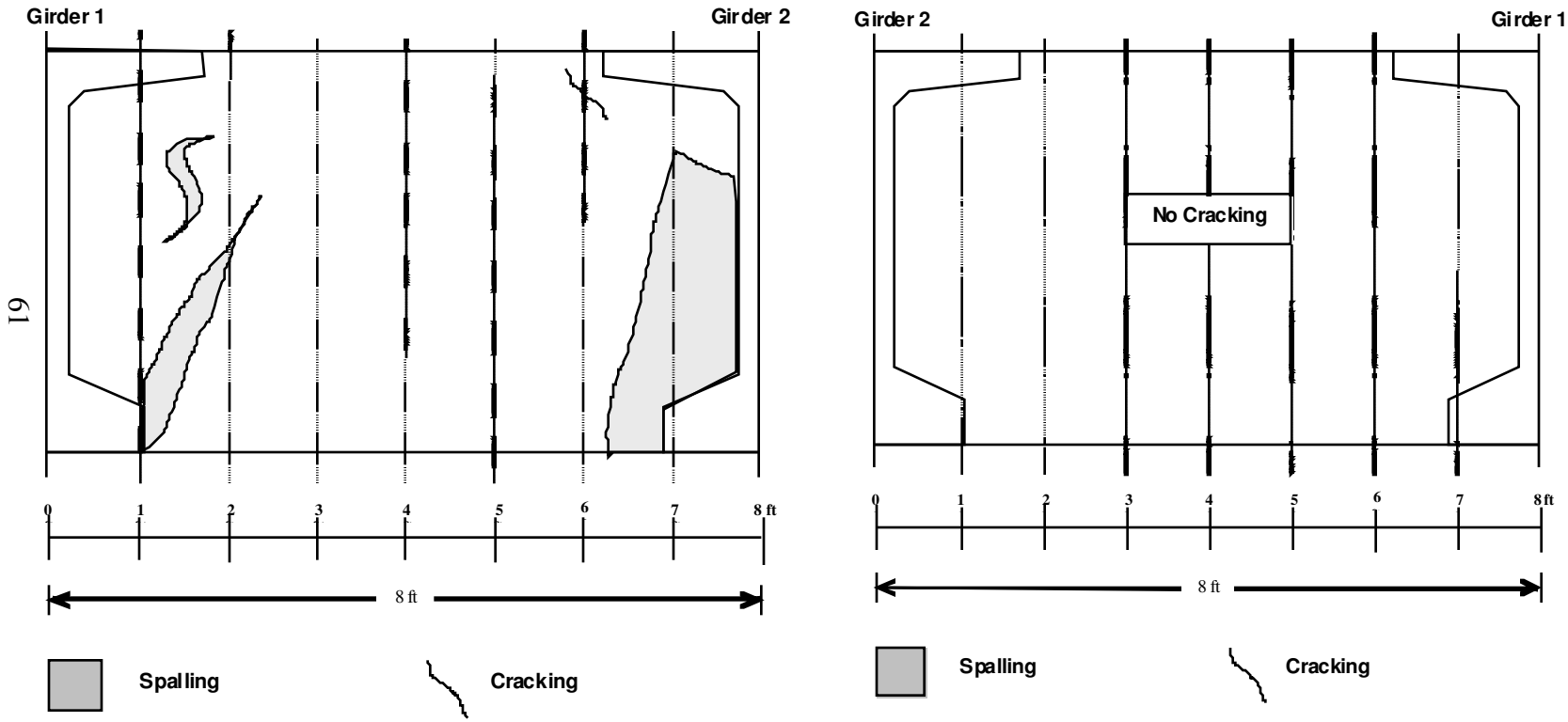


**Figure 3-19:** Continuity Diaphragm Between Girder Lines 1 and 2

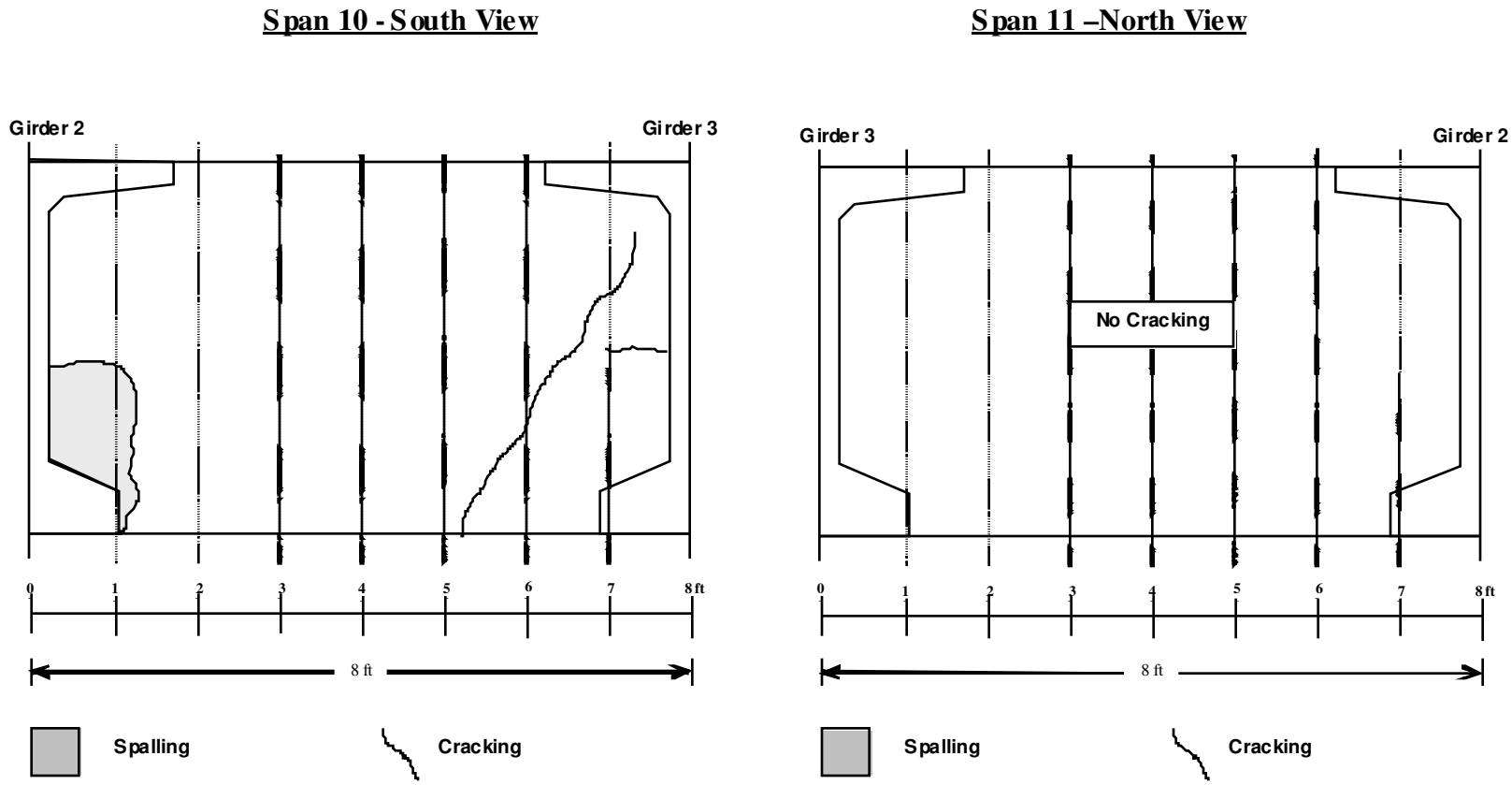


**Figure 3-20:** Continuity Diaphragm Between Girder Lines 2 and 3

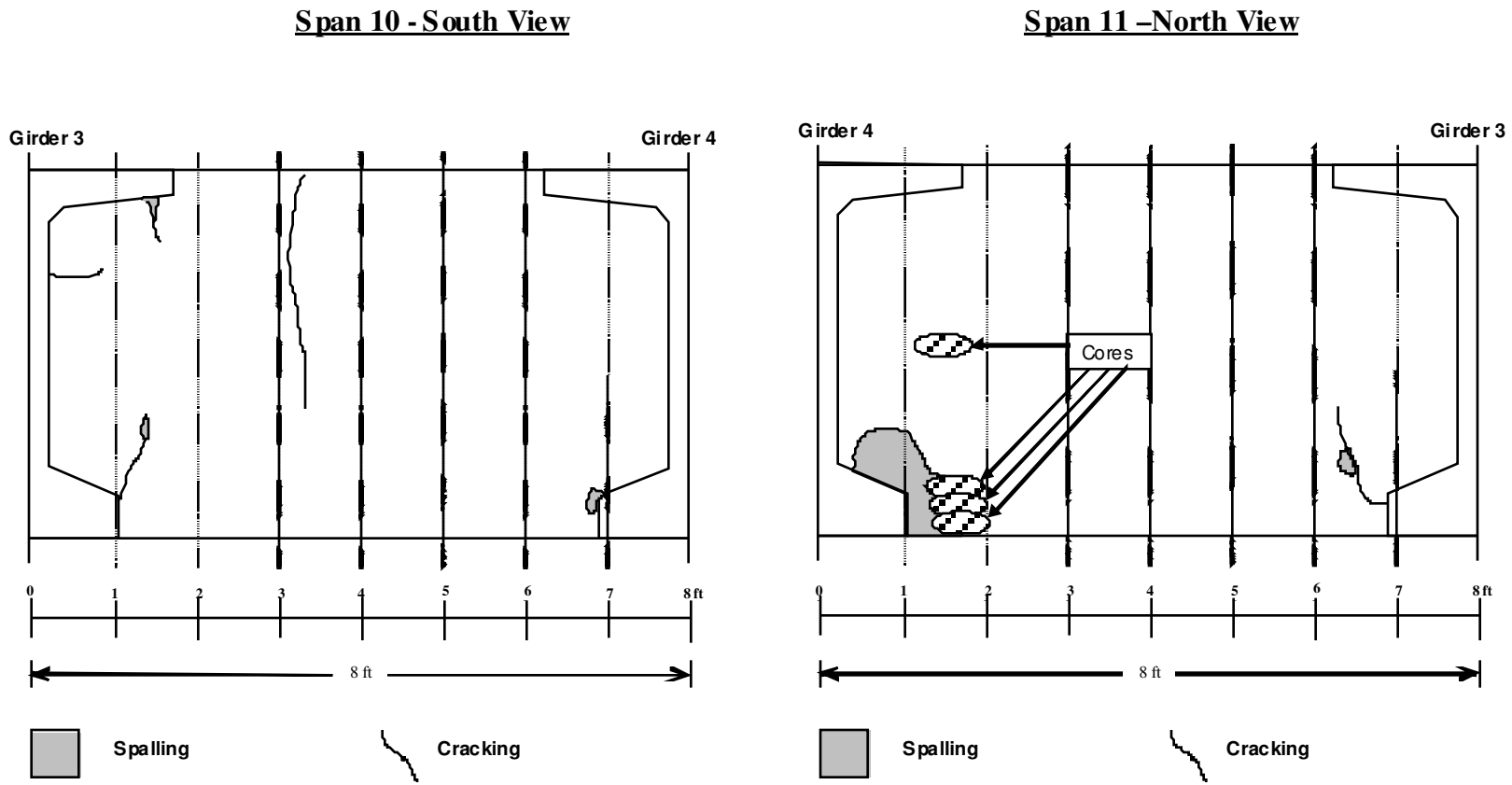


**Figure 3-21:** Continuity Diaphragm Between Girder Lines 3 and 4

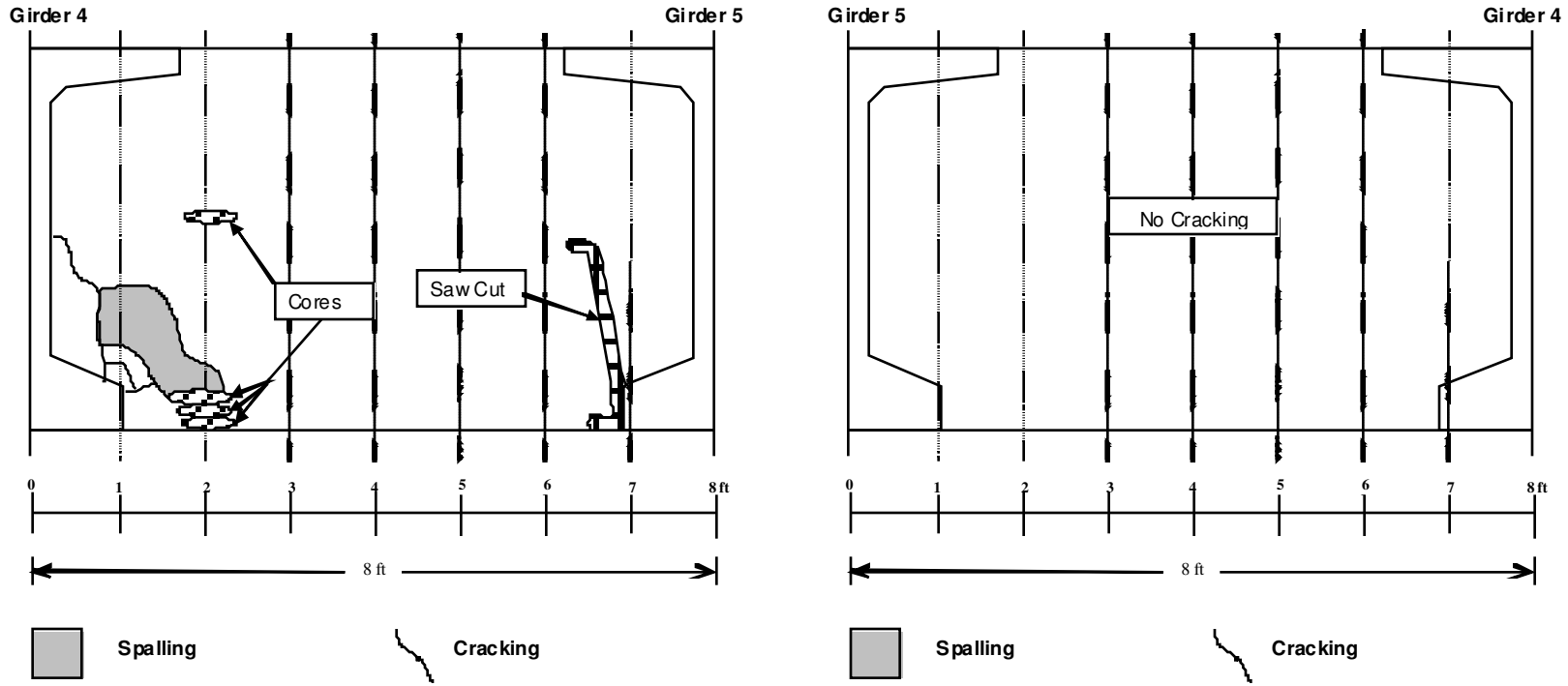


**Figure 3-22:** Continuity Diaphragm Between Girder Lines 4 and 5

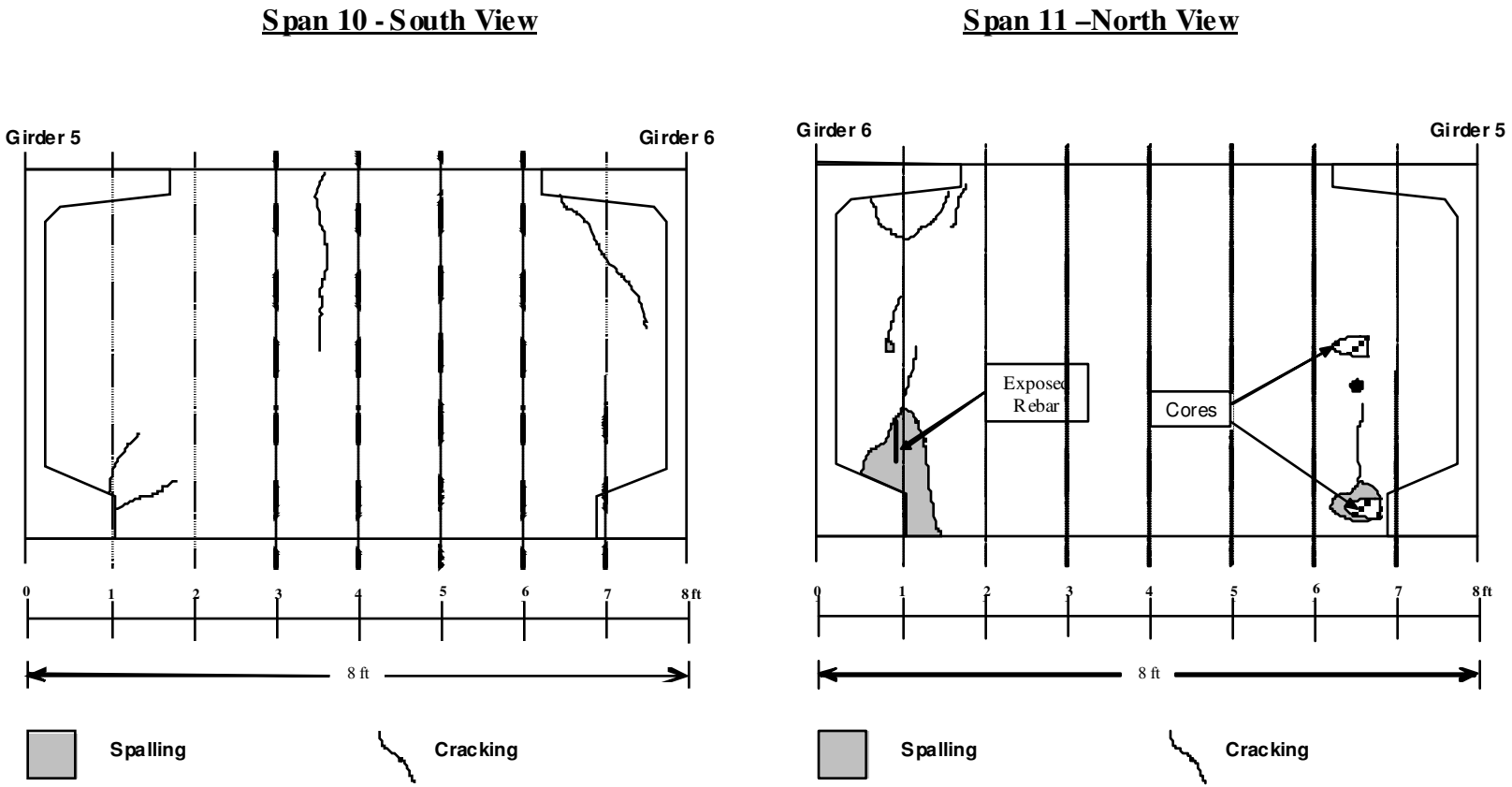


**Figure 3-23:** Continuity Diaphragm Between Girder Lines 5 and 6

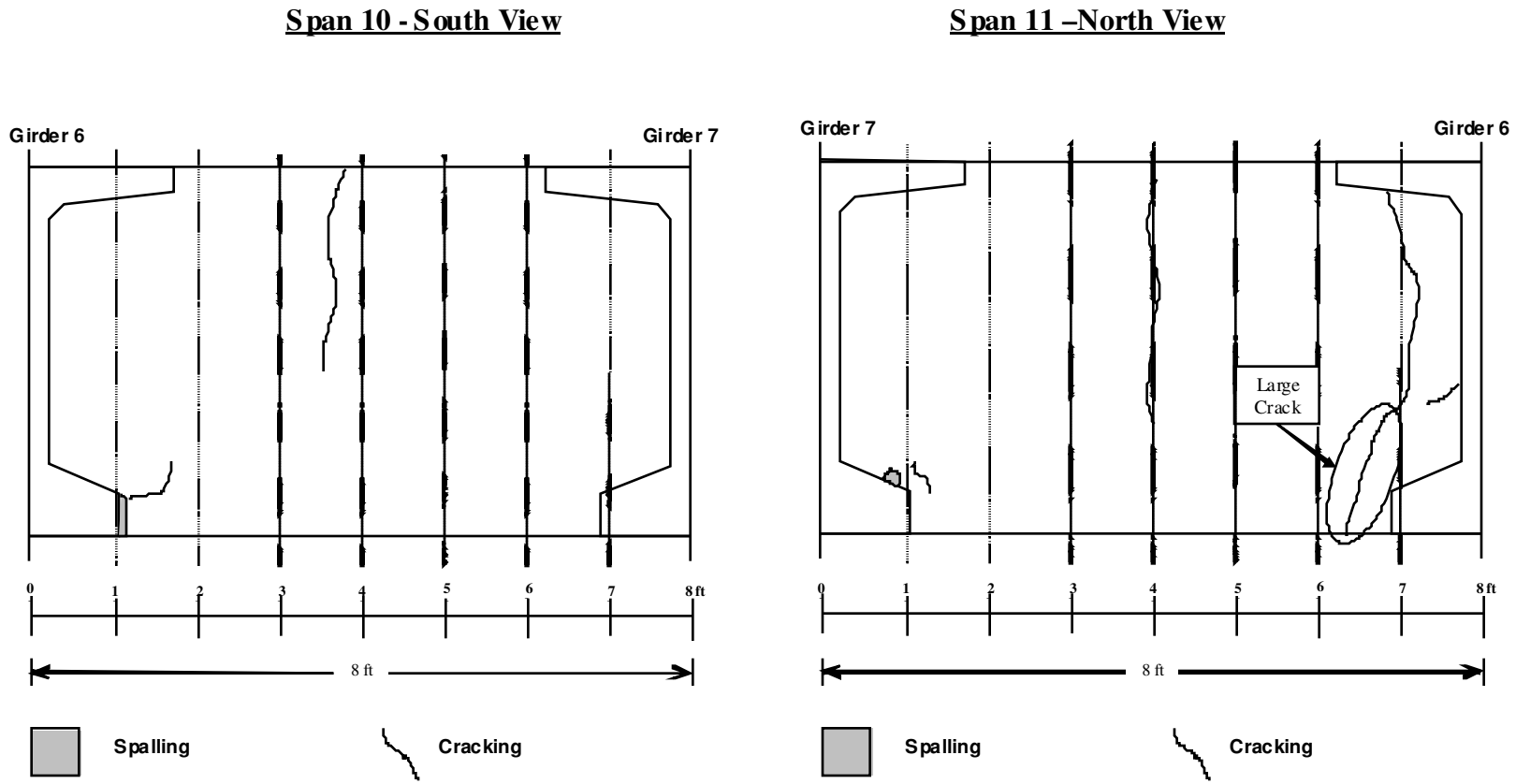


**Figure 3-24:** Continuity Diaphragm Between Girder Lines 6 and 7

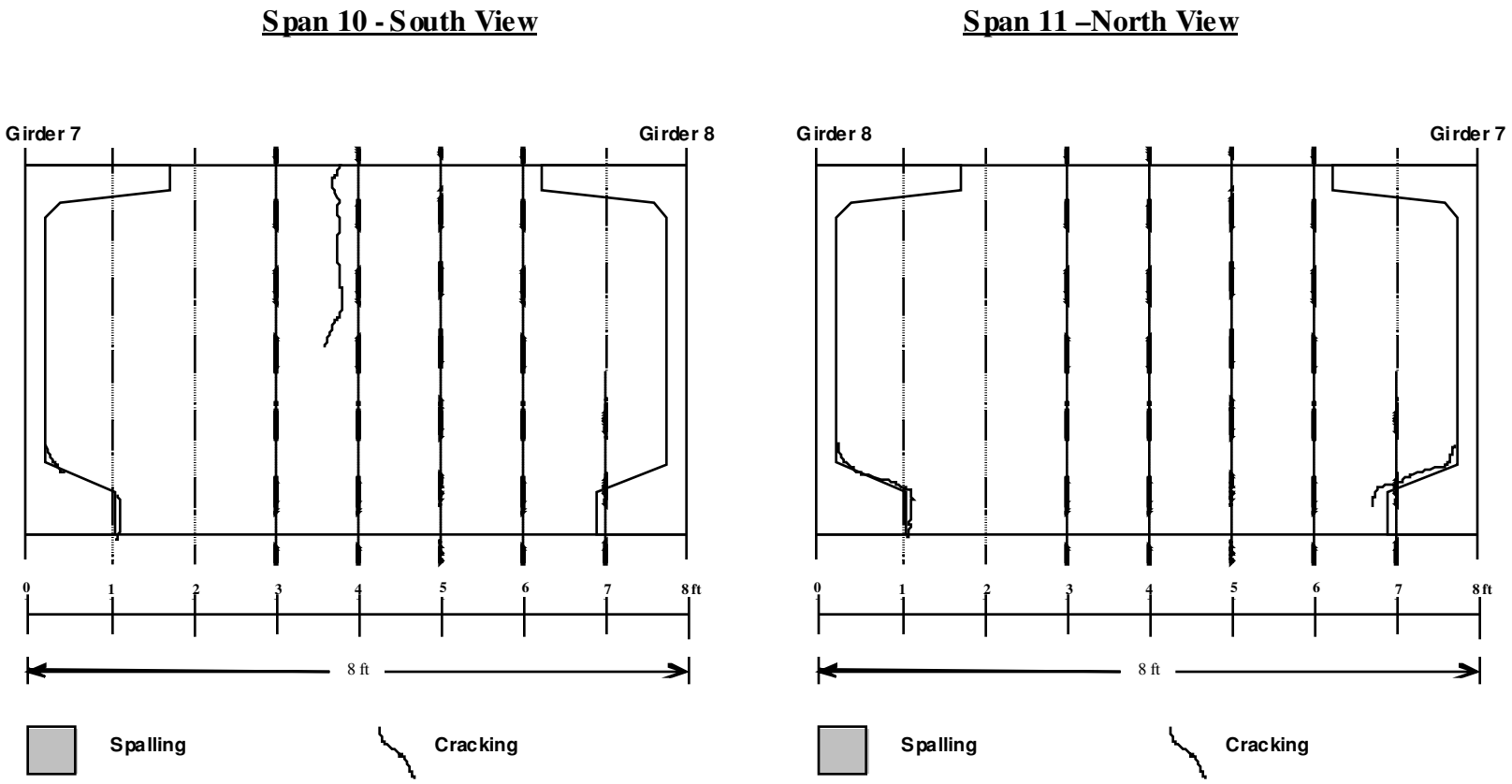


**Figure 3-25:** Continuity Diaphragm Between Girder Lines 7 and 8

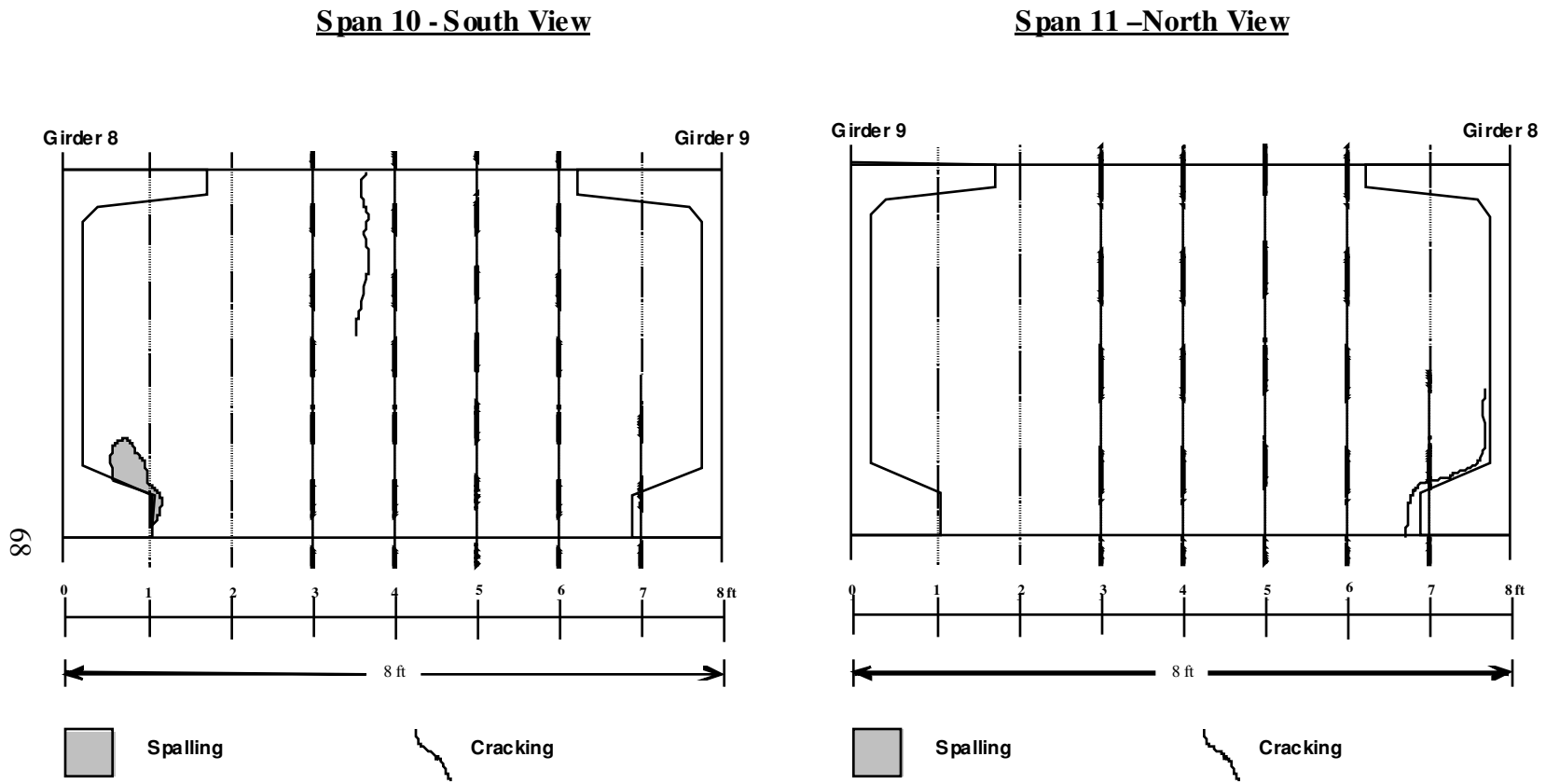


**Figure 3-26:** . Continuity Diaphragm Between Girder Lines 8 and 9

# CHAPTER 4

# LOAD-TESTING INSTRUMENTATION

Instrumentation was chosen to provide the most information about the behavior of the BT-54 girders during load testing. Gage locations were selected to help discern the type of behavior exhibited in the bridge from the several possibilities: two span continuous behavior, simply supported behavior, behavior consistent with the beam being continuous over the support with hinges at the cracked cross sections, or some combination of these conditions. Strain gages, deflectometers, and crack-opening measurement devices (COD's) were used to determine the behavior of the cracked prestressed BT-54 girders. The Optim Megadac® data acquisition system used for this test had seventy-two available 350-ohm channels. COD's were full-bridge gages. Strain gages and deflectometers were quarter-bridge instruments. Three-wire configurations were used with the quarter bridge strain gages to reduce lead-wire temperature effects on the strain gage readings.

With nine girders in each span, and eighteen total girder ends to be tested, a decision had to be made on whether or not to instrument every girder. For this test, it was decided that the use of more sensors on two girders would be more beneficial than having only a few gages on each girder. Two adjacent girders, Girder 7 and Girder 8, which exhibited a significant amount of cracking, were chosen to be instrumented. These girders are the second and third interior girders from the east edge of the bridge. The exterior girder

(Girder 9) was not chosen because of anticipated analytical complications related to the proximity of the barrier rail. Instrumenting two girders fairly close to the east edge of the bridge proved to be beneficial. Sample measurements indicated that the instrumented girders were practically unaffected by traffic in the westernmost lane. After the bridge setup was complete and prior to the static load test, strain gages reading were monitored as traffic passed in the westernmost lane. The effects of traffic in the westernmost lane did not affect Girders 7 and 8. No data was recorded at this time. With the low amounts of traffic during the early morning hours, it was acceptable to leave one lane open to traffic during load testing.

## 4.1 STRAIN GAGES

Several types of strain gages can be used in determining strains throughout a prestressed concrete girder. Because this bridge had been built and is currently in use, the most practical type of strain gage that could be used was a strain gage mounted directly to the surface of the concrete. With this in mind, electrical-resistance strain gages were chosen to be used to detect strains at different locations on the BT-54 girders, as described in Section 4.1.2.

Strain gages come in various lengths, but strain gages for concrete must be longer than those used for metals like steel or aluminum. Concrete is not a homogeneous material, but instead is made of several different materials combined, each with its own physical properties. Once hardened, the aggregate in the concrete is stiffer than the cement in the concrete. For that reason, strain gages should be 5 times as large as the largest coarse aggregate used in the concrete. Using longer gages gives an averaging effect that includes strains in both the aggregate and the cement. The Texas Instruments

gages used for this test were sixty-mm (2.36 inches) long quarter-bridge strain gages with a resistance of 350 Ω (MFLA-60•350-1L). A typical strain gage used in the test can be seen in Figure 4-1. The gages applied for this test were intended to be used in the post-FRP repair test as well. For that reason it is very important that the gages, once applied, are weather-resistant.

**Figure 4-1:** Typical Strain Gage Before Being Protected

Strains measured by each gage were helpful in determining the behavior of the girders. Positive strains correlate to tension, or a reduced amount of compression, due to the applied load, and negative strains correlate to compression, or an reduced amount of tension at that location in the girder. Strain readings from known locations on the girders under applied load cases give valuable insight into the overall behavior of the bridge.

### 4.1.1 STRAIN GAGE INSTALLATION

Strain gages must be applied very carefully to achieve acceptable results. A step by step strain gage application is shown later in this chapter. The first step in strain gage application was to clearly mark each gage location. To seal the gage against water, a base coat of 100% solids epoxy was applied to the gage location before the gage was applied. Concrete is a porous material, which allows moisture to reach the gage if the gage is applied directly to the concrete surface. With no voids, a 100% solid epoxy will not allow water to pass through. The thin layer of epoxy between the gage and the concrete will prevent moisture from reaching the gage on the concrete side of the gage.

After the base coat of epoxy was applied, each gage location was slightly abraded with sandpaper, providing a slightly roughened surface for the gage bonding. Following the abrading, the surface was carefully cleaned (M-Prep Conditioner A) and neutralized (M-Prep Neutralizer B).

Following surface preparation, the gages were applied to the girders. Each gage was individually removed from its package and taped to a clean glass plate. The tape must be smooth and bubble free. The gage and tape were then carefully removed from the glass plate and taped in the desired location on the girder. The tape is then carefully peeled back, revealing the underside of the strain gage. A standard 5-minute epoxy was used to attach the gage to the prepared concrete surface. A light coat of epoxy was then applied to both the gage surface and the concrete surface. The gage is then placed into position and held firmly in place until the gage is attached properly. The epoxy is given sufficient time to dry.

Following the application of the gages, moisture and mechanical protection was applied in order to increase the durability of the gages and to prevent moisture invasion. Once the epoxy is dry, the tape is peeled away from the gage and concrete. Immediately, a layer of RTV silicone rubber was applied to the gage to provide moisture resistance, as seen in Figure 4-2. A final application of mastic tape was applied to provide mechanical protection, as seen in Figure 4-3.


**Figure 4-2:** Strain Gage After Being Coated with RTV for Moisture Protection

## STEP BY STEP STRAIN GAGE INSTALLATION PROCEDURE

**Prepare Concrete**

1. Mark area for gage.
2. Spray gaging area with degreaser.
3. Brush area with wire brush.
4. Smooth area with grinder if needed to remove irregularities or epoxy.
5. Blow loose dust from surface.
6. Generously apply Conditioner.
7. Scrub with wire brush.
8. Blot area with gauze sponges.
9. Rinse area thoroughly with clean water.
10. Scrub surface with Surface Neutralizer.
11. Blot area with gauze sponges.
12. Rinse with water.
13. Dry surface thoroughly (warming surface with heat gun may help).

**Apply 100% solids epoxy adhesive**

14. Apply adhesive to gaging area, work into voids, and smooth with putty knife.
15. Allow epoxy to cure.
16. Sand smooth with 320 grit sandpaper.
17. Using a Ball Point Pen draw layout lines.
18. Scrub with Conditioner.
19. Apply Neutralizer.
20. Dry as before.

**Mounting Gage**

21. Carefully mount strain gage to glass plate with Cellophane Tape.
22. Tape gage into correct location on concrete.
23. Peel tape and gage back to expose back of gage.
24. Mix 5-minute epoxy.
25. Place 5-minute epoxy on gage and concrete.
26. Gently place gage on concrete.
27. Hold pressure for 2 minutes.
28. After 1 hour or longer, remove tape.
29. Apply RTV silicone rubber (moisture sealer), and let dry.
30. Apply Mastic Tape.
31. Attach wire ends to mounted terminal strips.

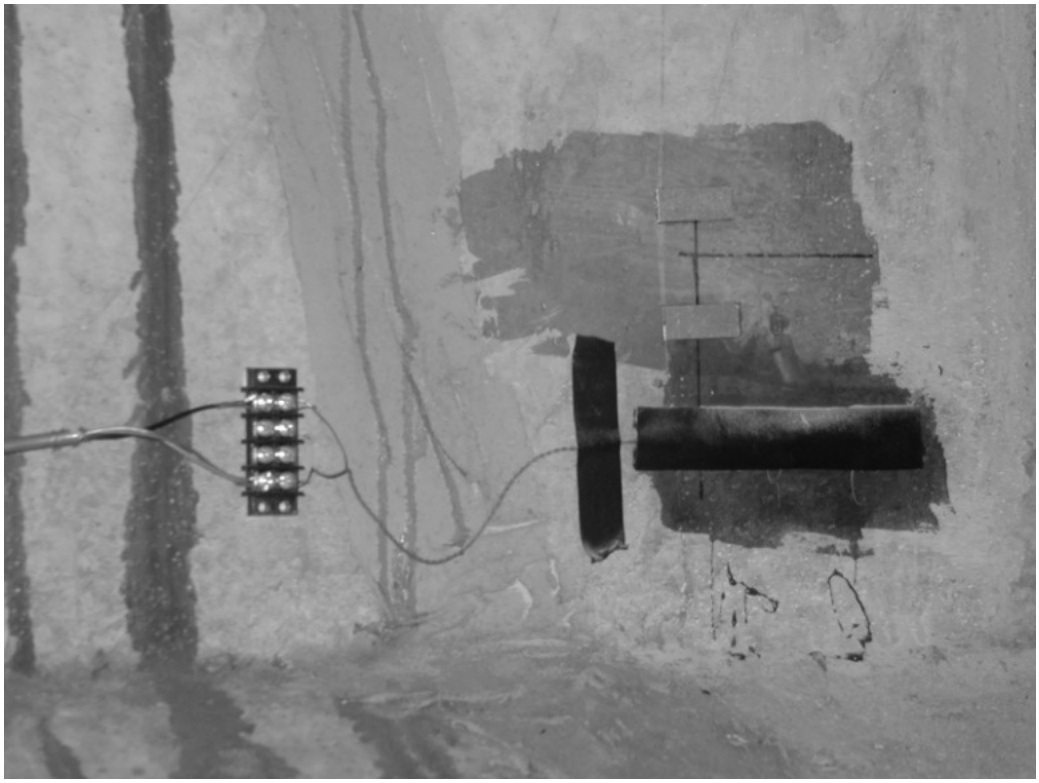

**Figure 4-3:** Strain Gage After Being Covered with Mastic Tape

### 4.1.2 STRAIN GAGE LOCATIONS

Because of the severe cracking in the end regions of the girders, these regions are the areas of the most concern in the girders. Consequently, the girder ends are more heavily instrumented than other locations in the girders. Each instrumented girder has two cross sections that are instrumented, one on each side of the cracking zones. Both girders in Span 11 have a line of strain gages along the bottom of the girders out to midspan. These multiple gages were positioned to obtain some insight into the overall behavior of the girders from the strain gage output instead of simply giving discrete, localized behaviors around the cracked regions.

Span 11 was chosen to be the primary span under investigation, and was more heavily instrumented than Span 10. Figure 4-4 shows the locations of instrumented cross

sections. Span 11 had six cross sections that were instrumented; Span 10 had only 2 cross sections instrumented. Table 4-1 provides the location of each instrumented cross section. The instrumented cross sections in Span 10 were located at distances of 6 in. (Cross Section 1) and 66 in. (Cross Section 2) from the face of the continuity diaphragm. The instrumented cross sections in Span 11 were located at distances of 6 in. (Cross Section 1), 66 in. (Cross Section 2), 8 ft (Cross Section 3), 22 ft (Cross Section 4), 36 ft (Cross Section 5), and 50ft (Cross Section 6) from the face of the continuity diaphragm.

Figure 4-5 diagrams the location of strain gages on Cross Section 1, located between the continuity diaphragm and the cracking. Figure 4-6 diagrams the locations of strain gages on Cross Section 2, located on the midspan side of cracking. Figure 4-7 diagrams the location of the strain gage on Cross Sections 3, 4, 5, and 6. Pictures of installed strain gages on Cross Sections 1 and 2 are shown in Figures 4-8 and 4-9, respectively.

Strain gages were located at each instrumented cross section. Cross Sections 1 and 2 in both spans have six strain gages, while Cross Sections 3, 4, 5, and 6 only had one strain gage located on the bottom center of the girder. Primary cracking in the girder ends of both spans was located between Cross Sections 1 and 2. Cross-section behaviors adjacent to the cracks were used to infer behavior in the cracked region. Strain gages located in Cross Sections 3, 4, 5, and 6 were used to determine the overall behavior of the loaded beam.

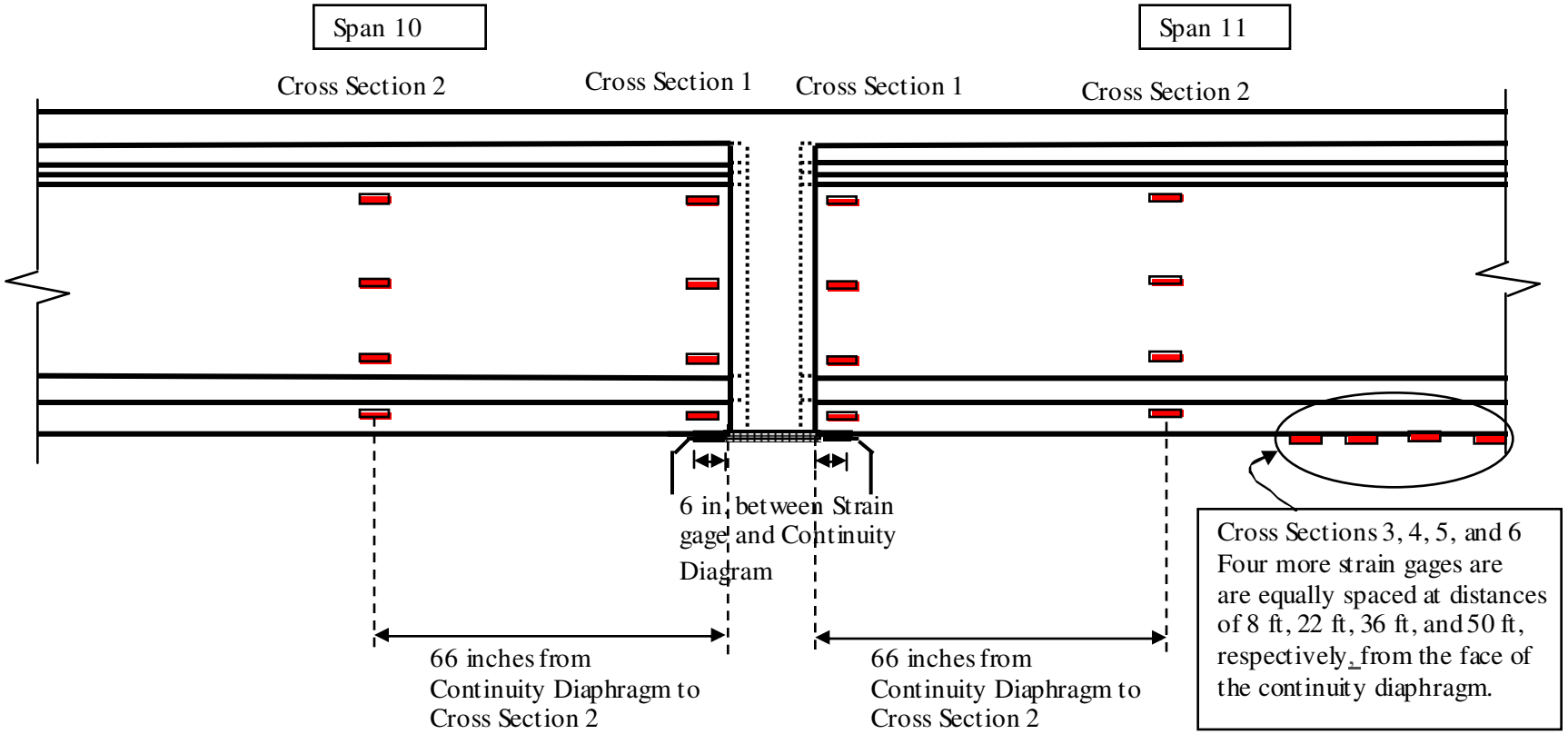


**Figure 4-4:** Strain Gage Instrumented Cross Sections for Girders 7 and 8

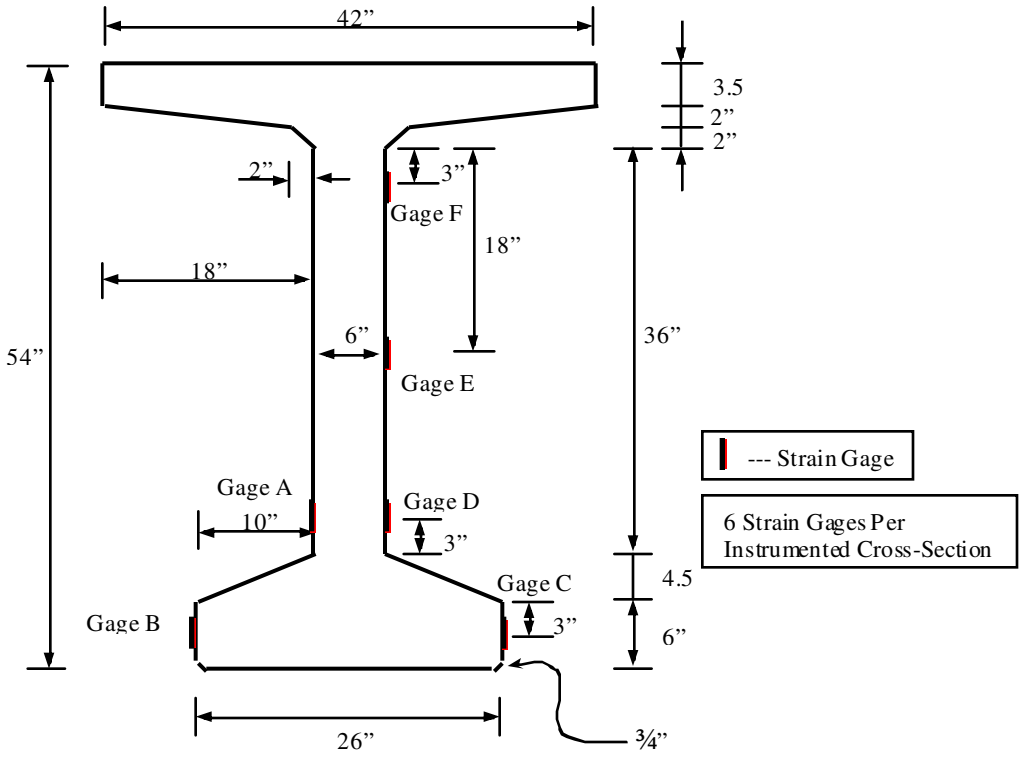


**Figure 4-5:** Strain Gage Layout - Span 10 and 11 Cross Section 1

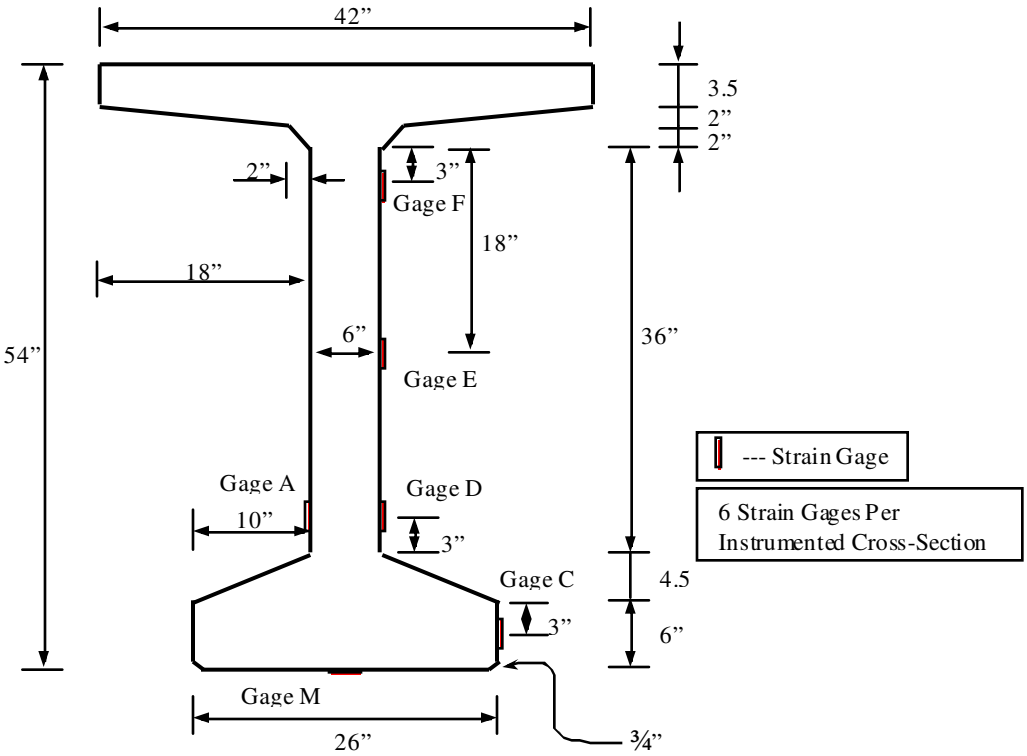


**Figure 4-6:** Strain Gage Layout - Span 10 and 11 Cross Section 2

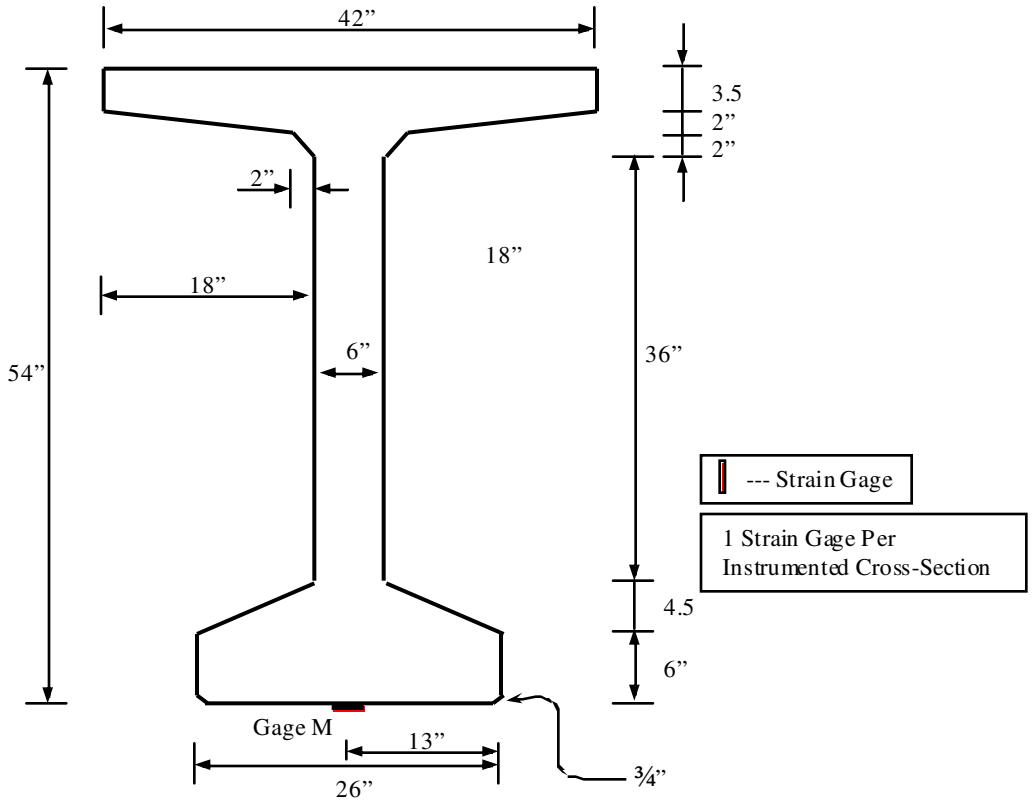


**Figure 4-7:** Strain Gage Layout - Span 11 Cross Sections 3, 4, 5, and 6

**Table 4-1:** Strain Gage Cross Section Locations

| | Span 10 Girders 7 and 8 | | Span 11 Girders 7 and 8 | | | | | |
|---|---|---|---|---|---|---|---|---|
| | Cross Section 1 | Cross Section 2 | Cross Section 1 | Cross Section 2 | Cross Section 3 | Cross Section 4 | Cross Section 5 | Cross Section 6 |
| Distance from face of continuity diaphragm to cross section | 6 in. | 66 in. | 6 in. | 66 in. | 96 in. | 264 in. | 432 in. | 600 in. |

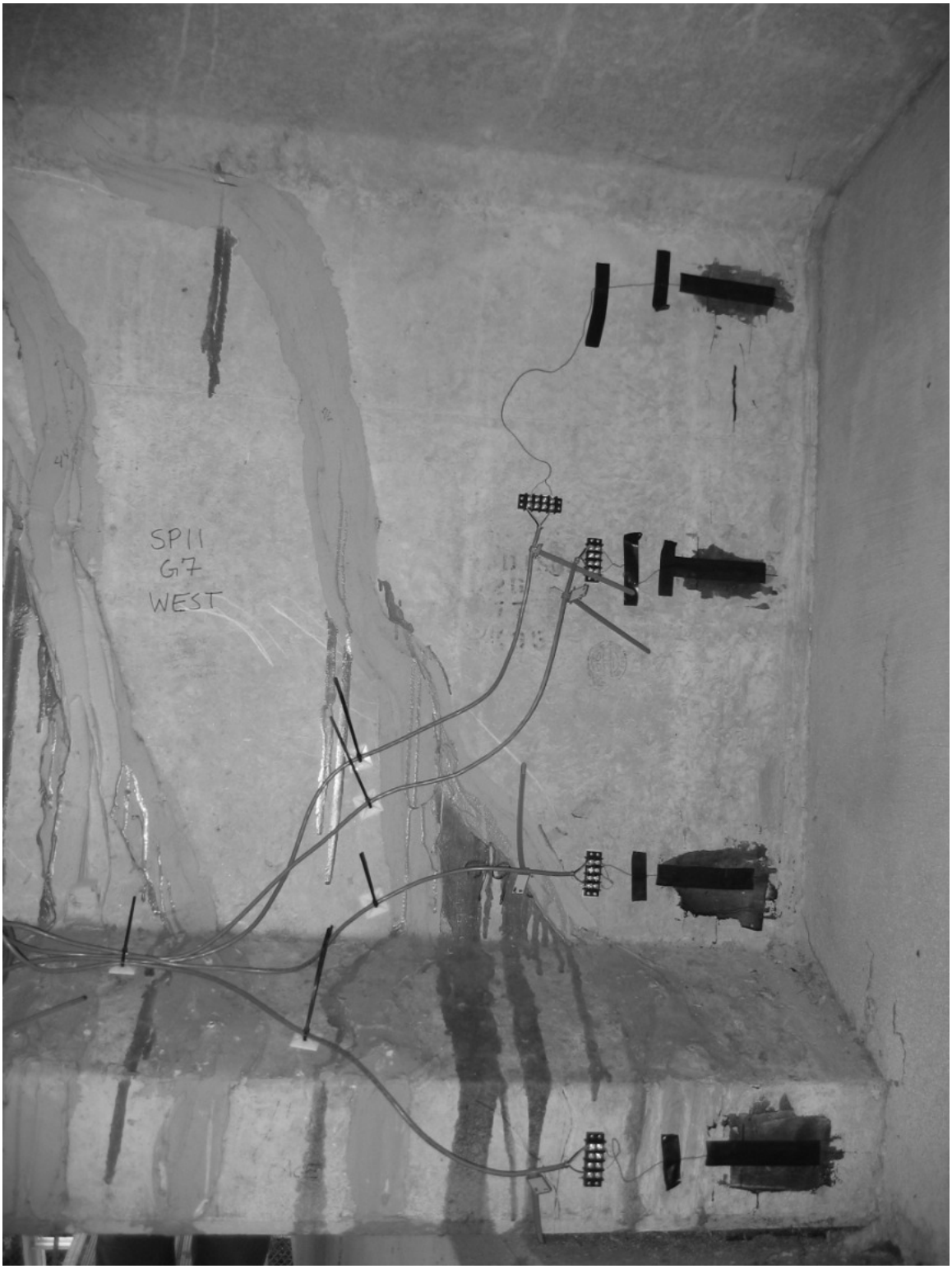


**Figure 4-8:** Strain Gages - Cross Section 1

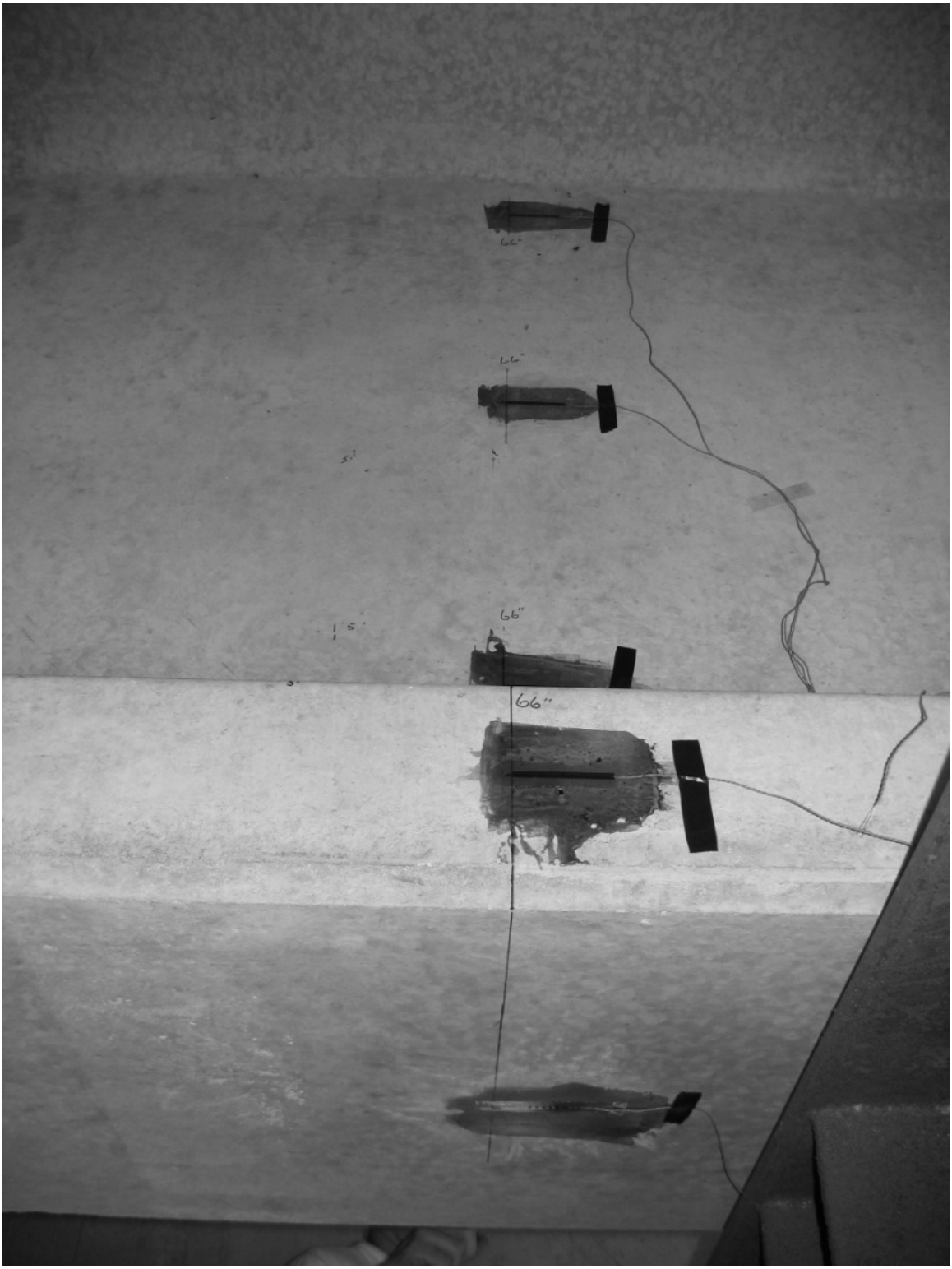


**Figure 4-9:** Strain Gages - Cross Section 2

## 4.2 DEFLECTOMETERS

Deflectometers were used to measure deflections at specific points along the girders. Deflections were considered to be the amount of movement, either up or down, that a particular point in the bridge is subjected to by a certain loading condition. Positive deflections imply that the bridge is deflecting upward, and negative deflections indicate that the bridge is deflecting downward. Deflection measurements can be very helpful in determining the behavior of the bridge. For example, a true simply supported span's deflections would graph as a concave-up shape, while a truly continuous two-span girder's deflections would graph as concave-down over the center support and concave-up in the midspan regions.

Deflectometers are a very simply constructed device. A picture of a typical deflectometer is shown in Figure 4-10. They are constructed of a prismatic bar (for this test aluminum was used) with a strain gage attached to the underside. These deflectometers used a single quarter-bridge strain gage. Often a full-bridge setup (four strain gages) is used for deflectometers. For the purpose of this project, it was determined that a quarter-bridge setup would provide the necessary accuracy. An eye bolt is attached to the end of the bar. The bar is anchored to a base that holds the unit firmly to the ground. A wire is then attached from the underside of the bridge girder to the eye bolt on the deflectometer.

For a deflectometer to work properly the aluminum bar must be bent elastically, producing tensile strains in the bottom of the bar at the location of the strain gage. This is accomplished by tensioning the connection wire to bend the bar so that the tip is deflected up approximately four inches prior to testing. Once this is done, the

deflectometer is capable of reading both upward and downward deflection in the bridge girder while the strain gage remains in its working range. If the wire is not pretensioned, downward bridge deflections would result in slack in the connection wire, and the bar deflection and strain change would not correspond to the actual girder deflection.

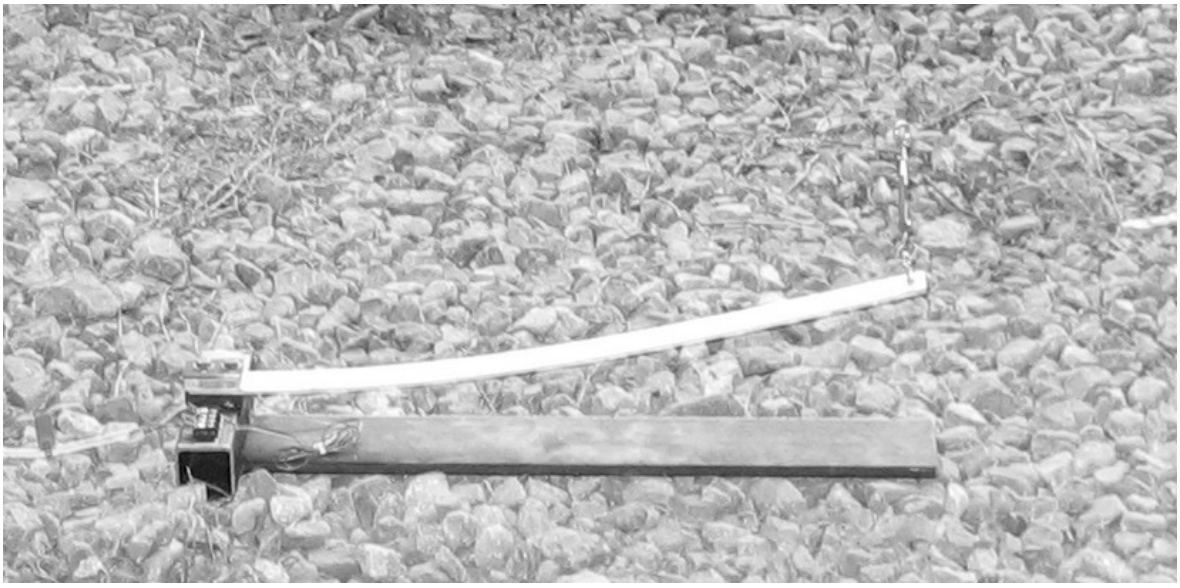

**Figure 4-10:** Deflectometer

Deflectometers must be calibrated in order to give usable readings. Calibration is achieved by pre-bending the aluminum bar and then moving the bar a known distance and taking a corresponding strain reading. If the deflectometer is set up properly, and the bar material is not bent past its proportional limit, there is a linear relationship between measured deflection and strain. Using this fact, an appropriate gage factor can be determined. With the proper gage factor, the change in strain measured from a particular load case gives a direct measurement of the deflections for that applied load.

### 4.2.1 DEFLECTOMETER INSTALLATION

Installation of a deflectometer is much less time consuming than that for a the strain gage. The first step is to locate the positions on the underside of the girder where deflections

will be measured. Next, a bracket is glued into place with 5-minute epoxy. Installation of the bracket is shown in Figure 4-11. Once the epoxy hardens, a wire is hung from each bracket down to the ground. A turnbuckle is attached to the end of each wire. The deflectometer is placed in the appropriate position on the ground. The deflectometer should sit solidly and not rock or move when the bar is bent. Finally, the turnbuckle is attached to the eyebolt, and the bar is pre-bent upward approximately four inches to the zero point. The deflectometer is then connected to the data-acquisition system with a 3-lead-wire cable.

**Figure 4-11:** Deflectometer Bracket Being Attached to the Underside of Girder 8

### 4.2.2 DEFLECTOMETER LOCATIONS

Twelve deflectometers were used in the preload test. The deflectometer positions are indicated in Figure 4-12. A picture of the actual layout of deflectometers during the load test is shown in Figure 4-13. The deflectometer locations for each girder are summarized in Table 4-2. Six deflectometers were used in each girder line. Girders 7 and 8 were instrumented identically. Two deflectometers were located in Span 10 of each girder line at distances of 25 ft and 50 ft from the face of the continuity diaphragm. Four deflectometers were located in Span 11 of each girder line at distances of 12.5 ft, 25 ft, 37.5 ft, and 50 ft from the face of the continuity diaphragm.

**Table 4-2:** Deflectometer Locations

| | Span 10 | | Span 11 | | | |
|---|---|---|---|---|---|---|
| | D-1 | D-2 | D-1 | D-2 | D-3 | D-4 |
| Girder 7 | 25 | 50 | 12.5 | 25 | 37.5 | 50 |
| Girder 8 | 25 | 50 | 12.5 | 25 | 37.5 | 50 |

Note: Locations are reported as distances (in feet) relative to the near face of the continuity diaphragm

## 4.3 CRACK OPENING DISPLACEMENT GAGES

Crack-opening displacement gages (COD's) were used to measure changes in crack width for each load case. The COD's used covered a 50-mm length between anchor screws. COD's were full-bridge setups and precalibrated. The COD's were capable of measuring changes in crack widths up to 2 mm. COD's provided valuable information on the opening and closing of cracks for each load case.

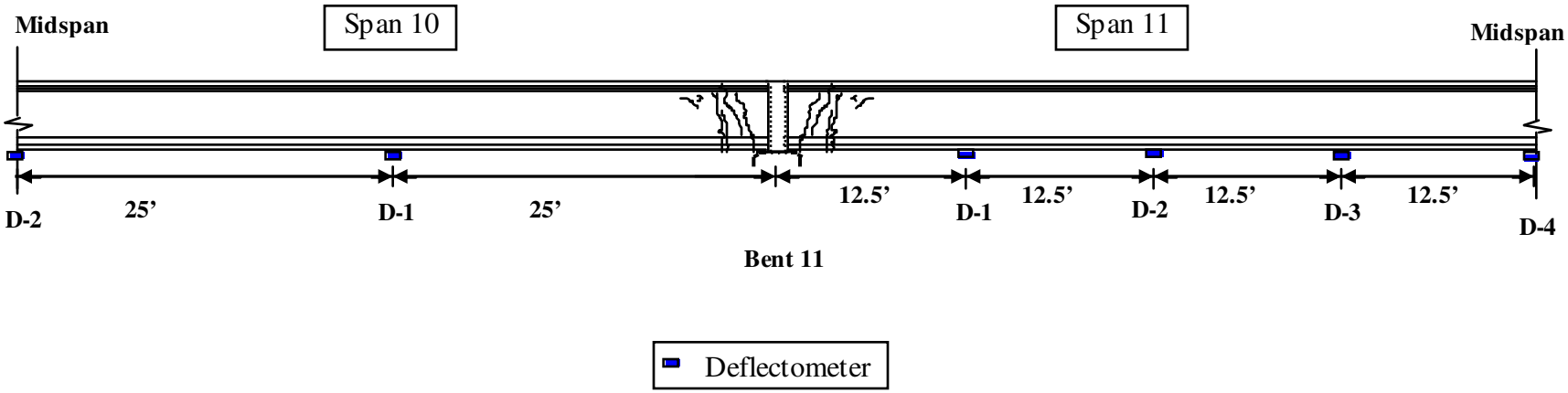


**Figure 4-12:** Girder 7 and 8 Deflectometer Locations

**Figure 4-13:** Deflectometers During Test

### 4.3.1 COD INSTALLATION

COD installation was the easiest of the three instruments. A reference bar was used to set the two anchor blocks in the exact locations. The two anchor blocks are screwed to the reference bar. The blocks are then attached to the surface with 5-minute epoxy. The crack should be located between the two anchor blocks. Once the epoxy is dry, the reference bar is removed, leaving the two anchor blocks attached to the concrete girder. A picture of the two anchor blocks without the COD attached is shown in Figure 4-14. Next, the COD is attached to the anchor blocks. A picture of an installed COD is displayed in Figure 4-15. Finally, the 4-wire strain gage cable is connected to the COD and the data-acquisition system. A diagram of the COD's used for the test is shown in Figure 4-16.

**Figure 4-14:** Anchor Blocks for COD

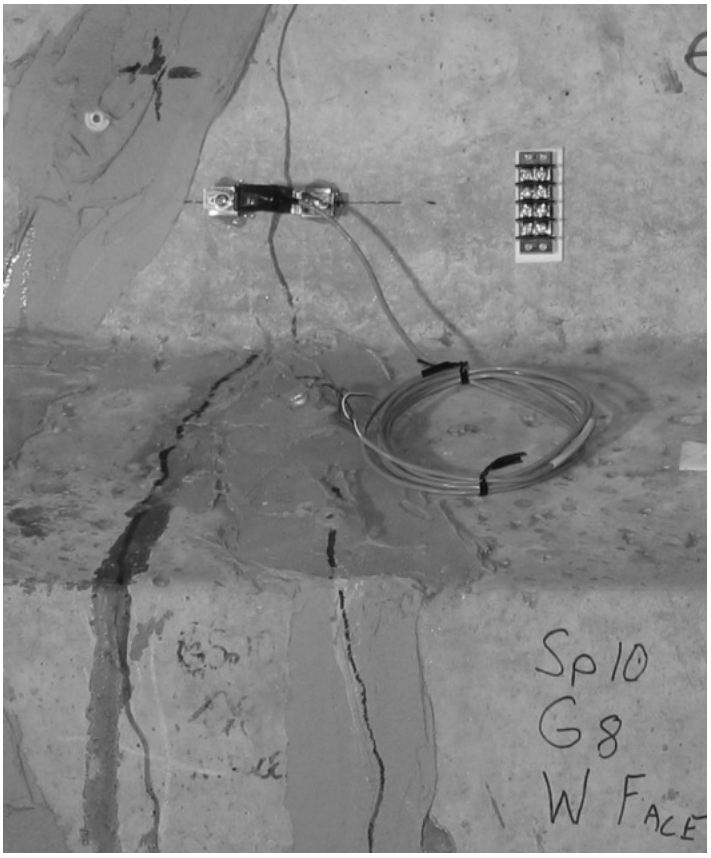


**Figure 4-15:** Crack Opening Device Installed on Girder


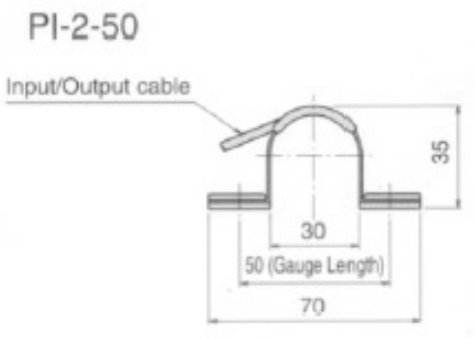


**Figure 4-16:** Crack Opening Devices (from Texas Measurements)

### 4.3.2 COD LOCATIONS

A total of four crack-opening gages were used in the pre-repair load test. There was one COD used on each girder end. Each was located directly over the primary crack in the girder end. Each COD is located three inches above the joint of the bottom flange and the web. The COD on Girder 8 Span 10 is located on the West face of the girder, while all other COD's are on the East face of the girder. Table 4-3 provides the location of each COD.

**Table 4-3:** Crack Opening Displacement Gage Locations

| | Span 10 | | Span 11 | |
|---|---|---|---|---|
| | Distance from Continuity Diaphragm | Face | Distance from Continuity Diaphragm | Face |
| Girder 7 | 49.5 in. | East | 47.75 in. | East |
| Girder 8 | 40 in. | West | 56 in. | East |

## 4.4 INSTRUMENTATION DESIGNATIONS

Each instrument was given a unique name. The instrument type was denoted by the letter or letters at the beginning of the instrument name: D for deflectometers, CO for crack opening devices, and S for strain gages. The number immediately following provides the girder on which the gage was located, either girder 7 or 8. An underscore follows the girder designation, and the numbers following the underscore provide the span in which the instrument is located, either span 10 or 11. An underscore follows the span designation. The final character indicates something different for each gage type. For deflectometers, it indicates the deflectometer number, 1 through 4. For crack opening devices, it indicates which face of the girder that it is located on, east or west face. For strain gages, it indicates the cross section, either 1 or 2, and the gage location as

described previously, A through F or M. An example for each instrument has been provided below for clarity.

Example:

D7_10_2 - Deflectometer, Girder 7, Span 10, Deflectometer #2

CO8_10_W - Crack Opening Device, Girder 8, Span 10, West Face

S7_10_1A - Strain Gage, Girder 7, Span 10, Cross Section 1, Gage Location A

## 4.5 DATA ACQUISTION SYSTEM

An Optim Megadac data-acquisition system was used to record data during the conventional static load test. During the test, each of the seventy-two channels recorded data at a rate of 240 scans per second. A picture of the van setup during the load test with all instrumentation cables attached can be seen in Figure 4-17. See Appendix B for channel layout.

**Figure 4-17:** Van Setup for Load Testing

# CHAPTER 5

# PRE-REPAIR LOAD TESTING PROCEDURE

Once instrumentation was complete, acoustic emissions (AE) tests as well as conventional static load tests were conducted in order to determine the behavior of the damaged bridge girders and to set a baseline from which post-repair load test results could be compared. The pre-test and post-test behavior will be compared in order to evaluate the benefits gained by FRP repairs.

Pre-repair load testing was conducted on two consecutive nights (early mornings of June 1 and 2, 2005). Acoustic emissions preloading was conducted the first night. The second night of testing consisted of marking all of the necessary lines for the static load test, the second round of the AE test, and finally the static load test.

## 5.1 TRAFFIC CONTROL

The two girders, Girders 7 and 8, to be tested are located on the east side of the bridge. The bridge has four lanes of traffic. In order to provide a safe area in which the trucks could drive and stop and in which workers could operate, all lanes with the exception of the far west lane were closed to traffic. It was realized that traffic loads can have a significant effect on readings taken during the load test. Initial planning had been to keep traffic completely off of the bridge during the test while data were being recorded. But, it was determined on the first night that traffic in the far west lane had a minimal influence on readings taken from the east side of the bridge. For this reason, it was decided to

leave the far west lane of traffic open throughout the entire test. In an attempt to further reduce traffic noise, data were taken during times when bridge traffic was minimal.

The bridge is located on I-565 in Huntsville. In this area, closing traffic down to one lane during the day would significantly affect the flow of traffic. Traffic data showed that the hours between 1 a.m. and 4 a.m. had the lowest traffic count. This led to the conclusion that the test should occur at this time. ALDOT began closing lanes at 11 p.m., and testing operations on the bridge deck began around midnight both nights. Testing was completed by 4 a.m. each night.

## 5.2 LOAD TEST TRUCKS

Two ALDOT trucks were used for the load test. The first was one of ALDOT's typical load testing trucks (ST-6400), shown in Figure 5-1. The second scheduled ALDOT load test truck was out of service at the time of the test, and an ALDOT Tool Trailer Truck (ST-6902), shown in Figure 5-2, had to be used in its place. The two trucks were slightly different in size and weight. The footprint of each truck was different; details are given in the following sections.

### 5.2.1 TRUCK WEIGHTS

Two load test trucks were used in the load test. Each truck has a slightly different weight and distribution of weight between the axles. Weights were changed between nights. Actual truck weight distributions may be seen in Table 5-1. The first night an LC-6.5 load truck configuration was used. This is not a standard ALDOT load test configuration and was used especially for the AE preload. The second night an LC-6 load truck configuration was used. The footprints of trucks ST-6400 and ST-6902 are shown in

Figures 5-3 and 5-4, respectively. After the test, the trucks' weights were measured at ALDOT headquarters in Montgomery using the portable scales.

**Figure 5-1:** ST-6400


**Figure 5-2:** ST-6902

**Table 5-1:** Load Distributions for LC-6 and LC-6.5

| Axle | Group | Tires | ST-6902 | | ST-6400 | |
|---|---|---|---|---|---|---|
| | | | LC-6 (lbs) | LC-6.5 (lbs) | LC-6 (lbs) | LC-6.5 (lbs) |
| Front | Left | Single | 7850 | 7575 | 10750 | 11500 |
| | Right | Single | 7450 | 7200 | 10900 | 11500 |
| Rear 1 | Left | Double | 19350 | 20300 | 18900 | 19450 |
| | Right | Double | 18750 | 19500 | 18350 | 19150 |
| Rear 2 | Left | Double | 18600 | 19450 | 17200 | 18000 |
| | Right | Double | 19250 | 20150 | 17500 | 17850 |
| | | Total = | 91250 | 94175 | 93600 | 97450 |

#### 5.2.1.1 First Night – AE preloading – LC-6.5

AE testing had two important loadings. On the first night of testing, the bridge was loaded with a load that was intended to be larger than any the bridge had ever experienced. The purpose of an unusually high load was to activate any cracks. The trucks were carefully backed into position without driving over the bent near the cracked girder ends.

#### 5.2.1.2 Second Night – AE loading and static load test – LC-6

The second night, the load was reduced to approximately 95 percent of the first night's load. The trucks were then carefully positioned in the same manner as the first night's load. Since no new cracks should have opened with a smaller load, there should not have been much AE activity. Too much AE activity could have been a sign that additional damage has occurred at the AE sensor location.

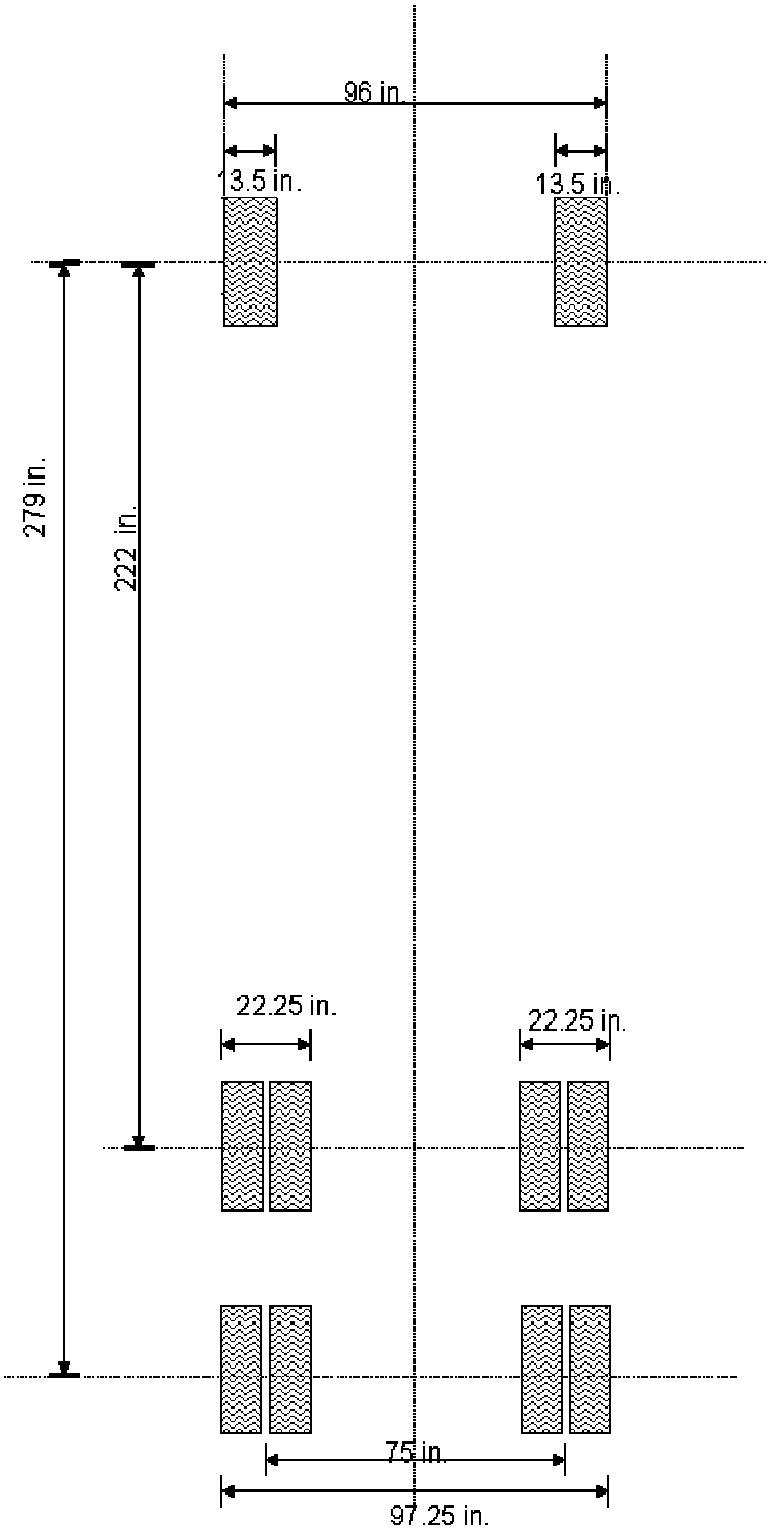


**Figure 5-3:** Footprint of Truck ST- 6400

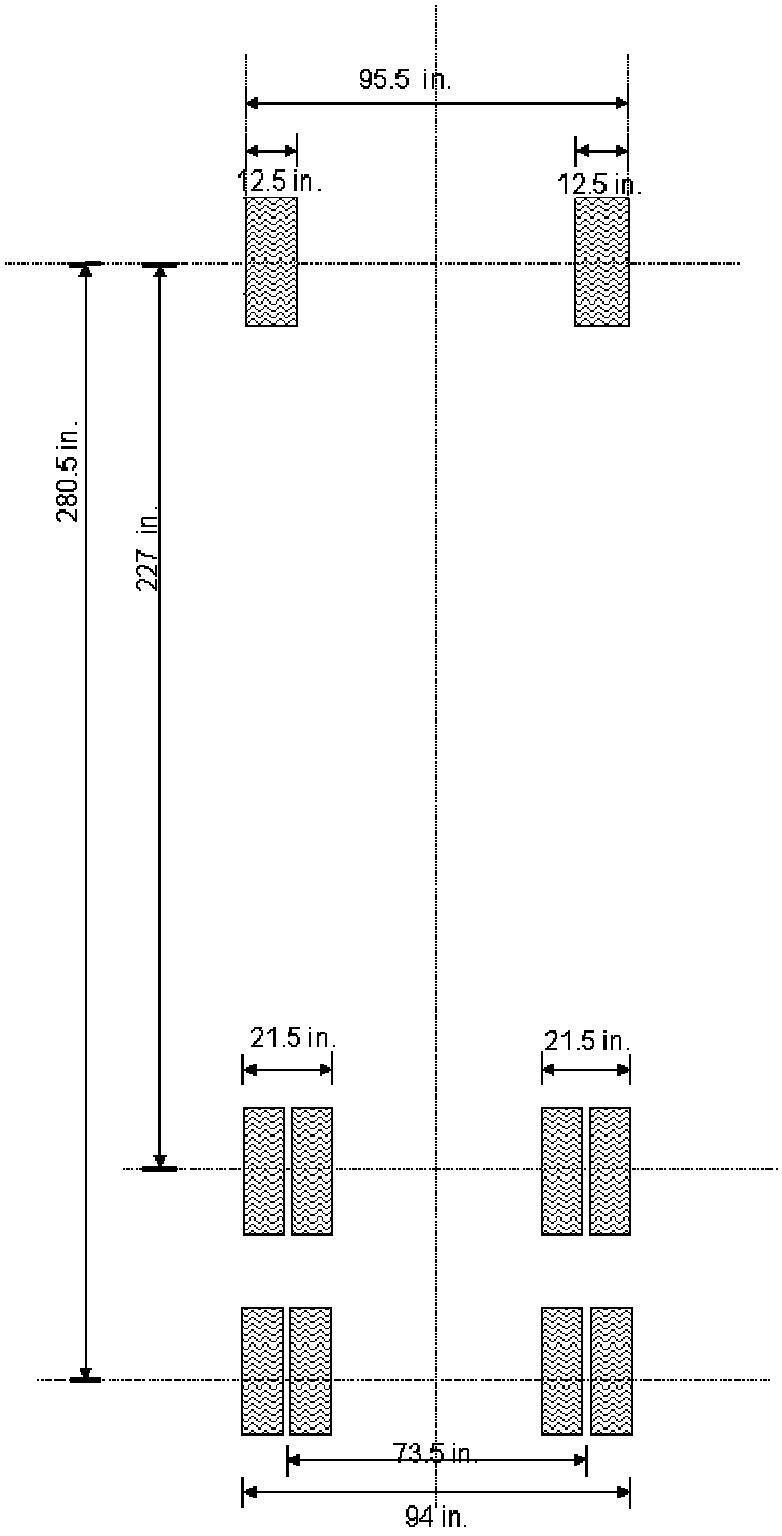


**Figure 5-4:** Footprint of Truck ST- 6902

#### 5.2.1.3 Truck Weight Limits

The load trucks used during testing were heavier than any legal truck on Alabama highways. For comparison purposes, Figure 5-5 shows the maximum truck weights for several different typical truck layouts. None of them match the load trucks used in this test, but the trucks used in this test were heavier than every truck combination shown. The maximum weight of a legal truck was 84 kips, while the minimum weight of a load test truck in the test was 91 kips.

## 5.3 STATIC LOAD TESTING

Pre-repair static load testing was performed on the bridge in order to 1) determine the behavior of the bridge and 2) set a base line to which the results of the post-repair static load test can be compared. During the test, the two trucks were placed side by side facing northbound. There were three lanes that the trucks drove down, Lanes A, B, and C, and there were nine longitudinal stop positions in each lane, Positions 1-9, giving a total of 27 total stop positions. Two North-South lines were spray painted on the deck for every lane, one line to align the east truck and one line to align the west truck. An East-West line was spray painted for every longitudinal stop position. These lines were used to position the trucks in the proper longitudinal position on the bridge. Figure 5-6 shows a picture of a load truck aligned properly with the driver's side tires on the line. As the trucks traveled down a lane with the edge of the driver's side tires centered on the North-South painted line, they stopped at each stop position, centering the center axle over each East-West longitudinal line. Data were recorded for at least three seconds at each position.

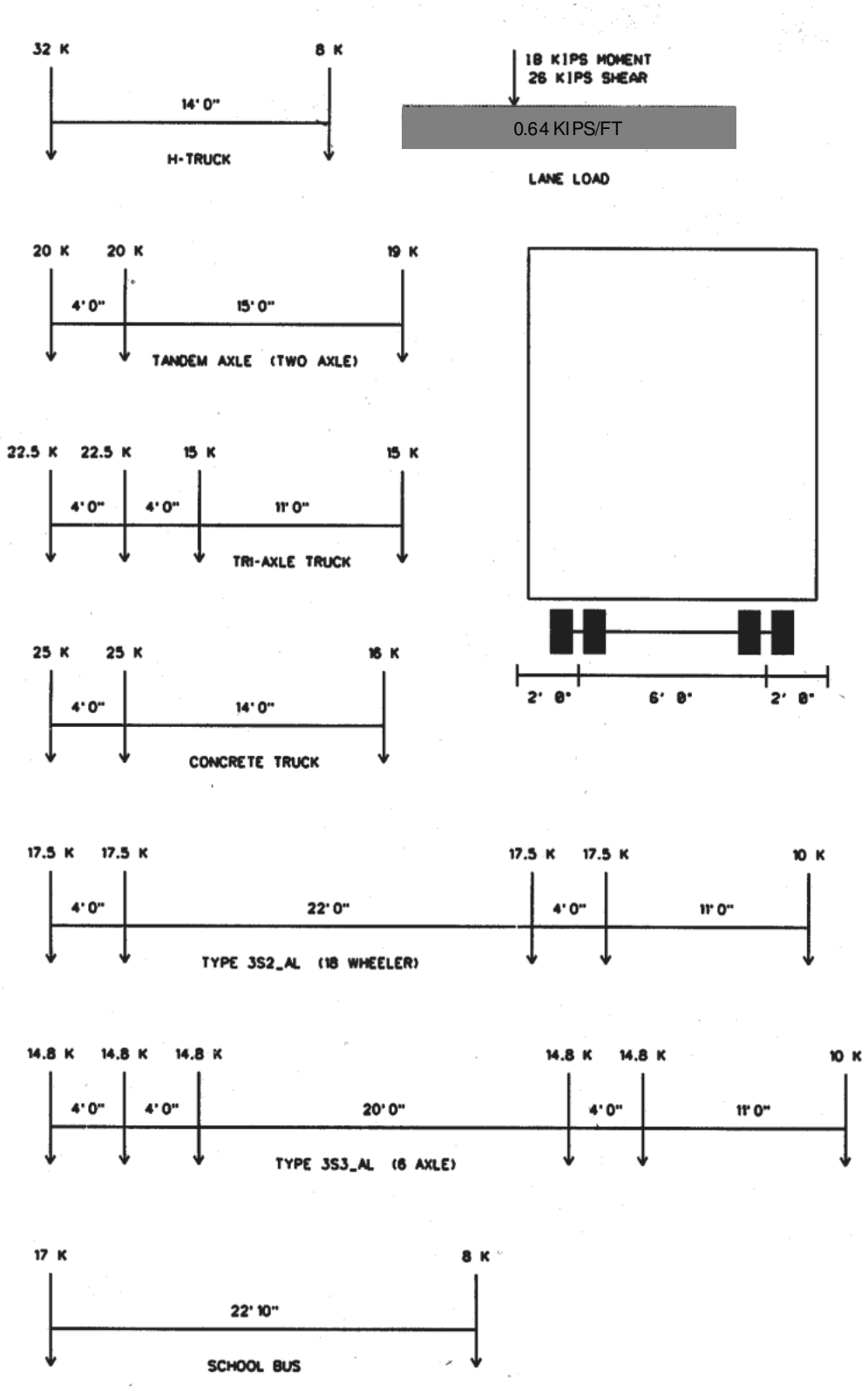


**Figure 5-5:** ALDOT Legal Truck Weight Limits

**Figure 5-6:** Load truck aligned with driver's side rear tires on lane line

### 5.3.1 TRUCK LANES

In order to apply the maximum load onto each girder, three transverse truck lanes were used. Figures 5-7, 5-8, and 5-9 show the horizontal positioning of the trucks for Lanes A, B, and C, respectively. Truck ST-6400 was always the East truck, and truck ST-6902 was always the West truck. Lane A has the center of the west wheel group of the east truck located directly over Girder 7. Lane B has the center of the east wheel group of the west truck located directly over Girder 7. Trucks on either Lane A or B should have the maximum influence on Girder 7. Lane C has the center of the west wheel group of the east truck located directly over Girder 8. Ideally, there would have been a Lane D with the west truck positioned over Girder 8. AASHTO design specifications do not require

trucks to be placed closer than 4 feet apart. Therefore, there was not room to fit the east truck in if the west truck's east wheel group was centered over Girder 8.

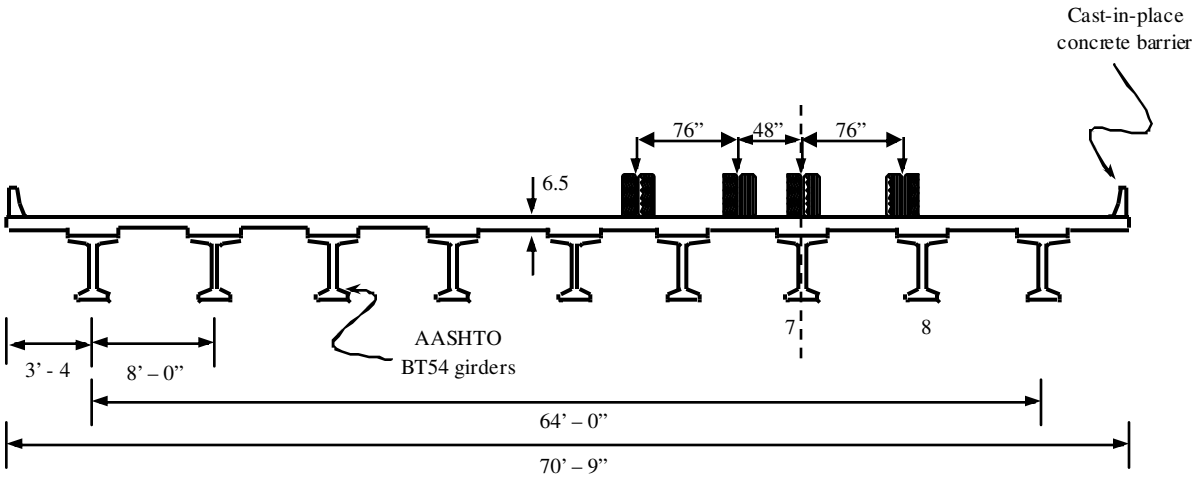


**Figure 5-7:** Lane A – Horizontal Truck Positioning (Static Test only)

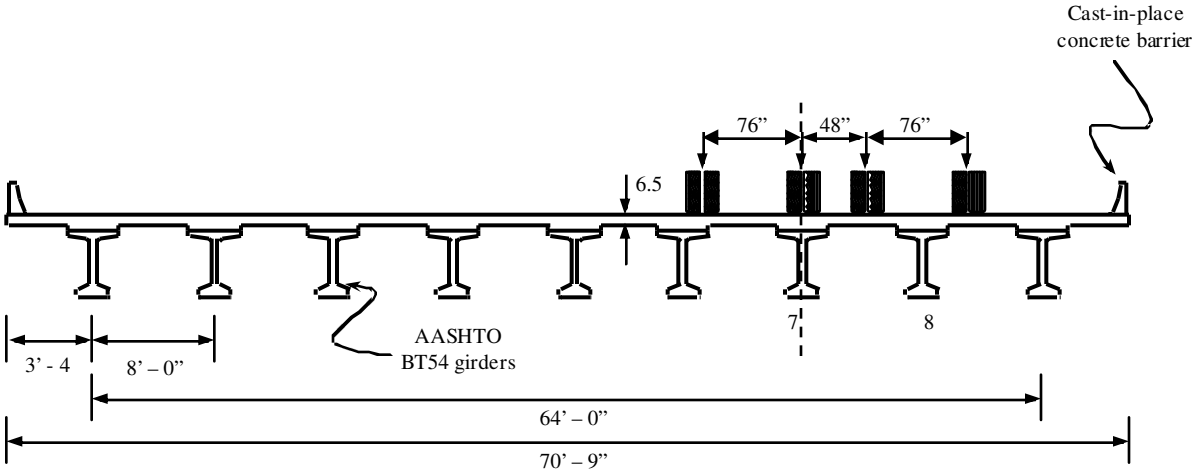


**Figure 5-8:** Lane B – Horizontal Truck Positioning (Static Test only)

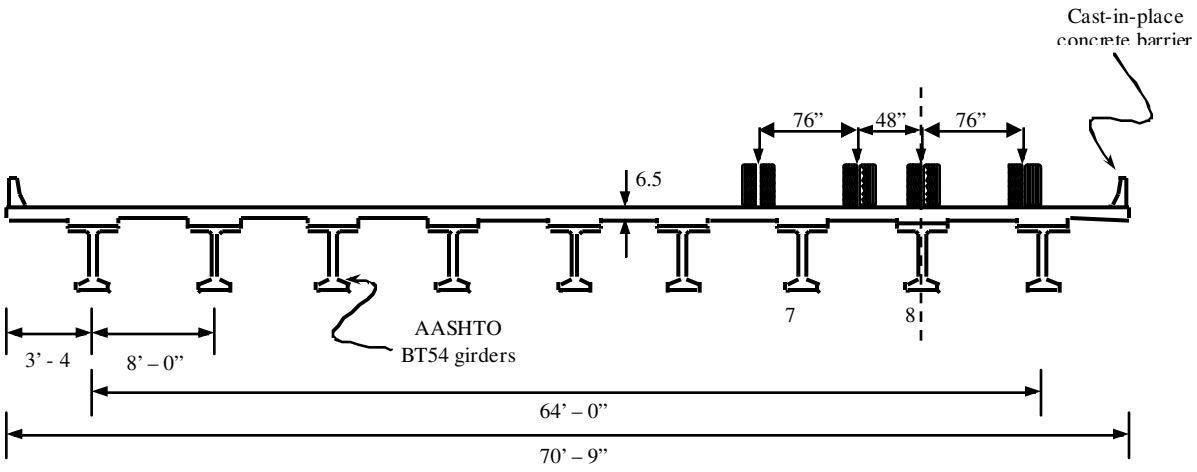


**Figure 5-9:** Lane C – Horizontal Truck Positioning (Static and AE Test)

### 5.3.2 TRUCK STOP POSITIONS

Data in a static load test are taken with the trucks sitting still. There were nine longitudinal stop positions for each truck lane. Trucks were stopped with their center axle over each stop position. Positions were chosen to give loading conditions that would assist in determining the behavior of the bridge. Table 5-2 and Figure 5-10 diagram the longitudinal location of each stop position.

### 5.3.3 DATA COLLECTION

Once a truck was stopped in position, data were recorded for spurts of at least three seconds. The data was recorded at a rate of 240 scans per second. Therefore, each of the seventy-two channels was read a total of at least 720 times for each position. Theoretically, each reading should be exactly the same. That is not the case in practice. Therefore, all of the readings for a single channel and single position were averaged to get a final reading for each stop position for each cycle.

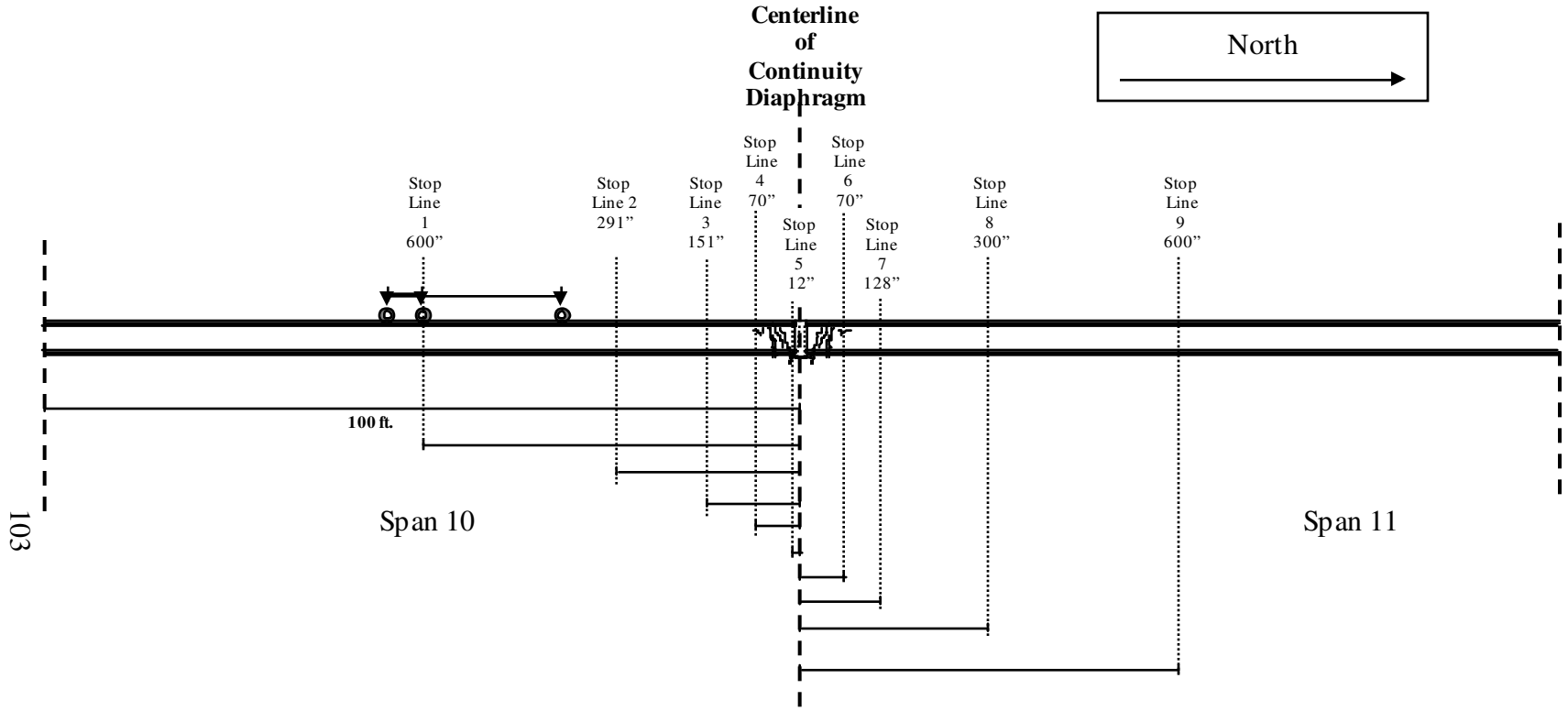


**Figure 5-10:** Truck Stop Positions

**Table 5-2:** Truck Stop Positions

| Stop Position | Position Description | Span To Mark | Distance from Center of Continuity Diaphragm | Distance from Center of Span |
|---|---|---|---|---|
| 1 | Middle tire near Midspan Span 10 | 10 | 600” | 50’-00” |
| 2 | Front Tire over Cross Section 2 Span 10 | 10 | 291” | 24’-03” |
| 3 | Front Tire over Cross Section 2 Span 11 | 10 | 151” | 12’-07” |
| 4 | Middle Tire on Cross Section 2 Span 10 | 10 | 70” | 5’-10” |
| 5 | Rear Tire over Cross Section 2 Span 10 | 10 | 12” | 1’-00” |
| 6 | Middle Tire over Cross Section 2 Span 11 | 11 | 70” | 5’-10” |
| 7 | Rear Tire over Cross Section 2 Span 11 | 11 | 128” | 10’-08” |
| 8 | Middle tire over Quarter-span Span 11 | 11 | 300” | 25’-00” |
| 9 | Middle tire near Midspan Span 11 | 11 | 600” | 50’-00” |

### 5.3.4 REPEATED CYCLES OF STATIC LOAD TESTING

One cycle of static load testing consists of both trucks driving down each lane and stopping at all nine positions in each lane and recording data. After averaging, each cycle gives one data reading for each channel at each of the twenty-seven stop positions. Three cycles were completed during the static load test. This gives three data readings for each channel at each of the twenty-seven stop positions. It is ideal to have at least three data points. With no other data to confirm it, one data reading may be questionable. If there are two data readings, and they differ, it is difficult to determine which data reading is correct. With three data readings, an outlier data point can be eliminated.

### 5.3.5 TESTING PROCEDURE

The following is a step-by-step procedure for the static load test

1. Paint all necessary lines on bridge deck (Truck Lanes and Stop Positions).

Cycle 1

2. Balance all sensors with trucks off structure.
3. Align both load trucks to Lane A.
4. Pull trucks to stop position 1 and record data for 3 seconds.
5. Repeat step 4 for stop positions 2 – 9.
6. Pull trucks off span and record a data reading.
7. Align both load trucks to Lane B.
8. Repeat steps 3 – 6.
9. Align both load trucks to Lane C.
10. Repeat steps 3 – 6.

Cycle 2

11. Repeat steps 2 – 10.

Cycle 3

12. Repeat steps 2 – 10.

End Load Test

## 5.4 ACOUSTIC EMISSIONS TESTING

During the two nights of AE loadings, both trucks were backed into two positions and remained stationary for six minutes. Coming from the south, both trucks were backed along lane C and stopped when their rear wheels were centered over Stop Line 4, being careful not to cross the line. The trucks sat in position for approximately 6 minutes while AE data was recorded. The trucks were then pulled forward off of the span in the direction from which they originally came. Then each truck was driven north across Spans 10 and 11, one at a time, through the lane furthest from the instrumented girders until they were off the structure on the far (north) side of Span 11. Coming from the

north, both trucks were backed along lane C and stopped when their rear wheels were centered over Stop Line 6, being careful not to cross the line. The trucks remained still for 6 minutes while AE data were recorded. The trucks were then pulled off of the span to the north (the direction from which they came when loading the span).

### 5.5 SUPERPOSITION TESTING

Once the static load test was completed, a short test was completed to determine the effectiveness of superpositioning. Load trucks were aligned along the east lane of lane A as shown in Figure 5-11. Load truck ST-6400 was pulled into position A9, and data were recorded. While ST-6400 was still on position A9, ST-6902 was then pulled into position A1. Data were recorded with both trucks on the spans. ST-6400 was then pulled completely off of the span, and data was recorded. The two sets of data recorded with only one truck on the spans are added together and compared to the data recorded with both trucks on the span. Theoretically, if the bridge's behavior was linear-elastic, the sum of the readings of the two individual trucks should equal the readings when both trucks were on the span. This test was only conducted once.

### 5.6 WEATHER CONDITIONS

Large temperature gradients cause severe effects in the damaged locations of the girders. During the days of the test, temperatures were mild and the weather was cloudy. Cloudy, rainy conditions led to a low variation of temperature throughout the test days. Cracks in the girders were visibly smaller than on earlier days when instrumentation was installed. Table 5-3 shows weather data for the days of the test. Testing began around 11 p.m. on the night of May 31 and ended around 5 a.m. on the morning of June 2.

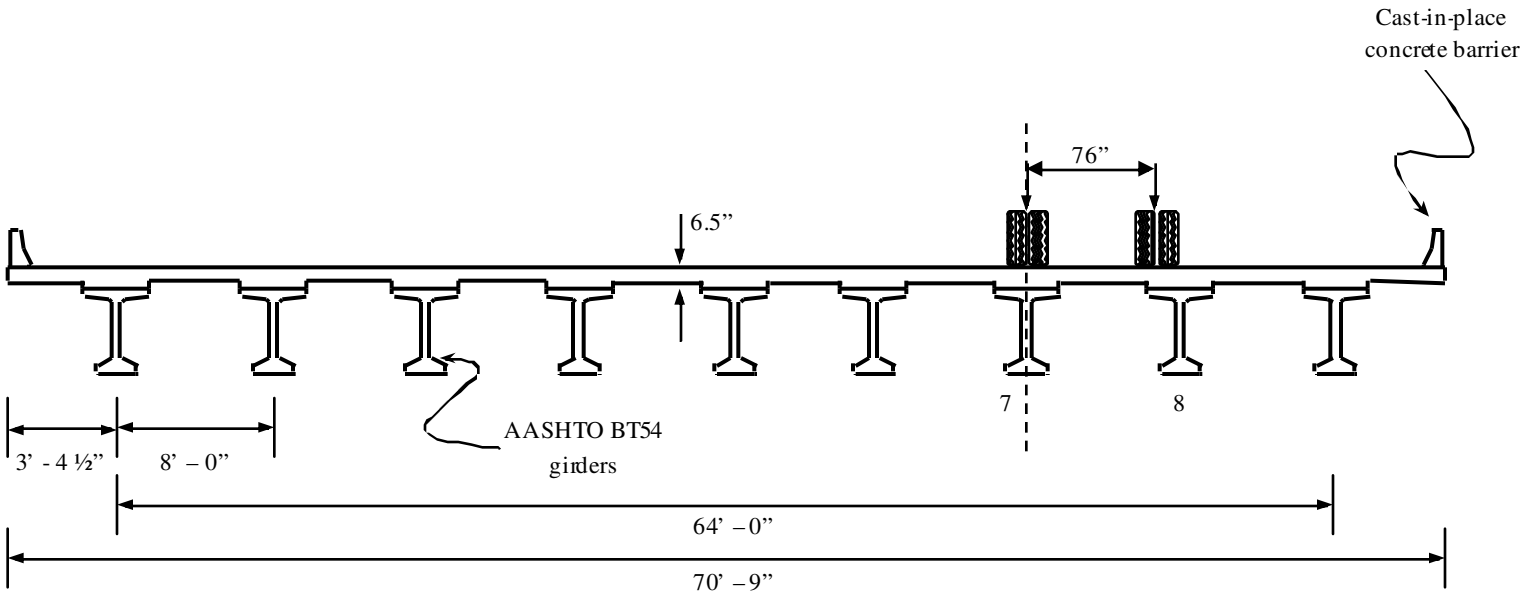


**Figure 5-11:** Superpositioning Test Lane – Horizontal Truck Positioning

**Table 5-3:** Temperature and Weather Data for Days of Load Test (NOAA)

| Date | Minimum Temperature (°F) | Maximum Temperature (°F) | Mean Temperature (°F) | Clouds | Rain |
|---|---|---|---|---|---|
| May 31, 2005 | 61 | 77 | 69 | Yes | 0.02 in. |
| June 1, 2005 | 63 | 70 | 67 | Yes | 0.093 in. |
| June 2, 2005 | 63 | 81 | 67 | Yes | 0.04 in. |

## 5.7 EFFECTS OF BEARING PADS AND FALSE SUPPORTS

Prior to the pre-FRP application load test, there was an attempt to remove the bearing pad atop the false supports under each girder. Only the bearing pad under Girder 8 in Span 10 was removed completely. The east half of the bearing pad under Girder 7 Span 10 was also removed. The west half of the bearing pad under Girder 7 Span 10, as well as both bearing pads in Span 11, remained in place. Many holes were drilled in these pads in an attempt to reduce their effective stiffness. The moderate, overcast weather during this time was not conducive to upward movement of the span, keeping the gaps between the pads and the girder rather small. With such a small gap and the fact that the bearing pads were glued to the false supports, removing the bearing pad with the available equipment was not possible prior to the scheduled load testing. Without removing the bearing pads, the behavior of the bulb-tee girders could possibly be affected if the girders are resting on the bearing pads and false supports.

# CHAPTER 6

# RESULTS AND DISCUSSION

## 6.1 ACOUSTIC EMISSIONS TESTING

Test data were recorded for two stop positions on each night, one stop position each in Spans 10 and 11, resulting in data from a total of four stop positions. The stop positions for the AE test are shown in Figure 6-1. As discussed earlier, truck weights were heavier the first night than the second night.

Also, data from the second night is more reliable than data from the first night. During the first night of testing, there were very significant amounts of noise in the recorded data. The cause for the noisy data was unknown, but the data was much less noisy the second night.

### 6.1.1 DEFORMATIONS MEASURED DURING AE TESTING

Tabular results from the AE test truck loadings can be seen in Table 6-1. During AE loadings, all COD's except for CO8_10W experienced crack openings when the loading was placed in the span containing COD's. When the load trucks were backed into stop position C4, with the rear wheels resting over the cracked section in Span 10, placing all of the load in Span 10, cracks in Girder 7 of span 10 opened while cracks in Girder 8 of Span 10 closed. During the same loading, cracks in both girders in Span 11 closed.

When the trucks were placed with their rear wheels on Stop Position 6 in Span 11, placing all of the load in Span 11, cracks in both girders of Span 11 opened, while cracks

in both girders of Span 10 closed. With the load placed directly over the crack, only cracks in Girder 8 Span 10 closed. This leads one to believe that Girder 8 Span 10 is behaving differently than the other 3 girder ends. If this is true, the girders cannot be said to all be acting in the same manner.

The only observed difference between Girder 8 Span 10 and the other 3 tested girders was that the bearing pad for Girder 8 Span 10 was completely removed, while the other bearing pads were drilled to reduce stiffness. If the cracks at Girder 8 Span 10 had opened, that would suggest that the false supports were providing support of the bridge girders.

If the girders are sitting on the false supports, which is highly likely, considering the fact that the bearing pads could not be removed because there was no gap between the two, the false supports may actually be acting as supports. Once the load is placed directly placed over the cracks, the load is roughly centered between two support points, the bent and the false supports. A load between the supports would induce positive moment at the crack location, causing the cracks to open. On the other hand, on Girder 8 Span 10, where the bearing pad was removed, the cracks closed when the load was placed directly over them. This would support the idea that the false supports were not being loaded by that girder. The cracks closed because of their proximity to the bent. At this distance, the loads cause negative moment at the crack location, causing the cracks to close.

It should be noted that the COD on Girder 8 Span 10 is located on the west face of the girder while the other three COD's are located on the east side of their respective girders. Another cause for the differences in readings could be out of plane bending or twisting of

the girder. Considering the results, this seems unlikely. At stop positions 3, 4, and 5 in all lanes, C07_10E opened and CO8_10W closed. The three lanes shift the center of the load from one side of Girder 7 to the other, depending on the load lane. As the center of the load shifts from one side of the girder to the other, one would expect the COD's to open and close depending on the location of the load relative to Girder 7. This is good evidence that out of plane bending or twisting is causing the CO8_10W to behave uniquely. However, the center of the load is always to the west of girder 8, possibly inducing the same direction of twist into the girder in all lanes. Furthermore, Lanes A and B are almost exactly opposite when comparing the possible "direction of twist" induced into Girder 7. In Lane A, the center of the two trucks is 2 ft to the west of Girder 7, and the center is 2 ft to the east of Girder 7 in Lane B. If "twist" was causing the crack openings, one would expect crack openings in Lane A lanes to become crack closings in Lane B. This doesn't happen though. CO7_11E only opens at Stop Positions 6 and 7, and this happens for both Lanes A and B. CO7_10E only opens at Stop Positions 3,4 and 5, and this happens for both Lanes A and B. Further finite element investigation may provide insight into this issue.

It can be concluded from the crack opening data that the false supports are having a significant affect on the pre-repair static load test results, and that the existence of these supports must be considered when drawing conclusions based on the pre-repair static load test.

**Table 6-1:** Deformations Measured during Acoustic Emissions Testing

| Position | | C4 - Span 10 | | C6 - Span 11 | | Position | | C4 - Span 10 | | C6 - Span 11 | |
|---|---|---|---|---|---|---|---|---|---|---|---|
| Night | | First | Second | First | Second | Night | | First | Second | First | Second |
| D7_11_1 | in | 0.00 | 0.01 | -0.07 | -0.06 | S8_10_2C | με | 14.1 | 12.7 | -15.6 | -15.4 |
| D7_11_2 | in | 0.01 | 0.02 | -0.11 | -0.09 | S8_10_2D | με | 9.7 | 8.2 | -16.6 | -12.8 |
| D7_11_3 | in | 0.01 | 0.02 | -0.12 | -0.10 | S8_10_2E | με | 2.3 | -13.4 | -11.5 | -23.4 |
| D7_11_4 | in | 0.01 | 0.03 | -0.12 | -0.08 | S8_10_2F | με | -7.2 | -7.7 | -1.1 | -0.5 |
| D8_11_1 | in | 0.01 | 0.02 | -0.07 | -0.07 | S7_11_1A | με | -4.2 | -5.6 | -0.3 | 1.0 |
| D8_11_2 | in | 0.02 | 0.02 | -0.12 | -0.10 | S7_11_1B | με | -13.4 | -12.1 | -2.1 | -2.1 |
| D8_11_3 | in | 0.02 | 0.03 | -0.14 | -0.12 | S7_11_1C | με | -7.3 | -8.3 | -10.5 | -10.6 |
| D8_11_4 | in | 0.03 | 0.03 | -0.11 | -0.10 | S7_11_1D | με | -10.4 | -9.4 | 2.8 | 2.8 |
| D7_10_1 | in | -0.10 | -0.09 | 0.01 | 0.02 | S7_11_1E | με | 0.9 | -1.3 | 0.7 | -0.9 |
| D7_10_2 | in | -0.11 | -0.09 | 0.01 | 0.02 | S7_11_1F | με | --[2] | -0.5 | ---[2] | 1.8 |
| D8_10_1 | in | -0.11 | -0.10 | 0.02 | 0.02 | S7_11_2A | με | -7.0 | -7.6 | 5.8 | 5.0 |
| D8_10_2 | in | -0.12 | -0.11 | 0.02 | 0.03 | S7_11_2M | με | -13.3 | -12.5 | 19.3 | 19.7 |
| CO8_10W | mm | -0.0118 | -0.0058 | -0.0183 | -0.0106 | S7_11_2C | με | -11.4 | -13.0 | 19.3 | 15.5 |
| CO8_11E | mm | -0.0141 | -0.0080 | 0.0038 | 0.0087 | S7_11_2D | με | -9.6 | -8.5 | 3.6 | 5.3 |
| CO7_10E | mm | 0.0157 | 0.0197 | -0.0265 | -0.0135 | S7_11_2E | με | -6.0 | -4.6 | -2.0 | -0.2 |
| CO7_11E | mm | -0.0280 | -0.0161 | 0.0119 | 0.0187 | S7_11_2F | με | -4.1 | -0.2 | -10.4 | -3.8 |
| S7_10_1A | με | 4.8 | 0.0 | 14.3 | 2.4 | S8_11_1A | με | -78.5 | -49.5 | -35.1 | 1.7 |
| S7_10_1B | με | -8.1 | -7.3 | -13.4 | -12.8 | S8_11_1B | με | -12.8 | -10.4 | -17.5 | -15.5 |
| S7_10_1C | με | -74.4 | -72.5 | -53.7 | -50.5 | S8_11_1C | με | -15.6 | -16.5 | -9.6 | -10.7 |
| S7_10_1D | με | -2.1 | -0.6 | -7.2 | -5.6 | S8_11_1D | με | -12.6 | -12.0 | -8.9 | -8.6 |
| S7_10_1E | με | 2.6 | 3.0 | -2.5 | -1.6 | S8_11_1E | με | -61.6 | -34.7 | -53.7 | -24.6 |
| S7_10_1F | με | -7.1 | -5.5 | -2.9 | -1.7 | S8_11_1F | με | 0.5 | -0.7 | -2.2 | -4.6 |
| S7_10_2A | με | 9.0 | 10.7 | -10.8 | -7.0 | S8_11_2A | με | -9.3 | -12.5 | 5.2 | 2.4 |
| S7_10_2M | με | 10.5 | 11.6 | -7.1 | -7.5 | S8_11_2M | με | -22.2 | -20.6 | 36.7 | 35.0 |
| S7_10_2C | με | 24.2 | 21.7 | -11.4 | -10.9 | S8_11_2C | με | -37.0 | -34.9 | 32.8 | 31.5 |
| S7_10_2D | με | 20.6 | 17.0 | -11.1 | -11.9 | S8_11_2D | με | -17.8 | -16.8 | 6.1 | 8.0 |
| S7_10_2E | με | 6.0 | 6.1 | -6.7 | -4.7 | S8_11_2E | με | -7.1 | -6.1 | -13.7 | -12.3 |
| S7_10_2F | με | -12.5 | -9.1 | -4.7 | -0.6 | S8_11_2F | με | -2.6 | -1.0 | -7.2 | -4.0 |
| S8_10_1A | με | 5.4 | 6.3 | -8.6 | -7.2 | S7_11_3M | με | -10.4 | -12.9 | 29.0 | 23.8 |
| S8_10_1B | με | -13.7 | -11.7 | -17.8 | -15.9 | S7_11_4M | με | -14.0 | -11.0 | 23.8 | 30.6 |
| S8_10_1C | με | -15.8 | -13.6 | -16.5 | -15.4 | S7_11_5M | με | -8.9 | -7.7 | 24.6 | 29.0 |
| S8_10_1D | με | 3.8 | 6.1 | -12.2 | -9.1 | S7_11_6M | με | -8.1 | -9.6 | 14.7 | 17.8 |
| S8_10_1E | με | 6.0 | 5.2 | 0.6 | -1.4 | S8_11_3M | με | -17.1 | -18.2 | 30.3 | 28.8 |
| S8_10_1F | με | -4.8 | -5.9 | -4.3 | -2.8 | S8_11_4M | με | -14.1 | -12.8 | 38.5 | 39.2 |
| S8_10_2A | με | 8.7 | 9.2 | -16.8 | -14.7 | S8_11_5M | με | -8.4 | -8.2 | 33.9 | 35.2 |
| S8_10_2M | με | 23.5 | 21.2 | -16.3 | -17.2 | S8_11_6M | με | -1.2 | -6.6 | -10.2 | 15.6 |

Notes:

1. Sign Convention: Positive = upward deflection, crack opening, or tensile strain; Negative = downward deflection, crack closing, or compression strain
2. --- = Unreliable Reading
3. με = microstrain (inch/inch x $10^{-6}$)

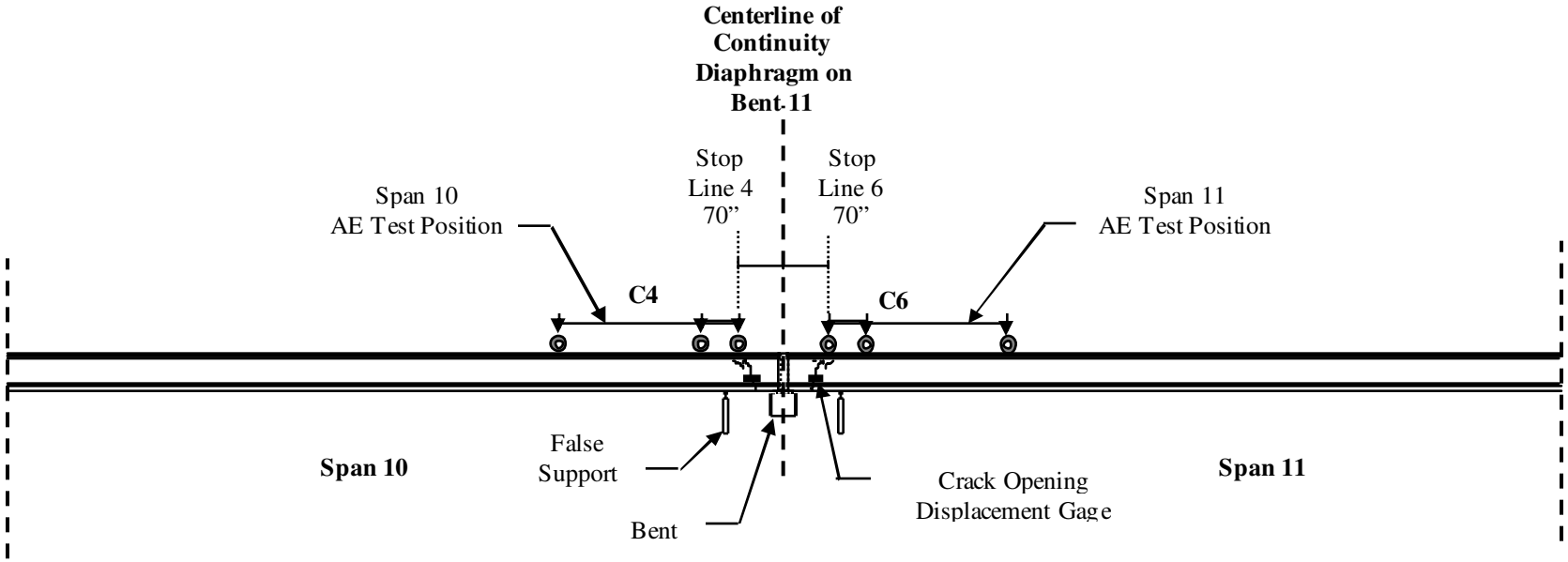


**Figure 6-1:** Elevation of Bridge Showing AE Truck Positions

## 6.2 STATIC LOAD TEST RESULTS

During the static load test, large amounts of data were recorded for each stop position. Data were reduced to one reading for each gage at each stop position for all three loading lanes. The static load test results may be seen in tabular format in Tables C-1 through C-9 of Appendix C. For each stop position, several graphs were constructed to help further analyze the data. These graphs included graphs of girder deflections, graphs of bottom fiber strains, and graphs of strains over Cross Sections 1 and 2 for Girders 7 and 8. These graphs are located in Appendix D.

### 6.2.1 DEFLECTIONS

The deflectometers provided very consistent deflection readings when comparing each of the three runs. These results were also very predictable, with no unexpected results. Midspan loadings, Stop Positions 1 and 9, always provided the maximum deflections in Spans 10 and 11, respectively. Downward deflection was always observed in the loaded span, while upward deflection was seen in the adjacent span from the loading. Load Lanes A and B produced very similar deflections for Girder 7, while producing the maximum deflections for this girder. Load Lane C produced the maximum effects on Girder 8.

#### 6.2.1.1 Maximum Deflections

Maximum deflections, either upward or downward, were always recorded under midspan loadings, Stop Positions 1 and 9. The downward deflection was recorded in the loaded span, and the upward deflection was recorded in the adjacent span. The maximum downward deflection, -0.31 in., in Girder 7 was seen during loadings A1 and B1. The maximum downward deflection, -0.33 in., in Girder 8 was seen during loading C1. The

maximum upward deflection, 0.07 in., in Girder 7 was seen during loading B1. The maximum upward deflection, 0.07 in., in Girder 8 was seen during loading C1.

#### 6.2.1.2 Implications of Deflection Behavior

Deflections consistently show evidence of continuous behavior. The opposite span from the one loaded, always deflected upward. For example, see Load Position A1. The truck is in the stop position near the midspan of Span 10. Both deflectometers in Span 10 deflect downward, with the deflectometer at midspan D7_10_2 deflecting downward the most. While the deflectometers in Span 10 deflect downward, every deflectometer in Span 11 shows upward deflection. Figure 6-2 shows this continuous behavior well. This is clear evidence of continuous behavior in the two-span bridge. However, from these deflection results alone, it is impossible to determine if the bridge is acting fully continuous, partially continuous with a reduced stiffness at the cracked section, or hinged at the cracked section. Simply supported behavior can be clearly ruled out.

### 6.2.2 CRACK OPENINGS GAGES

Crack openings provide a unique look into bridge behavior. Crack closing should occur in areas experiencing negative moments, and crack opening should occur in areas of positive moment. Larger crack closings mean larger negative moments at the cracked section, while larger crack openings mean larger positive moments at the cracked section.

#### 6.2.2.1 Crack Openings

Cracks only opened when trucks were positioned close to the cracks, stop positions 3, 4, 5, 6, and 7. With the load placed directly over the crack, positive moment forms at the crack, causing the cracks to open. Girder 8 span 10 never recorded a crack opening. The maximum crack opening of 0.0212 inches occurred at stop position B7 at crack opening

gage CO7_11E, in Girder 7 Span 11. Maximum crack openings for all crack opening gages were recorded with loads near the crack location, stop positions 4 and 7. As one would expect from continuous behavior, it can be determined that loads close to midspan create increased negative moments at the cracked sections, when compared to loads closer to the bent. It would be helpful if COD's were provided on both faces of the girders for future testing.

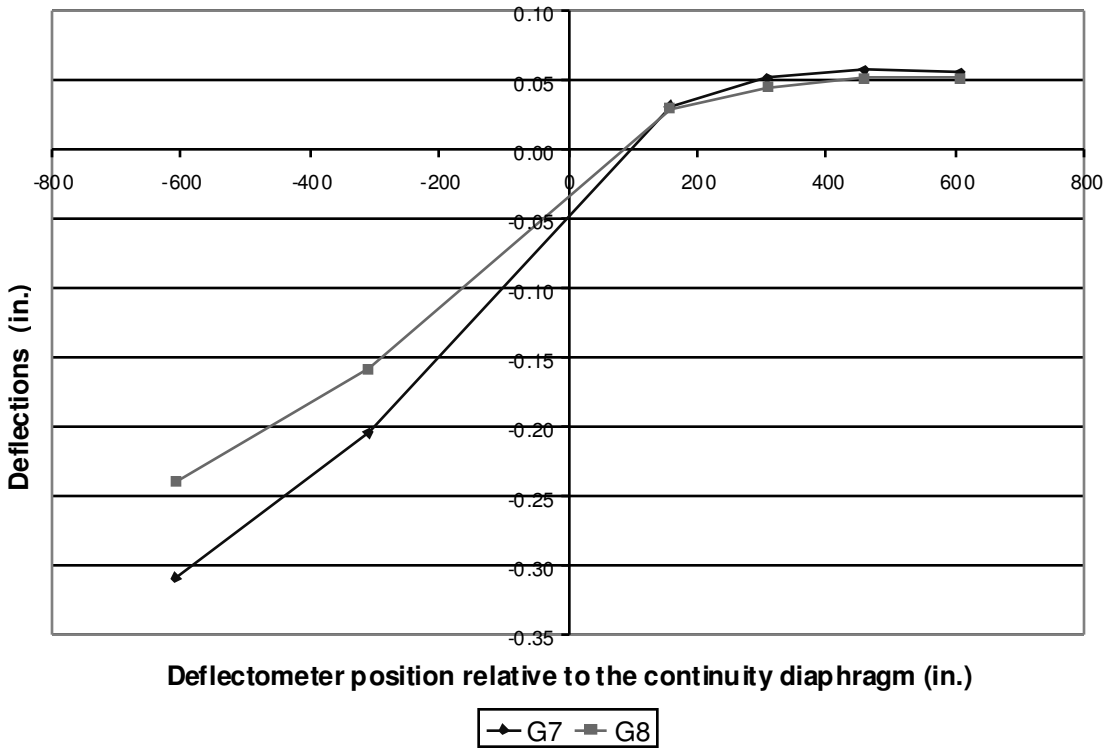


**Figure 6-2:** Stop Position A1 Deflections

#### 6.2.2.2 Crack Closings

The maximum crack closing of -0.0222 inches occurred at stop position B1 at crack opening gage CO7_11, in Girder 7 Span 11. Maximum crack closings for all crack opening gages were recorded with loads near midspan, stop positions 1 and 9. As one

would expect from continuous behavior, it can be determined that loads close to midspan create increased negative moments at the cracked sections, when compared to loads closer to the bent.

#### 6.2.2.3 Crack Opening Observations

Crack opening gage CO8_10W never opened, while the other three gages opened at some load position. Girder 8 Span 10 was the only girder end where the bearing pad on the false support was actually removed. This leads one to believe that the false supports have a significant impact on the test data.

Some cracks open and close more than others. This may be attributed to the fact that crack openings were measured across the largest crack at each girder end, but some girder ends have more smaller cracks while others have less but larger cracks. The total crack openings at those locations may be distributed over several cracks.

#### 6.2.2.4 Loadings that Most Influenced Crack Openings

Loads positions 2, 3, 4, 5, 6, and 7 all produced crack openings along at least one load lane in the test. Crack openings would induce tension in the FRP. Load positions 1 and 9 induce the maximum crack closures. Data from all of the stop positions should be analyzed after the post-repair load test to determine the effectiveness of the FRP repair. All three lane loadings should be repeated during follow-up tests. Lane A loading provides the maximum influence on Girder 7. Lane B loading provides a load almost exactly opposite of Lane A loading for comparing the "direction of twist" in Girder 7. Lane B loading also causes the maximum crack openings and closings. Lane C loading provides the maximum influence on Girder 8.

#### 6.2.2.5 Implications of Crack Opening Displacements

The crack opening displacement results support the idea that the false supports had a significant effect on the results from the static load test. The crack closings also supported the idea that the bridge acts in a continuous manner by being able to carry negative moment through the cracked section. Through crack opening displacement results alone, it is impossible to determine if the bridge is behaving as fully continuous, partially continuous, or hinged at the cracked cross section.

### 6.2.3 STRAINS

Strains represent the longitudinal elongation or shortening per unit length of the portion of concrete to which the gage is attached. From the strains, one can infer whether the portion of concrete is undergoing axial tension or compression, the relative magnitude of tensile and compressive stresses, and the sign of the bending moment at the cracked section.

#### 6.2.3.1 Strain Gages Close to the Bent

Gages close to the bent, cross section 1, consistently reported compressive strains near the bottom flange. Negative moment is apparent at this location because of the bottom flange being in compression. From this it can be determined that the girder is acting continuously directly over the support.

The amount of compressive strains indicate the relative magnitude of the negative moment, with the negative moment getting more negative as the load location approaches midspan, and the moment approaching zero as the load location nears the bent. This is shown in Figure 6-3 for Lane A loading.

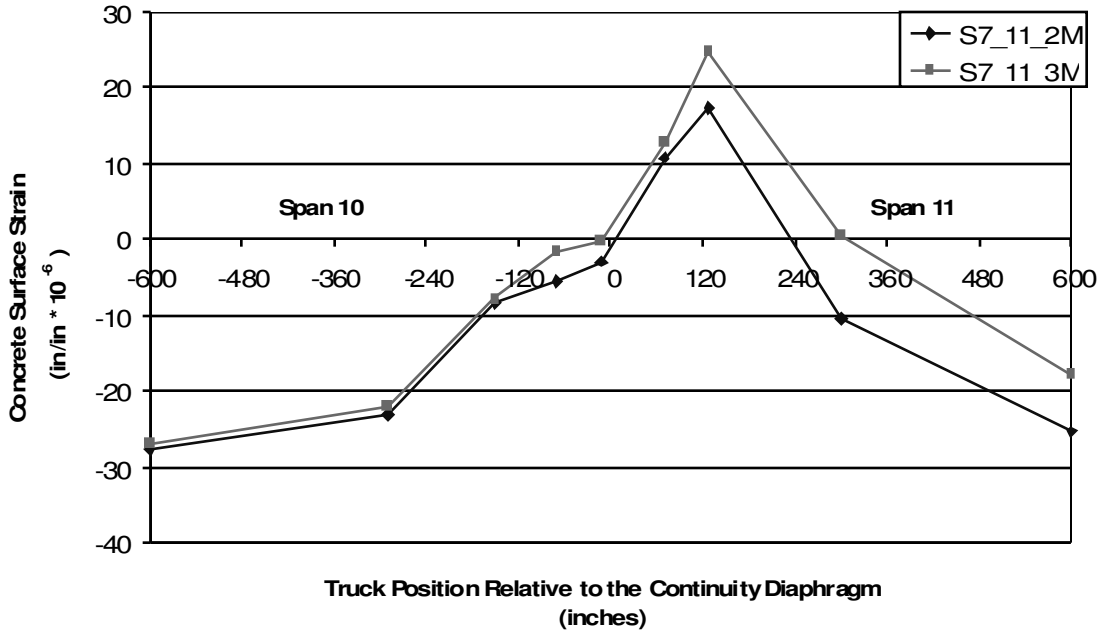


**Figure 6-3:** Strain versus Load Application Location

#### 6.2.3.2 Implications of Strains

It is apparent from the strain data that the cracked section can support negative moment under service-level loads, and that the bridge acts as a continuous structure when negative moments are induced at the cracked locations. This can be clearly seen with two examples.

At truck position B1, the load is placed at the midspan of Span 10. From the deflection data, we know that Span 11 deflects upward. From the strain data we can see that all of the strain gages in Span 11 at position M, positioned at the bottom center of the bottom flange, report compression under the B1 loading. Gages B and C at cross section 1 also report compression. With all of the bottom strain gages reading negative strains, indicating negative moments, it is clear that the negative moment can be transmitted

through the cracks and that the bridge is acting in a continuous manner, either fully continuous or partially continuous under this loading.

Secondly, at truck position B9, the load is placed at the midspan of Span 11. For this loading, assuming continuous behavior, one would expect negative moment at the bent with a transition to positive moment near midspan of Span 11. This is exactly what is seen at truck position B9, as shown in Figure 6-4. Specifically looking at Girder 8, Gages S8_11_1B, S8_11_2M, S8_11_3M all report compressive strains in the bottom flange of the girder. Strain gages S8_11_4M, S8_11_5M, and S8_11_6M all report tensile strains. From this behavior, it is clear that the beam is acting continuously with some negative moment being transferred through the cracked section. It is also apparent that the inflection point is located roughly halfway between cross sections 3 and 4, approximately 16 feet from the centerline of the continuity diaphragm.

At cross section 1, strain gages B and C are located at the same height and on opposite sides of the girder, B on the East and C on the West. Theoretically, these two gages should read the exact same strains. This is not the case, however. This could be attributed to out-of-plane bending effects, but as discussed earlier, this is not thought to be an issue. A glance through the tables in Appendix C shows that these two gages hardly ever read similar strains. The strains are always of the same sign, but the magnitude of the two often differs. For example, at truck stop position A1, gage S8_10_1B read a strain of 33 με while gage S8_10_1C read a strain of 16 με, less than half of gage S8_10_1B. Therefore, strains gages should not be used to determine exact strains and stresses at a particular point, and should be used more for determination of

overall behavior (e.g., high compressive strains, low compressive strains, high tensile strains, low tensile strains, etc.).

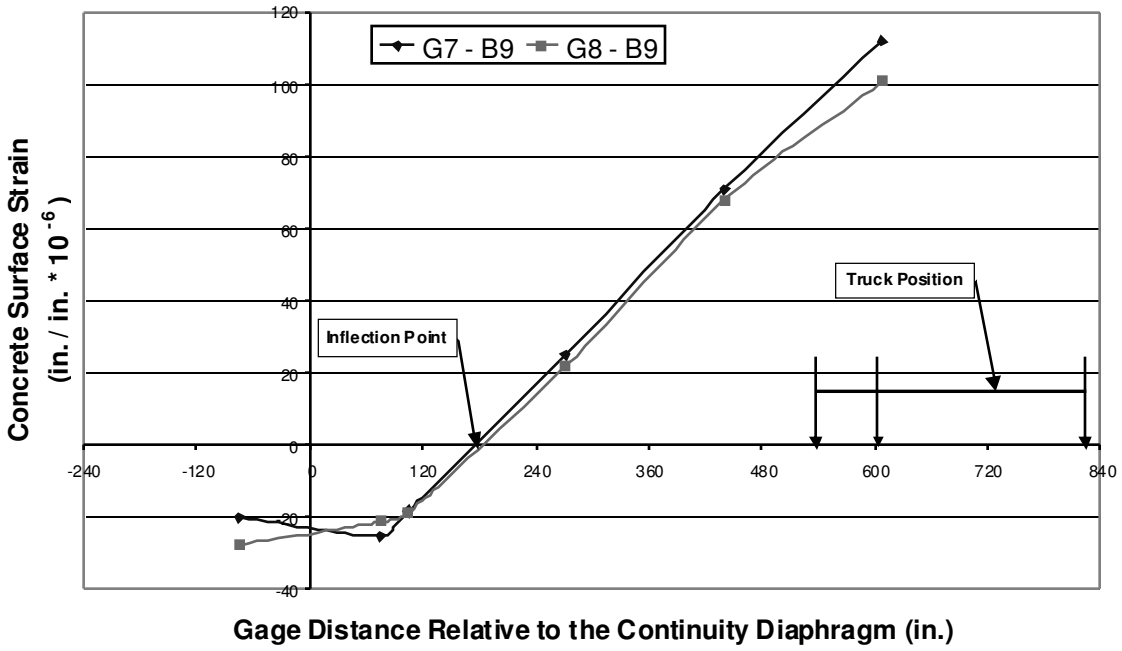


**Figure 6-4:** Bottom-Fiber Strains for Load Position B9

## 6.3 SUPERPOSITION OF TEST RESULTS

Once the static load testing was completed, a simple test was conducted to test the validity of superposition of load test readings. If the bridge is behaving linear-elastically, superposition should be effective. Theoretically, if the bridge superstructure was exhibiting linear structural response, the sum of the first and third measurements at each gage should equal the second measurement (both trucks present) at each gage. This test was conducted twice. The data from each round of testing were combined to give an average for each truck position. To illuminate the effectiveness of this test, each type of

deformation measurement is discussed individually. Two trucks were aligned along the east end of Lane A. The first truck was initially driven to stop position A9 near the center of Span 11. Data for the single truck were recorded. A second truck was then driven to position A1 near the center of Span 10. Data were recorded with both trucks on the bridge. The first truck (position A9) was then driven off of the bridge, and data were recorded with only the second truck on the bridge at position A1.

### 6.3.1 DEFLECTIONS

The final deflections for the superposition test are shown in Table 6-2. It can be seen that the results predicted by superposition are accurate. The average difference between the deflections predicted by superposition and the deflections recorded with trucks in positions A1 and A9 simultaneously was only -0.002 inches. The average percent difference is 2.3 percent. The max difference is 0.006 inches for the deflectometer located at position 3 along Girder 7 in Span 11. The maximum percent difference is roughly 6 percent at position 2 along Girder 7 in Span 11.

**Table 6-2:** Deflection Superposition Results

| Deflectometer Location | Truck Position A1 (in.) | Truck Position A9 (in.) | Superposition A1+A9 (in.) | Truck Position A1 and A9 (in.) | Difference (in.) | Percent Difference |
|---|---|---|---|---|---|---|
| D7_11_1 | 0.015 | -0.051 | -0.036 | -0.035 | -0.001 | 4 |
| D7_11_2 | 0.022 | -0.108 | -0.086 | -0.081 | -0.005 | 6 |
| D7_11_3 | 0.023 | -0.146 | -0.122 | -0.117 | -0.006 | 5 |
| D7_11_4 | 0.032 | -0.161 | -0.129 | -0.133 | 0.003 | -2 |
| D8_11_1 | 0.018 | -0.051 | -0.032 | -0.033 | 0.001 | -2 |
| D8_11_2 | 0.023 | -0.103 | -0.080 | -0.076 | -0.003 | 5 |
| D8_11_3 | 0.024 | -0.146 | -0.122 | -0.117 | -0.005 | 4 |
| D8_11_4 | 0.030 | -0.159 | -0.129 | -0.130 | 0.001 | -1 |
| D7_10_1 | -0.113 | 0.024 | -0.089 | -0.086 | -0.003 | 4 |
| D7_10_2 | -0.172 | 0.025 | -0.147 | -0.143 | -0.004 | 3 |
| D8_10_1 | -0.106 | 0.026 | -0.080 | -0.077 | -0.003 | 4 |
| D8_10_2 | -0.160 | 0.030 | -0.130 | -0.129 | -0.001 | 0 |

From this data it can be determined that superposition works well in predicting service-load bridge deflections, even with the level of damage observed in this structure. Which means that the bridge is behaving linear-elastically.

### 6.3.2 CRACK OPENINGS

The final crack openings for the superposition test are shown in Table 6-3. When comparing the average percent differences, the crack openings predicted by superposition are not as accurate as the deflections shown earlier. The average difference was -0.002 mm, but the average percent difference was 14 percent. The maximum difference between the crack opening predicted by superposition and the crack opening reading taken with both trucks on the bridge was 0.004 mm. The maximum percent difference between the two was 35%. Both of these maximums occurred at the crack location on Girder 8 Span 10. At all four locations, the cracks closed less than predicted by superposition.

Analysis by superposition would predict that all four of the cracks would close more than the crack closings that were recorded with both trucks on the bridge. This phenomenon can best be explained by understanding that the cracked zone does not act linearly. It acts more closely to a nonlinear spring in which the stiffness factor increases with deflection. As the cracks close, more and more compression can be transferred across the crack, until finally the crack is closed completely and the full girder section is capable of transferring compression. Therefore, adding additional load does not have a linear effect as predicted with superposition. Adding the second truck does not have as large an effect on the crack closing as it would without the first truck being in place.

**Table 6-3:** Crack Opening Superposition Results

| COD Location | Truck Position A1 (mm) | Truck Position A9 (mm) | Superposition A1+A9 (mm) | Truck Position A1 and A9 (mm) | Difference (mm) | Percent Difference |
|---|---|---|---|---|---|---|
| CO8_10 | -0.008 | -0.007 | -0.015 | -0.011 | -0.004 | 35 |
| CO8_11 | -0.005 | -0.005 | -0.010 | -0.009 | -0.001 | 6 |
| CO7_10 | -0.010 | -0.011 | -0.022 | -0.020 | -0.002 | 8 |
| CO7_11 | -0.014 | -0.011 | -0.024 | -0.022 | -0.002 | 9 |

### 6.3.3 STRAINS

The final strains for the superposition test are shown in Table 6-4. Based on percent differences, the strain readings obtained by a superposition analysis are the least accurate of the measurements taken during the superposition testing. When looking at actual strain differences, the results were fairly accurate, with an average difference between the superposition-predicted value and the actual recorded value of only about 3 microstrain ($3 \times 10^{-6}$ in./in.). The maximum difference in strains was 17 microstrain recorded at strain gage S7_10_1B. As one would expect, the percent differences varied widely with the overall magnitude of the strain reading. With larger strain readings, the percent differences were typically smaller. With smaller strain readings, the percent differences were typically larger. For strain gages near the bottom of the girder in compression zones, the strains obtained from superposition were typically less than the compressive strains. These gages with both trucks in place typically produced compressive strains that exceeded the superimposed strains, as seen with the negative percent differences. This may be attributed to the influence of the false supports providing support for the girder, as discussed below.

**Table 6-4:** Strain Superposition Results

| Strain Gage Location | Truck Position A1 (με) | Truck Position A9 (με) | Superposition A1+A9 (με) | Truck Position A1 and A9 (με) | Difference (με) | Percent Difference |
|---|---|---|---|---|---|---|
| S7_10_1A | 4 | -1 | 4 | 1 | 2 | 200 |
| S7_10_1B | -6 | -9 | -15 | -32 | 17 | -54 |
| S7_10_1C | -73 | -49 | -122 | -124 | 1 | -1 |
| S7_10_1D | -3 | -8 | -11 | -13 | 2 | -20 |
| S7_10_1E | 0 | -2 | -2 | -1 | -1 | 50 |
| S7_10_1F | -1 | -2 | -3 | -3 | 0 | -1 |
| S7_10_2A | -5 | -8 | -13 | -18 | 5 | -30 |
| S7_10_2M | -6 | -9 | -15 | -20 | 5 | -30 |
| S7_10_2C | -9 | -13 | -22 | -27 | 5 | -20 |
| S7_10_2D | -11 | -14 | -25 | -30 | 5 | -20 |
| S7_10_2E | -6 | -6 | -12 | -14 | 2 | -20 |
| S7_10_2F | -5 | -1 | -5 | -6 | 1 | -20 |
| S8_10_1A | 0 | -8 | -9 | -12 | 3 | -30 |
| S8_10_1B | -13 | -9 | -22 | -34 | 12 | -35 |
| S8_10_1C | -12 | -14 | -25 | -31 | 5 | -20 |
| S8_10_1D | -2 | -11 | -12 | -12 | 0 | 1 |
| S8_10_1E | 0 | -3 | -2 | -2 | -1 | 40 |
| S8_10_1F | -2 | -2 | -4 | -4 | 0 | -5 |
| S8_10_2A | -11 | -12 | -24 | -27 | 3 | -10 |
| S8_10_2M | -12 | -14 | -26 | -30 | 4 | -10 |
| S8_10_2C | -9 | -14 | -23 | -26 | 3 | -10 |
| S8_10_2D | -7 | -11 | -19 | -24 | 5 | -20 |
| S8_10_2E | -7 | -6 | -13 | -14 | 1 | -9 |
| S8_10_2F | -4 | 0 | -4 | -5 | 0 | -7 |
| S7_11_1A | -12 | -2 | -14 | -18 | 4 | -20 |
| S7_11_1B | -9 | -5 | -14 | -23 | 9 | -40 |
| S7_11_1C | -9 | -12 | -21 | -36 | 15 | -42 |
| S7_11_1D | -15 | -5 | -19 | -22 | 2 | -10 |
| S7_11_1E | -3 | 0 | -3 | -4 | 1 | -30 |
| S7_11_1F | -1 | -1 | -2 | -3 | 1 | -40 |
| S7_11_2A | -8 | -6 | -14 | -20 | 6 | -30 |
| S7_11_2M | -12 | -12 | -25 | -29 | 4 | -10 |
| S7_11_2C | -13 | -13 | -26 | -31 | 5 | -20 |
| S7_11_2D | -9 | -7 | -16 | -20 | 4 | -20 |
| S7_11_2E | -5 | -4 | -10 | -13 | 3 | -20 |
| S7_11_2F | 0 | -1 | -1 | -3 | 2 | -50 |
| S8_11_1A | -44 | -25 | -69 | -69 | 0 | 0 |
| S8_11_1B | -7 | -15 | -22 | -27 | 5 | -20 |
| S8_11_1C | -14 | -11 | -25 | -30 | 4 | -20 |
| S8_11_1D | -16 | -7 | -23 | -25 | 2 | -6 |
| S8_11_1E | -22 | -13 | -35 | -31 | -4 | 10 |
| S8_11_1F | -1 | -1 | -2 | -1 | -1 | 200 |
| S8_11_2A | -10 | -10 | -20 | -22 | 2 | -8 |
| S8_11_2M | -17 | -11 | -28 | -31 | 3 | -10 |
| S8_11_2C | -29 | -22 | -51 | -53 | 2 | -4 |
| S8_11_2D | -14 | -13 | -27 | -29 | 1 | -5 |
| S8_11_2E | -5 | -9 | -14 | -17 | 3 | -20 |
| S8_11_2F | -2 | -5 | -7 | -7 | 0 | -1 |
| S7_11_3M | -12 | -9 | -21 | -25 | 5 | -20 |
| S7_11_4M | -11 | 14 | 3 | 0 | 3 | -1000 |
| S7_11_5M | -7 | 40 | 33 | 31 | 2 | 7 |
| S7_11_6M | -3 | 64 | 61 | 58 | 3 | 5 |
| S8_11_3M | -15 | -10 | -25 | -28 | 4 | -10 |
| S8_11_4M | -11 | 13 | 2 | -1 | 2 | -400 |
| S8_11_5M | -7 | 40 | 33 | 30 | 3 | 10 |
| S8_11_6M | 6 | 61 | 67 | 54 | 13 | 25 |

In Table 6-2, notice that the deflectometers recorded larger deflections when a single truck was loading the span in which the deflection was being recorded than when both trucks were in position on opposite spans. In other words, Girder 10 deflections were larger when a single truck was in Position A1, and Girder 11 deflections were larger when a single truck was in Position A9. The afternoon before the bridge testing was conducted, an unsuccessful attempt was made to remove the bearing pads from the top of the false supports. Because of the moderate rainy weather, the girders had not deflected upward, and the girders were flush against the bearing pads, making removal of some of these pads impossible. During the test, the deflections were a maximum in a span when only one truck was positioned in that span. If it is assumed that the bearing pad and false support system acts as a spring, the false supports in a span would absorb more load when only that span is loaded, because the increased deflection would cause the bearing pad and false support to deflect downward more, therefore transferring more load. As the false supports take more load, the loads and moments transmitted through the beam to the bent would in turn be reduced. Therefore, with reduced loads and moments, there would be less strain in the superposition predictions than during the actual load test with two trucks in place. This can be clearly seen in Table 6-4 at Gages B and C at Cross Section 1 of all four girder ends. Superposition predicts less compression than what was recorded with both trucks on the span, Truck Position A1 and A9. For example, Gage S7_10_1B had a superimposed strain of -15 microstrain, while the strain recorded with both trucks on the span was -32 microstrain.

### 6.3.4 SUPERPOSITION SUMMARY AND CONCLUSIONS

Superposition reliability was investigated for strains, deflections, and crack openings. Superposition appears to be the most accurate when predicting large-scale behaviors, such as bridge deflection. Deflection is the result of an accumulation of the response curvatures of all the cross sections. Thus, discrepancies at individual, critical cross sections are effectively averaged out across the entire structure. Superposition does not predict smaller, more localized measurements such as strains and crack openings quite as well. The complexities of this bridge, including the extreme cracking, epoxy injection, and uncertain support conditions, reduce one's ability to assess if it exhibits linear-elastic behavior.

During the analysis of the superposition data, it became quite evident that the false supports were having a significant effect on the reported strains and deflections. This could prove to have a significant effect on the overall test results.

## 6.4 BRIDGE BEHAVIOR

Several types of structural response behavior of the two-span girder system have been considered when investigating and analyzing the bridge girders. These possible behavior types are discussed below.

### 6.4.1 SIMPLY SUPPORTED

Simply supported behavior can easily be ruled out when looking at the test data. In order for the bridge to act as if simply supported, there can be no negative moment in any portion of either bridge span. Negative (compression) strains below the neutral axis can be seen throughout the test data. Therefore the bridge is not behaving as if simply supported under service-level loads.

### 6.4.2 FULLY CONTINUOUS

The bridge was originally designed to act as a continuous structure under live loads. The test data supports the fact that the bridge is acting in a continuous manner. For example, during the superposition testing, the results for position A1 & A9 (both trucks positioned simultaneously) showed the inflection point in the beam near Cross Section 4, as indicated in Figure 6-5. The strain gages at that location showed very little strain. In order for negative moment to end that far out into the span, negative moment would have to be carried through the cracked section. This supports the idea that the bridge is acting continuously. It can be concluded from the test data that at the time of the test the bridge was not acting as though there were a hinge at the cracked region. A hinge at the cracked region would imply that vertical downward load applied near midspan would cause negative moments at cross section 1 on the bent side of the cracks and positive moments at cross section 2 on the midspan side of the cracks. It was common to see negative moments in both cross sections.

### 6.4.3 FACTOR THAT COULD INFLUENCE CONTINUITY OF CRACKED CROSS SECTIONS

It is likely that the behavior of a bridge having girders with such extensive cracking can vary depending on the load, location of the load, and the thermal conditions. Differential heat transfer across the cross section of the bridge causes the cracks to open and close. At times when the top of the girder is at a higher temperature than the bottom of the girder, the crack opens. When the cracks are open, the girder is allowed to act as if hinged, and the girder is allowed to rotate at the crack until a vertical load large enough to close the crack is seen. At times with uniform temperatures throughout the girder, the cracks close and compression is carried across the crack through the bottom flange of the

girder, thus causing the bridge to act in a continuous manner. As the cracks become smaller and even close, it is likely that the bridge acts as a continuous structure. The cracks close, and the cracked cross section carries both compression and negative moment across the cracks. As the cracks open, it is more likely that the normal service loads do not close the cracks completely, and therefore the cracked section acts as if hinged, not transferring compression across the cracks.

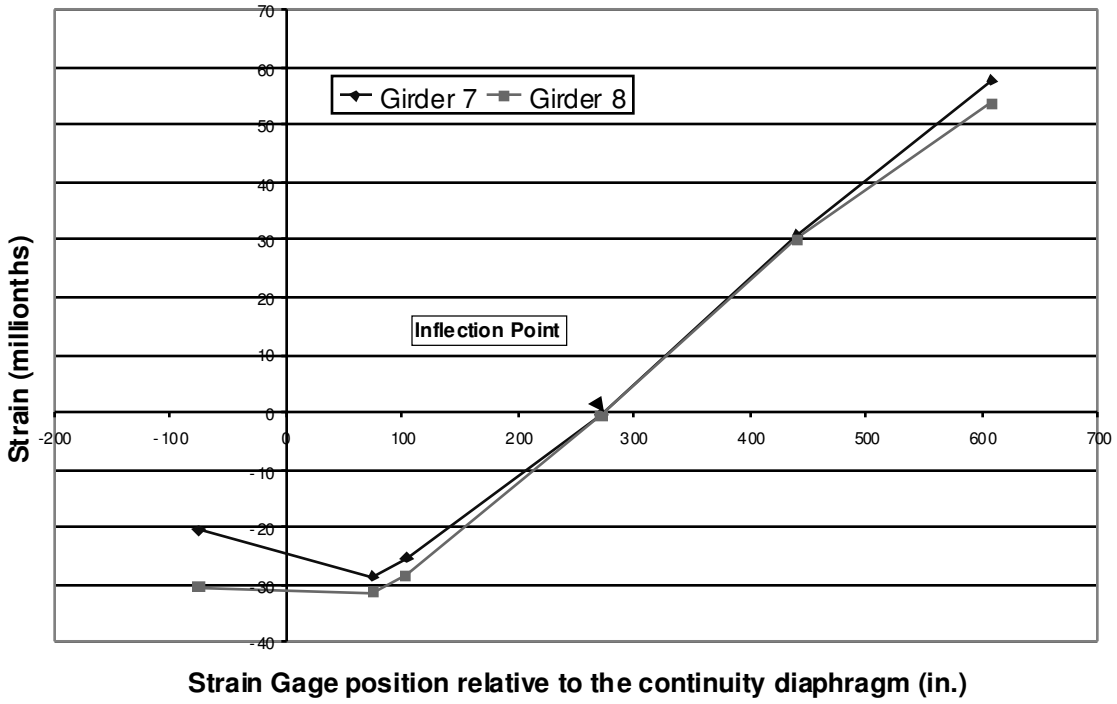


**Figure 6-5:** Bottom Fiber Strains for Load Position A1 & A9

The days leading up to and the night of the testing were moderate and rainy, and continuous behavior might be expected. As a result of the moderate rainy weather, the cracks were noticeably smaller than during any point during the instrumentation process. It is not surprising, then, that the bottom strain gages outside of the cracked section; gages S7_10_2M, S8_10_2M, S7_11_2M, and S8_11_2M; were commonly in

compression. This would imply that negative moment and compression were being transferred through the cracked section. Based on the data collected from the superposition tests, it was evident that the inflection point of the girders in Span 11 was very near Cross Section 4. Strain gages S7_11_4M and S8_11_4M reported strains very near zero. The strain gages closer to midspan reported tension, and those closer to the bent reported compression. These results would further support the conclusion that both compression and negative moments were being transferred through the cracked section on the night of the pre-repair static load test. The same test on a hot sunny afternoon may have given different results.

### 6.5 FRP EVALUATION

The purpose of the external FRP strengthening system is to provide the horizontal tension tie required to develop the required shear strength at the cracked cross section. Evaluation of the effectiveness of the FRP strengthening will be difficult, considering the fact that almost all truck positions produce negative moment at the crack location under service-level loads, therefore causing compression in the region where the FRP will be placed. In order to properly determine the effectiveness of the FRP repair, the bridge should be tested under the thermal conditions that caused it to crack. In order to do this properly, a second pre-repair test would need to be conducted that record the strains throughout the course of a hot, sunny day. This test should begin early in the morning, before daylight, when thermal effects are minimized. Once the FRP repair has been completed, a post-repair test should be conducted that would more clearly show the effectiveness of the FRP repair.

## 6.6 FALSE SUPPORTS

During initial test preparation, a strain gage was placed on one column of the false supports. As a large truck drove over the bridge, a small compression strain was induced in the false support column, thus proving that the false supports were providing some support during normal traffic conditions. At that time, this test provided no real concern about the upcoming bridge test. The plan was to remove the bearing pads between the false supports and the prestressed concrete bridge girders on the day of the test, allowing the girders to behave freely from the false supports. Unfortunately, when the time came to remove the pads, only the bearing pad for one girder end was removed completely.

The effects of false supports could easily cause an increase in the stiffness of the girder that Shapiro (2007) had assumed to be the result of prestressed tendons being bonded and acting like non-prestressed reinforcement. Swenson's (2003) work had the objective of determining the strength of the existing bridge without the false supports, so they were not included in his analyses.

## 6.7 COMPARISONS TO PREVIOUS RESEARCH

Based on the recorded strains, crack openings, and deflections it may be possible to determine a slight change in overall behavior resulting from the FRP repair as suggested by Shapiro (2007). It is difficult to extrapolate a change in shear strength from this change in service-load response. Shapiro (2007) discussed the compression induced in the FRP under the truck loads, and that the FRP would be able to transfer the resulting compression over the short crack distance. Shapiro's finite-element analyses and the static load test offer little information for determining the effectiveness of the FRP repair. Both of these investigations provide more information about the cracked bridge behavior

rather than providing information pertinent to the original objective of the research: to strengthen the bridge (in shear) that has been weakened by cracking that resulted from upward deflection due to differential heating across the depth of the bridge girders. The conclusions drawn from Shapiro's finite element work essentially conflict with Swenson's worst-case assumption of girder behavior. Swenson (2003) based his strut-and-tie design models on the assumption that extreme (factored) downward truck loads may induce very large tensile forces in the bottom flange of the girders. Shapiro's finite-element analyses indicated that there would be compression in the FRP under service-load conditions once installed on the bottom flange of the girders.

The static load test results agree with Shapiro's results more so than Swenson's worst-case design assumptions. In both the load test and Shapiro's work, loads near midspan created compression in the bottom flange near the bent, and partial closing of cracks. Assuming the tendons slipped during the opening of the original wide cracks and therefore have limited bond capacity, the bridge in its current state does not have any steel in the bottom flange that can be conservatively relied upon to act as a tensile tie under factored design loads. Swenson predicted very high tensile forces in the bottom flange of the girder with his strut and tie analysis. For that reason, Swenson designed an FRP retrofit to provide the required reinforcement to handle the tensile forces. The strains from the load test did not agree with Swenson's predictions. All loads near midspan created negative moment and compression in the bottom flange of the girders. After reviewing the test results, the analysis methods and assumptions from Swenson's work may not accurately predict the behavior and stresses within the bridge under vertical truck loadings. Much of this discrepancy can be attributed to the fact that much

of Swenson's design and analysis was based on simply supported behavior, which appears to be an inaccurate representation of the actual girder behavior based on the load test results.

# CHAPTER 7

# SUMMARY AND CONCLUSIONS

## 7.1 SUMMARY

Construction began on I-565 in Huntsville, Alabama in January of 1988. After slightly more than 3 years of construction, the elevated highway was completed on March 27, 1991. Bridges spans were composed of either steel or prestressed concrete and were designed to act as simply supported, two-, three-, or four-span continuous structures.

A bridge inspection in 1992 revealed small cracks in the continuous ends of many of the prestressed concrete bulb-tee girders. Approximately 18 months later, during March and April of 1994, a second inspection revealed much more serious cracking, with cracks as wide as 0.25 inches. A survey was then performed on all spans to record size and locations of the cracks.

ALDOT personnel then instrumented the bridges in an attempt to determine the cause of the severe cracking. Engineers at ALDOT found that a nonlinear temperature distribution caused by the sun warming the top of the bridge more than the underside was the likely cause. Later research by Gao (2003) from Auburn University supported ALDOT's findings. Gao (2003) reported that the temperature distributions in the bridges caused the spans to deflect upward, a behavior known as "sun cambering". The upward deflection caused large positive restraint moments in the girders that ultimately led to cracking.

Swenson (2003) of Auburn University examined the strength effects on the bridge caused by the cracking. He concluded that the longitudinal reinforcement in the bottom flange of the girders is likely not adequate developed at the cracked girder ends to provide dependable shear resistance in these regions. In order to alleviate this problem, Swenson designed a 4-ply FRP system to strengthen the girders.

The research described in this thesis consisted of load testing the bridge before the FRP was installed. This load testing provided a baseline to which later post-repair load tests can be compared. The load tests also provided valuable data about the pre-repair behavior of the cracked girders.

## 7.2 CONCLUSIONS

### 7.2.1 OVERALL BRIDGE BEHAVIOR

After reviewing the test results, it is clear that the bridge is not acting as if the girders are simply supported. At the time of the test, the bridge was not acting as if it was hinged at the cracks. It is difficult to determine whether the bridge is acting in a fully continuous manner or acting in a partially continuous manner with reduced stiffness at the cracked section. It is probable, based on the visual observations throughout the research and instrumentation process, that the bridge acts in varying manners depending on the weather conditions and the relative behavior of the bridge at that time i.e., acting hinged at times when there is a large difference between the temperature at the top of the girders and that at the bottom of the girders and acting continuously at times when the temperature throughout the girder is uniform.

### 7.2.2 FALSE SUPPORTS

The test data indicate that the false supports had a significant effect on the bridge behavior. In order to apply the FRP, the bearing pads were removed completely. This fact alone makes it doubtful that post-repair load test results can be accurately compared to the intended baseline, the pre-repair load test results. In order to use the pre-repair test results as a baseline for the post-repair tests results, the bearing pads would have to be replaced in the same position as they were located in the pre-repair load test. In order for the post-repair test to provide the most information about the effectiveness of the FRP repair, the bearing pads would need to be removed completely. At that time, the pre-repair results may no longer serve as a good baseline for the post-repair results.

### 7.2.3 COMPARISONS TO PREVIOUS RESEARCH

Based on the recorded strains, crack openings, and deflections, it may be possible to determine a slight change in overall behavior resulting from the FRP repair as suggested by Shapiro (2007). It will be difficult to predict the increase in shear strength from this change in behavior alone. Shapiro (2007) predicted compression in the FRP at the cracked section, while Swenson's analysis was based on the conservative assumption of simply supported behavior; Swenson (2003) concluded that there would be high tensile forces located in the FRP at the cracked section under factored design loads. The static load test results agree with Shapiro's work. The test results indicate that the analysis methods and assumptions made in Swenson's work may not accurately predict the behavior and stresses within the bridge under vertical truck loadings. However, it is difficult to extrapolate ultimate response from the linear-elastic response under service-level test loads. Much of this discrepancy can be attributed to the fact that much of

Swenson's design and analysis was based on simply supported behavior, which has been observed not to be the actual behavior exhibited by the bridge girders.

### 7.2.4 General Conclusions

Static load tests of in-service bridges only offer direct insight about bridge response under heavy service-load conditions. For a bridge that is deficient in shear strength, like the one being examined here, it is very difficult to draw conclusions about the shear strength based on a normal static load test. Longitudinal strains provide more information about moments within the structure and provide little directly useful information about shear. Therefore, once a post-repair test is completed, it will be virtually impossible to determine the increase in shear strength resulting from the FRP repair.

There are too many variables to gain useful data in a post-repair load test. The false supports have had a significant effect on the data obtained during the pre-repair testing. It has also been shown that the behavior of the bridge can vary with thermal conditions within the bridge. It will not be possible to match the exact weather conditions of the pre-repair test when the post-repair test is conducted, and the effects of this difference will be impossible to consider during the comparison of the test data. These effects make the pre-repair data a very poor baseline to which the post-repair tests can be compared to. The strengthening benefits provided by the FRP retrofit will be difficult to determine using service-level test loads.

In general, there were no areas of abnormally high strains, deflections, or crack openings as result of the applied static loads. The results of the pre-repair static load test seem to be similar to the results one would expect from a normal undamaged bridge

during a static load test. Considering the relatively small strains recorded throughout the bridge during the load test and the accuracy with which these strains are measured, it is likely that there will be very little significant change in behavior from the pre-repair test to the post-repair test. In Shapiro's study, all models typically exhibited very similar behavior, and the difference was small enough that deciphering between the types of behavior from static load test data alone would be nearly impossible.

# CHAPTER 8

# RECOMMENDATIONS

The primary benefit to conducting a post-repair static load test would be to verify the predicted changes in Shapiro's various bridge models. But, even if the post-repair data strongly agrees with Shapiro's work, it does very little to provide insight into the effectiveness of the FRP retrofit.

## 8.1 POST-REPAIR LOAD TEST INSTRUMENTATION

In the event that a post-repair load static load test is conducted, some channels will have to be opened in order to place strain gages on the FRP. Shapiro provided a good analysis that can be used to determine which strain gages should be abandoned and where new strain gages should be placed. To summarize, the top strain gage, gage F, should be abandoned at all locations, freeing up 8 data channels. These channels should then be used for strain gages placed directly on the FRP to determine the FRP strains. Shapiro suggested that gages should be placed on the FRP directly above gages S8_11_2M, S7_11_2M, S8_11_3M, and S7_11_3M. These 4 gages will give comparative strains between the FRP and the concrete below at the same location. The other 4 gages shall be placed on the FRP directly over the primary crack, one at each of the four girder ends that have been instrumented.

All lanes and stop positions used for the pre-repair static load test should be repeated during the post-repair test. The stop positions close to the bent and the cracks are likely

to provide the most useful comparisons i.e., stop positions 3,4,5,6, and 7. These positions produced crack openings and tensile strains in the bottom of cross section 2, and therefore, could induce stresses into the FRP. This is likely to provide the best data on the development of forces in the FRP.

## 8.2 FURTHER RESEARCH

If possible, additional research should be performed to better understand the effectiveness of the FRP repair.

### 8.2.1 REVIEW OF SWENSON'S ANALYSIS AND DESIGN

Swenson's FRP design was based on excessive bottom flange tensile forces caused by factored loads under a conservative simply supported analysis. These results were not seen in the test data nor were predicted by the finite element analysis conducted by Shapiro, both of which were service-load analysis. A review of Swenson's FRP design should be completed in order to determine the variations between his analysis and the test data. A modification to the FRP design could be required. As noted previously, his design could be overly conservative.

### 8.2.2 PRE-REPAIR AND POST-REPAIR THERMAL TEST

Results collected by instrumenting the bridge throughout the warming cycle of a full day will help to further understand the behavior of the bridge girders. If hinged at the cracks, cross section 1 will probably only show small positive moments, Cross Section 2 will have small negative moments, and COD's will open. These data should be compared to a data collected just before daylight, before any thermal heating of the bridge can occur. This should be the point at which the bridge has cooled the most. This test should also

occur on a sunny day. This type of monitoring should also be done after the FRP repair. It may help to determine the force in the FRP caused by thermal effects.

### 8.2.3 Finite Element Analysis Considering Thermal Effects

Shapiro (2007); did not address the effects that the temperature distribution causes within the bridge girders. A finite element analysis that included the temperature distribution throughout the beam and deck would provide very beneficial data on the distribution of stresses through the cross section, as well as providing forces in the FRP in the post-repair model. These models would better serve to show the effectiveness of the FRP repair.

### 8.2.4 Lab Controlled Testing

Testing structures to failure provides very useful information. In a static load test of an in-service bridge, the test data only provide service level results. From that data, it is up to the engineer to predict the ultimate behaviors of the structure. In a load test to failure, the ultimate loads are determined directly. Laboratory controlled load testing of scaled bridge girders would provide valuable information on the strengthening effects of the FRP. An artificial crack can be made in the two span continuous test girders. An un-repaired girder can be tested to failure to create a baseline. Later a repaired girder should be tested to determine the effectiveness of the FRP repair.

# REFERENCES


ACI Committee 440. 2002. Guide for the design and construction of externally bonded FRP systems for strengthening concrete structures (ACI 440.2R-02). Farmington Hills, MI: American Concrete Institute (ACI).

Alabama Department of Transportation (ALDOT) (1994a). "Summary of Field Survey – I565-45-11.5 A&B." Montgomery, Alabama. ALDOT Maintenance Bureau – Bridge Rating and Load Testing.

Alabama Department of Transportation (ALDOT) (1994b). Interoffice Memorandum, May 3.

Alabama Department of Transportation (ALDOT) (1994c). "Summary of Investigation of I-565-45-11.5 A&B June 14&15 1994." Montgomery, Alabama.

Alabama Department of Transportation (ALDOT) (1994d). "Cracks in Precast Prestressed Bulb Tee Girders on Structure No.'s I-565-45-11.5 A. & B. on I-565 in Huntsville, Alabama." Montgomery, Alabama.

Barnes, R.W. (2007). FRP strengthening of concrete bridges in Alabama. In Proceedings of the Polymer Composites Conference IV: Composite Applications and Fundamentals, Morgantown, WV, March 20-22, 2007. Constructed Facilities Center, West Virginia University (http://www.cemr.wvu.edu/cfc/conference/).

Elbadry, M.M. and A. Ghali. 1989. "Serviceability design of continuous prestressed concrete structures." PCI Journal 34(1): 54-91.

Freyermuth, C. 1969. "Design of continuous highway bridges with precast, prestressed concrete girders." PCI Journal 14(2): 14-39.

Fyfe Co. 2004. Suggested construction specifications for installation of fiber reinforced polymer (FRP) composite material. San Diego: Fyfe Co. LLC. Obtained March 2004.

Gao, N. 2003. Investigation of cracking in precast prestressed girders made continuous for live load. Master's thesis, Auburn University.

Ma, Zhongguo, Xiaoming Huo, Maher K. Tadros, and Mantu Baishya. 1998. "Restraint moments in precast/prestressed concrete continuous bridges." PCI Journal 43(6): 40-57.

Mirmiran, Amir, Siddharth Kulkarni, Reid Castrodale, Richard Miller, and Makarand Hastak. 2001. "Nonlinear continuity analysis of precast prestressed concrete girders with cast-in-place decks and diaphragms." PCI Journal, September-October, P. 60-80.

National Oceanic and Atmospheric Administraion (NOAA), "Huntsville, Alabama Climatology", (http://www.srh.noaa.gov/hun/climate/hsvcli.php).

Oesterle, R.G., J.D. Gilkins, and S.C. Larson. 1989. "Design of precast prestressed bridge girders made continuous." NCHRP Report 322. Washington: Transportation Research Board.

Potgieter, I.C., and W.L. Gamble. 1989. "Nonlinear temperature distributions in bridges at different locations in the United States." PCI Journal July-August, p.80-103.

Shapiro, K.A. 2007. Finite-element modeling of a damaged prestressed concrete bridge. Master's thesis, Auburn University.

Swenson, K.S. 2003a. Feasibility of externally bonded FRP reinforcement for repair of cracked prestressed concrete girders. Master's thesis, Auburn University.

Swenson, K.S. 2003b. Report on Repair of Huntsville I-565 Cracked PC Bulb-tee Girders. Report, Auburn University.

## APPENDIX A

## BRIDGE LAYOUT

The Figure A-1 below shows a plan view of the bridge providing the girder, span, and bent numbering and orientation.

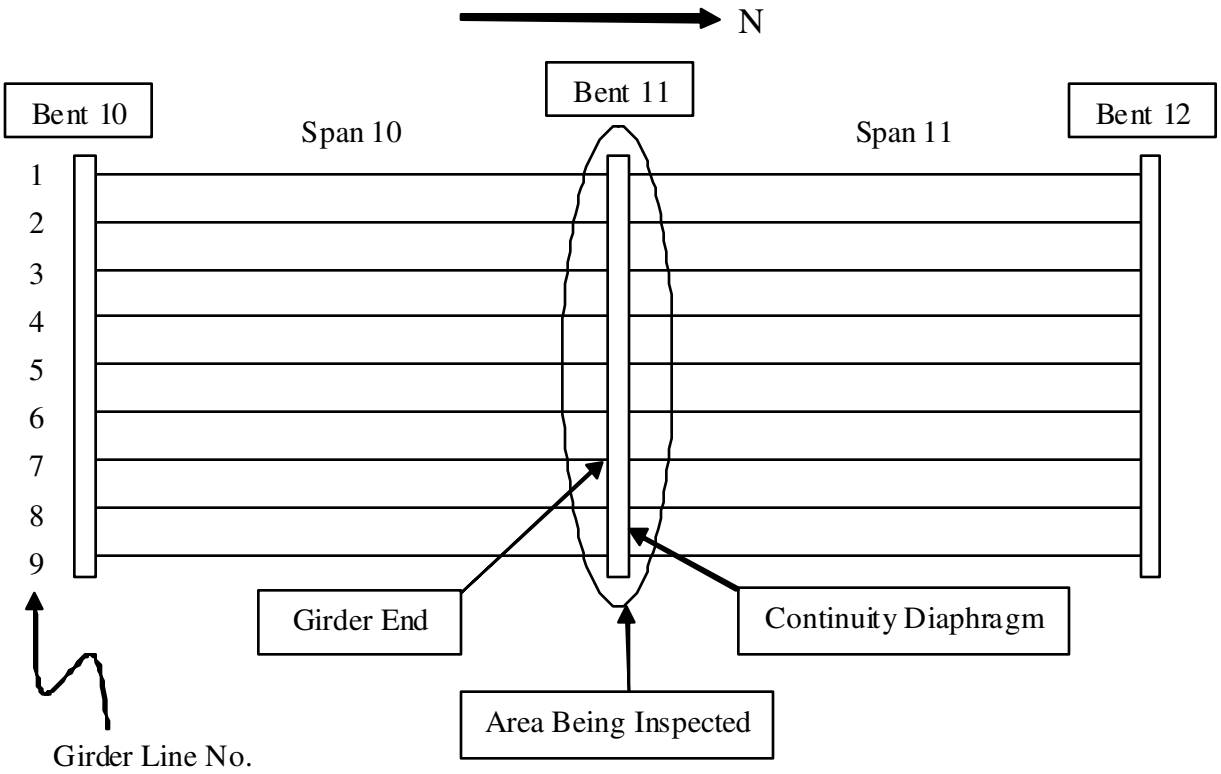


**Figure A-1:** Bridge Layout

## APPENDIX B

## MEGADAC CHANNEL LAYOUT

The table below provides the megadac channel used for each individual gage.

| Megadac Channel | Instrumentation Device | Units | Megadac Channel | Instrumentation Device | Units |
|---|---|---|---|---|---|
| 0 | D7_11_1 | in | 36 | S8_10_2C | uE |
| 1 | D7_11_2 | in | 37 | S8_10_2D | uE |
| 2 | D7_11_3 | in | 38 | S8_10_2E | uE |
| 3 | D7_11_4 | in | 39 | S8_10_2F | uE |
| 4 | D8_11_1 | in | 40 | S7_11_1A | uE |
| 5 | D8_11_2 | in | 41 | S7_11_1B | uE |
| 6 | D8_11_3 | in | 42 | S7_11_1C | uE |
| 7 | D8_11_4 | in | 43 | S7_11_1D | uE |
| 8 | D7_10_1 | in | 44 | S7_11_1E | uE |
| 9 | D7_10_2 | in | 45 | S7_11_1F | uE |
| 10 | D8_10_1 | in | 46 | S7_11_2A | uE |
| 11 | D8_10_2 | in | 47 | S7_11_2M | uE |
| 12 | CO8_10 | mm | 48 | S7_11_2C | uE |
| 13 | CO8_11 | mm | 49 | S7_11_2D | uE |
| 14 | CO7_10 | mm | 50 | S7_11_2E | uE |
| 15 | CO7_11 | mm | 51 | S7_11_2F | uE |
| 16 | S7_10_1A | uE | 52 | S8_11_1A | uE |
| 17 | S7_10_1B | uE | 53 | S8_11_1B | uE |
| 18 | S7_10_1C | uE | 54 | S8_11_1C | uE |
| 19 | S7_10_1D | uE | 55 | S8_11_1D | uE |
| 20 | S7_10_1E | uE | 56 | S8_11_1E | uE |
| 21 | S7_10_1F | uE | 57 | S8_11_1F | uE |
| 22 | S7_10_2A | uE | 58 | S8_11_2A | uE |
| 23 | S7_10_2M | uE | 59 | S8_11_2M | uE |
| 24 | S7_10_2C | uE | 60 | S8_11_2C | uE |
| 25 | S7_10_2D | uE | 61 | S8_11_2D | uE |
| 26 | S7_10_2E | uE | 62 | S8_11_2E | uE |
| 27 | S7_10_2F | uE | 63 | S8_11_2F | uE |
| 28 | S8_10_1A | uE | 64 | S7_11_3M | uE |
| 29 | S8_10_1B | uE | 65 | S7_11_4M | uE |
| 30 | S8_10_1C | uE | 66 | S7_11_5M | uE |
| 31 | S8_10_1D | uE | 67 | S7_11_6M | uE |
| 32 | S8_10_1E | uE | 68 | S8_11_3M | uE |
| 33 | S8_10_1F | uE | 69 | S8_11_4M | uE |
| 34 | S8_10_2A | uE | 70 | S8_11_5M | uE |
| 35 | S8_10_2M | uE | 71 | S8_11_6M | uE |

# APPENDIX C

# TEST RESULTS

Appendix C contains test data for each of the 72 channels from each of the nine stopping points on all three load test lanes. The different types of data included for each loading position are the following: deflections, crack opening gages, and strain gage readings. Precise Locations for strain gages are included.

**Code for Gage Name**

Ex: D7_10_2 - Deflectometer, Girder 7, Span 10, Deflectometer #2

CO8_10_W - Crack Opening Device, Girder 8, Span 10, West Face

S7_10_1A - Strain Gage, Girder 7, Span 10, Cross Section 1, Gage Location A

## C.1 LANE A – DEFLOCTOMETER AND CRACK OPENING DEVICE

**Table C-1:** Lane A - Crack Openings and Deflections

| | | Gage | Height of gage from bottom of girder | Distance along girder from center of continuity diaphragm to gage. (in. ) (-) Span 10 (+) Span 11 | Units | A1 | A2 | A3 | A4 | A5 | A6 | A7 | A8 | A9 |
|---|---|---|---|---|---|---|---|---|---|---|---|---|---|---|
| Deflectometers | Girder 7 | D7_10_2 | n/a | -608.0000 | in | -0.31 | -0.18 | -0.10 | -0.05 | -0.02 | 0.01 | 0.02 | 0.05 | 0.05 |
| | | D7_10_1 | n/a | -308.0000 | in | -0.20 | -0.17 | -0.10 | -0.05 | -0.02 | 0.01 | 0.02 | 0.04 | 0.05 |
| | | D7_11_1 | n/a | 158.0000 | in | 0.03 | 0.02 | 0.00 | -0.01 | -0.02 | -0.04 | -0.06 | -0.10 | -0.09 |
| | | D7_11_2 | n/a | 308.0000 | in | 0.05 | 0.04 | 0.01 | -0.01 | -0.03 | -0.06 | -0.10 | -0.18 | -0.20 |
| | | D7_11_3 | n/a | 458.0000 | in | 0.06 | 0.04 | 0.02 | -0.01 | -0.03 | -0.06 | -0.10 | -0.20 | -0.27 |
| | | D7_11_4 | n/a | 608.0000 | in | 0.06 | 0.04 | 0.02 | -0.01 | -0.02 | -0.06 | -0.09 | -0.20 | -0.30 |
| | Girder 8 | D8_10_2 | n/a | -608.0000 | in | -0.24 | -0.14 | -0.08 | -0.04 | -0.01 | 0.01 | 0.02 | 0.05 | 0.05 |
| | | D8_10_1 | n/a | -308.0000 | in | -0.16 | -0.12 | -0.07 | -0.04 | -0.02 | 0.01 | 0.02 | 0.04 | 0.04 |
| | | D8_11_1 | n/a | 158.0000 | in | 0.03 | 0.02 | 0.01 | -0.01 | -0.01 | -0.03 | -0.05 | -0.07 | -0.08 |
| | | D8_11_2 | n/a | 308.0000 | in | 0.05 | 0.03 | 0.01 | -0.01 | -0.02 | -0.04 | -0.07 | -0.13 | -0.15 |
| | | D8_11_3 | n/a | 458.0000 | in | 0.05 | 0.04 | 0.02 | 0.00 | -0.02 | -0.05 | -0.08 | -0.16 | -0.21 |
| | | D8_11_4 | n/a | 608.0000 | in | 0.05 | 0.04 | 0.02 | 0.00 | -0.02 | -0.05 | -0.07 | -0.16 | -0.23 |
| Crack Gages | | CO8_10_W | 13.5000 | -40.0000 | mm | -0.0090 | -0.0069 | -0.0048 | -0.0025 | -0.0012 | -0.0034 | -0.0054 | -0.0083 | -0.0088 |
| | | CO8_11_E | 13.5000 | 56.0000 | mm | -0.0073 | -0.0062 | -0.0032 | -0.0026 | -0.0017 | 0.0025 | 0.0042 | -0.0036 | -0.0066 |
| | | CO7_10_E | 13.5000 | -49.5000 | mm | -0.0171 | -0.0029 | 0.0073 | 0.0206 | 0.0142 | -0.0048 | -0.0104 | -0.0186 | -0.0198 |
| | | CO7_11_E | 13.5000 | 47.7500 | mm | -0.0215 | -0.0196 | -0.0098 | -0.0078 | -0.0057 | 0.0118 | 0.0190 | -0.0095 | -0.0212 |

**Table C-2:** Lane A - Span 10 Strain Readings

| | | Gage | Height of gage from bottom of girder | Distance along girder from center of continuity diaphragm to gage. (in.) (-) Span 10 (+) Span 11 | Units | A1 | A2 | A3 | A4 | A5 | A6 | A7 | A8 | A9 |
|---|---|---|---|---|---|---|---|---|---|---|---|---|---|---|
| Span 10 | Girder 7 Cross Section 1 | S7_10_1A | 13.5000 | -12.7500 | uE | 4.9843 | 3.4347 | 2.7407 | -0.4084 | 0.8114 | 2.6502 | 0.5266 | -1.5684 | -2.5854 |
| | | S7_10_1B | 3.0000 | -12.7500 | uE | -39.0944 | -30.4320 | -20.3372 | -14.0080 | -9.7720 | -12.6455 | -16.3540 | -25.5549 | -22.3818 |
| | | S7_10_1C | 3.0000 | -12.7500 | uE | -116.8714 | -101.3267 | -77.2401 | -57.3592 | -35.0672 | -43.7219 | -62.7182 | -95.5035 | -93.2445 |
| | | S7_10_1D | 13.5000 | -12.7500 | uE | -8.4817 | -3.5126 | -2.2123 | -1.4889 | -0.6421 | -3.0833 | -7.1570 | -14.5419 | -15.5246 |
| | | S7_10_1E | 28.5000 | -12.7500 | uE | 1.6266 | 3.0024 | 2.7490 | 2.9310 | 3.7565 | -0.0612 | -0.9021 | -3.3502 | -4.2042 |
| | | S7_10_1F | 43.5000 | -12.7500 | uE | -1.2573 | -3.5065 | -3.4044 | -4.9561 | -0.6783 | 0.8259 | -1.2846 | -3.5118 | -4.3240 |
| | Girder 7 Cross Section 2 | S7_10_2A | 13.5000 | -75.2500 | uE | -14.3988 | -1.0030 | 5.3412 | 10.8497 | 5.8774 | -4.6490 | -8.2476 | -16.5715 | -17.3437 |
| | | S7_10_2M | 0.0000 | -75.2500 | uE | -16.8116 | -2.1196 | 4.3744 | 9.2114 | 5.1582 | -5.6375 | -9.4058 | -18.6069 | -19.5275 |
| | | S7_10_2C | 3.0000 | -75.2500 | uE | -21.4339 | 0.8687 | 10.1598 | 19.8167 | 10.9589 | -7.6406 | -13.7214 | -25.5108 | -26.0196 |
| | | S7_10_2D | 13.5000 | -75.2500 | uE | -22.6881 | -3.0031 | 6.1901 | 12.4669 | 6.3936 | -8.5163 | -14.7462 | -26.9541 | -27.5291 |
| | | S7_10_2E | 28.5000 | -75.2500 | uE | -12.0649 | -2.6820 | 0.8598 | 6.6523 | 5.3762 | -2.7175 | -5.4643 | -11.0108 | -11.7386 |
| | | S7_10_2F | 43.5000 | -75.2500 | uE | -10.0873 | -10.5701 | -15.4753 | -5.7939 | 4.0837 | 0.1641 | -0.0916 | -0.9451 | -1.1958 |
| | Girder 8 Cross Section 1 | S8_10_1A | 13.5000 | -12.7500 | uE | -2.6124 | 0.4761 | 1.8793 | 2.2547 | 3.7186 | -0.2662 | -3.7641 | -10.4653 | -12.8095 |
| | | S8_10_1B | 3.0000 | -12.7500 | uE | -33.1483 | -25.2387 | -15.5319 | -8.2518 | -3.1151 | -4.4770 | -8.0483 | -13.3715 | -13.9144 |
| | | S8_10_1C | 3.0000 | -12.7500 | uE | -15.5922 | -8.5928 | -6.9221 | -5.6179 | -4.0212 | -9.2453 | -13.7393 | -22.3433 | -22.1585 |
| | | S8_10_1D | 13.5000 | -12.7500 | uE | -0.4263 | 2.9033 | 2.8101 | 3.3362 | 3.0783 | -1.9568 | -6.2416 | -13.7122 | -15.9132 |
| | | S8_10_1E | 28.5000 | -12.7500 | uE | 1.4499 | 2.3778 | 1.8440 | 2.0887 | 1.9212 | -0.4310 | -1.3336 | -3.0415 | -3.4533 |
| | | S8_10_1F | 43.5000 | -12.7500 | uE | -2.4900 | -3.3758 | -3.3980 | -3.3284 | -1.5306 | -1.2951 | -1.6351 | -1.9448 | -1.7661 |
| | Girder 8 Cross Section 2 | S8_10_2A | 13.5000 | -75.2500 | uE | -16.7536 | -4.5271 | -0.1278 | 6.1886 | 4.1352 | -4.7023 | -8.9141 | -16.4733 | -17.8654 |
| | | S8_10_2M | 0.0000 | -75.2500 | uE | -18.1225 | -2.1472 | 3.1636 | 10.6073 | 6.2816 | -5.7411 | -10.7642 | -19.8003 | -21.2693 |
| | | S8_10_2C | 3.0000 | -75.2500 | uE | -12.9164 | -1.9856 | 0.3660 | 2.5071 | -0.1576 | -6.1797 | -10.4247 | -18.5910 | -20.0255 |
| | | S8_10_2D | 13.5000 | -75.2500 | uE | -13.7226 | -4.8223 | -0.2021 | 2.8251 | 1.0618 | -5.6310 | -8.5169 | -16.2295 | -17.4682 |
| | | S8_10_2E | 28.5000 | -75.2500 | uE | -8.9652 | -3.8164 | -1.3523 | -0.1500 | -0.1574 | -2.1392 | -4.3479 | -7.9400 | -8.7525 |
| | | S8_10_2F | 43.5000 | -75.2500 | uE | -5.8042 | -5.8689 | -7.5686 | -3.8890 | 0.2361 | -0.1195 | 0.0705 | 0.0917 | -0.2684 |

**Table C-3:** Lane A - Span 11 Strain Readings

| | | Gage | Height of gage from bottom of girder | Distance along girder from center of continuity diaphragm to gage. (in.) (-) Span 10 (+) Span 11 | Units | A1 | A2 | A3 | A4 | A5 | A6 | A7 | A8 | A9 |
|---|---|---|---|---|---|---|---|---|---|---|---|---|---|---|
| Span 11 | Girder 7 Cross Section 1 | S7_11_1A | 13.5000 | 12.7500 | uE | -23.9418 | -15.8761 | -6.1497 | -0.3642 | 5.3665 | 7.0120 | 0.9595 | -4.9021 | -6.8725 |
| | | S7_11_1B | 3.0000 | 12.7500 | uE | -23.0480 | -20.4601 | -13.7260 | -10.6766 | -6.3767 | -5.8085 | -10.1604 | -21.5772 | -20.5493 |
| | | S7_11_1C | 3.0000 | 12.7500 | uE | -27.5931 | -21.9610 | -13.7860 | -9.2506 | -5.1127 | -3.6532 | -8.9897 | -21.5981 | -22.2165 |
| | | S7_11_1D | 13.5000 | 12.7500 | uE | -26.9661 | -20.0136 | -8.1851 | -2.9835 | 3.6958 | 11.2122 | 6.7736 | -4.3162 | -9.7948 |
| | | S7_11_1E | 28.5000 | 12.7500 | uE | -7.4486 | -4.4002 | -1.9159 | -0.0099 | 2.1422 | 2.8512 | -0.4431 | -0.4719 | -0.3684 |
| | | S7_11_1F | 43.5000 | 12.7500 | uE | -3.3752 | -2.6150 | -1.2379 | -0.8788 | -0.2556 | 4.3124 | 2.5973 | -0.0127 | -1.7746 |
| | Girder 7 Cross Section 2 | S7_11_2A | 13.5000 | 75.2500 | uE | -19.4885 | -15.8906 | -6.4672 | -3.9048 | -1.5648 | 5.3246 | 5.3360 | -7.8120 | -15.2713 |
| | | S7_11_2M | 0.0000 | 75.2500 | uE | -27.8494 | -23.1975 | -8.4461 | -5.7075 | -2.9573 | 10.7778 | 17.3296 | -10.4205 | -25.3368 |
| | | S7_11_2C | 3.0000 | 75.2500 | uE | -28.3124 | -22.9996 | -9.9553 | -5.7838 | -2.9154 | 7.7672 | 11.9553 | -10.9627 | -24.8826 |
| | | S7_11_2D | 13.5000 | 75.2500 | uE | -19.0560 | -14.9589 | -6.4797 | -4.1931 | -1.4363 | 5.0222 | 4.7808 | -8.1143 | -15.1121 |
| | | S7_11_2E | 28.5000 | 75.2500 | uE | -11.0932 | -8.5037 | -2.7857 | -2.8041 | -1.1909 | 2.7718 | -0.6401 | -7.7045 | -9.9851 |
| | | S7_11_2F | 43.5000 | 78.7500 | uE | -0.7239 | -0.1319 | 2.0984 | -2.1342 | -1.5048 | 2.4147 | -4.3664 | -8.3242 | -3.5147 |
| | Girder 8 Cross Section 1 | S8_11_1A | 13.5000 | 12.7500 | uE | -58.9849 | -45.5072 | -23.4565 | -15.2023 | -5.7288 | 9.3387 | 5.6437 | -20.5342 | -35.0713 |
| | | S8_11_1B | 3.0000 | 12.7500 | uE | -12.2811 | -9.5198 | -8.1538 | -7.3800 | -4.9868 | -8.7091 | -16.7725 | -27.4058 | -25.8972 |
| | | S8_11_1C | 3.0000 | 12.7500 | uE | -23.4973 | -18.4807 | -10.9936 | -6.6268 | -2.8395 | -0.2760 | -1.0419 | -7.5288 | -11.8348 |
| | | S8_11_1D | 13.5000 | 12.7500 | uE | -24.7813 | -16.3427 | -9.0971 | -3.4697 | 1.3223 | 1.6023 | -2.2116 | -6.4856 | -7.7852 |
| | | S8_11_1E | 28.5000 | 12.7500 | uE | -28.2540 | -21.8186 | -13.5875 | -10.5268 | -6.4889 | -2.7159 | -3.2962 | -9.8605 | -14.8971 |
| | | S8_11_1F | 43.5000 | 12.7500 | uE | -1.2415 | -0.3251 | -0.1732 | -0.1399 | 0.3408 | -0.1456 | -1.4220 | -0.3502 | 0.0026 |
| | Girder 8 Cross Section 2 | S8_11_2A | 13.5000 | 75.2500 | uE | -16.2786 | -13.5129 | -5.2393 | -4.0344 | -1.4763 | 3.5759 | 2.5635 | -6.9928 | -11.0810 |
| | | S8_11_2M | 0.0000 | 75.2500 | uE | -26.5449 | -21.9547 | -8.9070 | -4.1713 | -1.0152 | 10.7553 | 19.8325 | -1.5242 | -14.1051 |
| | | S8_11_2C | 3.0000 | 75.2500 | uE | -43.1171 | -33.9156 | -18.1819 | -10.6450 | -5.0581 | 4.1092 | 6.3237 | -8.9753 | -27.7112 |
| | | S8_11_2D | 13.5000 | 75.2500 | uE | -21.9470 | -16.5425 | -7.9321 | -4.7672 | -2.7185 | 2.5939 | 2.8188 | -9.1611 | -17.2671 |
| | | S8_11_2E | 28.5000 | 75.2500 | uE | -8.0906 | -6.6834 | -3.0830 | -3.3406 | -3.1497 | -2.2371 | -9.2742 | -14.8022 | -12.3412 |
| | | S8_11_2F | 43.5000 | 78.7500 | uE | -1.1999 | -0.5465 | 1.8272 | -2.0149 | -1.9166 | 2.8640 | -1.4904 | -9.8201 | -6.9476 |
| | Girder 7 Midspan Gages | S7_11_3M | 0.0000 | 104.0000 | uE | -27.0171 | -22.2648 | -7.8451 | -1.6941 | -0.2818 | 12.7414 | 24.6390 | 0.4345 | -17.9353 |
| | | S7_11_4M | 0.0000 | 272.0000 | uE | -23.5571 | -19.2575 | -7.9442 | 2.2546 | 11.3500 | 27.3558 | 36.1573 | 75.0379 | 24.6588 |
| | | S7_11_5M | 0.0000 | 440.0000 | uE | -17.6504 | -14.3760 | -6.8346 | -0.1706 | 6.0546 | 18.7851 | 31.4550 | 66.5416 | 71.3442 |
| | | S7_11_6M | 0.0000 | 608.0000 | uE | -11.0135 | -8.4998 | -3.5258 | -0.5281 | 4.4680 | 12.4791 | 20.9725 | 52.9416 | 110.0126 |
| | Girder 8 Midspan Gages | S8_11_3M | 0.0000 | 104.0000 | uE | -25.1065 | -19.3861 | -7.6137 | -2.4107 | -0.3082 | 8.2149 | 16.1856 | -0.1965 | -13.3960 |
| | | S8_11_4M | 0.0000 | 272.0000 | uE | -19.1706 | -14.9728 | -6.7144 | 0.4644 | 7.5206 | 18.6787 | 24.0057 | 48.2336 | 18.3301 |
| | | S8_11_5M | 0.0000 | 440.0000 | uE | -14.1101 | -10.8887 | -4.8324 | 0.7840 | 5.2920 | 13.8228 | 23.3760 | 48.4411 | 53.9191 |
| | | S8_11_6M | 0.0000 | 608.0000 | uE | -6.4927 | -4.8592 | 0.7744 | 10.9479 | 8.8952 | 7.4938 | 17.3767 | 39.2256 | 73.9049 |

## C.2 LANE B – DEFLOCTOMETER AND CRACK OPENING DEVICE

**Table C-4:** Lane B - Crack Openings and Deflections

| | | Gage | Height of gage from bottom of girder | Distance along girder from center of continuity diaphragm to gage. (in.) (-) Span 10 (+) Span 11 | Units | B1 | B2 | B3 | B4 | B5 | B6 | B7 | B8 | B9 |
|---|---|---|---|---|---|---|---|---|---|---|---|---|---|---|
| Deflectometers | Girder 7 | D7_10_2 | n/a | -608.00 | in | -0.31 | -0.18 | -0.10 | -0.05 | -0.02 | 0.01 | 0.03 | 0.05 | 0.05 |
| | | D7_10_1 | n/a | -308.00 | in | -0.20 | -0.17 | -0.10 | -0.05 | -0.02 | 0.01 | 0.02 | 0.04 | 0.05 |
| | | D7_11_1 | n/a | 158.00 | in | 0.03 | 0.02 | 0.00 | -0.01 | -0.02 | -0.04 | -0.06 | -0.10 | -0.09 |
| | | D7_11_2 | n/a | 308.00 | in | 0.05 | 0.04 | 0.01 | -0.01 | -0.03 | -0.06 | -0.10 | -0.18 | -0.20 |
| | | D7_11_3 | n/a | 458.00 | in | 0.06 | 0.05 | 0.02 | -0.01 | -0.03 | -0.06 | -0.10 | -0.20 | -0.26 |
| | | D7_11_4 | n/a | 608.00 | in | 0.07 | 0.05 | 0.02 | -0.01 | -0.02 | -0.06 | -0.09 | -0.20 | -0.30 |
| | Girder 8 | D8_10_2 | n/a | -608.00 | in | -0.29 | -0.17 | -0.09 | -0.04 | -0.01 | 0.02 | 0.03 | 0.05 | 0.06 |
| | | D8_10_1 | n/a | -308.00 | in | -0.19 | -0.15 | -0.09 | -0.05 | -0.02 | 0.01 | 0.02 | 0.04 | 0.05 |
| | | D8_11_1 | n/a | 158.00 | in | 0.04 | 0.03 | 0.01 | -0.01 | -0.02 | -0.04 | -0.06 | -0.09 | -0.09 |
| | | D8_11_2 | n/a | 308.00 | in | 0.05 | 0.04 | 0.02 | -0.01 | -0.02 | -0.06 | -0.09 | -0.16 | -0.18 |
| | | D8_11_3 | n/a | 458.00 | in | 0.06 | 0.05 | 0.02 | -0.01 | -0.02 | -0.06 | -0.10 | -0.20 | -0.26 |
| | | D8_11_4 | n/a | 608.00 | in | 0.06 | 0.05 | 0.02 | 0.00 | -0.02 | -0.06 | -0.09 | -0.19 | -0.29 |
| Crack Gages | | CO8_10 | 13.5 | -40.00 | mm | -0.01045 | -0.00869 | -0.00660 | -0.00298 | -0.00070 | -0.00455 | -0.00711 | -0.00997 | -0.01012 |
| | | CO8_11 | 13.5 | 56.00 | mm | -0.00905 | -0.00816 | -0.00485 | -0.00333 | -0.00216 | 0.00324 | 0.00676 | -0.00322 | -0.00784 |
| | | CO7_10 | 13.5 | -49.50 | mm | -0.01574 | -0.00203 | 0.00836 | 0.02090 | 0.01300 | -0.00591 | -0.01148 | -0.01929 | -0.02032 |
| | | CO7_11 | 13.5 | 47.75 | mm | -0.02223 | -0.02064 | -0.01152 | -0.00872 | -0.00615 | 0.01336 | 0.02116 | -0.00731 | -0.01988 |

**Table C-5:** Lane B - Span 10 Strain Readings

| | | Gage | Height of gage from bottom of girder | Distance along girder from center of continuity diaphragm to gage. (in.) (-) Span 10 (+) Span 11 | Units | B1 | B2 | B3 | B4 | B5 | B6 | B7 | B8 | B9 |
|---|---|---|---|---|---|---|---|---|---|---|---|---|---|---|
| Span 10 | Girder 7 Cross Section 1 | S7_10_1A | 13.5 | -12.75 | uE | 4.73884 | 3.15855 | 1.99719 | -0.57650 | 1.21906 | 2.50252 | 0.90169 | -1.36402 | -2.34043 |
| | | S7_10_1B | 3.0 | -12.75 | uE | -29.95710 | -22.44776 | -15.57180 | -11.26512 | -7.73270 | -12.18828 | -16.32936 | -26.47693 | -23.37092 |
| | | S7_10_1C | 3.0 | -12.75 | uE | -125.53237 | -114.57467 | -87.68483 | -63.19863 | -35.24546 | -41.29227 | -62.01271 | -92.14485 | -89.89649 |
| | | S7_10_1D | 13.5 | -12.75 | uE | -8.14186 | -3.48937 | -1.79790 | -1.58957 | -0.35126 | -2.83896 | -7.32938 | -14.64309 | -15.55417 |
| | | S7_10_1E | 28.5 | -12.75 | uE | 1.21091 | 2.55735 | 2.60808 | 2.73092 | 3.54285 | -0.06363 | -0.94347 | -3.41642 | -4.20205 |
| | | S7_10_1F | 43.5 | -12.75 | uE | -1.11810 | -4.49371 | -3.99360 | -5.83068 | -1.13881 | -0.15775 | -1.25790 | -3.69847 | -4.47861 |
| | Girder 7 Cross Section 2 | S7_10_2A | 13.5 | -75.25 | uE | -13.56810 | -0.55957 | 5.43696 | 10.24500 | 5.86625 | -4.46109 | -8.72367 | -16.30673 | -17.11350 |
| | | S7_10_2M | 0.0 | -75.25 | uE | -15.10739 | -0.84332 | 5.71163 | 10.90070 | 5.58108 | -5.56552 | -10.45258 | -18.83444 | -20.06098 |
| | | S7_10_2C | 3.0 | -75.25 | uE | -20.59917 | 0.64586 | 10.85512 | 20.80673 | 10.20283 | -8.13596 | -14.22294 | -25.72875 | -26.18871 |
| | | S7_10_2D | 13.5 | -75.25 | uE | -22.94320 | -1.98953 | 7.93499 | 16.20393 | 7.75275 | -8.65960 | -15.46495 | -27.23832 | -27.77035 |
| | | S7_10_2E | 28.5 | -75.25 | uE | -12.05180 | -2.90345 | 0.73069 | 7.00372 | 5.08684 | -2.84595 | -5.77889 | -11.18899 | -11.87166 |
| | | S7_10_2F | 43.5 | -75.25 | uE | -9.74196 | -11.47806 | -15.83638 | -6.27893 | 2.98796 | -0.08351 | -0.27327 | -0.89803 | -1.52889 |
| | Girder 8 Cross Section 1 | S8_10_1A | 13.5 | -12.75 | uE | -3.16323 | 1.59722 | 3.01317 | 3.97576 | 4.64029 | -0.61982 | -5.68770 | -15.05359 | -17.35372 |
| | | S8_10_1B | 3.0 | -12.75 | uE | -35.05248 | -27.52154 | -16.33933 | -8.46037 | -3.26328 | -6.59638 | -12.59924 | -21.92099 | -21.62221 |
| | | S8_10_1C | 3.0 | -12.75 | uE | -26.32063 | -18.61647 | -14.73247 | -10.58283 | -6.38511 | -12.36359 | -19.31322 | -28.93679 | -26.46183 |
| | | S8_10_1D | 13.5 | -12.75 | uE | -2.49972 | 1.95063 | 2.26059 | 3.27606 | 4.50240 | -2.51768 | -8.42734 | -17.70944 | -19.58168 |
| | | S8_10_1E | 28.5 | -12.75 | uE | 0.88629 | 2.32916 | 1.92824 | 1.97485 | 2.36933 | -0.63839 | -1.91209 | -4.01177 | -4.48614 |
| | | S8_10_1F | 43.5 | -12.75 | uE | -3.35929 | -4.83162 | -4.43382 | -5.09977 | -1.74354 | -1.63948 | -2.37450 | -2.77054 | -2.69789 |
| | Girder 8 Cross Section 2 | S8_10_2A | 13.5 | -75.25 | uE | -21.63048 | -7.33556 | -0.18758 | 7.24782 | 4.61096 | -6.91905 | -12.65980 | -22.34816 | -22.88725 |
| | | S8_10_2M | 0.0 | -75.25 | uE | -23.01622 | -2.55088 | 5.66936 | 15.87022 | 9.11556 | -8.60684 | -15.39269 | -26.90779 | -27.66193 |
| | | S8_10_2C | 3.0 | -75.25 | uE | -18.96778 | -2.79563 | 3.37582 | 10.54597 | 5.31310 | -8.76778 | -14.75627 | -25.25347 | -25.55021 |
| | | S8_10_2D | 13.5 | -75.25 | uE | -18.69934 | -4.47540 | 0.34695 | 6.62976 | 3.30826 | -7.76580 | -13.19616 | -21.37993 | -23.03765 |
| | | S8_10_2E | 28.5 | -75.25 | uE | -12.03642 | -4.76302 | -2.42257 | 2.33621 | 2.50294 | -3.58744 | -6.39356 | -11.26265 | -11.54974 |
| | | S8_10_2F | 43.5 | -75.25 | uE | -7.22470 | -7.40020 | -10.24284 | -4.51264 | 1.29904 | -0.24626 | -0.24882 | -0.44463 | -0.42501 |

**Table C-6:** Lane B - Span 11 Strain Readings

| | | Gage | Height of gage from bottom of girder | Distance along girder from center of continuity diaphragm to gage. (in.) (-) Span 10 (+) Span 11 | Units | B1 | B2 | B3 | B4 | B5 | B6 | B7 | B8 | B9 |
|---|---|---|---|---|---|---|---|---|---|---|---|---|---|---|
| Span 11 | Girder 7 Cross Section 1 | S7_11_1A | 13.5 | 12.75 | uE | -23.94999 | -16.59946 | -6.86516 | -0.75580 | 5.45231 | 6.87722 | 1.89187 | -4.07378 | -5.89591 |
| | | S7_11_1B | 3.0 | 12.75 | uE | -24.02777 | -21.85675 | -13.41485 | -9.48506 | -5.61960 | -2.99698 | -5.80659 | -14.96727 | -15.37691 |
| | | S7_11_1C | 3.0 | 12.75 | uE | -25.26100 | -21.38462 | -14.49981 | -10.98195 | -5.26459 | -5.68162 | -12.59072 | -28.19418 | -28.37718 |
| | | S7_11_1D | 13.5 | 12.75 | uE | -26.07387 | -21.05766 | -8.75485 | -4.21424 | 3.06230 | 11.21314 | 6.09531 | -5.95430 | -10.85507 |
| | | S7_11_1E | 28.5 | 12.75 | uE | -6.40895 | -3.19529 | -2.32428 | 0.08346 | 2.54160 | 3.34114 | -0.84611 | -0.64890 | -0.42476 |
| | | S7_11_1F | 43.5 | 12.75 | uE | -1.37963 | -1.08413 | -0.53156 | -0.48744 | -0.53614 | 4.57273 | 2.14498 | -0.94547 | -2.23463 |
| | Girder 7 Cross Section 2 | S7_11_2A | 13.5 | 75.25 | uE | -18.22262 | -14.88212 | -6.27096 | -4.33116 | -1.70228 | 5.16037 | 4.77017 | -8.04243 | -15.69933 |
| | | S7_11_2M | 0.0 | 75.25 | uE | -27.30458 | -22.54369 | -7.72767 | -5.73893 | -2.66369 | 11.68897 | 18.78223 | -9.92381 | -25.23995 |
| | | S7_11_2C | 3.0 | 75.25 | uE | -28.53271 | -24.13252 | -9.10934 | -5.79685 | -3.10162 | 9.74566 | 15.38875 | -12.04210 | -26.03141 |
| | | S7_11_2D | 13.5 | 75.25 | uE | -19.16548 | -15.89424 | -6.89104 | -4.30471 | -1.35690 | 5.90799 | 5.79239 | -7.64146 | -14.37129 |
| | | S7_11_2E | 28.5 | 75.25 | uE | -11.59771 | -9.61379 | -3.40180 | -3.02263 | -1.38044 | 3.14903 | -0.40789 | -7.28672 | -9.80806 |
| | | S7_11_2F | 43.5 | 78.75 | uE | -0.65481 | -0.22749 | 1.99874 | -2.17148 | -1.08959 | 3.23340 | -3.56064 | -7.61240 | -2.65293 |
| | Girder 8 Cross Section 1 | S8_11_1A | 13.5 | 12.75 | uE | -74.53848 | -60.88771 | -32.53346 | -21.17903 | -7.92896 | 12.92207 | 10.47367 | -25.24107 | -44.77430 |
| | | S8_11_1B | 3.0 | 12.75 | uE | -17.44027 | -14.28933 | -10.62280 | -8.43817 | -5.35186 | -8.90731 | -17.12125 | -29.56701 | -27.78905 |
| | | S8_11_1C | 3.0 | 12.75 | uE | -27.21497 | -24.07642 | -16.68478 | -12.38313 | -6.19583 | -3.23686 | -8.84624 | -19.48427 | -22.56137 |
| | | S8_11_1D | 13.5 | 12.75 | uE | -30.66575 | -21.75115 | -12.66655 | -5.54937 | 1.69870 | 1.70325 | -6.15103 | -11.34141 | -11.73087 |
| | | S8_11_1E | 28.5 | 12.75 | uE | -36.68933 | -31.19714 | -20.57159 | -15.47999 | -9.13559 | -0.19729 | -2.90664 | -13.74623 | -19.73568 |
| | | S8_11_1F | 43.5 | 12.75 | uE | -1.94403 | -1.69336 | -1.84887 | -1.06126 | -0.38040 | -1.17702 | -2.72522 | -1.47874 | -0.31459 |
| | Girder 8 Cross Section 2 | S8_11_2A | 13.5 | 75.25 | uE | -20.74888 | -17.01400 | -8.97810 | -6.54784 | -3.62967 | 2.60433 | 0.74742 | -11.96321 | -17.03510 |
| | | S8_11_2M | 0.0 | 75.25 | uE | -32.98862 | -27.03987 | -11.61670 | -5.92825 | -1.41426 | 16.03009 | 27.31685 | -1.71935 | -21.24252 |
| | | S8_11_2C | 3.0 | 75.25 | uE | -54.26077 | -46.41196 | -20.93592 | -12.63901 | -6.81417 | 16.07947 | 28.28114 | -14.27968 | -39.51960 |
| | | S8_11_2D | 13.5 | 75.25 | uE | -27.90203 | -23.77018 | -11.71518 | -7.59307 | -3.49283 | 5.43904 | 6.10945 | -12.88329 | -23.09472 |
| | | S8_11_2E | 28.5 | 75.25 | uE | -12.42695 | -9.90023 | -5.74995 | -7.67933 | -5.07748 | -2.95280 | -10.95233 | -20.01542 | -15.64401 |
| | | S8_11_2F | 43.5 | 78.75 | uE | -1.67292 | -1.42891 | 1.38642 | -3.57487 | -2.37373 | 2.43085 | -4.36542 | -12.87890 | -8.74216 |
| | Girder 7 Midspan Gages | S7_11_3M | 0.0 | 104.00 | uE | -27.25916 | -23.03928 | -8.53143 | -2.53866 | -0.60665 | 13.51531 | 26.13093 | 0.61825 | -18.36035 |
| | | S7_11_4M | 0.0 | 272.00 | uE | -23.97592 | -19.71576 | -8.47171 | 1.37732 | 10.92597 | 26.74238 | 35.84611 | 75.74025 | 24.89571 |
| | | S7_11_5M | 0.0 | 440.00 | uE | -17.75327 | -14.53890 | -6.55171 | 0.10726 | 6.17016 | 18.50007 | 30.78472 | 65.95888 | 70.66198 |
| | | S7_11_6M | 0.0 | 608.00 | uE | -14.29286 | -10.42302 | -5.46733 | 1.49433 | 5.36858 | 13.20314 | 22.91262 | 53.94313 | 111.92794 |
| | Girder 8 Midspan Gages | S8_11_3M | 0.0 | 104.00 | uE | -31.26225 | -25.78396 | -10.30547 | -3.12549 | -0.44138 | 12.11927 | 23.08816 | -0.34913 | -18.78734 |
| | | S8_11_4M | 0.0 | 272.00 | uE | -23.39548 | -19.04599 | -8.05996 | 2.05285 | 10.71705 | 25.16205 | 32.79541 | 67.78644 | 22.01850 |
| | | S8_11_5M | 0.0 | 440.00 | uE | -17.09127 | -13.22619 | -5.76070 | 0.86880 | 6.82993 | 18.21786 | 29.85147 | 63.21705 | 67.72608 |
| | | S8_11_6M | 0.0 | 608.00 | uE | -3.57060 | 4.23788 | 4.25825 | 5.19933 | 11.98486 | 18.22713 | 24.73407 | 52.90679 | 100.55288 |

## C.3 LANE B – DEFLOCTOMETER AND CRACK OPENING DEVICE

**Table C-7:** Lane C - Crack Openings and Deflections

| | | Gage | Height of gage from bottom of girder | Distance along girder from center of continuity diaphragm to gage. (in.) (-) Span 10 (+) Span 11 | Units | C1 | C2 | C3 | C4 | C5 | C6 | C7 | C8 | C9 |
|---|---|---|---|---|---|---|---|---|---|---|---|---|---|---|
| Deflectometers | Girder 7 | D7_10_2 | n/a | -608.0000 | in | -0.28 | -0.17 | -0.09 | -0.05 | -0.02 | 0.01 | 0.02 | 0.05 | 0.05 |
| | | D7_10_1 | n/a | -308.0000 | in | -0.19 | -0.15 | -0.09 | -0.05 | -0.02 | 0.01 | 0.02 | 0.04 | 0.05 |
| | | D7_11_1 | n/a | 158.0000 | in | 0.03 | 0.02 | 0.00 | -0.01 | -0.02 | -0.04 | -0.06 | -0.09 | -0.09 |
| | | D7_11_2 | n/a | 308.0000 | in | 0.05 | 0.04 | 0.01 | -0.01 | -0.02 | -0.06 | -0.08 | -0.16 | -0.18 |
| | | D7_11_3 | n/a | 458.0000 | in | 0.06 | 0.05 | 0.02 | 0.00 | -0.02 | -0.06 | -0.09 | -0.18 | -0.24 |
| | | D7_11_4 | n/a | 608.0000 | in | 0.06 | 0.04 | 0.02 | 0.00 | -0.02 | -0.05 | -0.08 | -0.18 | -0.27 |
| | Girder 8 | D8_10_2 | n/a | -608.0000 | in | -0.33 | -0.19 | -0.10 | -0.05 | -0.02 | 0.02 | 0.03 | 0.06 | 0.06 |
| | | D8_10_1 | n/a | -308.0000 | in | -0.21 | -0.17 | -0.10 | -0.06 | -0.02 | 0.01 | 0.02 | 0.05 | 0.05 |
| | | D8_11_1 | n/a | 158.0000 | in | 0.04 | 0.03 | 0.01 | -0.01 | -0.02 | -0.04 | -0.07 | -0.11 | -0.10 |
| | | D8_11_2 | n/a | 308.0000 | in | 0.06 | 0.05 | 0.02 | -0.01 | -0.03 | -0.06 | -0.10 | -0.18 | -0.21 |
| | | D8_11_3 | n/a | 458.0000 | in | 0.07 | 0.05 | 0.02 | -0.01 | -0.03 | -0.07 | -0.11 | -0.22 | -0.29 |
| | | D8_11_4 | n/a | 608.0000 | in | 0.07 | 0.05 | 0.02 | 0.00 | -0.02 | -0.06 | -0.10 | -0.21 | -0.32 |
| Crack Gages | | CO8_10 | 13.5000 | -40.0000 | mm | -0.01131 | -0.00979 | -0.00757 | -0.00371 | -0.00120 | -0.00502 | -0.00776 | -0.01083 | -0.01100 |
| | | CO8_11 | 13.5000 | 56.0000 | mm | -0.01017 | -0.00936 | -0.00563 | -0.00438 | -0.00283 | 0.00471 | 0.00989 | -0.00294 | -0.00807 |
| | | CO7_10 | 13.5000 | -49.5000 | mm | -0.01122 | 0.00087 | 0.00883 | 0.01942 | 0.01212 | -0.00491 | -0.00999 | -0.01778 | -0.01885 |
| | | CO7_11 | 13.5000 | 47.7500 | mm | -0.02044 | -0.01883 | -0.01069 | -0.00829 | -0.00563 | 0.01249 | 0.02046 | -0.00428 | -0.01608 |

**Table C-8:** Lane C - Span 10 Strain Readings

| | | Gage | Height of gage from bottom of girder | Distance along girder from center of continuity diaphragm to gage. (in.) (-) Span 10 (+) Span 11 | Units | C1 | C2 | C3 | C4 | C5 | C6 | C7 | C8 | C9 |
|---|---|---|---|---|---|---|---|---|---|---|---|---|---|---|
| Span 10 | Girder 7 Cross Section 1 | S7_10_1A | 13.5000 | -12.7500 | uE | 4.17762 | 2.40480 | 1.23548 | -0.77169 | 0.48606 | 2.09631 | 0.83426 | -1.12874 | -1.97594 |
| | | S7_10_1B | 3.0000 | -12.7500 | uE | -16.20372 | -11.46988 | -8.88851 | -6.52808 | -4.81580 | -9.57753 | -12.92791 | -22.54520 | -21.20001 |
| | | S7_10_1C | 3.0000 | -12.7500 | uE | -118.79855 | -106.59231 | -78.83410 | -54.18692 | -27.91610 | -30.78178 | -48.06756 | -76.08097 | -76.24788 |
| | | S7_10_1D | 13.5000 | -12.7500 | uE | -6.88776 | -2.81594 | -1.56298 | -1.29320 | -0.47877 | -2.79874 | -6.56994 | -13.22132 | -14.17311 |
| | | S7_10_1E | 28.5000 | -12.7500 | uE | 0.70878 | 2.15252 | 2.01328 | 2.28992 | 2.68531 | -0.15900 | -1.12681 | -3.29999 | -4.08548 |
| | | S7_10_1F | 43.5000 | -12.7500 | uE | -1.03190 | -3.65011 | -3.85012 | -5.27278 | -1.81838 | -0.11225 | -1.21232 | -3.25157 | -3.97374 |
| | Girder 7 Cross Section 2 | S7_10_2A | 13.5000 | -75.2500 | uE | -10.64860 | -1.68239 | 4.56232 | 9.22245 | 5.54708 | -4.88667 | -7.91473 | -13.94431 | -15.71783 |
| | | S7_10_2M | 0.0000 | -75.2500 | uE | -13.55037 | -2.17806 | 5.03404 | 9.47643 | 5.38243 | -5.65950 | -8.99436 | -17.91157 | -17.69952 |
| | | S7_10_2C | 3.0000 | -75.2500 | uE | -16.45877 | 0.26878 | 9.66964 | 18.78453 | 9.25743 | -7.07626 | -12.23687 | -22.62698 | -23.45949 |
| | | S7_10_2D | 13.5000 | -75.2500 | uE | -20.38643 | -3.47429 | 7.34709 | 13.86597 | 5.99198 | -7.98231 | -13.93487 | -25.12397 | -25.65666 |
| | | S7_10_2E | 28.5000 | -75.2500 | uE | -9.79810 | -2.58572 | 1.06916 | 6.13481 | 4.58378 | -2.27948 | -4.76418 | -9.52782 | -10.18285 |
| | | S7_10_2F | 43.5000 | -75.2500 | uE | -7.87559 | -9.41637 | -13.79453 | -6.56961 | 3.16945 | -0.14227 | -0.19318 | -0.64390 | -0.81337 |
| | Girder 8 Cross Section 1 | S8_10_1A | 13.5000 | -12.7500 | uE | -2.32437 | 2.20961 | 3.35355 | 4.33761 | 6.01137 | -0.99056 | -7.42529 | -19.07939 | -21.15016 |
| | | S8_10_1B | 3.0000 | -12.7500 | uE | -28.77619 | -23.44978 | -14.93698 | -7.32930 | -1.86023 | -7.39586 | -15.67964 | -29.02105 | -28.79486 |
| | | S8_10_1C | 3.0000 | -12.7500 | uE | -41.14145 | -28.22616 | -19.19726 | -12.20731 | -6.90454 | -12.32970 | -18.98806 | -29.17240 | -26.64271 |
| | | S8_10_1D | 13.5000 | -12.7500 | uE | -4.97185 | -0.00772 | 1.62936 | 3.50387 | 4.90227 | -3.15005 | -9.41331 | -19.99727 | -22.00844 |
| | | S8_10_1E | 28.5000 | -12.7500 | uE | 0.75754 | 2.72490 | 2.52570 | 2.72862 | 3.32100 | -0.69709 | -2.08584 | -4.70896 | -5.16239 |
| | | S8_10_1F | 43.5000 | -12.7500 | uE | -3.35483 | -5.18107 | -5.09397 | -5.62330 | -1.40056 | -2.45857 | -3.02733 | -3.85101 | -3.62155 |
| | Girder 8 Cross Section 2 | S8_10_2A | 13.5000 | -75.2500 | uE | -24.44423 | -8.48234 | -0.24792 | 8.87390 | 5.68208 | -7.81783 | -14.57625 | -26.11615 | -26.33888 |
| | | S8_10_2M | 0.0000 | -75.2500 | uE | -25.33597 | -2.33875 | 7.12207 | 19.12997 | 10.75484 | -9.61981 | -17.50459 | -31.44443 | -31.69394 |
| | | S8_10_2C | 3.0000 | -75.2500 | uE | -24.37669 | -4.79902 | 4.18249 | 10.86276 | 5.45518 | -9.67599 | -16.61334 | -28.86490 | -29.03530 |
| | | S8_10_2D | 13.5000 | -75.2500 | uE | -22.67112 | -8.06574 | -0.30481 | 7.38037 | 3.83842 | -7.81938 | -14.26916 | -24.02532 | -25.09692 |
| | | S8_10_2E | 28.5000 | -75.2500 | uE | -14.42423 | -6.75758 | -2.83547 | 1.82142 | 2.01918 | -4.35563 | -7.78737 | -13.40830 | -13.56271 |
| | | S8_10_2F | 43.5000 | -75.2500 | uE | -7.67724 | -7.94089 | -11.61979 | -5.05455 | 2.11593 | -0.51610 | -0.56963 | -0.80282 | -0.89479 |

**Table C-9:** Lane C - Span 11 Strain Readings

| | | Gage | Height of gage from bottom of girder | Distance along girder from center of continuity diaphragm to gage. (in.) (-) Span 10 (+) Span 11 | Units | C1 | C2 | C3 | C4 | C5 | C6 | C7 | C8 | C9 |
|---|---|---|---|---|---|---|---|---|---|---|---|---|---|---|
| Span 11 | Girder 7 Cross Section 1 | S7_11_1A | 13.5000 | 12.7500 | uE | -21.24299 | -14.27831 | -5.91950 | -0.90802 | 4.62569 | 6.59096 | 1.44191 | -1.88801 | -3.71048 |
| | | S7_11_1B | 3.0000 | 12.7500 | uE | -22.16517 | -18.97446 | -11.11600 | -7.34494 | -3.28888 | -0.30279 | -2.56907 | -6.52558 | -7.85964 |
| | | S7_11_1C | 3.0000 | 12.7500 | uE | -18.43363 | -15.28890 | -10.86773 | -7.75817 | -4.45210 | -4.77382 | -11.55824 | -29.53275 | -29.09566 |
| | | S7_11_1D | 13.5000 | 12.7500 | uE | -23.79422 | -18.19524 | -7.31690 | -3.64681 | 2.67261 | 7.37748 | 4.18439 | -6.60308 | -11.19743 |
| | | S7_11_1E | 28.5000 | 12.7500 | uE | -5.92954 | -3.92173 | -2.48241 | -0.26101 | 1.34538 | 2.18437 | -0.96517 | -0.89144 | 0.13173 |
| | | S7_11_1F | 43.5000 | 12.7500 | uE | -1.68603 | -1.11601 | -0.56341 | -0.24830 | -0.72365 | 2.87564 | 1.35691 | -1.68270 | -2.99144 |
| | Girder 7 Cross Section 2 | S7_11_2A | 13.5000 | 75.2500 | uE | -15.28989 | -12.94937 | -6.00356 | -4.68185 | -1.63036 | 4.39540 | 4.22793 | -7.13157 | -13.19600 |
| | | S7_11_2M | 0.0000 | 75.2500 | uE | -23.76048 | -20.07496 | -8.99016 | -5.62308 | -3.33794 | 10.17400 | 16.97229 | -7.96945 | -21.43248 |
| | | S7_11_2C | 3.0000 | 75.2500 | uE | -25.91199 | -22.05123 | -10.52766 | -6.65072 | -3.26844 | 8.20751 | 13.36772 | -10.59919 | -24.06577 |
| | | S7_11_2D | 13.5000 | 75.2500 | uE | -16.93636 | -13.82475 | -6.66038 | -4.15883 | -1.72012 | 5.10763 | 5.37085 | -5.66583 | -12.18660 |
| | | S7_11_2E | 28.5000 | 75.2500 | uE | -9.50986 | -8.18510 | -3.48323 | -2.94279 | -1.13081 | 3.48079 | -0.18165 | -5.10587 | -7.75179 |
| | | S7_11_2F | 43.5000 | 78.7500 | uE | -0.18260 | -0.14838 | 1.33731 | -1.75639 | -1.00666 | 3.36474 | -2.73499 | -5.92375 | -1.86792 |
| | Girder 8 Cross Section 1 | S8_11_1A | 13.5000 | 12.7500 | uE | -86.94658 | -72.71672 | -40.37367 | -26.74599 | -10.03792 | 15.47180 | 12.01653 | -27.07895 | -49.19327 |
| | | S8_11_1B | 3.0000 | 12.7500 | uE | -21.04894 | -18.01691 | -12.99939 | -9.86382 | -5.11920 | -8.19550 | -17.03207 | -28.03993 | -25.46939 |
| | | S8_11_1C | 3.0000 | 12.7500 | uE | -27.56400 | -24.39716 | -16.96745 | -12.64844 | -6.33676 | -3.71758 | -10.83030 | -29.36459 | -34.37010 |
| | | S8_11_1D | 13.5000 | 12.7500 | uE | -34.67229 | -24.92356 | -14.61256 | -6.57672 | 1.64804 | 1.68721 | -7.35081 | -15.10820 | -15.34291 |
| | | S8_11_1E | 28.5000 | 12.7500 | uE | -42.88791 | -36.24454 | -24.26631 | -18.06968 | -11.03741 | -0.42960 | -4.06354 | -16.83468 | -24.60987 |
| | | S8_11_1F | 43.5000 | 12.7500 | uE | -1.08374 | -1.17675 | -1.25447 | -0.79629 | 0.02660 | 0.46471 | -3.08931 | -1.58151 | -0.45517 |
| | Girder 8 Cross Section 2 | S8_11_2A | 13.5000 | 75.2500 | uE | -23.44756 | -19.89810 | -9.72230 | -8.14942 | -4.22796 | 2.81647 | 0.60529 | -15.11203 | -21.60615 |
| | | S8_11_2M | 0.0000 | 75.2500 | uE | -37.77865 | -32.39109 | -13.46940 | -7.46001 | -2.82554 | 17.52206 | 32.87475 | -3.61611 | -26.54296 |
| | | S8_11_2C | 3.0000 | 75.2500 | uE | -61.48523 | -54.25008 | -28.31536 | -17.44163 | -8.46771 | 16.90309 | 28.43285 | -18.05199 | -49.74137 |
| | | S8_11_2D | 13.5000 | 75.2500 | uE | -31.30266 | -26.52953 | -13.26529 | -7.84911 | -4.45884 | 6.67030 | 8.17951 | -14.65693 | -26.13753 |
| | | S8_11_2E | 28.5000 | 75.2500 | uE | -13.51308 | -11.43886 | -5.86880 | -7.85465 | -4.41251 | -1.66925 | -12.65406 | -21.56399 | -18.51964 |
| | | S8_11_2F | 43.5000 | 78.7500 | uE | -2.17949 | -2.11639 | 1.94754 | -3.95340 | -3.38393 | 3.75470 | -4.16534 | -14.74673 | -9.11426 |
| | Girder 7 Midspan Gages | S7_11_3M | 0.0000 | 104.0000 | uE | -24.51336 | -20.56495 | -8.31989 | -3.28799 | -0.99052 | 11.52556 | 23.01303 | 0.90507 | -15.61067 |
| | | S7_11_4M | 0.0000 | 272.0000 | uE | -21.92456 | -18.07034 | -7.97565 | 0.55157 | 9.01353 | 22.29144 | 30.81150 | 68.20256 | 23.35221 |
| | | S7_11_5M | 0.0000 | 440.0000 | uE | -16.97873 | -13.26546 | -6.47404 | -0.24226 | 5.40258 | 16.56841 | 27.10705 | 58.32980 | 64.32412 |
| | | S7_11_6M | 0.0000 | 608.0000 | uE | -12.17511 | -9.21994 | -3.38729 | 0.16871 | 4.98851 | 12.28905 | 21.22474 | 48.04123 | 100.70022 |
| | Girder 8 Midspan Gages | S8_11_3M | 0.0000 | 104.0000 | uE | -35.59116 | -30.07513 | -12.30074 | -4.16307 | -0.86764 | 13.58219 | 26.70549 | -0.60878 | -22.75278 |
| | | S8_11_4M | 0.0000 | 272.0000 | uE | -26.64738 | -21.71794 | -9.78395 | 1.65667 | 11.85284 | 28.76734 | 37.57544 | 79.19151 | 24.74795 |
| | | S8_11_5M | 0.0000 | 440.0000 | uE | -19.39500 | -15.22809 | -6.78747 | 1.21677 | 7.33172 | 19.88834 | 32.75341 | 71.61521 | 76.56388 |
| | | S8_11_6M | 0.0000 | 608.0000 | uE | -14.40541 | -9.83620 | -0.37493 | 6.71723 | 11.48035 | 8.77868 | 19.73418 | 54.38946 | 110.69655 |

# APPENDIX D

## GRAPHS OF TEST DATA

Appendix D contains graphs of test data from each of the nine stopping points on all three load test lanes. The different types of graphs included for each loading position are the following: deflections vs. position in span; bottom stresses vs. position in span; and a graph of strains vs. depth in cross section for all eight cross sections, 2 on each girder end.

## D.1 LANE A

### D.1.1 POSITION A1

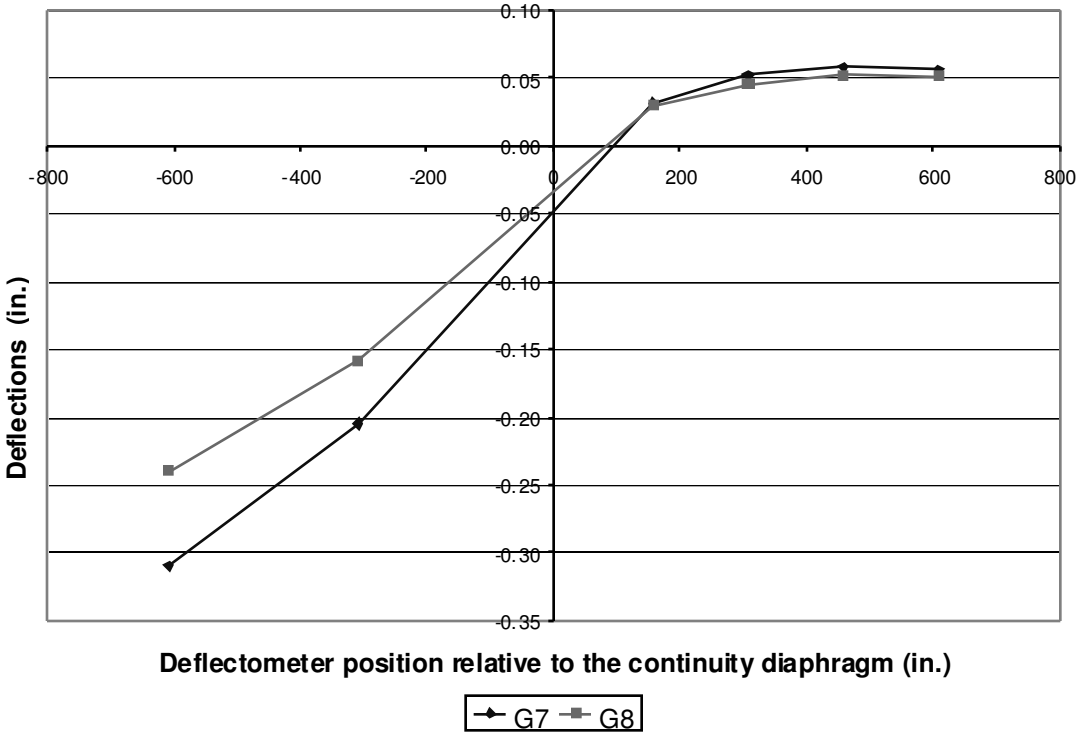


**Figure D-1:** A1 Deflections

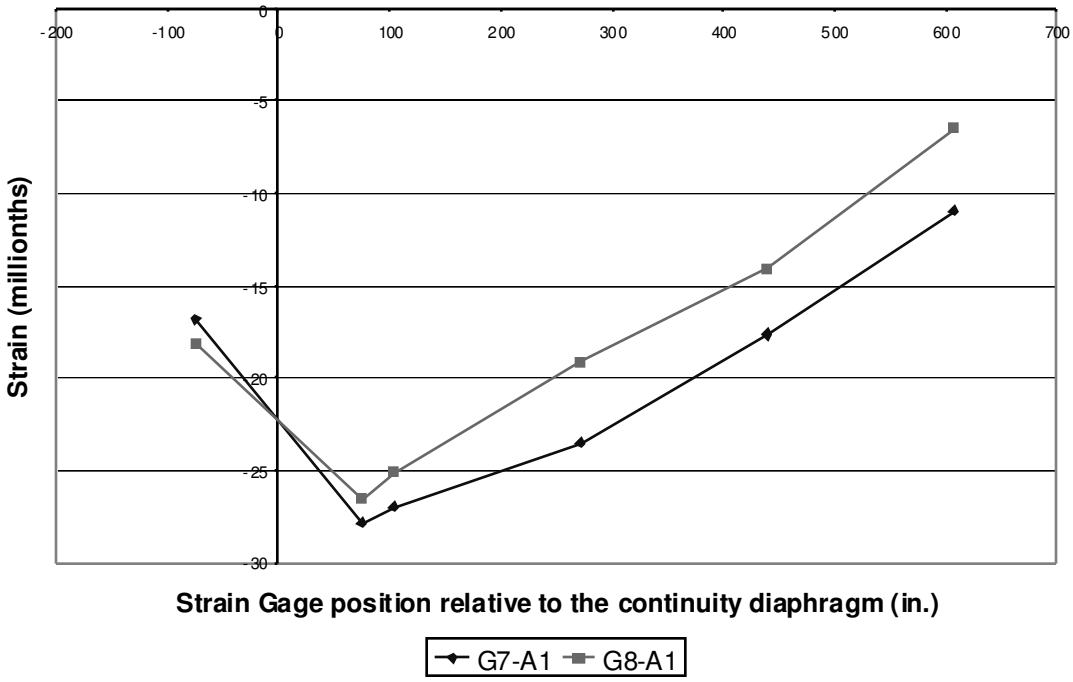


**Figure D-2:** A1 Bottom Fiber Strains

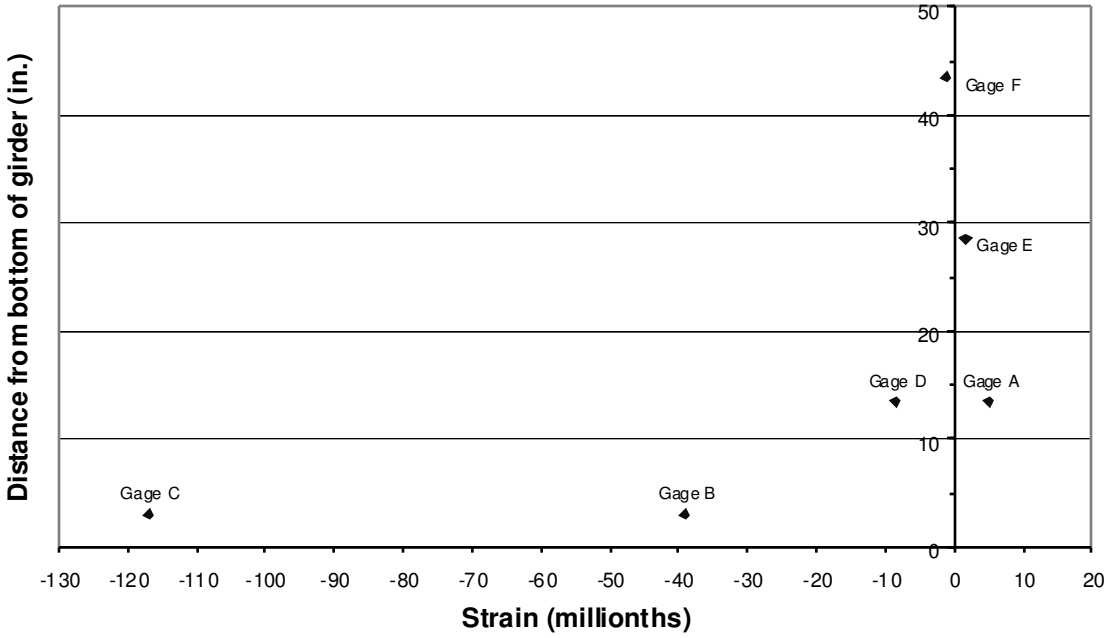


**Figure D-3:** A1 Span 10 Girder 7 Cross Section1

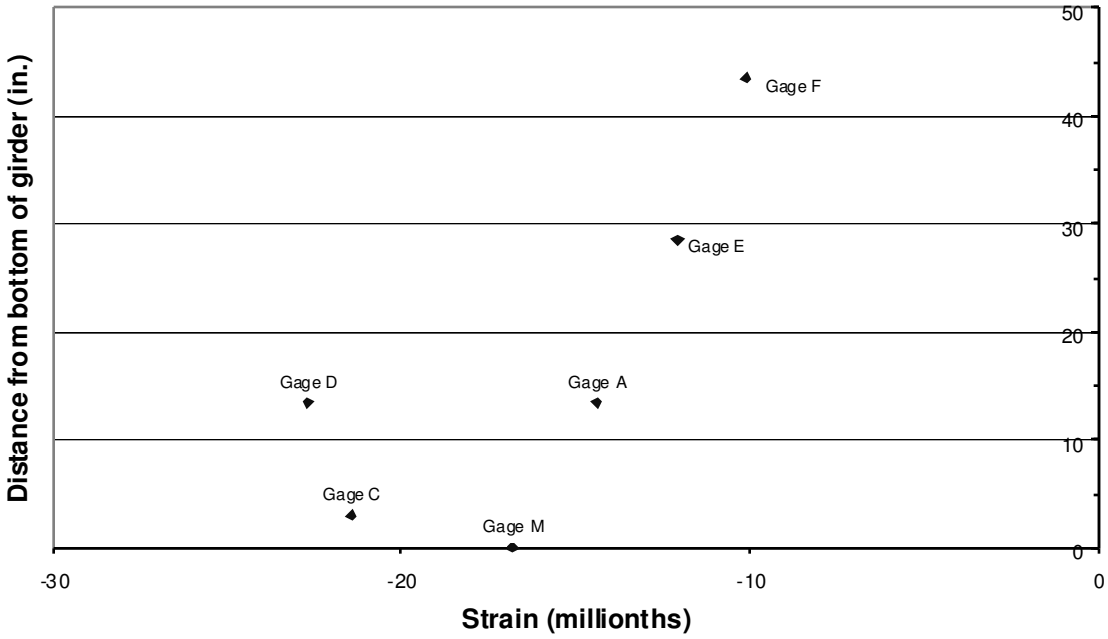


**Figure D-4:** A1 Span 10 Girder 7 Cross Section 2

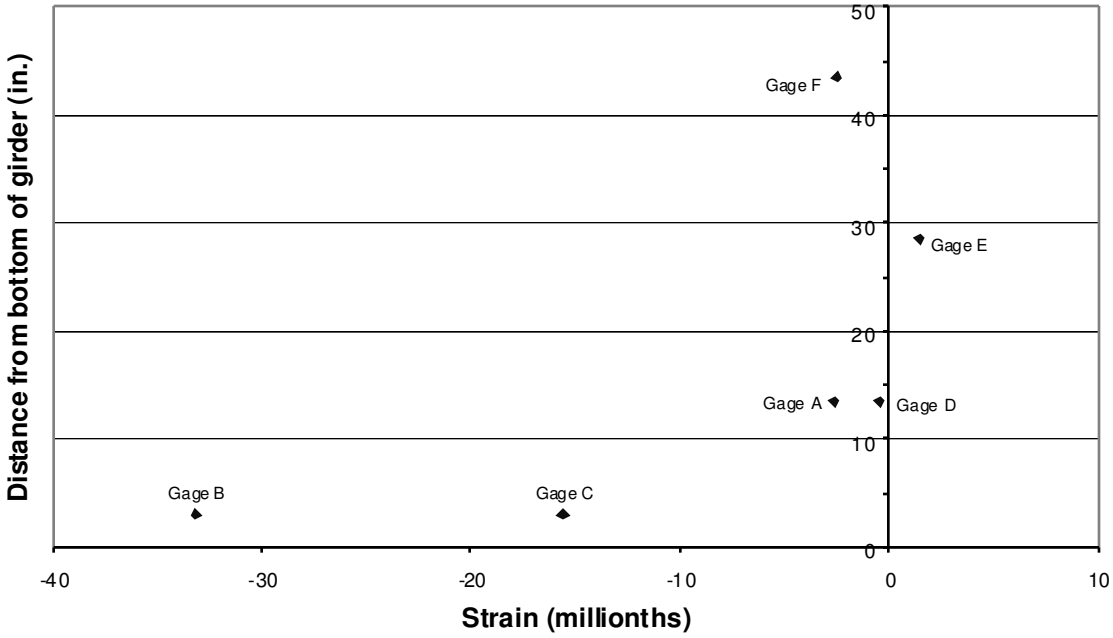


**Figure D-5:** A1 Span 10 Girder 8 Cross Section 1

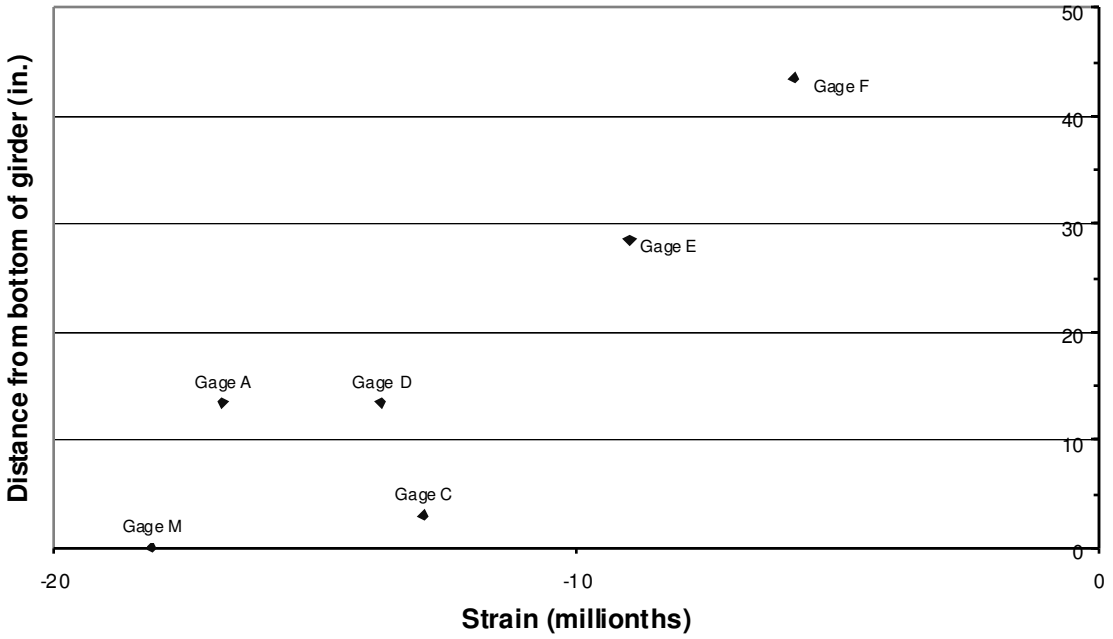


**Figure D-6:** A1 Span 10 Girder 8 Cross Section 2

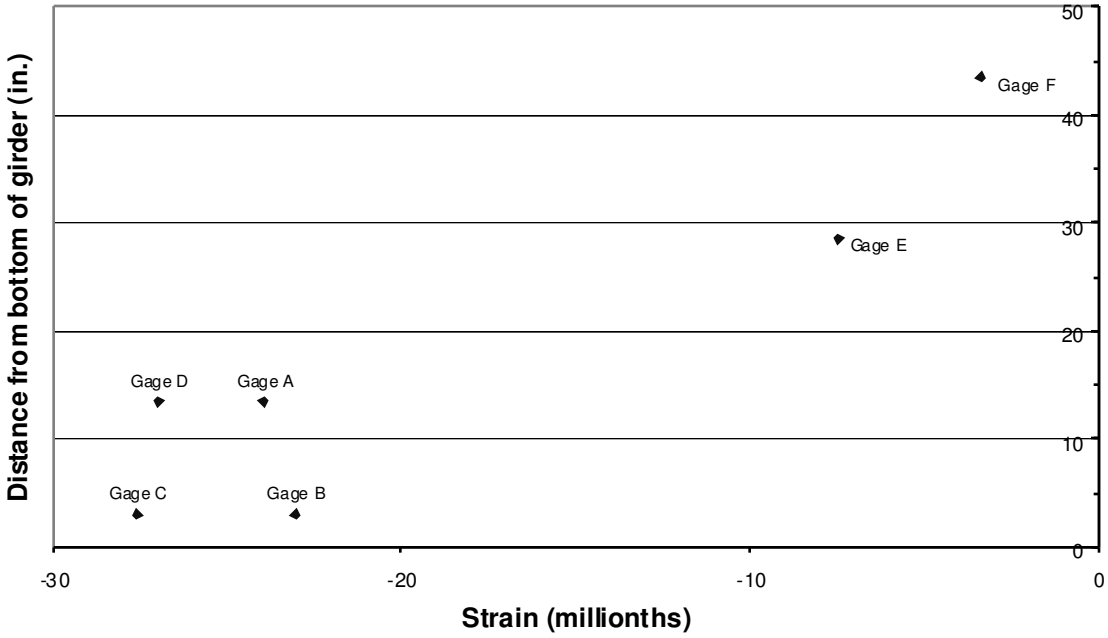


**Figure D-7:** A1 Span 11 Girder 7 Cross Section 1

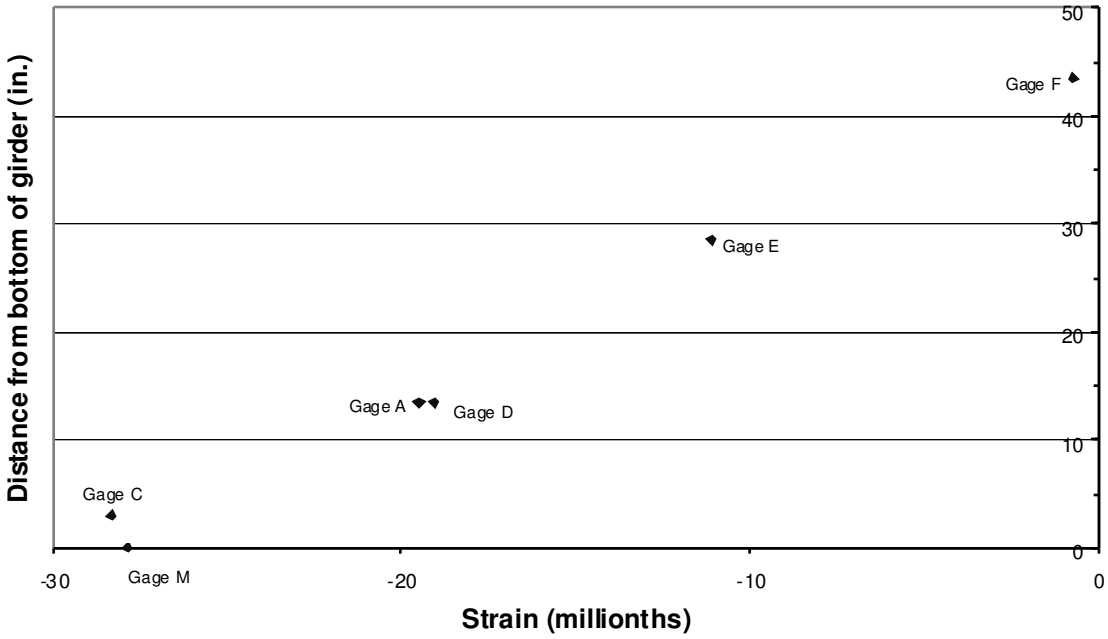


**Figure D-8:** A1 Span 11 Girder 7 Cross Section 2

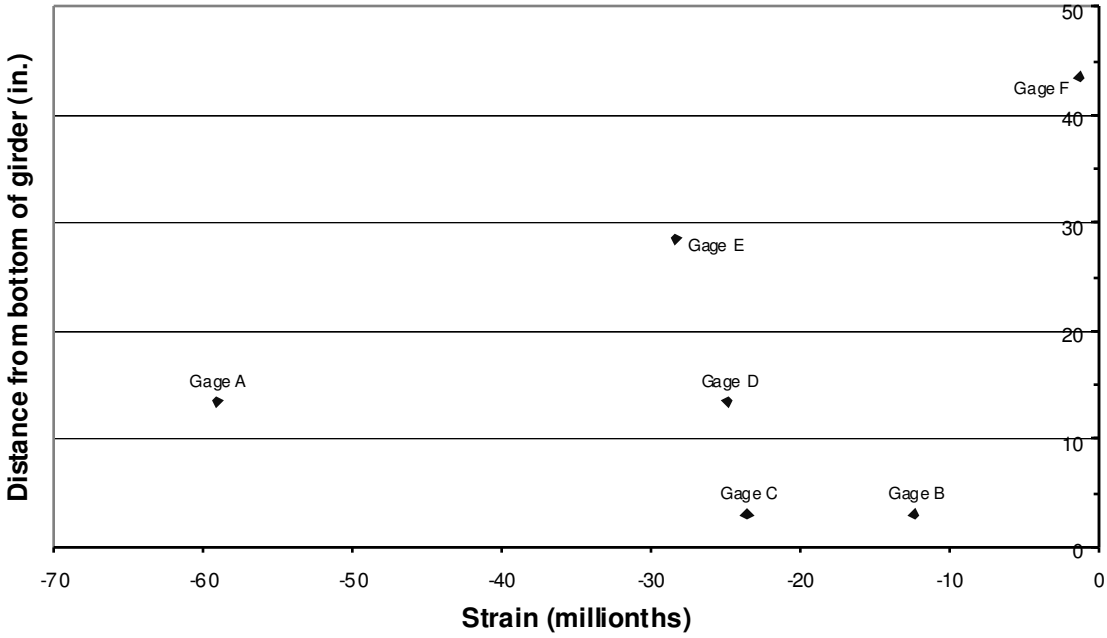


**Figure D-9:** A1 Span 11 Girder 8 Cross Section 1

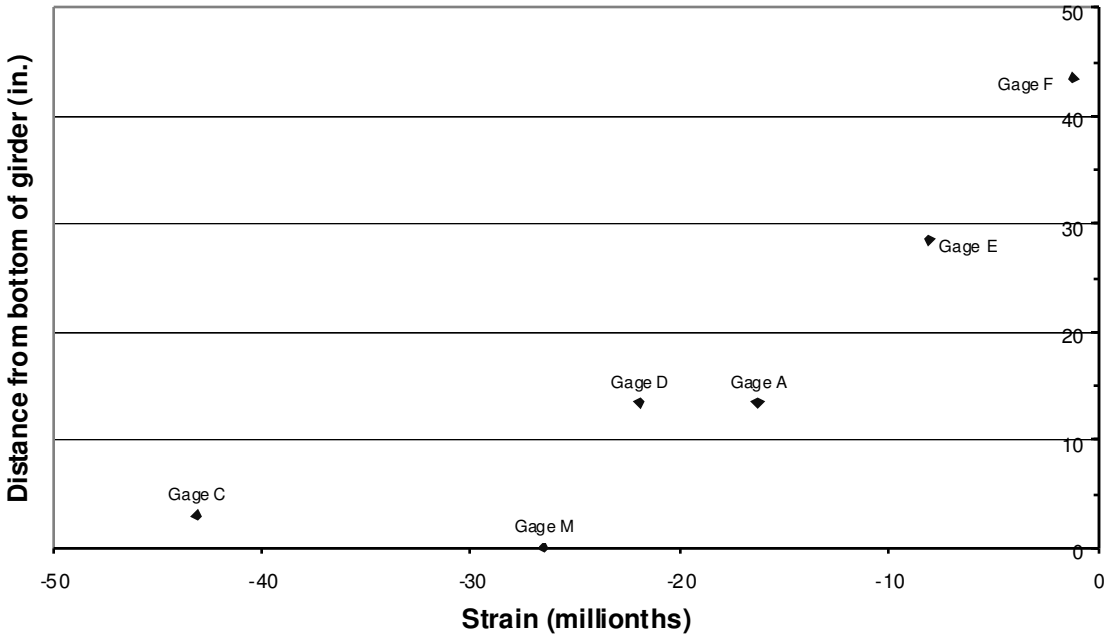


**Figure D-10:** A1 Span 11 Girder 8 Cross Section 2

### D.1.2 POSITION A2

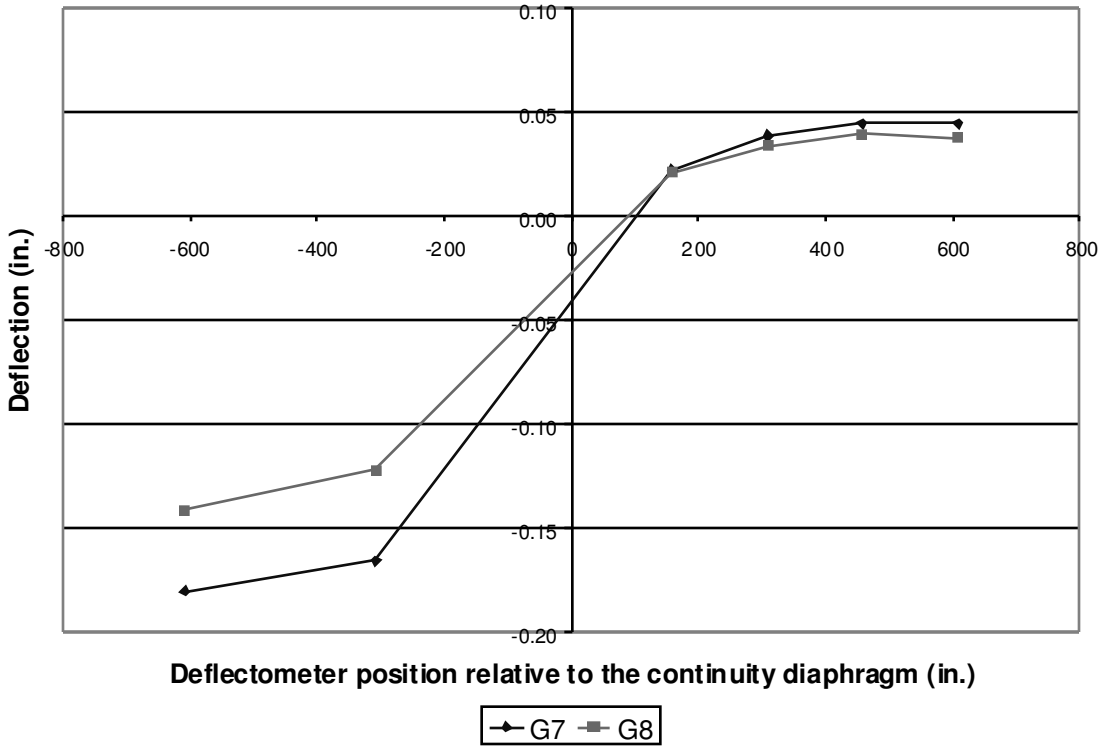


**Figure D-11:** A2 Deflections

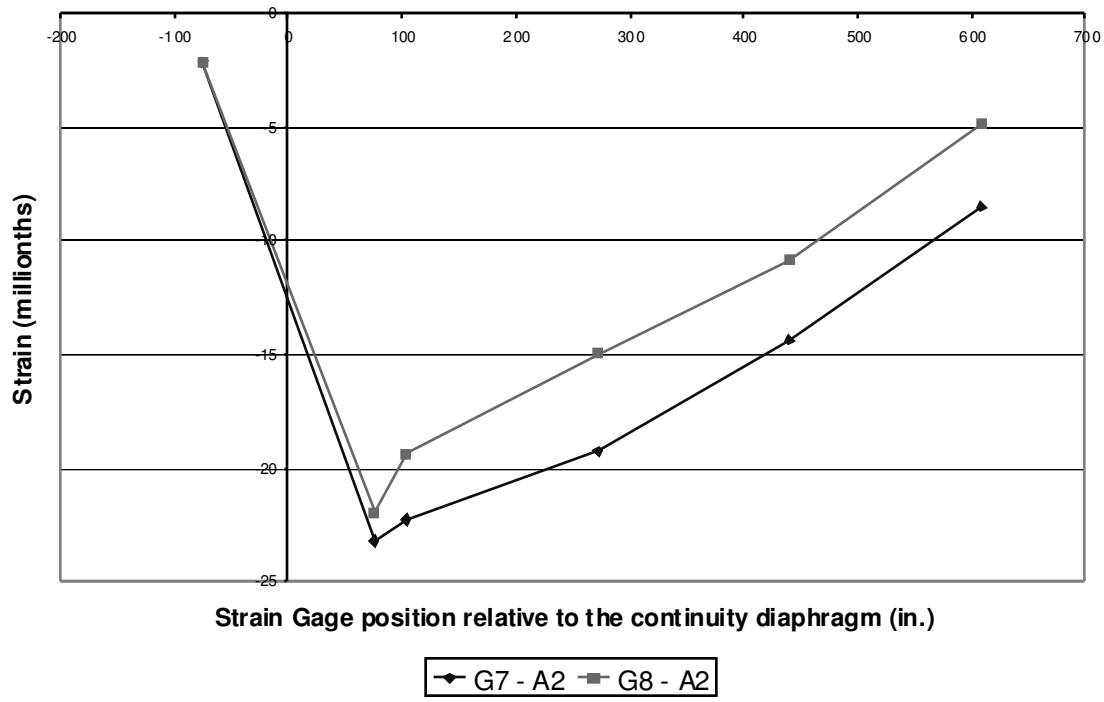


**Figure D-12:** A2 Bottom Fiber Strains

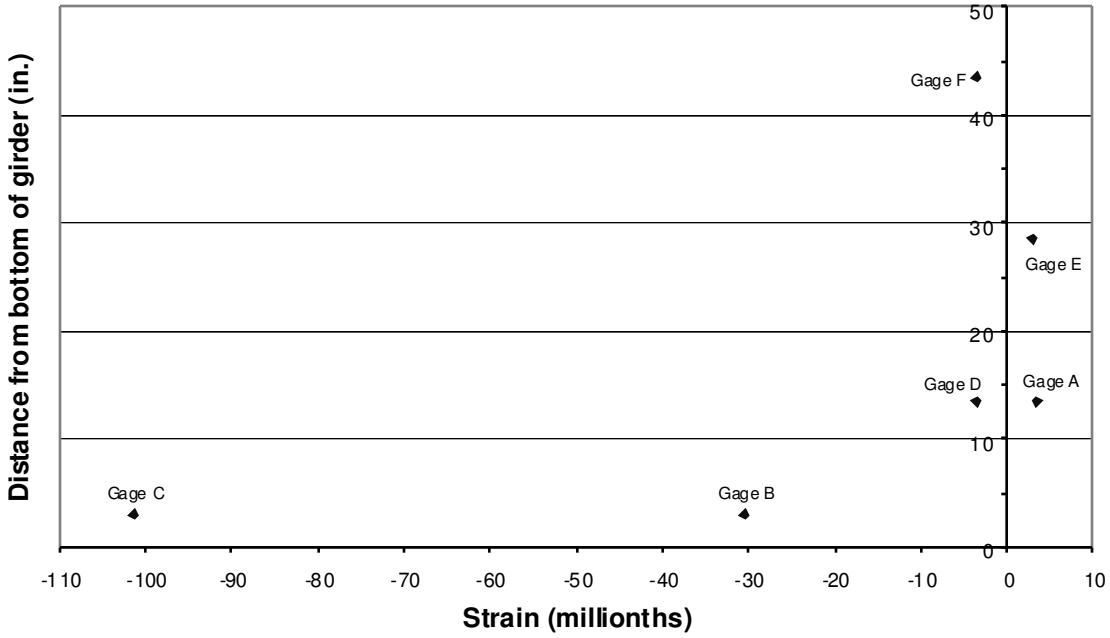


**Figure D-13:** A2 Span 10 Girder 7 Cross Section1

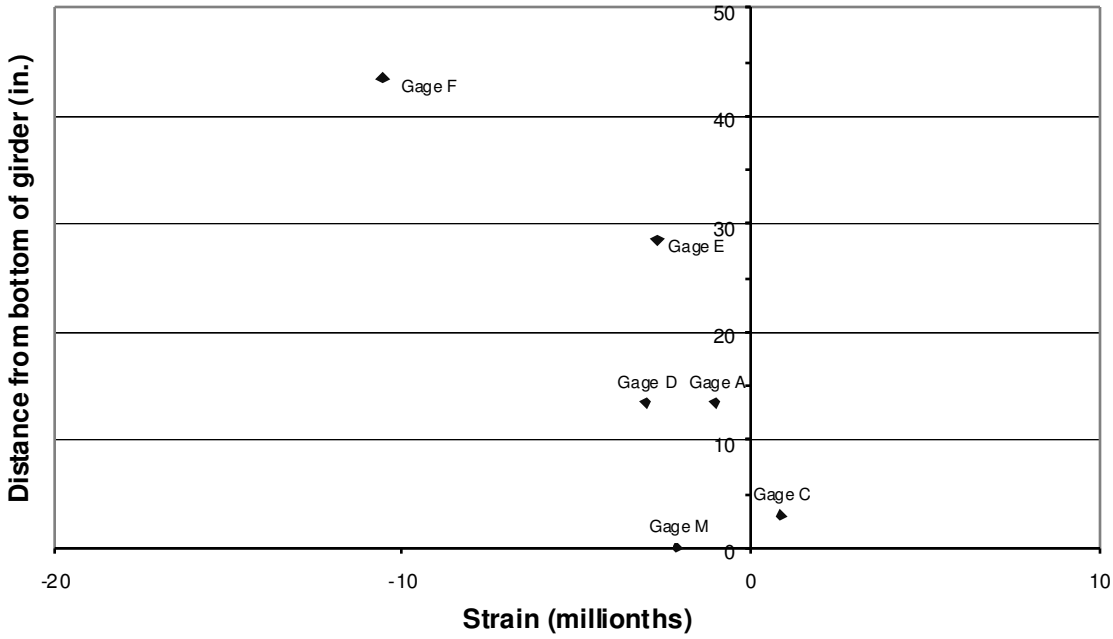


**Figure D-14:** A2 Span 10 Girder 7 Cross Section 2

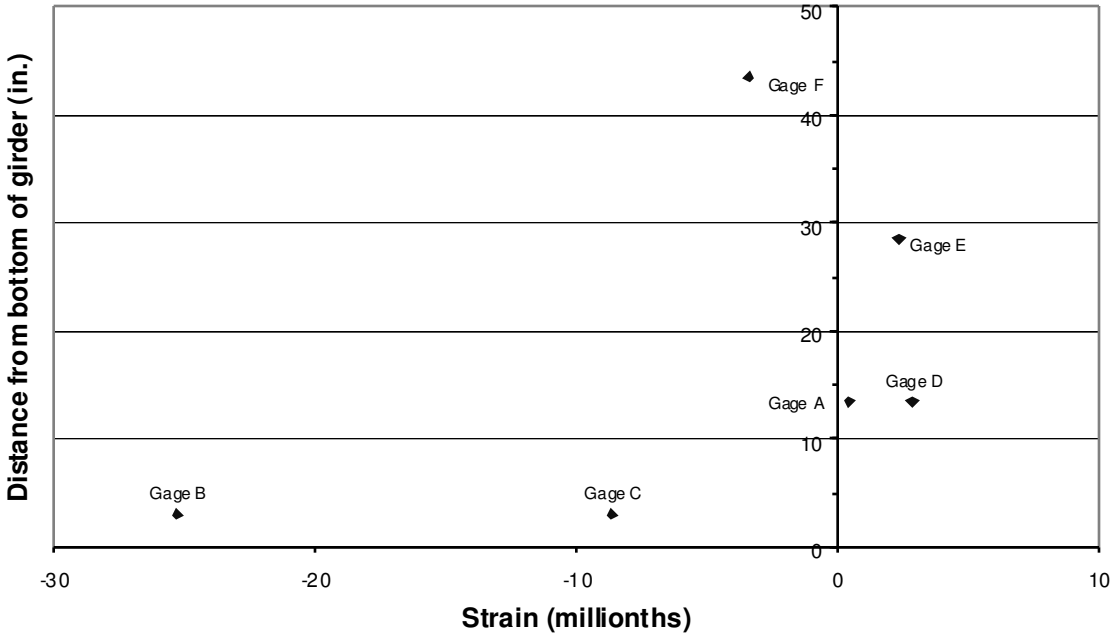


**Figure D-15:** A2 Span 10 Girder 8 Cross Section 1

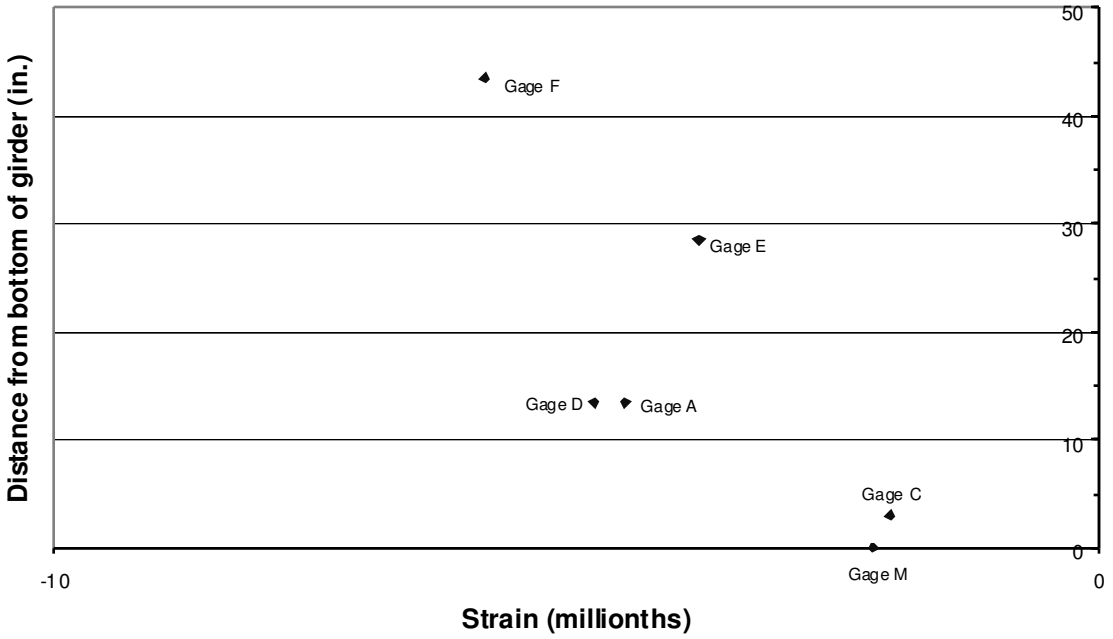


**Figure D-16:** A2 Span 10 Girder 8 Cross Section 2

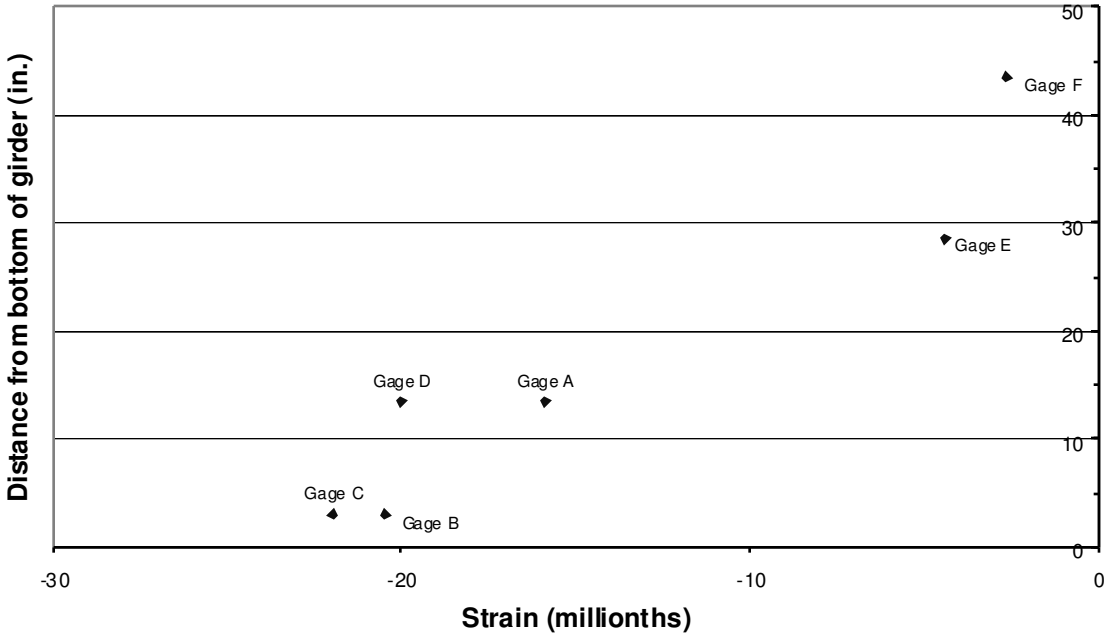


**Figure D-17:** A2 Span 11 Girder 7 Cross Section 1

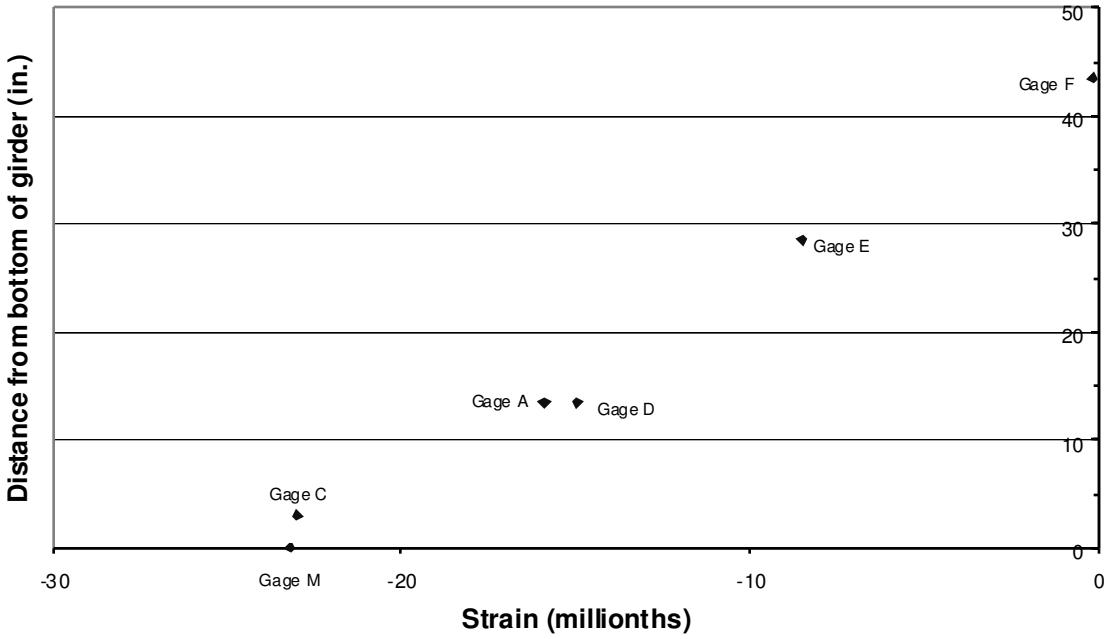


**Figure D-18:** A2 Span 11 Girder 7 Cross Section 2

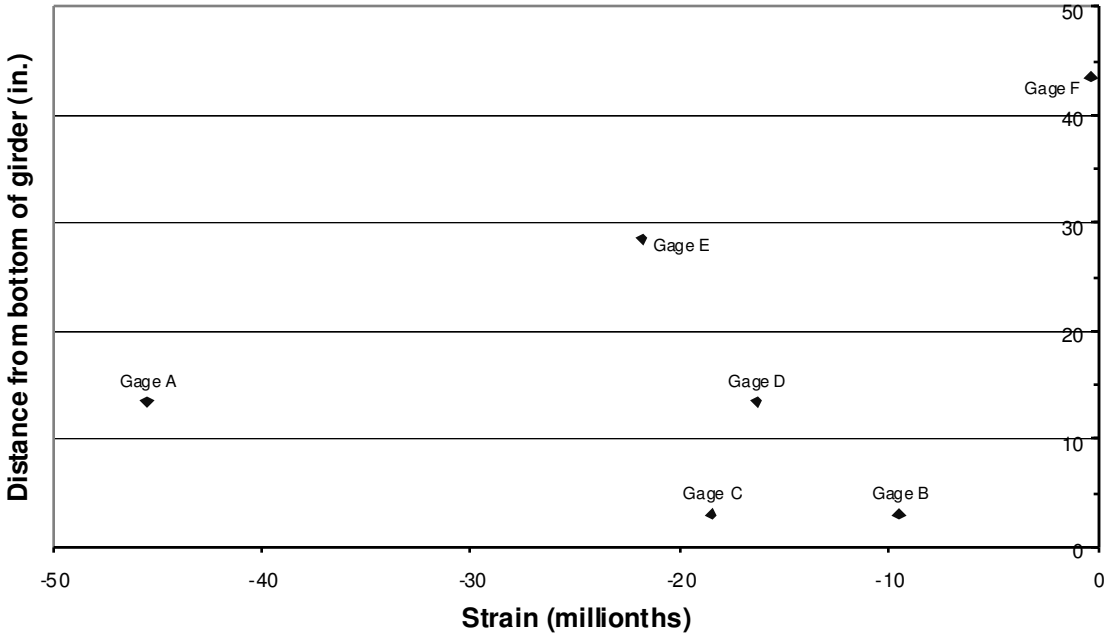


**Figure D-19:** A2 Span 11 Girder 8 Cross Section 1

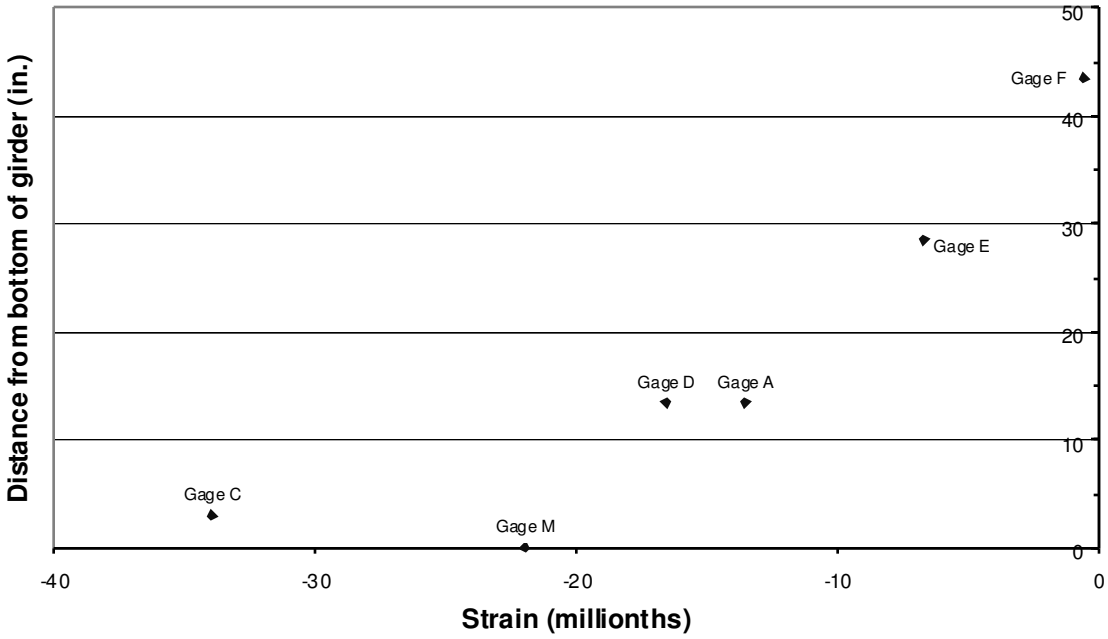


**Figure D-20:** A2 Span 11 Girder 8 Cross Section 2

### D.1.3 POSITION A3

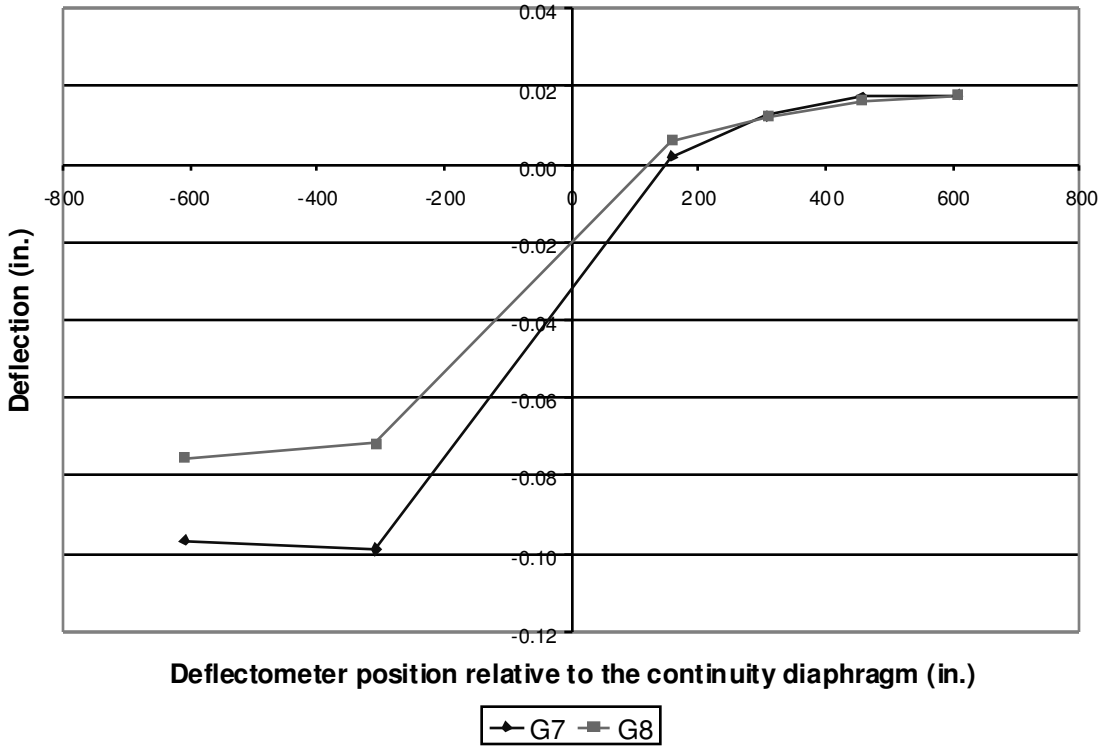


**Figure D-21:** A3 Deflections

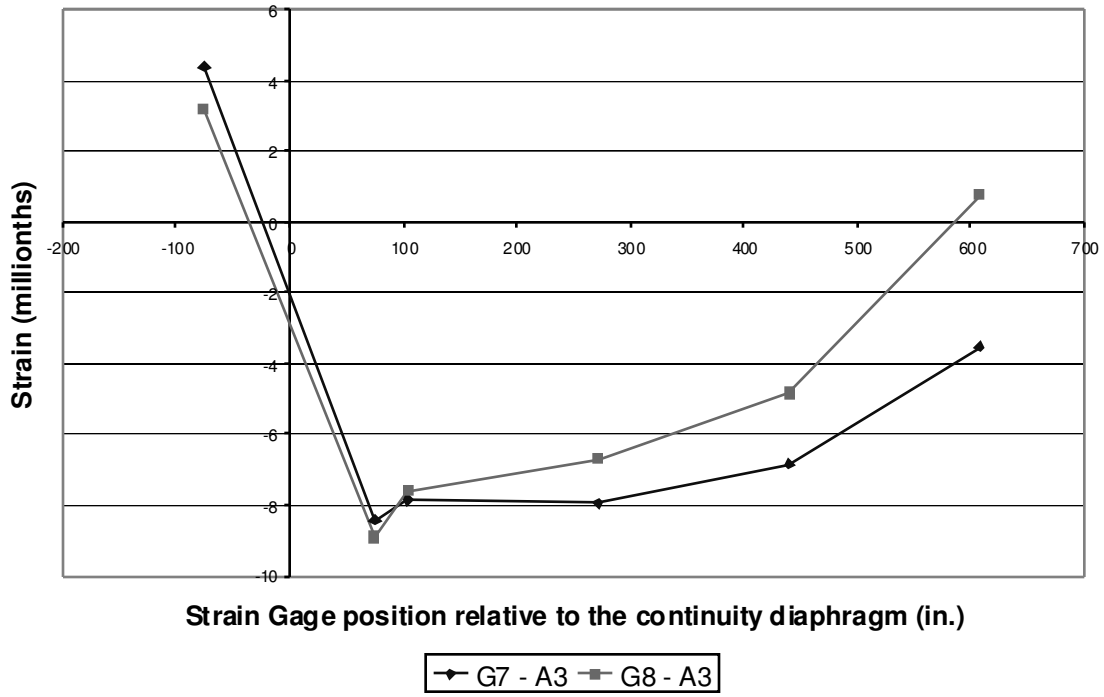


**Figure D-22:** A3 Bottom Fiber Strains

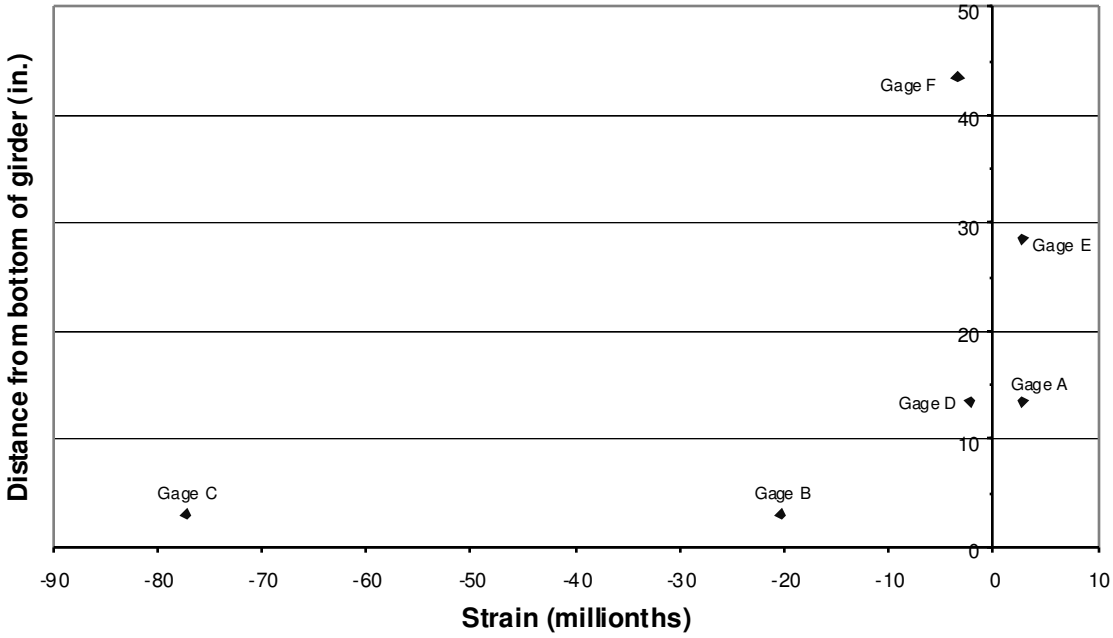


**Figure D-23:** A3 Span 10 Girder 7 Cross Section1

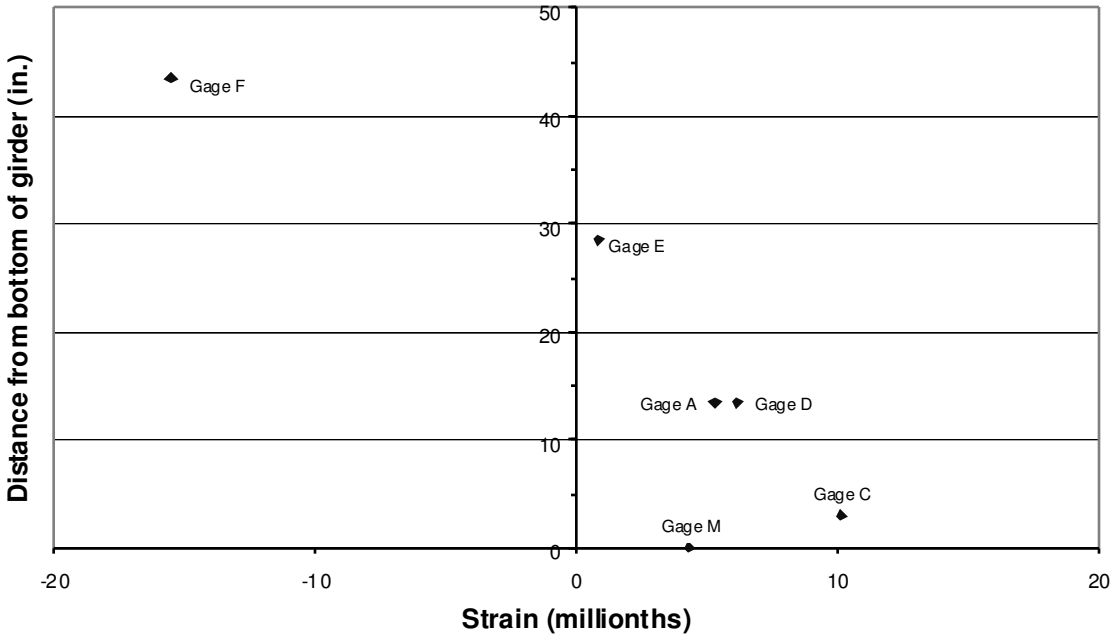


**Figure D-24:** A3 Span 10 Girder 7 Cross Section 2

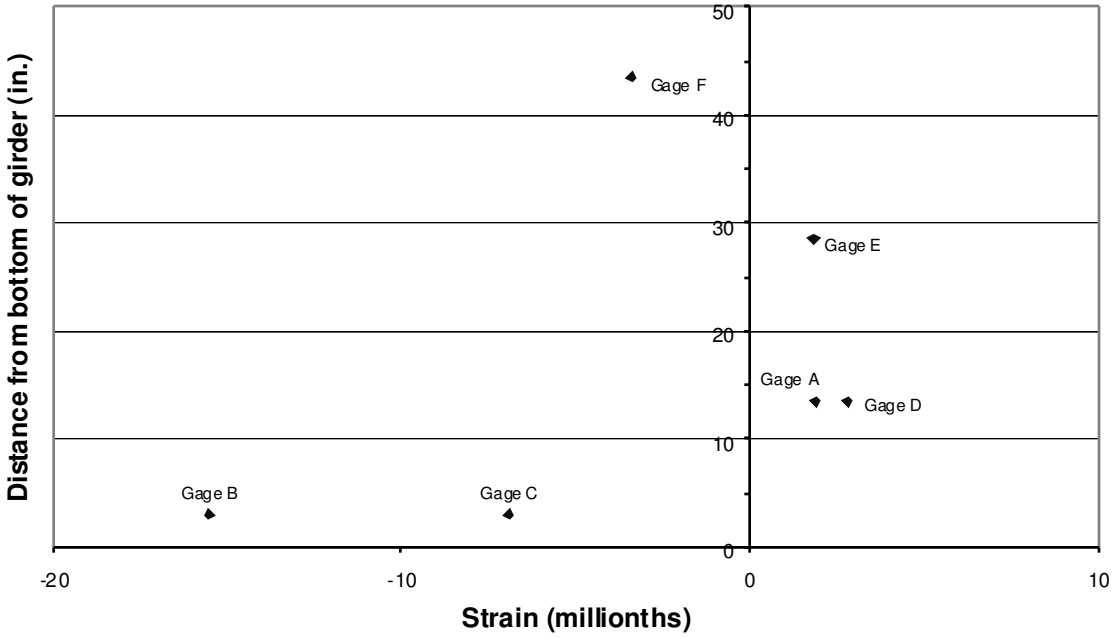


**Figure D-25:** A3 Span 10 Girder 8 Cross Section 1

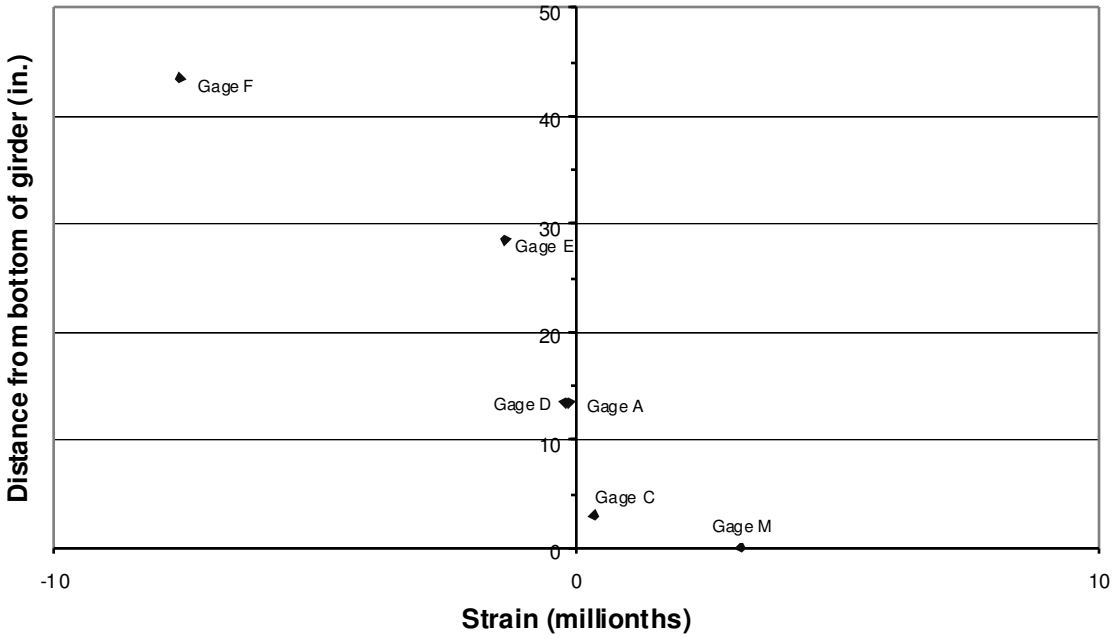


**Figure D-26:** A3 Span 10 Girder 8 Cross Section 2

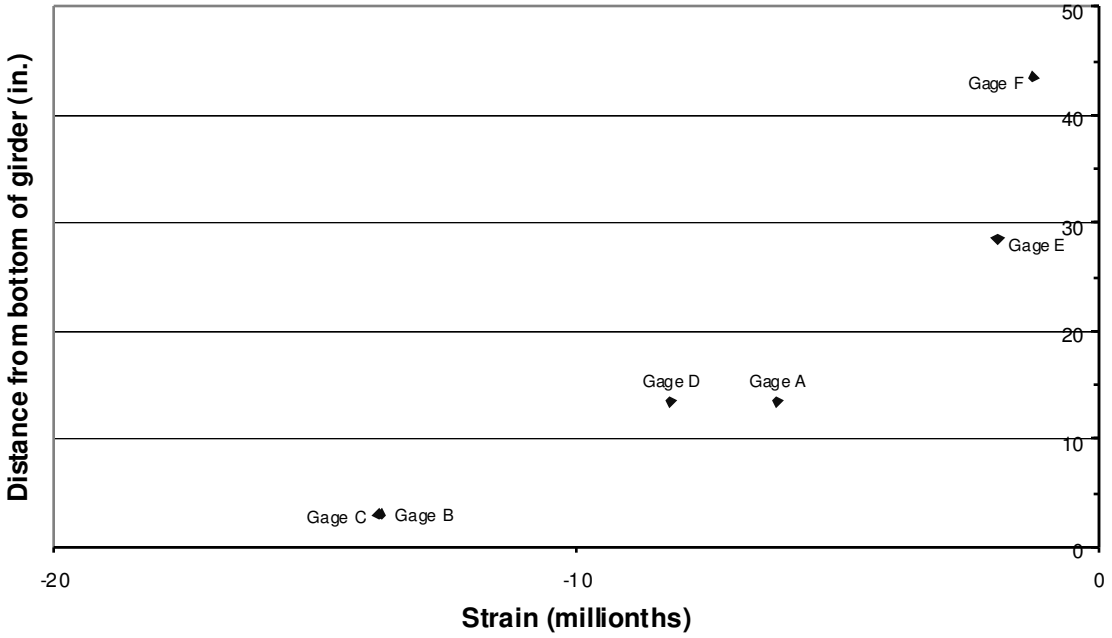


**Figure D-27:** A3 Span 11 Girder 7 Cross Section 1

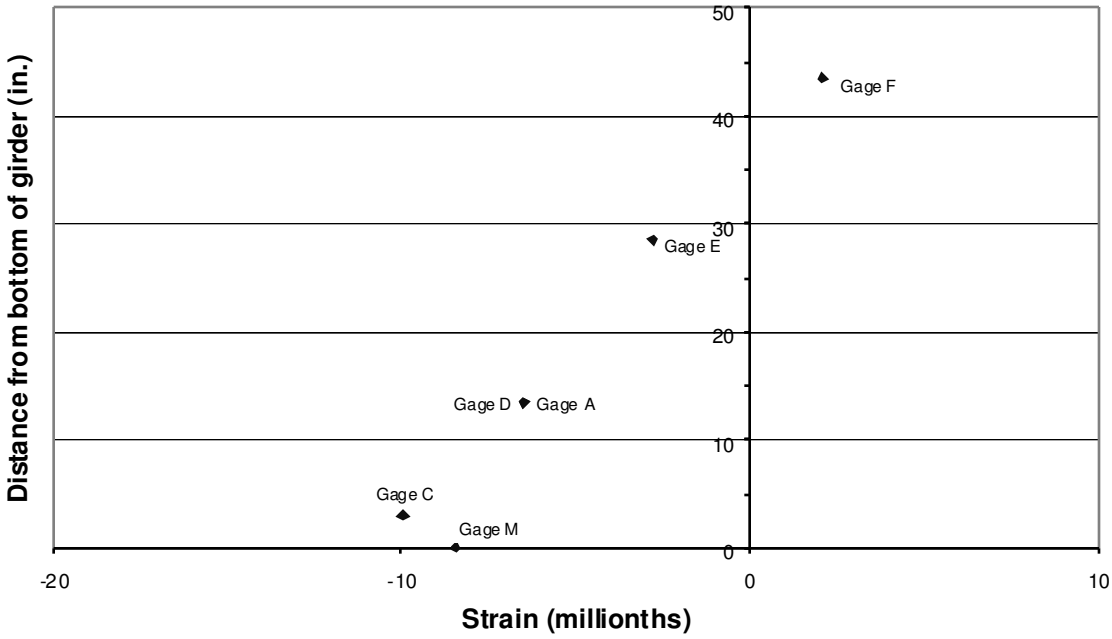


**Figure D-28:** A3 Span 11 Girder 7 Cross Section 2

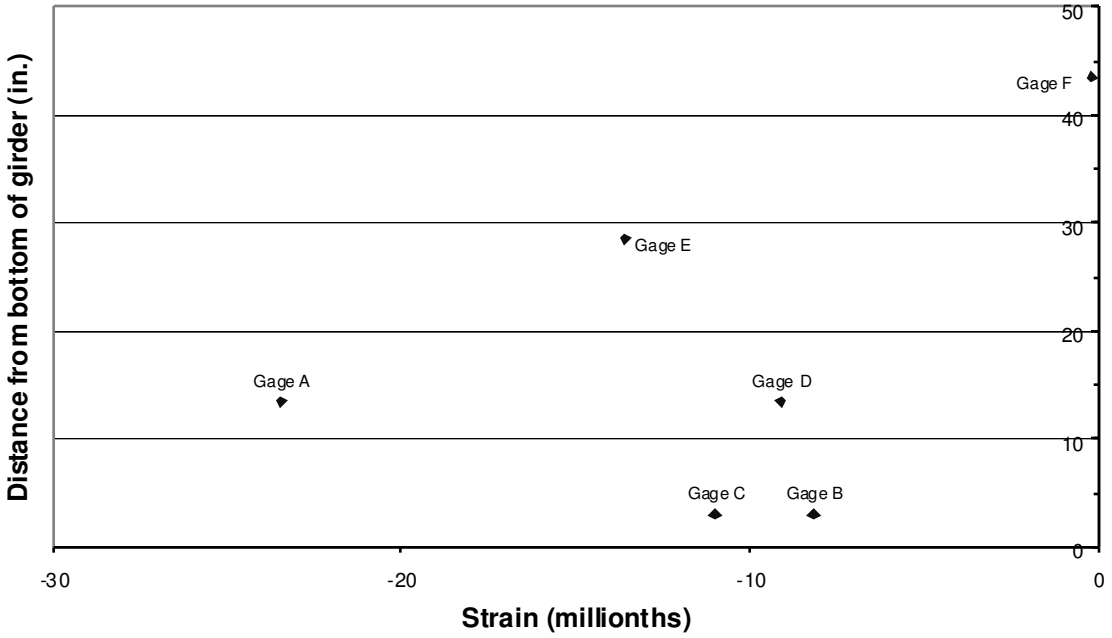


**Figure D-29:** A3 Span 11 Girder 8 Cross Section 1

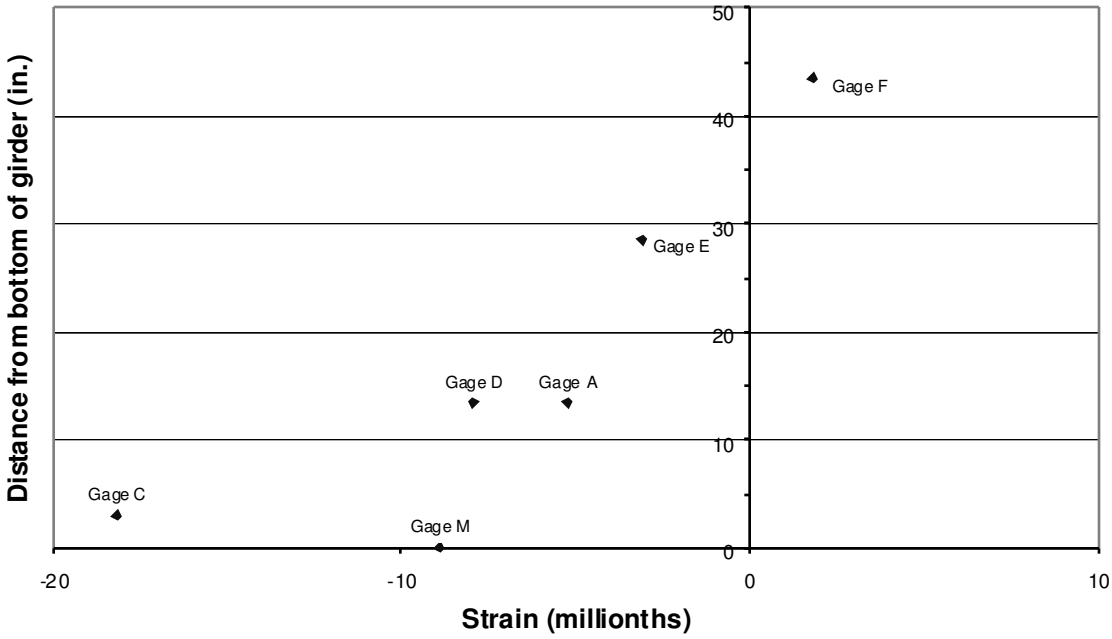


**Figure D-30:** A3 Span 11 Girder 8 Cross Section 2

### D.1.4 POSITION A4

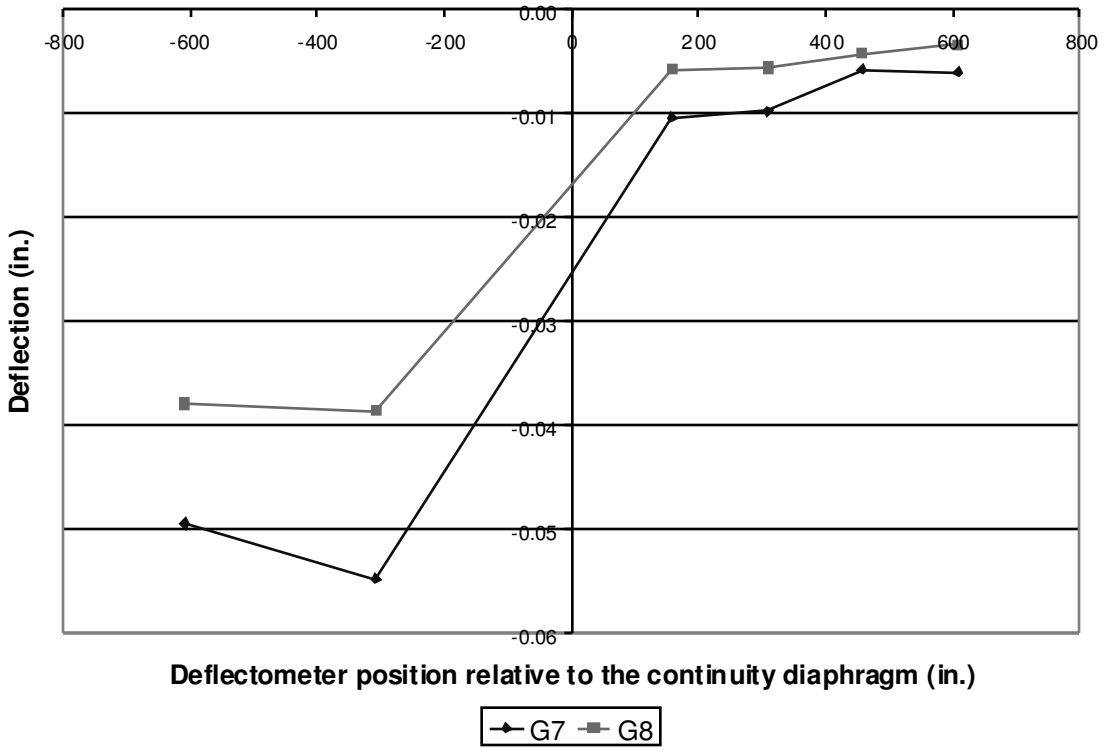


**Figure D-31:** A4 Deflections

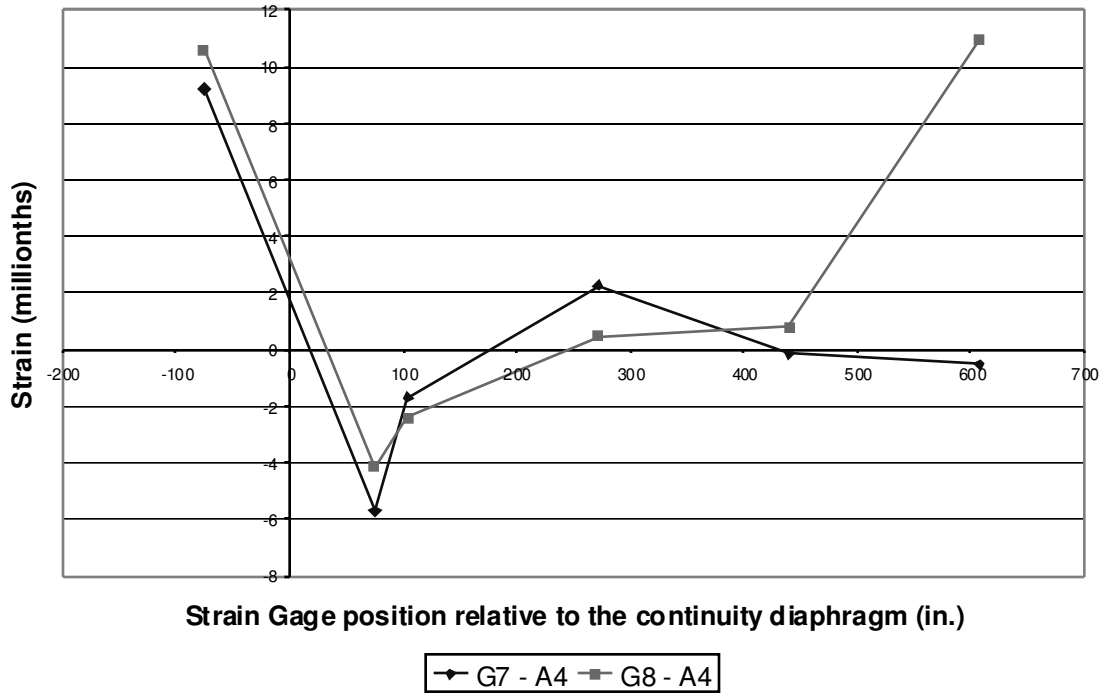


**Figure D-32:** A4 Bottom Fiber Strains

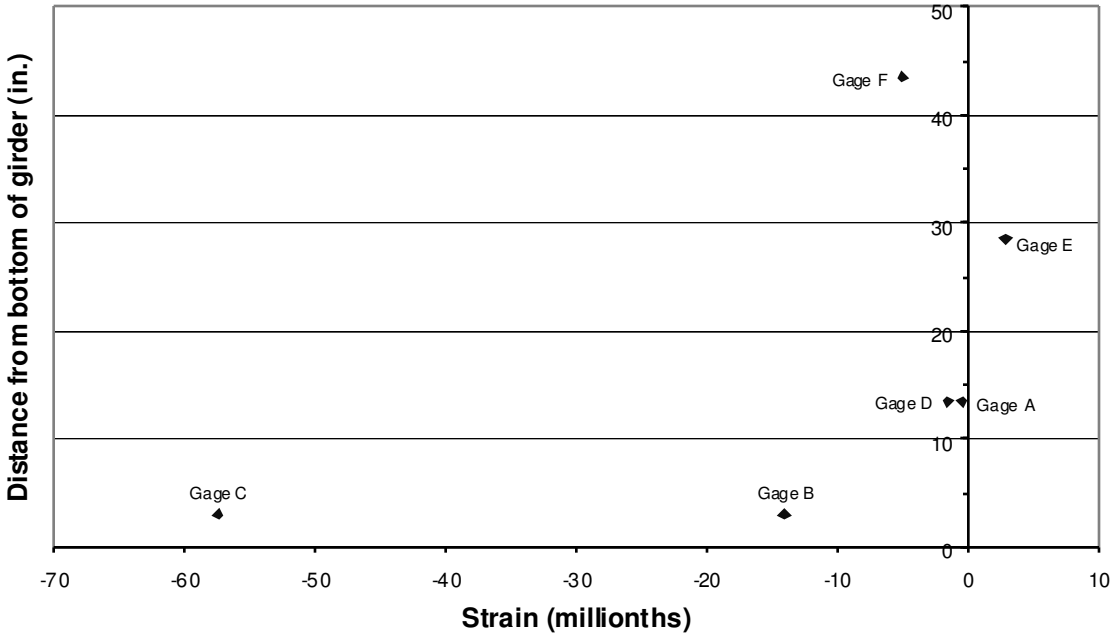


**Figure D-33:** A4 Span 10 Girder 7 Cross Section1

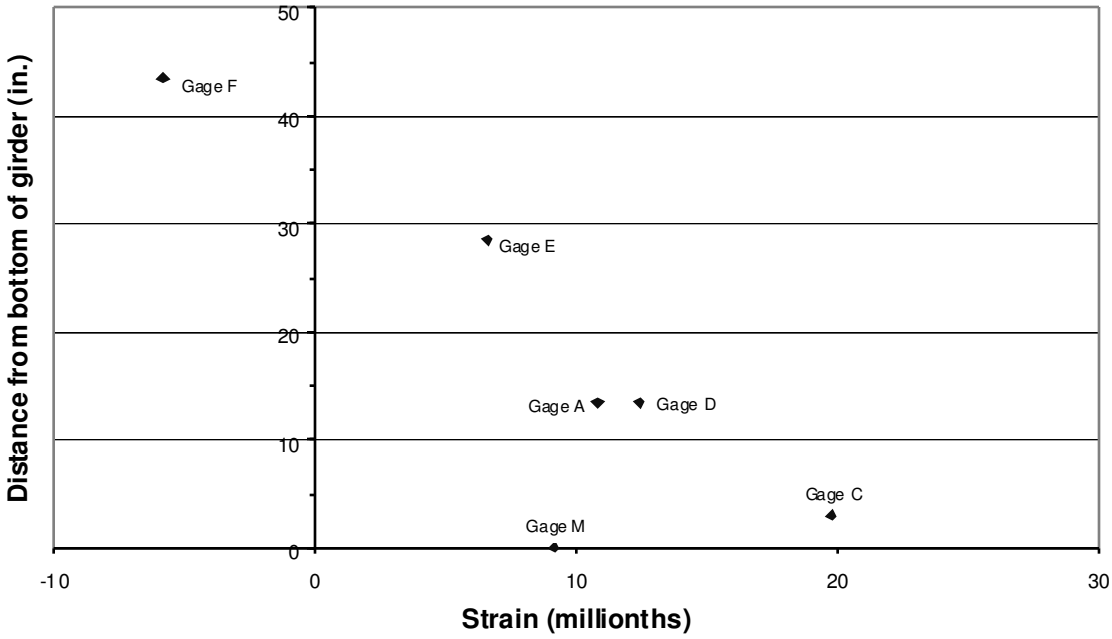


**Figure D-34:** A4 Span 10 Girder 7 Cross Section 2

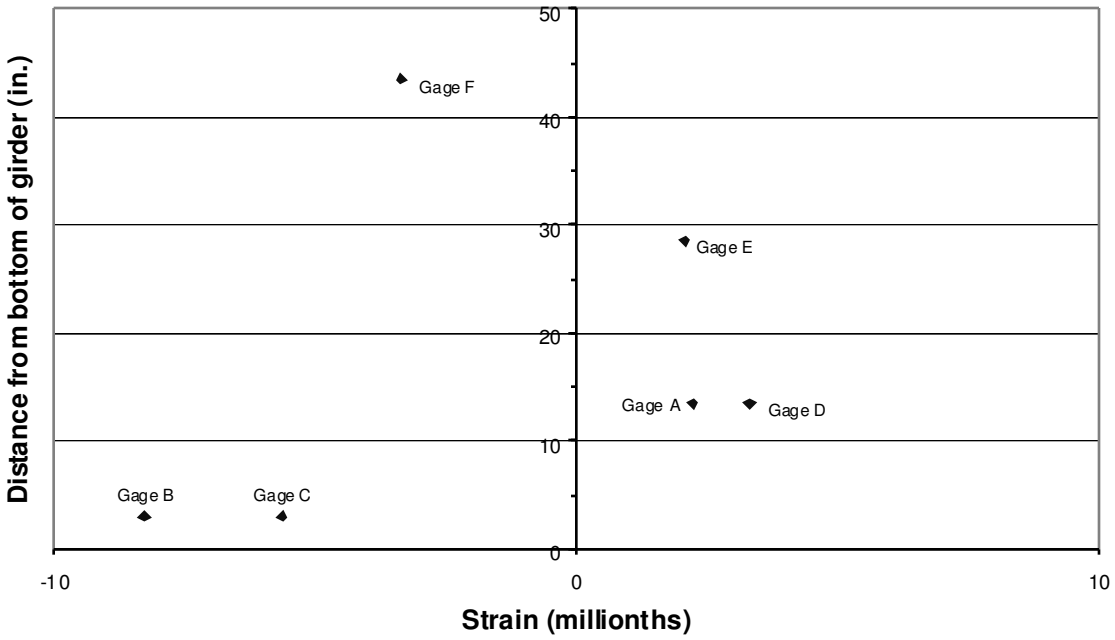


**Figure D-35:** A4 Span 10 Girder 8 Cross Section 1

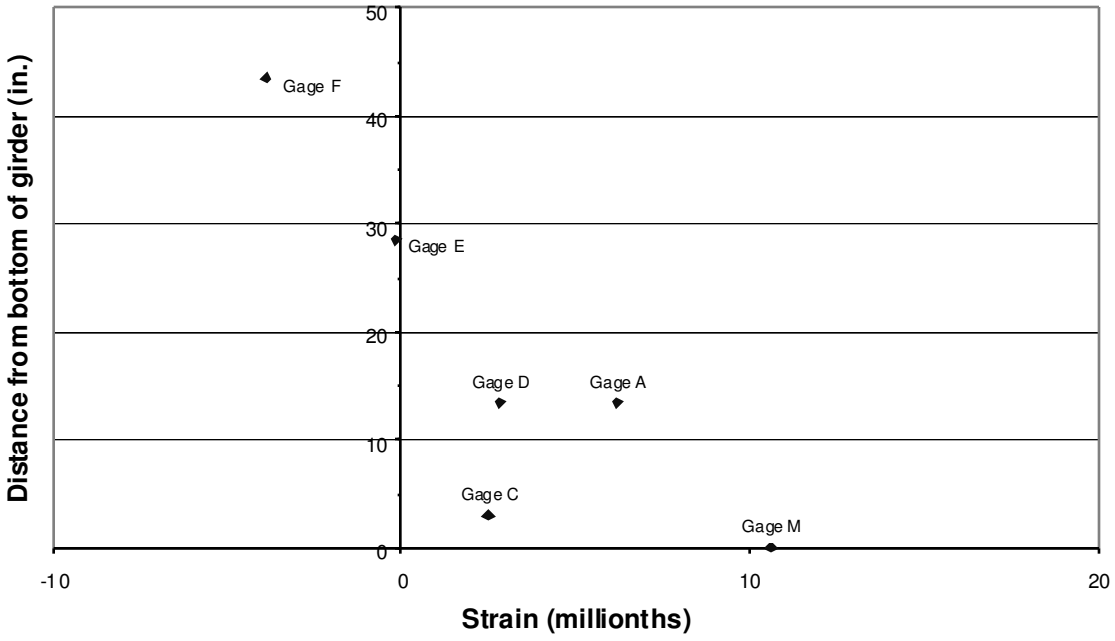


**Figure D-36:** A4 Span 10 Girder 8 Cross Section 2

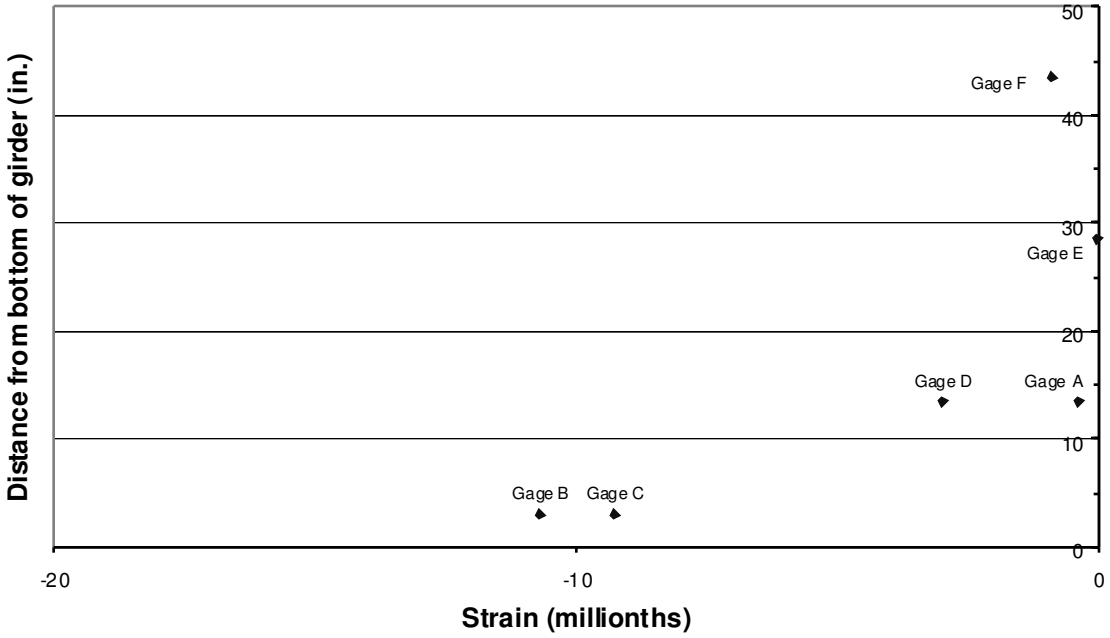


**Figure D-37:** A4 Span 11 Girder 7 Cross Section 1

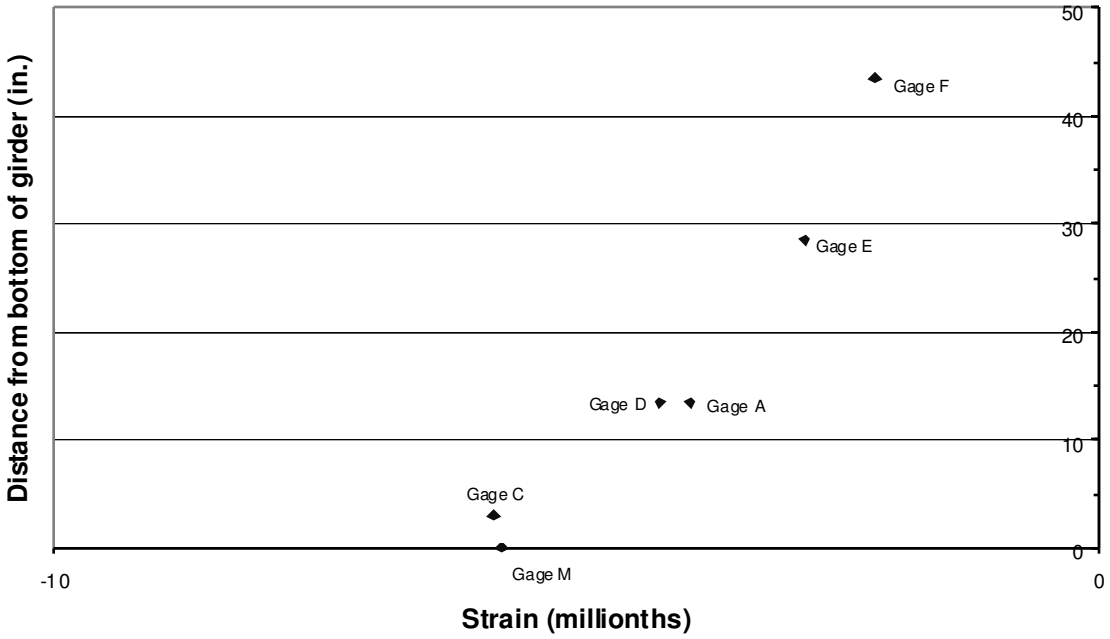


**Figure D-38:** A4 Span 11 Girder 7 Cross Section 2

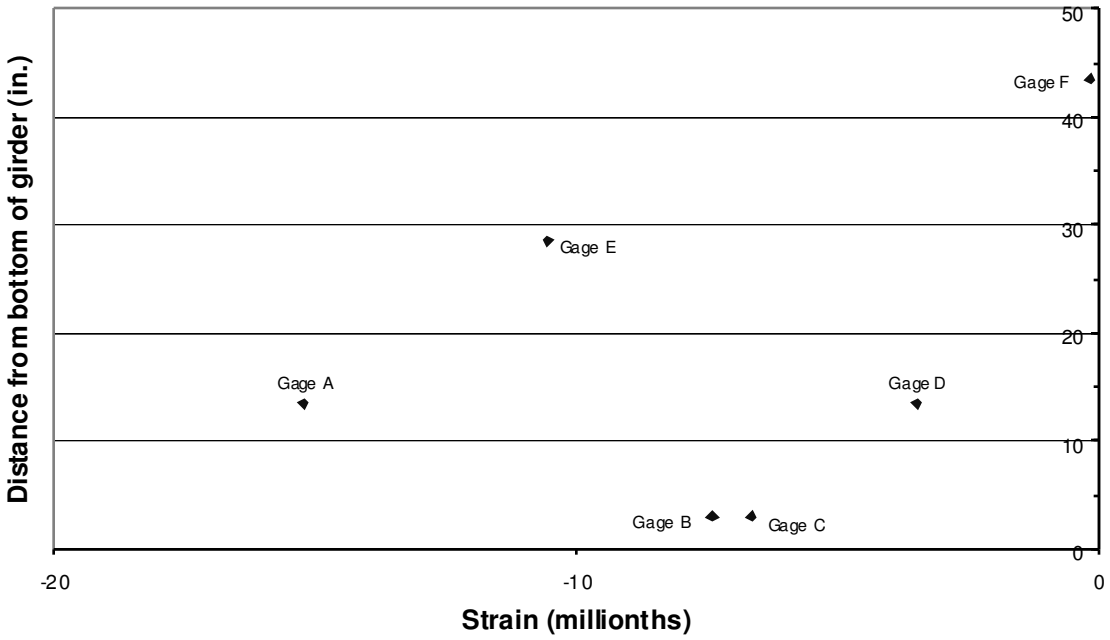


**Figure D-39:** A4 Span 11 Girder 8 Cross Section 1

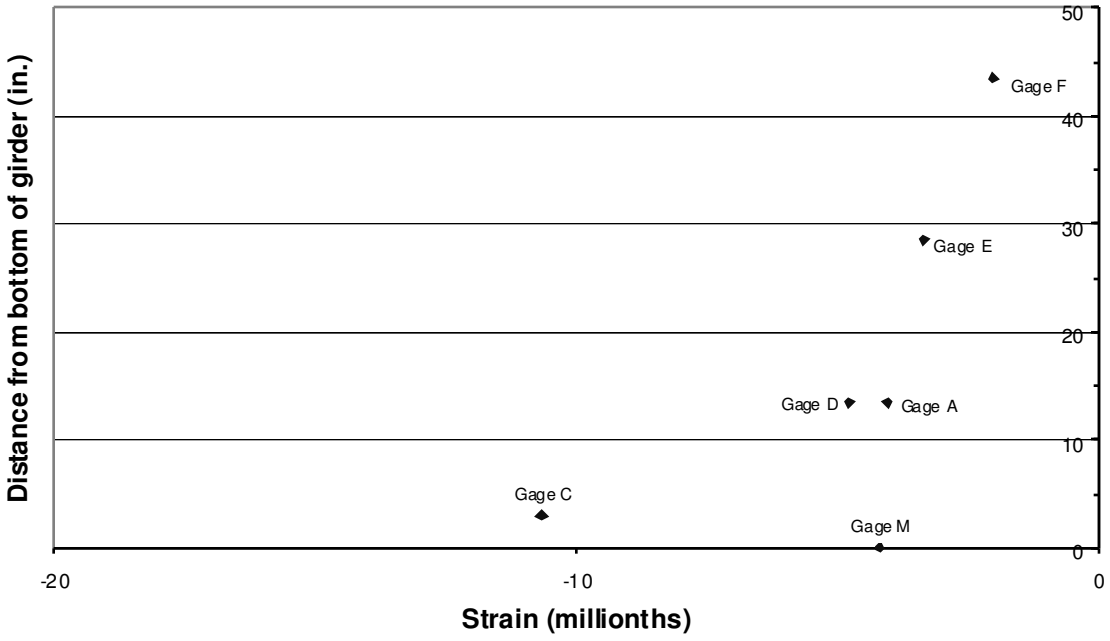


**Figure D-40:** A4 Span 11 Girder 8 Cross Section 2

### D.1.5 POSITION A5

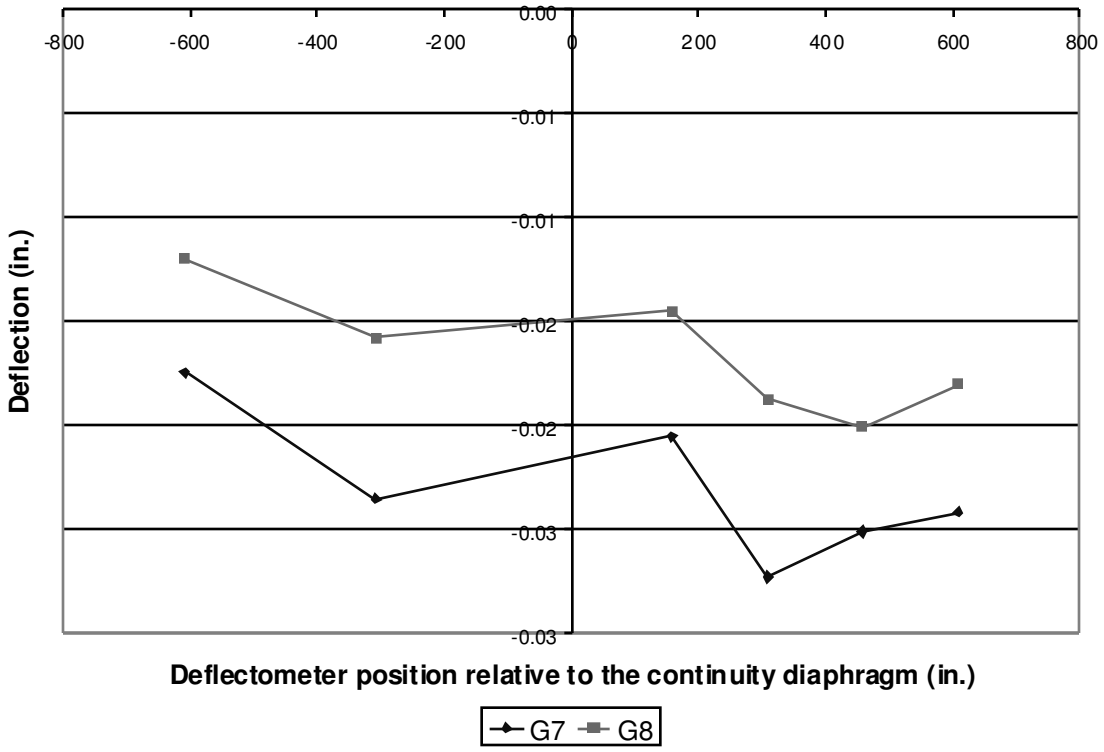


**Figure D-41:** A5 Deflections

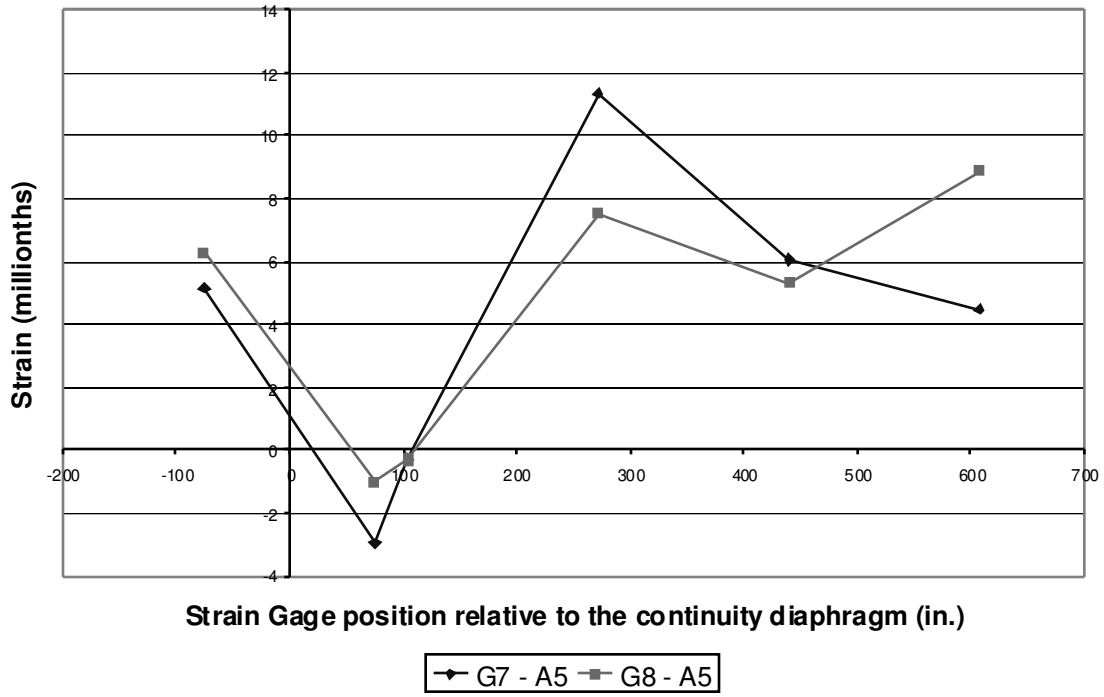


**Figure D-42:** A5 Bottom Fiber Strains

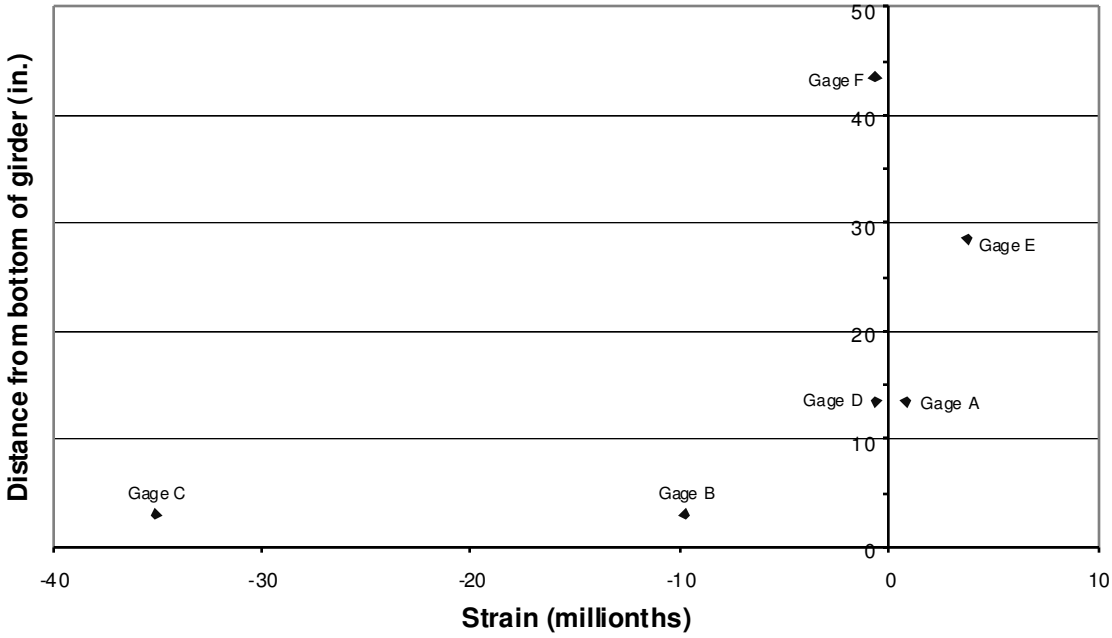


**Figure D-43:** A5 Span 10 Girder 7 Cross Section1

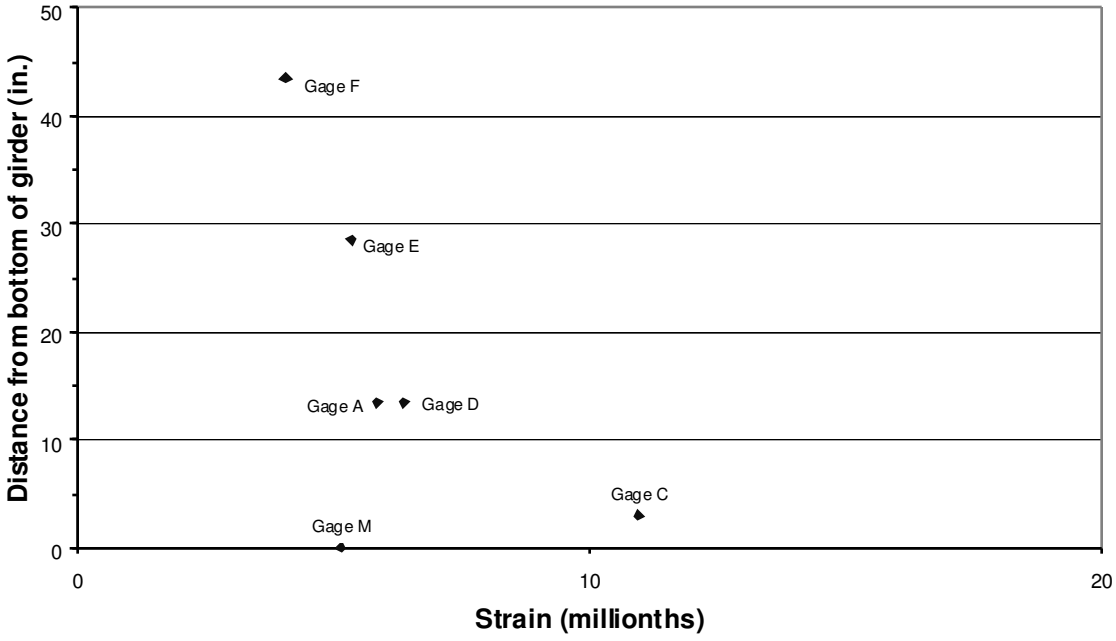


**Figure D-44:** A5 Span 10 Girder 7 Cross Section 2

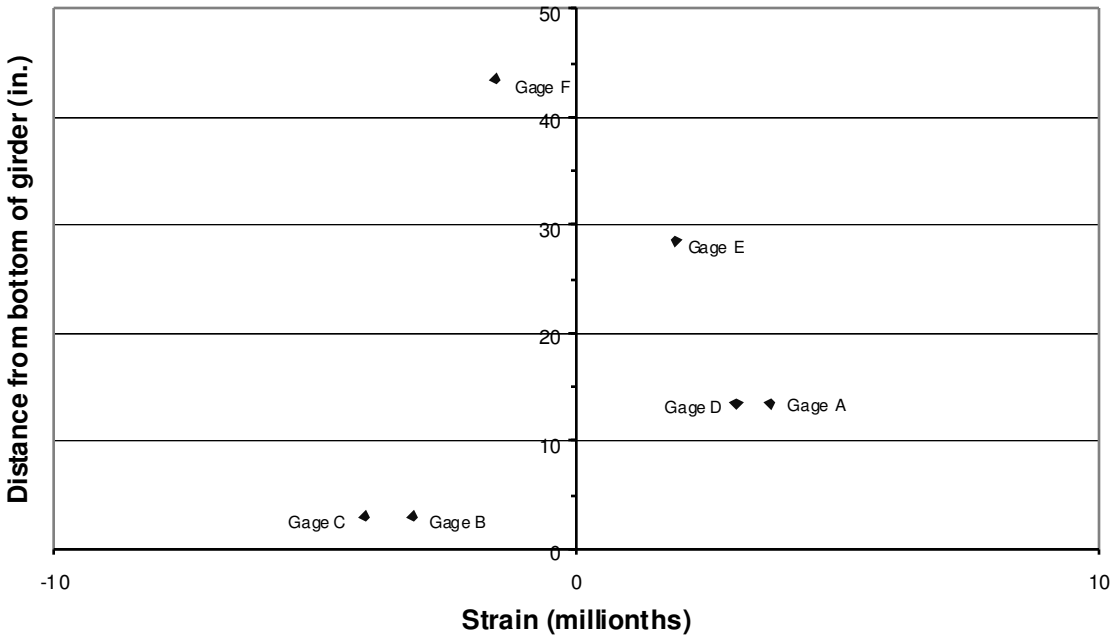


**Figure D-45:** A5 Span 10 Girder 8 Cross Section 1

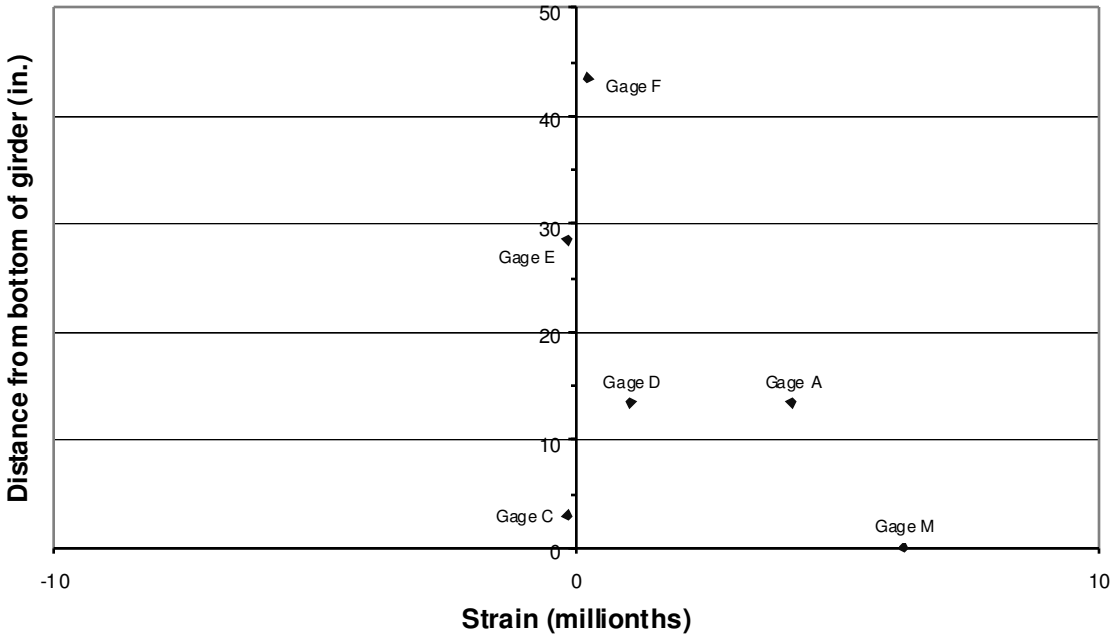


**Figure D-46:** A5 Span 10 Girder 8 Cross Section 2

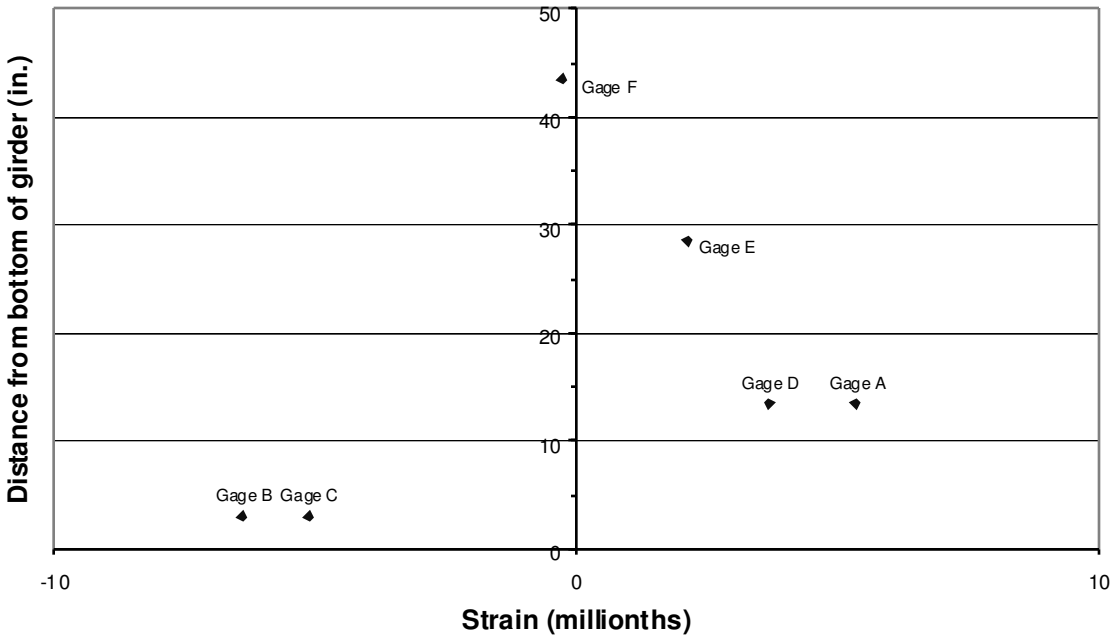


**Figure D-47:** A5 Span 11 Girder 7 Cross Section 1

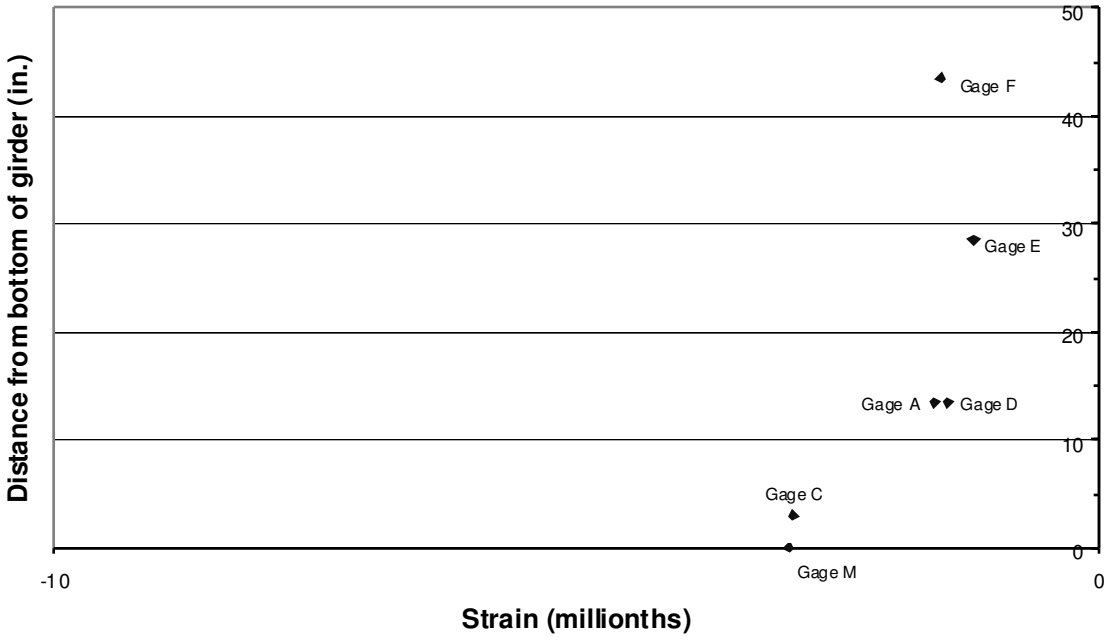


**Figure D-48:** A5 Span 11 Girder 7 Cross Section 2

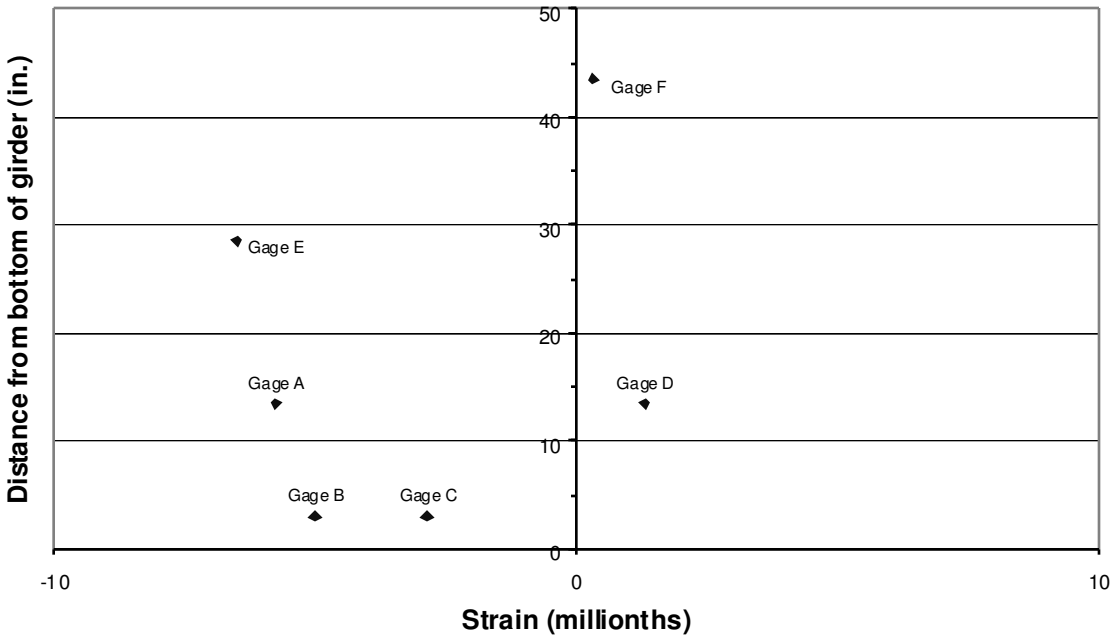


**Figure D-49:** A5 Span 11 Girder 8 Cross Section 1

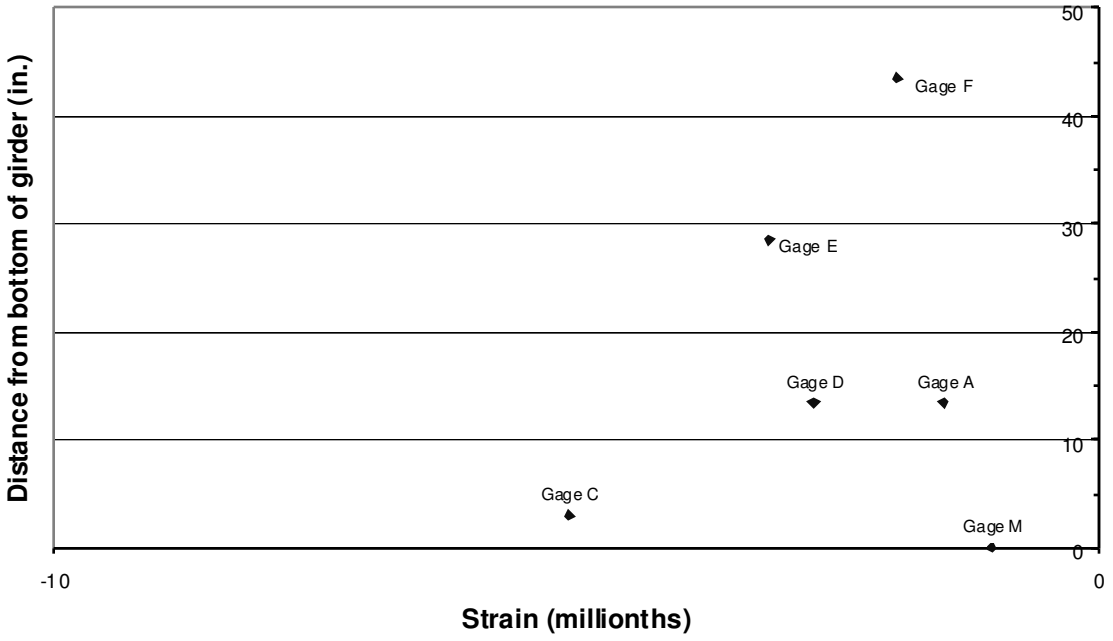


**Figure D-50:** A5 Span 11 Girder 8 Cross Section 2

### D.1.6 POSITION A6

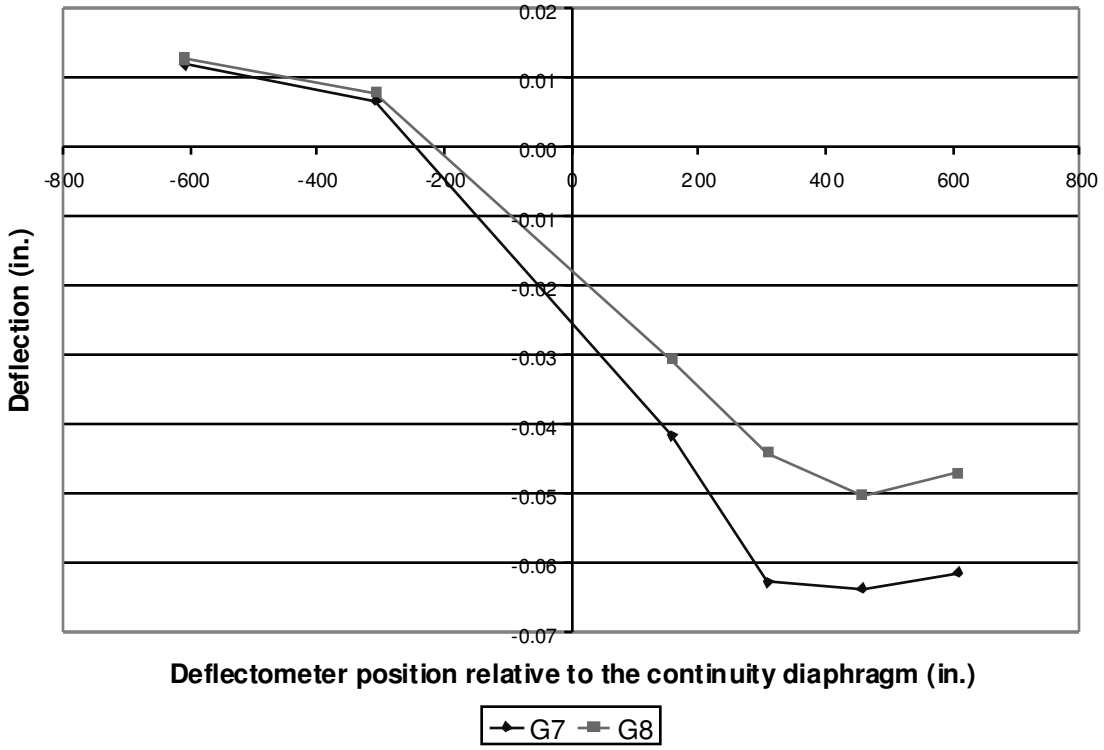


**Figure D-51:** A6 Deflections

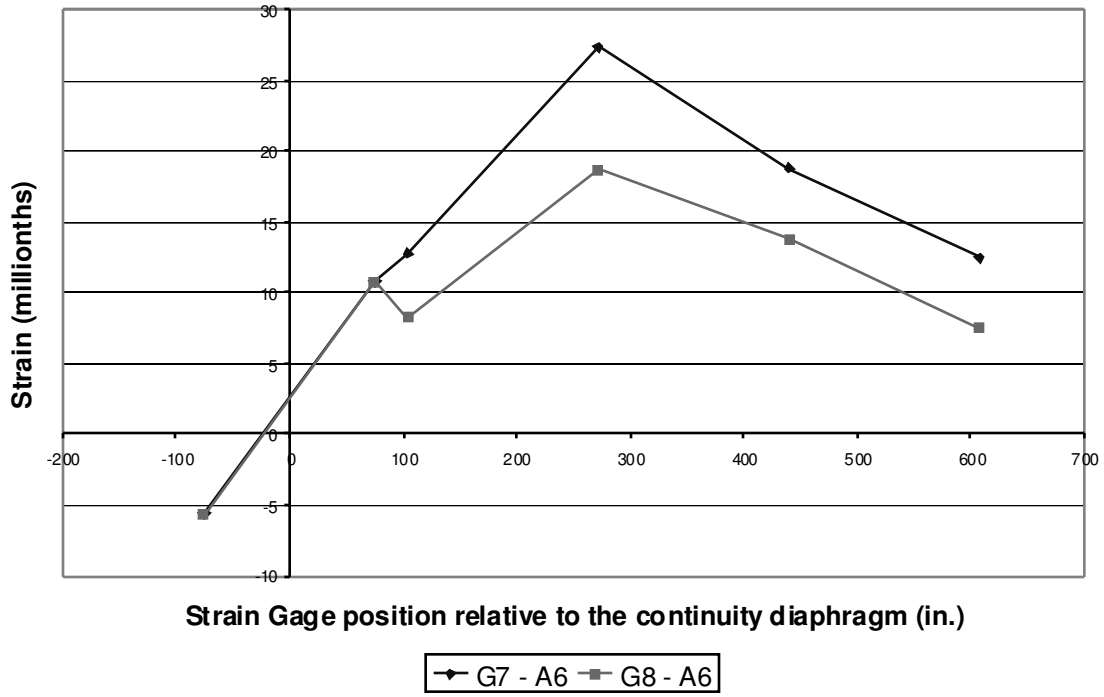


**Figure D-52:** A6 Bottom Fiber Strains

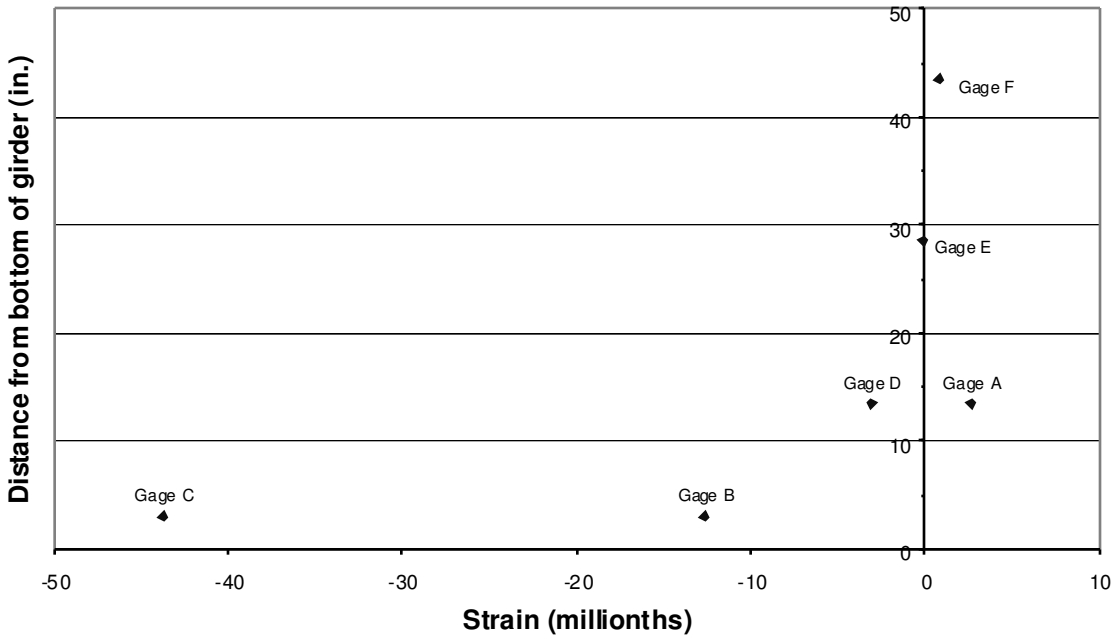


**Figure D-53:** A6 Span 10 Girder 7 Cross Section1

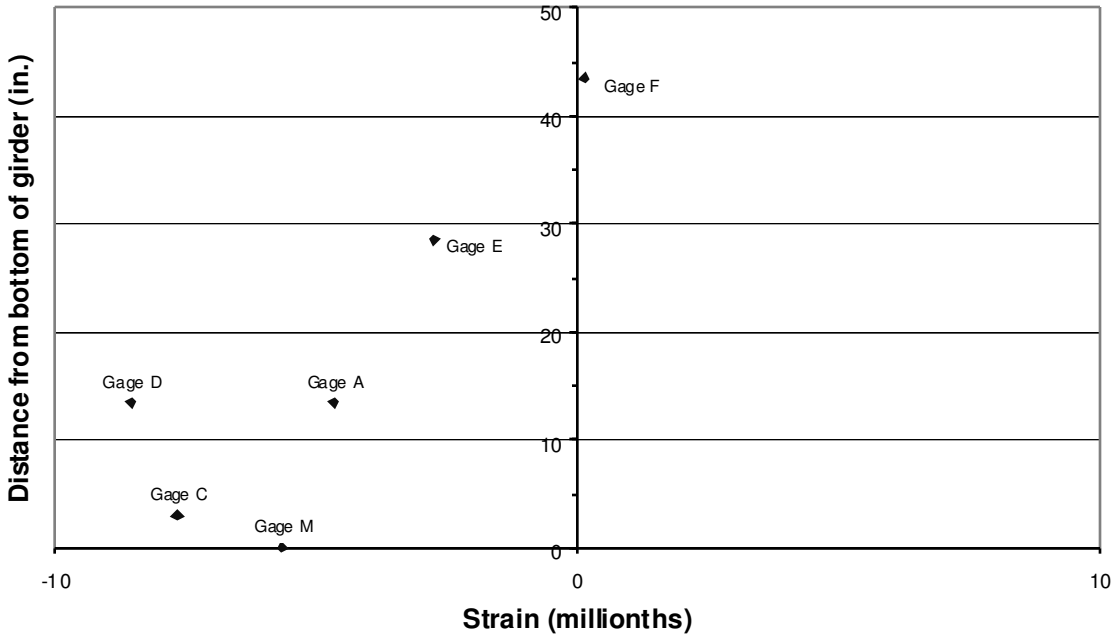


**Figure D-54:** A6 Span 10 Girder 7 Cross Section 2

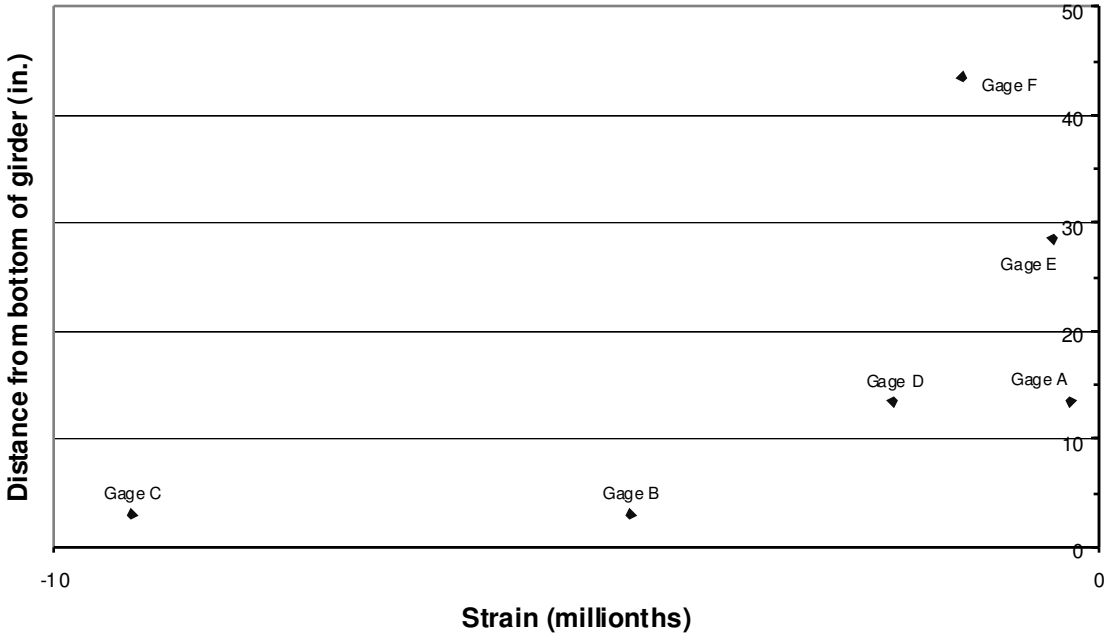


**Figure D-55:** A6 Span 10 Girder 8 Cross Section 1

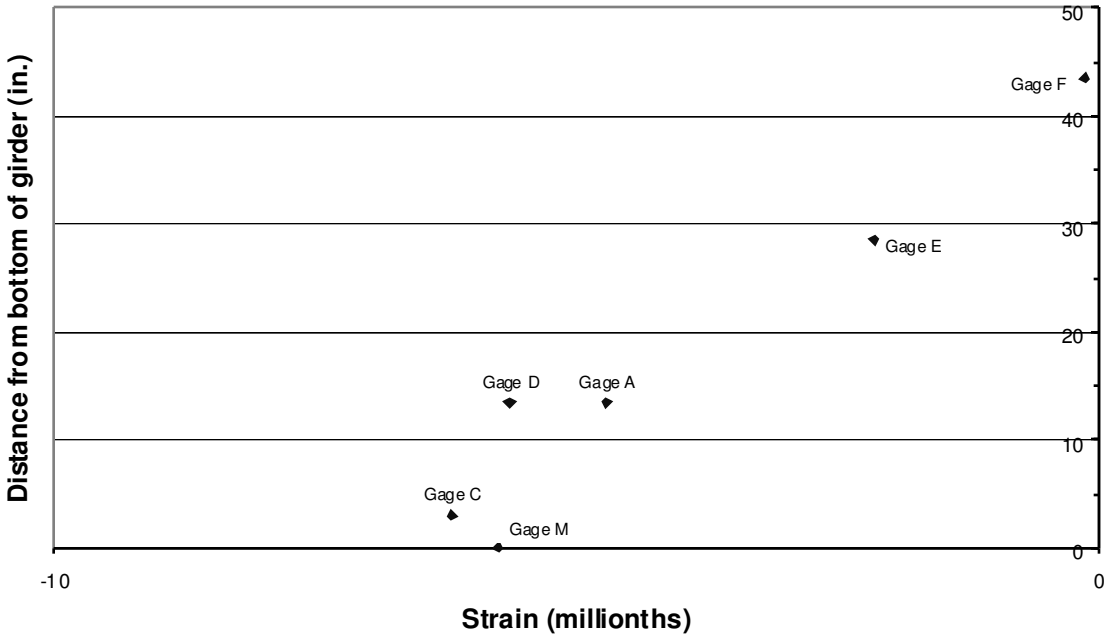


**Figure D-56:** A6 Span 10 Girder 8 Cross Section 2

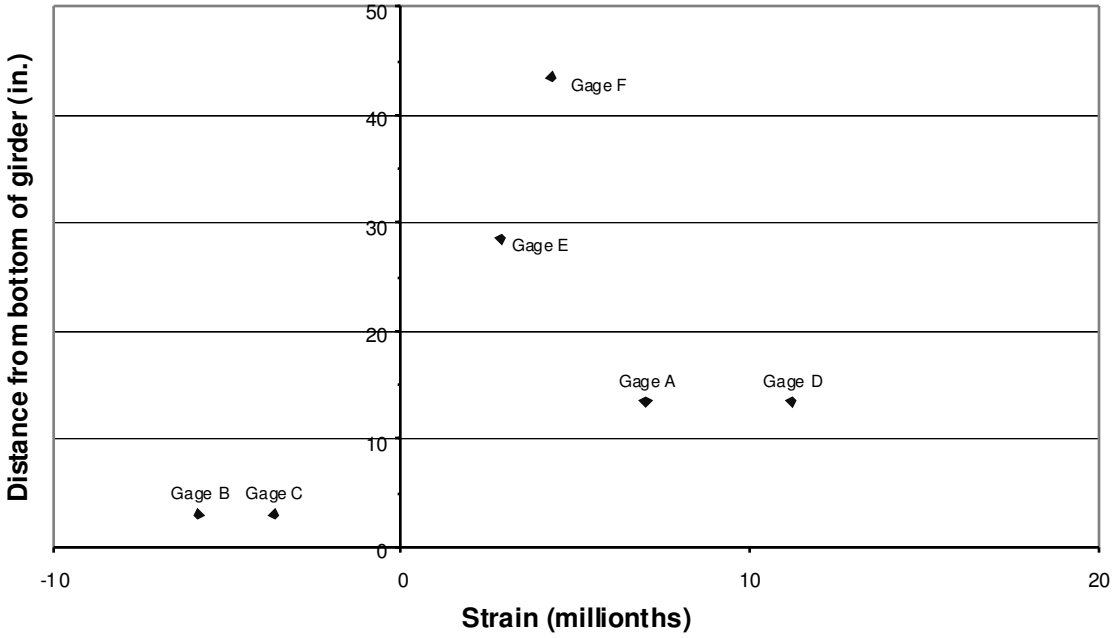


**Figure D-57:** A6 Span 11 Girder 7 Cross Section 1

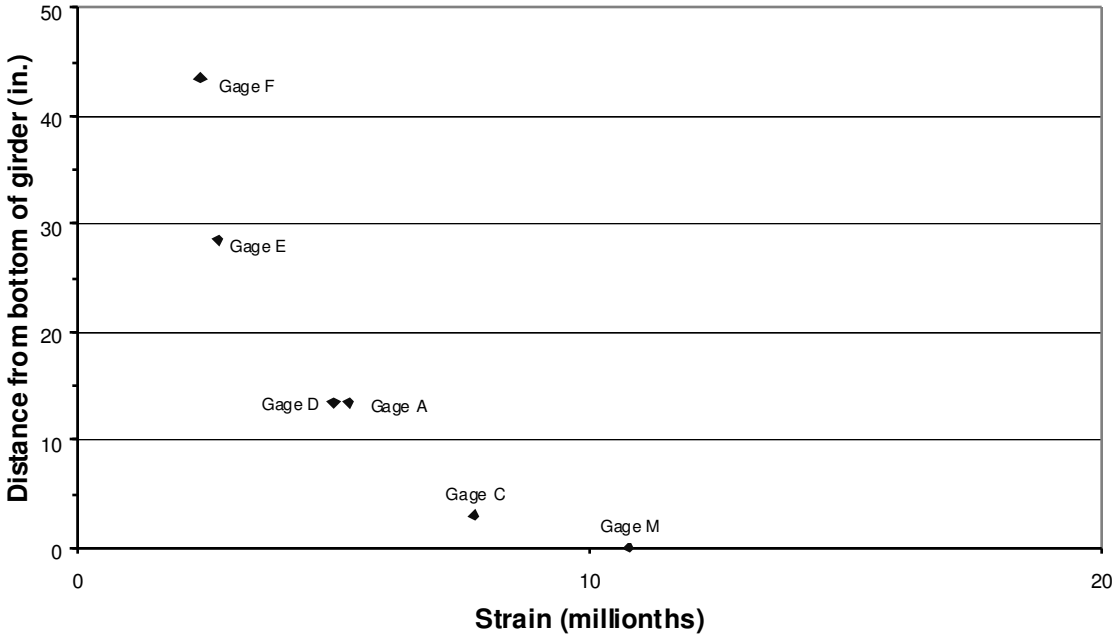


**Figure D-58:** A6 Span 11 Girder 7 Cross Section 2

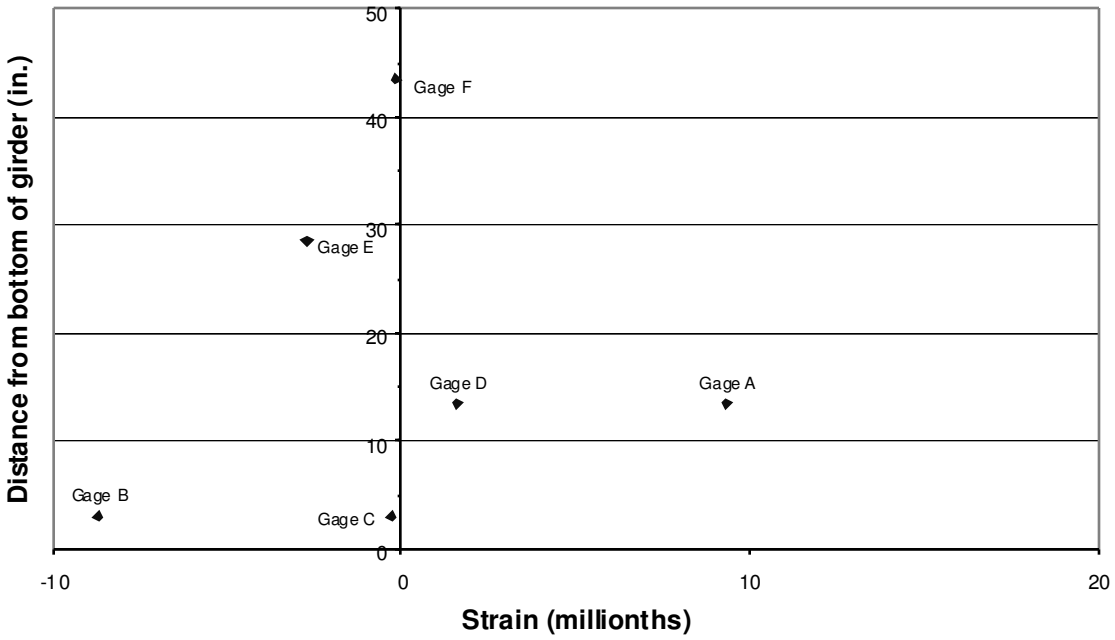


**Figure D-59:** A6 Span 11 Girder 8 Cross Section 1

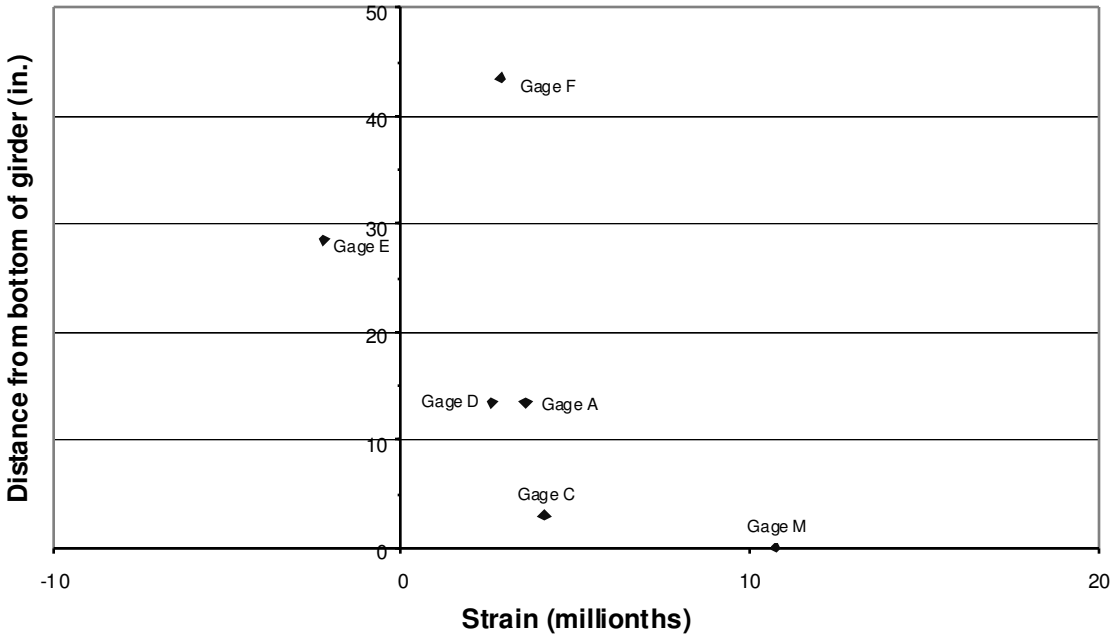


**Figure D-60:** A6 Span 11 Girder 8 Cross Section 2

### D.1.7 POSITION A7

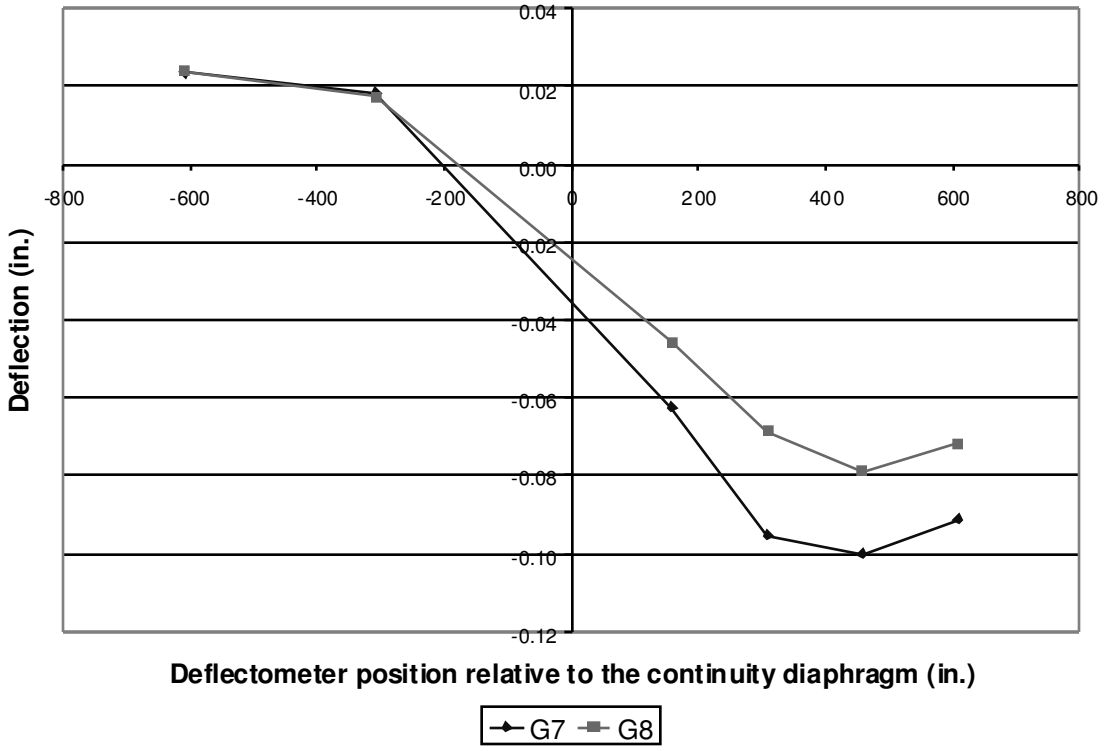


**Figure D-61:** A7 Deflections

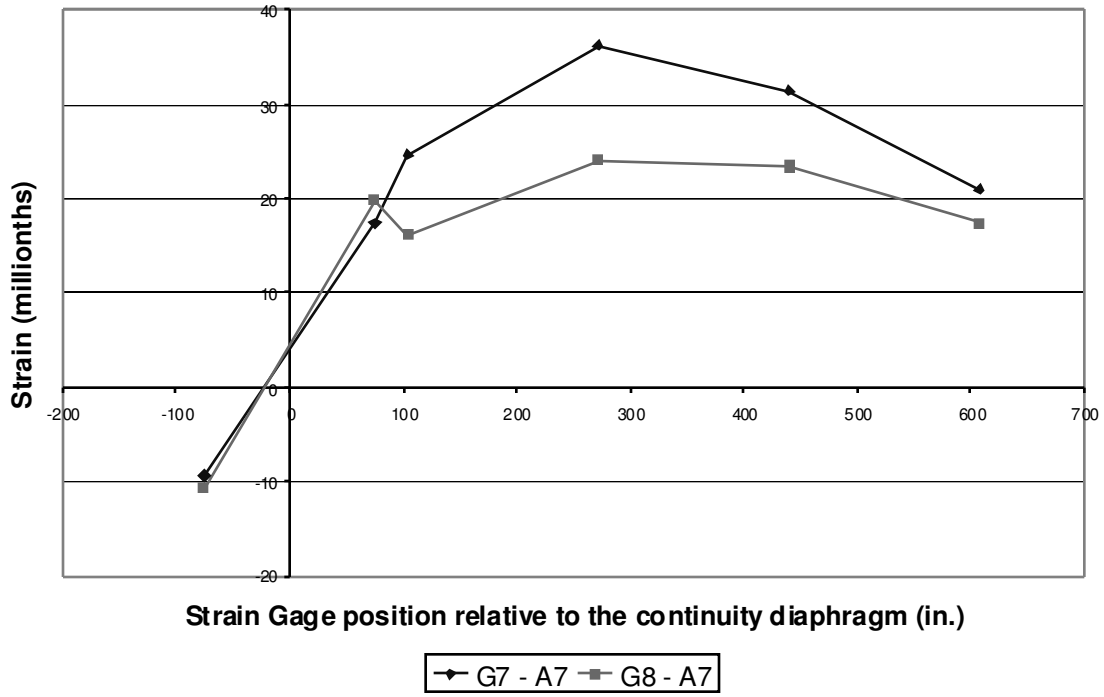


**Figure D-62:** A7 Bottom Fiber Strains

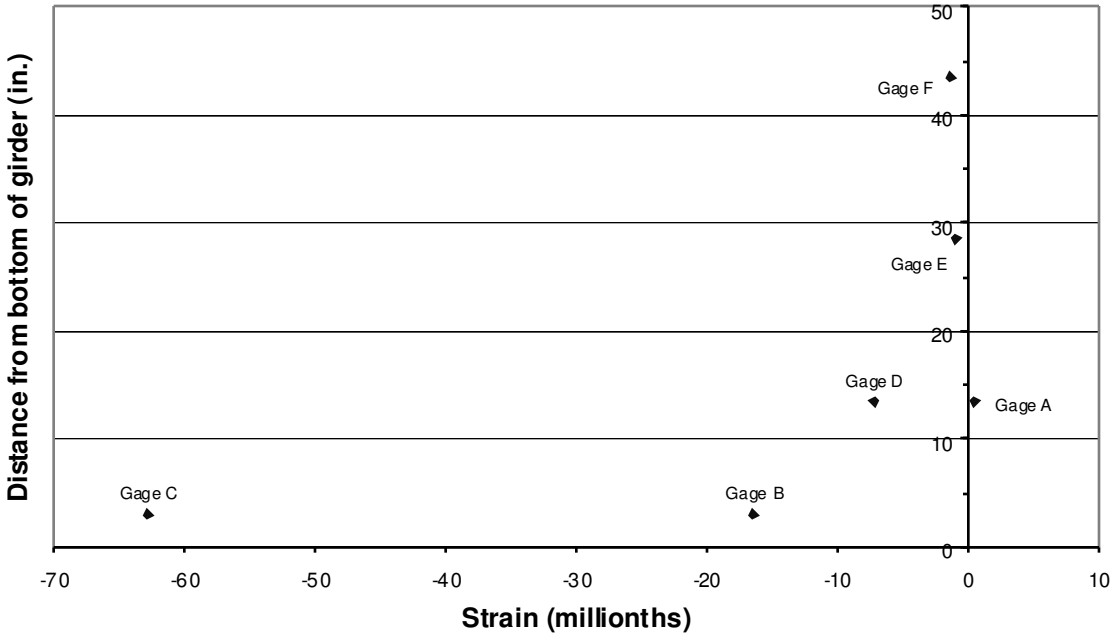


**Figure D-63:** A7 Span 10 Girder 7 Cross Section1

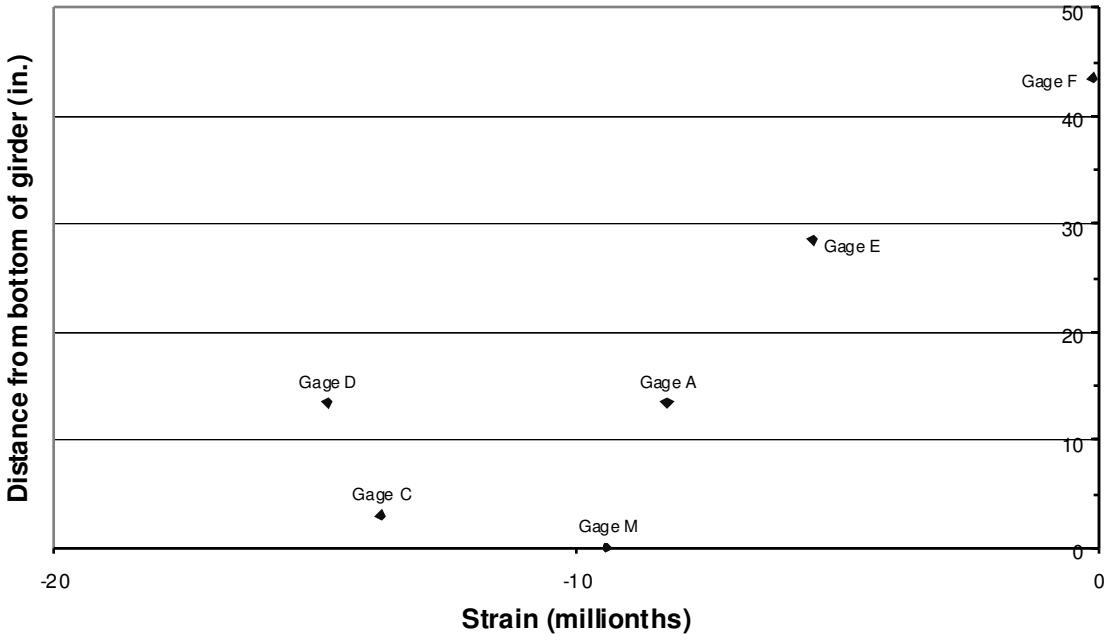


**Figure D-64:** A7 Span 10 Girder 7 Cross Section 2

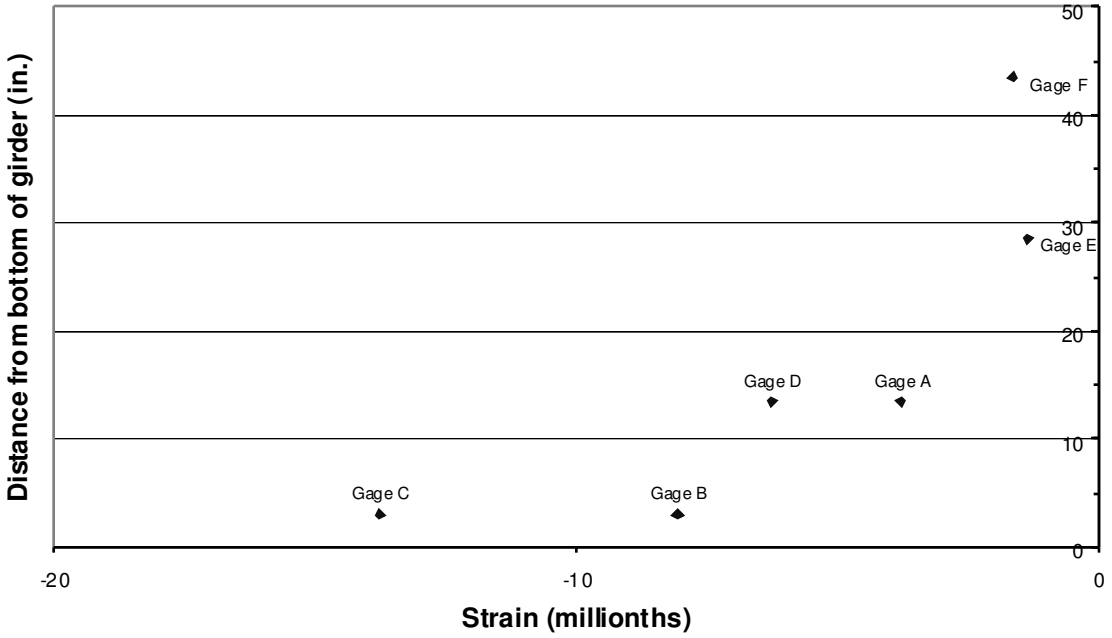


**Figure D-65:** A7 Span 10 Girder 8 Cross Section 1

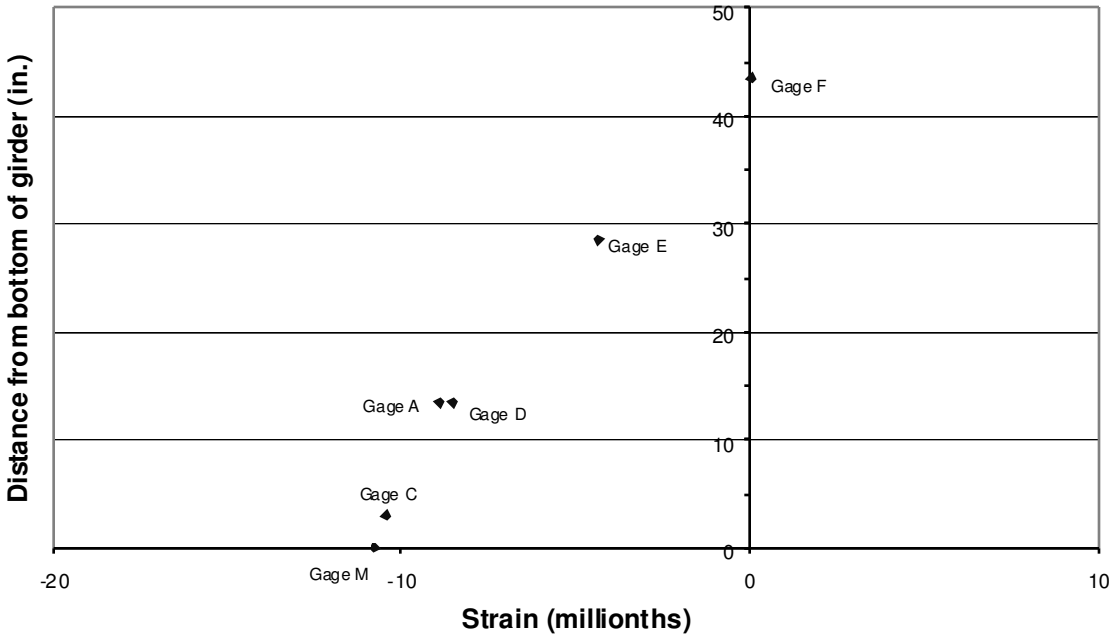


**Figure D-66:** A7 Span 10 Girder 8 Cross Section 2

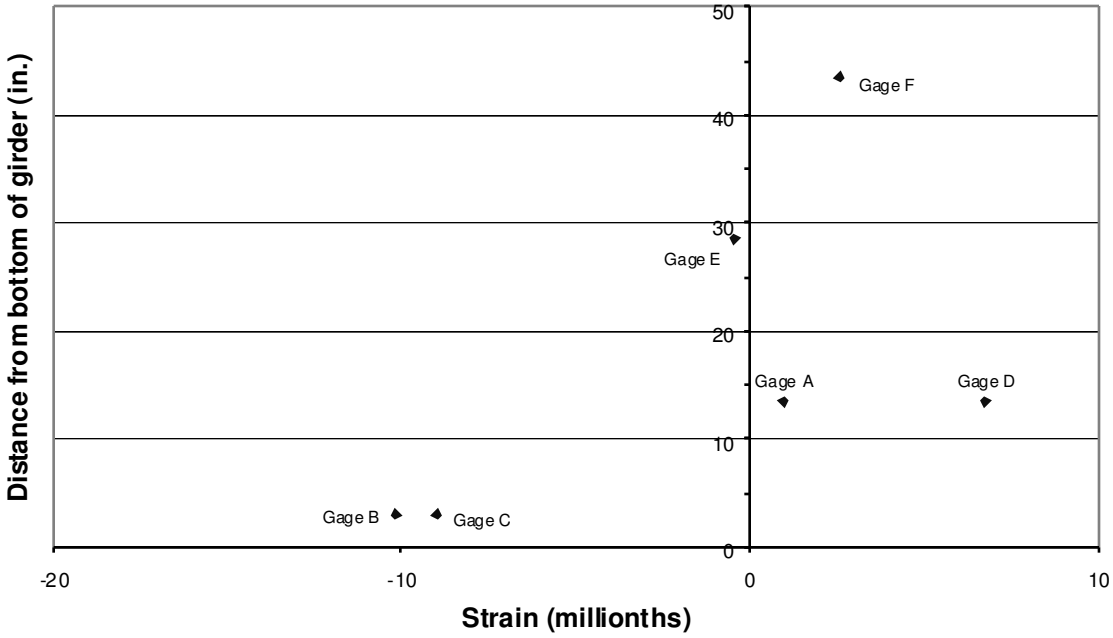


**Figure D-67:** A7 Span 11 Girder 7 Cross Section 1

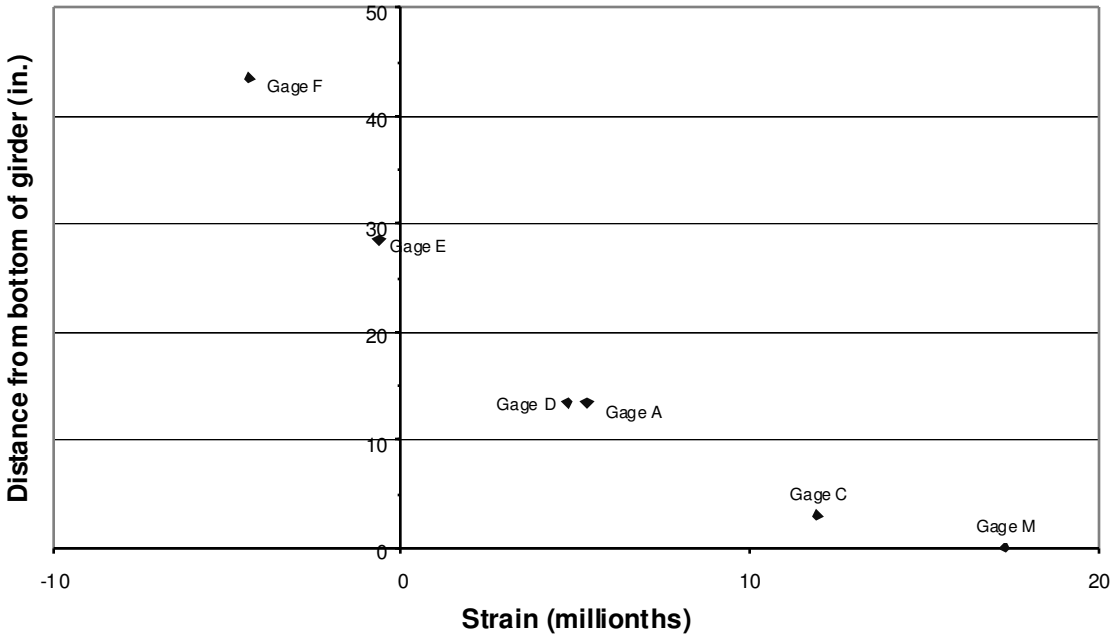


**Figure D-68:** A7 Span 11 Girder 7 Cross Section 2

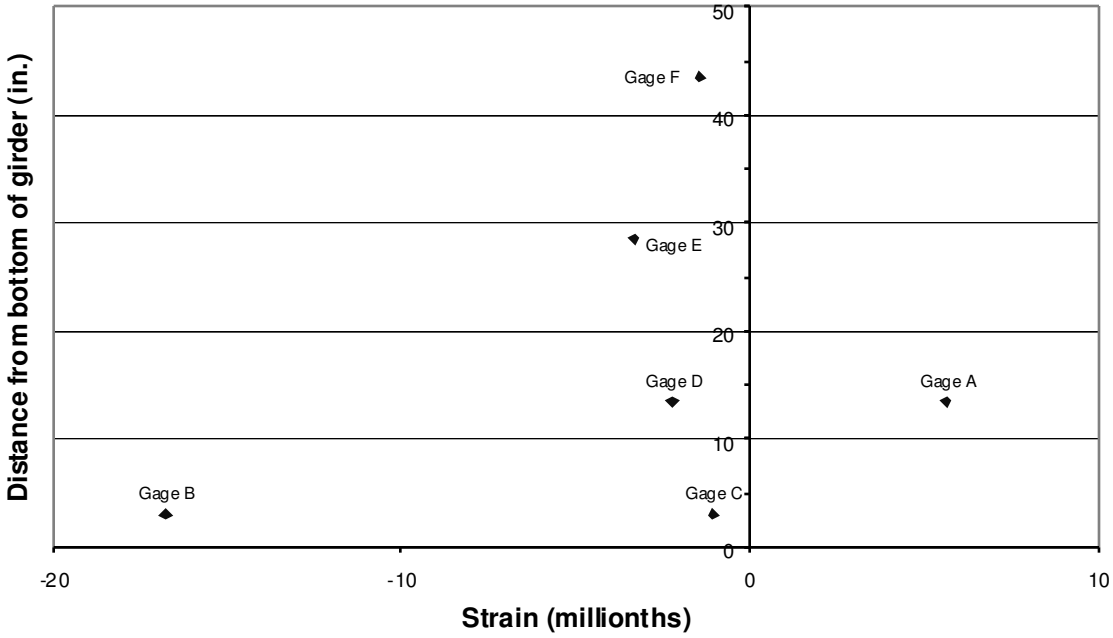


**Figure D-69:** A7 Span 11 Girder 8 Cross Section 1

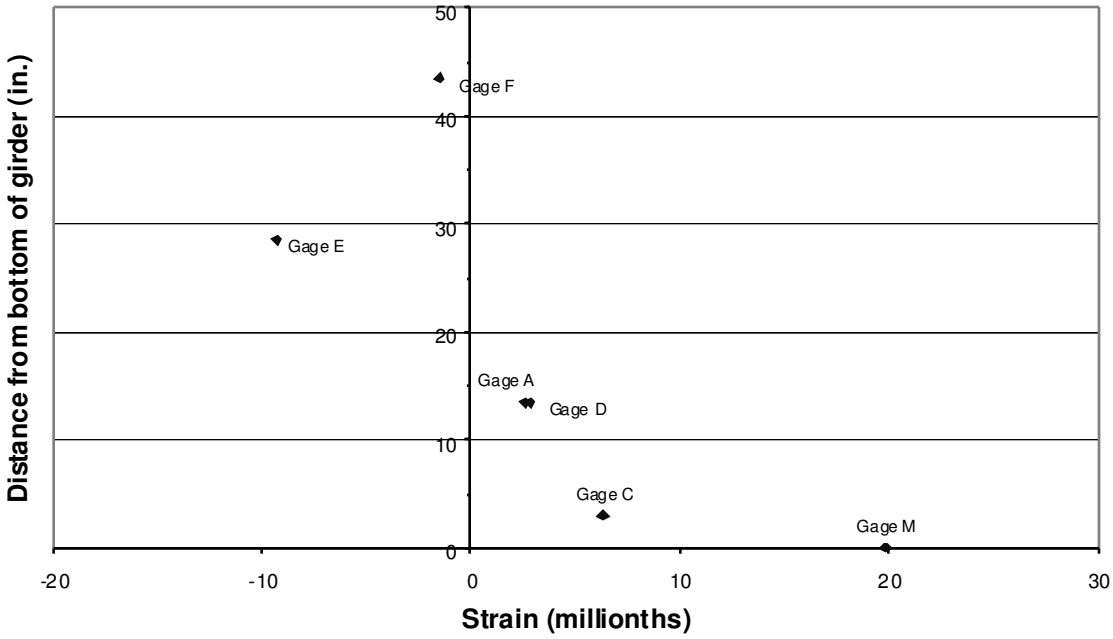


**Figure D-70:** A7 Span 11 Girder 8 Cross Section 2

### D.1.8 POSITION A8

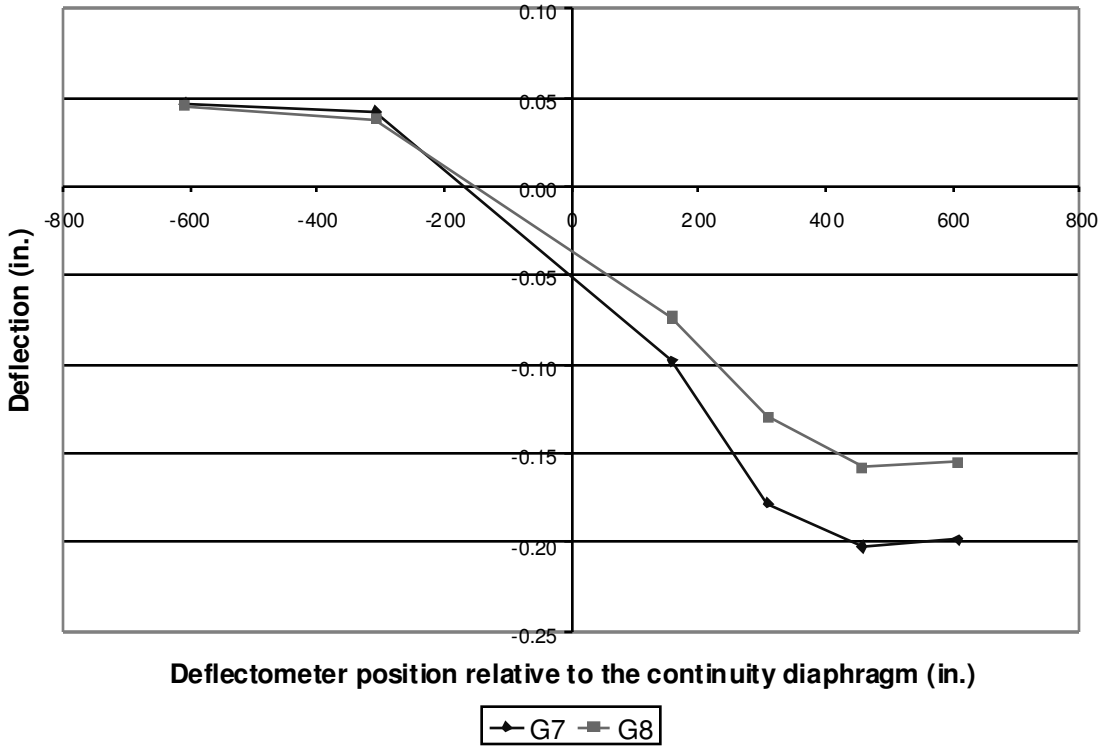


**Figure D-71:** A8 Deflections

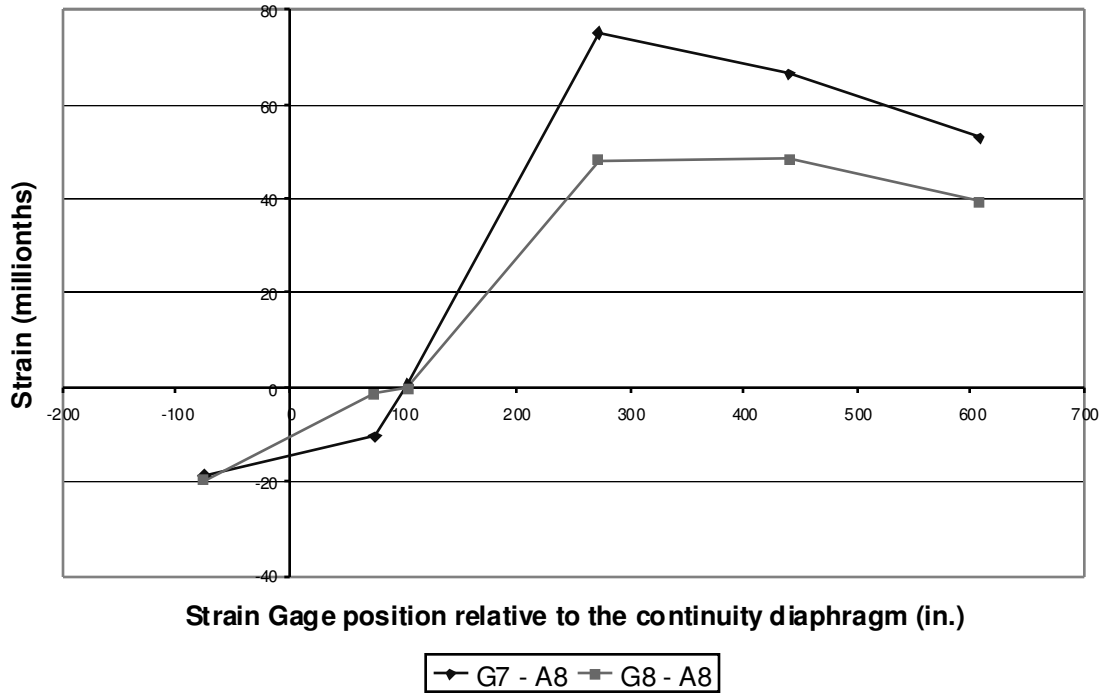


**Figure D-72:** A8 Bottom Fiber Strains

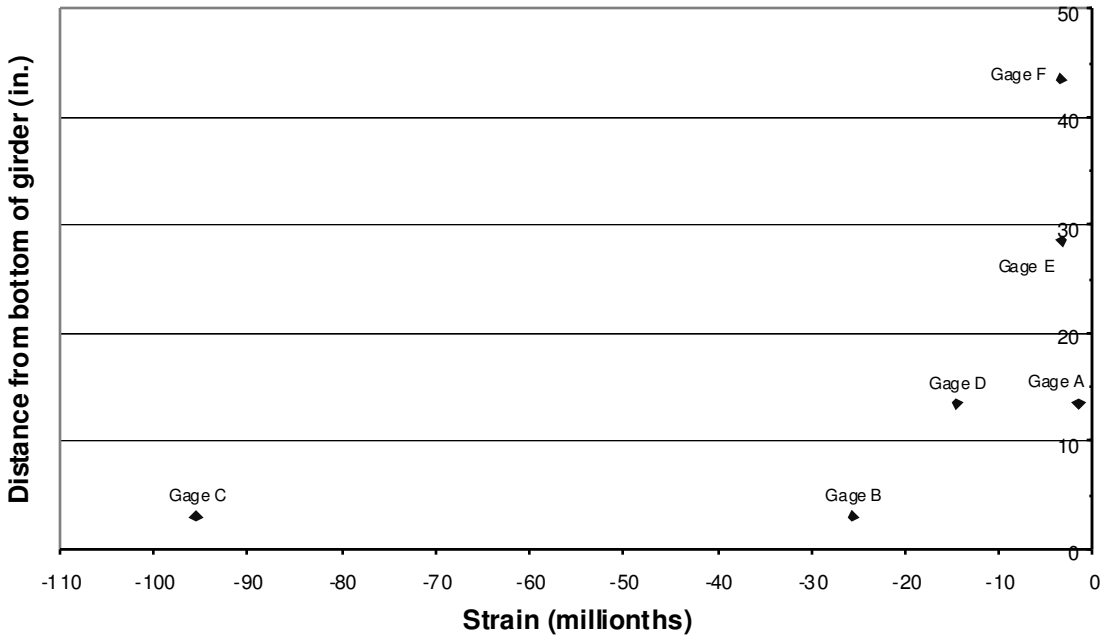


**Figure D-73:** A8 Span 10 Girder 7 Cross Section1

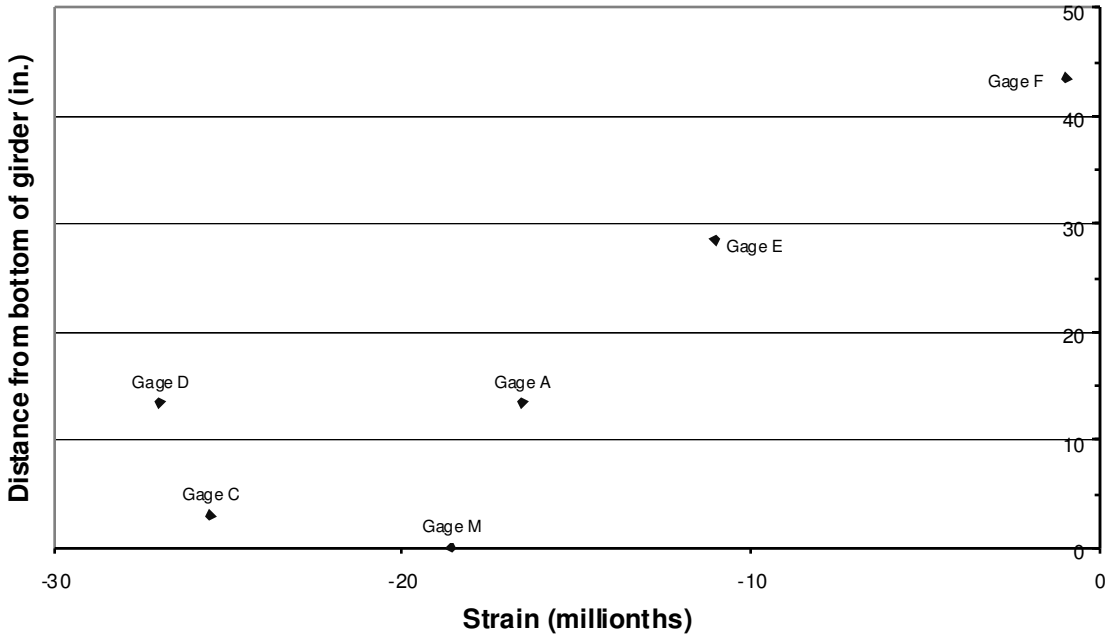


**Figure D-74:** A8 Span 10 Girder 7 Cross Section 2

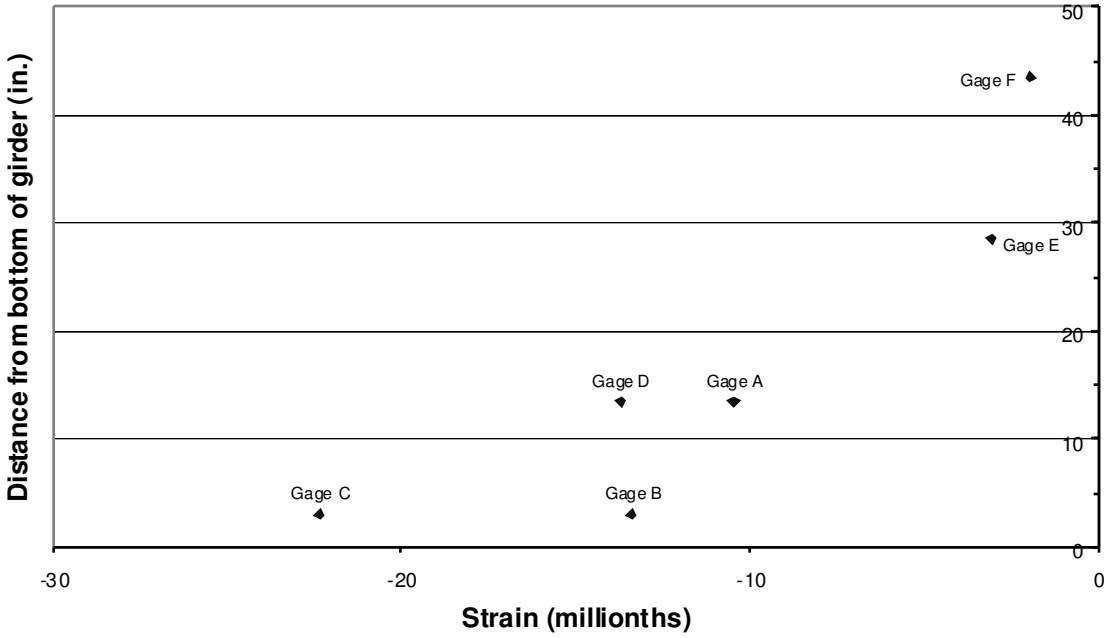


**Figure D-75:** A8 Span 10 Girder 8 Cross Section 1

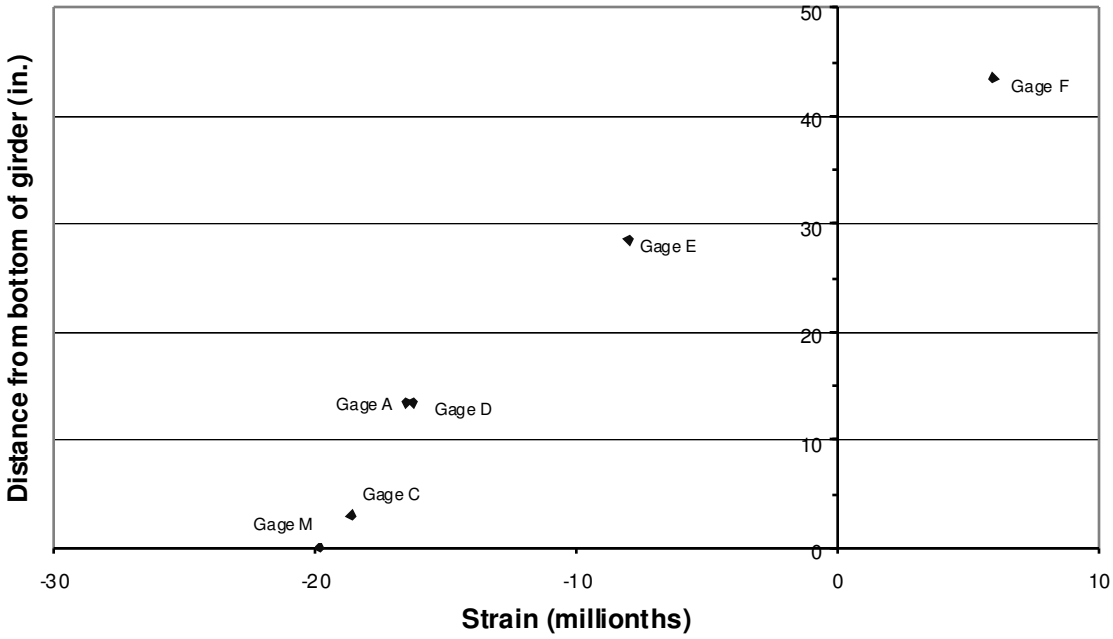


**Figure D-76:** A8 Span 10 Girder 8 Cross Section 2

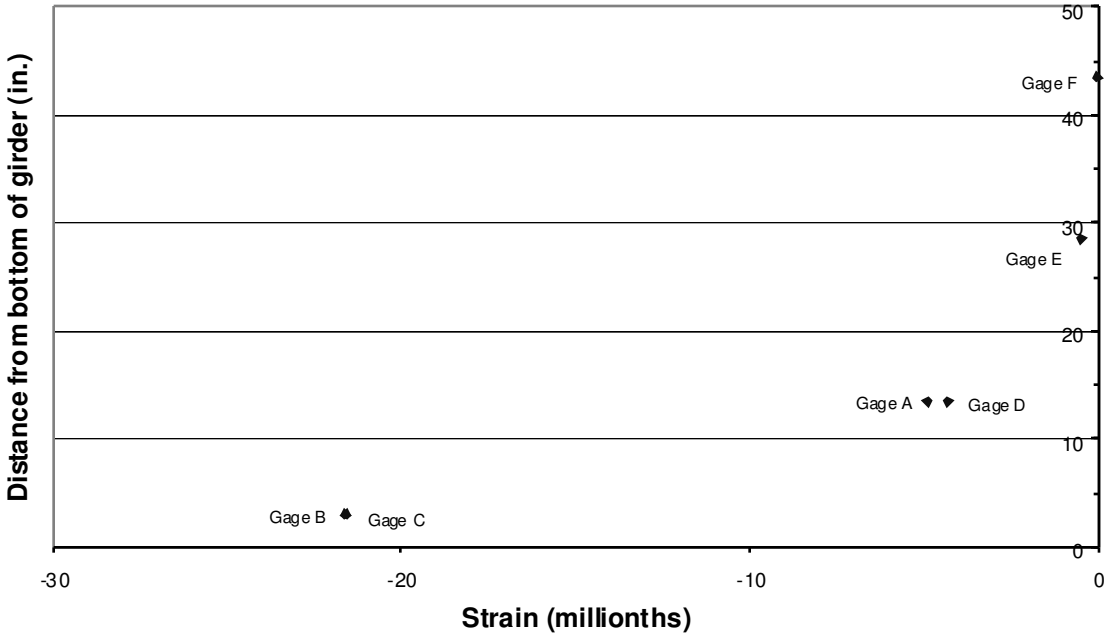


**Figure D-77:** A8 Span 11 Girder 7 Cross Section 1

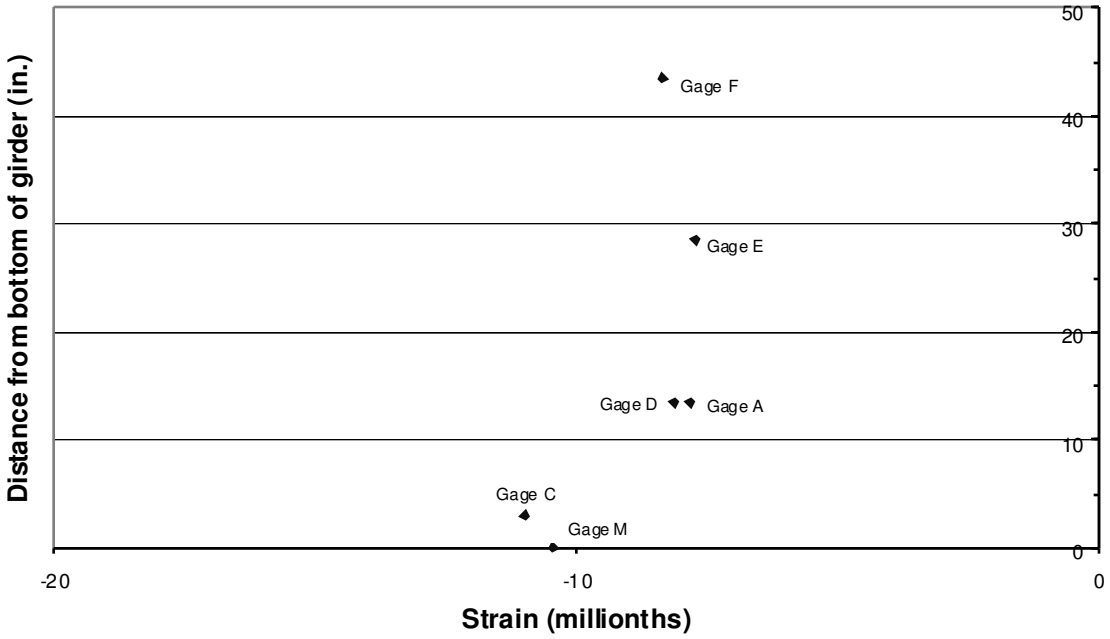


**Figure D-78:** A8 Span 11 Girder 7 Cross Section 2

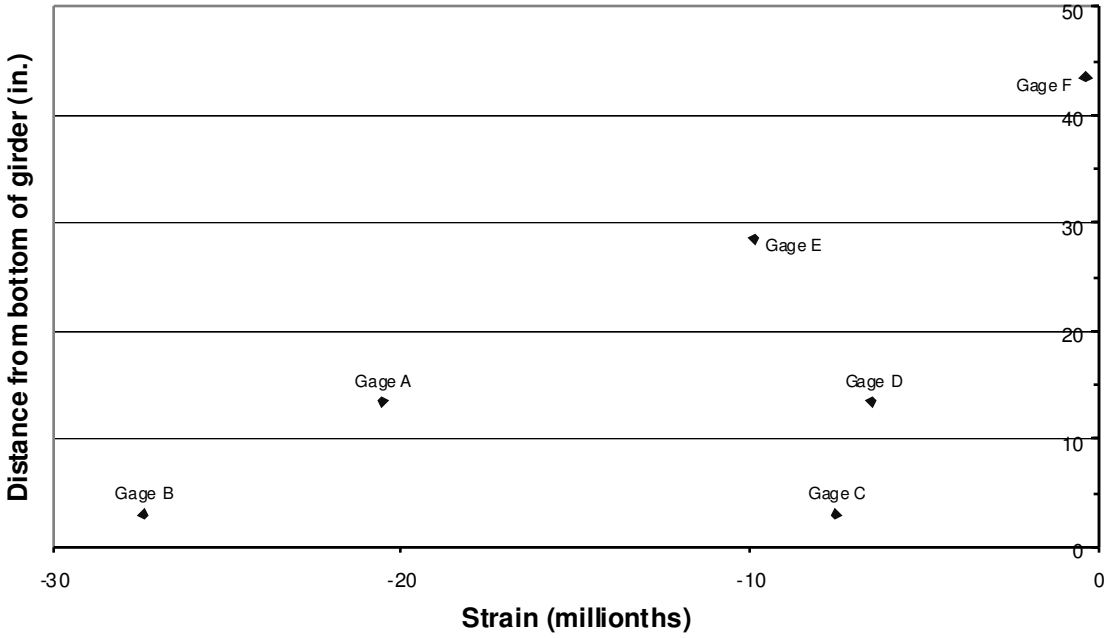


**Figure D-79:** A8 Span 11 Girder 8 Cross Section 1

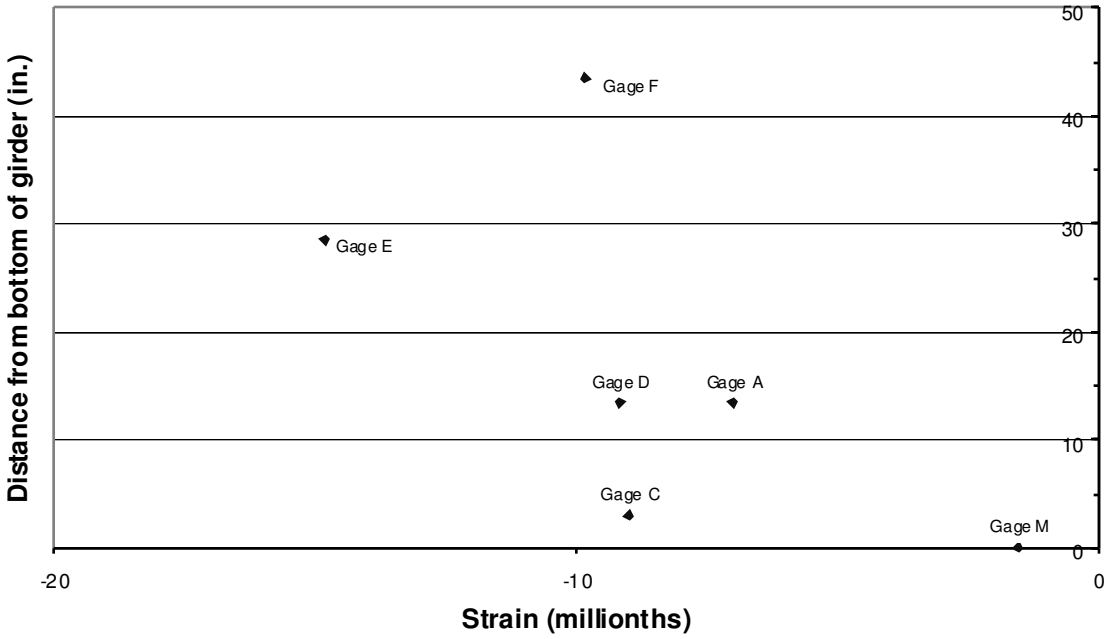


**Figure D-80:** A8 Span 11 Girder 8 Cross Section 2

### D.1.9 POSITION A9

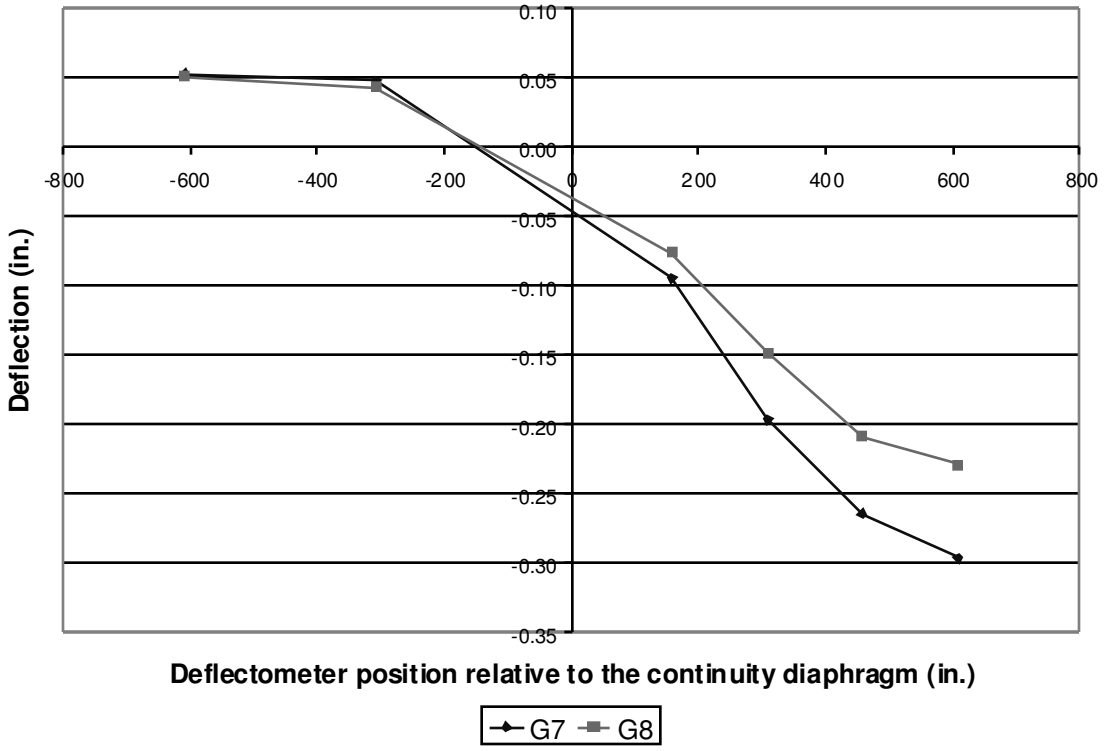


**Figure D-81:** A9 Deflections

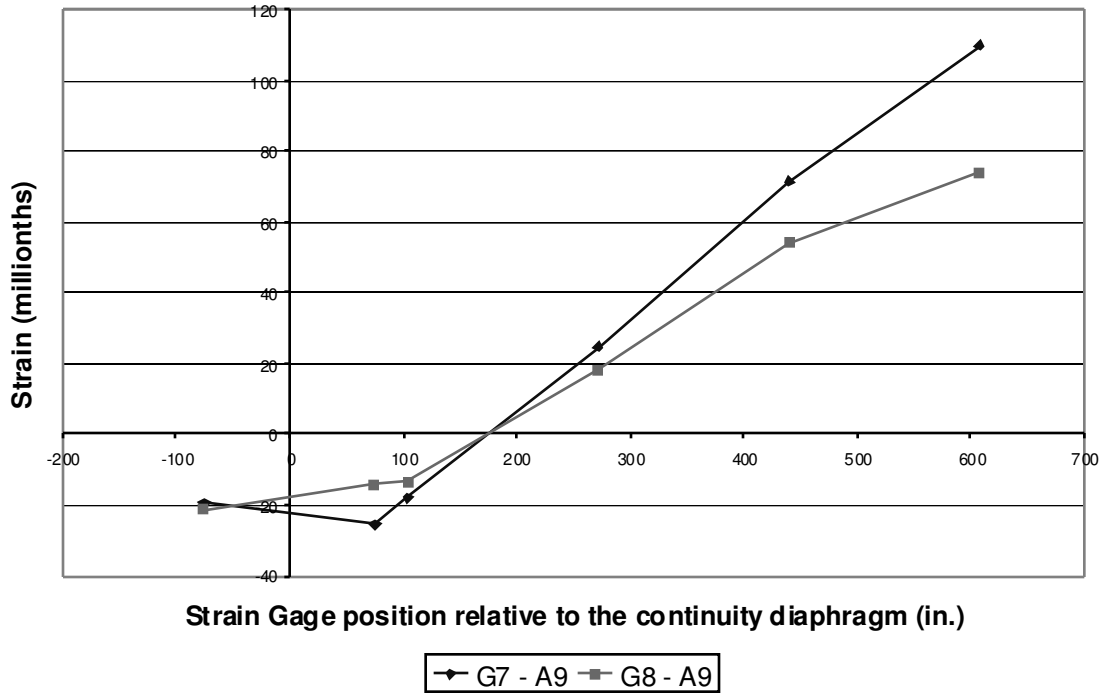


**Figure D-82:** A9 Bottom Fiber Strains

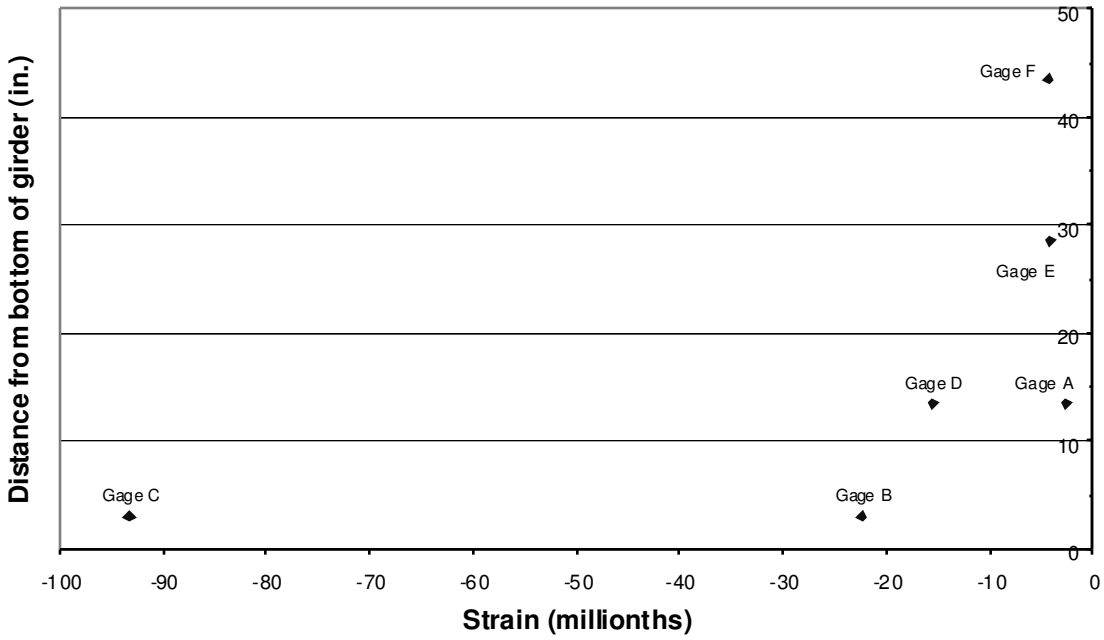


**Figure D-83:** A9 Span 10 Girder 7 Cross Section1

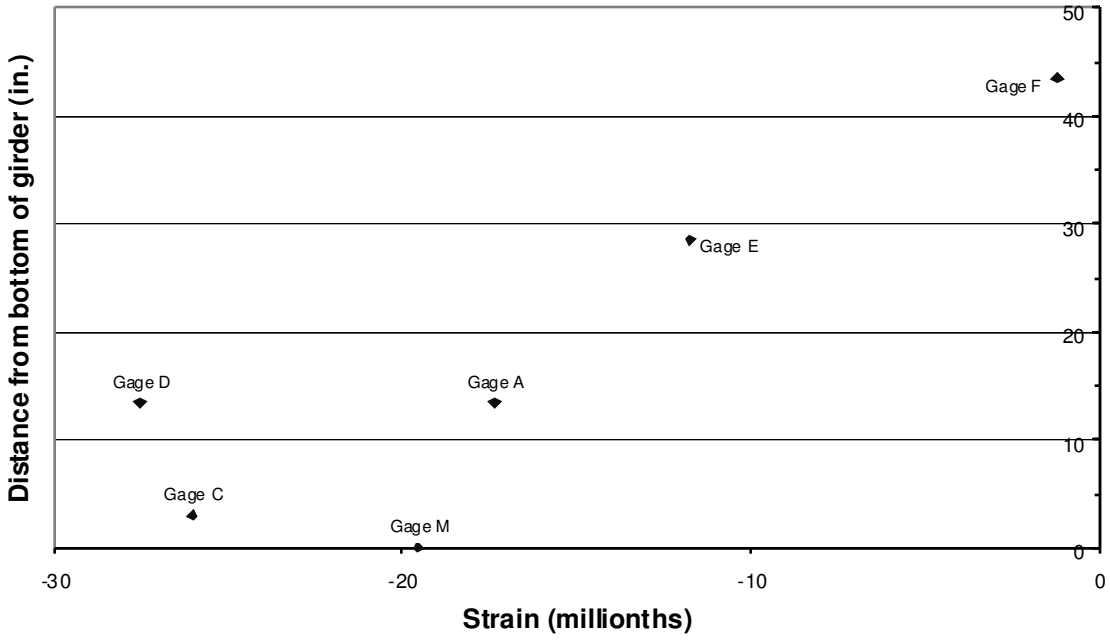


**Figure D-84:** A9 Span 10 Girder 7 Cross Section 2

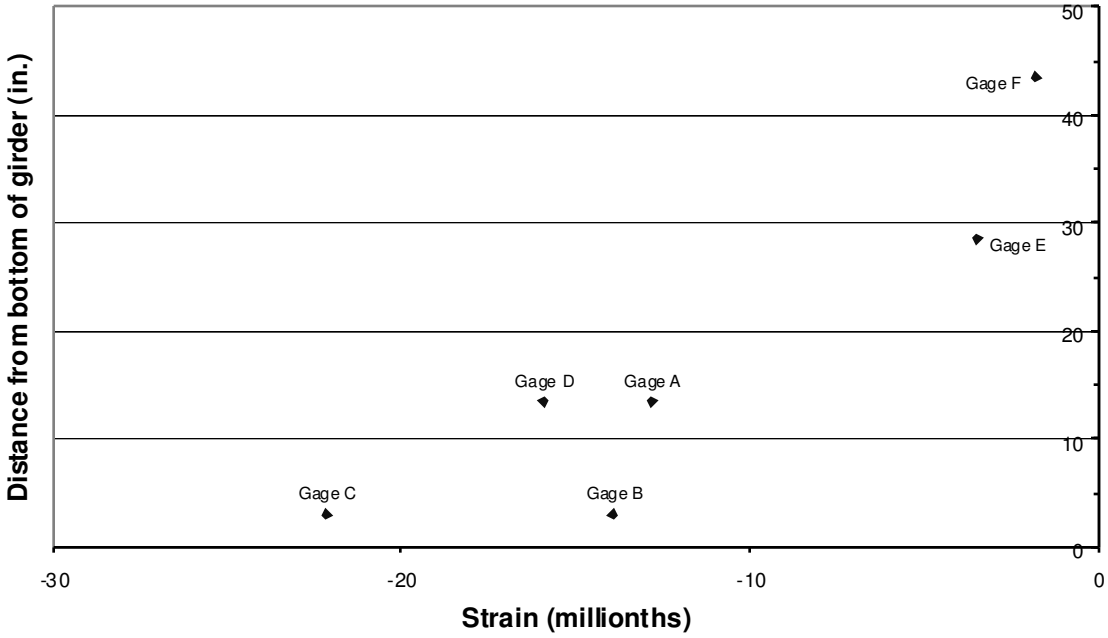


**Figure D-85:** A9 Span 10 Girder 8 Cross Section 1

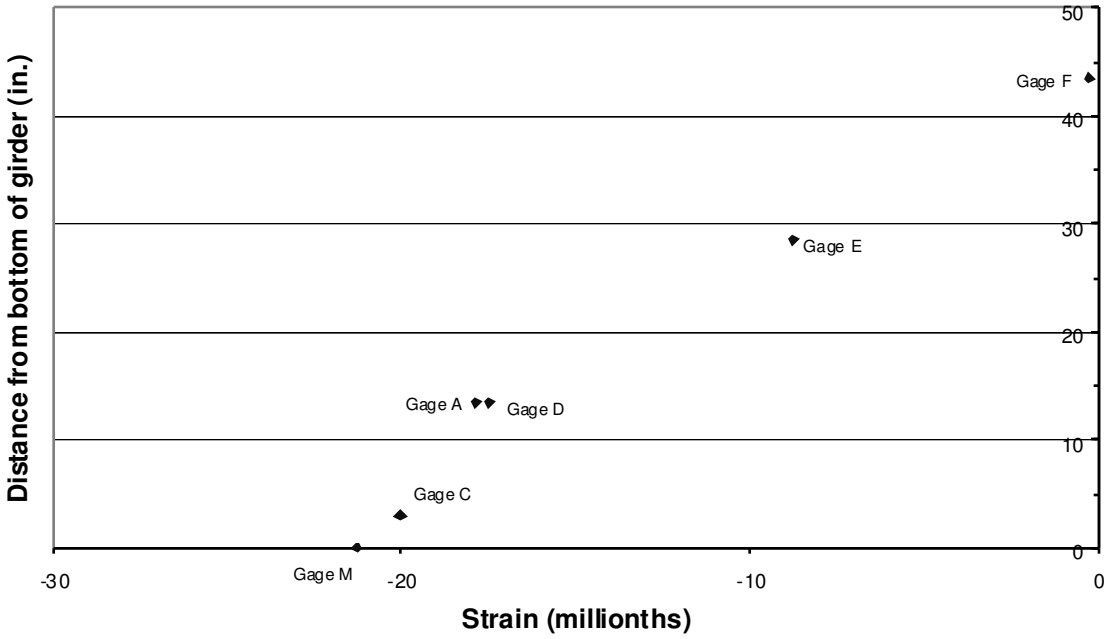


**Figure D-86:** A9 Span 10 Girder 8 Cross Section 2

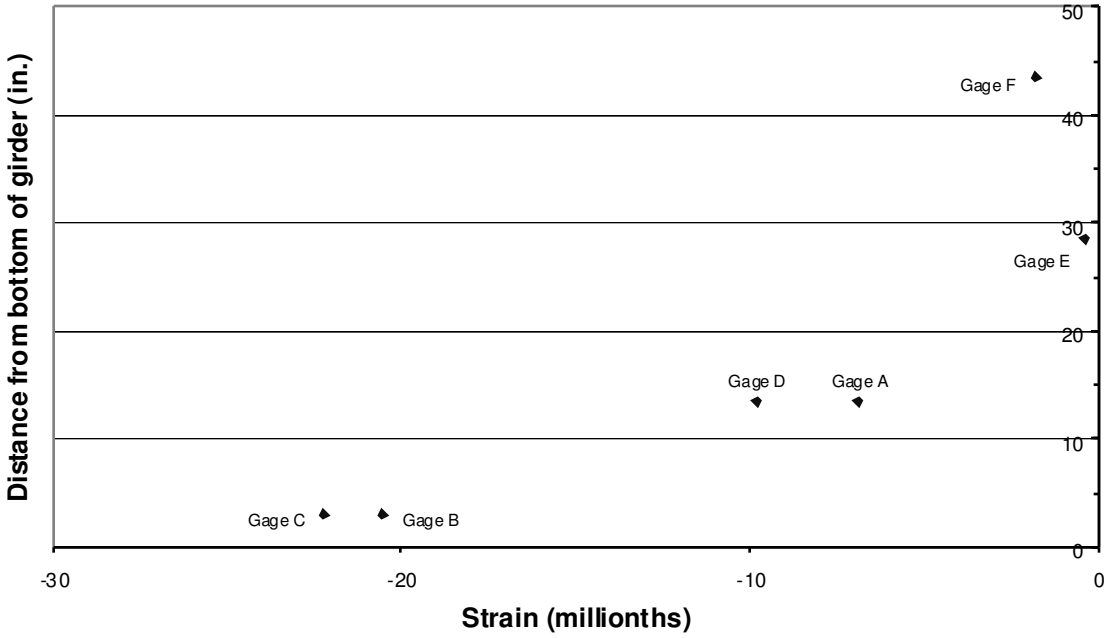


**Figure D-87:** A9 Span 11 Girder 7 Cross Section 1

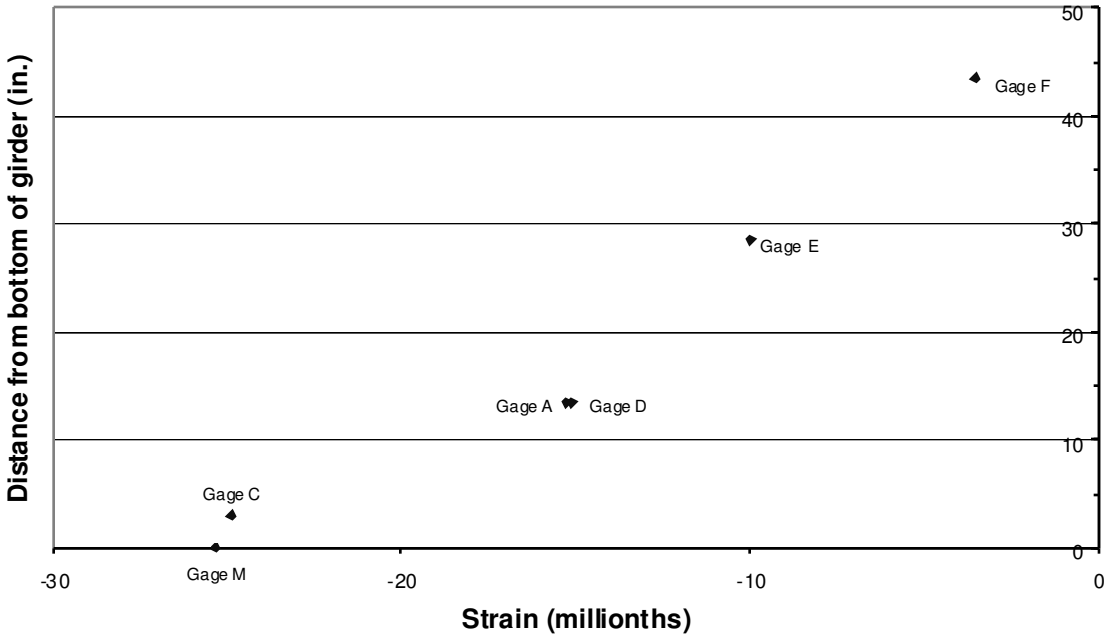


**Figure D-88:** A9 Span 11 Girder 7 Cross Section 2

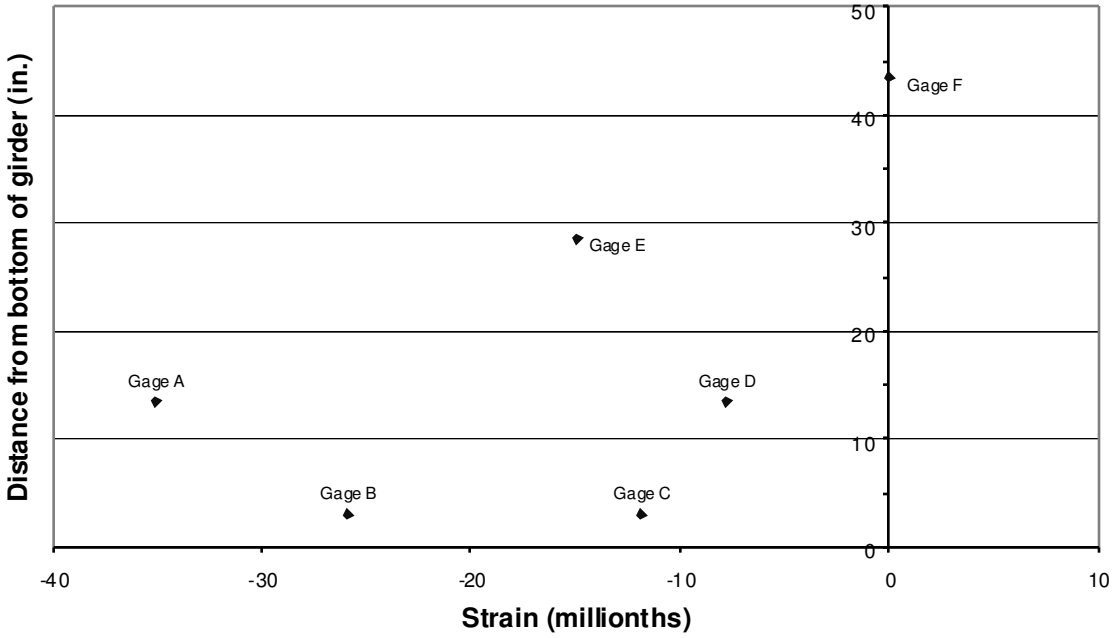


**Figure D-89:** A9 Span 11 Girder 8 Cross Section 1

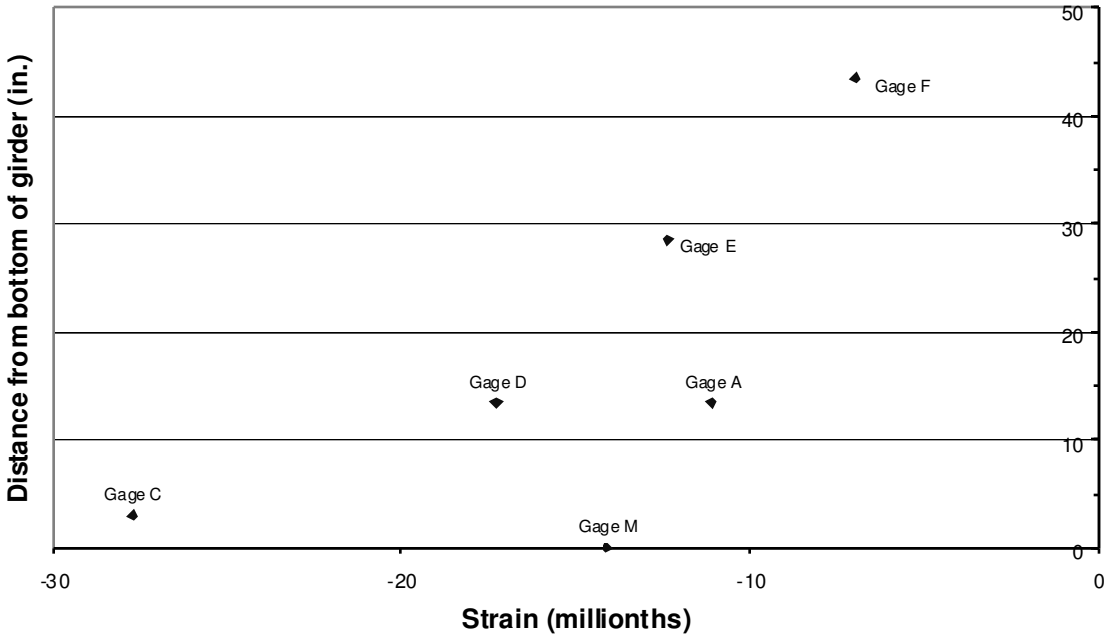


**Figure D-90:** A9 Span 11 Girder 8 Cross Section 2

## D.2 LANE B

### D.2.1 POSITION B1

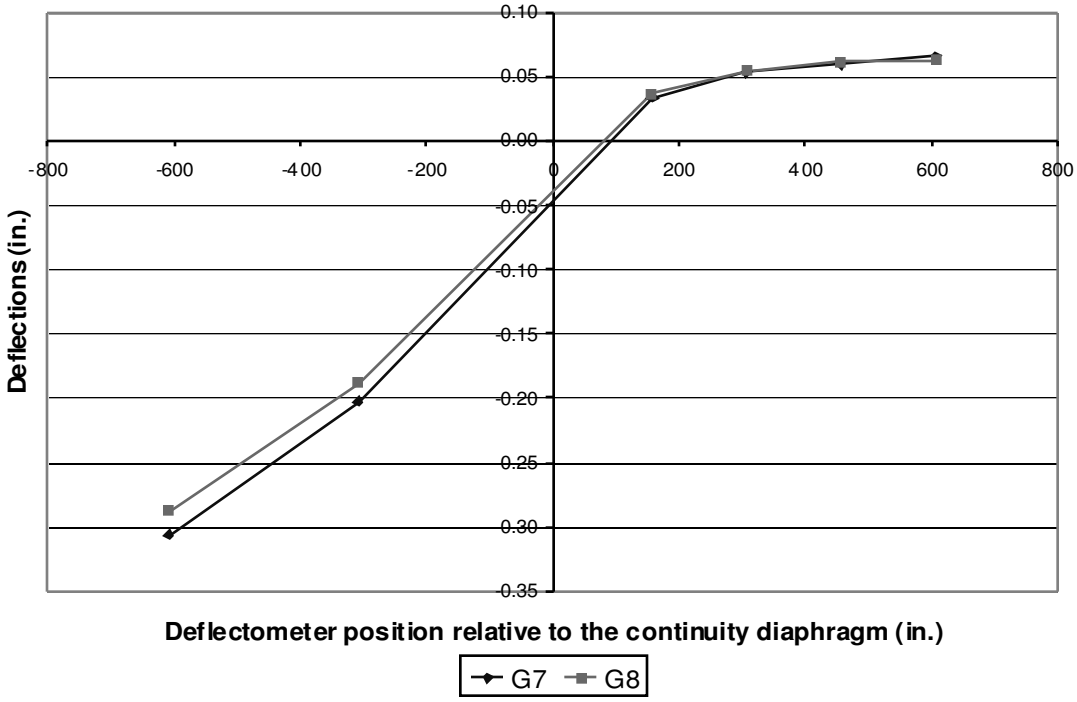


**Figure D-91:** B1 Deflections

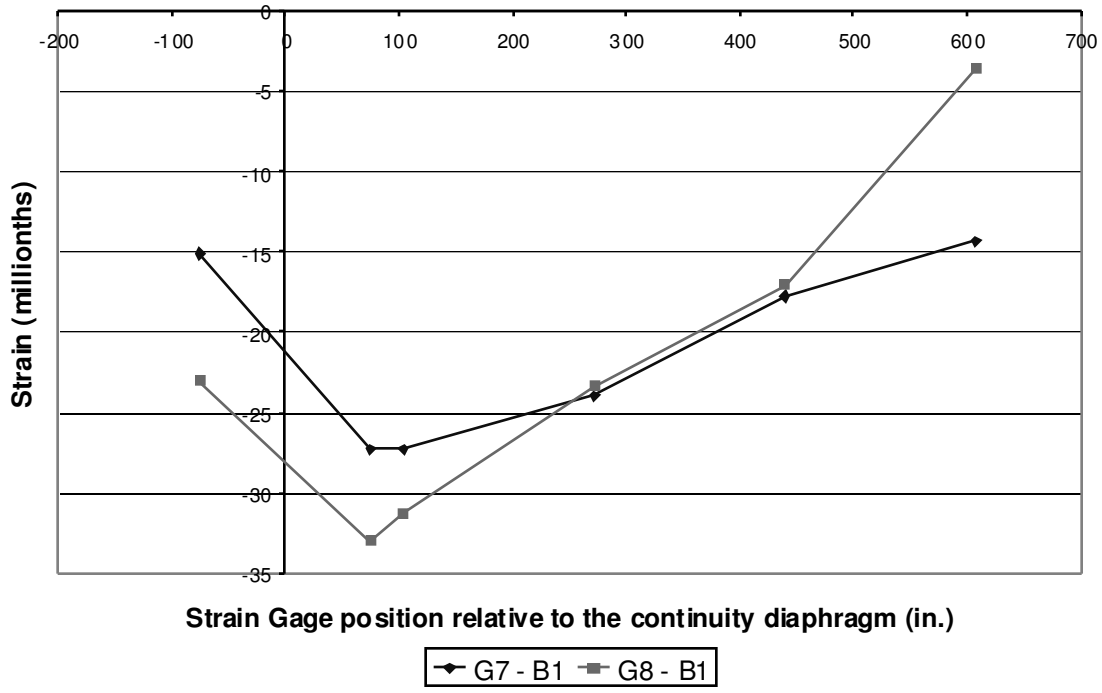


**Figure D-92:** B1 Bottom Fiber Strains

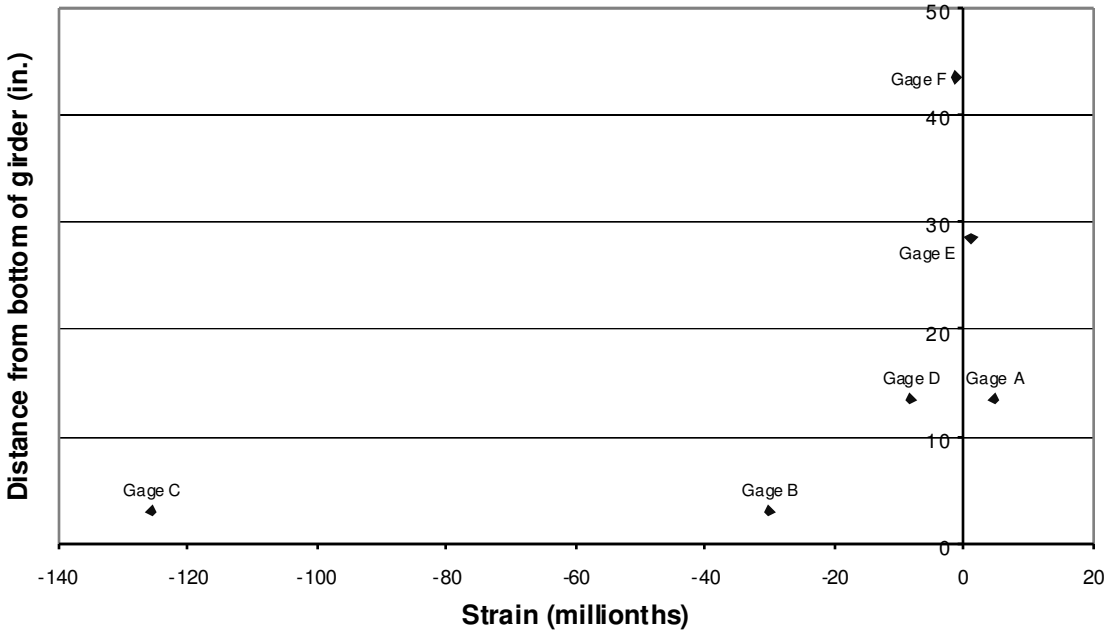


**Figure D-93:** B1 Span 10 Girder 7 Cross Section1

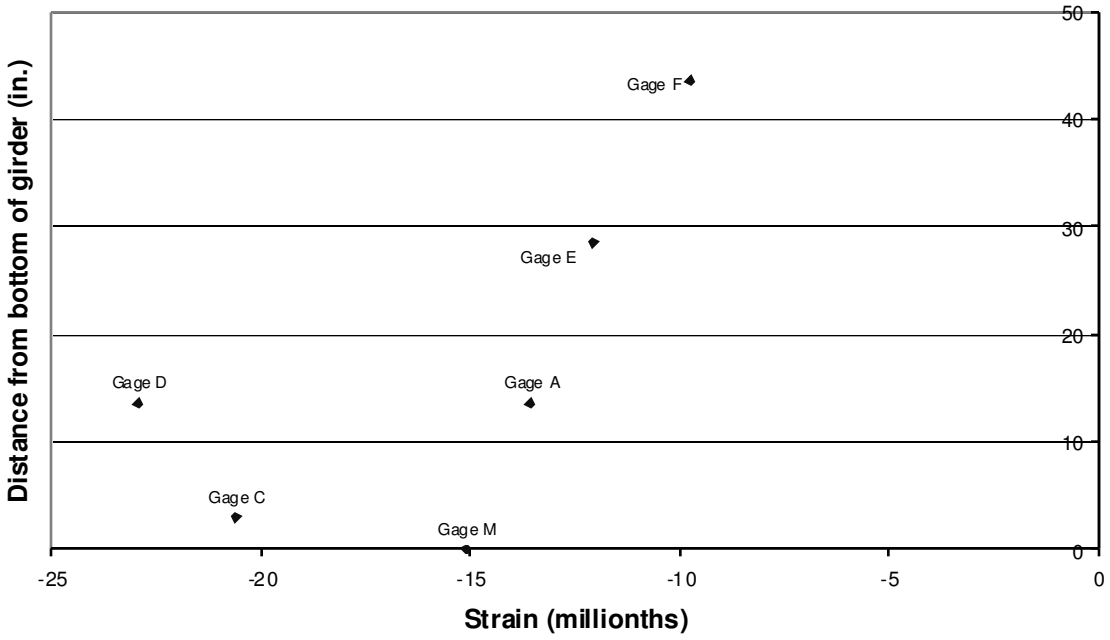


**Figure D-94:** B1 Span 10 Girder 7 Cross Section 2

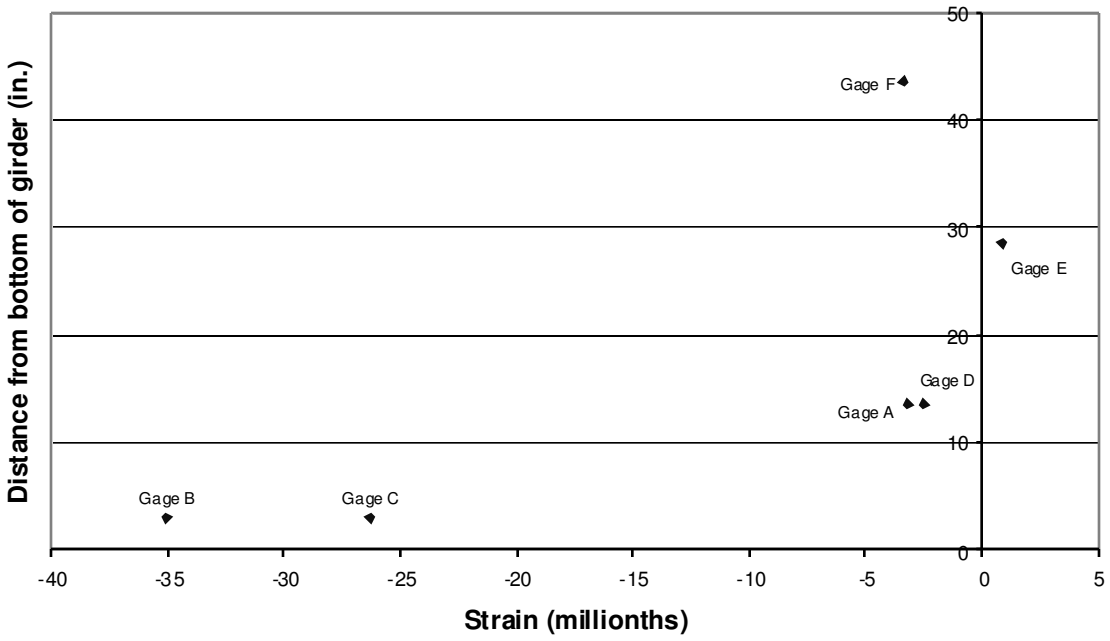


**Figure D-95:** B1 Span 10 Girder 8 Cross Section 1

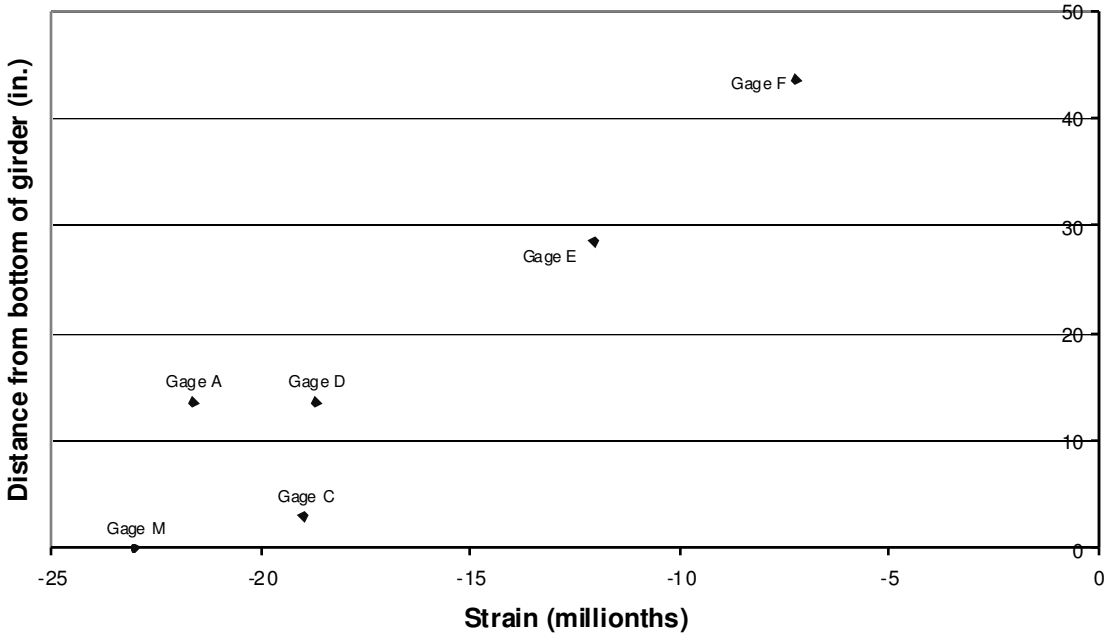


**Figure D-96:** B1 Span 10 Girder 8 Cross Section 2

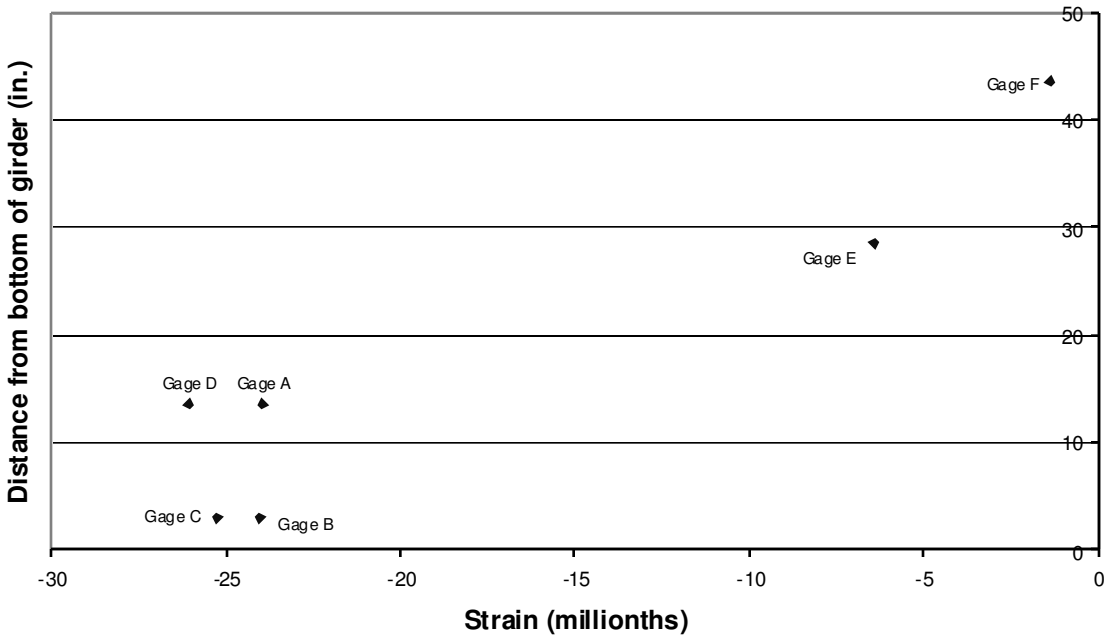


**Figure D-97:** B1 Span 11 Girder 7 Cross Section 1

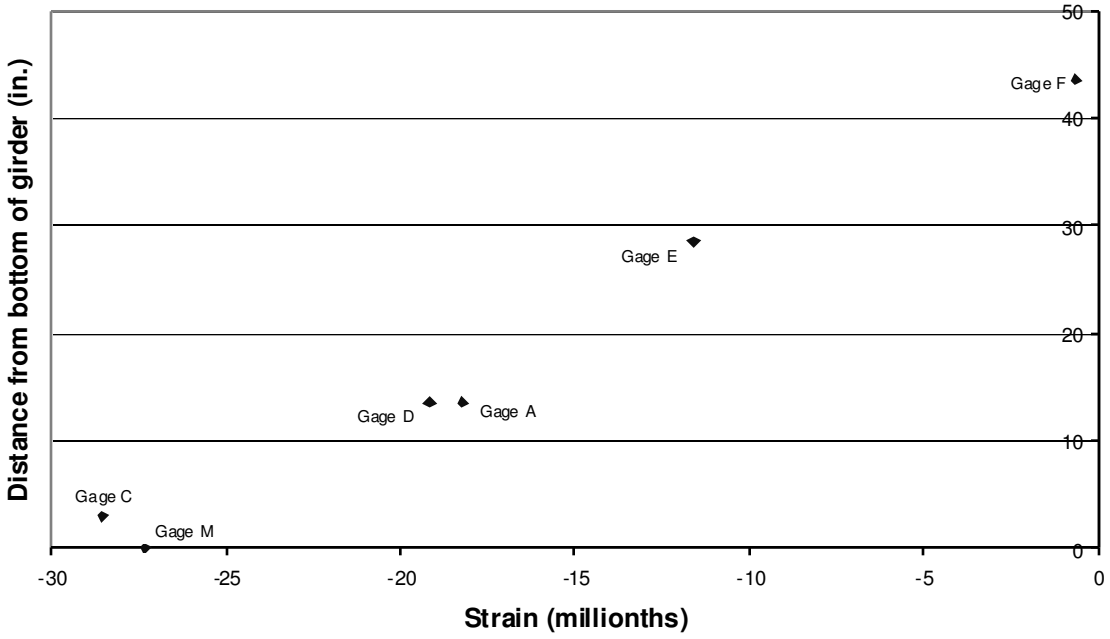


**Figure D-98:** B1 Span 11 Girder 7 Cross Section 2

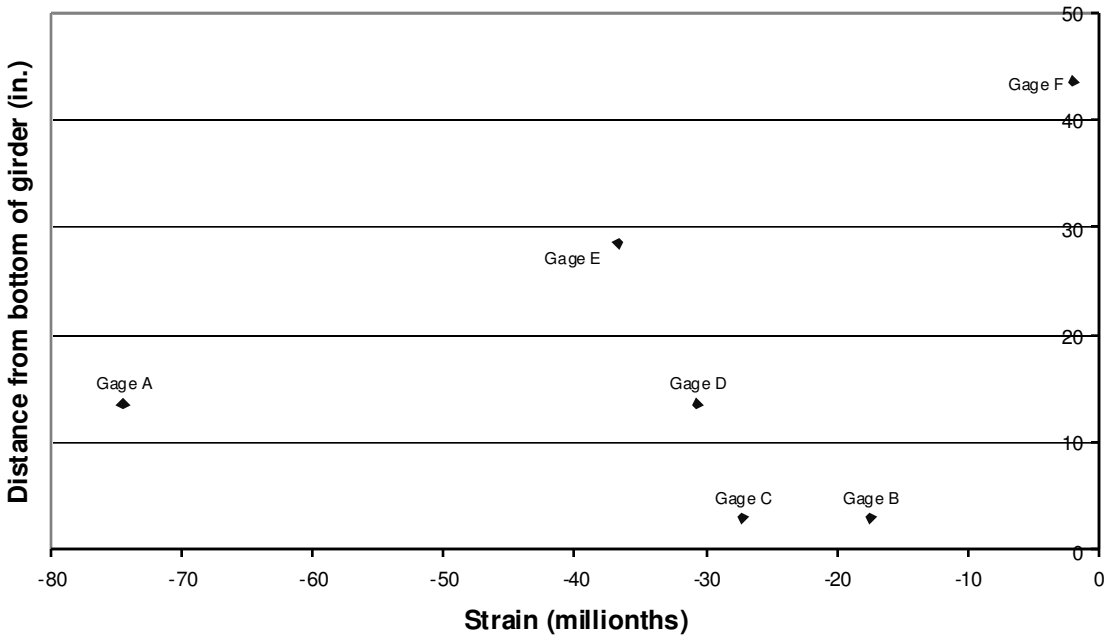


**Figure D-99:** B1 Span 11 Girder 8 Cross Section 1

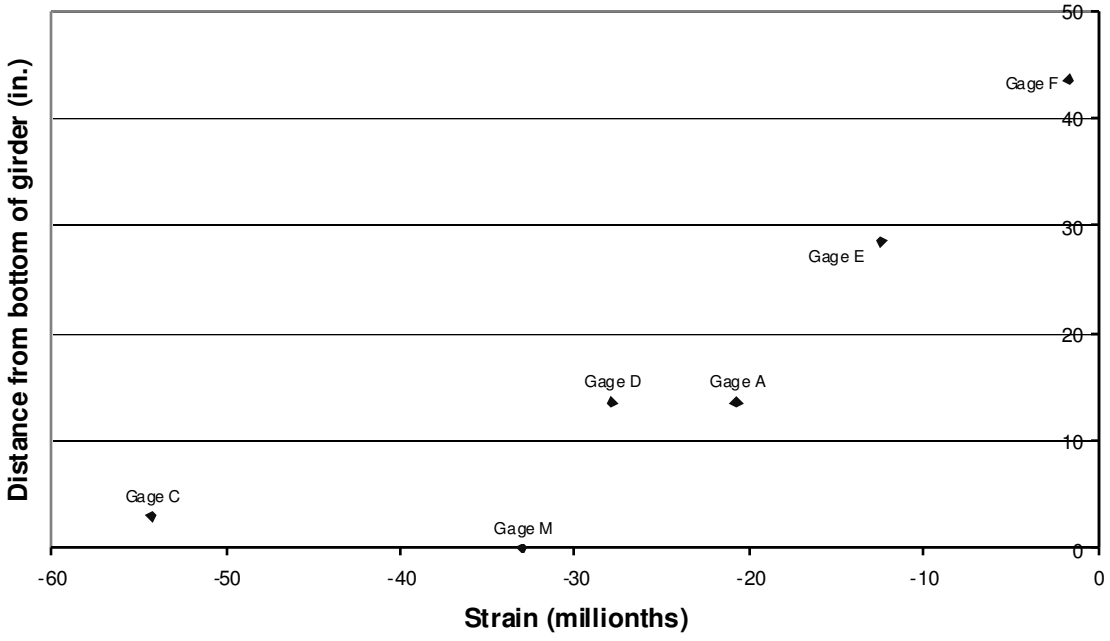


**Figure D-100:** B1 Span 11 Girder 8 Cross Section 2

### D.2.2 POSITION B2

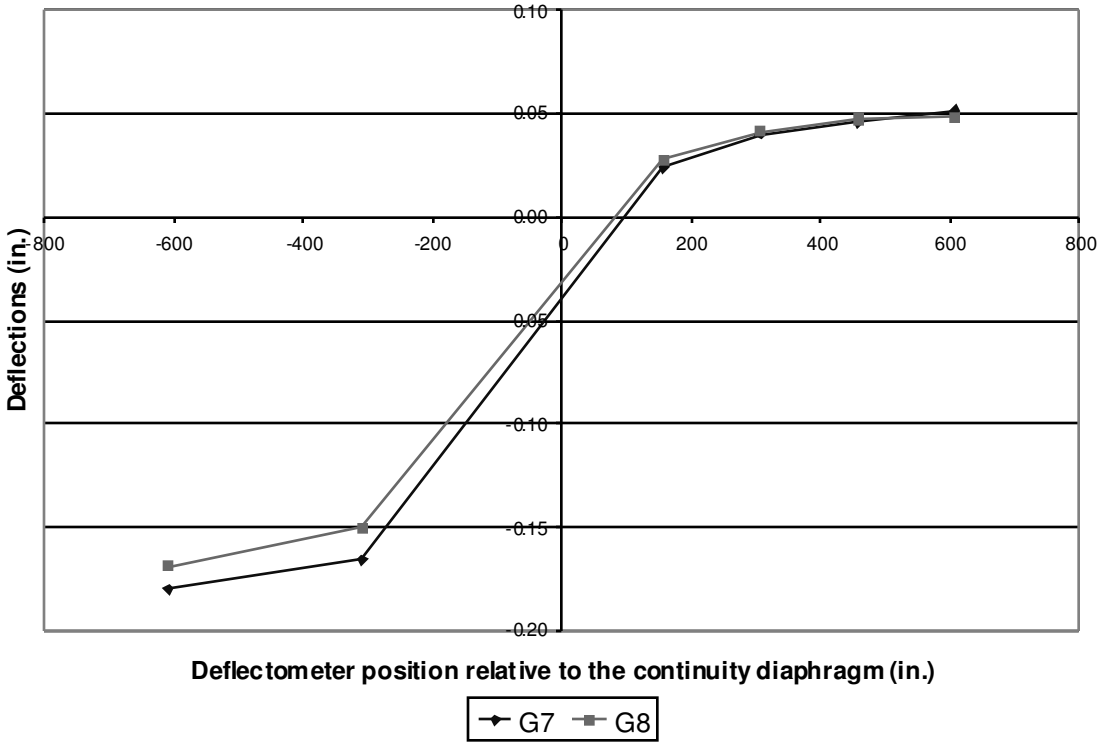


**Figure D-101:** B2 Deflections

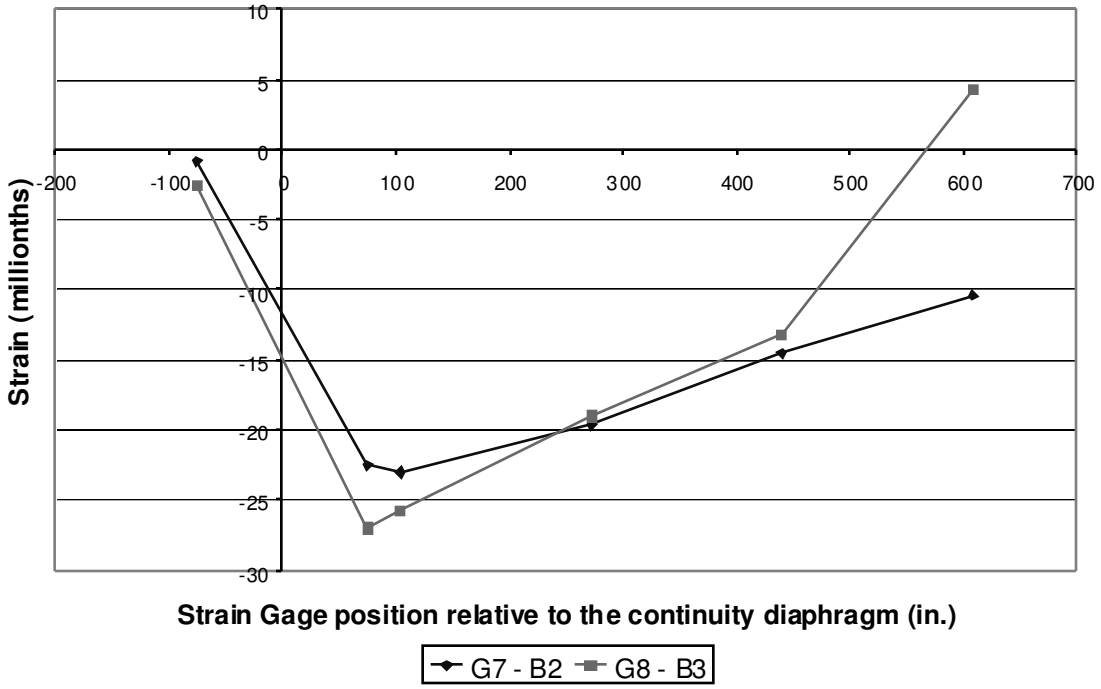


**Figure D-102:** B2 Bottom Fiber Strains

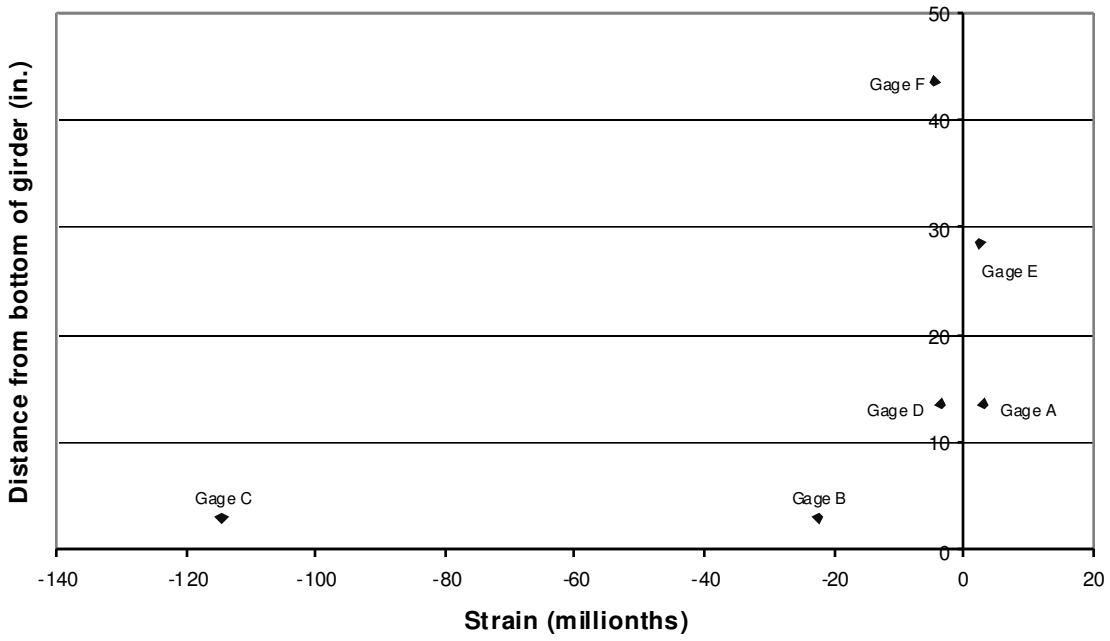


**Figure D-103:** B2 Span 10 Girder 7 Cross Section1

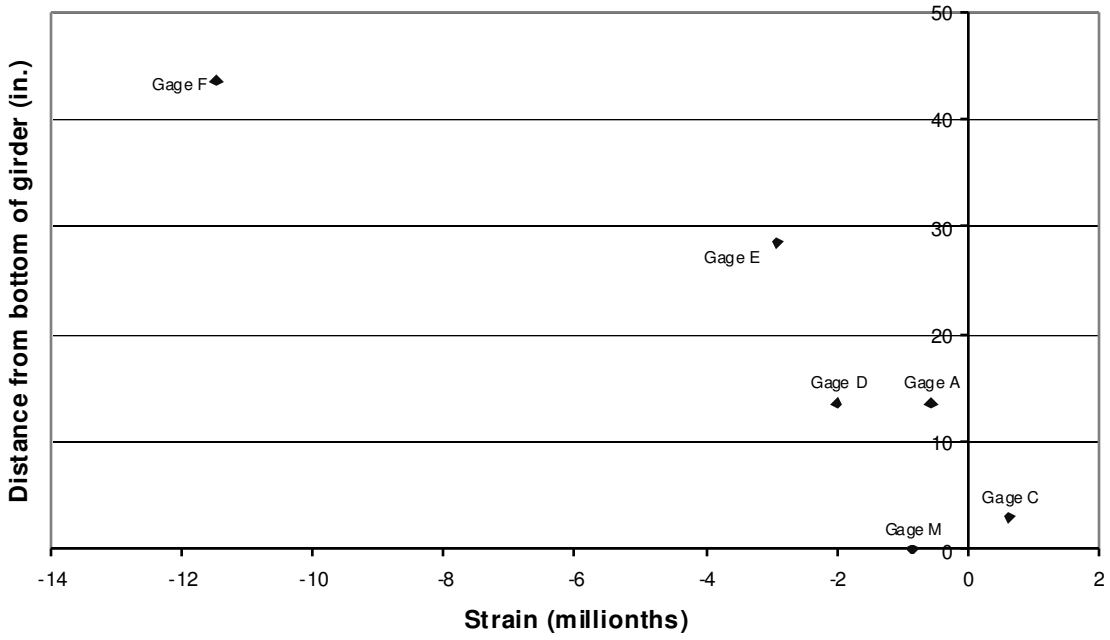


**Figure D-104:** B2 Span 10 Girder 7 Cross Section 2

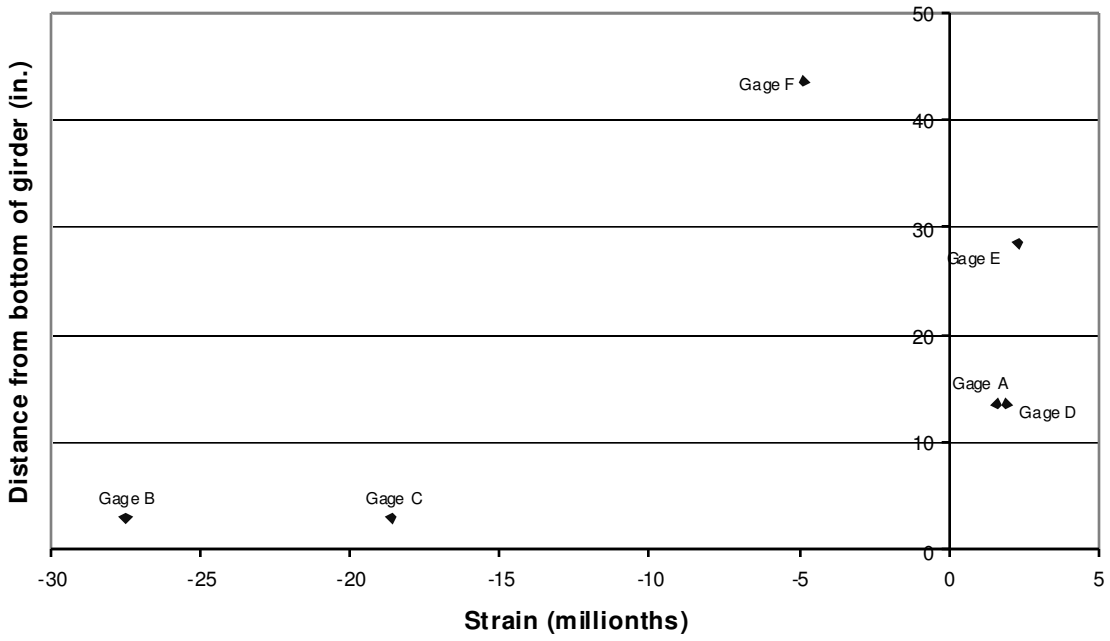


**Figure D-105:** B2 Span 10 Girder 8 Cross Section 1

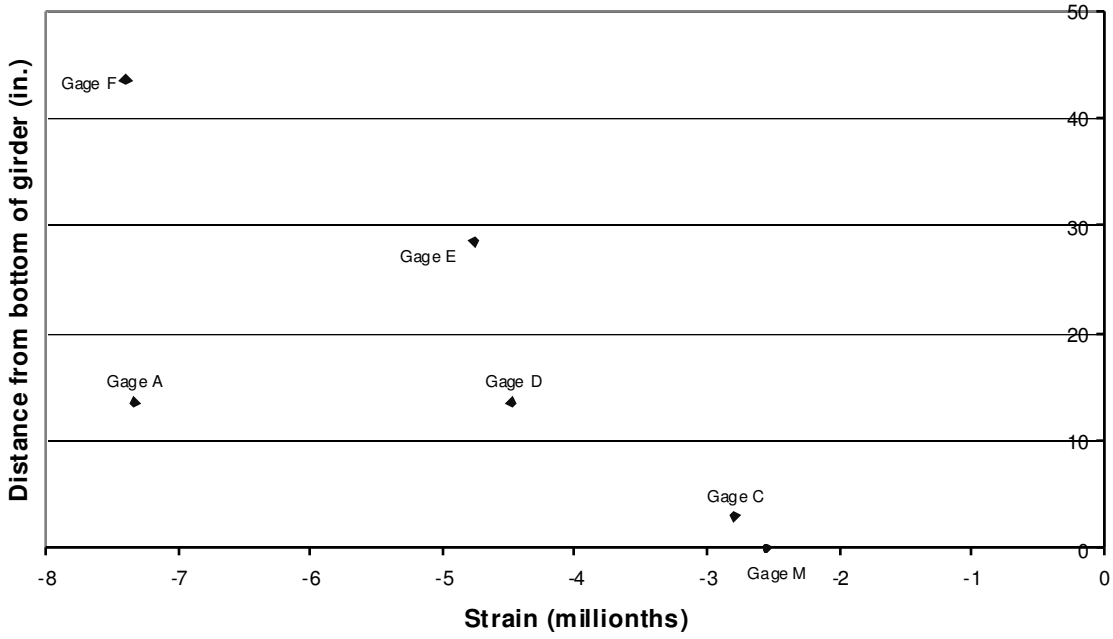


**Figure D-106:** B2 Span 10 Girder 8 Cross Section 2

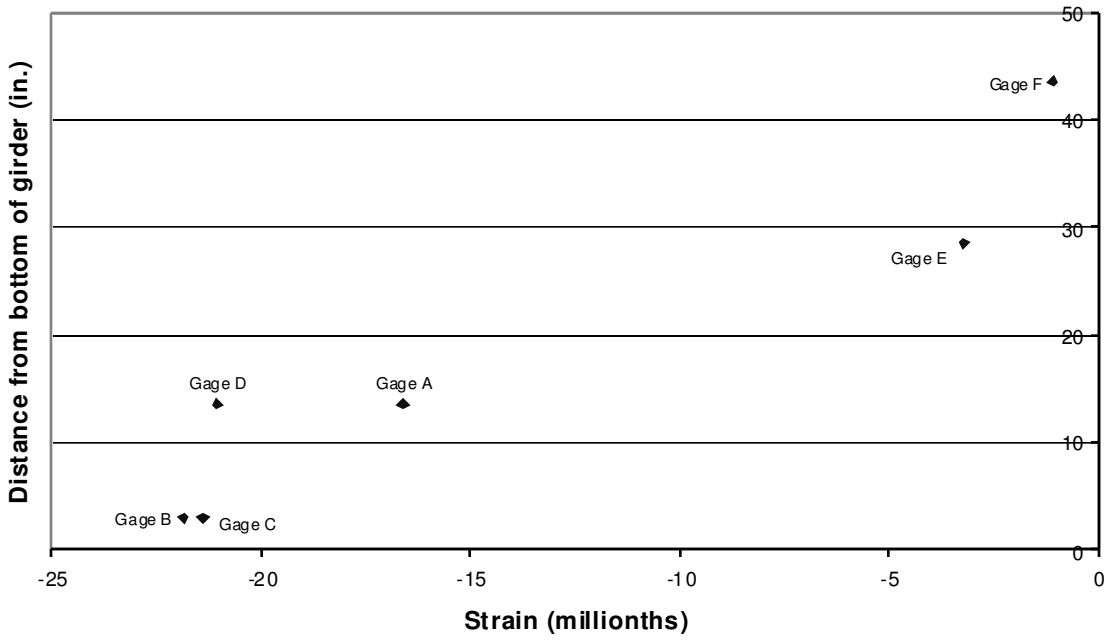


**Figure D-107:** B2 Span 11 Girder 7 Cross Section 1

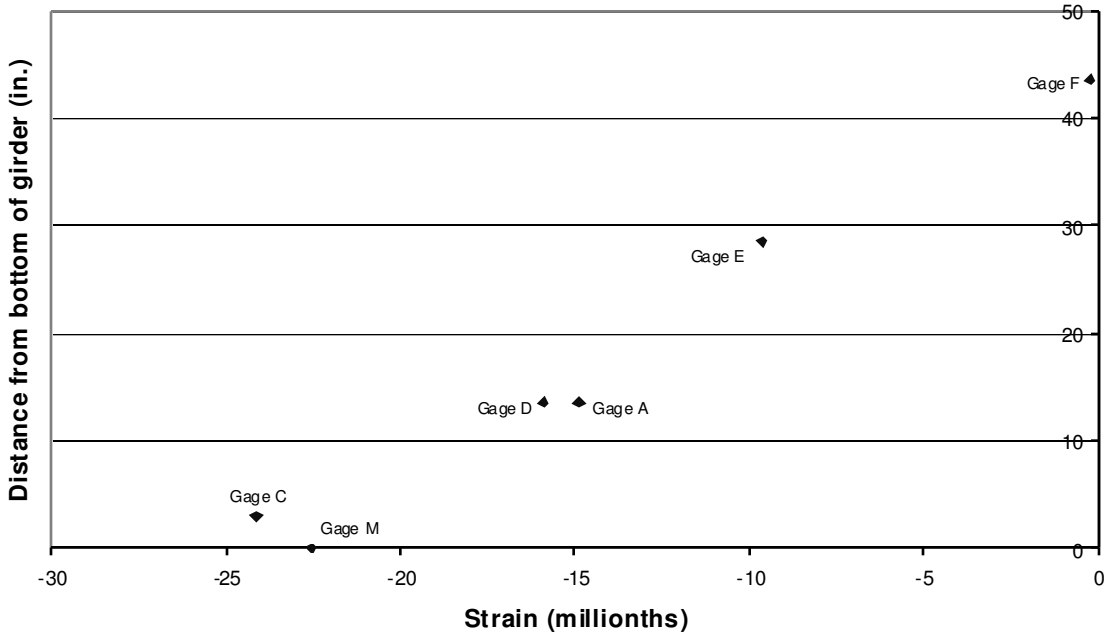


**Figure D-108:** B2 Span 11 Girder 7 Cross Section 2

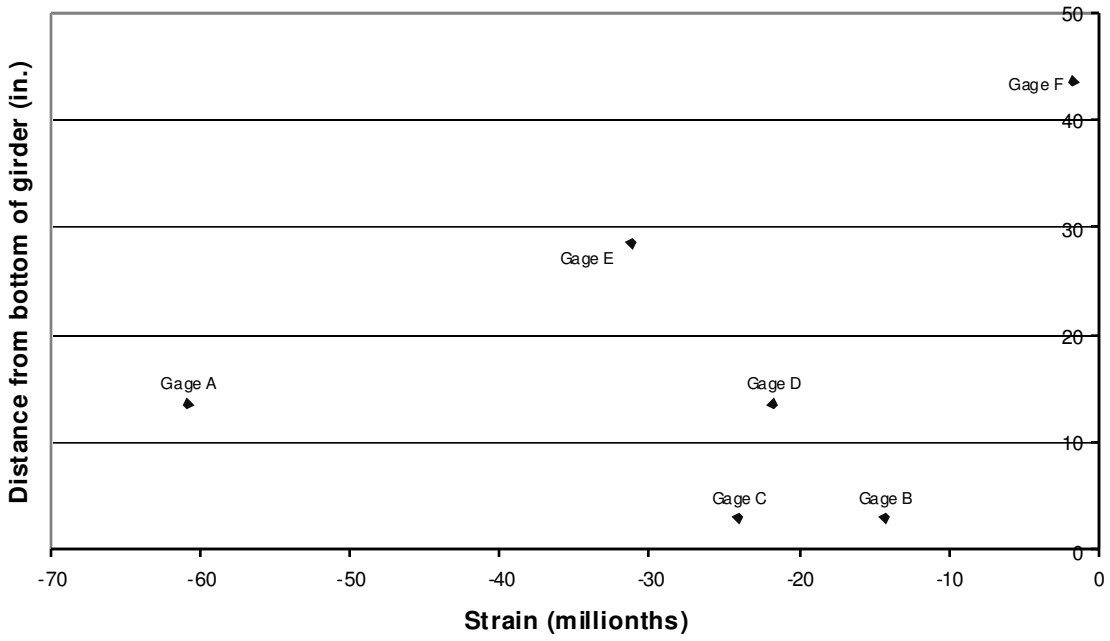


**Figure D-109:** B2 Span 11 Girder 8 Cross Section 1

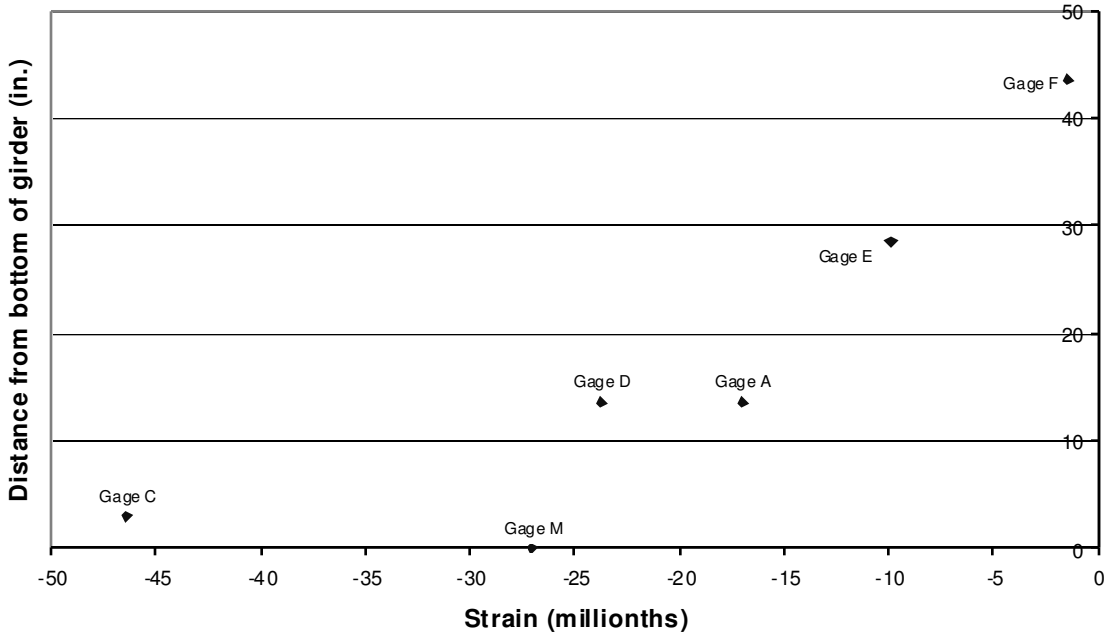


**Figure D-110:** B2 Span 11 Girder 8 Cross Section 2

### D.2.3 POSITION B3

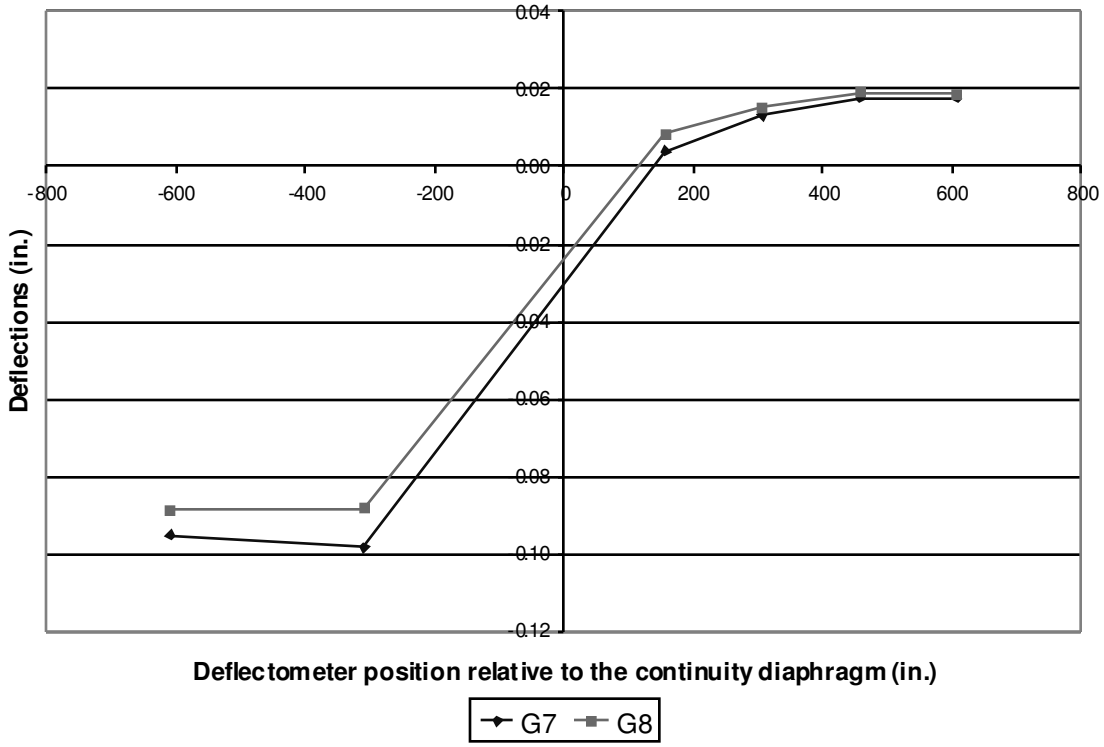


**Figure D-111:** B3 Deflections

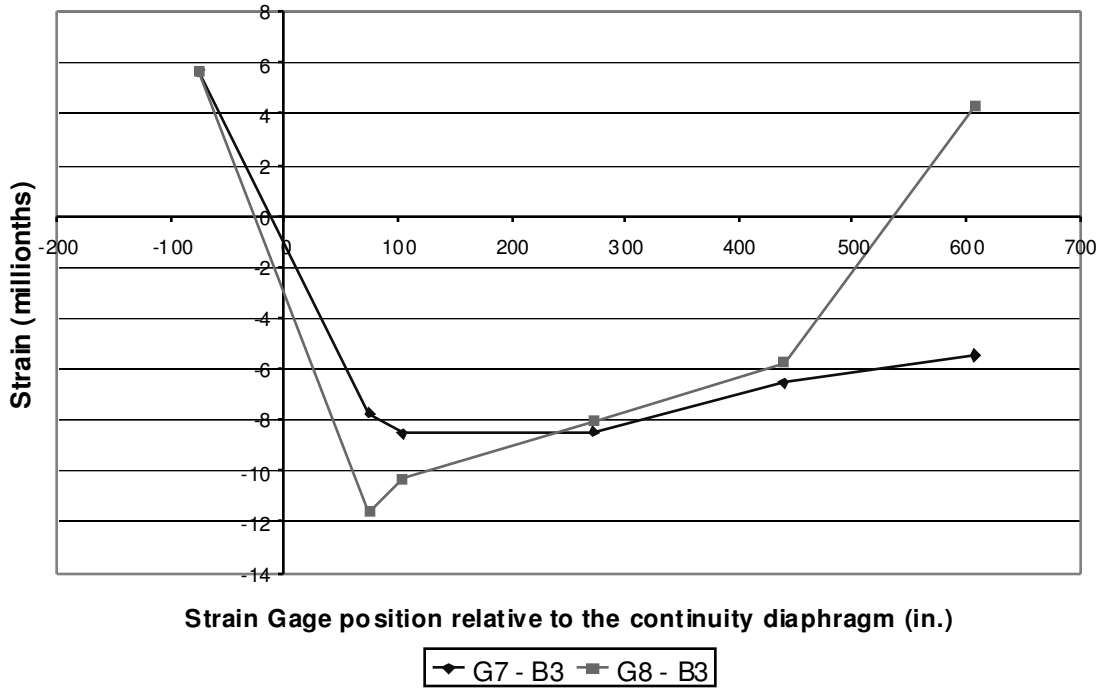


**Figure D-112:** B3 Bottom Fiber Strains

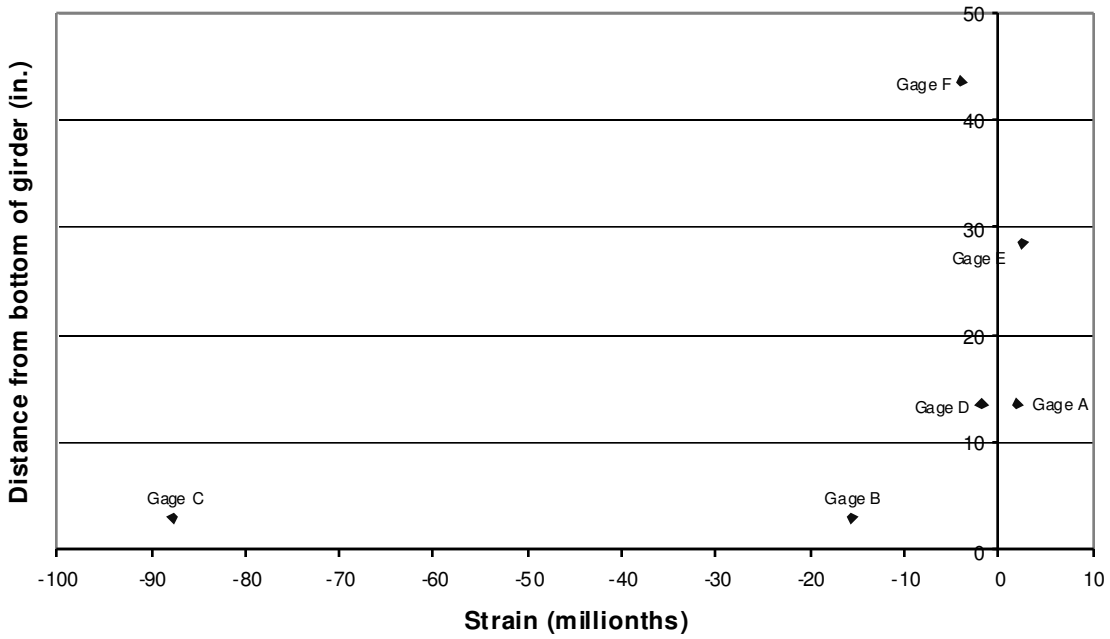


**Figure D-113:** B3 Span 10 Girder 7 Cross Section1

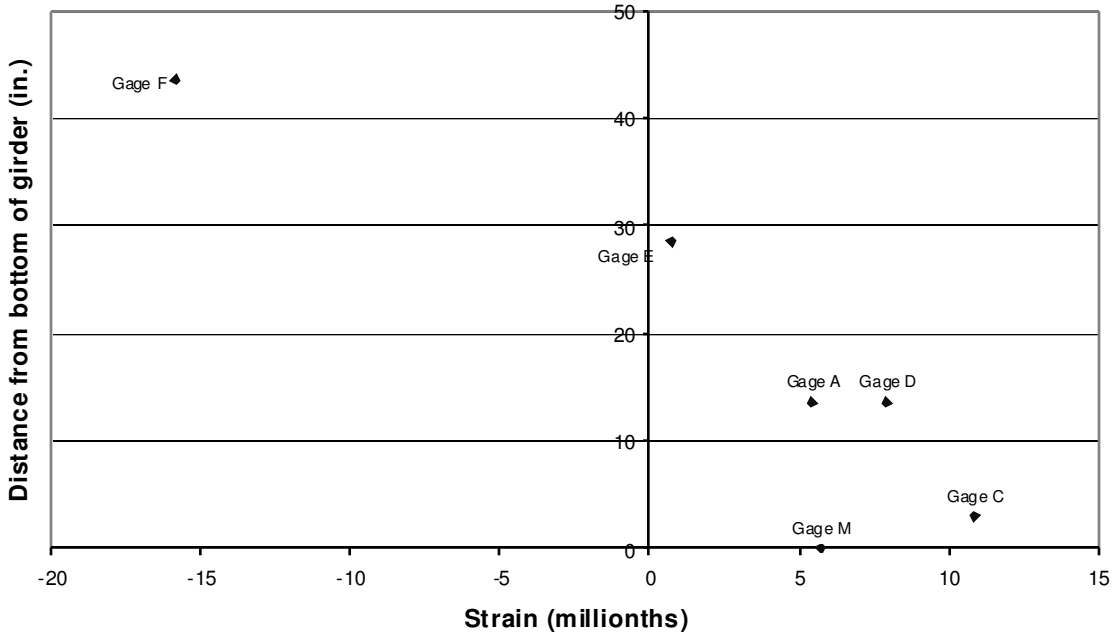


**Figure D-114:** B3 Span 10 Girder 7 Cross Section 2

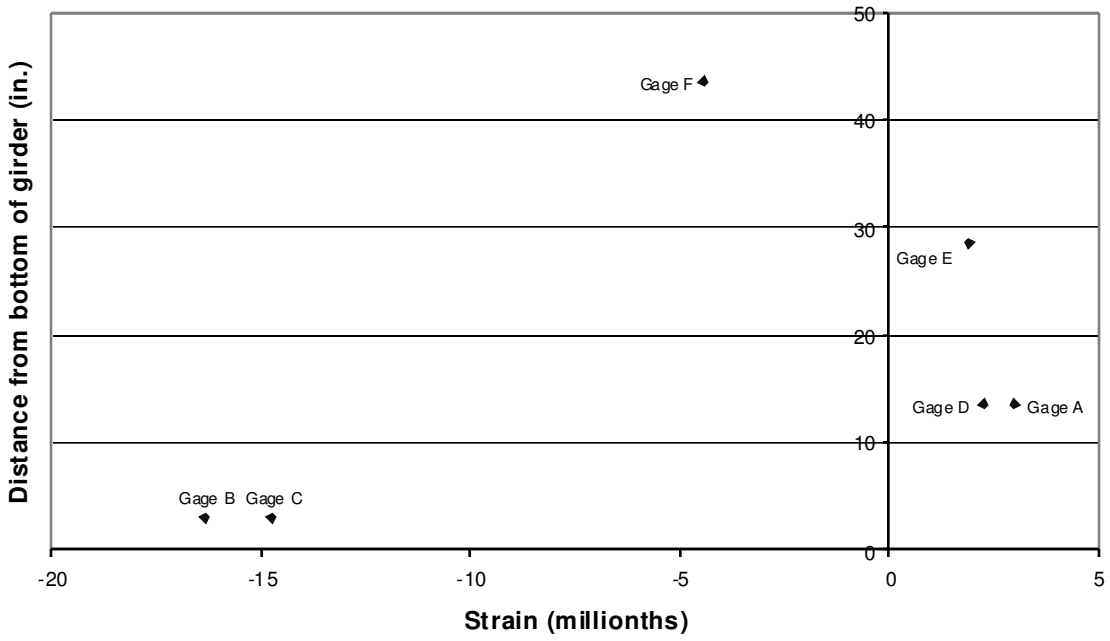


**Figure D-115:** B3 Span 10 Girder 8 Cross Section 1

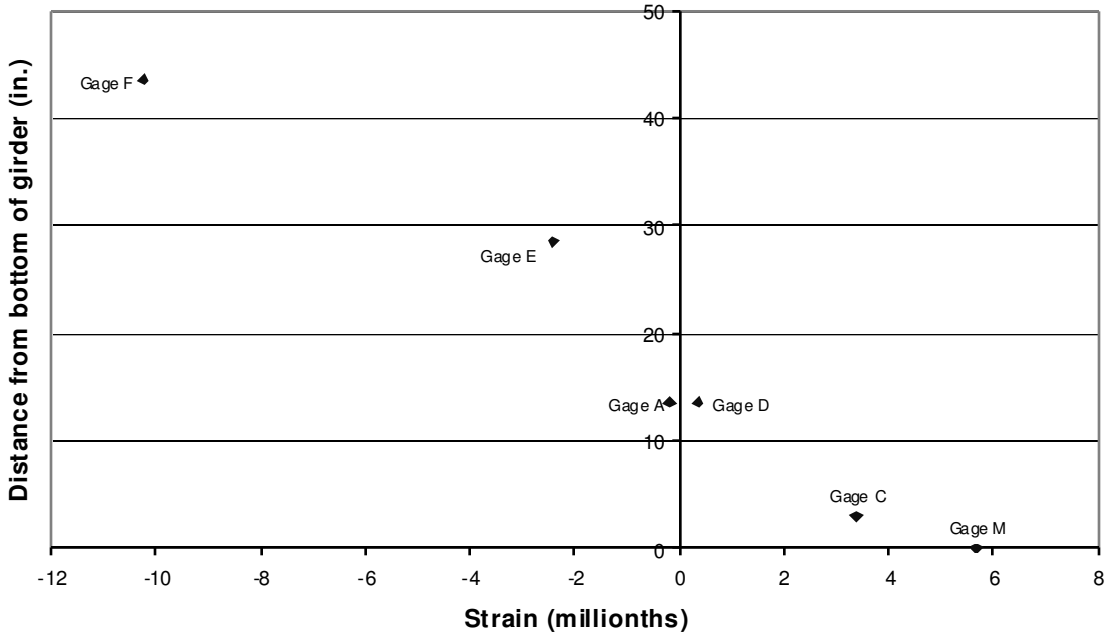


**Figure D-116:** B3 Span 10 Girder 8 Cross Section 2

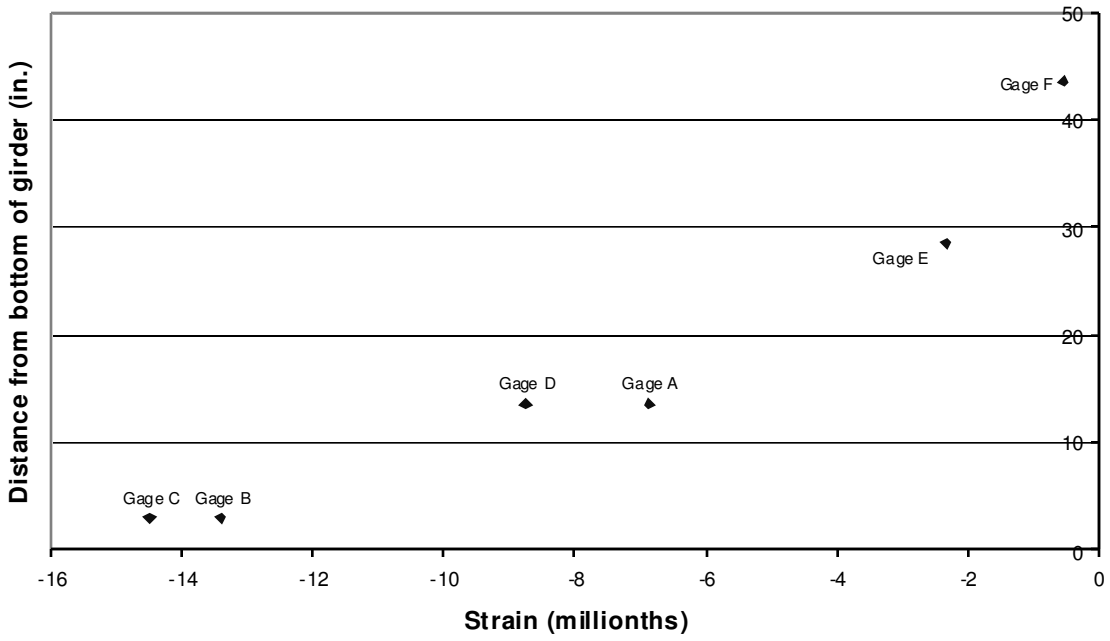


**Figure D-117:** B3 Span 11 Girder 7 Cross Section 1

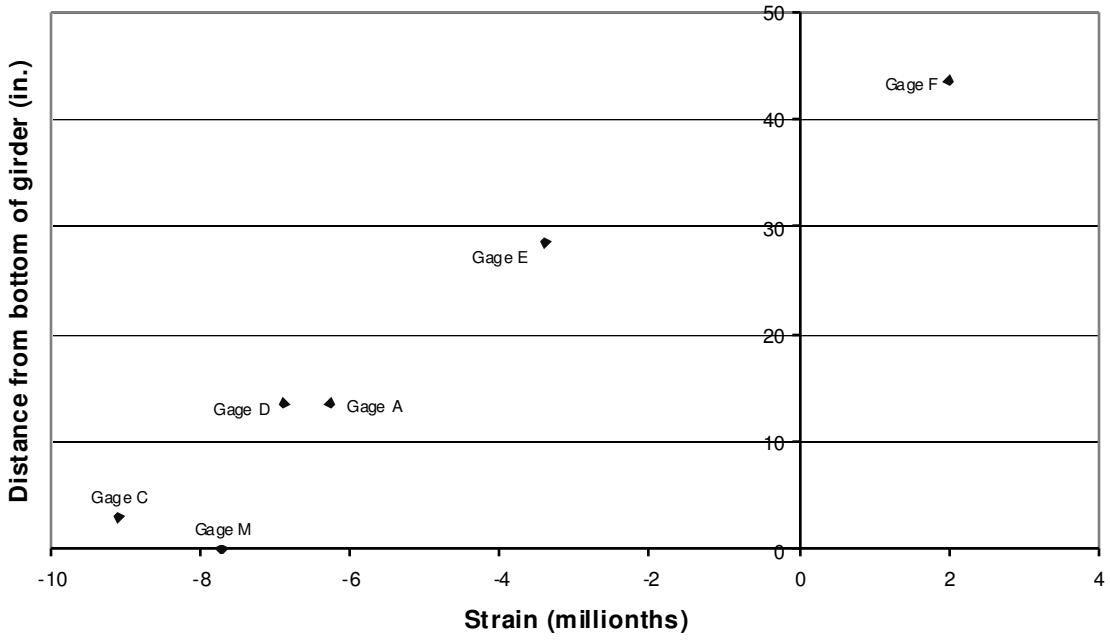


**Figure D-118:** B3 Span 11 Girder 7 Cross Section 2

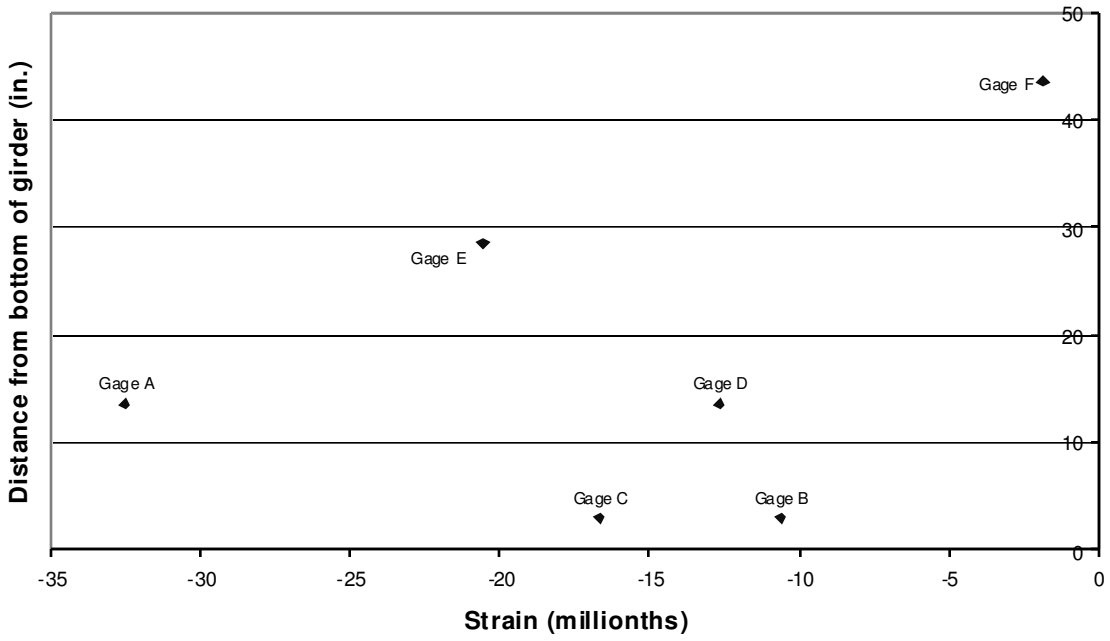


**Figure D-119:** B3 Span 11 Girder 8 Cross Section 1

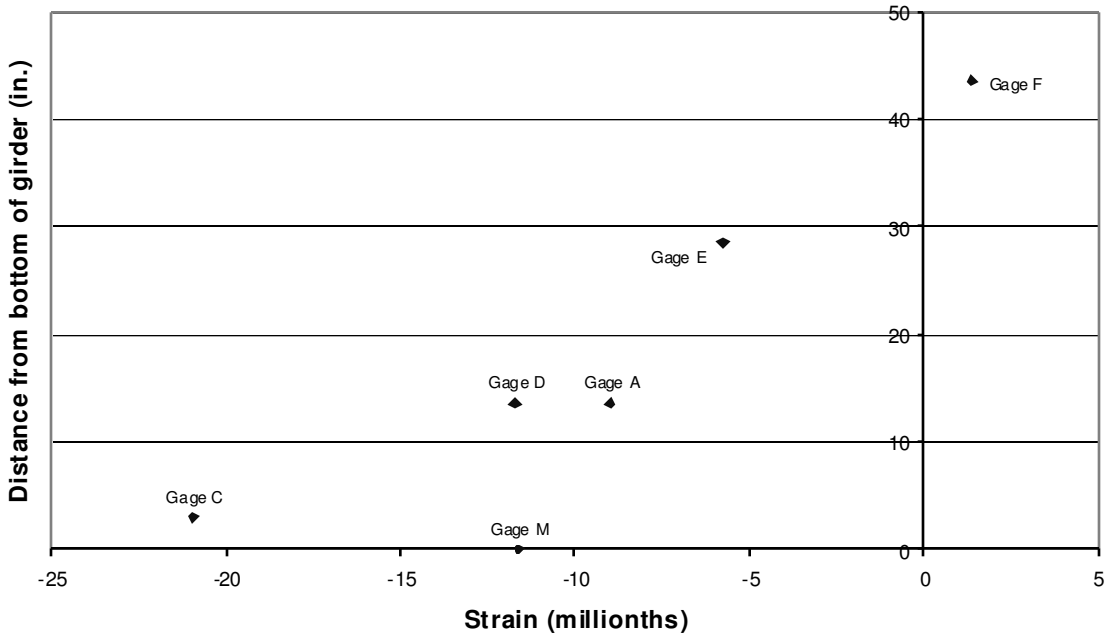


**Figure D-120:** B3 Span 11 Girder 8 Cross Section 2

### D.2.4 POSITION B4

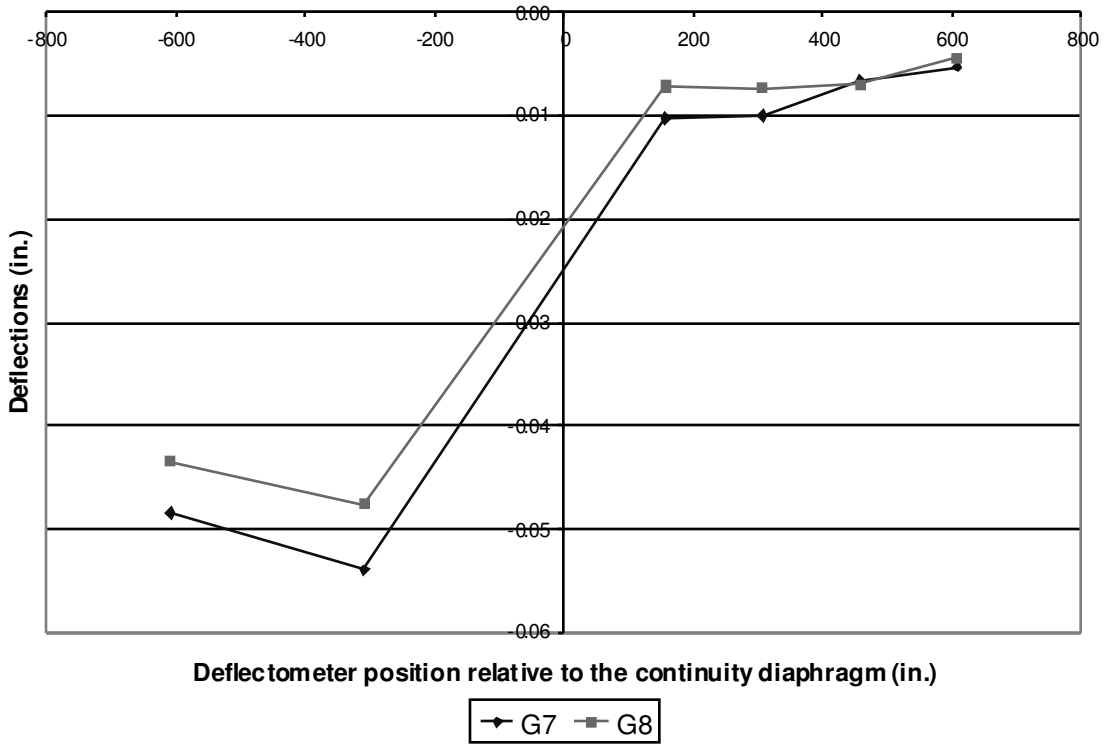


**Figure D-121:** B4 Deflections

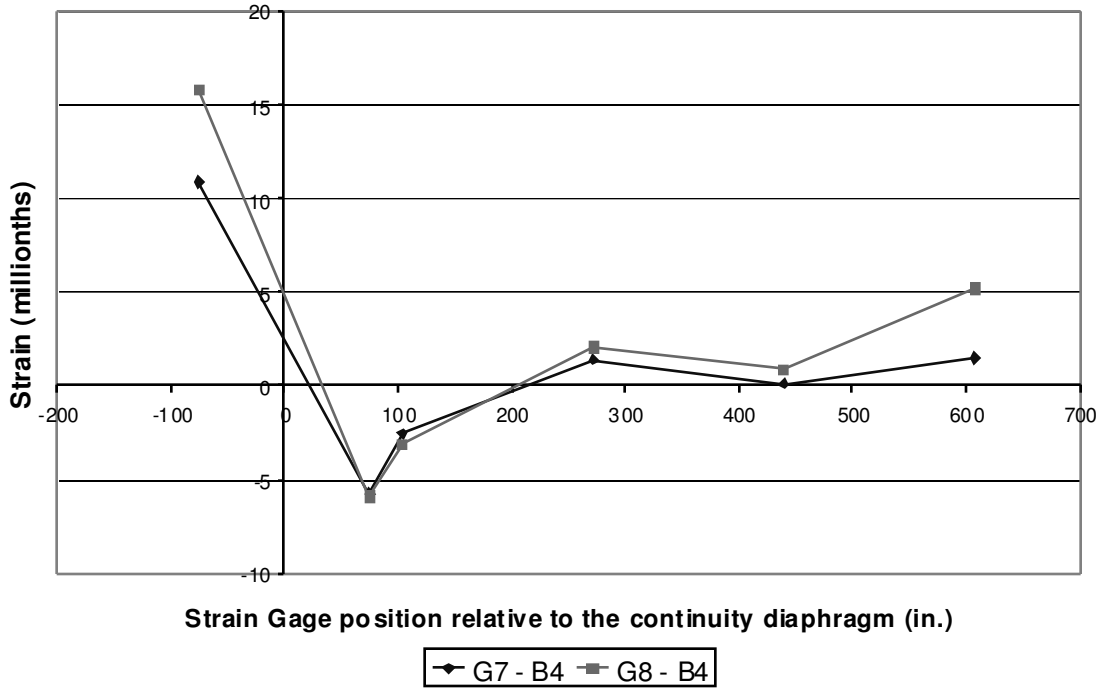


**Figure D-122:** B4 Bottom Fiber Strains

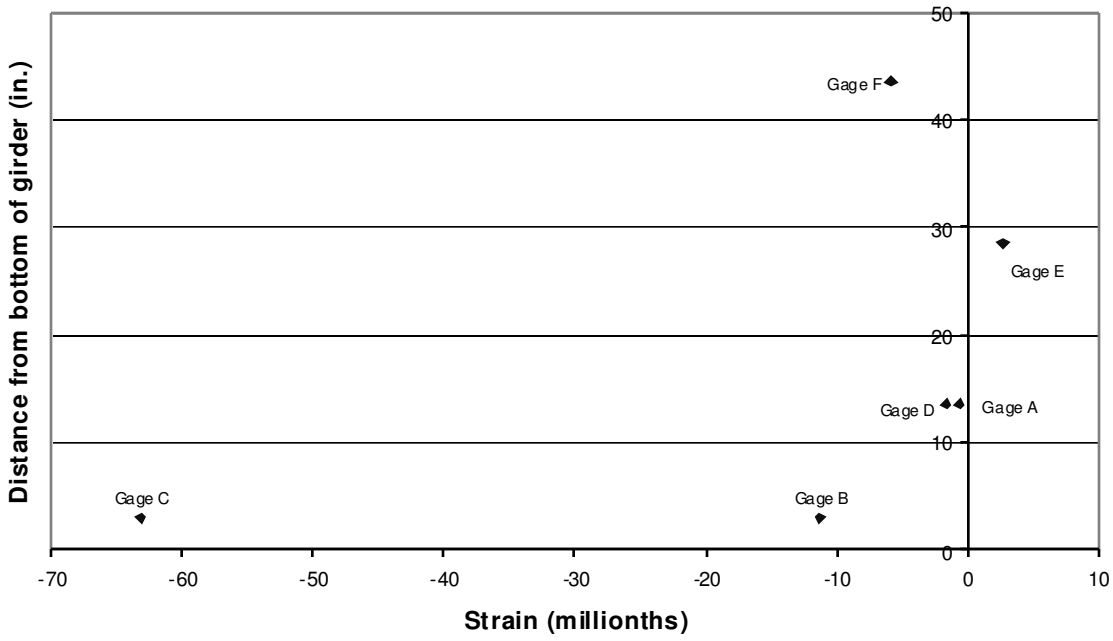


**Figure D-123:** B4 Span 10 Girder 7 Cross Section1

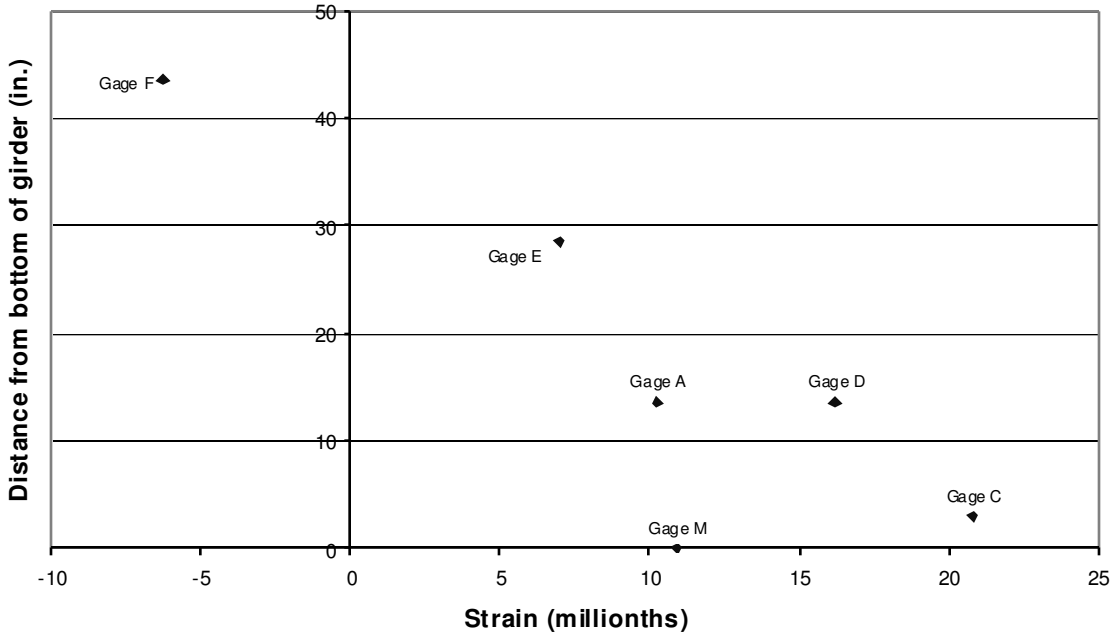


**Figure D-124:** B4 Span 10 Girder 7 Cross Section 2

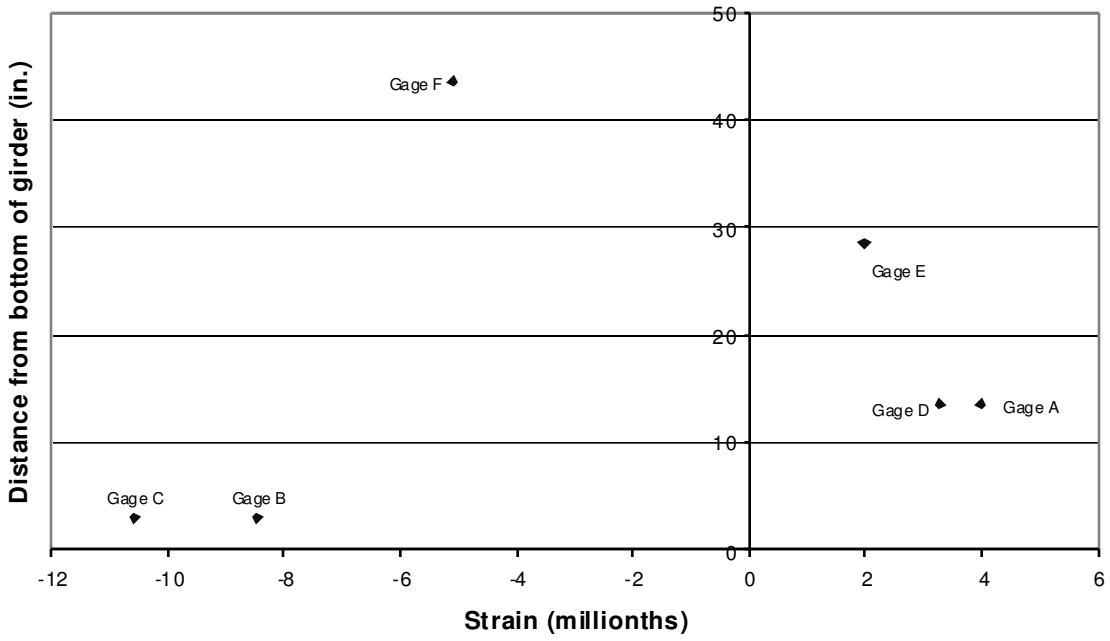


**Figure D-125:** B4 Span 10 Girder 8 Cross Section 1

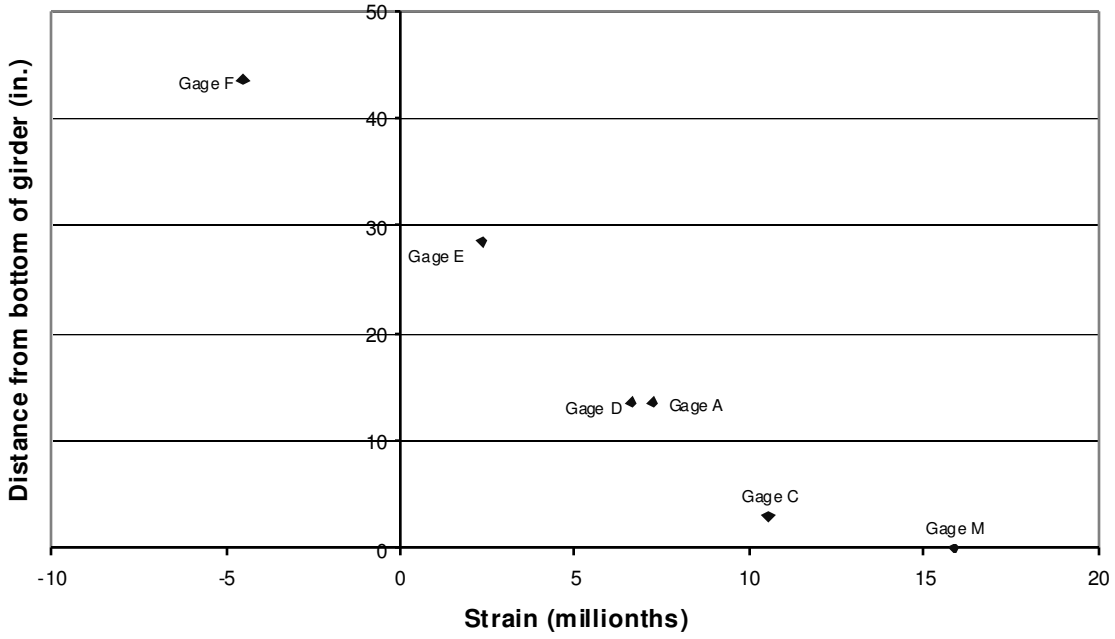


**Figure D-126:** B4 Span 10 Girder 8 Cross Section 2

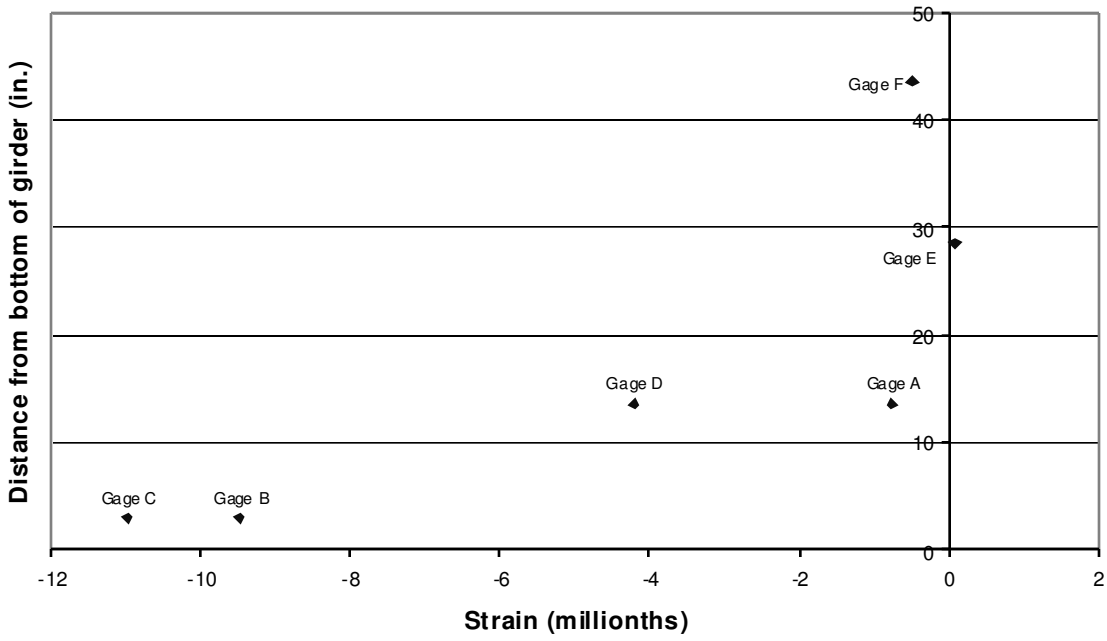


**Figure D-127:** B4 Span 11 Girder 7 Cross Section 1

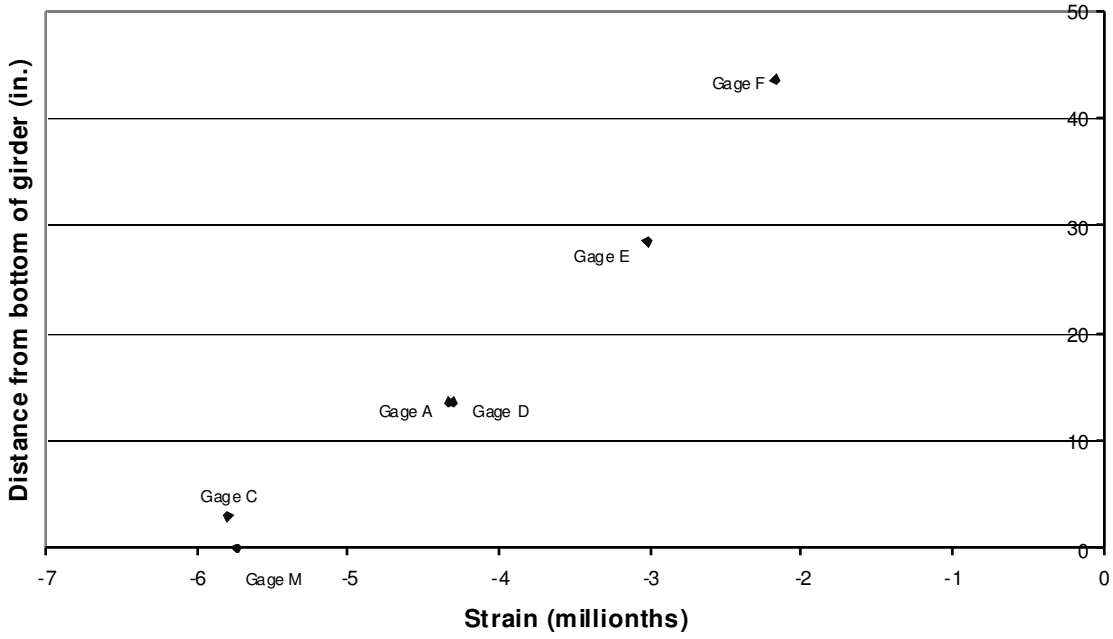


**Figure D-128:** B4 Span 11 Girder 7 Cross Section 2

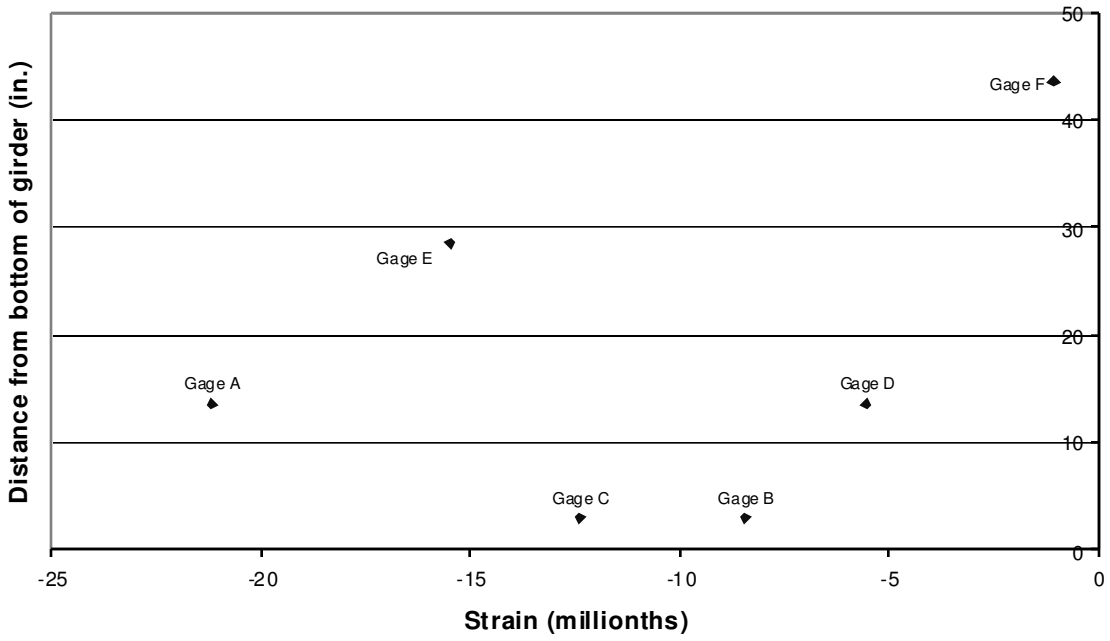


**Figure D-129:** B4 Span 11 Girder 8 Cross Section 1

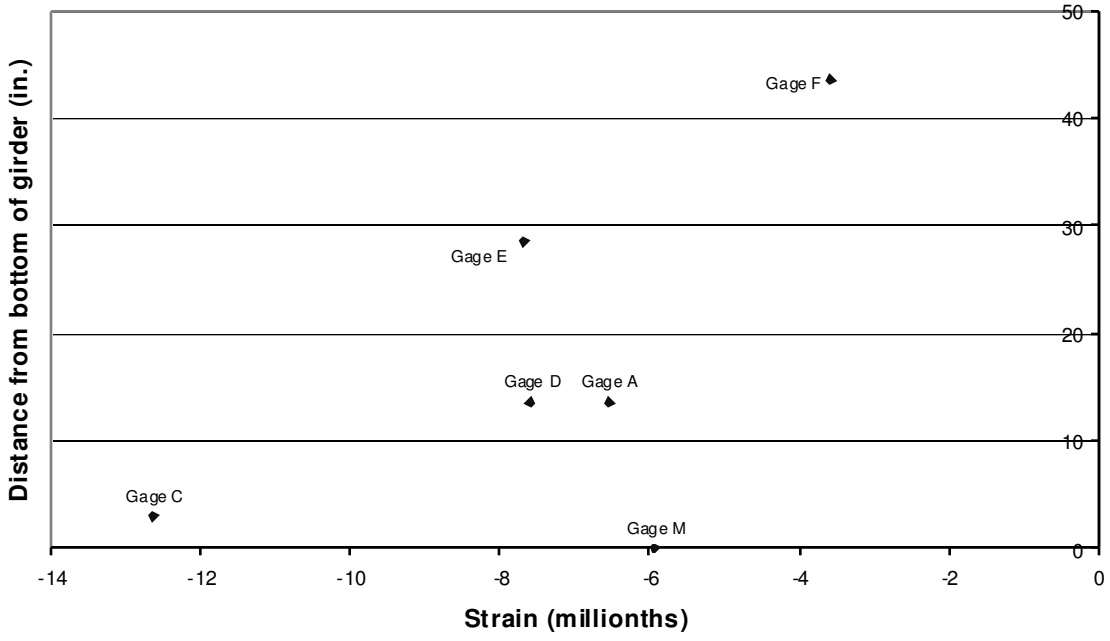


**Figure D-130:** B4 Span 11 Girder 8 Cross Section 2

### D.2.5 POSITION B5

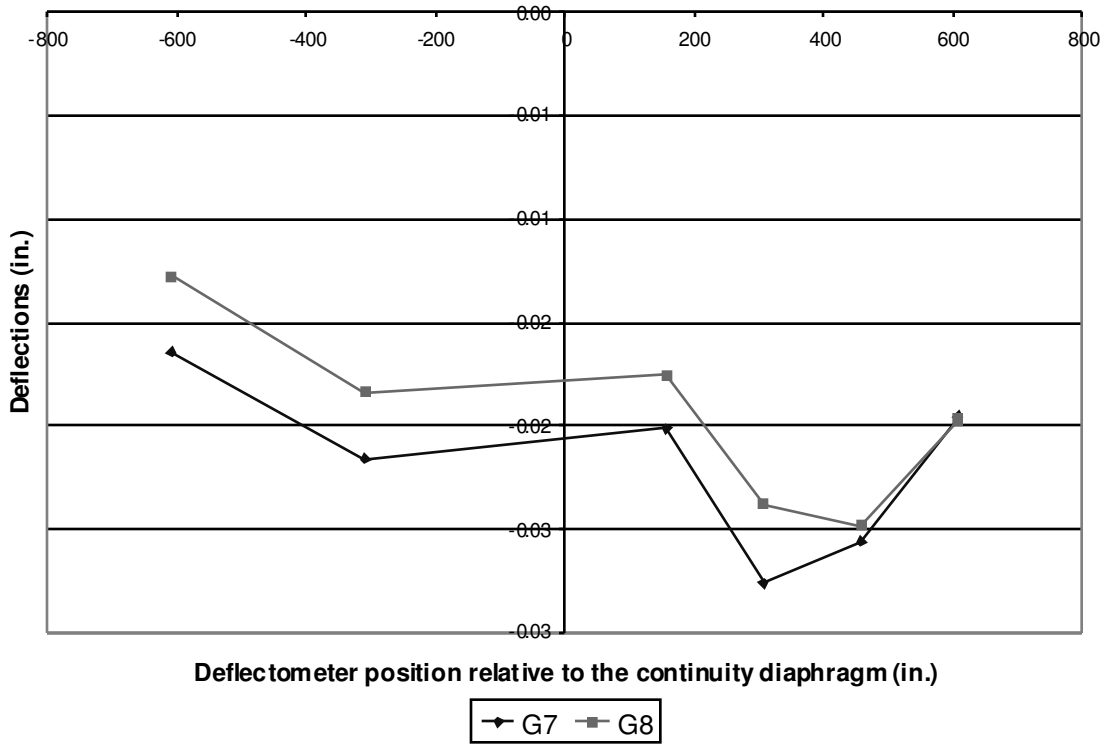


**Figure D-131:** B5 Deflections

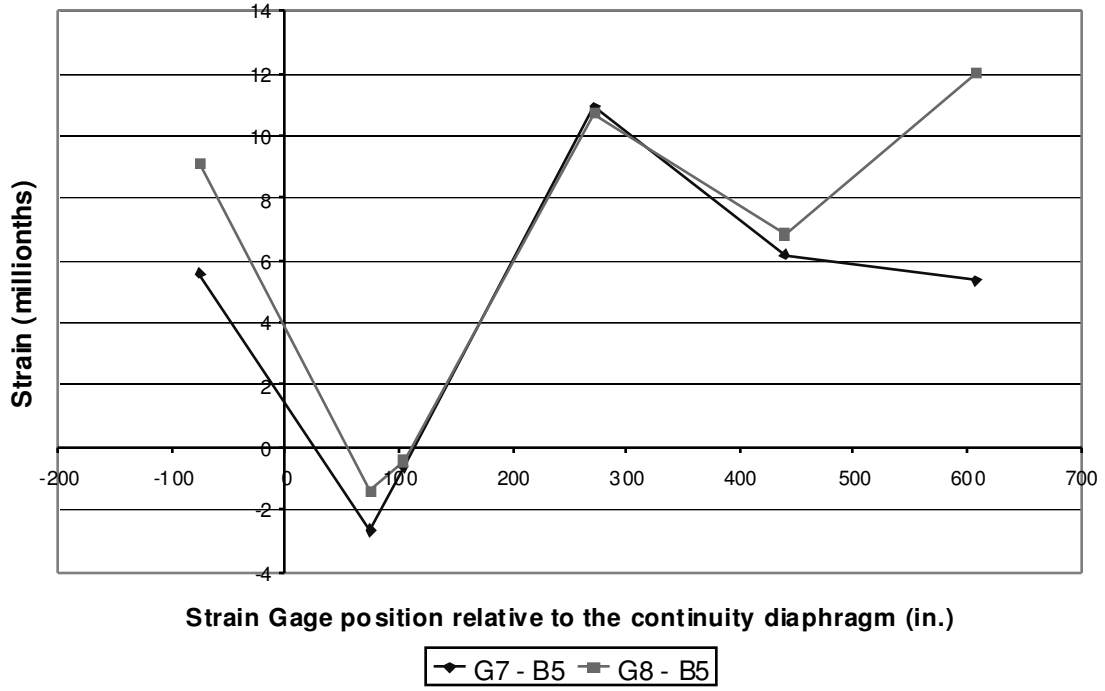


**Figure D-132:** B5 Bottom Fiber Strains

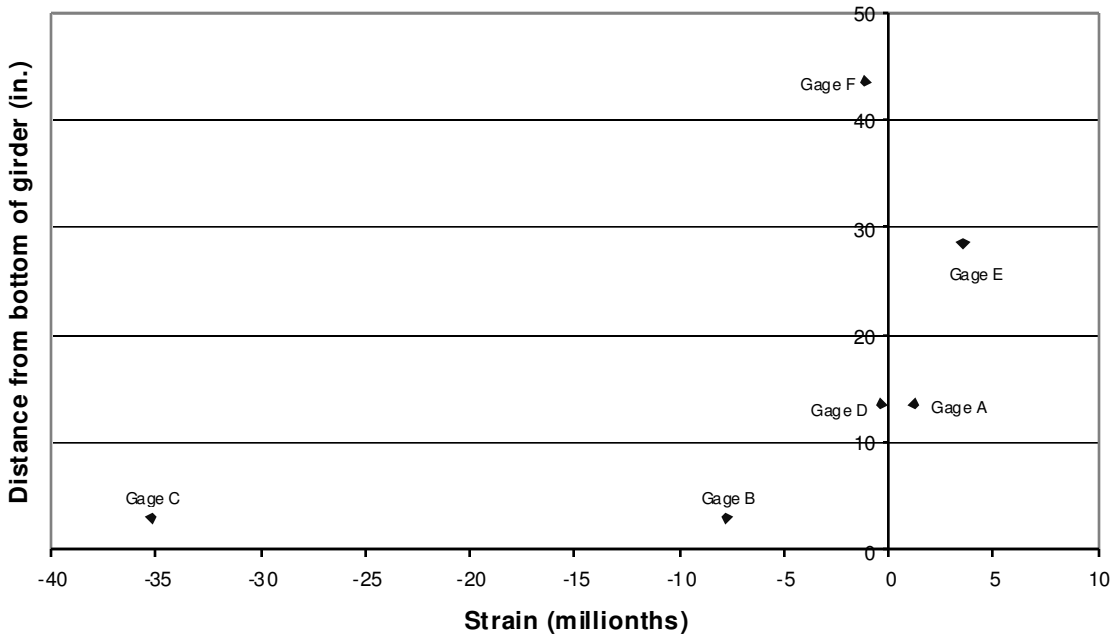


**Figure D-133:** B5 Span 10 Girder 7 Cross Section1

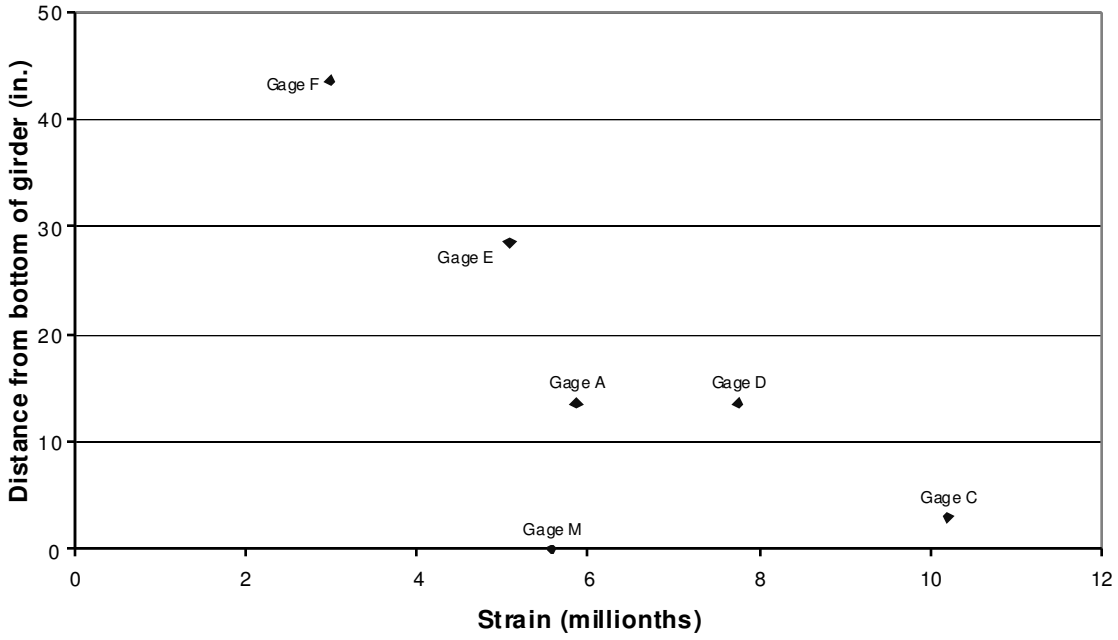


**Figure D-134:** B5 Span 10 Girder 7 Cross Section 2

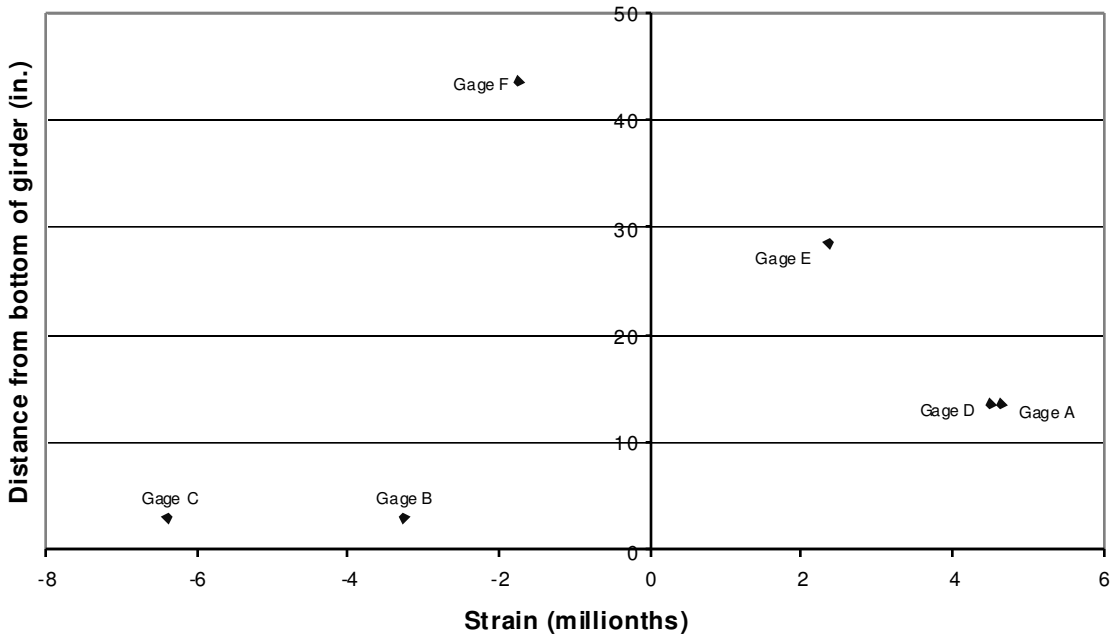


**Figure D-135:** B5 Span 10 Girder 8 Cross Section 1

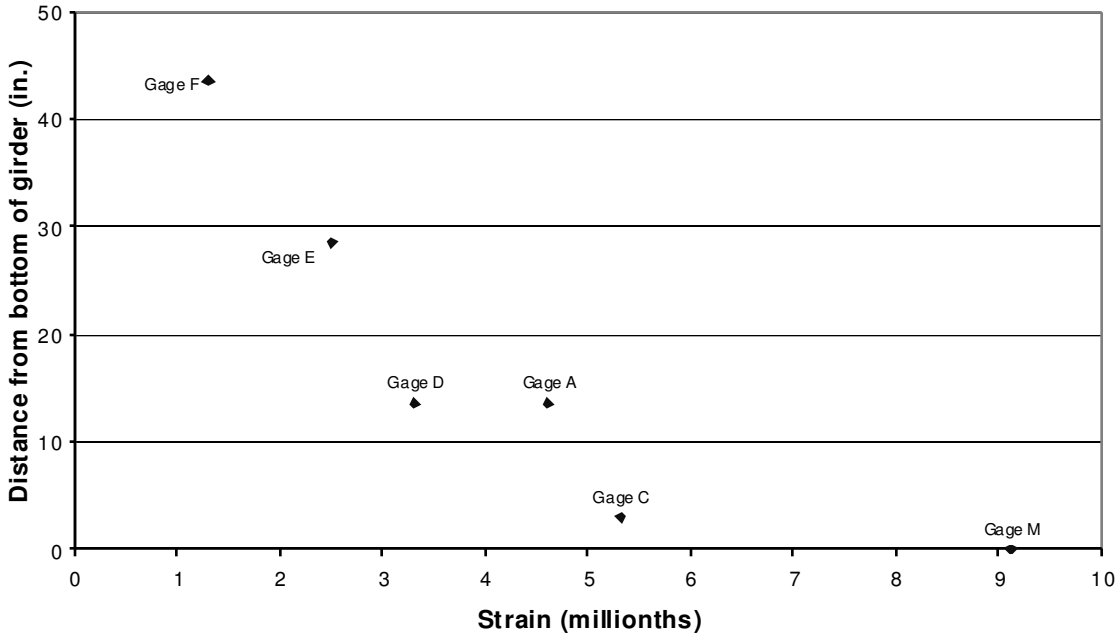


**Figure D-136:** B5 Span 10 Girder 8 Cross Section 2

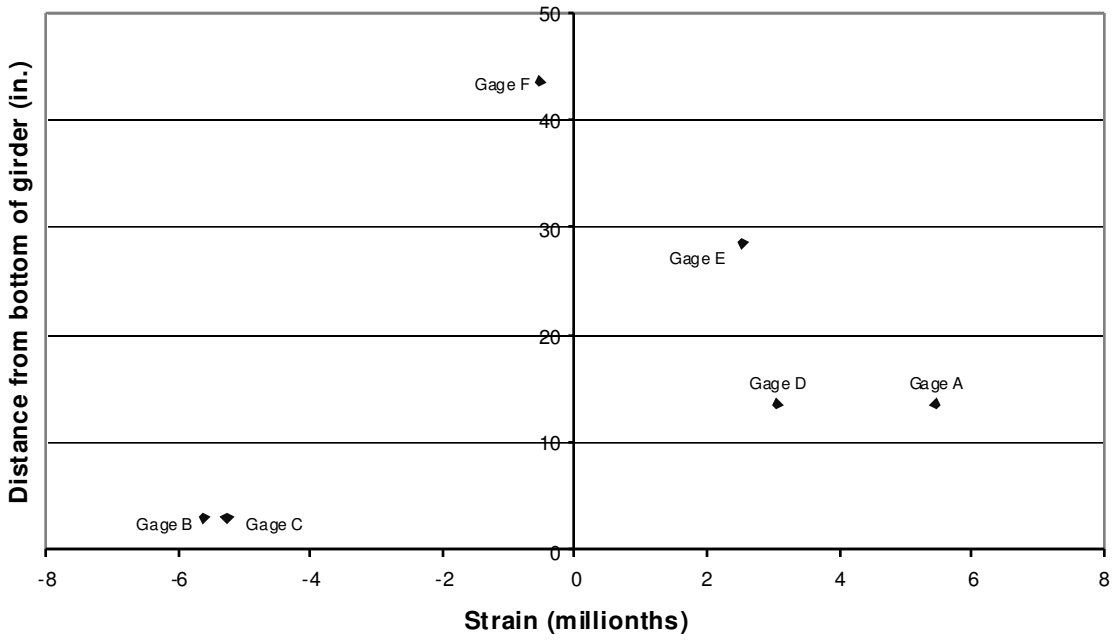


**Figure D-137:** B5 Span 11 Girder 7 Cross Section 1

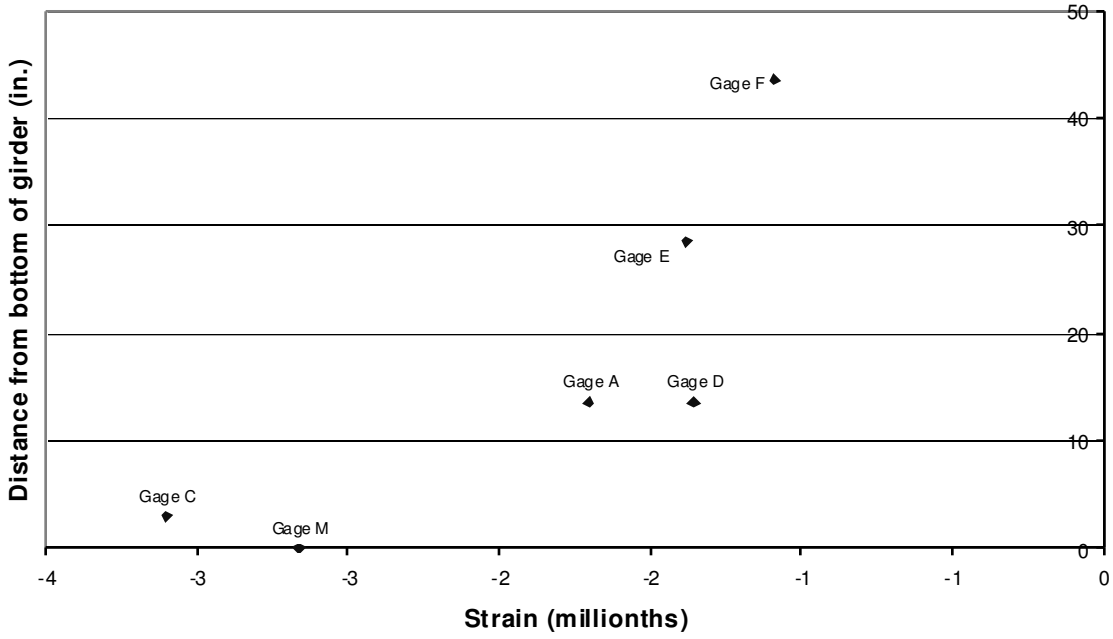


**Figure D-138:** B5 Span 11 Girder 7 Cross Section 2

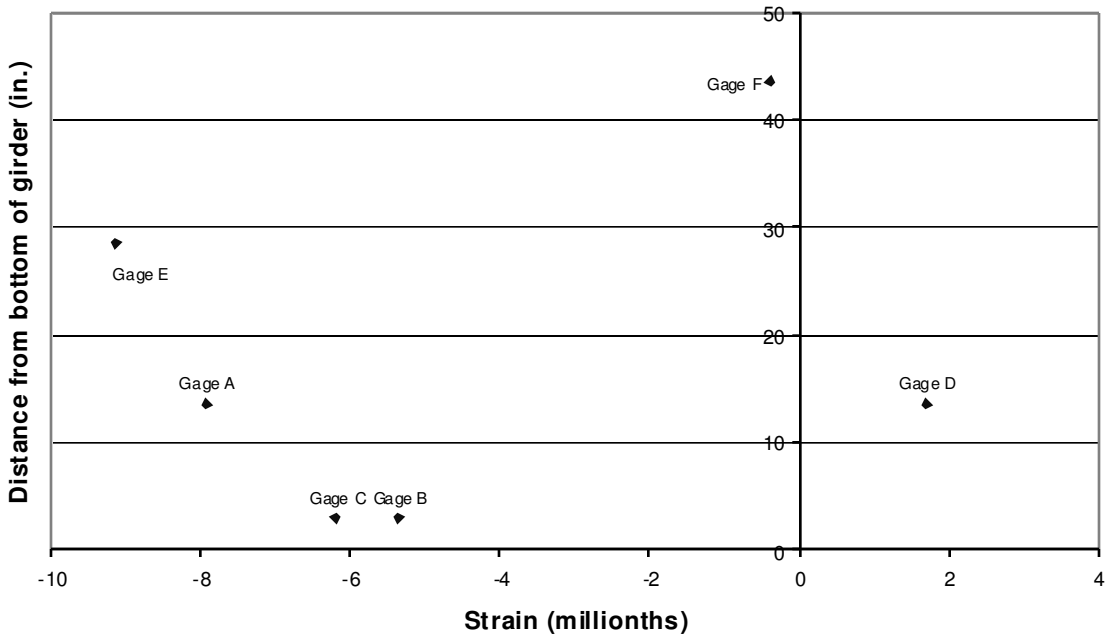


**Figure D-139:** B5 Span 11 Girder 8 Cross Section 1

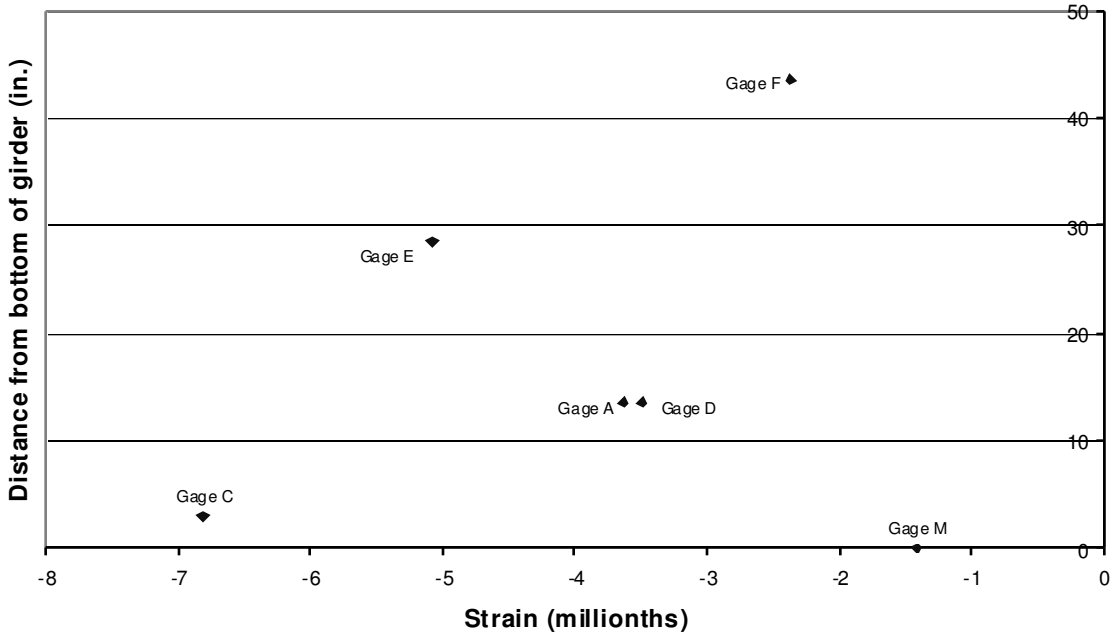


**Figure D-140:** B5 Span 11 Girder 8 Cross Section 2

### D.2.6 POSITION B6

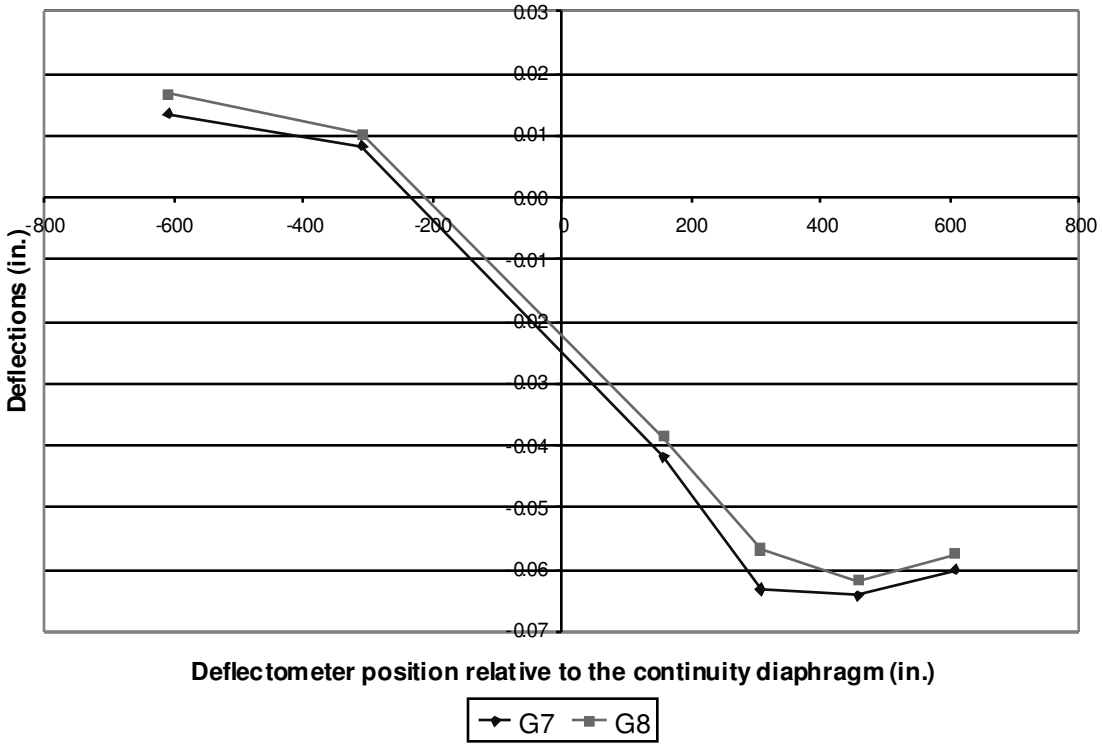


**Figure D-141:** B6 Deflections

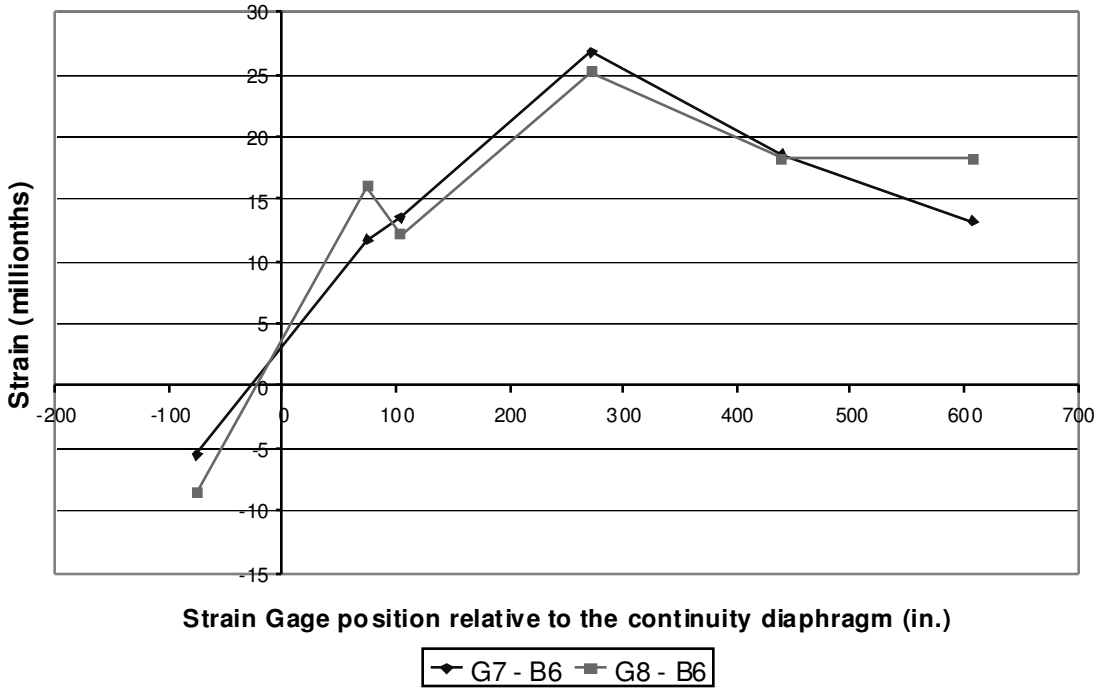


**Figure D-142:** B6 Bottom Fiber Strains

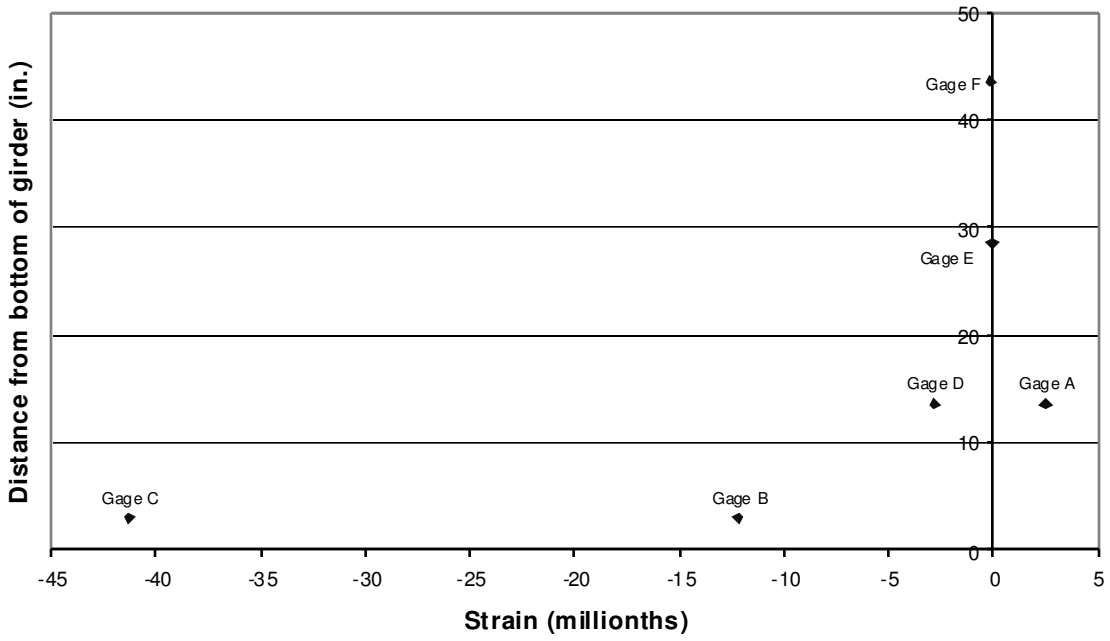


**Figure D-143:** B6 Span 10 Girder 7 Cross Section1

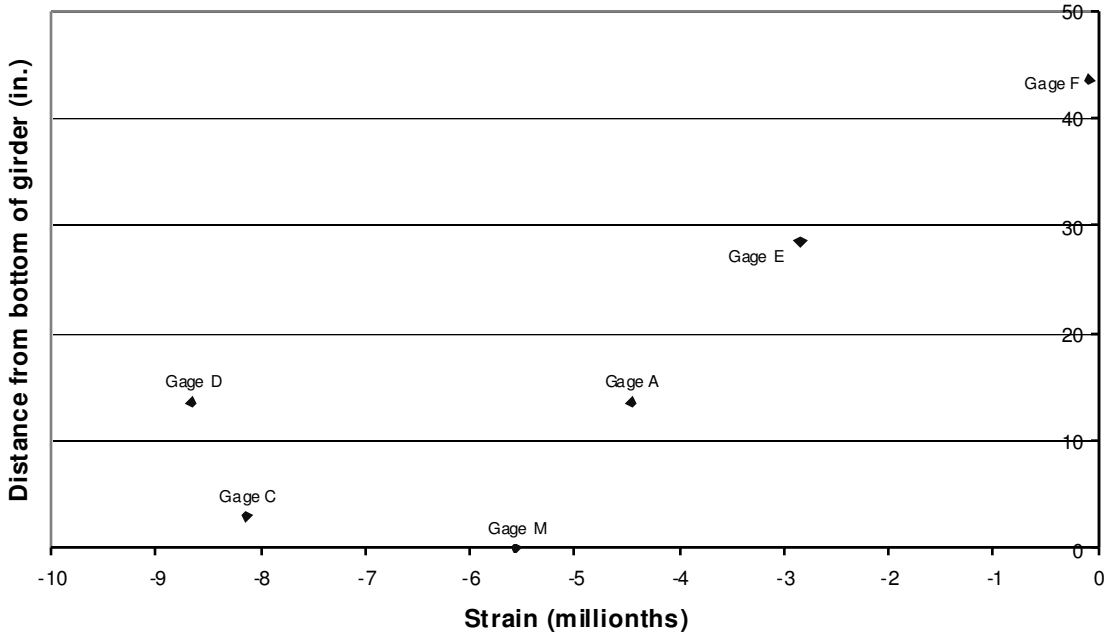


**Figure D-144:** B6 Span 10 Girder 7 Cross Section 2

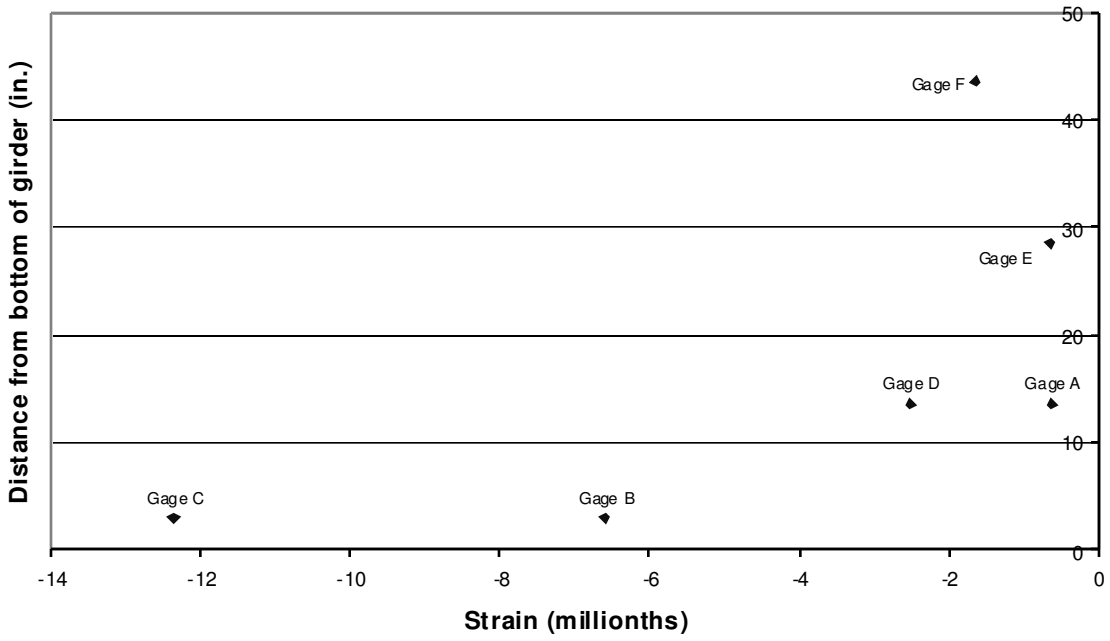


**Figure D-145:** B6 Span 10 Girder 8 Cross Section 1

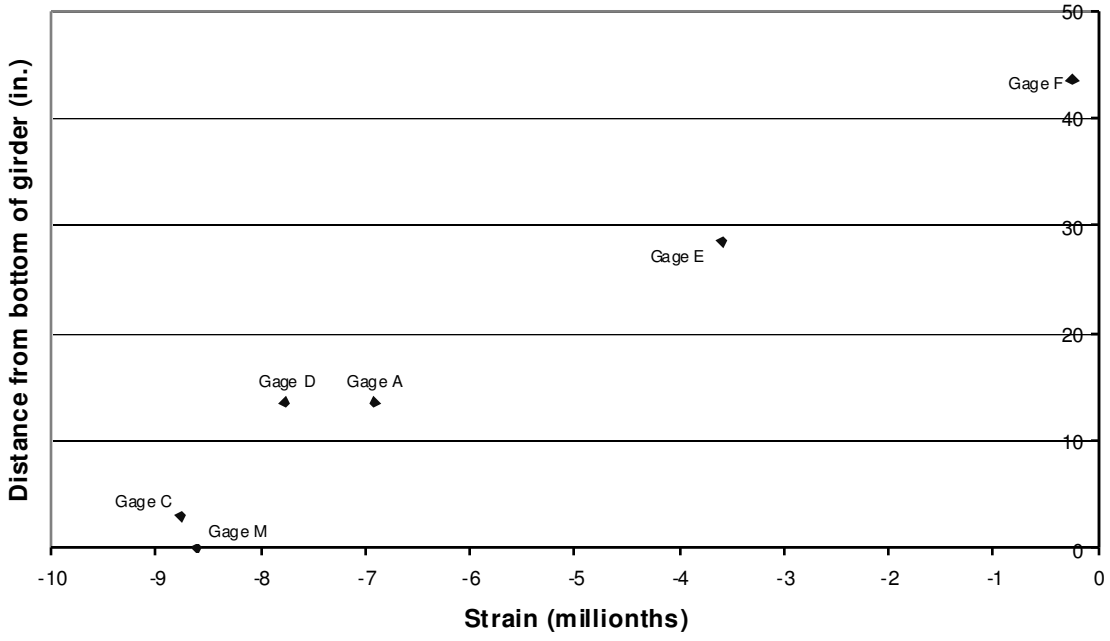


**Figure D-146:** B6 Span 10 Girder 8 Cross Section 2

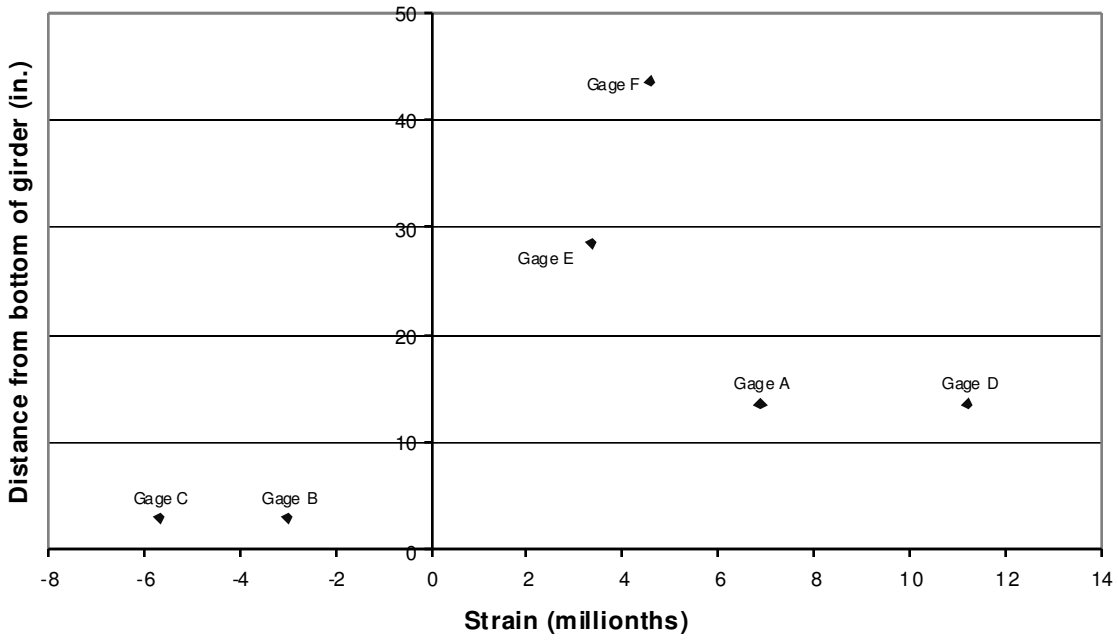


**Figure D-147:** B6 Span 11 Girder 7 Cross Section 1

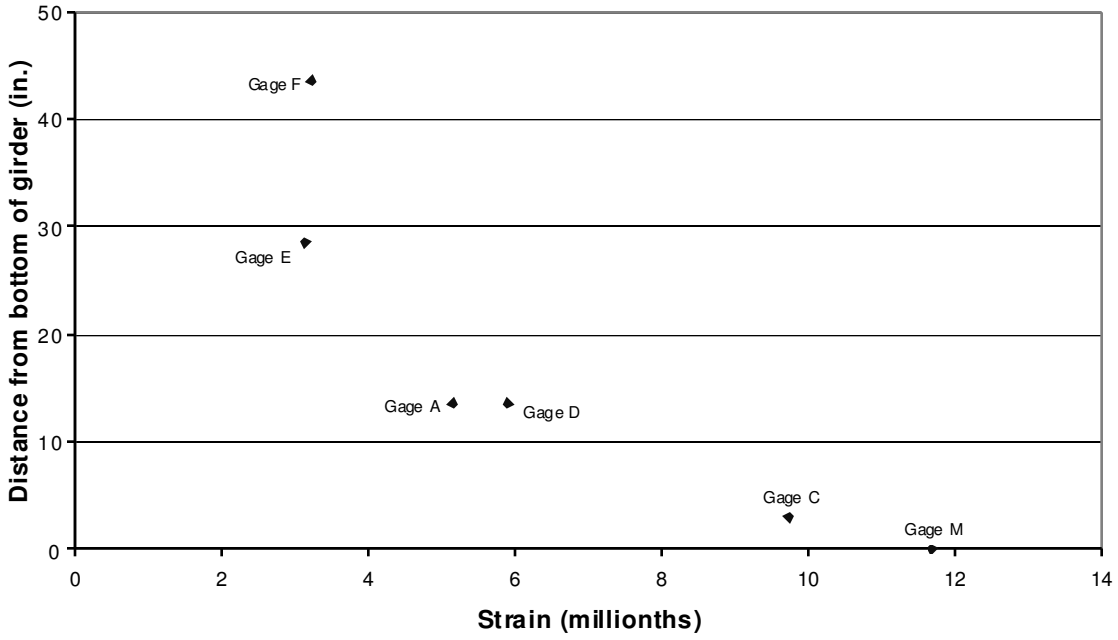


**Figure D-148:** B6 Span 11 Girder 7 Cross Section 2

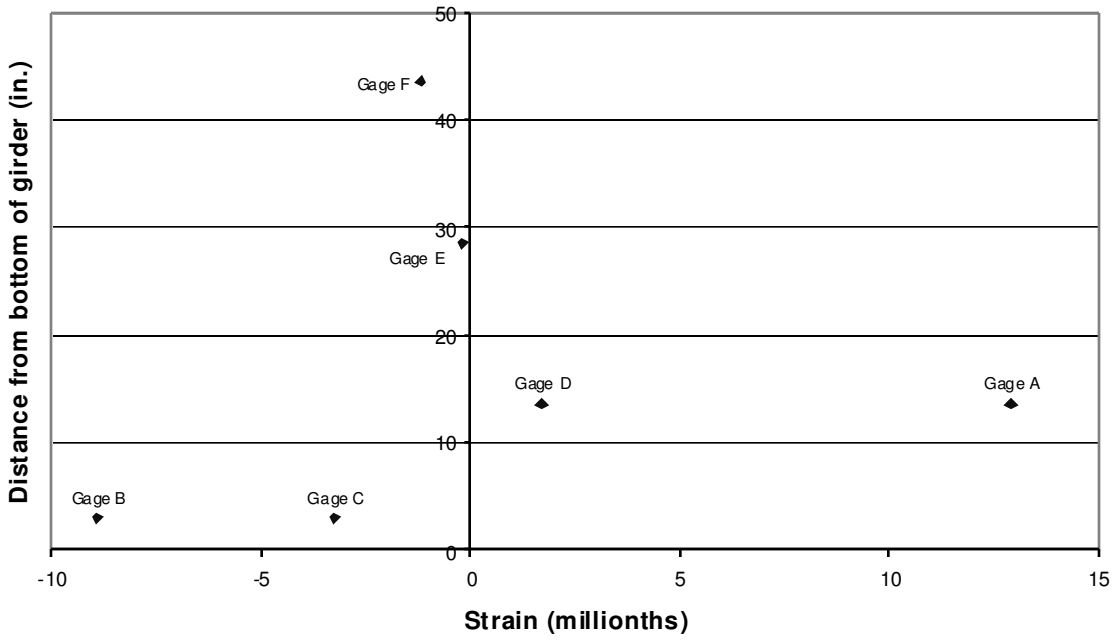


**Figure D-149:** B6 Span 11 Girder 8 Cross Section 1

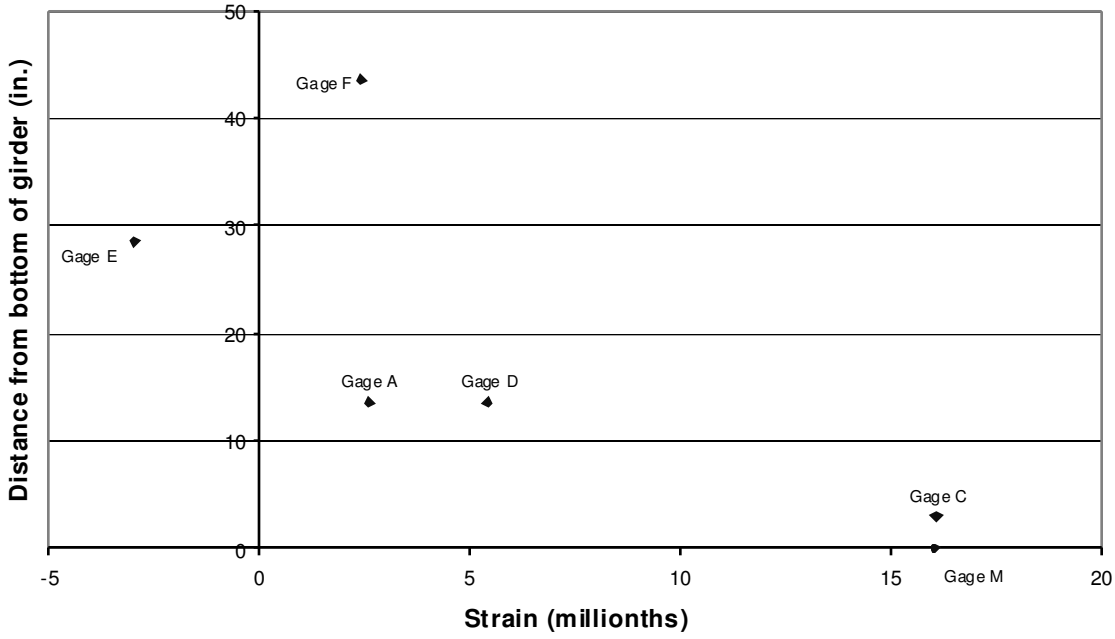


**Figure D-150:** B6 Span 11 Girder 8 Cross Section 2

### D.2.7 POSITION B7

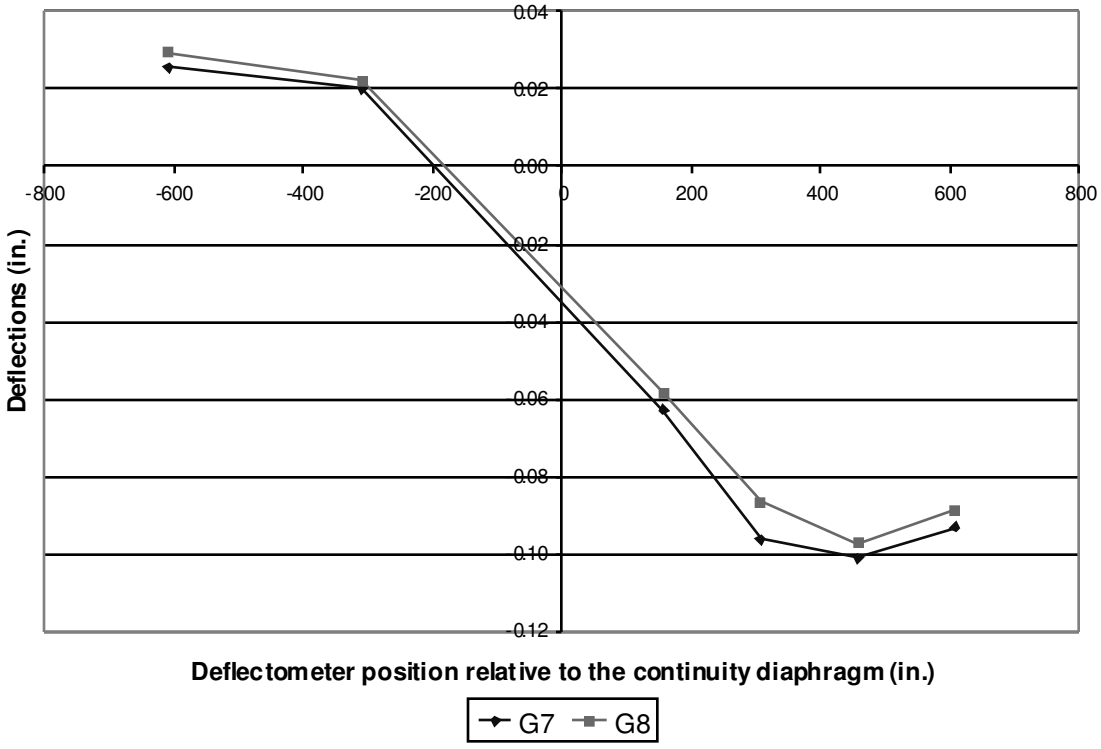


**Figure D-151:** B7 Deflections

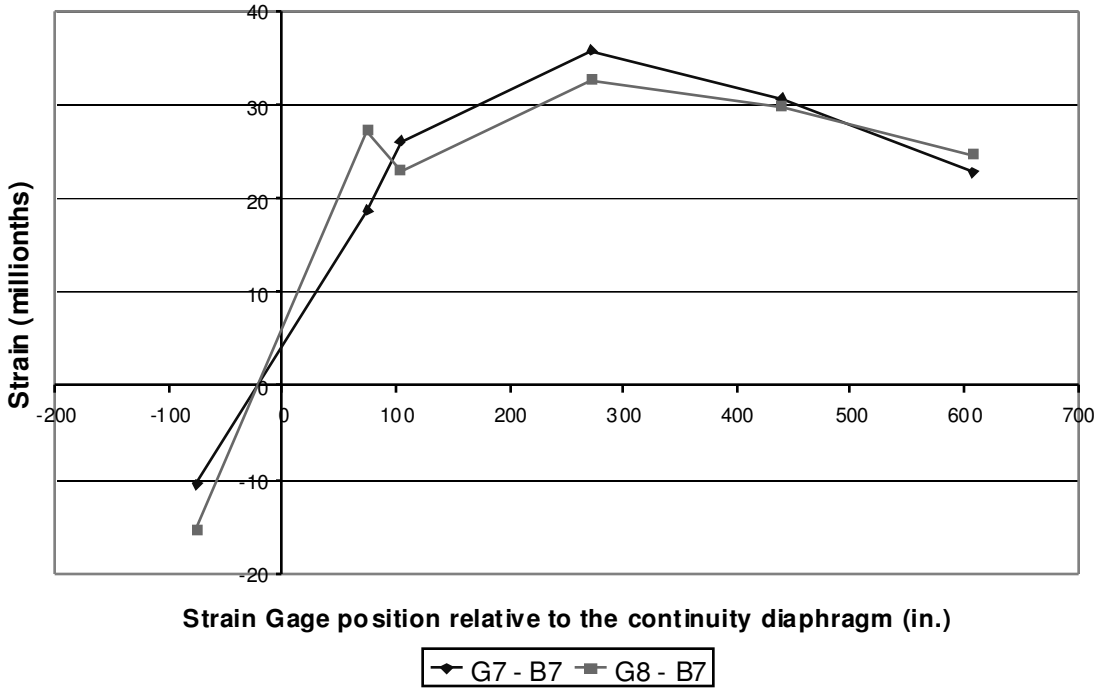


**Figure D-152:** B7 Bottom Fiber Strains

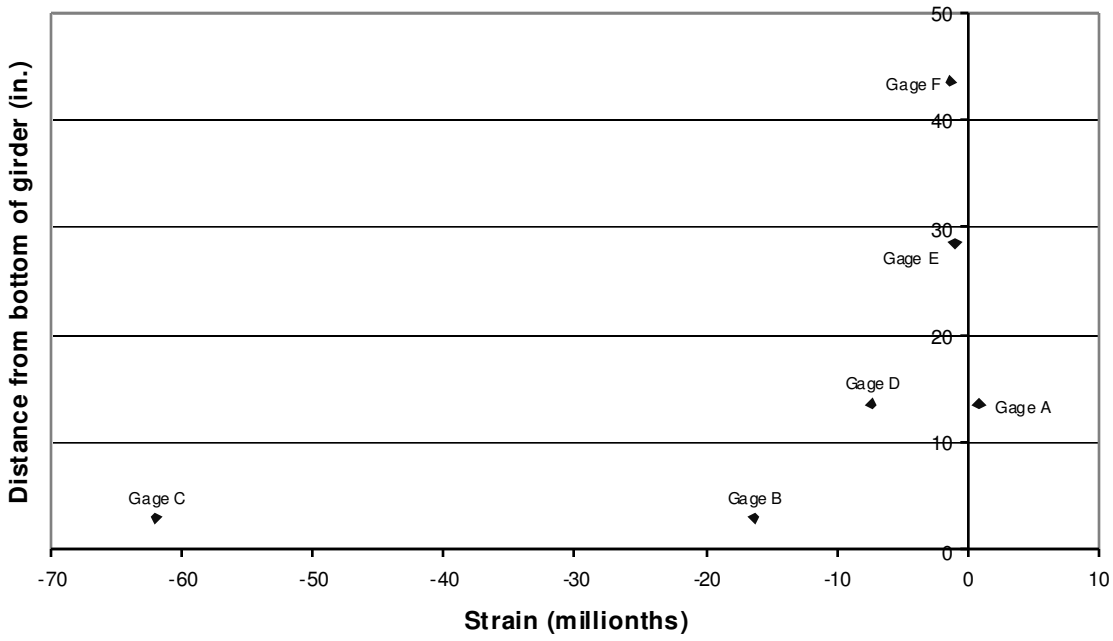


**Figure D-153:** B7 Span 10 Girder 7 Cross Section1

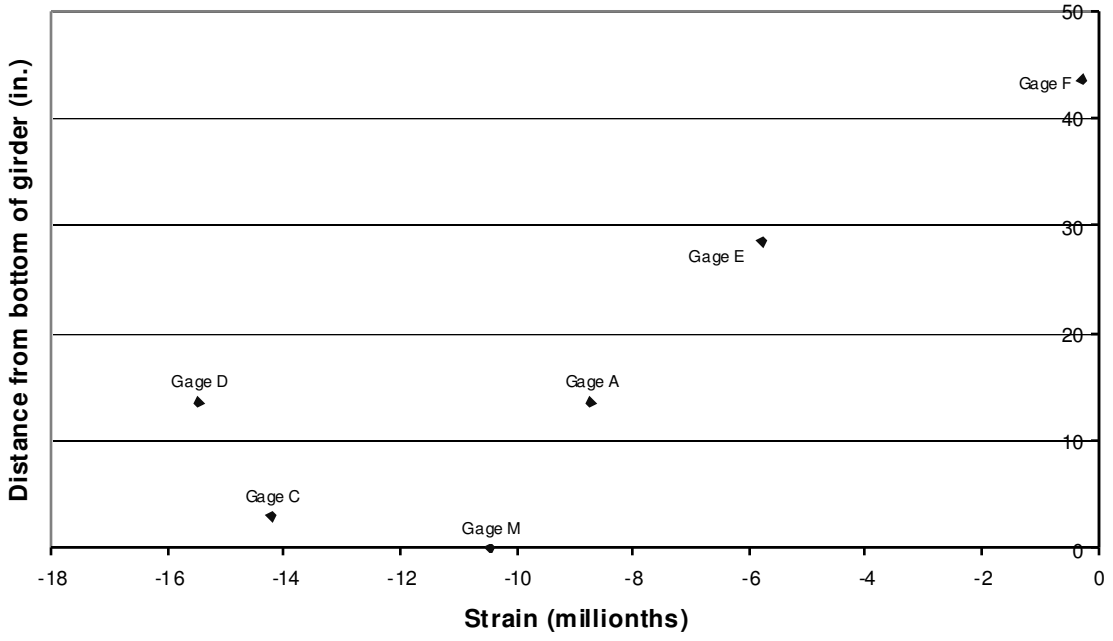


**Figure D-154:** B7 Span 10 Girder 7 Cross Section 2

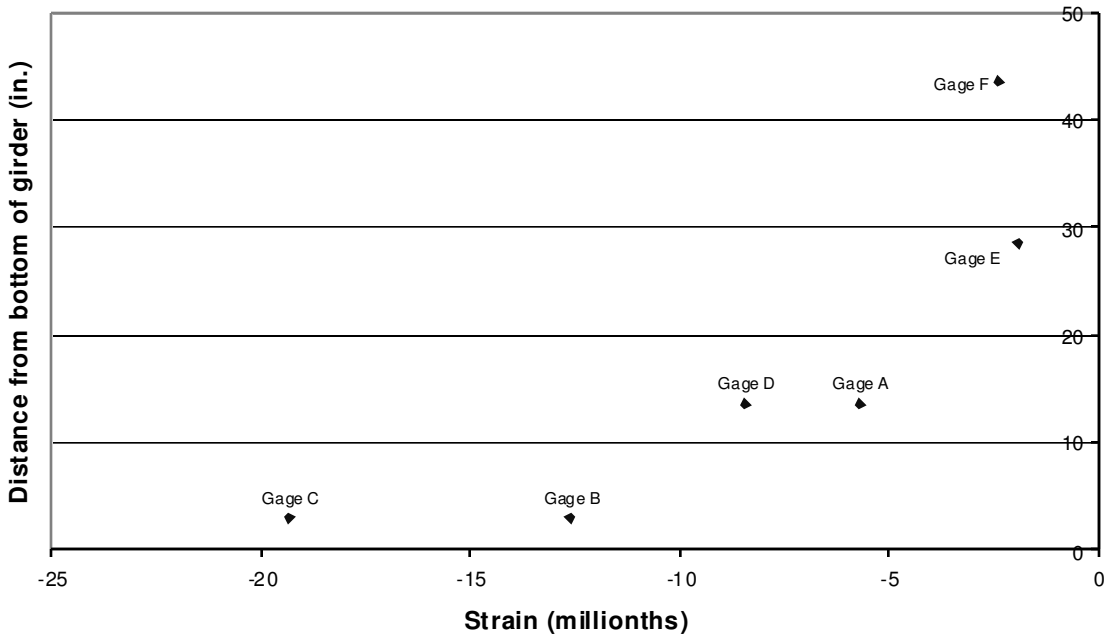


**Figure D-155:** B7 Span 10 Girder 8 Cross Section 1

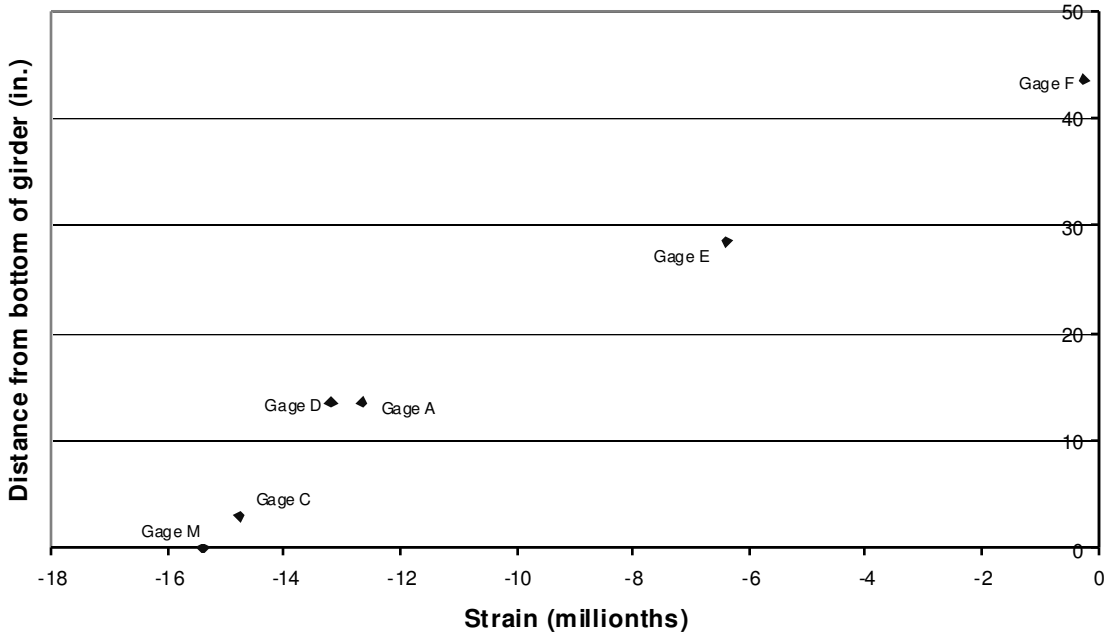


**Figure D-156:** B7 Span 10 Girder 8 Cross Section 2

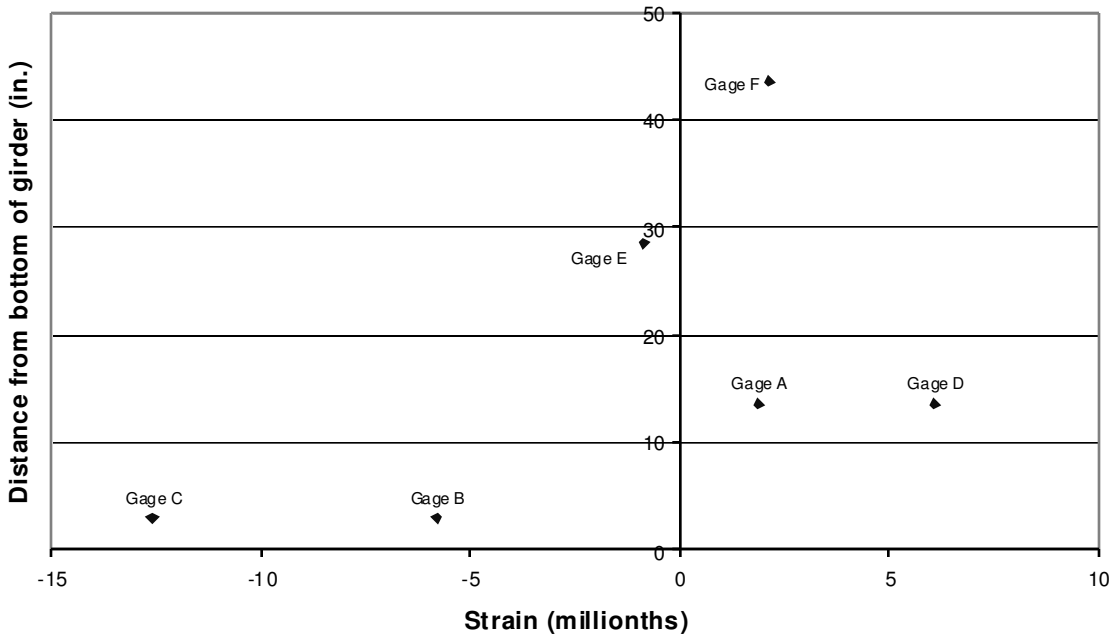


**Figure D-157:** B7 Span 11 Girder 7 Cross Section 1

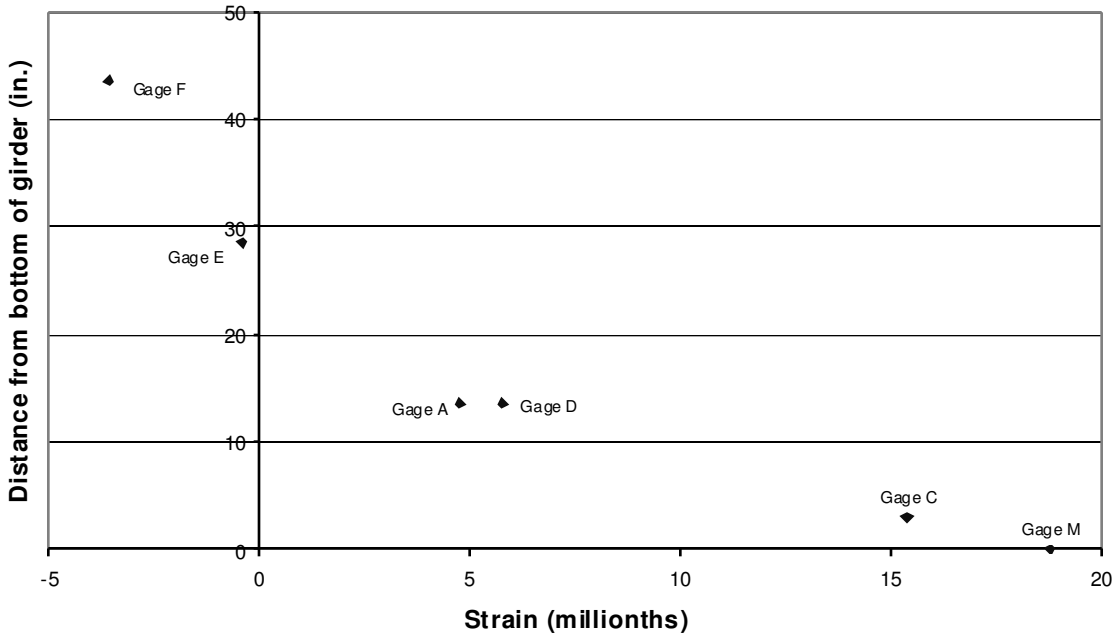


**Figure D-158:** B7 Span 11 Girder 7 Cross Section 2

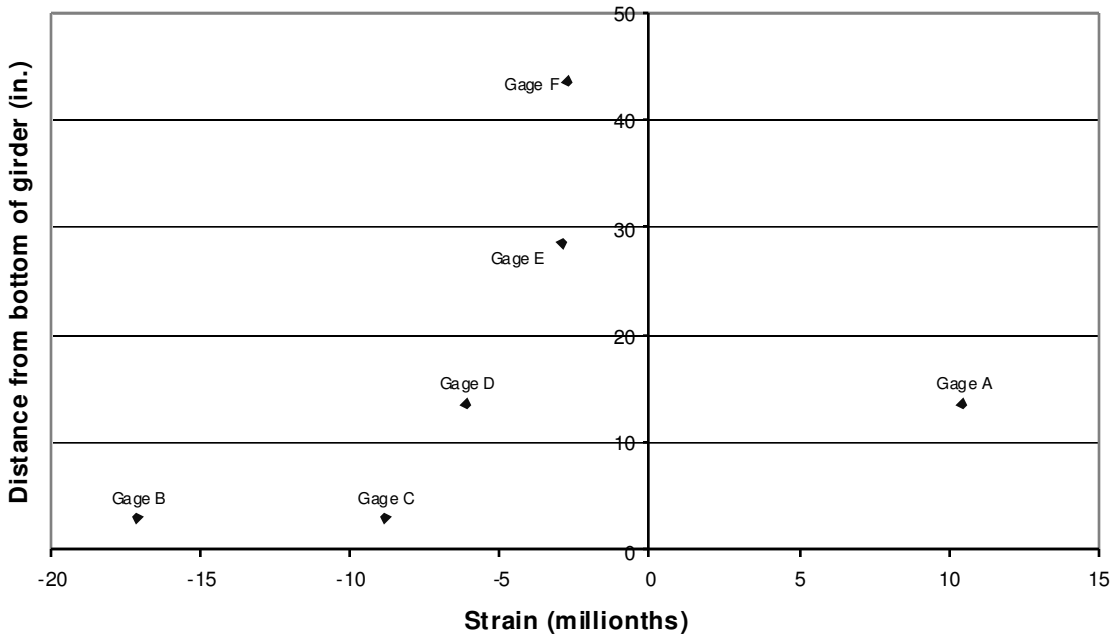


**Figure D-159:** B7 Span 11 Girder 8 Cross Section 1

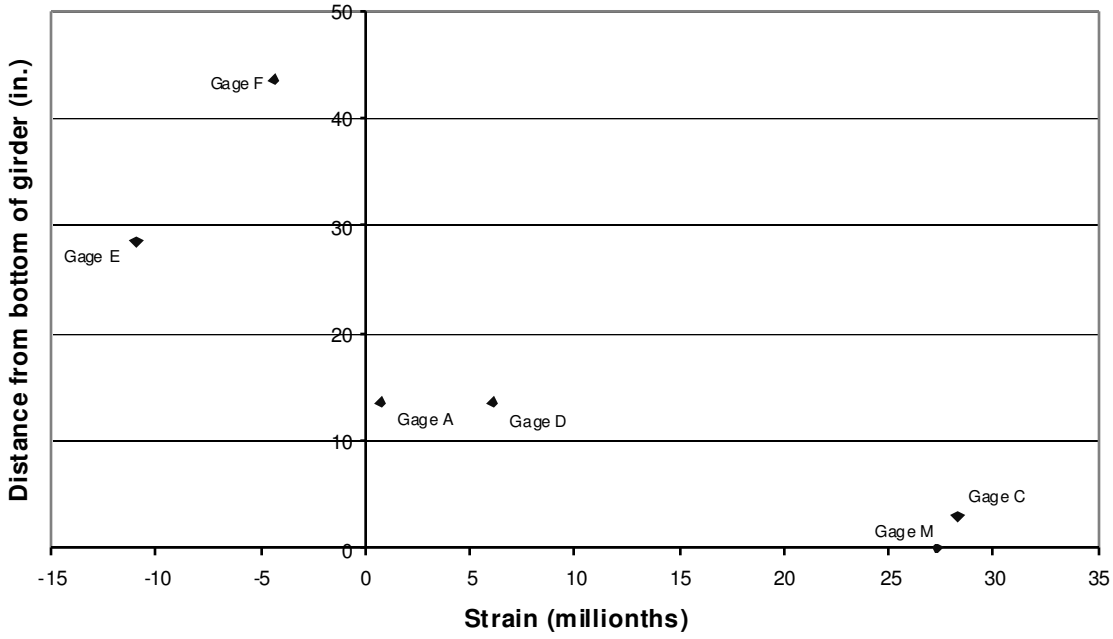


**Figure D-160:** B7 Span 11 Girder 8 Cross Section 2

### D.2.8 POSITION B8

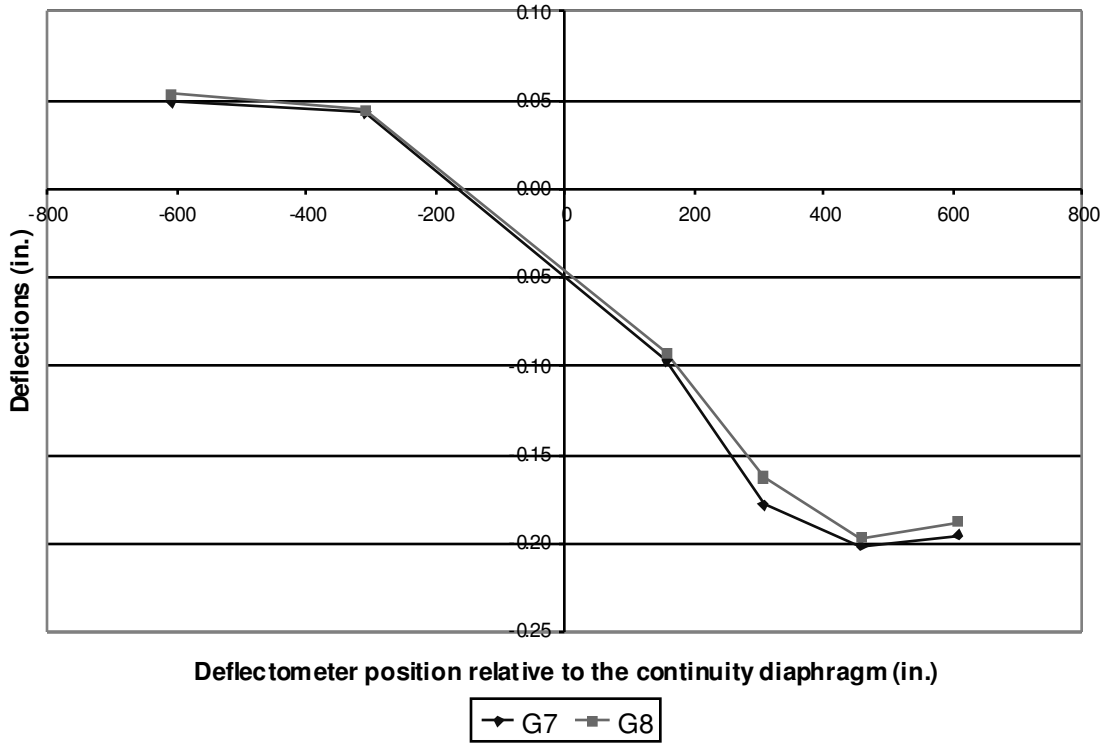


**Figure D-161:** B8 Deflections

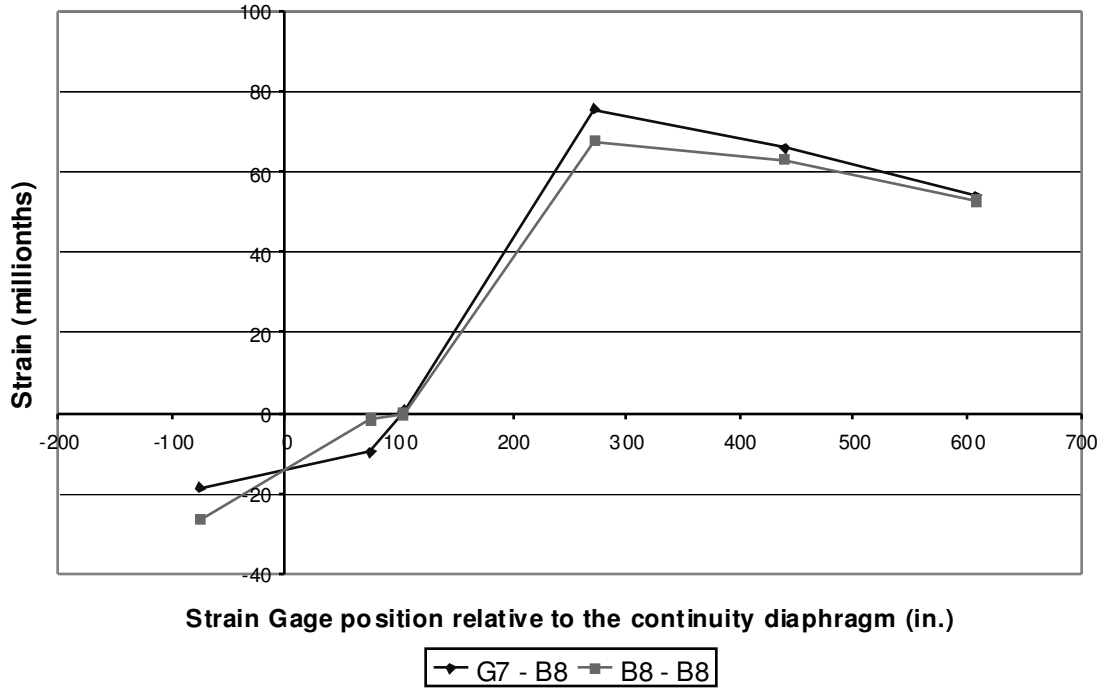


**Figure D-162:** B8 Bottom Fiber Strains

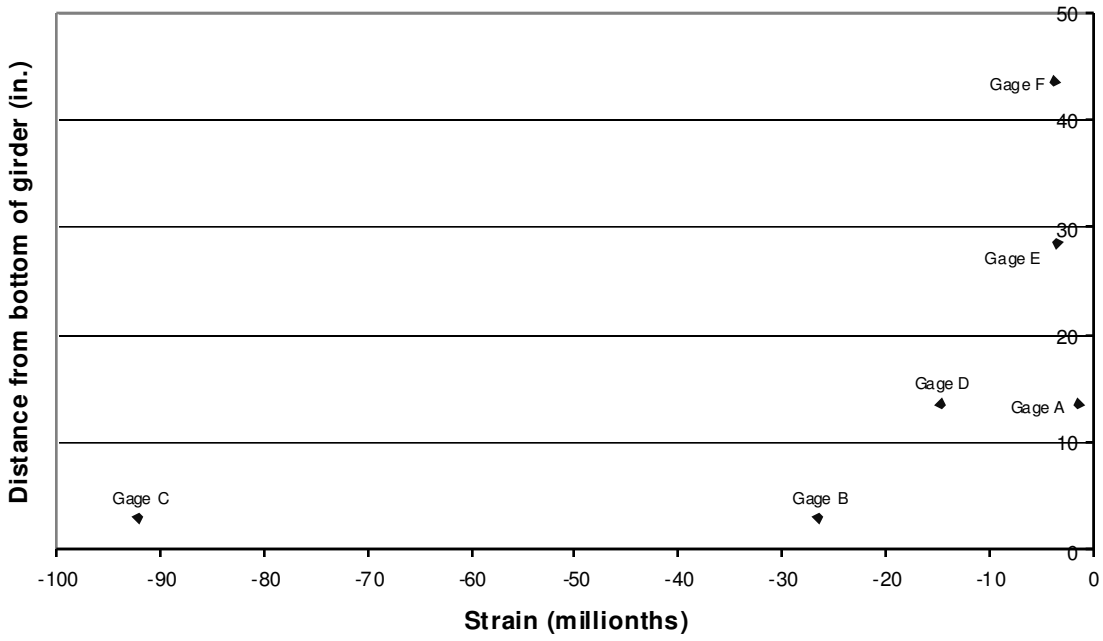


**Figure D-163:** B8 Span 10 Girder 7 Cross Section1

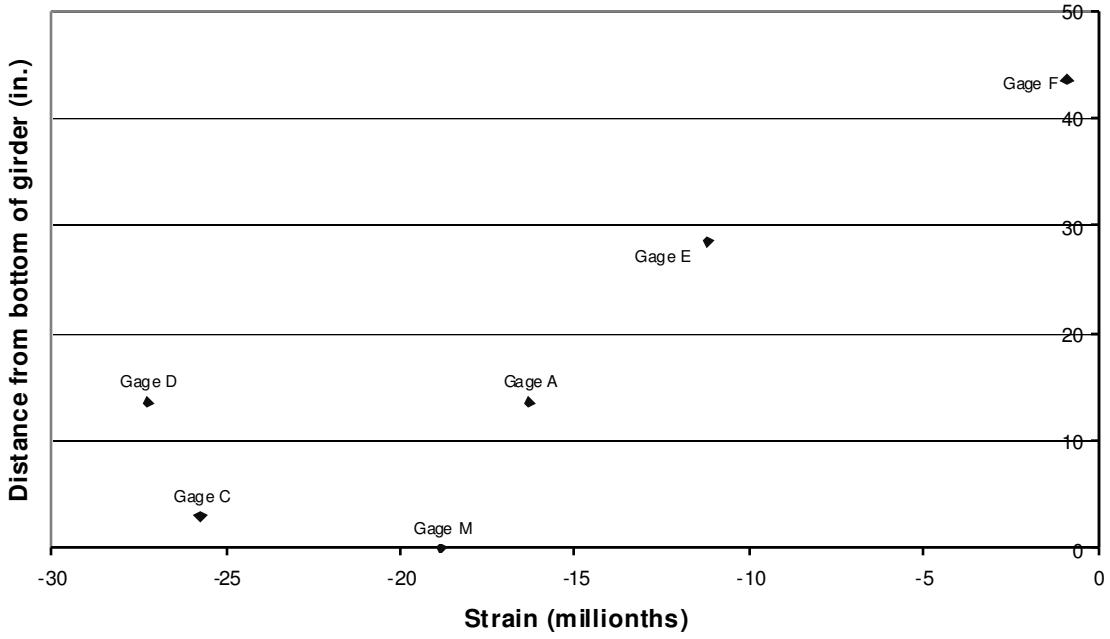


**Figure D-164:** B8 Span 10 Girder 7 Cross Section 2

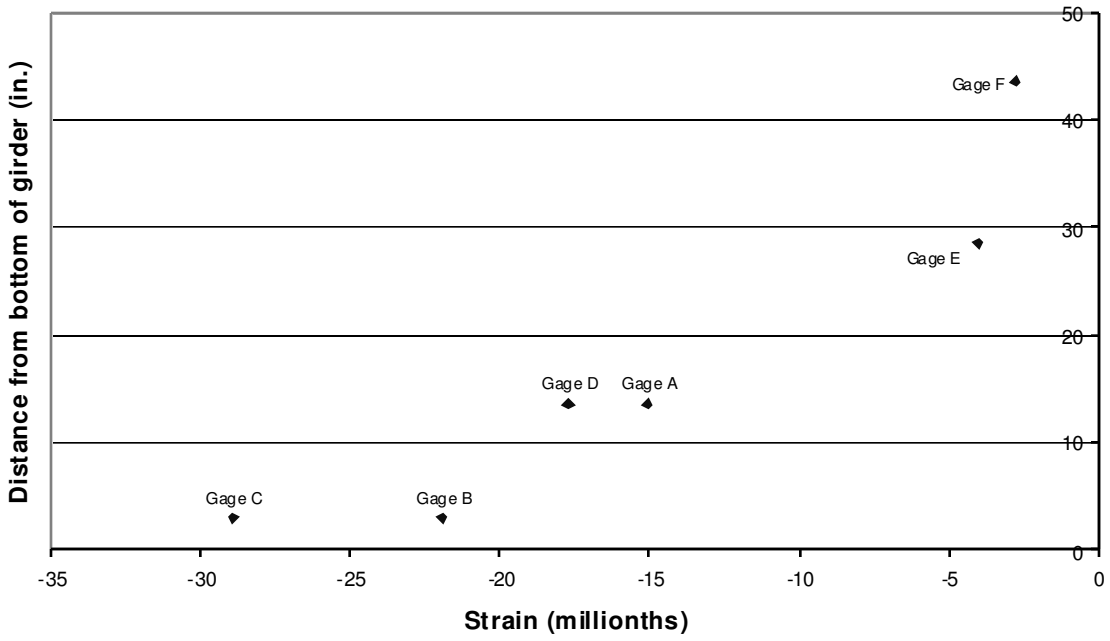


**Figure D-165:** B8 Span 10 Girder 8 Cross Section 1

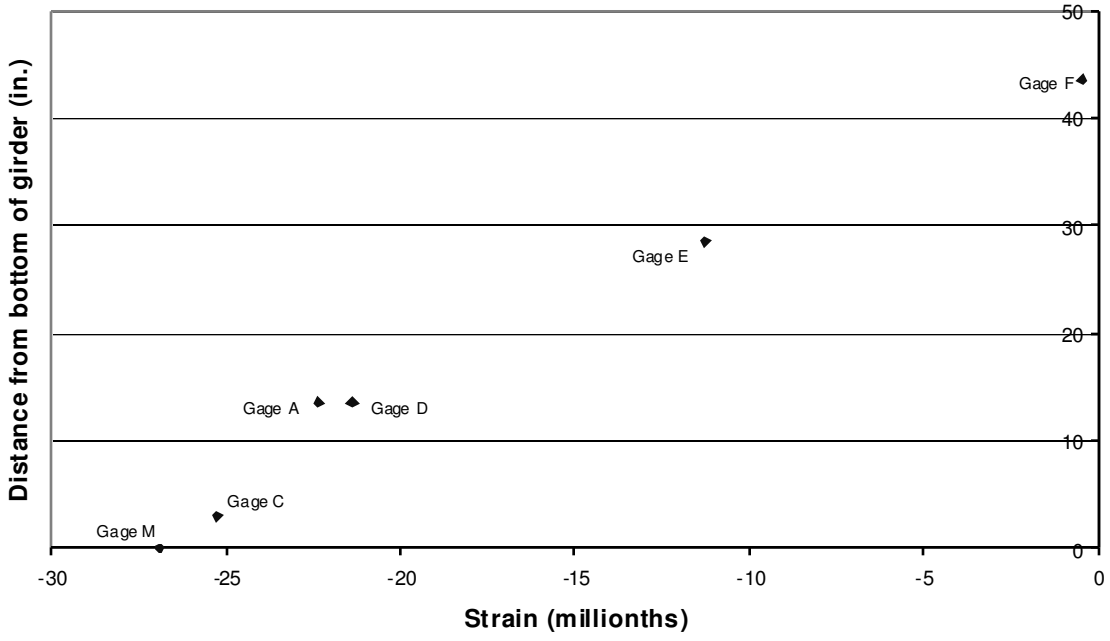


**Figure D-166:** B8 Span 10 Girder 8 Cross Section 2

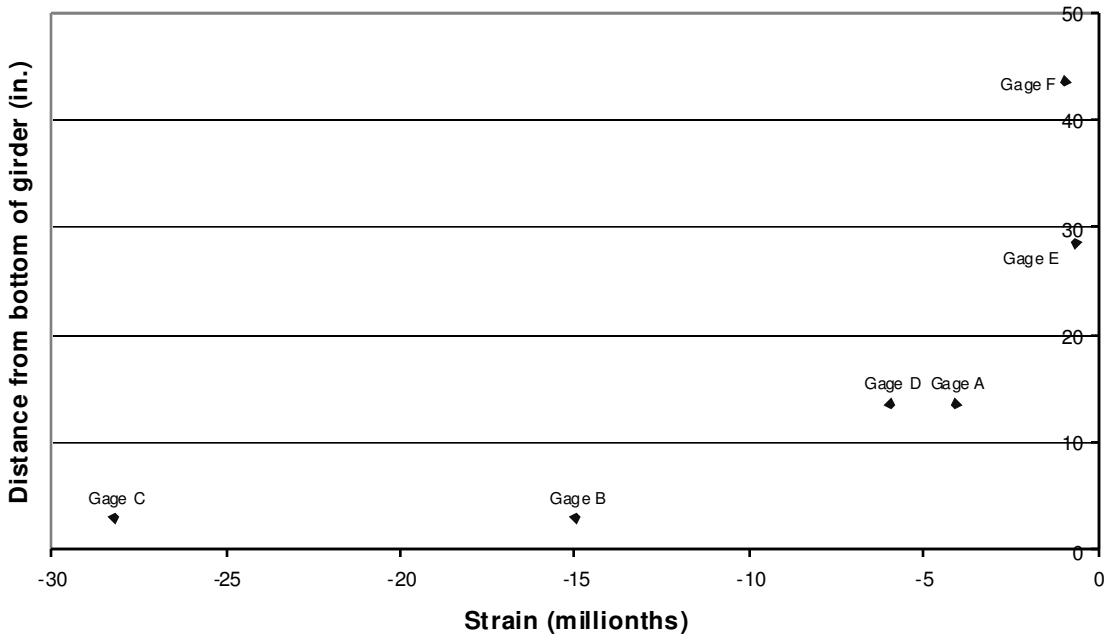


**Figure D-167:** B8 Span 11 Girder 7 Cross Section 1

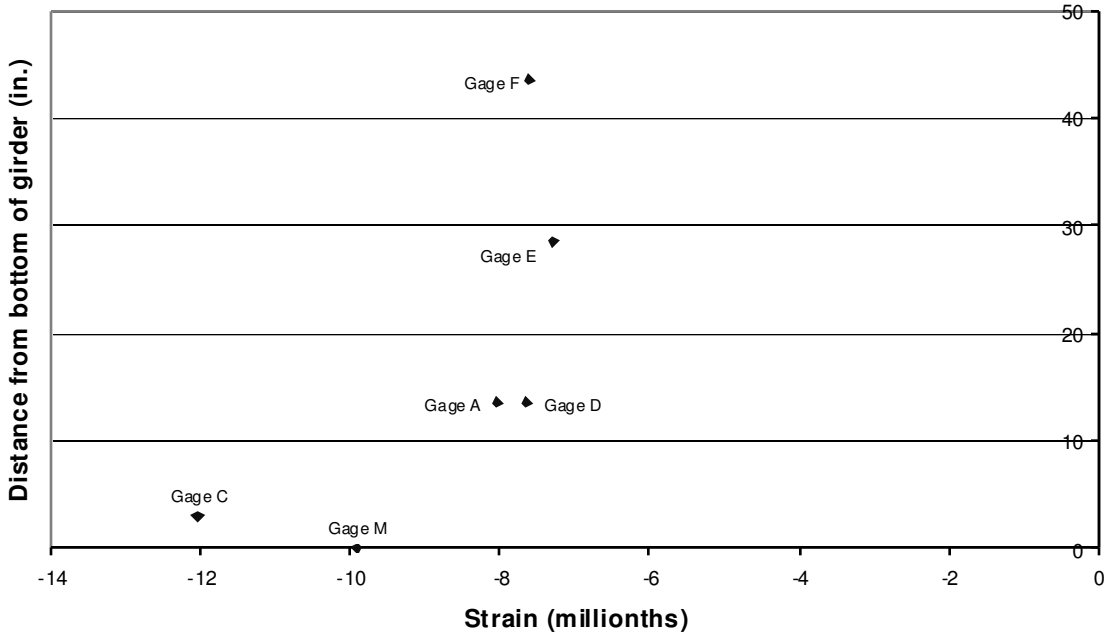


**Figure D-168:** B8 Span 11 Girder 7 Cross Section 2

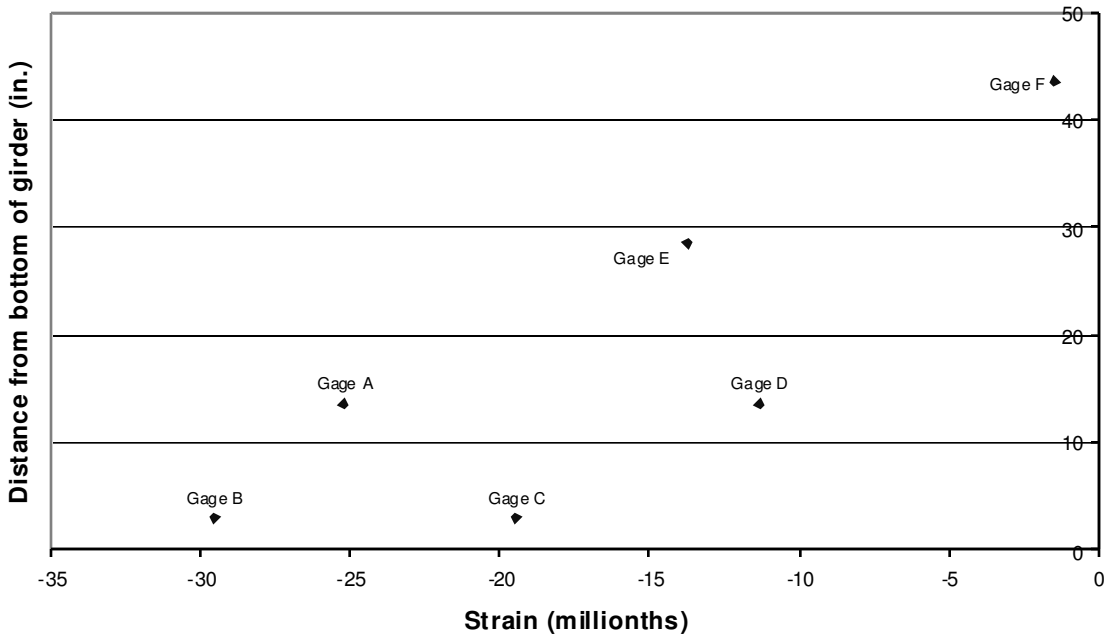


**Figure D-169:** B8 Span 11 Girder 8 Cross Section 1

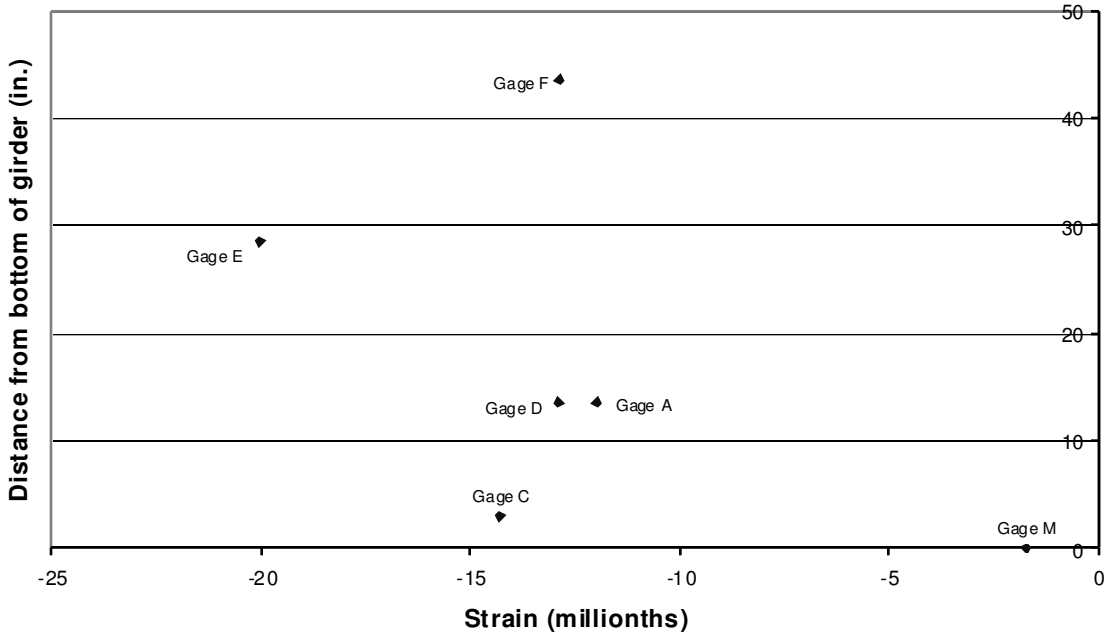


**Figure D-170:** B8 Span 11 Girder 8 Cross Section 2

### D.2.9 POSITION B9

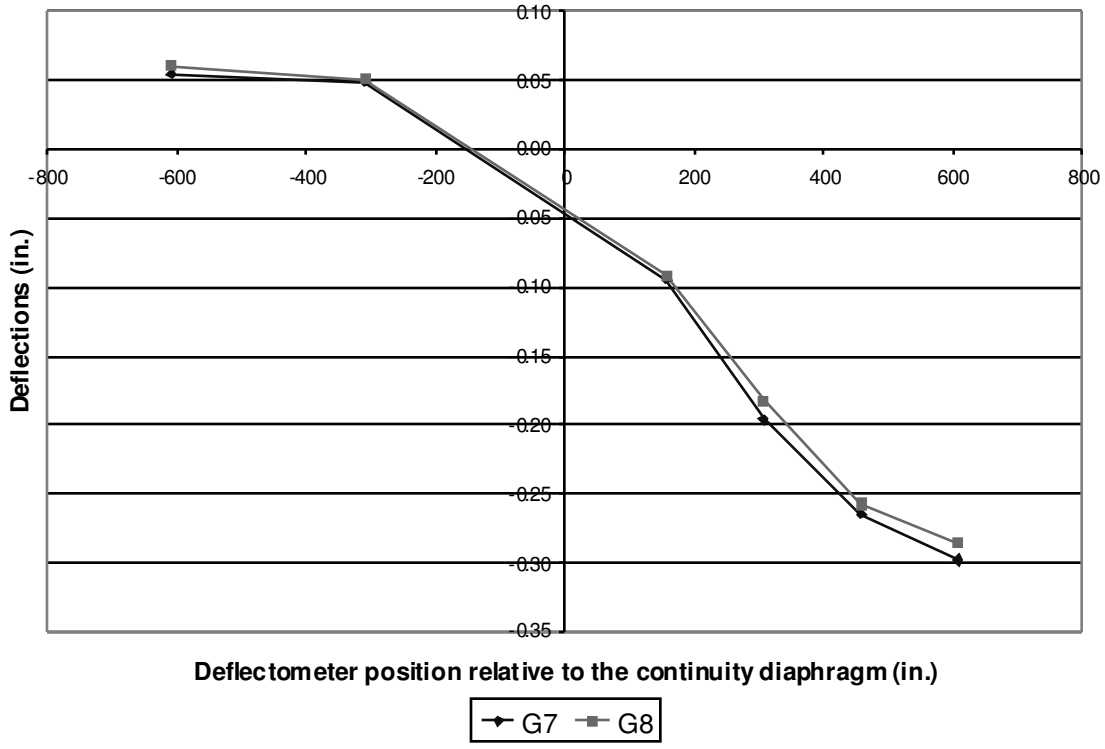


**Figure D-171:** B9 Deflections

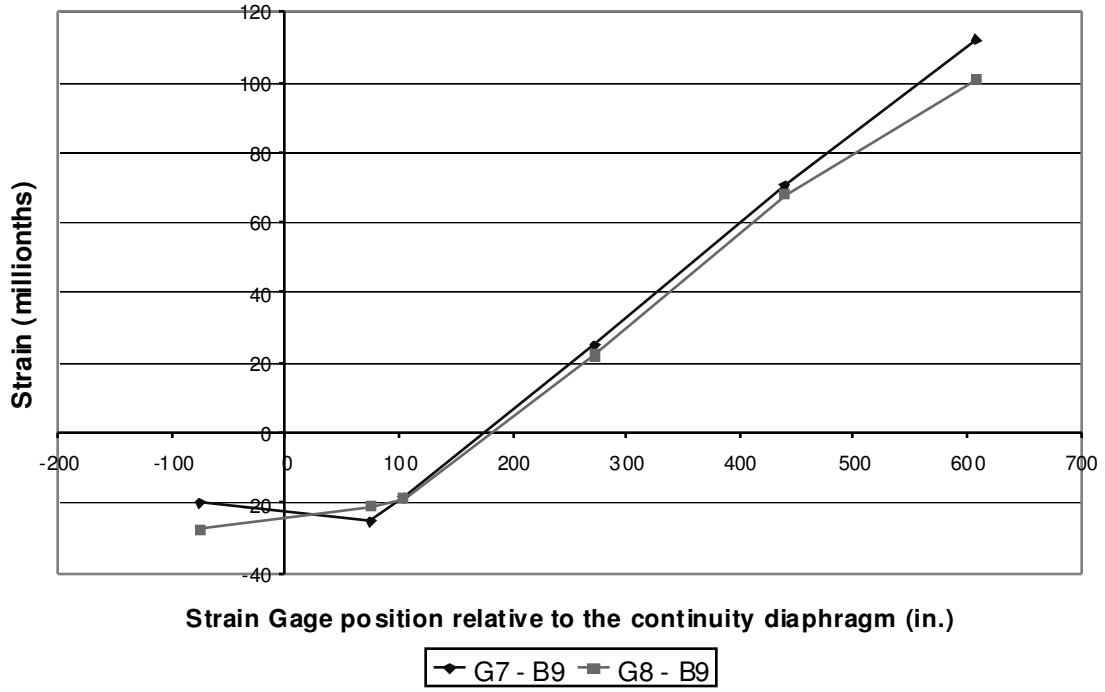


**Figure D-172:** B9 Bottom Fiber Strains

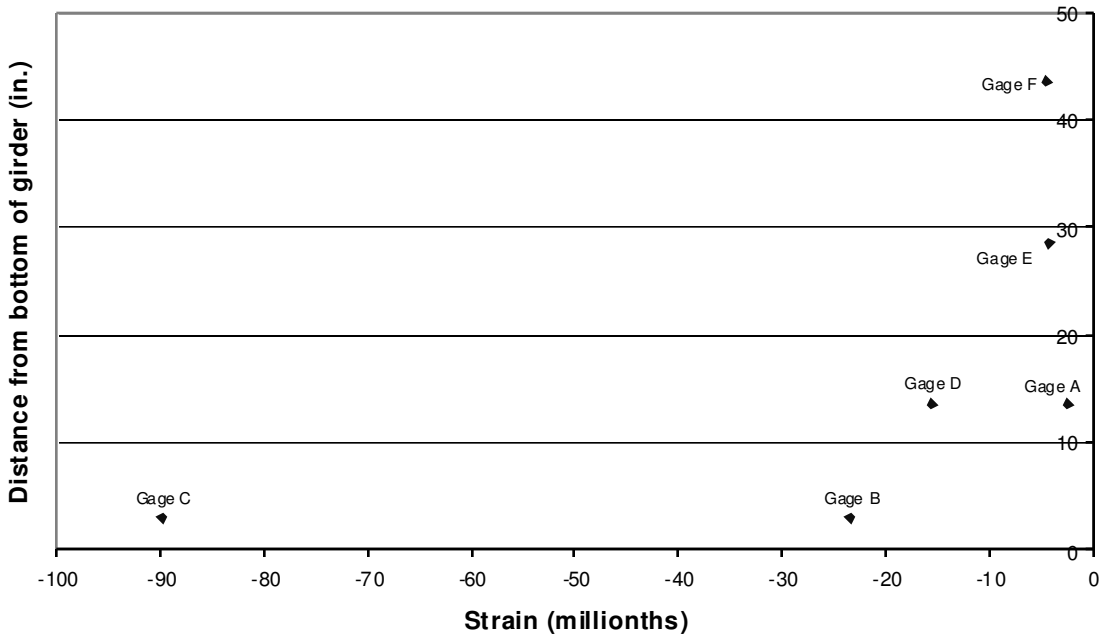


**Figure D-173:** B9 Span 10 Girder 7 Cross Section1

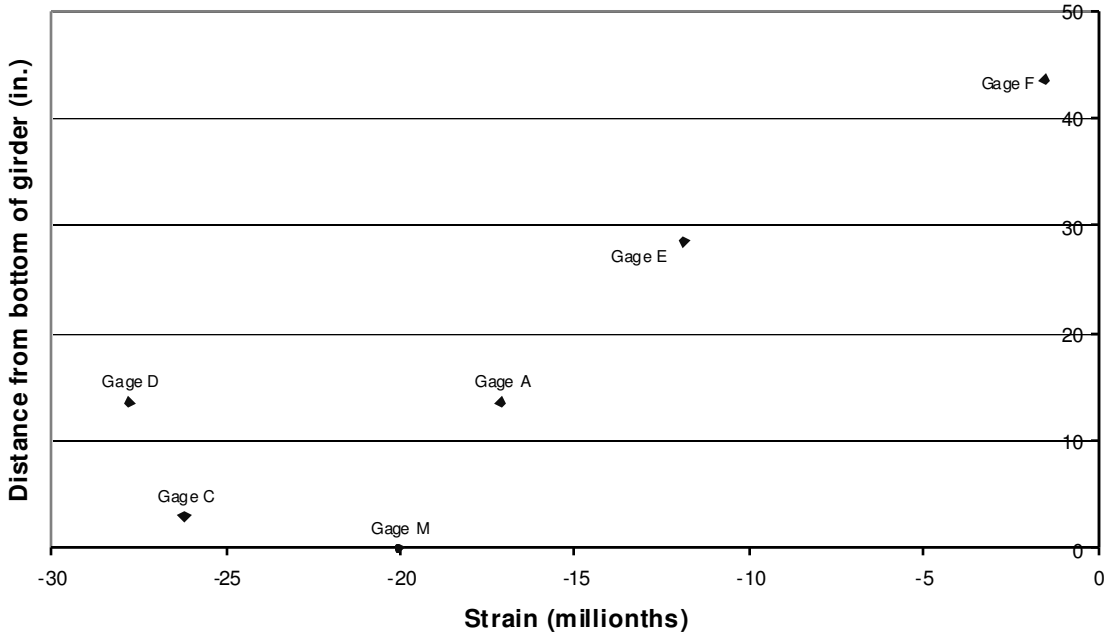


**Figure D-174:** B9 Span 10 Girder 7 Cross Section 2

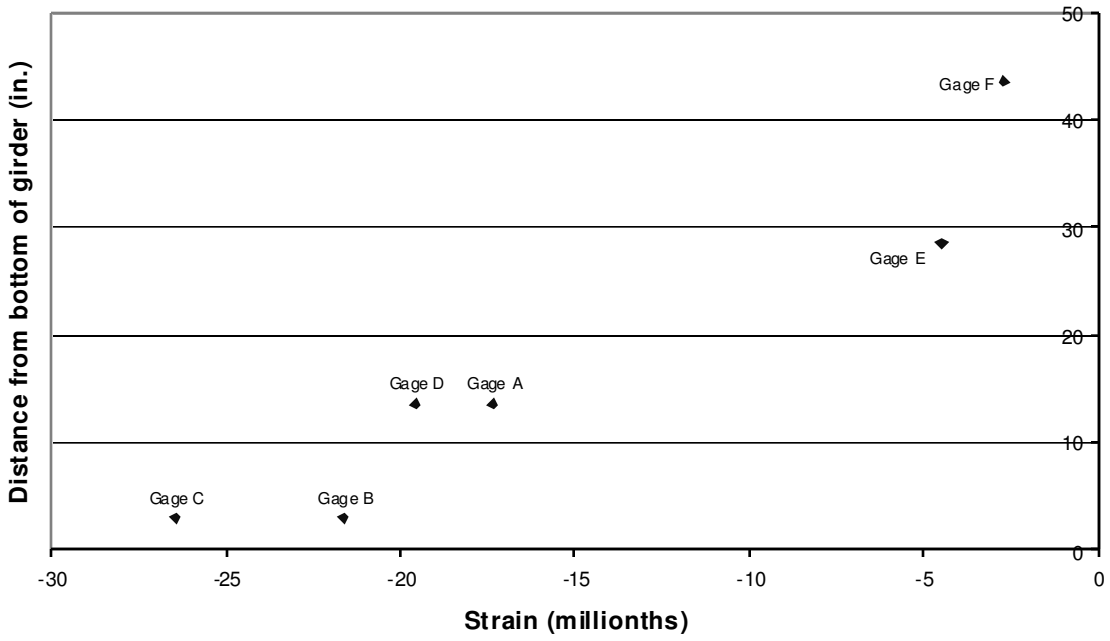


**Figure D-175:** B9 Span 10 Girder 8 Cross Section 1

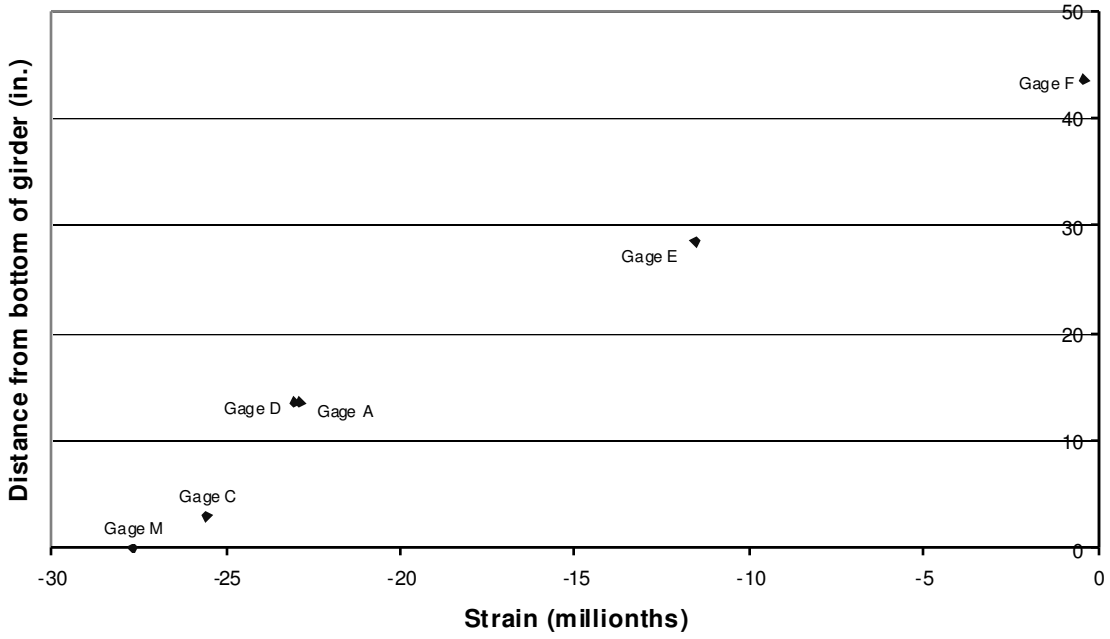


**Figure D-176:** B9 Span 10 Girder 8 Cross Section 2

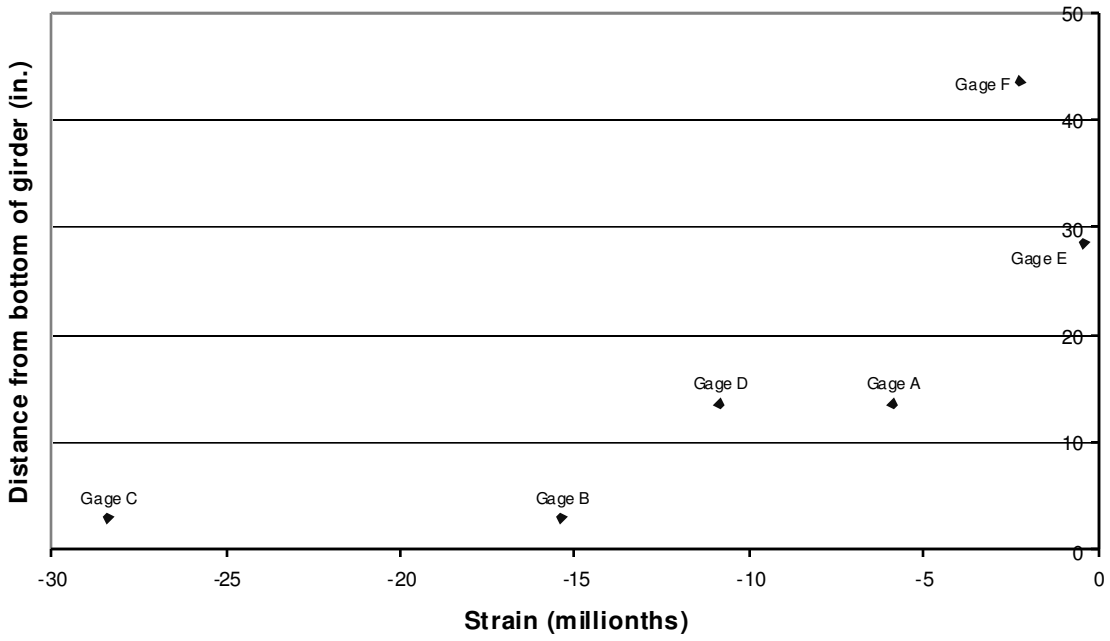


**Figure D-177:** B9 Span 11 Girder 7 Cross Section 1

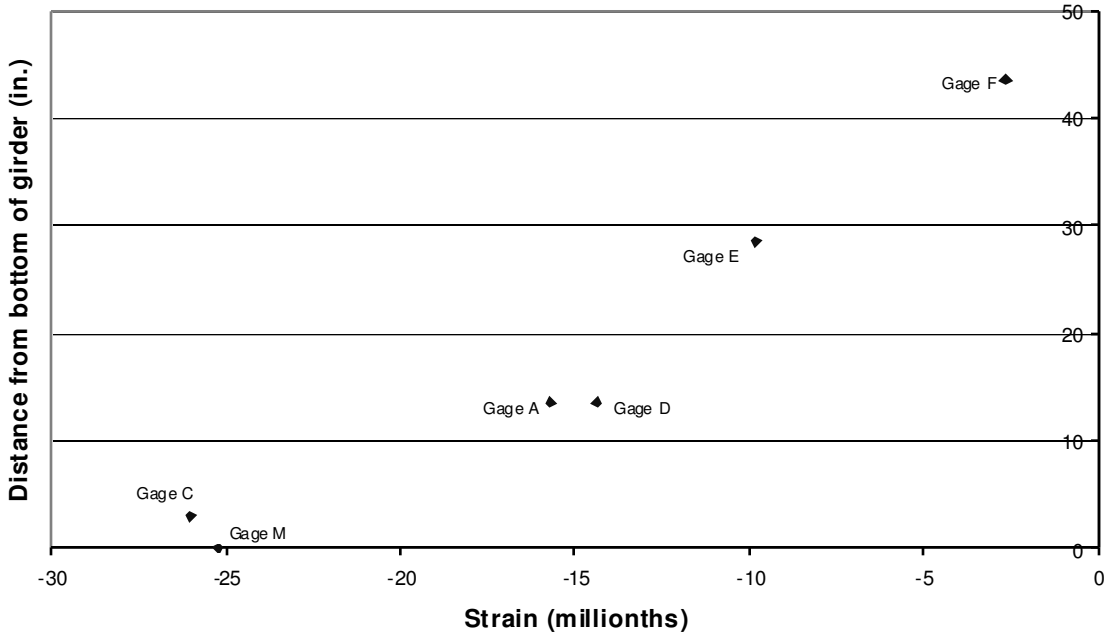


**Figure D-178:** B9 Span 11 Girder 7 Cross Section 2

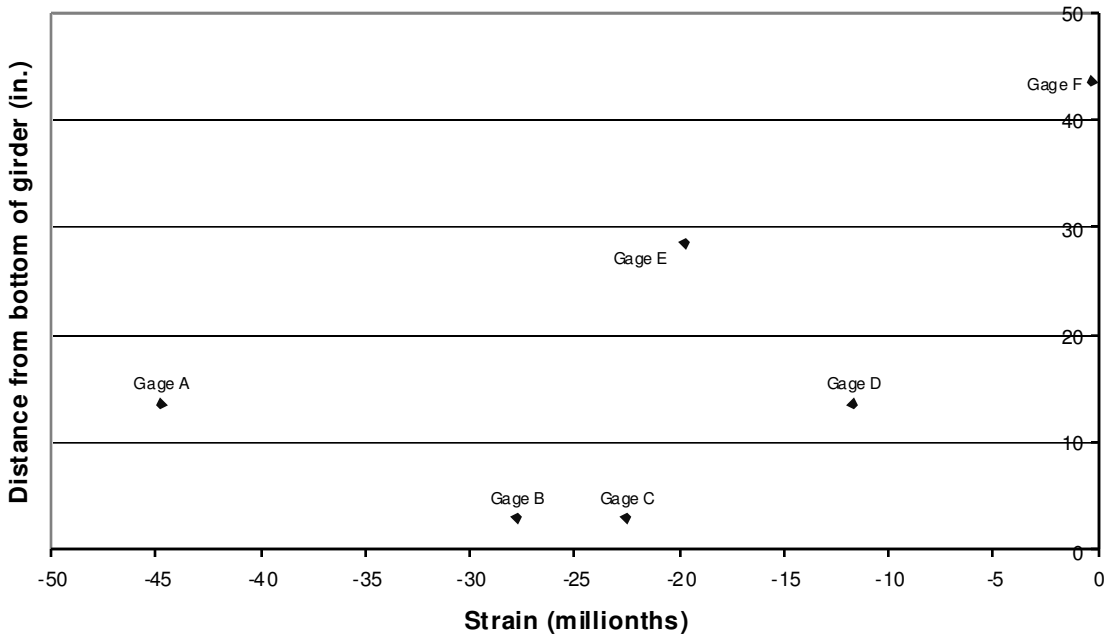


**Figure D-179:** B9 Span 11 Girder 8 Cross Section 1

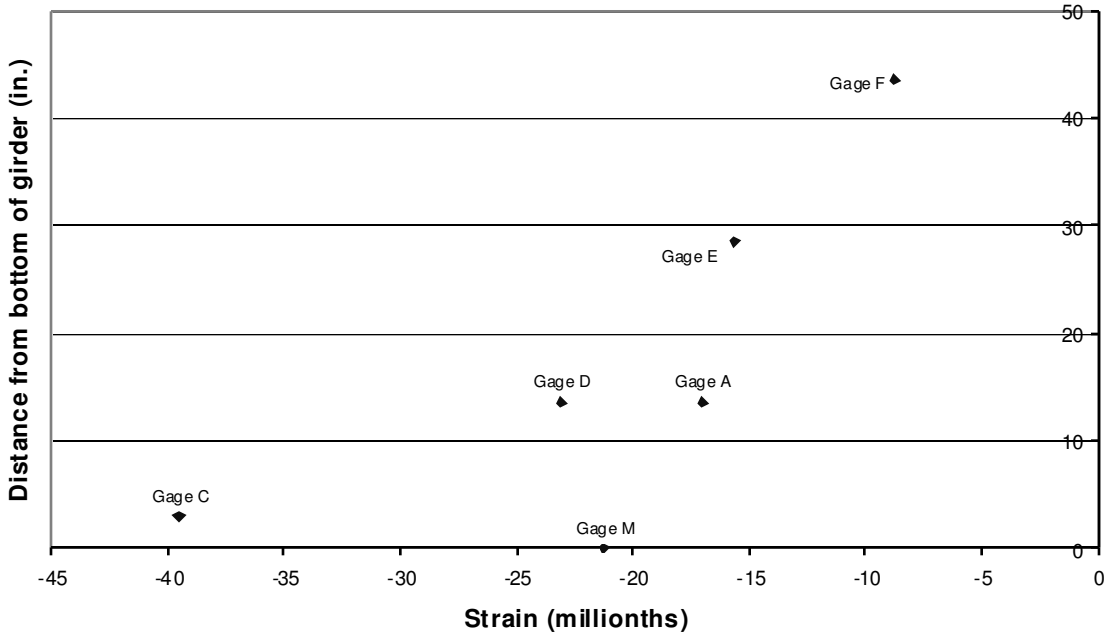


**Figure D-180:** B9 Span 11 Girder 8 Cross Section 2

## D.3 LANE C

### D.3.1 POSITION C1

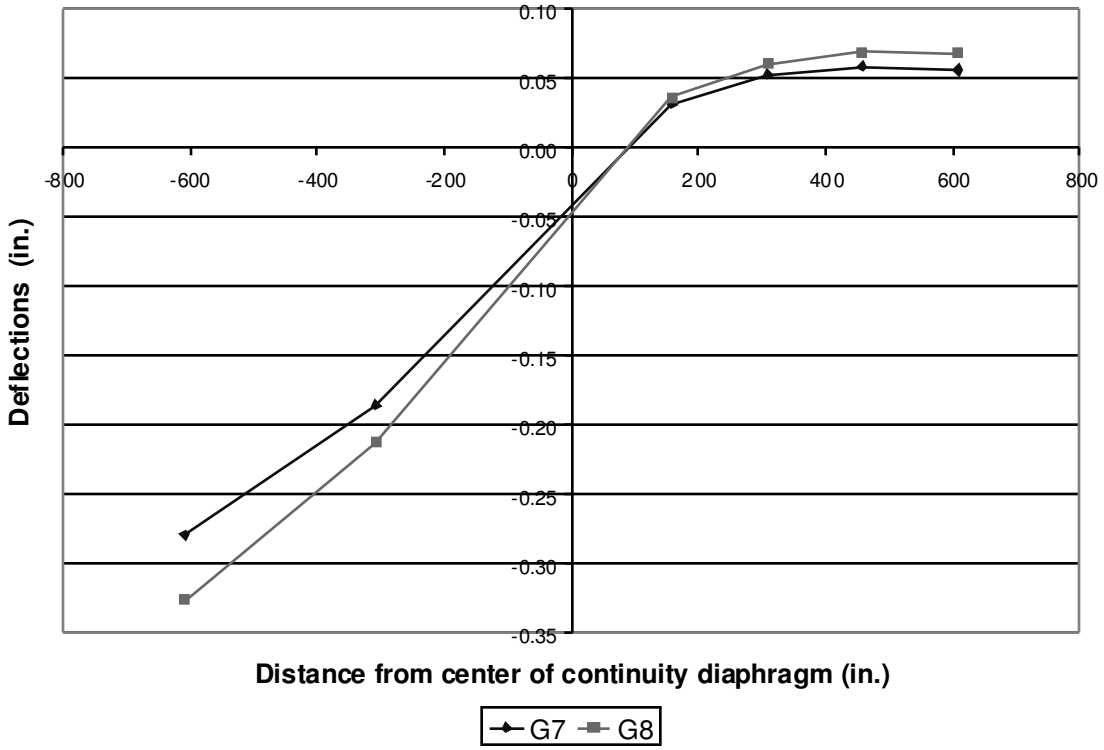


**Figure D-181:** C1 Deflections

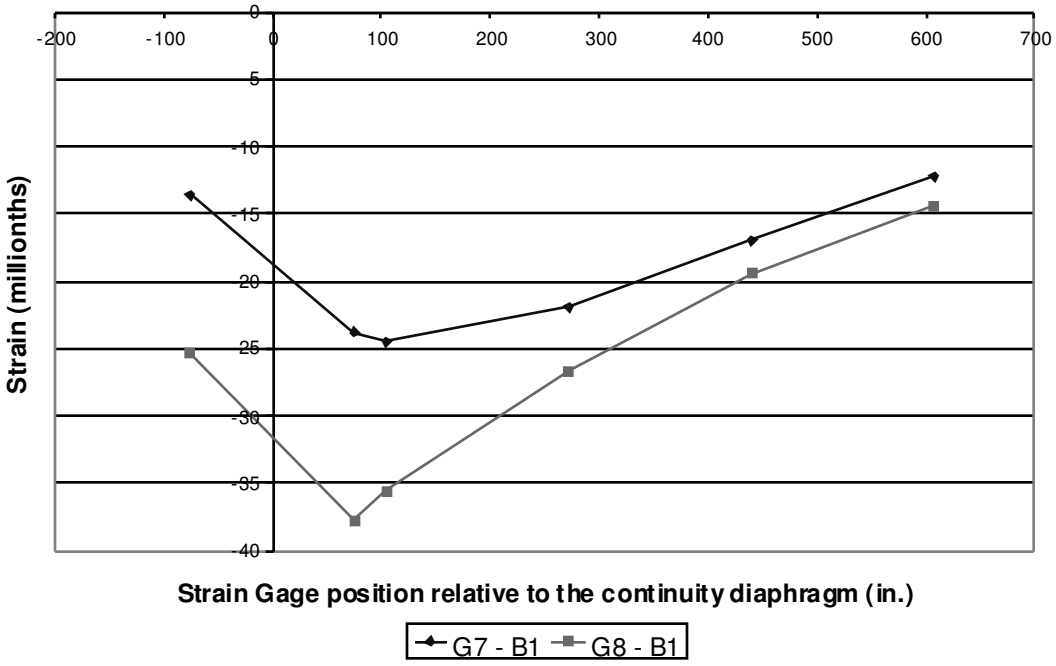


**Figure D-182:** C1 Bottom Fiber Strains

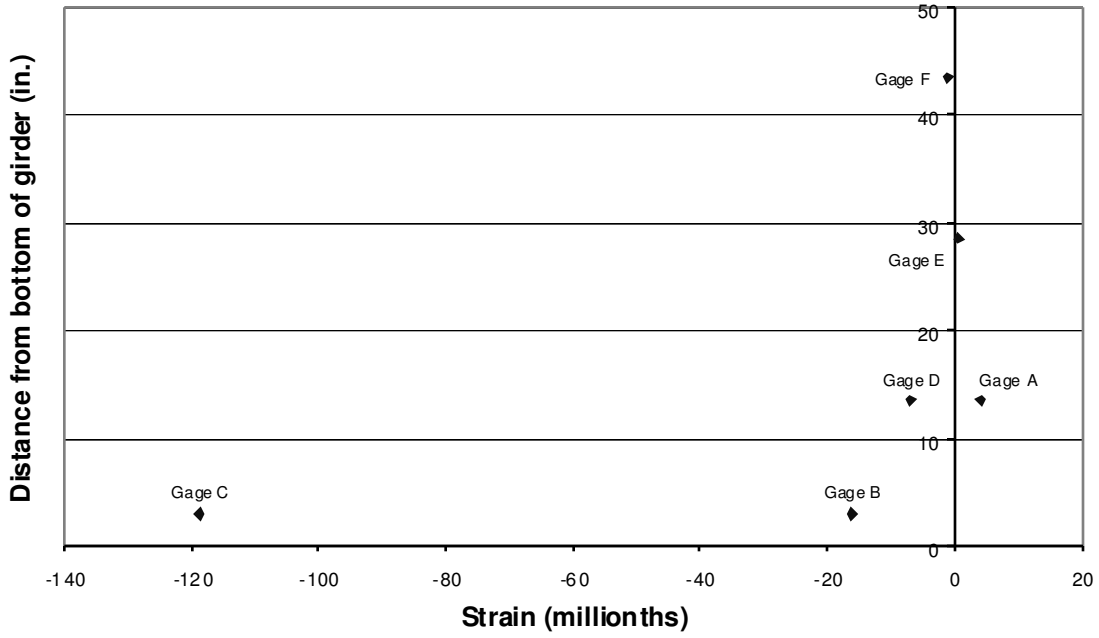


**Figure D-183:** C1 Span 10 Girder 7 Cross Section1

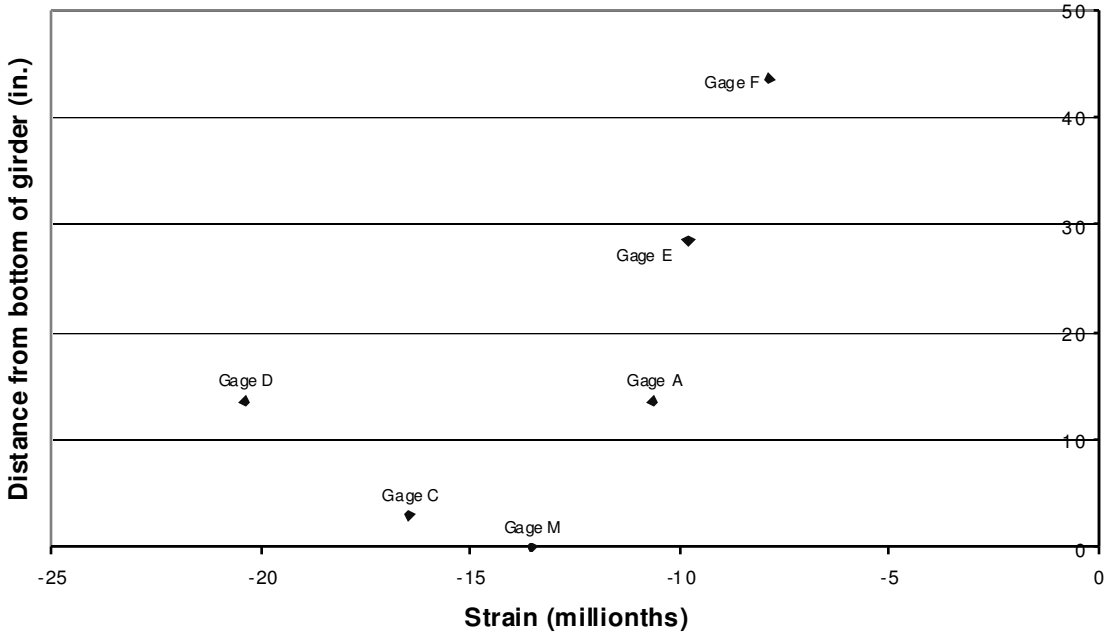


**Figure D-184:** C1 Span 10 Girder 7 Cross Section 2

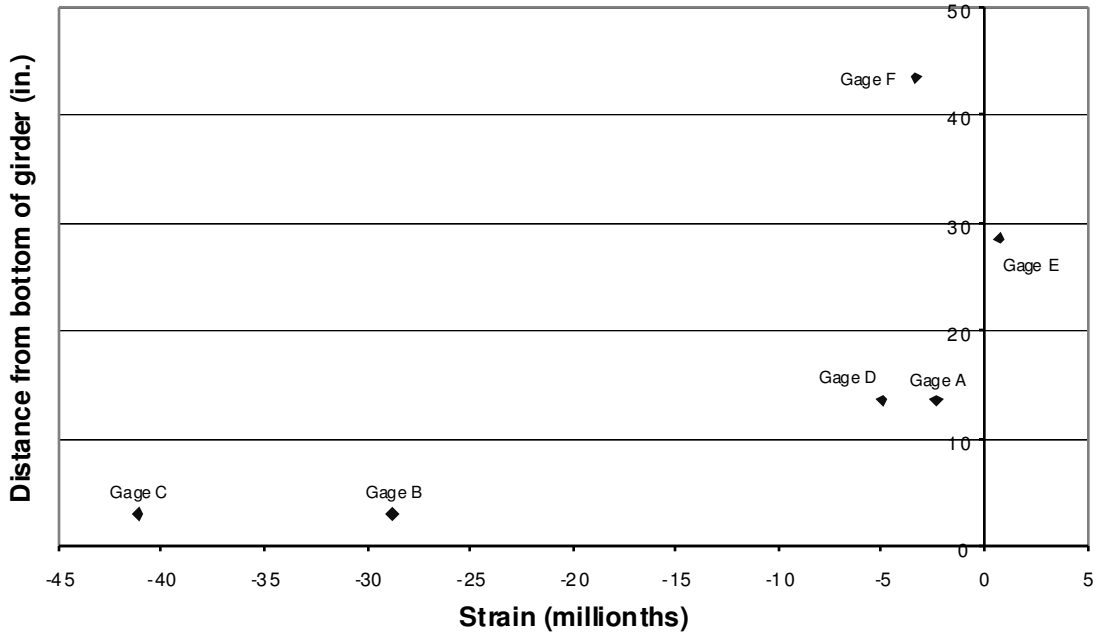


**Figure D-185:** C1 Span 10 Girder 8 Cross Section 1

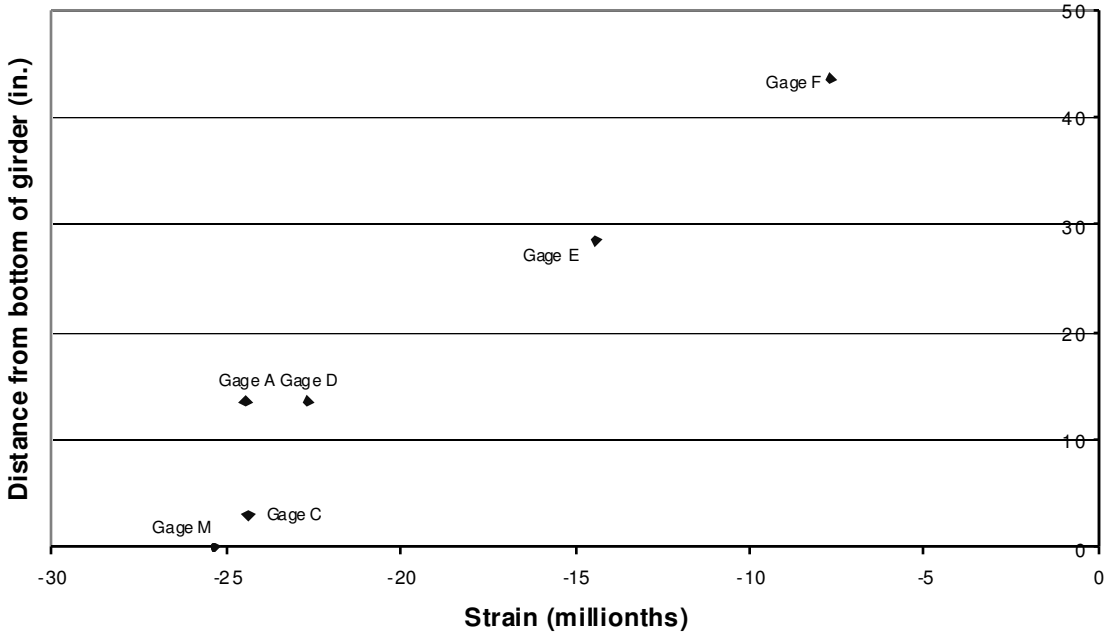


**Figure D-186:** C1 Span 10 Girder 8 Cross Section 2

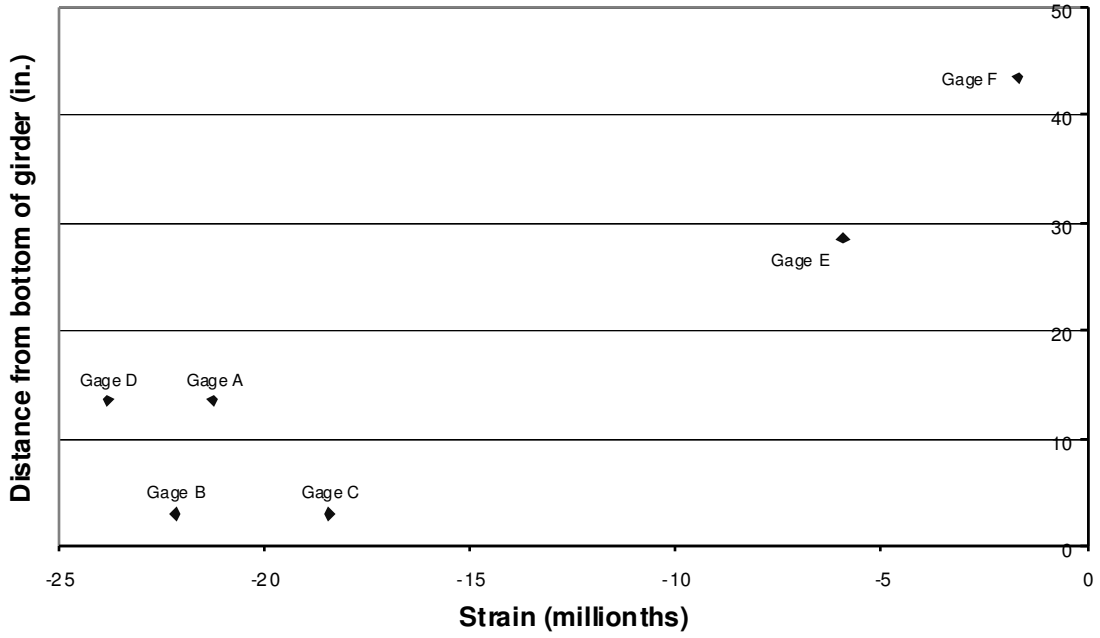


**Figure D-187:** C1 Span 11 Girder 7 Cross Section 1

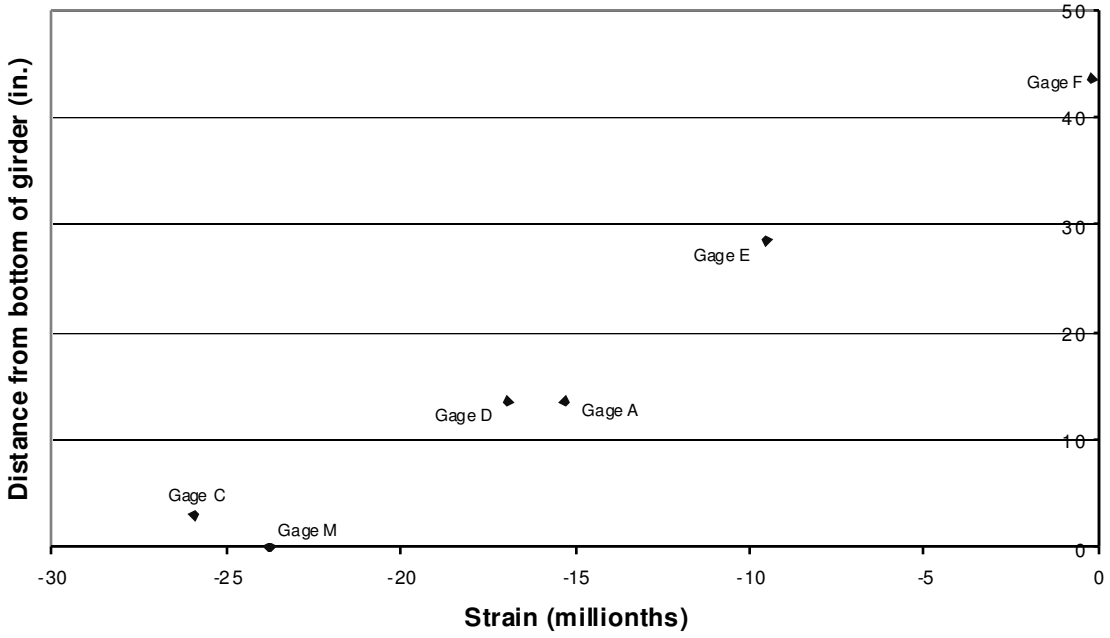


**Figure D-188:** C1 Span 11 Girder 7 Cross Section 2

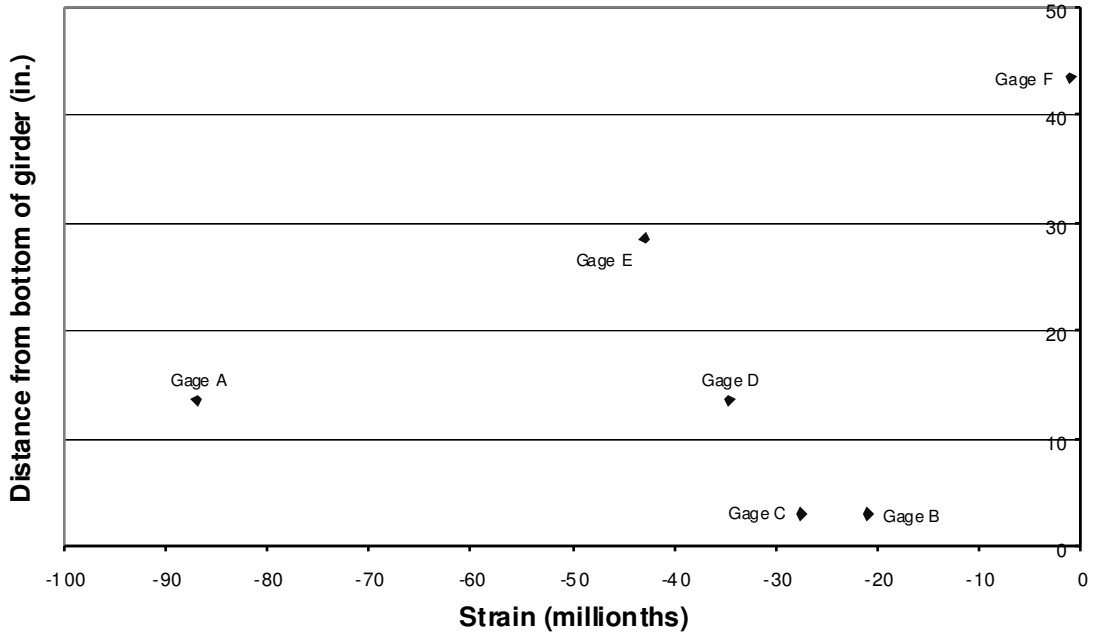


**Figure D-189:** C1 Span 11 Girder 8 Cross Section 1

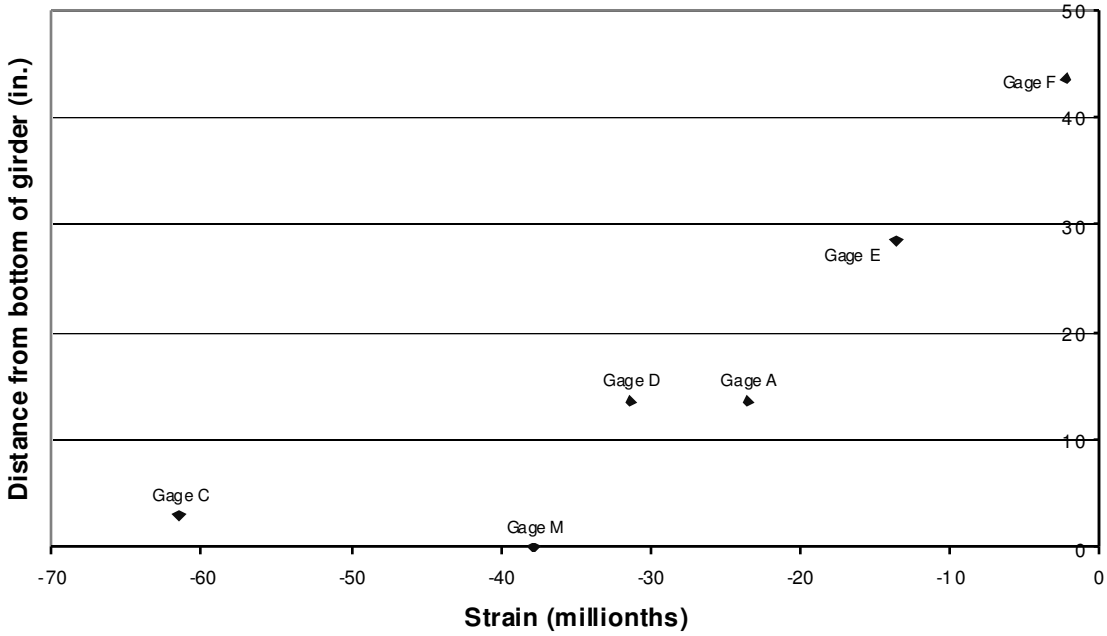


**Figure D-190:** C1 Span 11 Girder 8 Cross Section 2

### D.3.2 POSITION C2

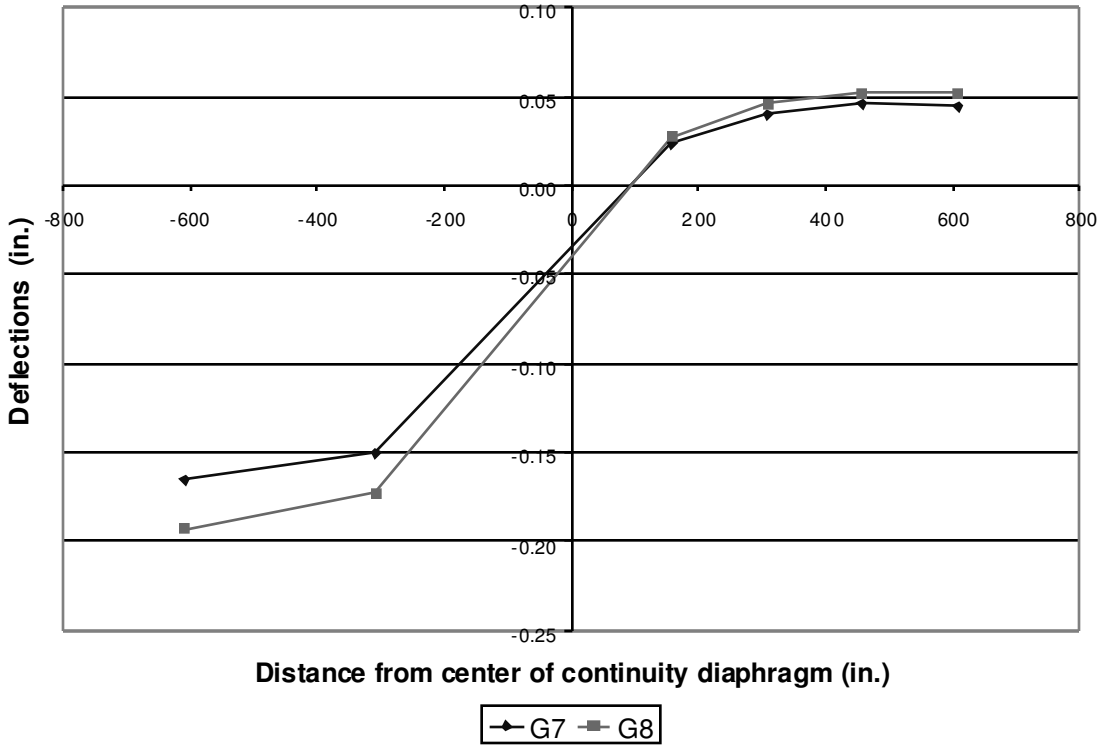


**Figure D-191:** C2 Deflections

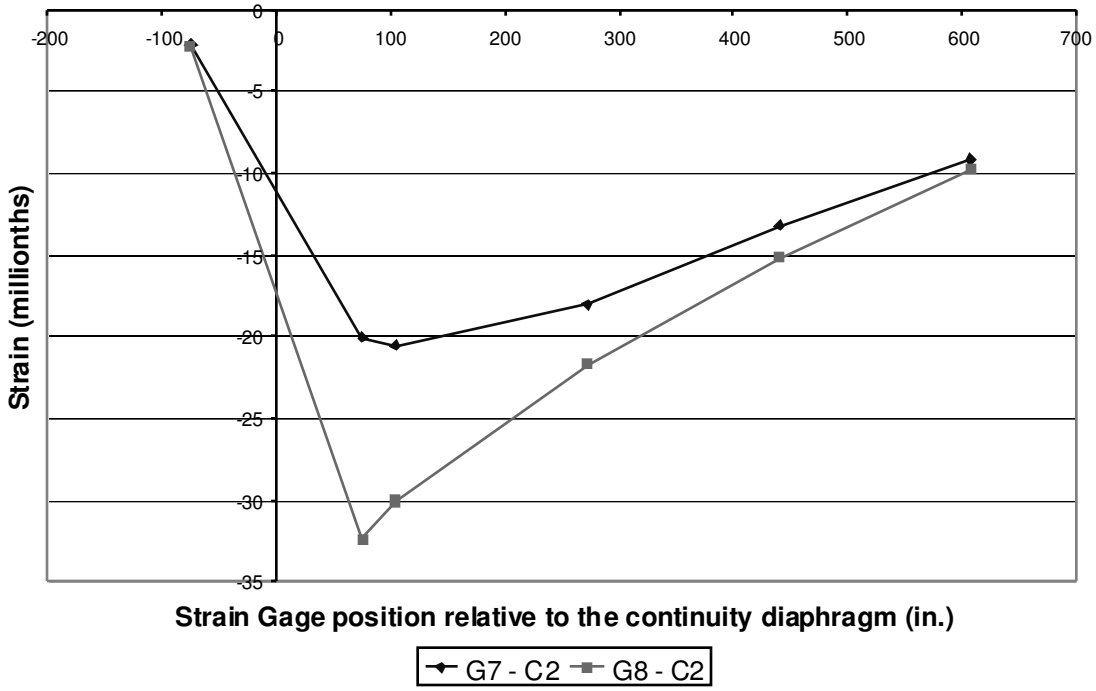


**Figure D-192:** C2 Bottom Fiber Strains

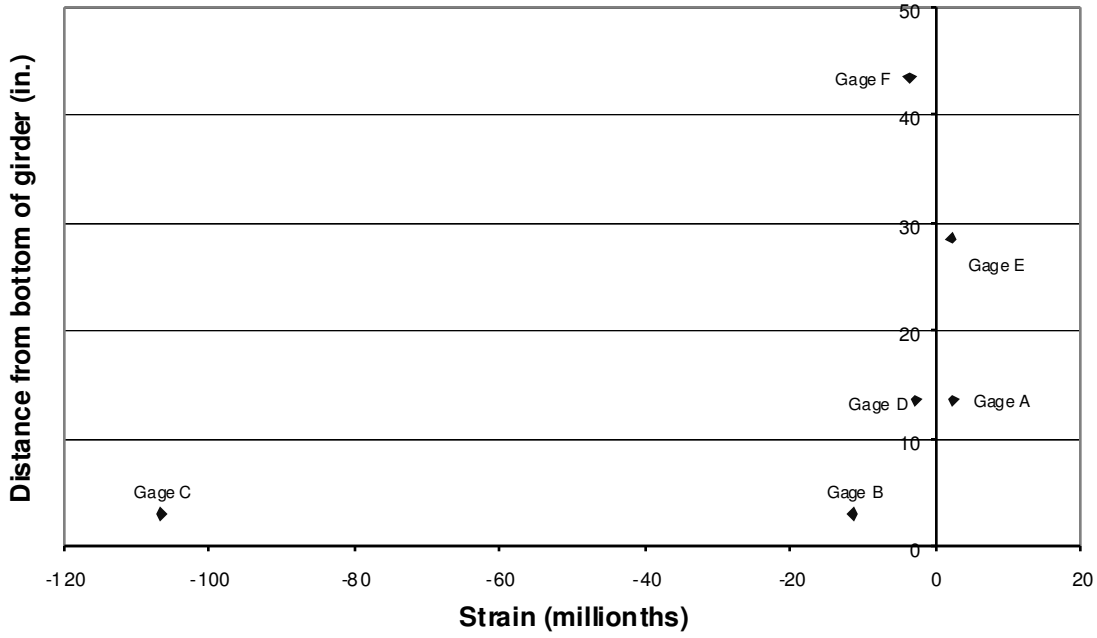


**Figure D-193:** C2 Span 10 Girder 7 Cross Section1

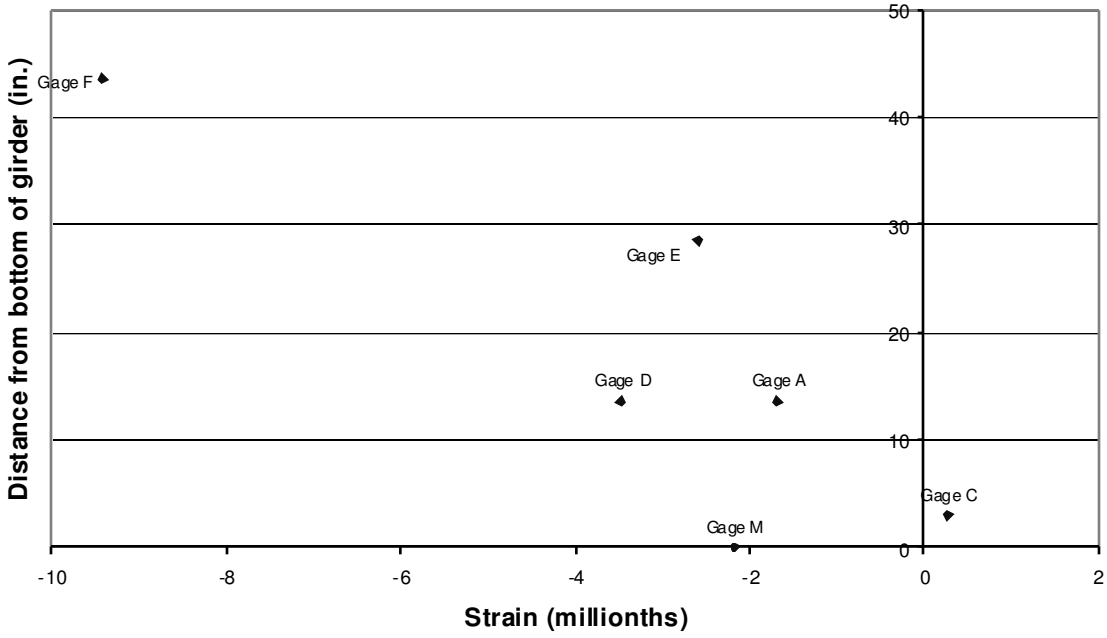


**Figure D-194:** C2 Span 10 Girder 7 Cross Section 2

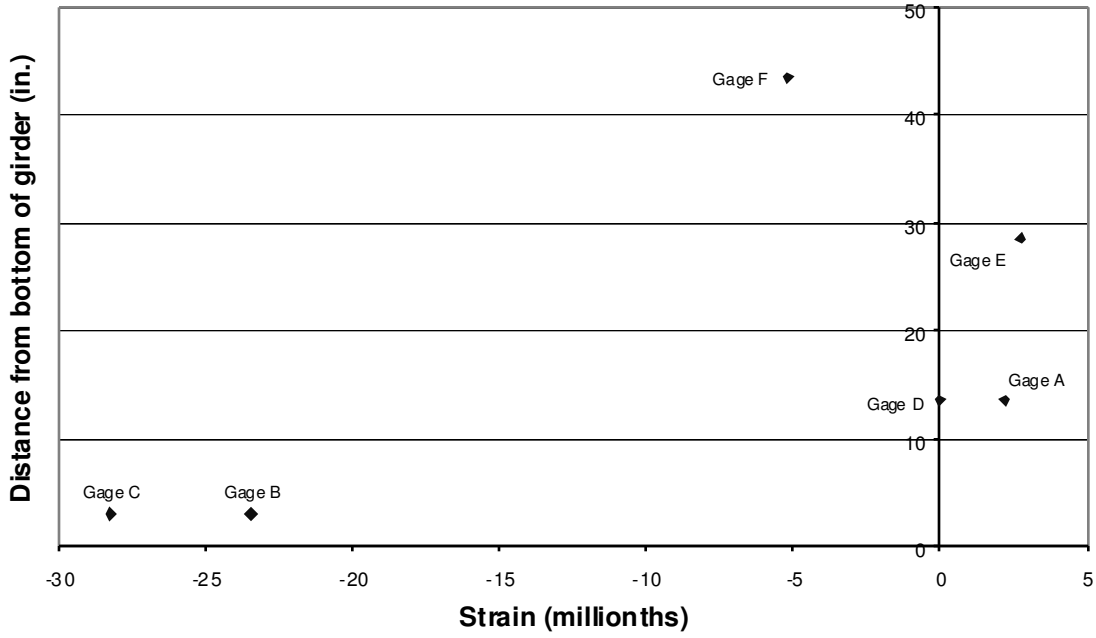


**Figure D-195:** C2 Span 10 Girder 8 Cross Section 1

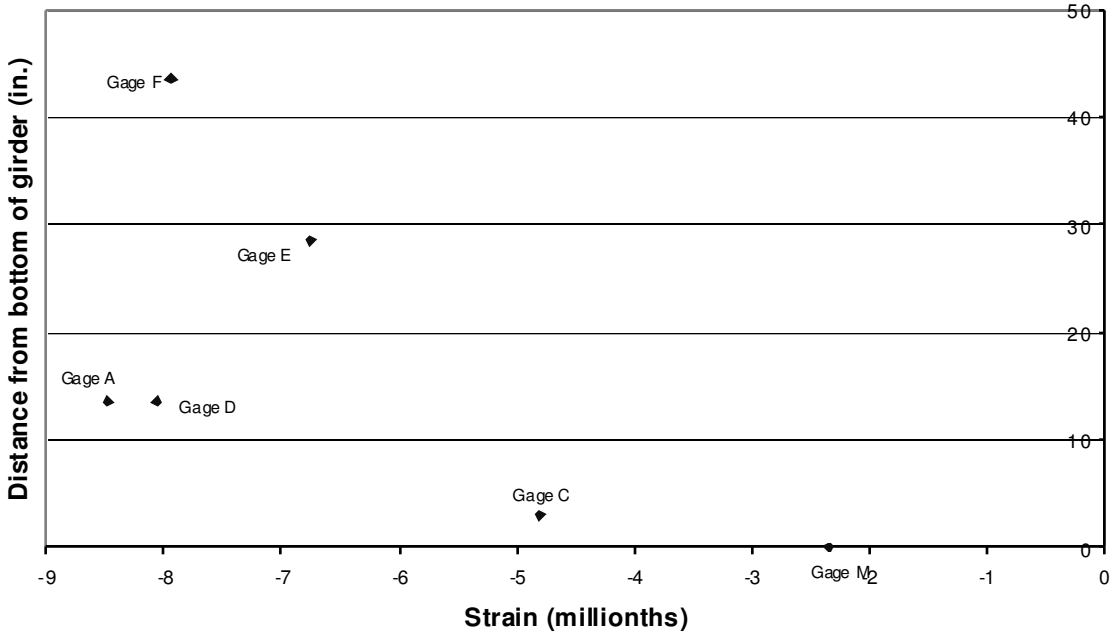


**Figure D-196:** C2 Span 10 Girder 8 Cross Section 2

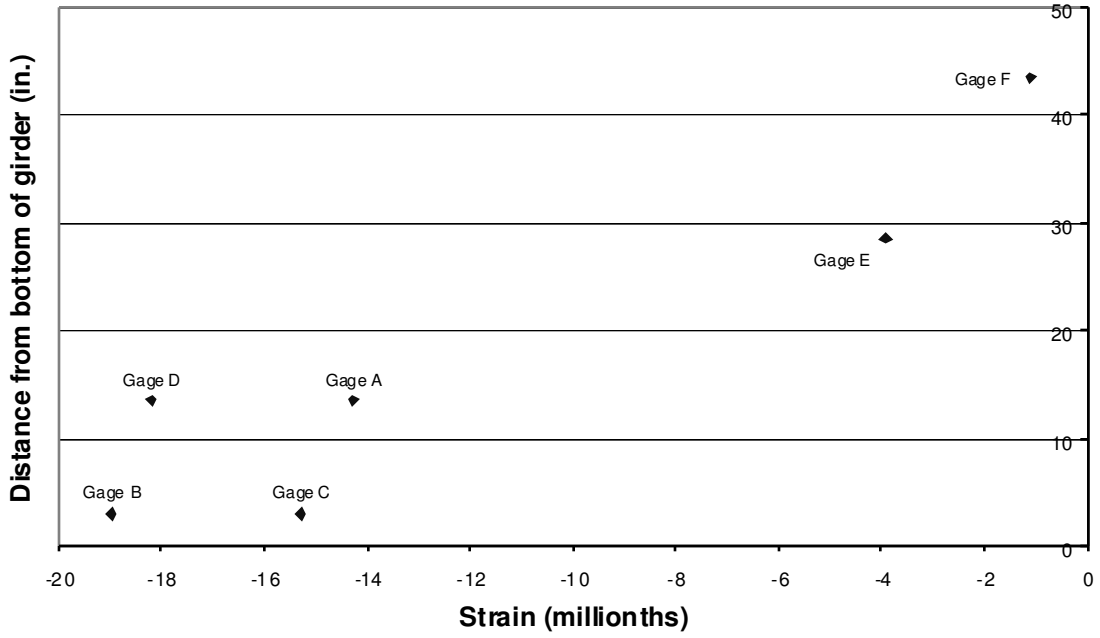


**Figure D-197:** C2 Span 11 Girder 7 Cross Section 1

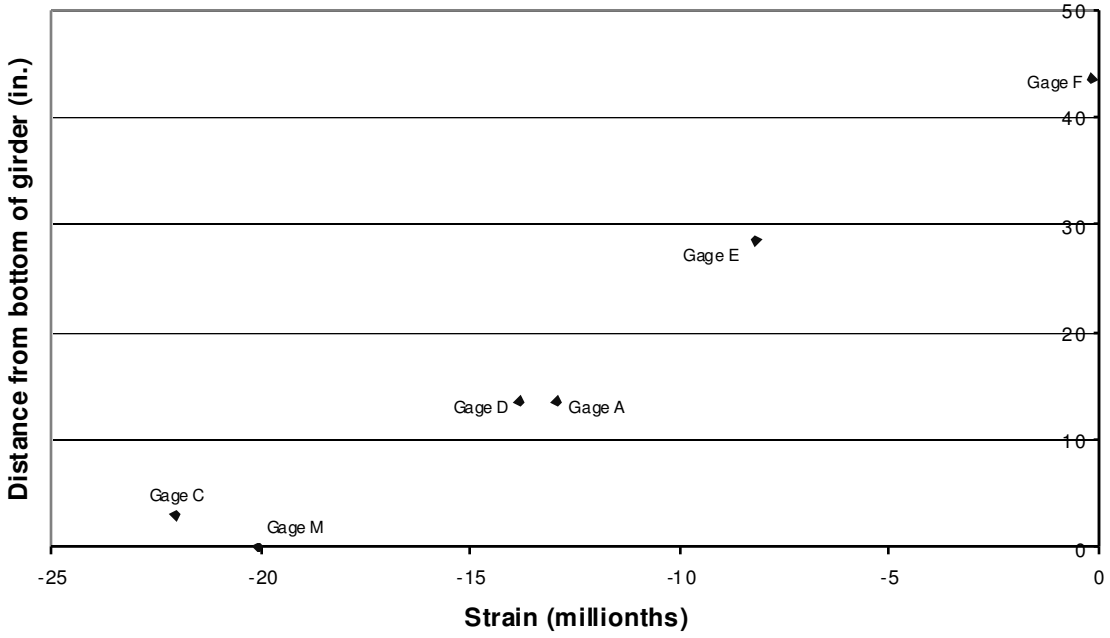


**Figure D-198:** C2 Span 11 Girder 7 Cross Section 2

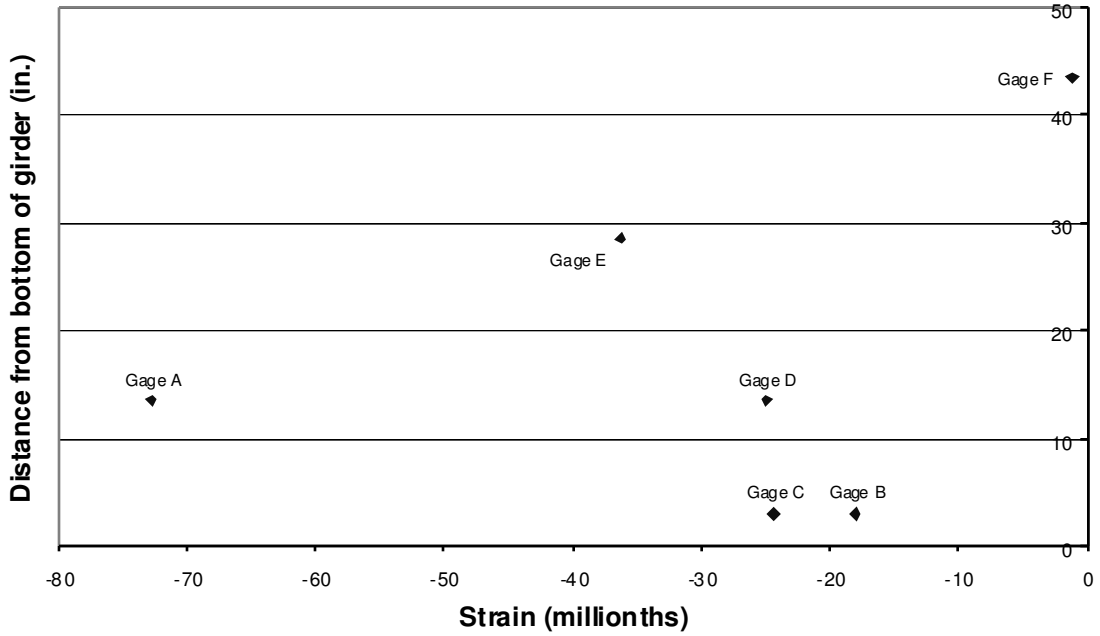


**Figure D-199:** C2 Span 11 Girder 8 Cross Section 1

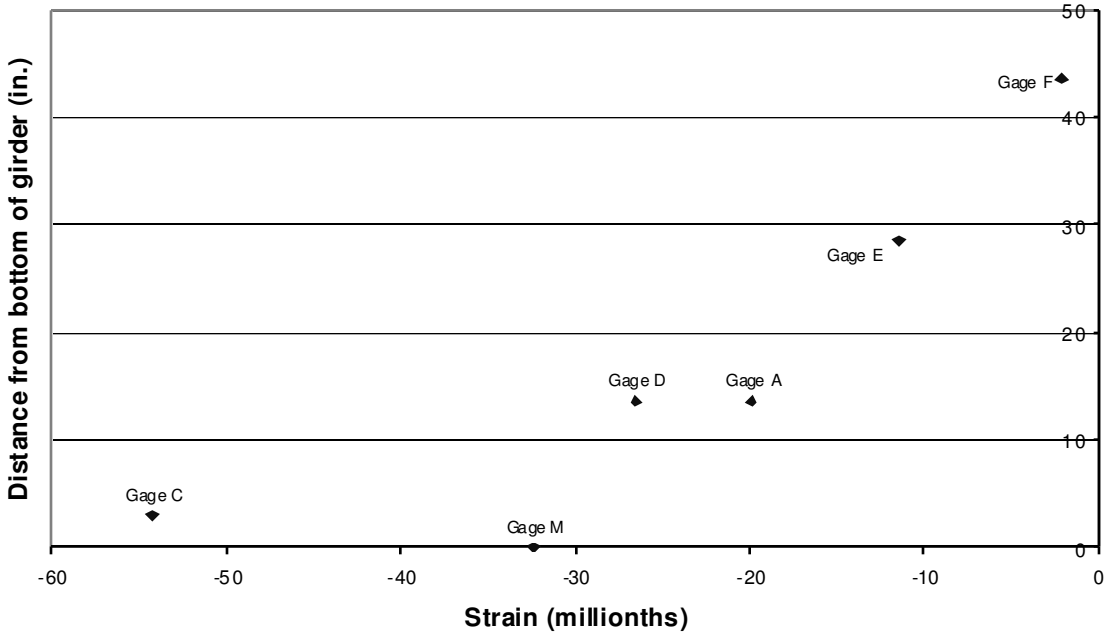


**Figure D-200:** C2 Span 11 Girder 8 Cross Section 2

### D.3.3 POSITION C3

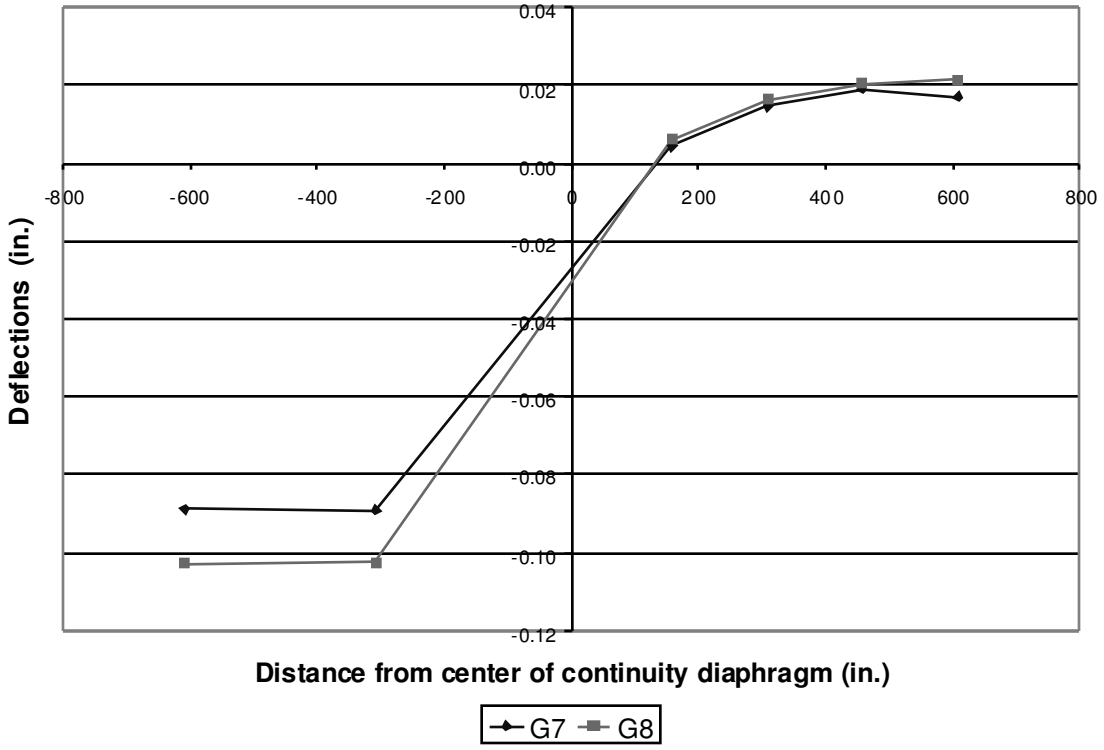


**Figure D-201:** C3 Deflections

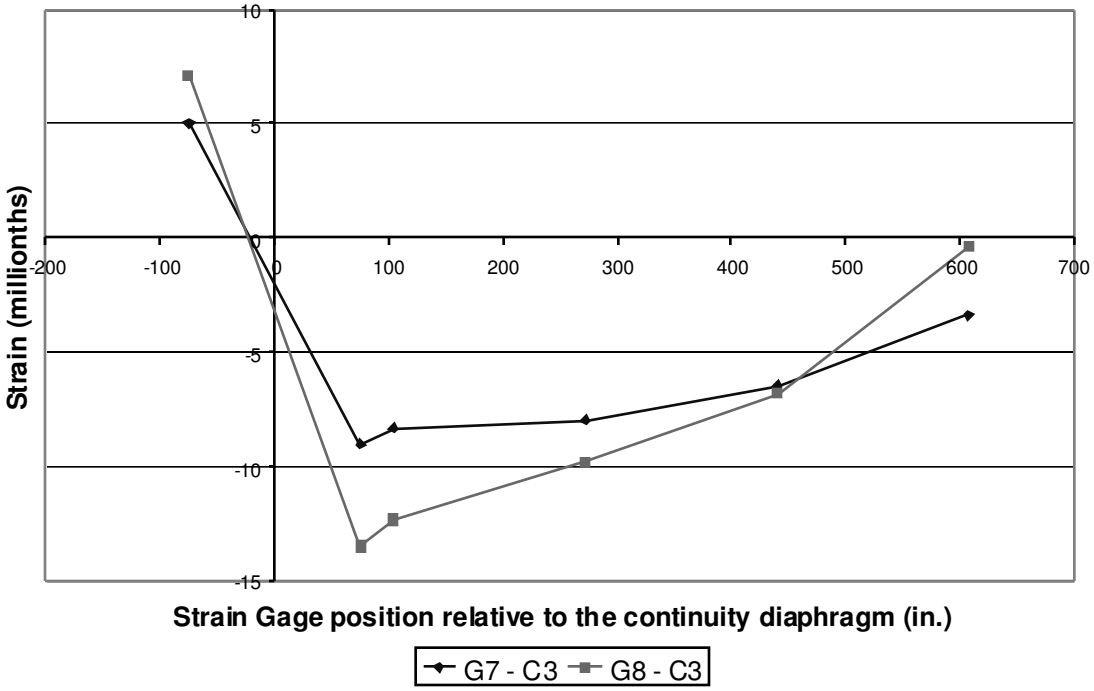


**Figure D-202:** C3 Bottom Fiber Strains

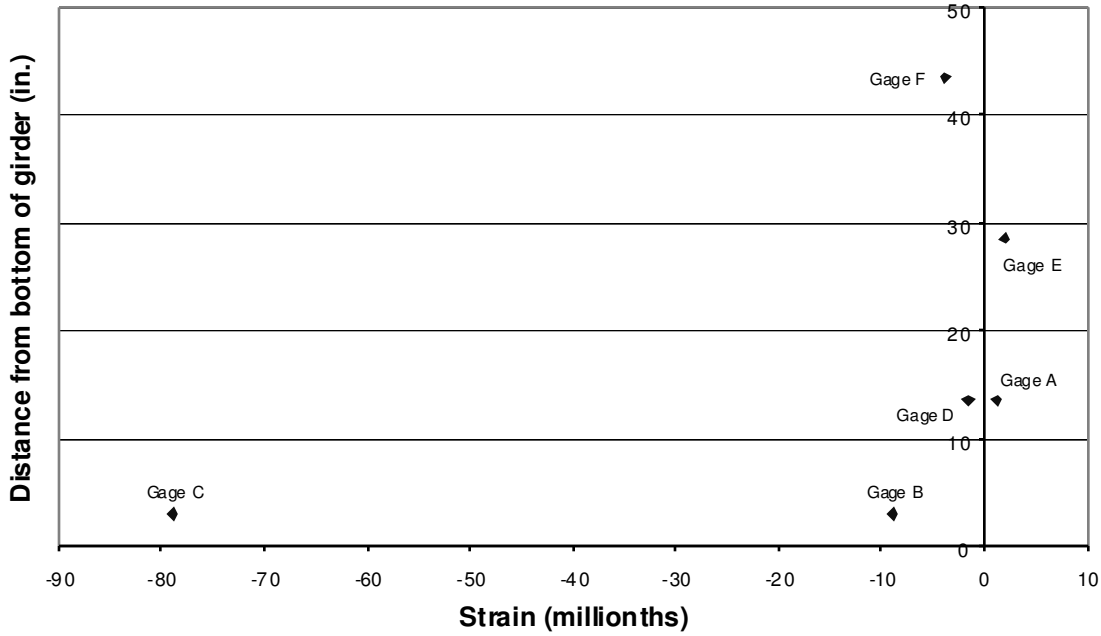


**Figure D-203:** C3 Span 10 Girder 7 Cross Section1

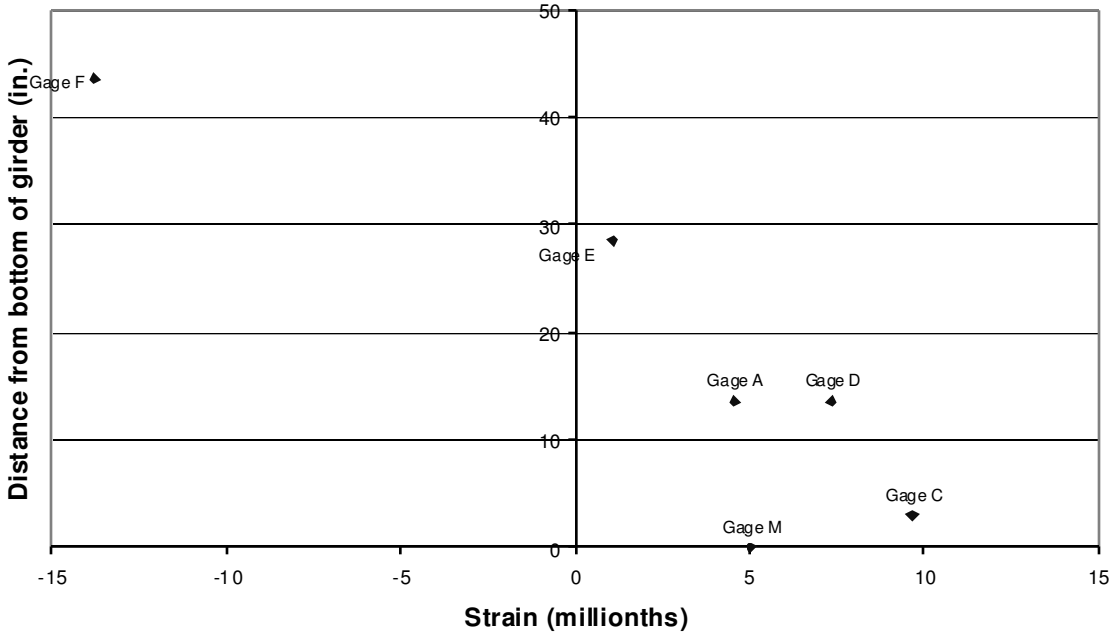


**Figure D-204:** C3 Span 10 Girder 7 Cross Section 2

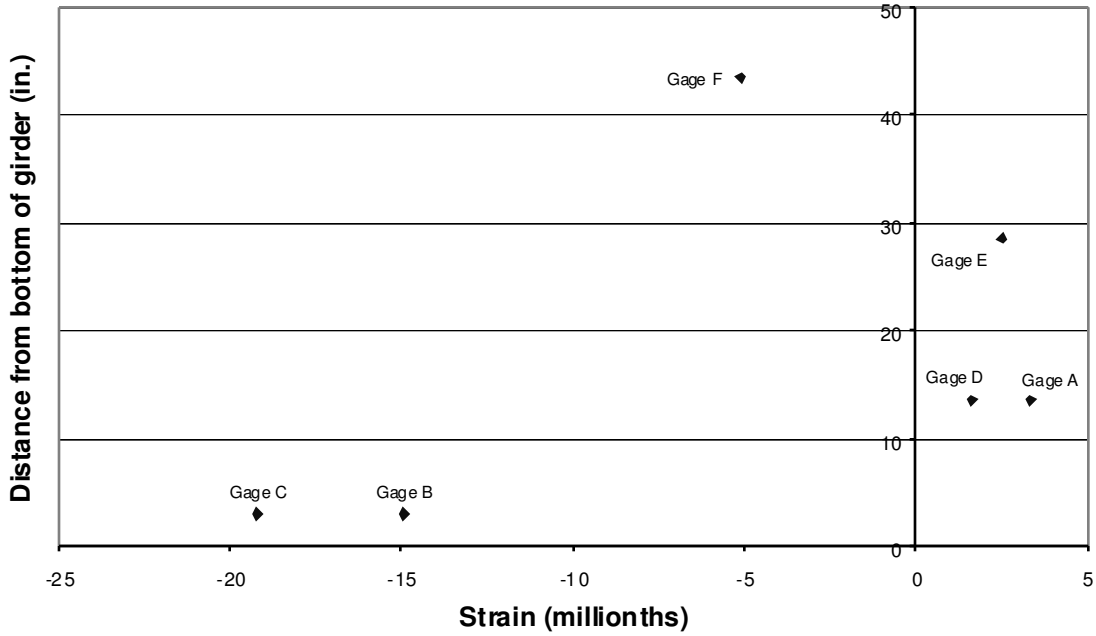


**Figure D-205:** C3 Span 10 Girder 8 Cross Section 1

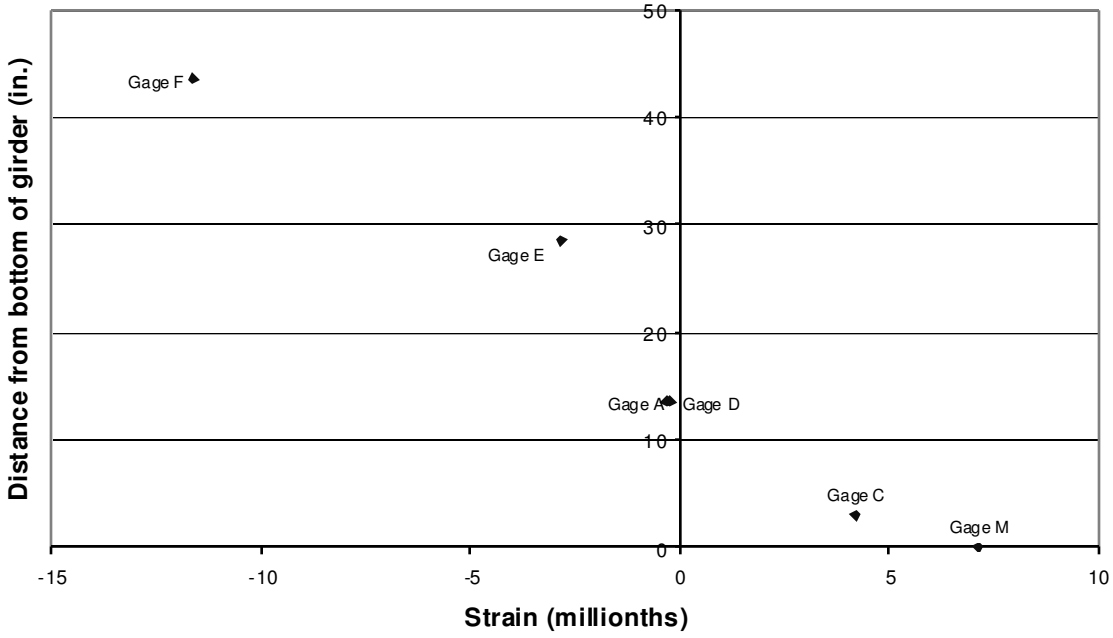


**Figure D-206:** C3 Span 10 Girder 8 Cross Section 2

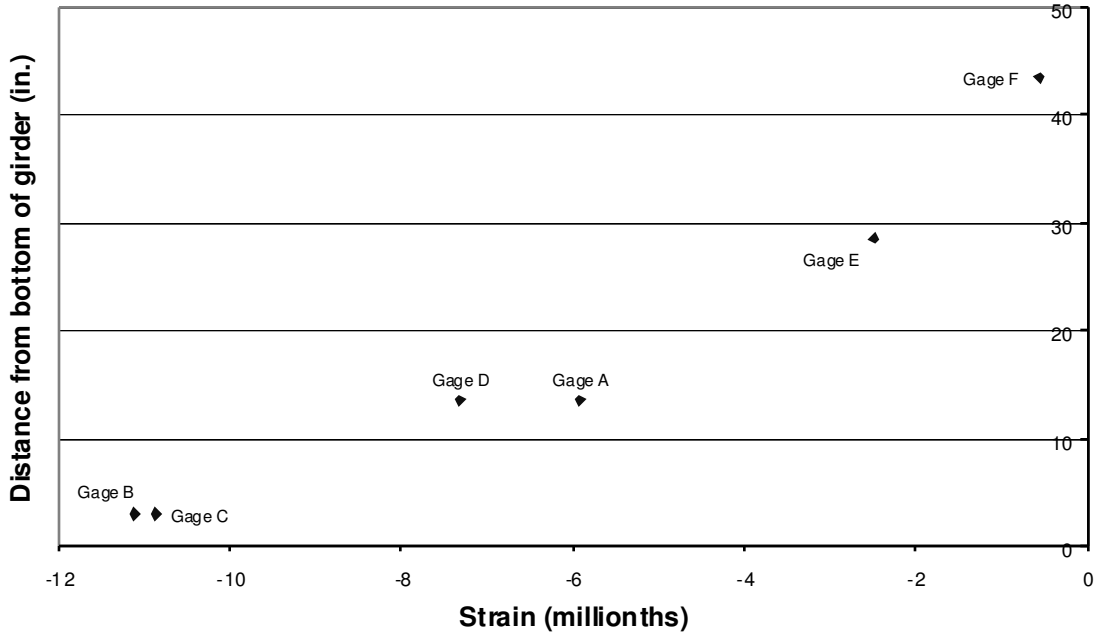


**Figure D-207:** C3 Span 11 Girder 7 Cross Section 1

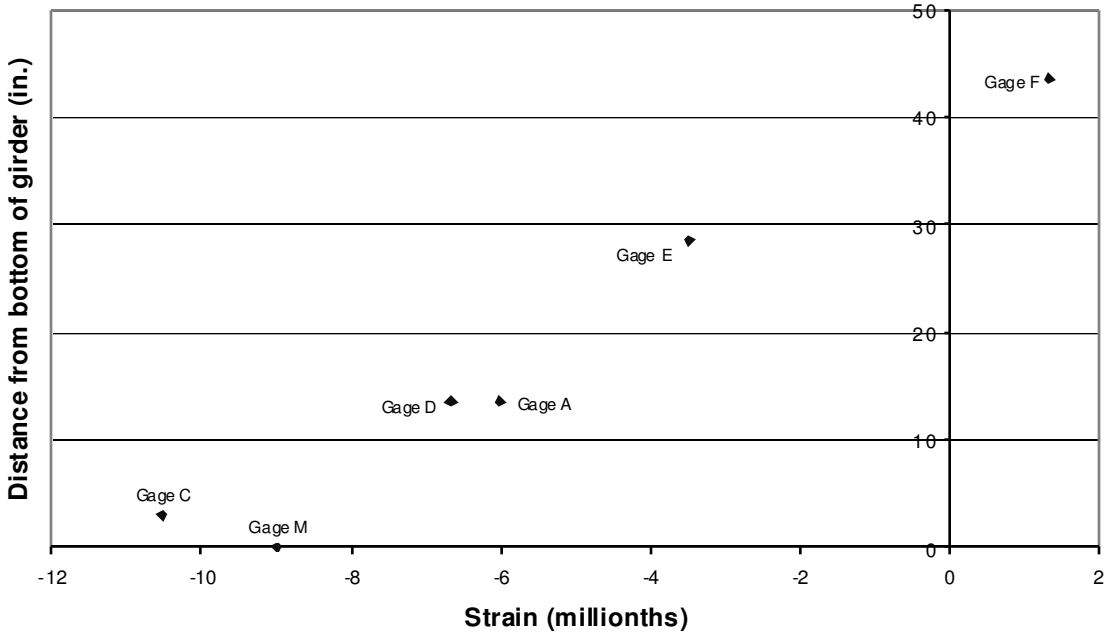


**Figure D-208:** C3 Span 11 Girder 7 Cross Section 2

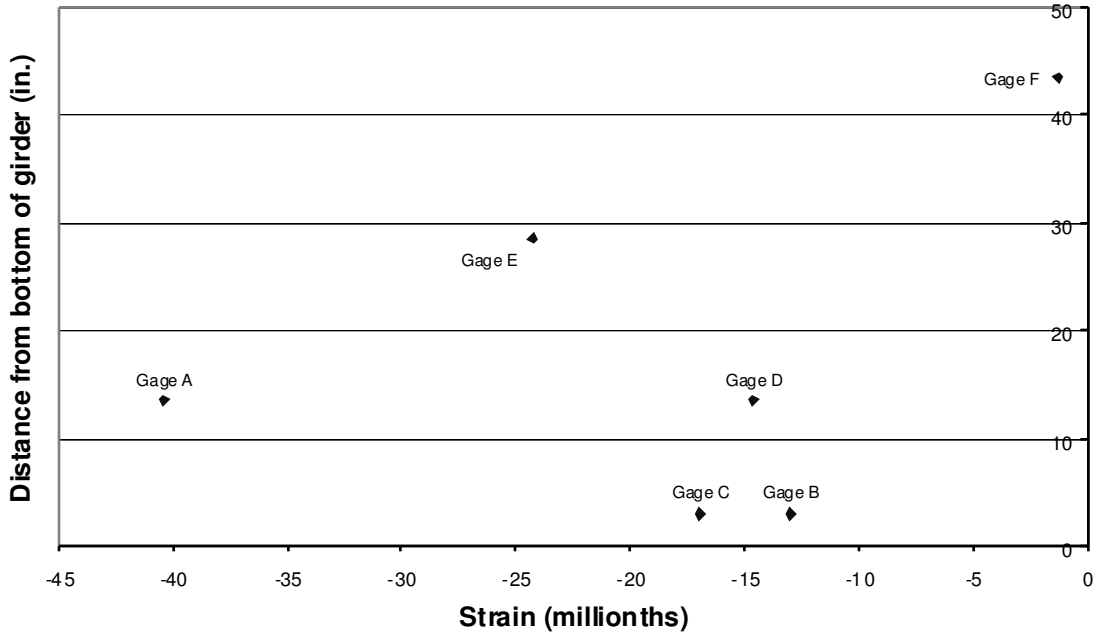


**Figure D-209:** C3 Span 11 Girder 8 Cross Section 1

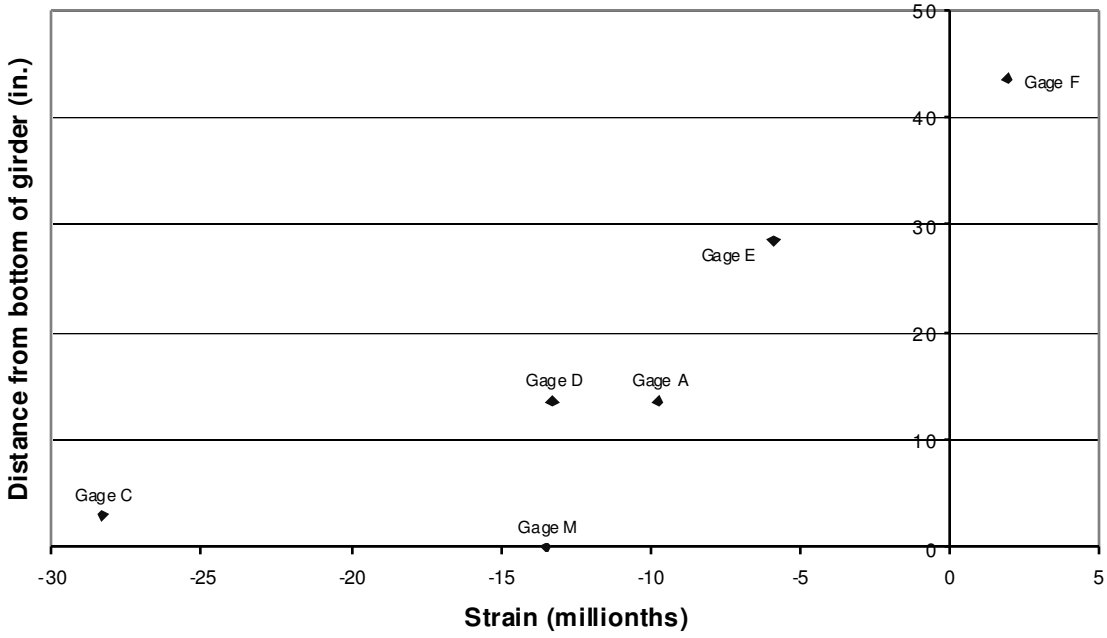


**Figure D-210:** C3 Span 11 Girder 8 Cross Section 2

### D.3.4 POSITION C4

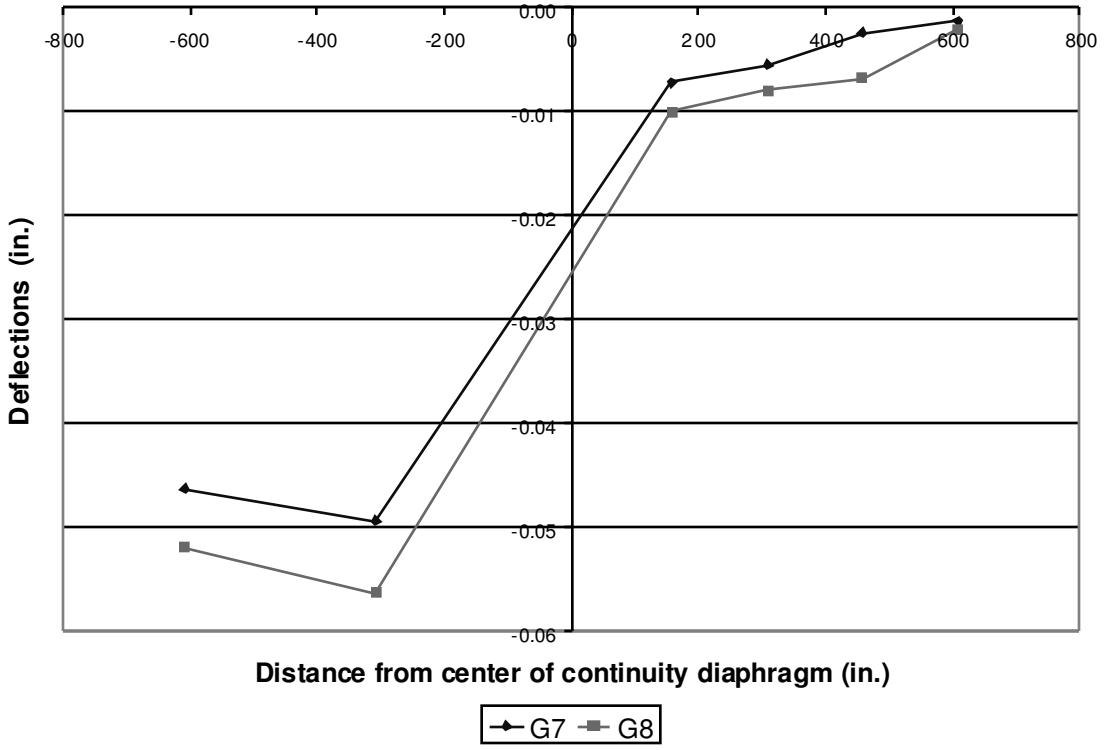


**Figure D-211:** C4 Deflections

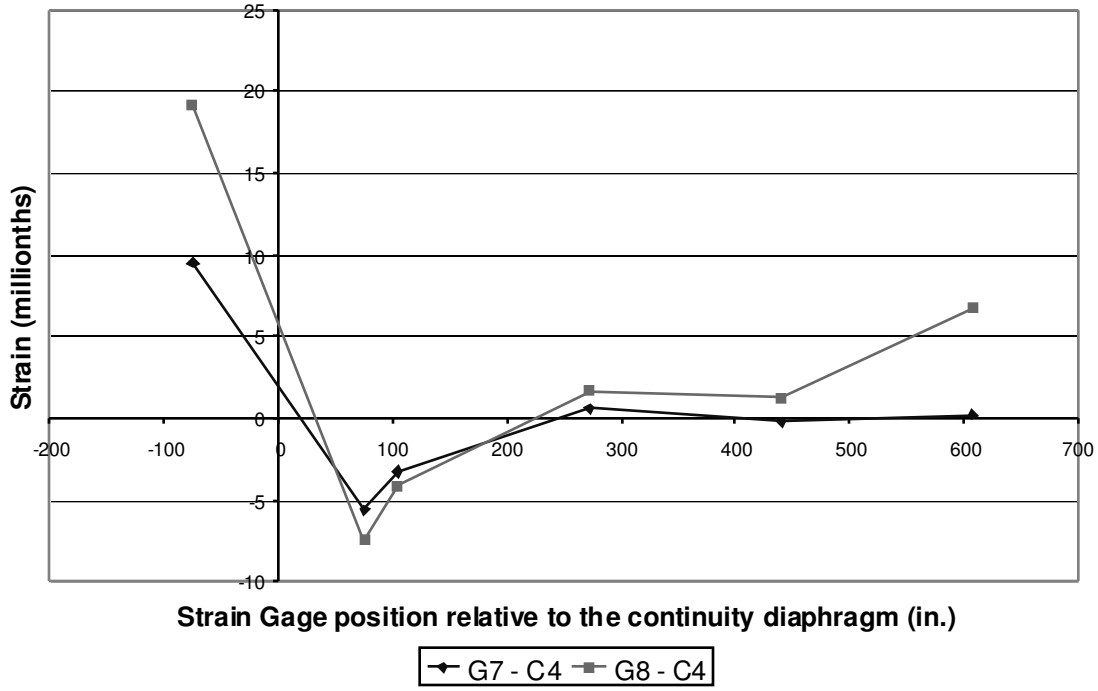


**Figure D-212:** C4 Bottom Fiber Strains

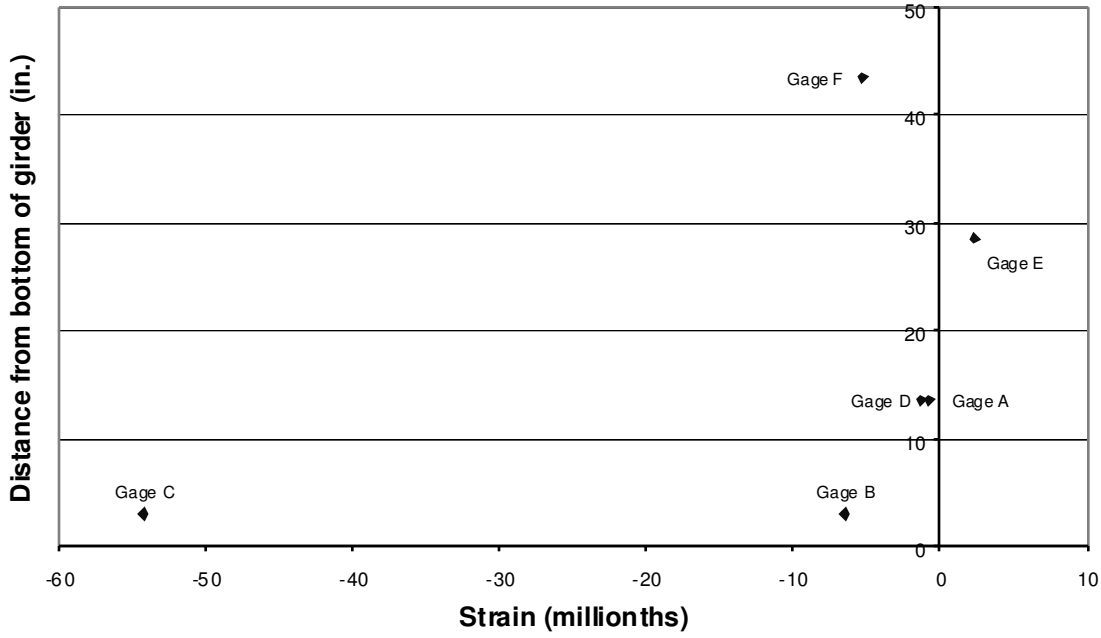


**Figure D-213:** C4 Span 10 Girder 7 Cross Section1

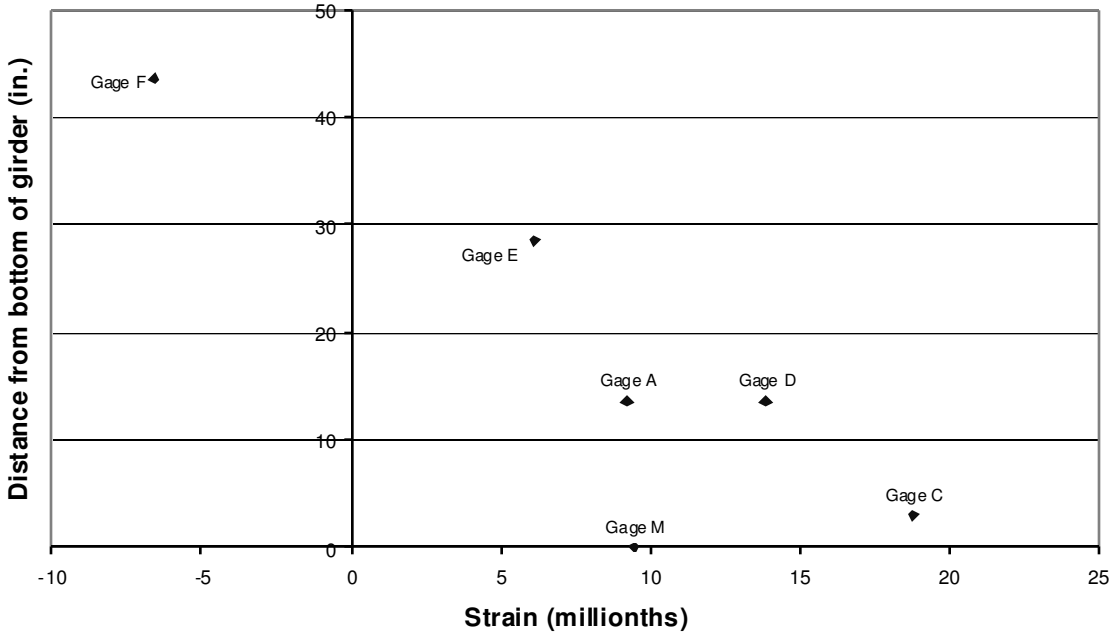


**Figure D-214:** C4 Span 10 Girder 7 Cross Section 2

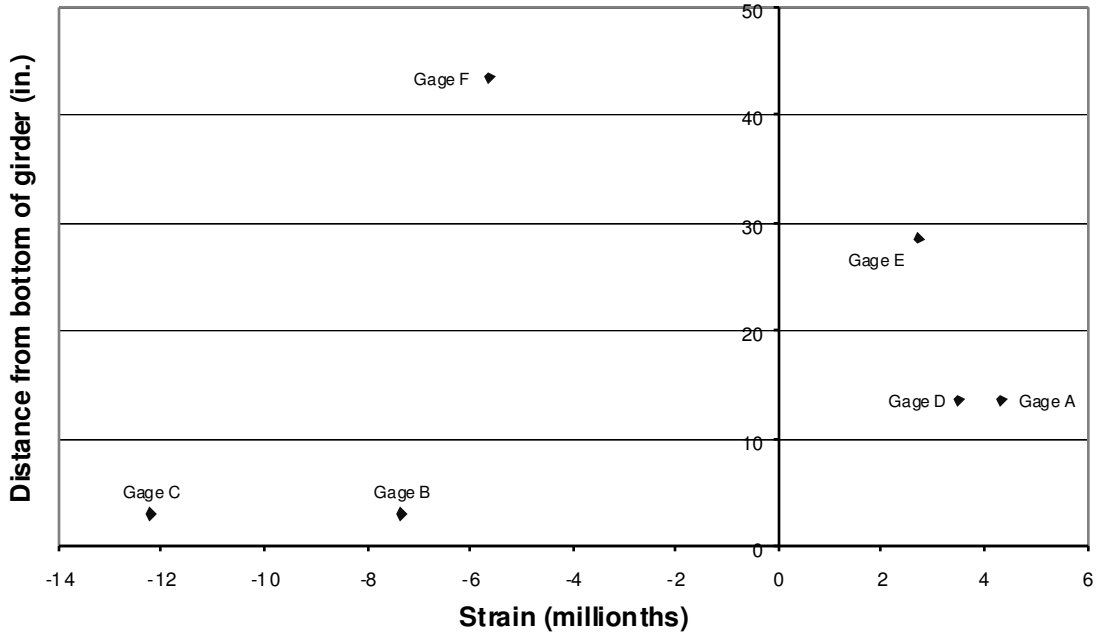


**Figure D-215:** C4 Span 10 Girder 8 Cross Section 1

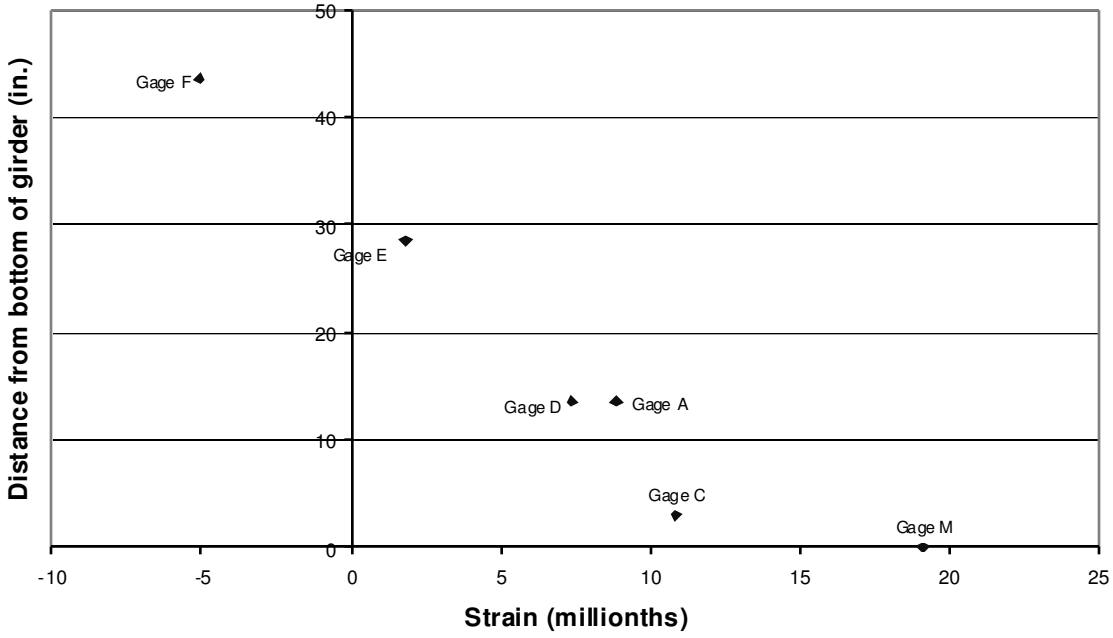


**Figure D-216:** C4 Span 10 Girder 8 Cross Section 2

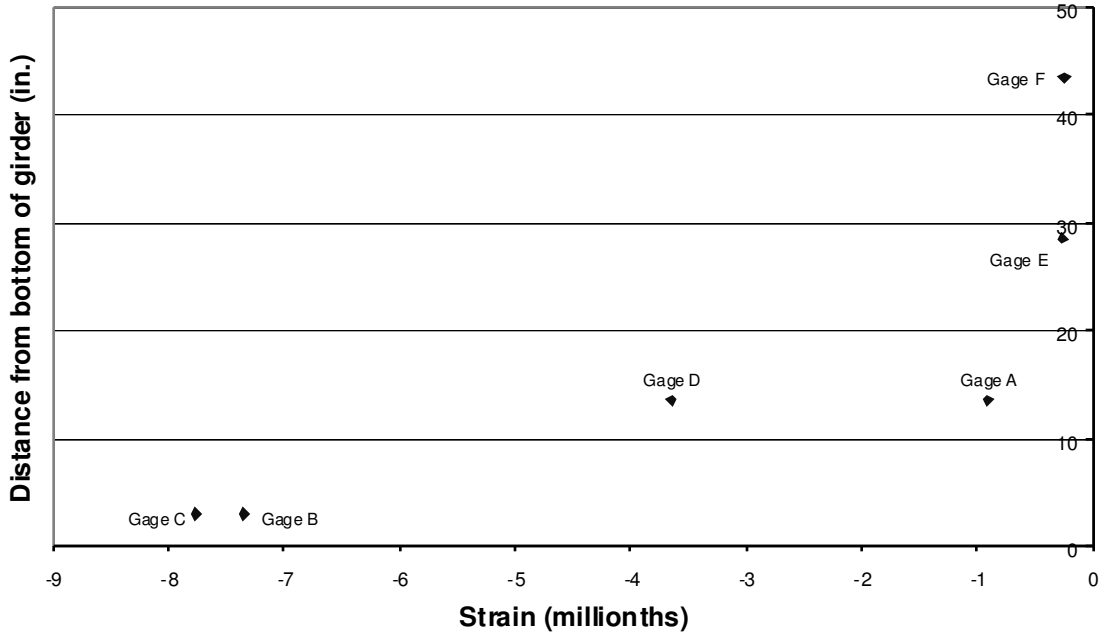


**Figure D-217:** C4 Span 11 Girder 7 Cross Section 1

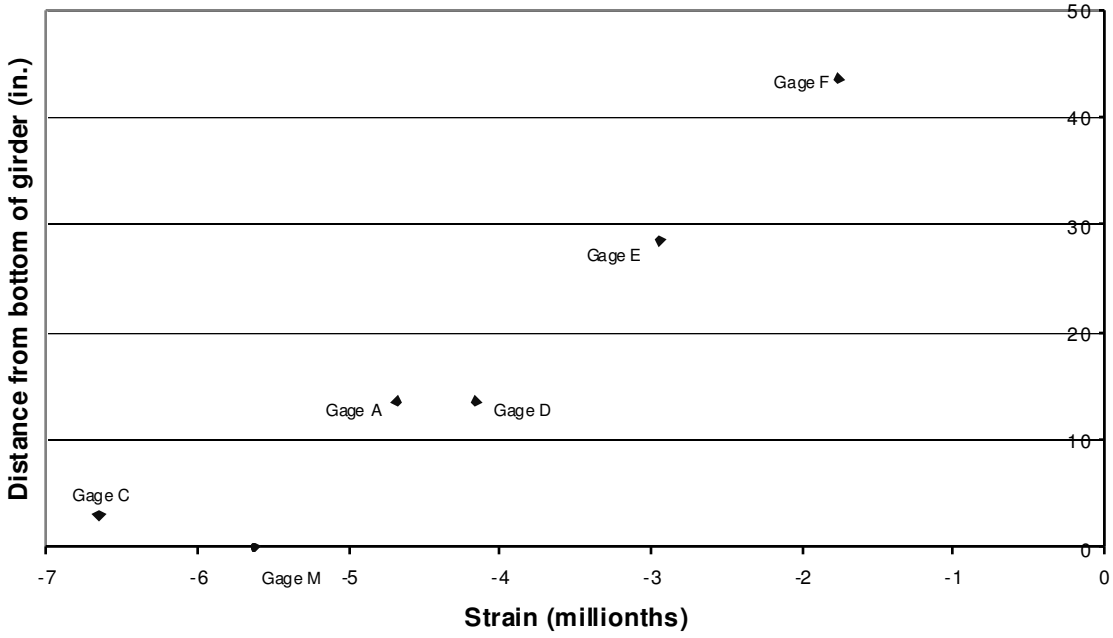


**Figure D-218:** C4 Span 11 Girder 7 Cross Section 2

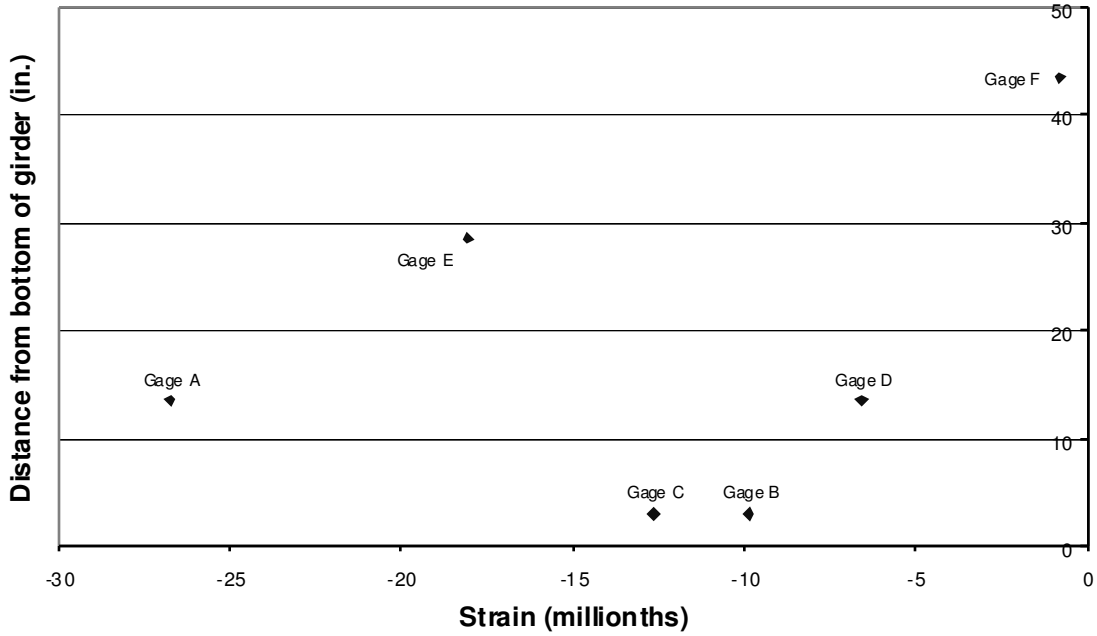


**Figure D-219:** C4 Span 11 Girder 8 Cross Section 1

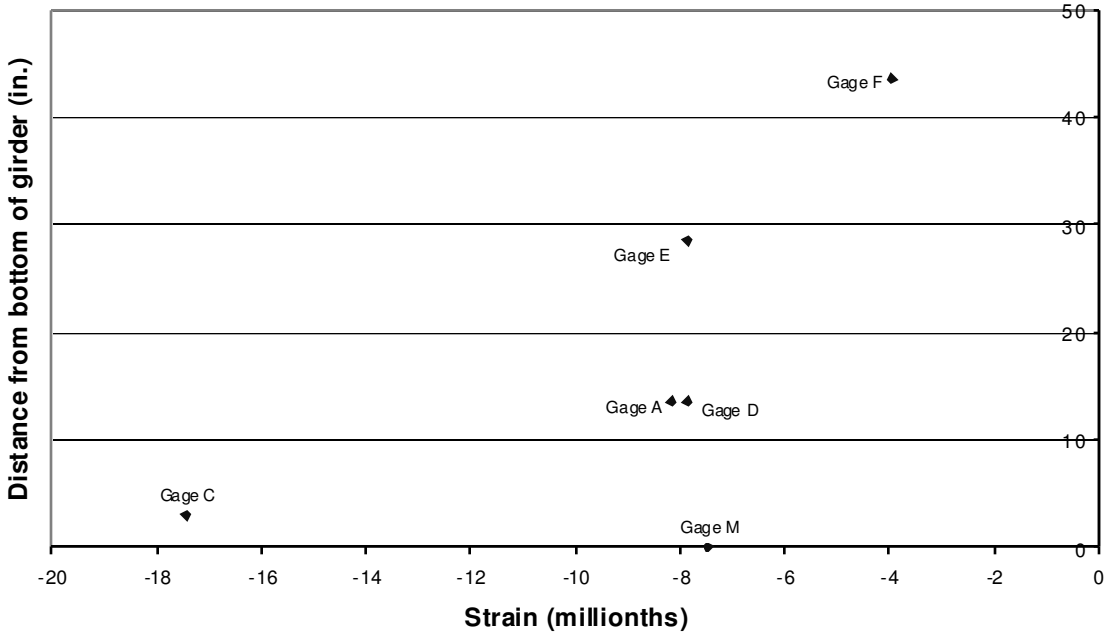


**Figure D-220:** C4 Span 11 Girder 8 Cross Section 2

### D.3.5 POSITION C5

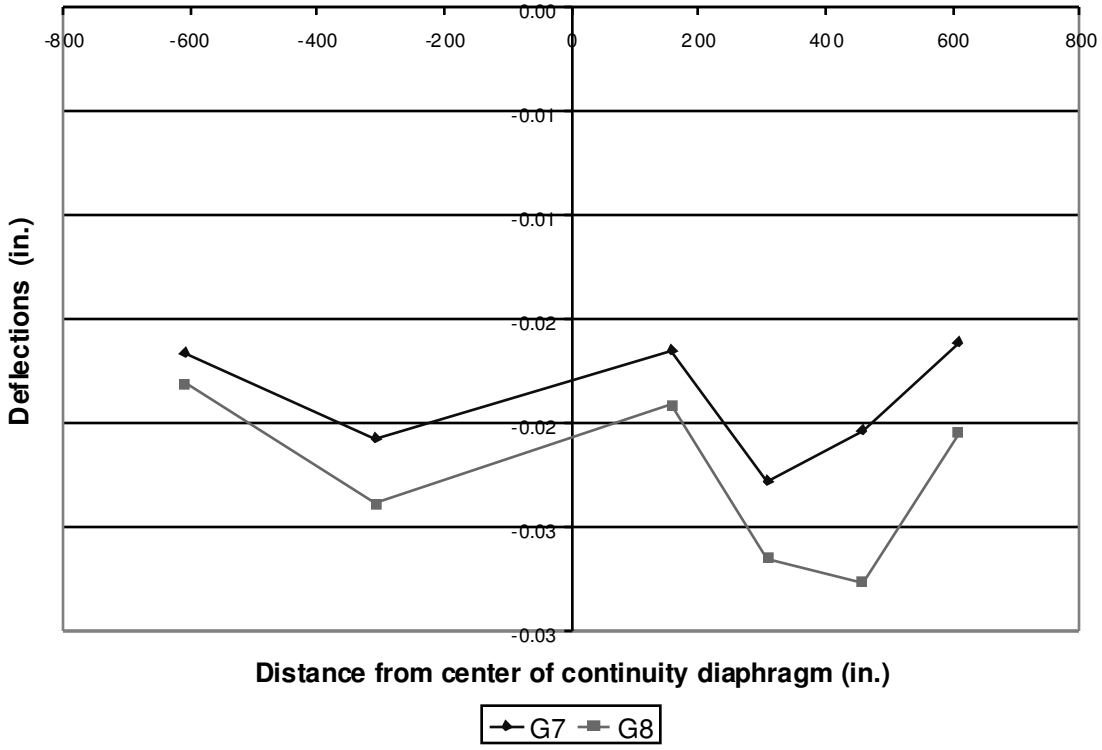


**Figure D-221:** C5 Deflections

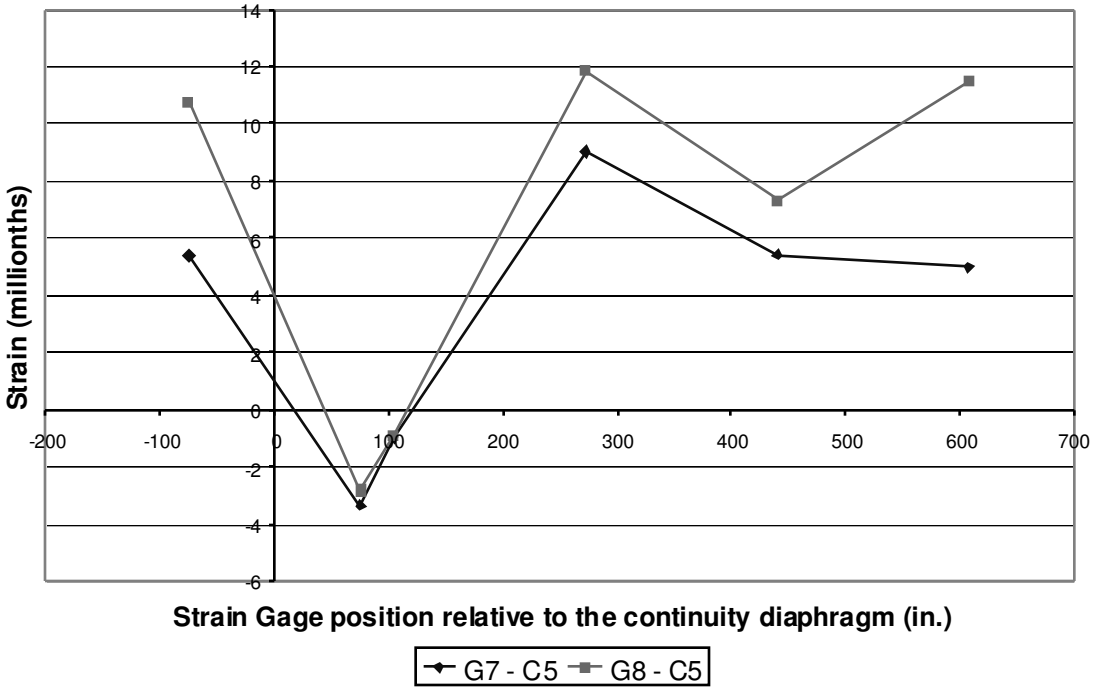


**Figure D-222:** C5 Bottom Fiber Strains

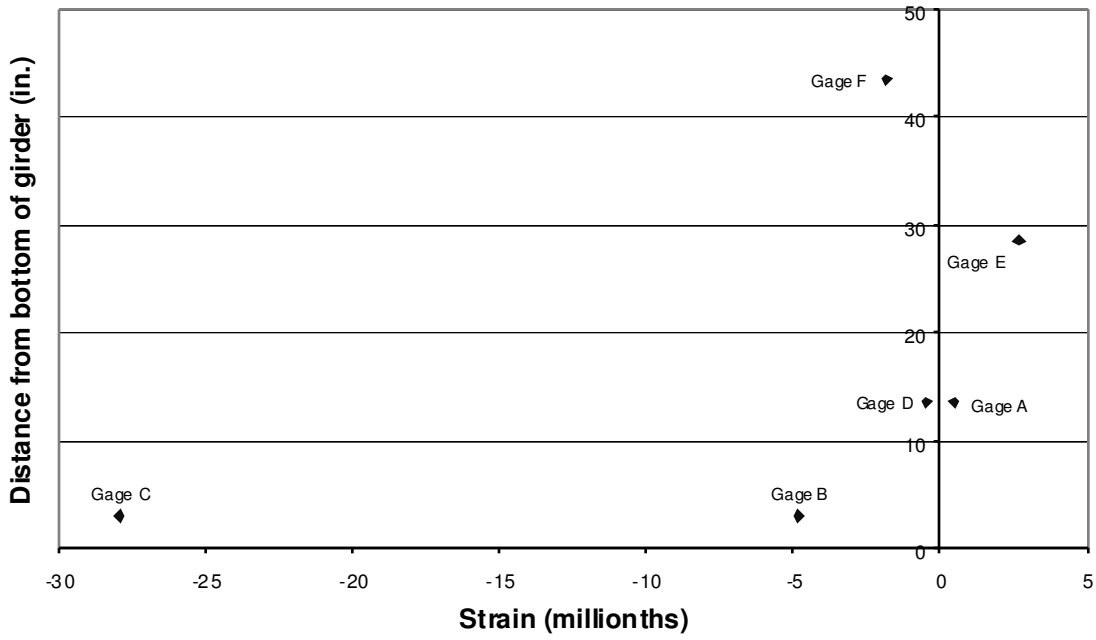


**Figure D-223:** C5 Span 10 Girder 7 Cross Section1

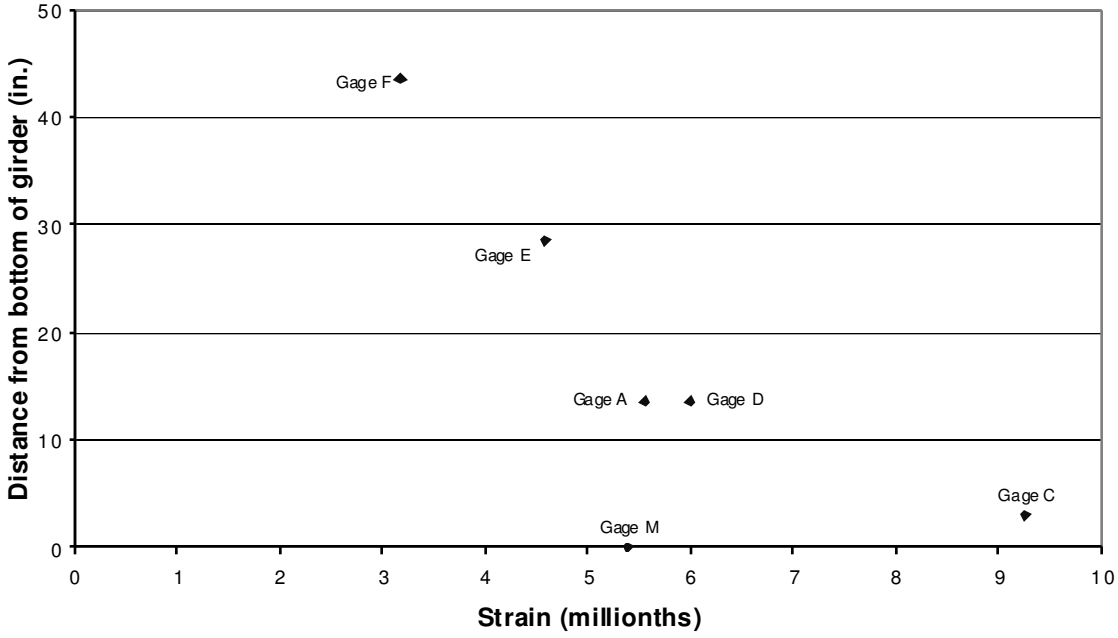


**Figure D-224:** C5 Span 10 Girder 7 Cross Section 2

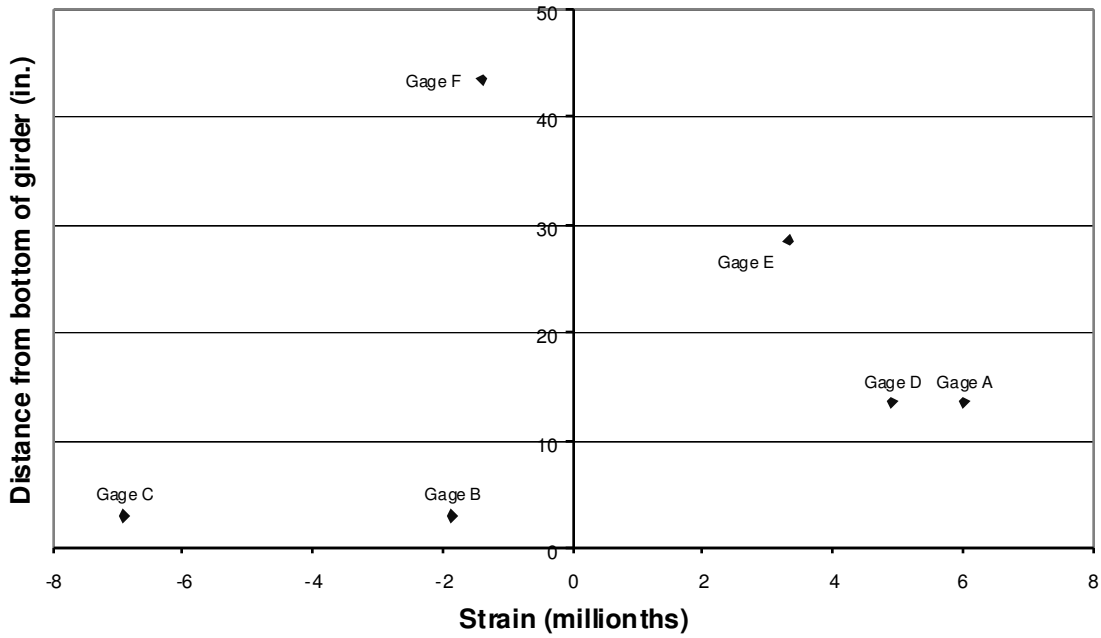


**Figure D-225:** C5 Span 10 Girder 8 Cross Section 1

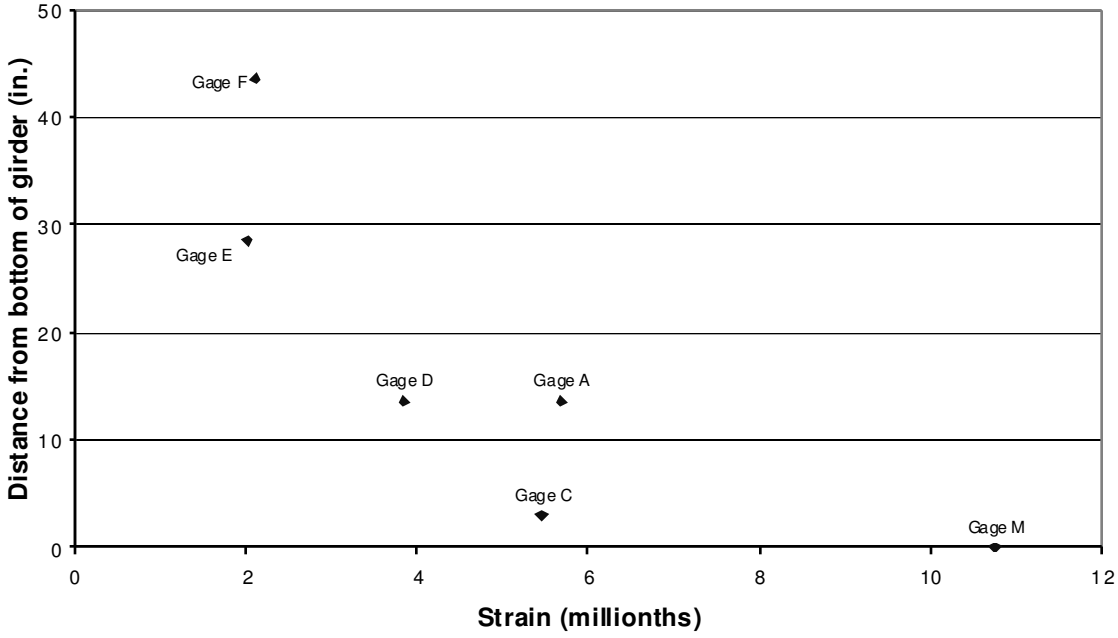


**Figure D-226:** C5 Span 10 Girder 8 Cross Section 2

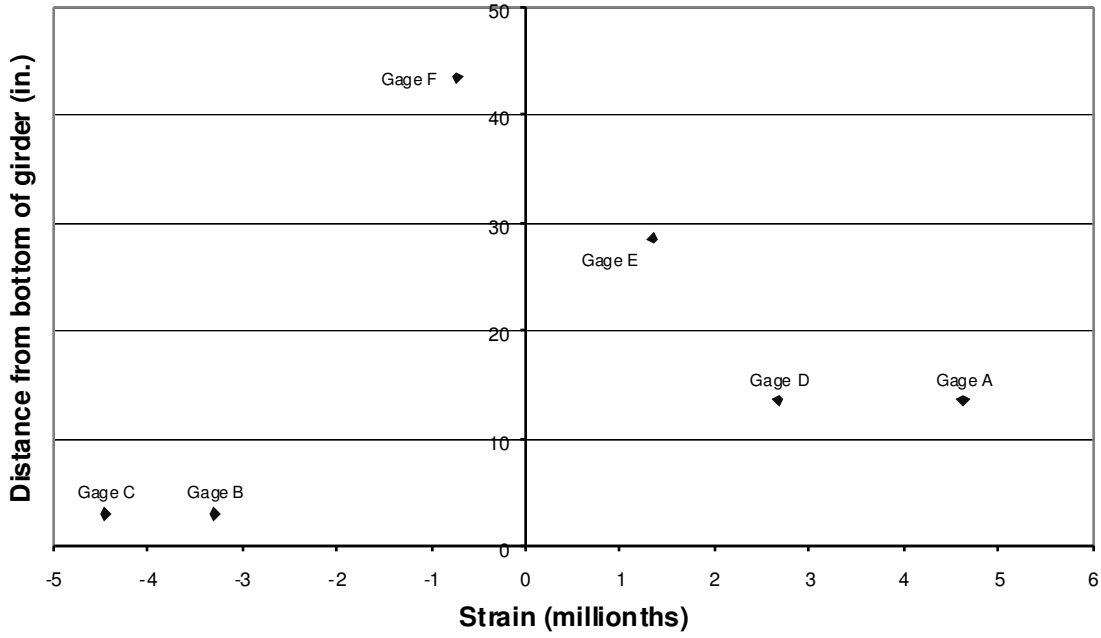


**Figure D-227:** C5 Span 11 Girder 7 Cross Section 1

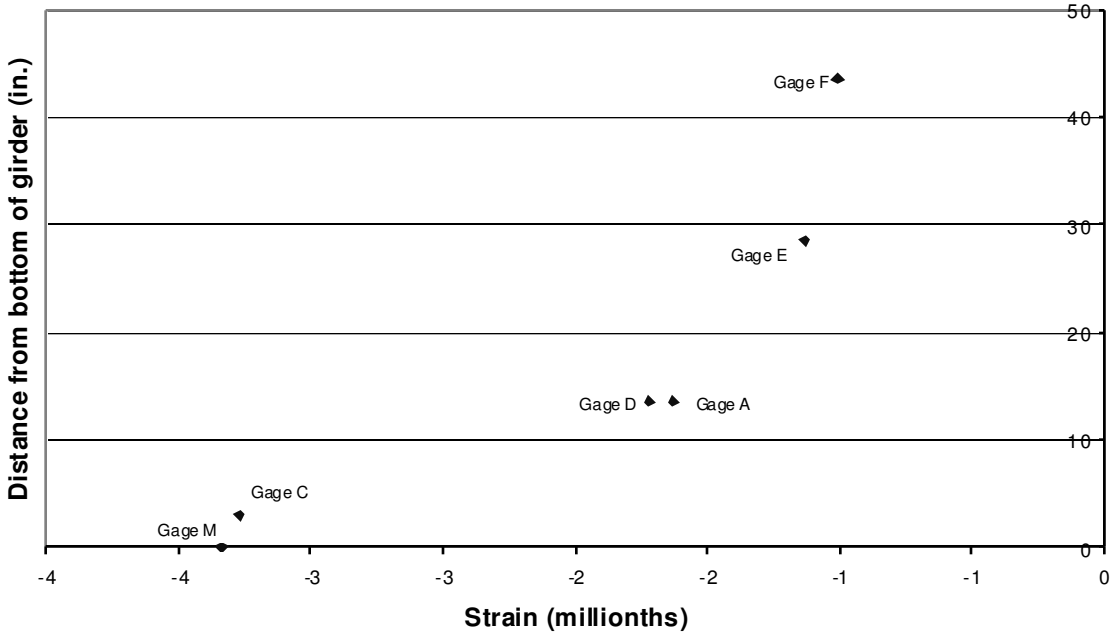


**Figure D-228:** C5 Span 11 Girder 7 Cross Section 2

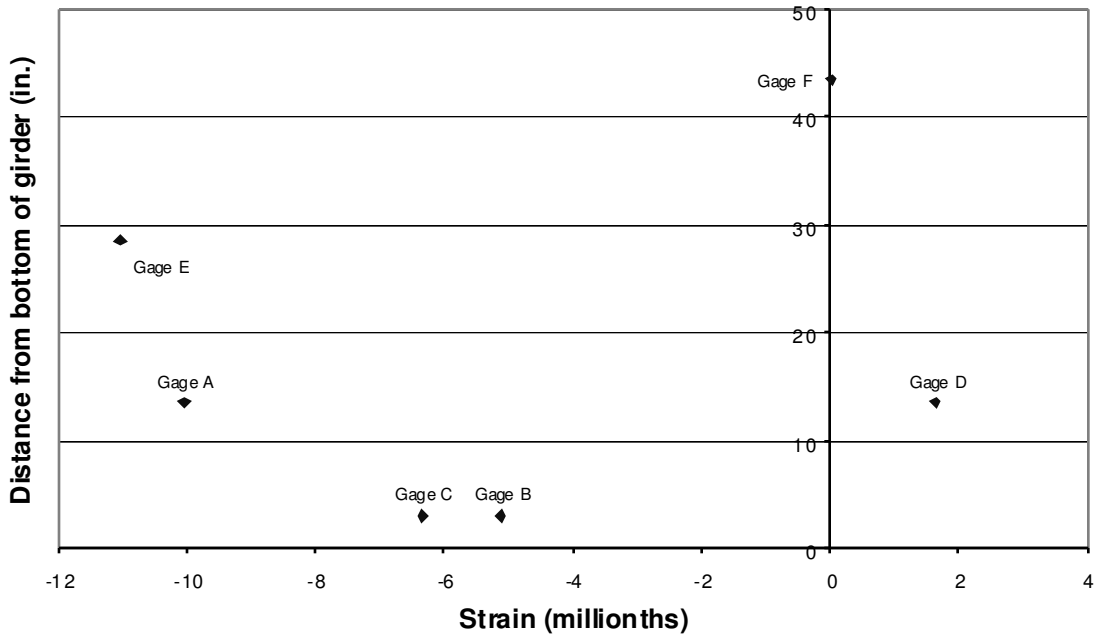


**Figure D-229:** C5 Span 11 Girder 8 Cross Section 1

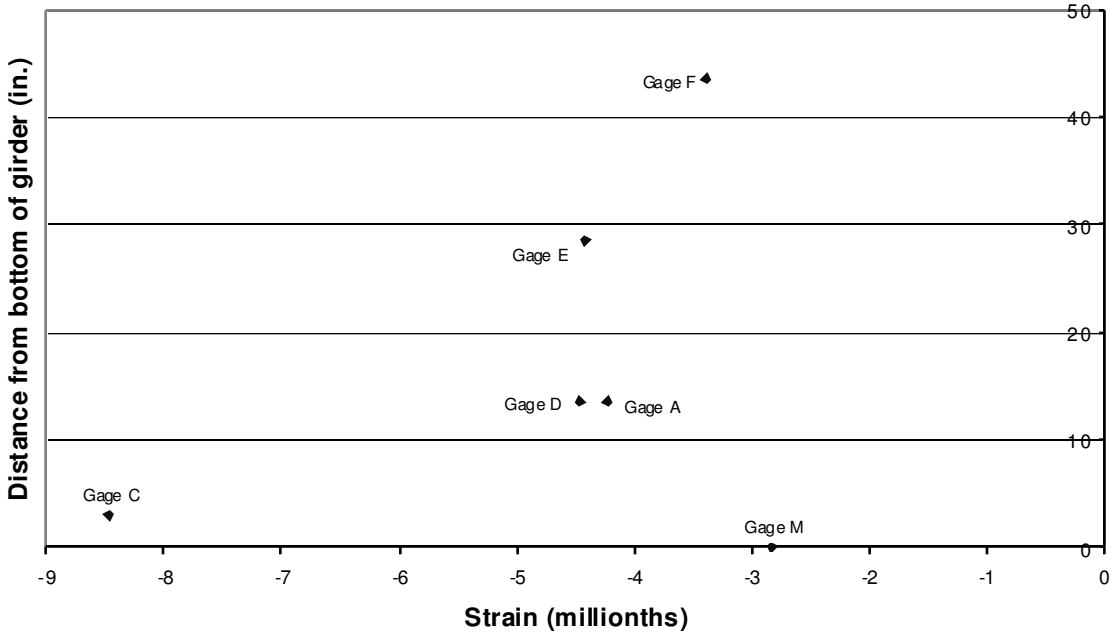


**Figure D-230:** C5 Span 11 Girder 8 Cross Section 2

### D.3.6 POSITION C6

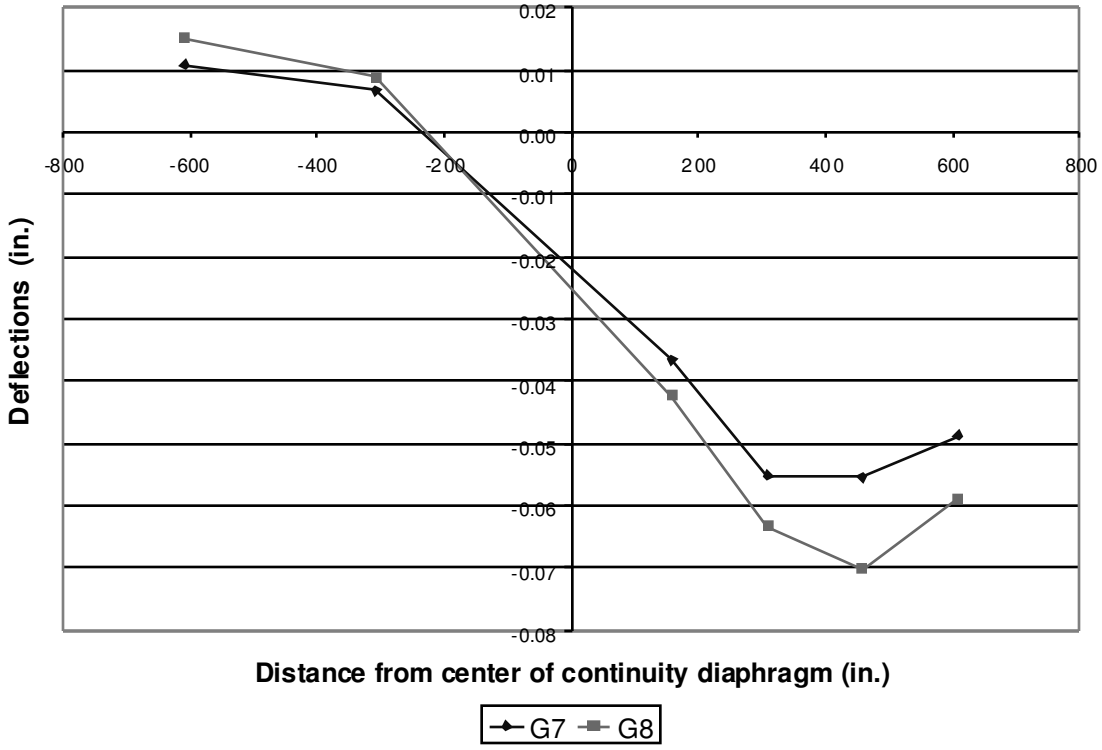


**Figure D-231:** C6 Deflections

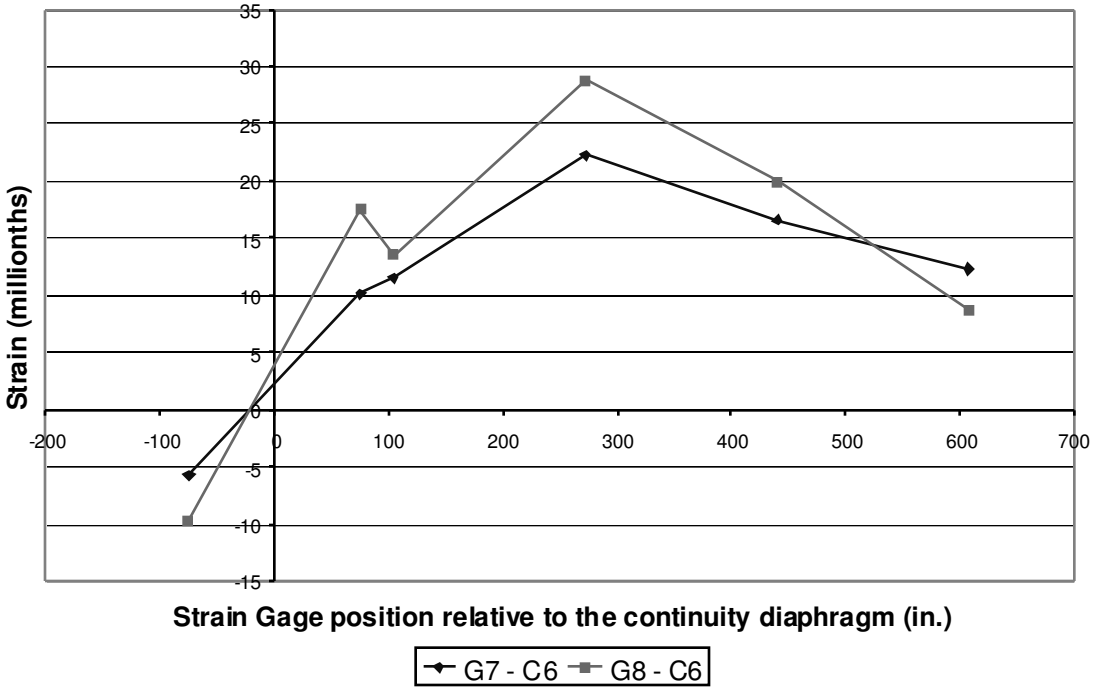


**Figure D-232:** C6 Bottom Fiber Strains

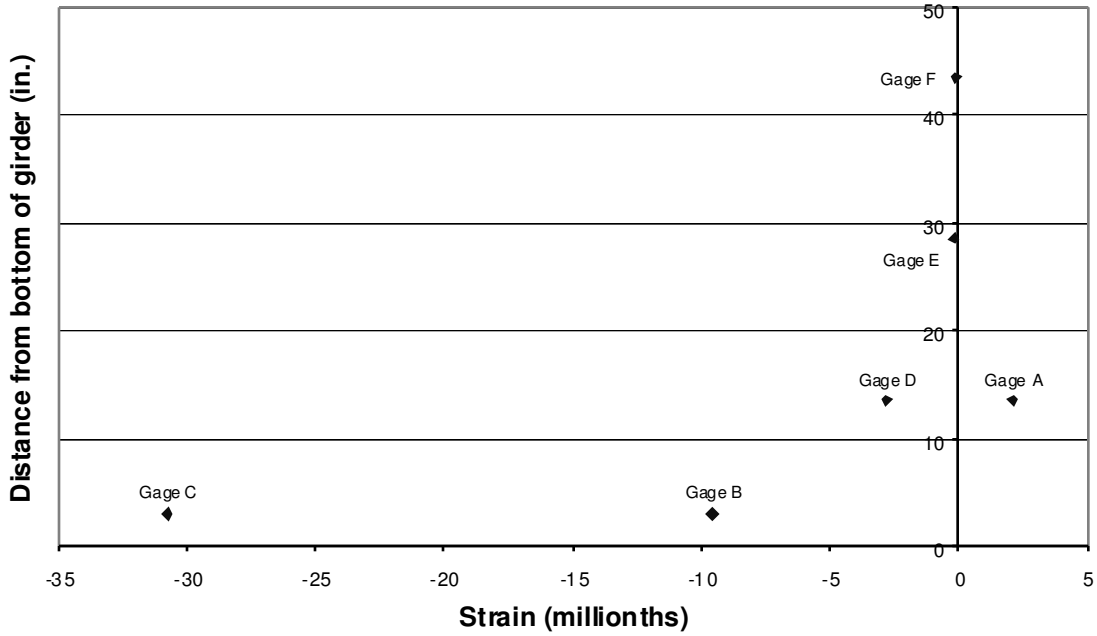


**Figure D-233:** C6 Span 10 Girder 7 Cross Section1

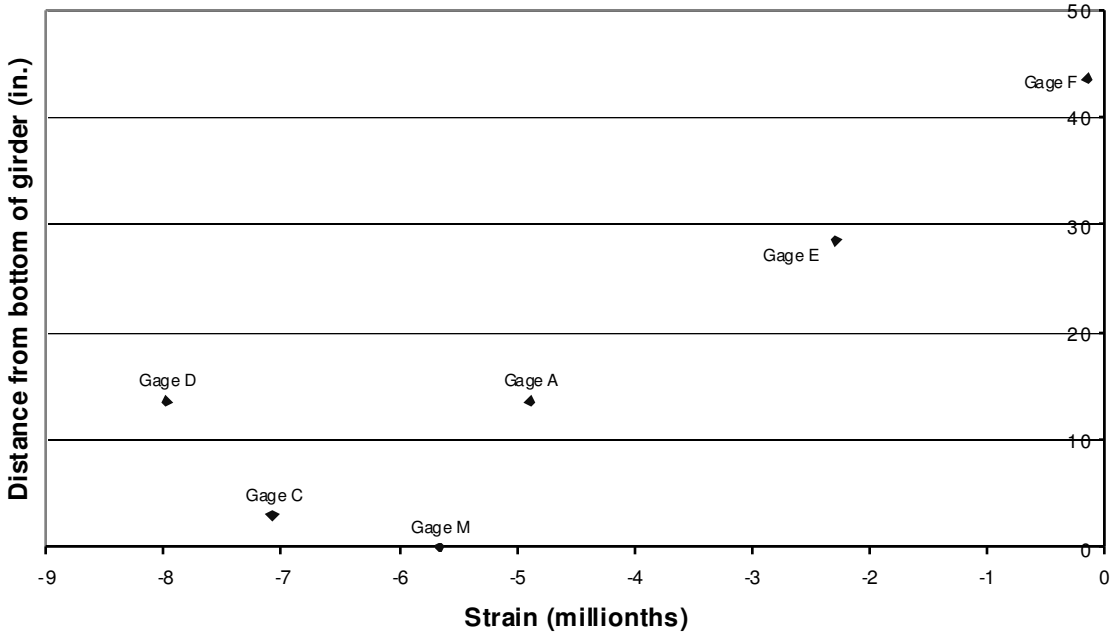


**Figure D-234:** C6 Span 10 Girder 7 Cross Section 2

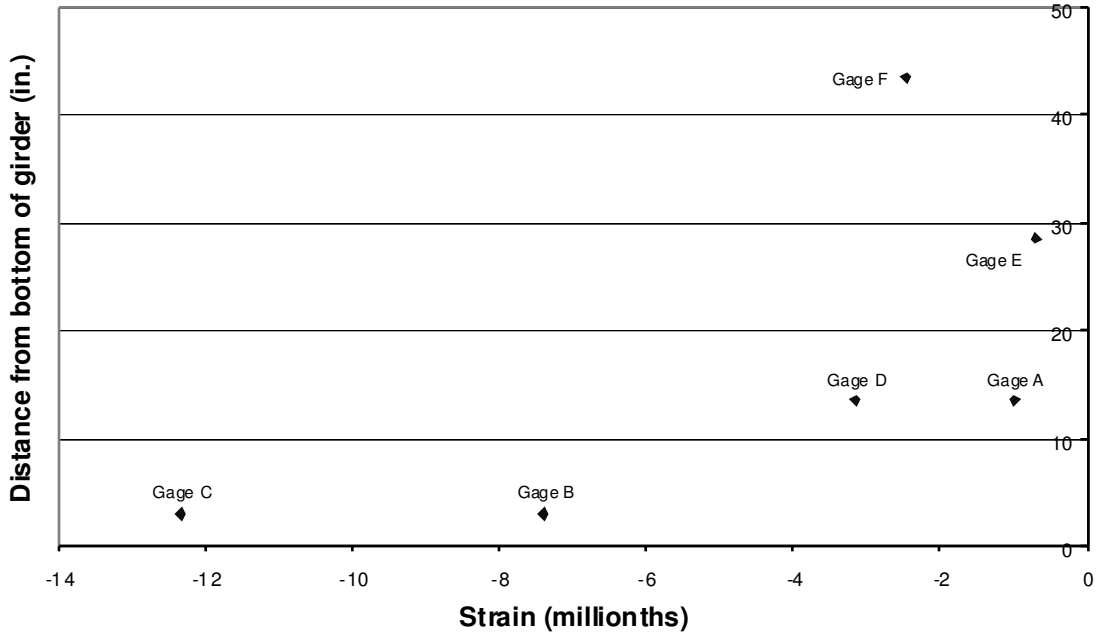


**Figure D-235:** C6 Span 10 Girder 8 Cross Section 1

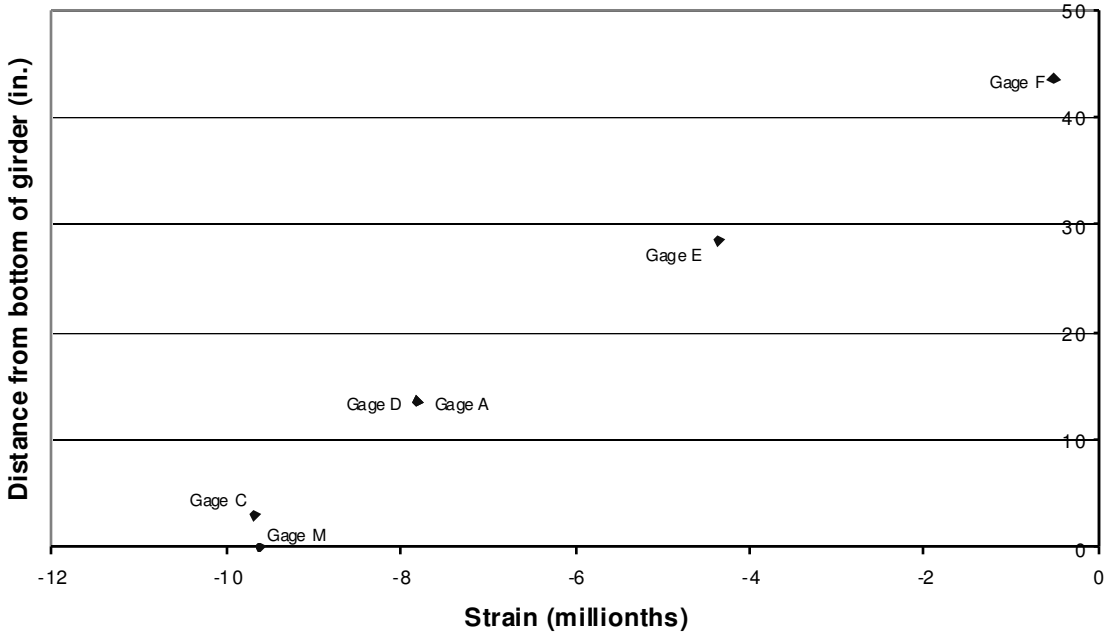


**Figure D-236:** C6 Span 10 Girder 8 Cross Section 2

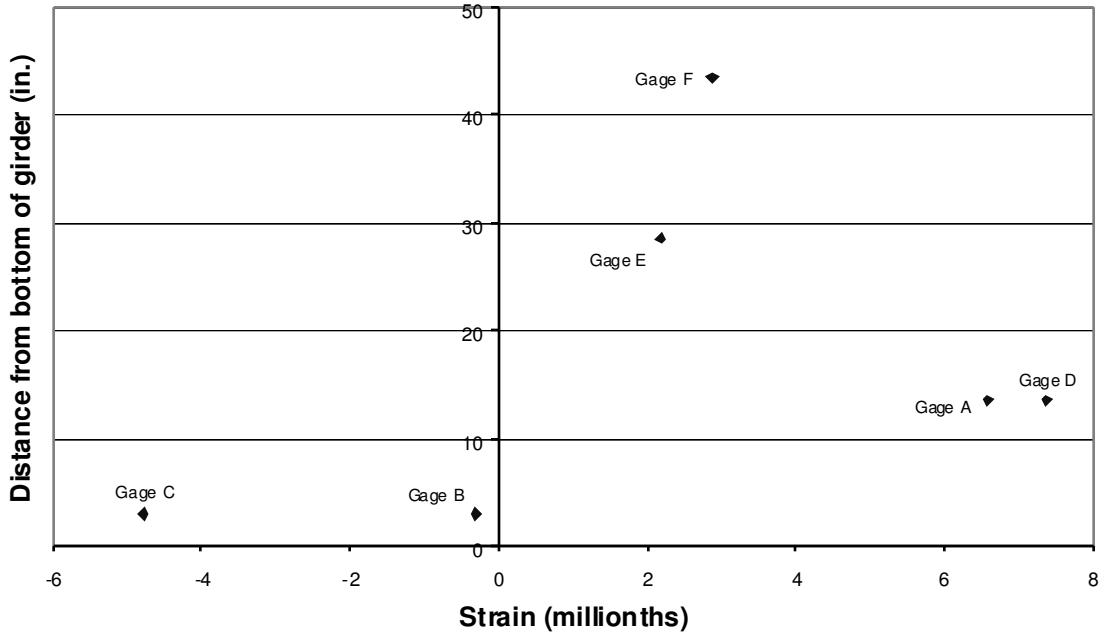


**Figure D-237:** C6 Span 11 Girder 7 Cross Section 1

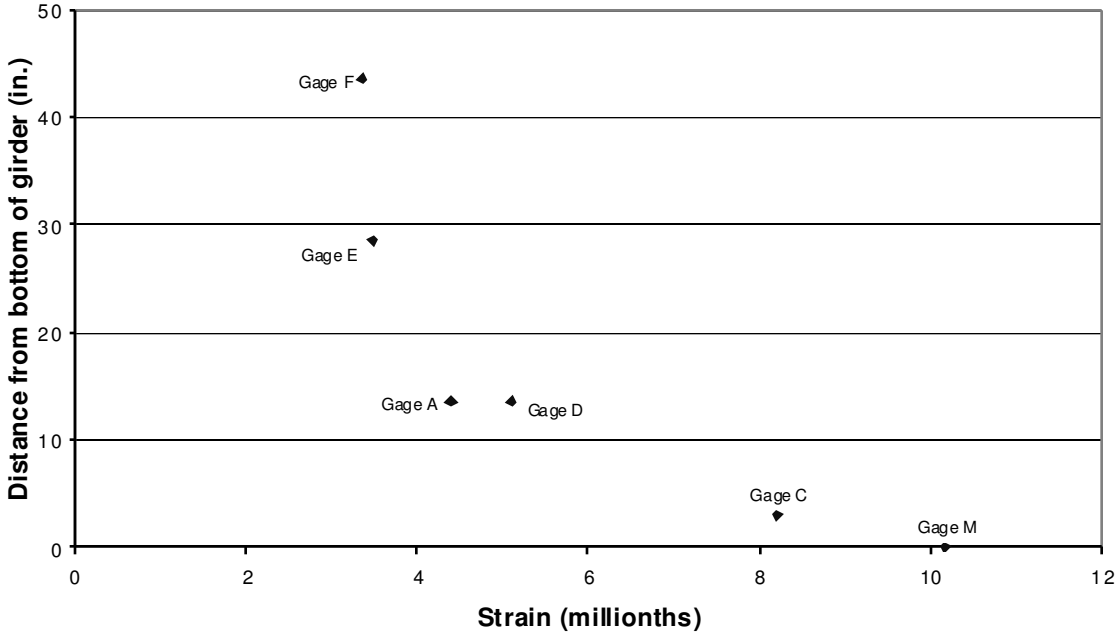


**Figure D-238:** C6 Span 11 Girder 7 Cross Section 2

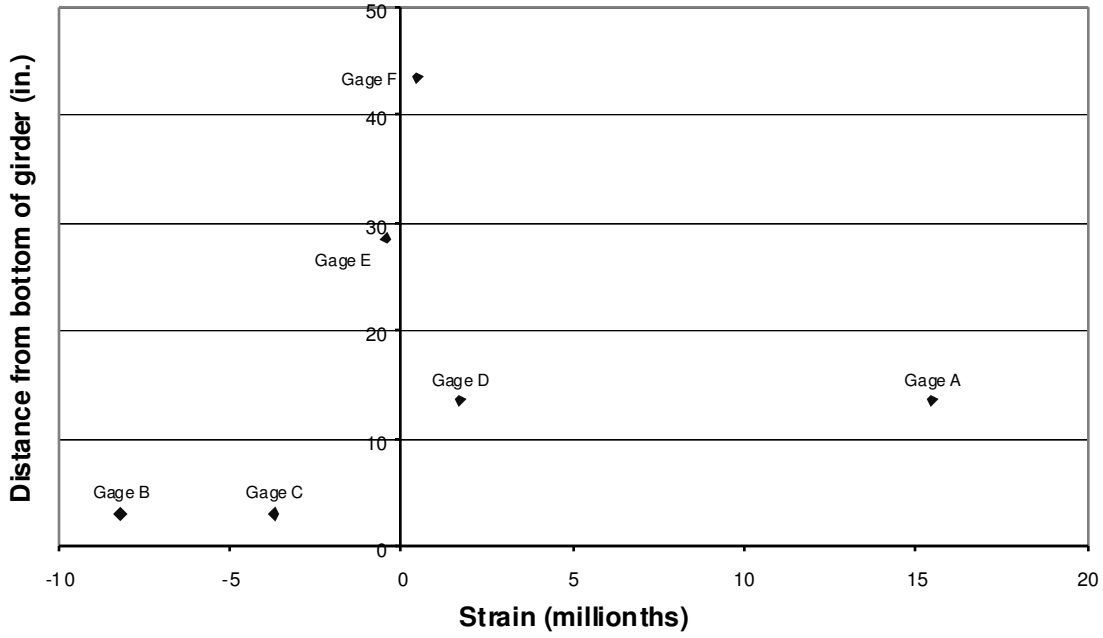


**Figure D-239:** C6 Span 11 Girder 8 Cross Section 1

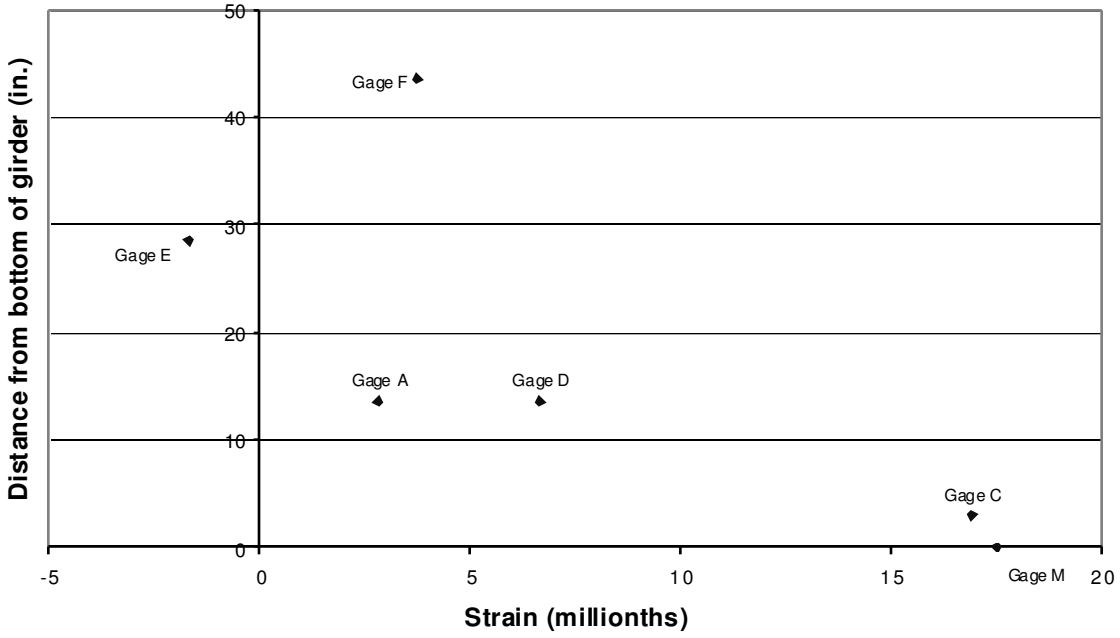


**Figure D-240:** C6 Span 11 Girder 8 Cross Section 2

### D.3.7 POSITION C7

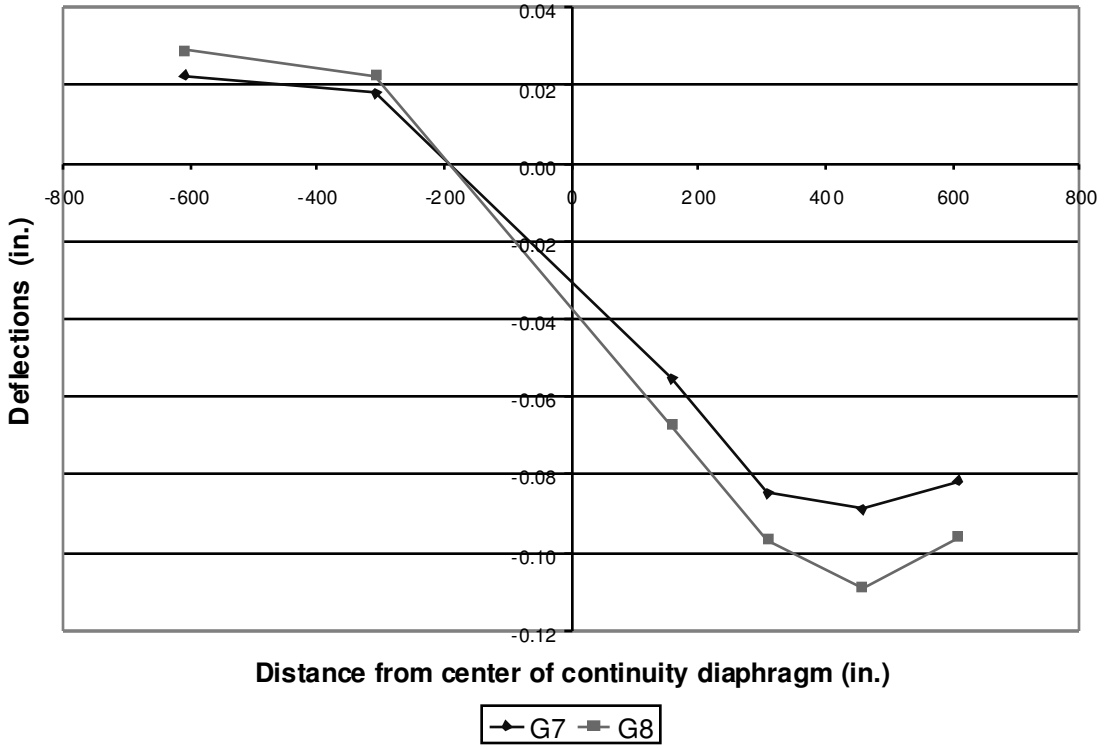


**Figure D-241:** C7 Deflections

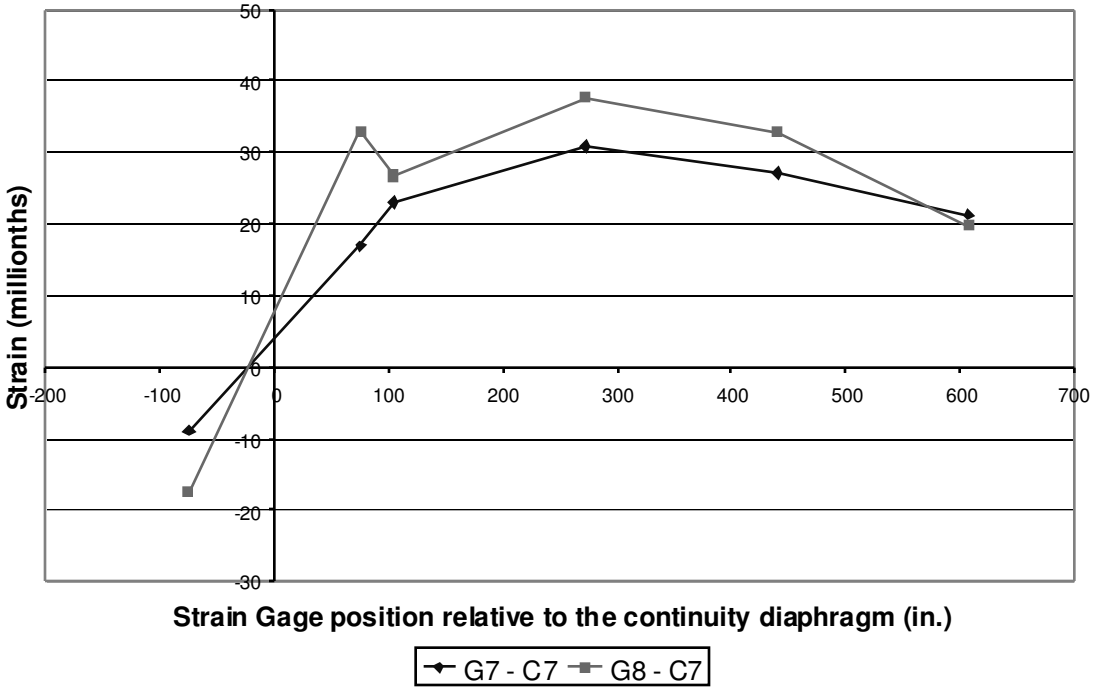


**Figure D-242:** C7 Bottom Fiber Strains

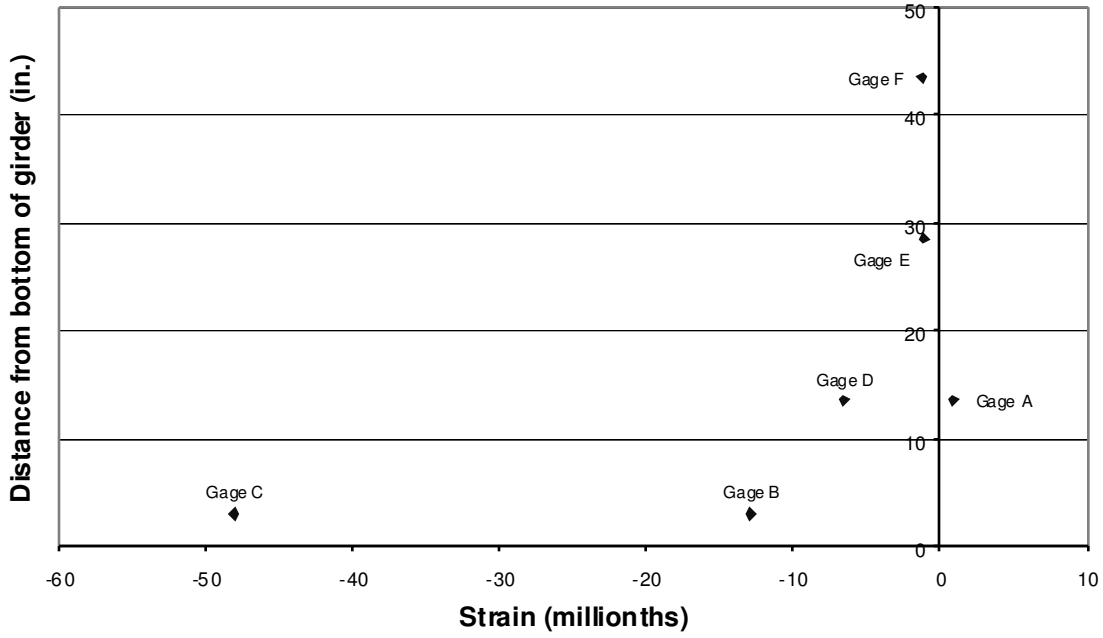


**Figure D-243:** C7 Span 10 Girder 7 Cross Section1

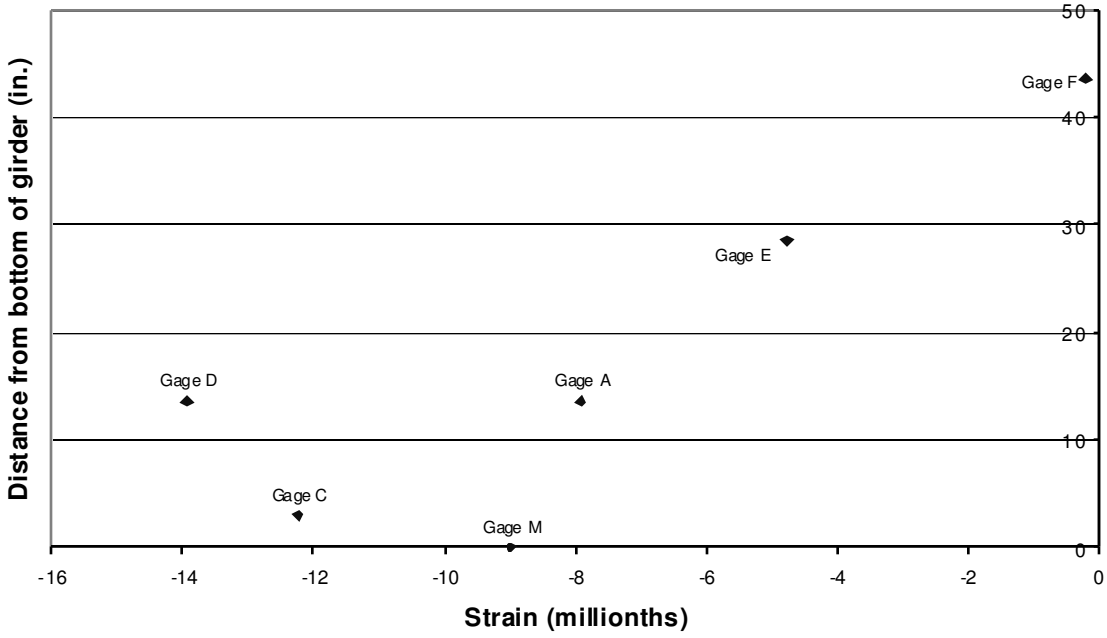


**Figure D-244:** C7 Span 10 Girder 7 Cross Section 2

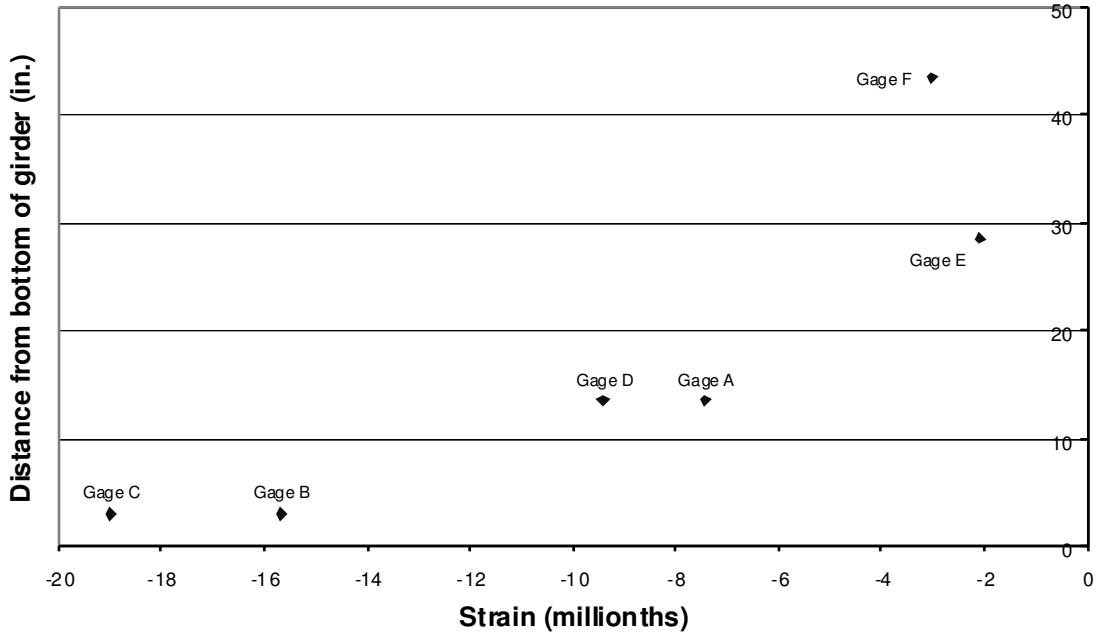


**Figure D-245:** C7 Span 10 Girder 8 Cross Section 1

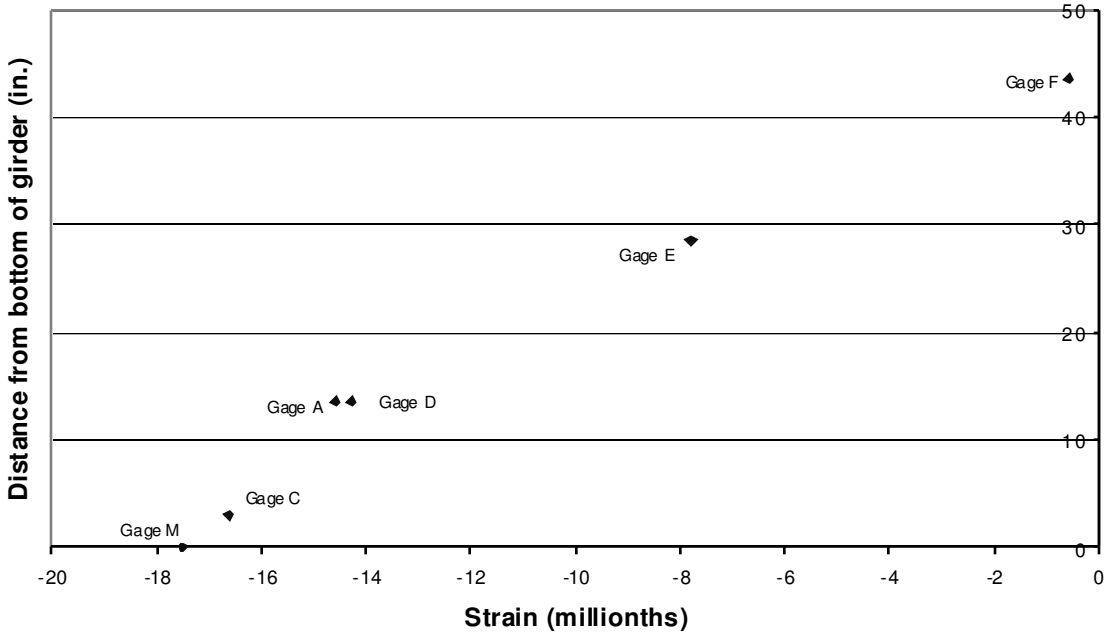


**Figure D-246:** C7 Span 10 Girder 8 Cross Section 2

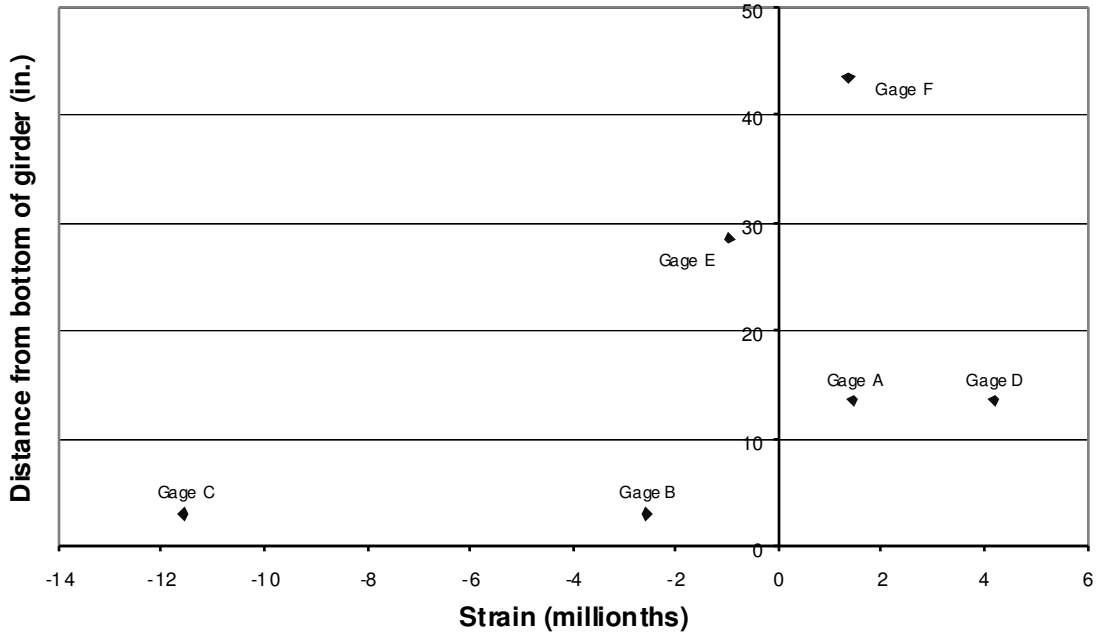


**Figure D-247:** C7 Span 11 Girder 7 Cross Section 1

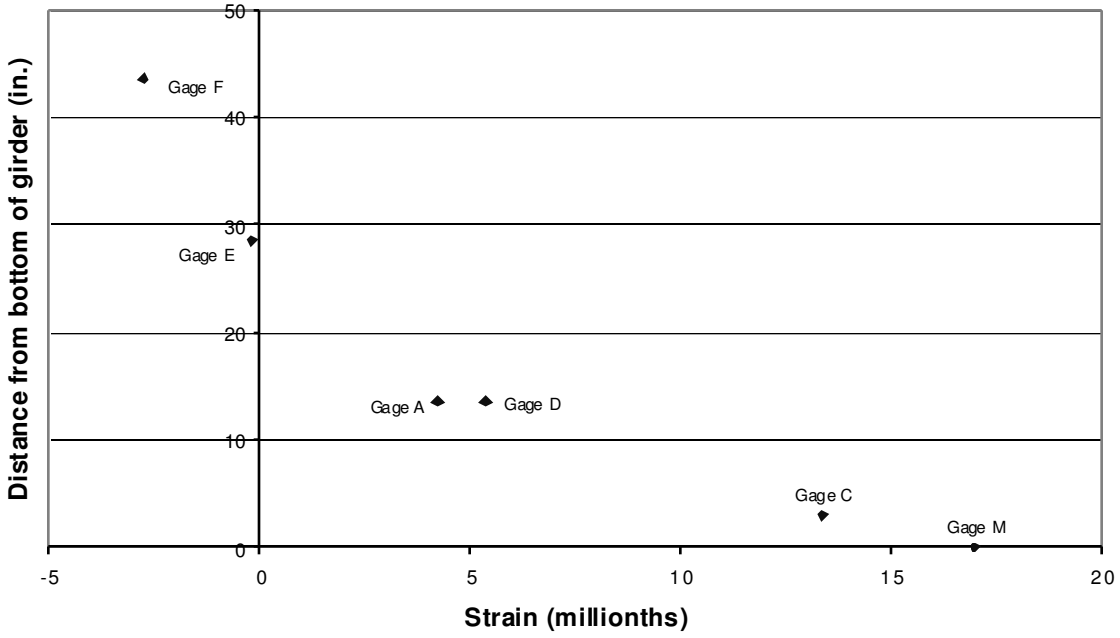


**Figure D-248:** C7 Span 11 Girder 7 Cross Section 2

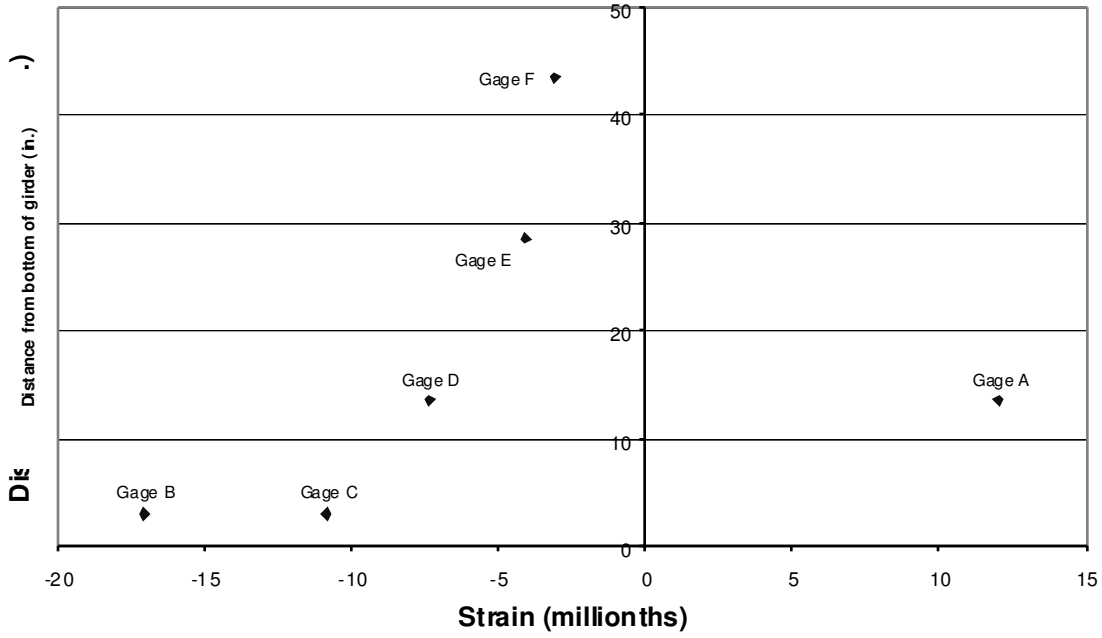


**Figure D-249:** C7 Span 11 Girder 8 Cross Section 1

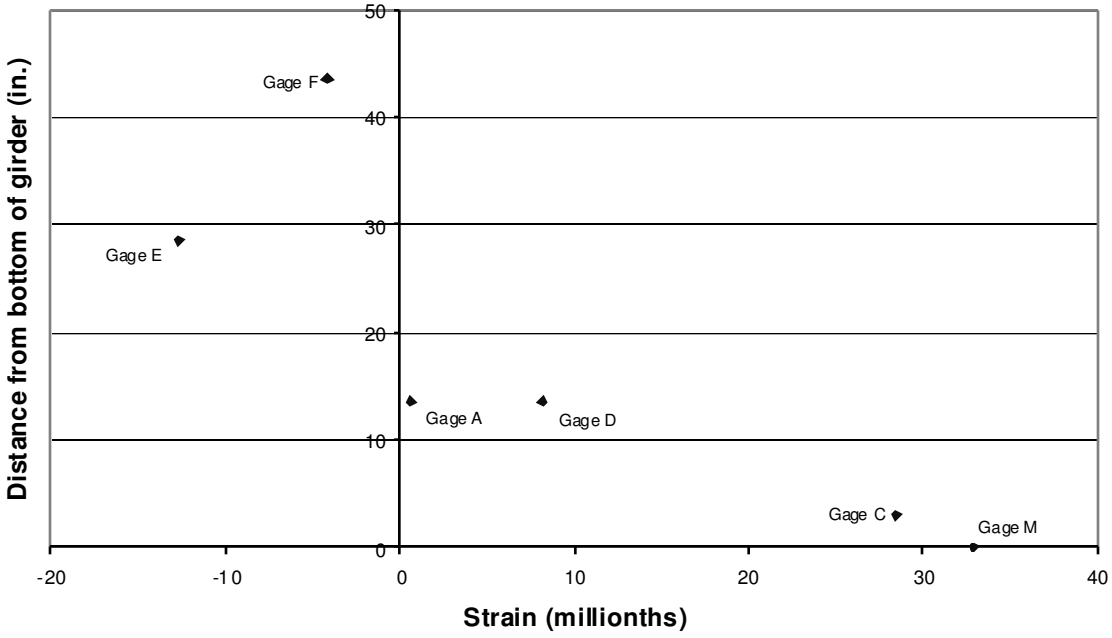


**Figure D-250:** C7 Span 11 Girder 8 Cross Section 2

### D.3.8 POSITION C8

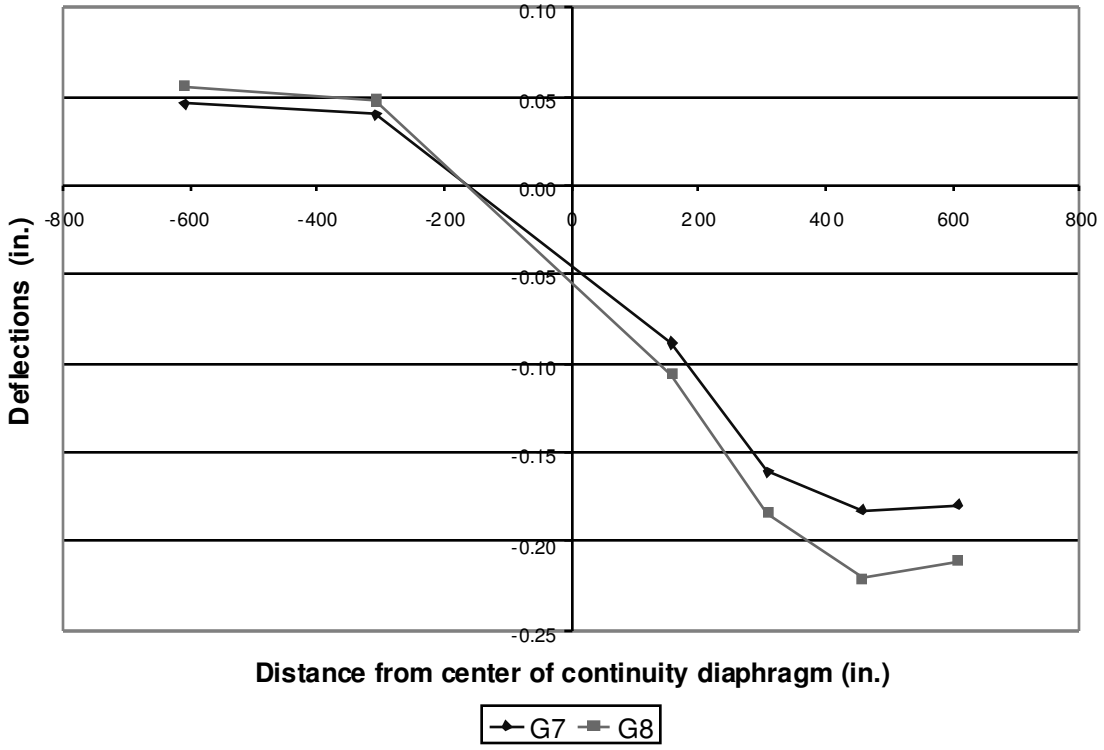


**Figure D-251:** C8 Deflections

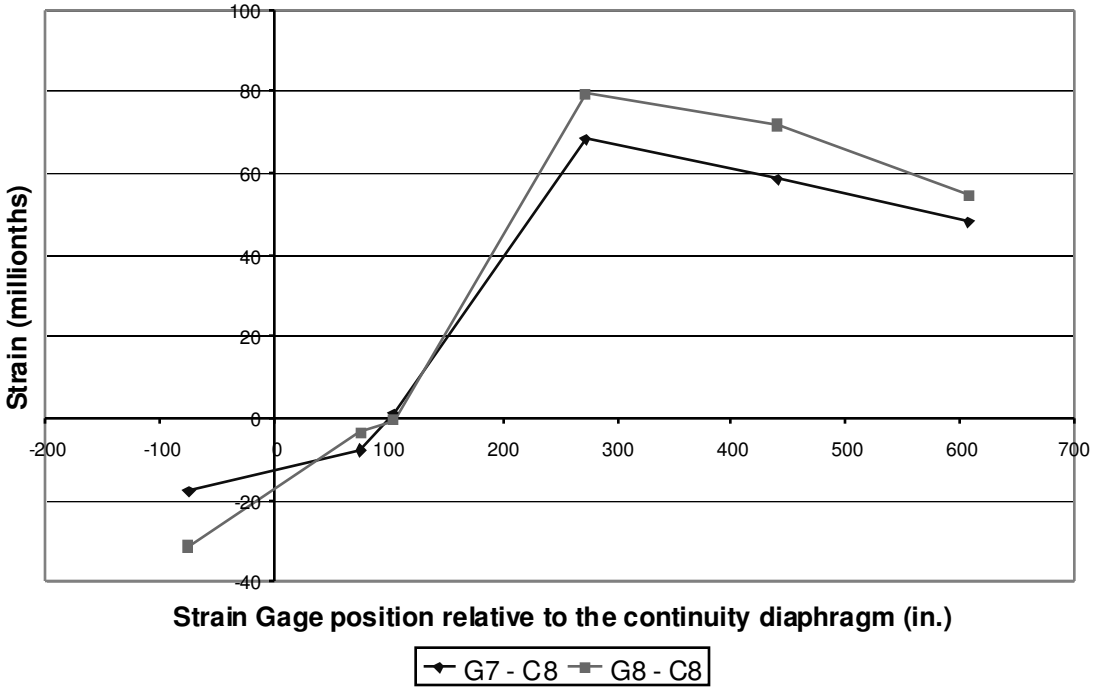


**Figure D-252:** C8 Bottom Fiber Strains

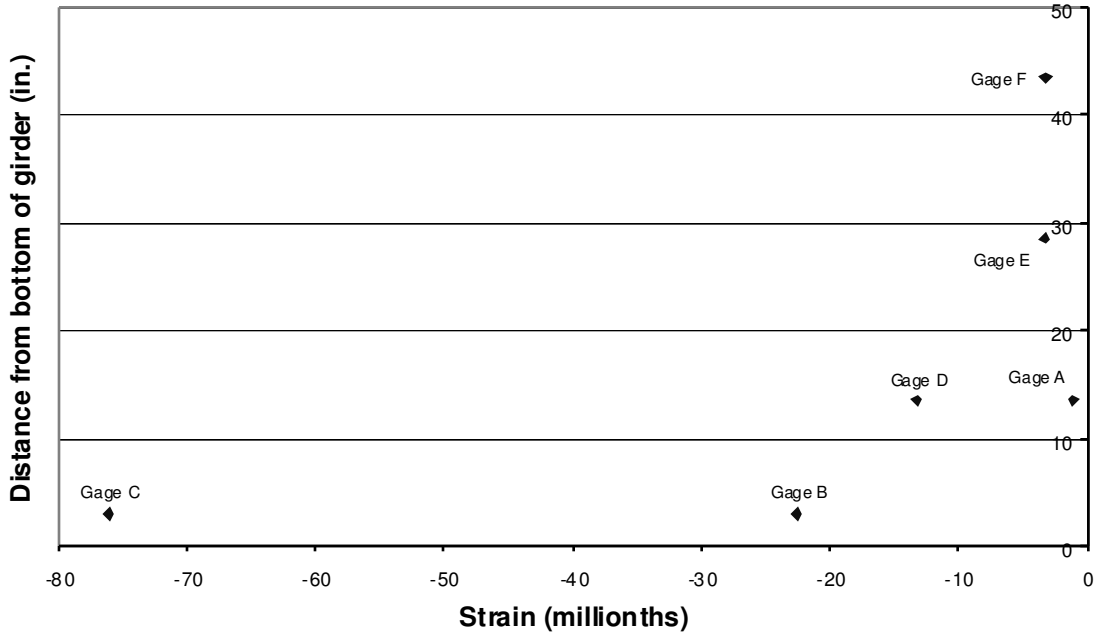


**Figure D-253:** C8 Span 10 Girder 7 Cross Section1

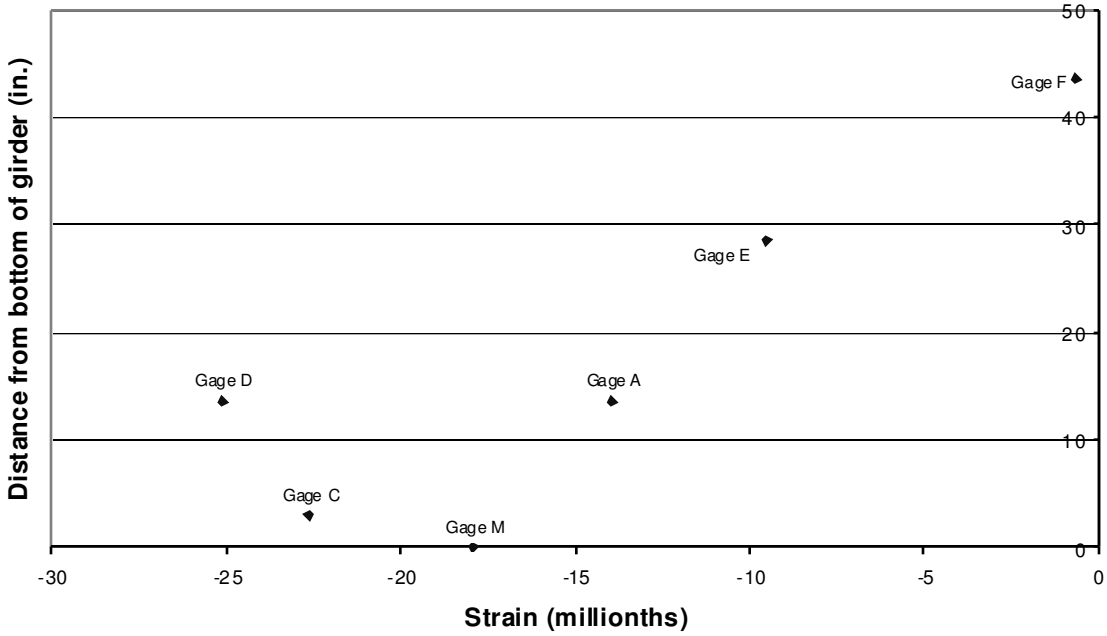


**Figure D-254:** C8 Span 10 Girder 7 Cross Section 2

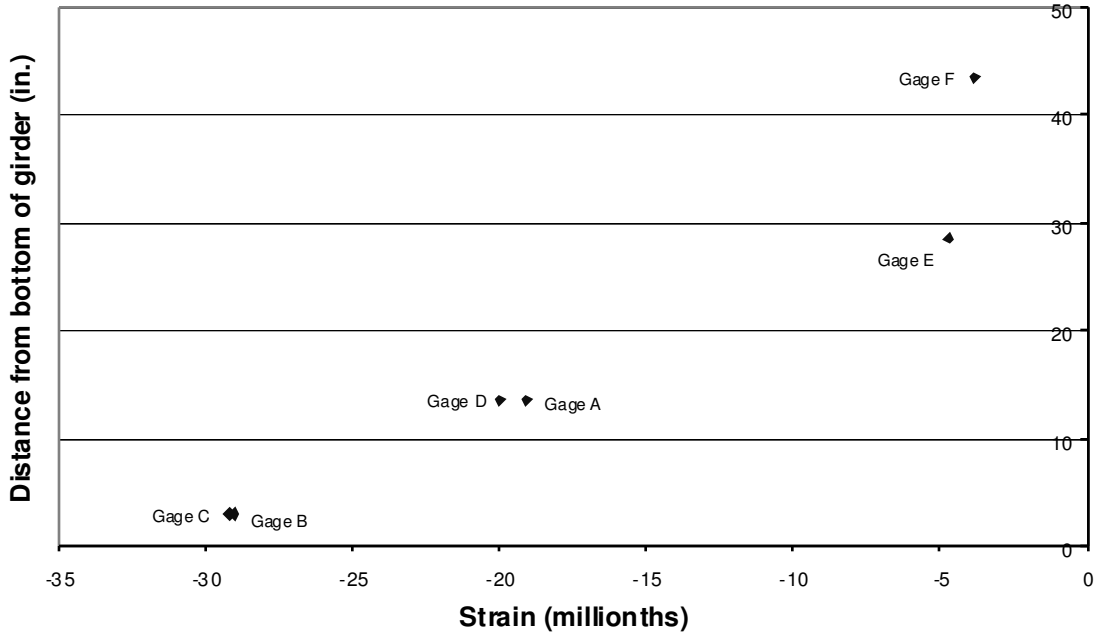


**Figure D-255:** C8 Span 10 Girder 8 Cross Section 1

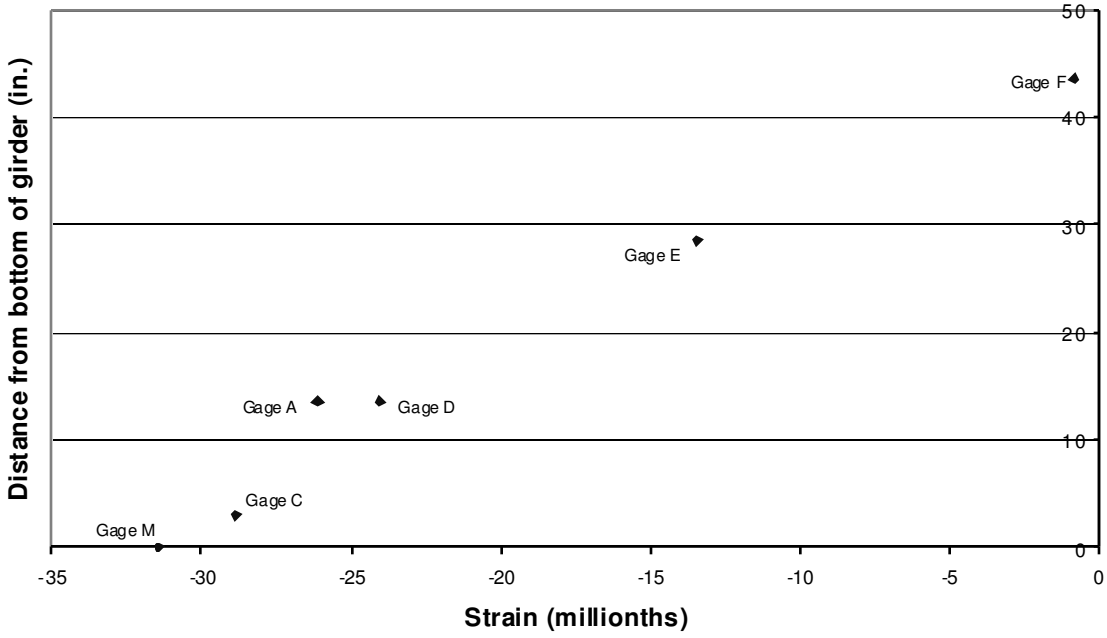


**Figure D-256:** C8 Span 10 Girder 8 Cross Section 2

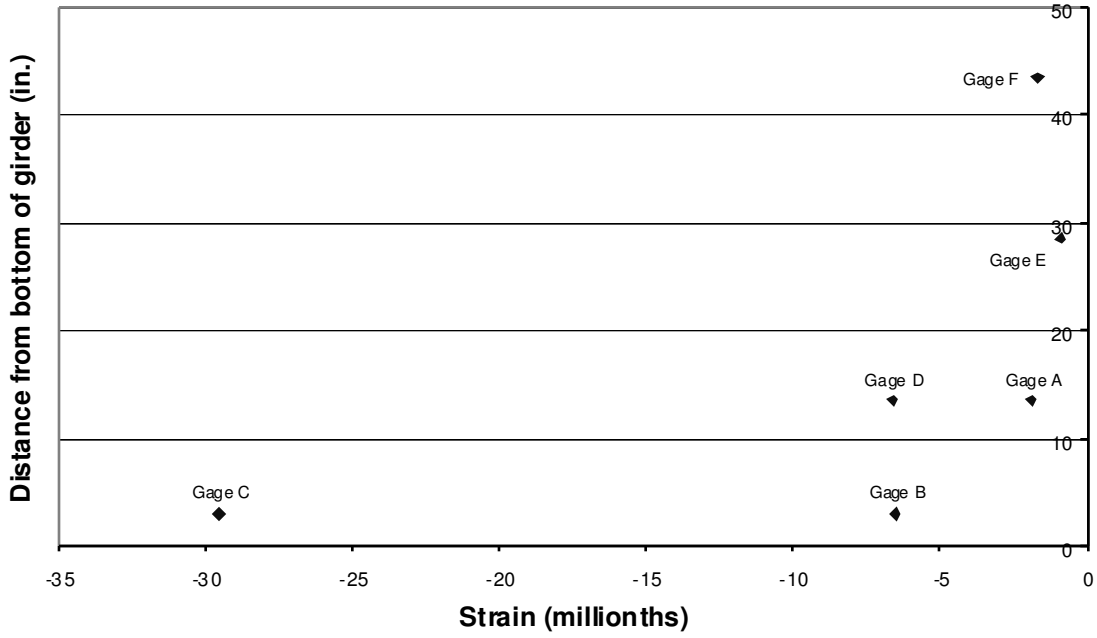


**Figure D-257:** C8 Span 11 Girder 7 Cross Section 1

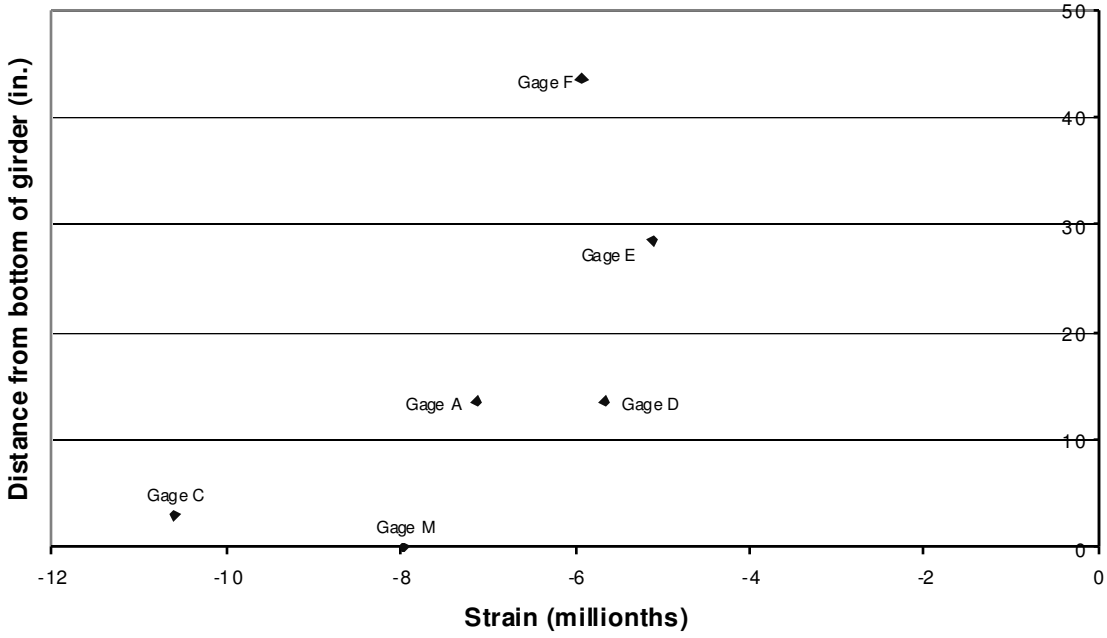


**Figure D-258:** C8 Span 11 Girder 7 Cross Section 2

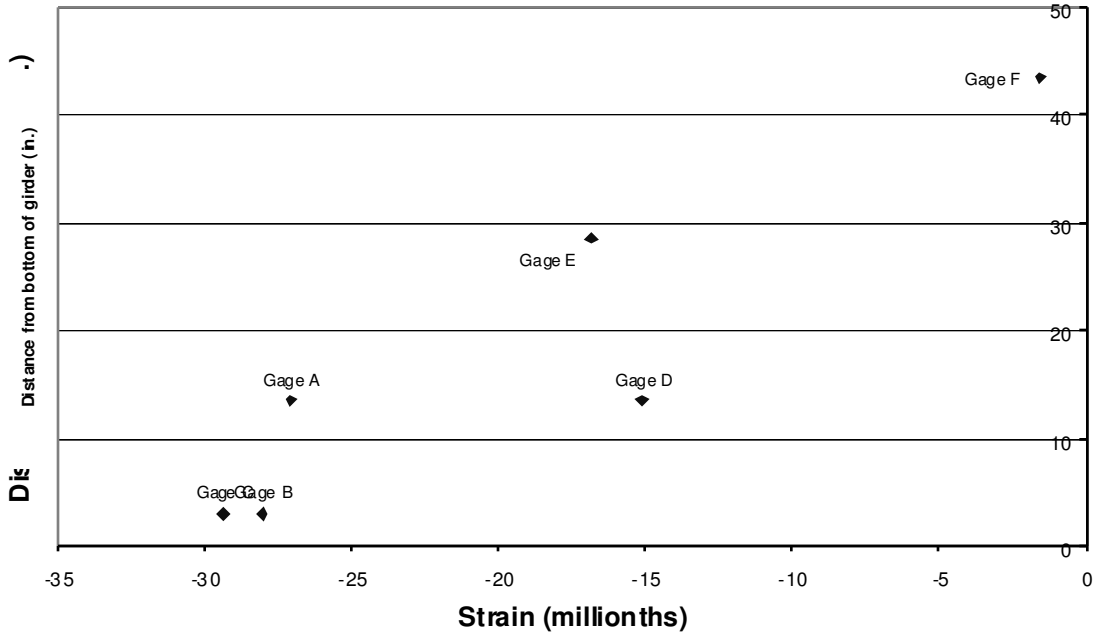


**Figure D-259:** C8 Span 11 Girder 8 Cross Section 1

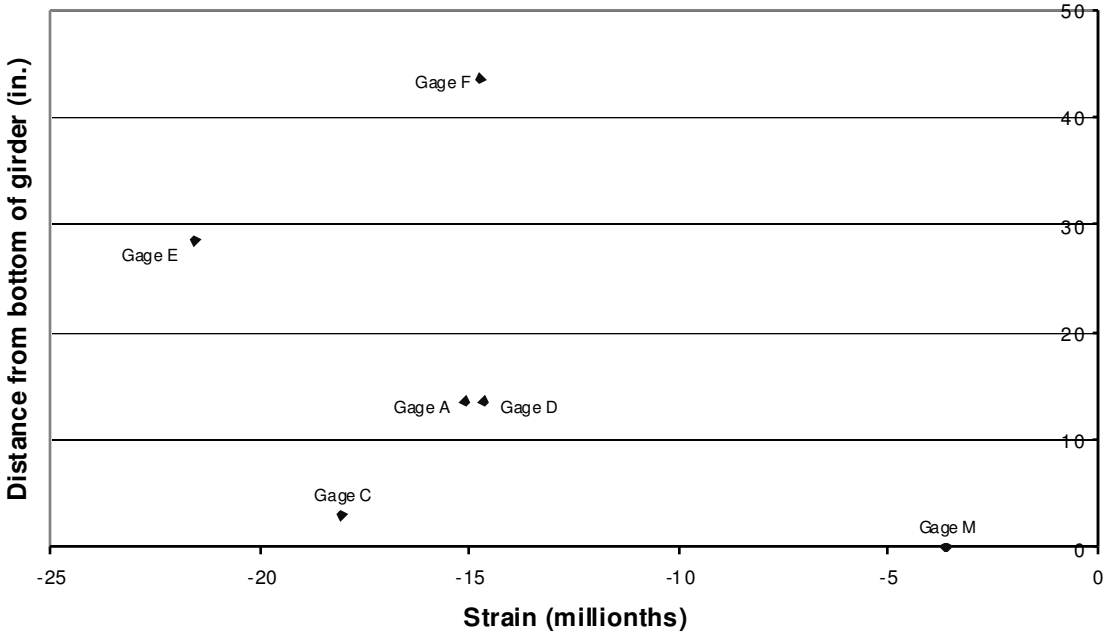


**Figure D-260:** C8 Span 11 Girder 8 Cross Section 2

### D.3.9 POSITION C9

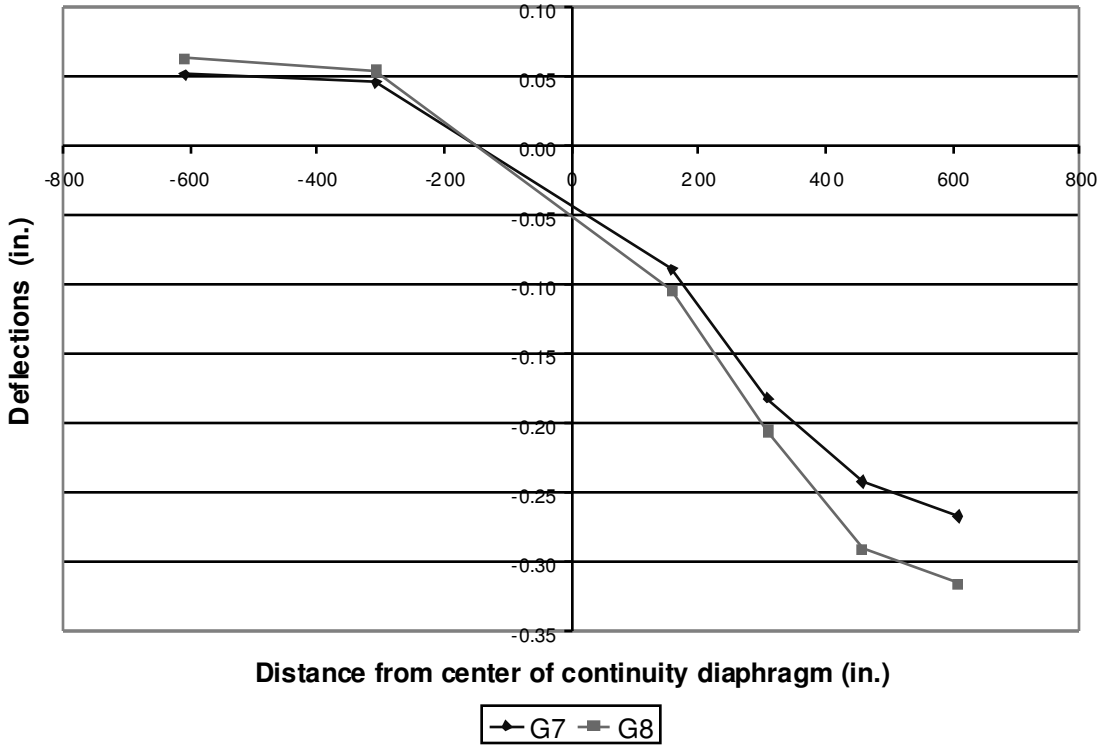


**Figure D-261:** C9 Deflections

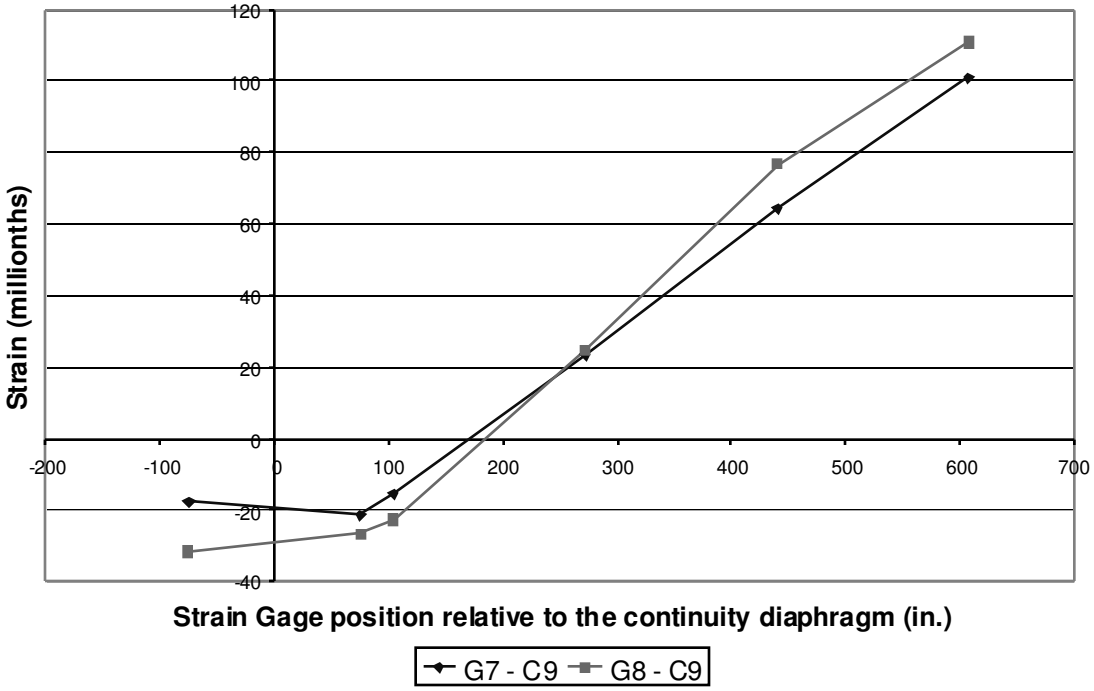


**Figure D-262:** C9 Bottom Fiber Strains

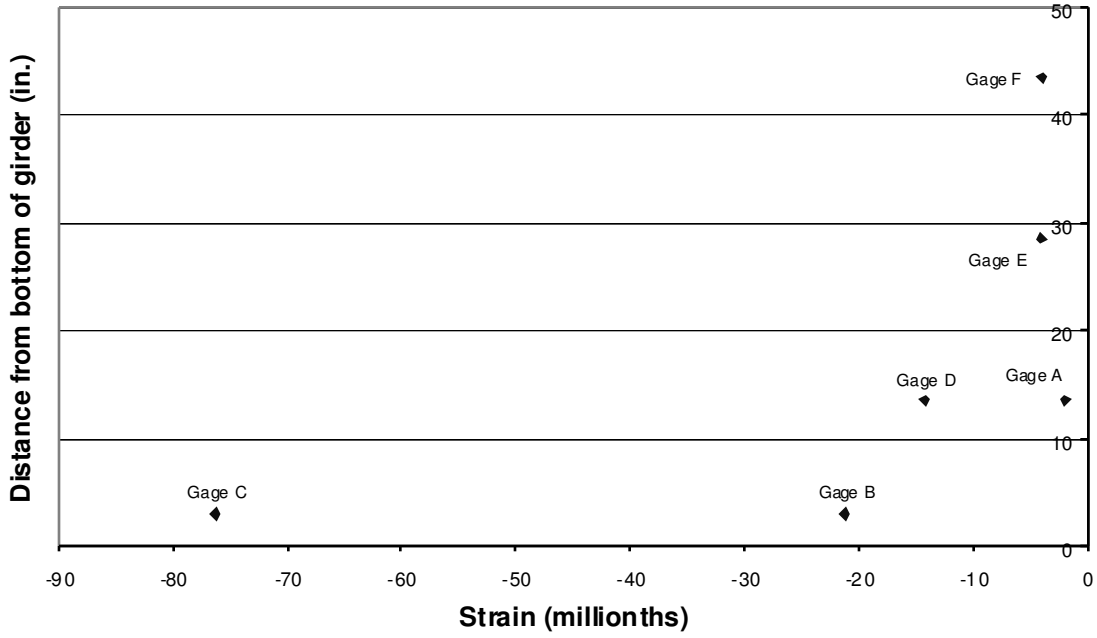


**Figure D-263:** C9 Span 10 Girder 7 Cross Section1

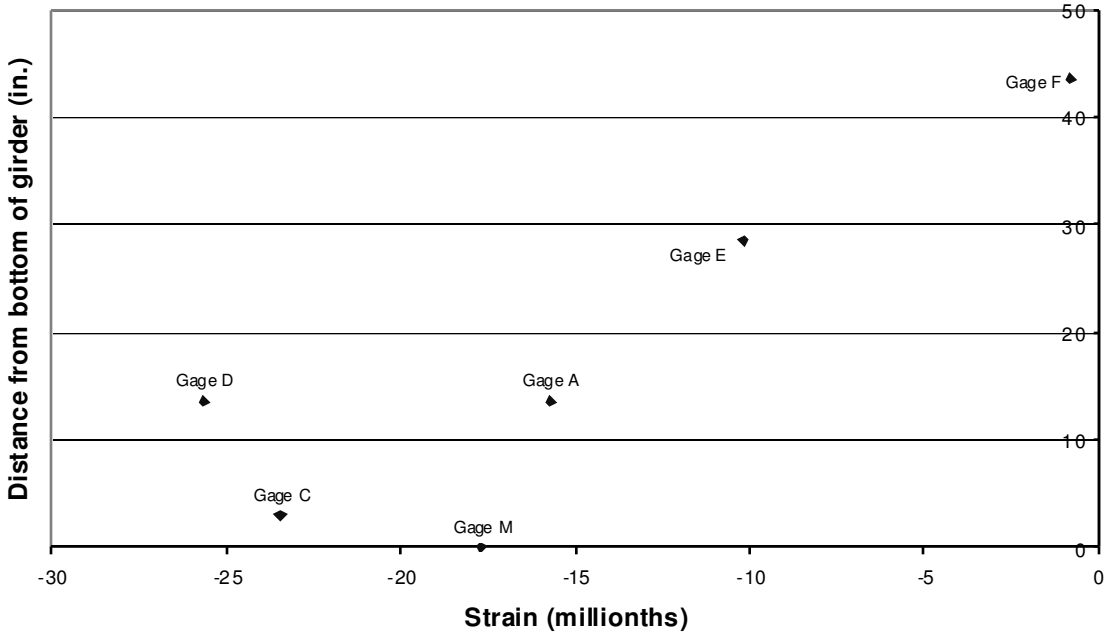


**Figure D-264:** C9 Span 10 Girder 7 Cross Section 2

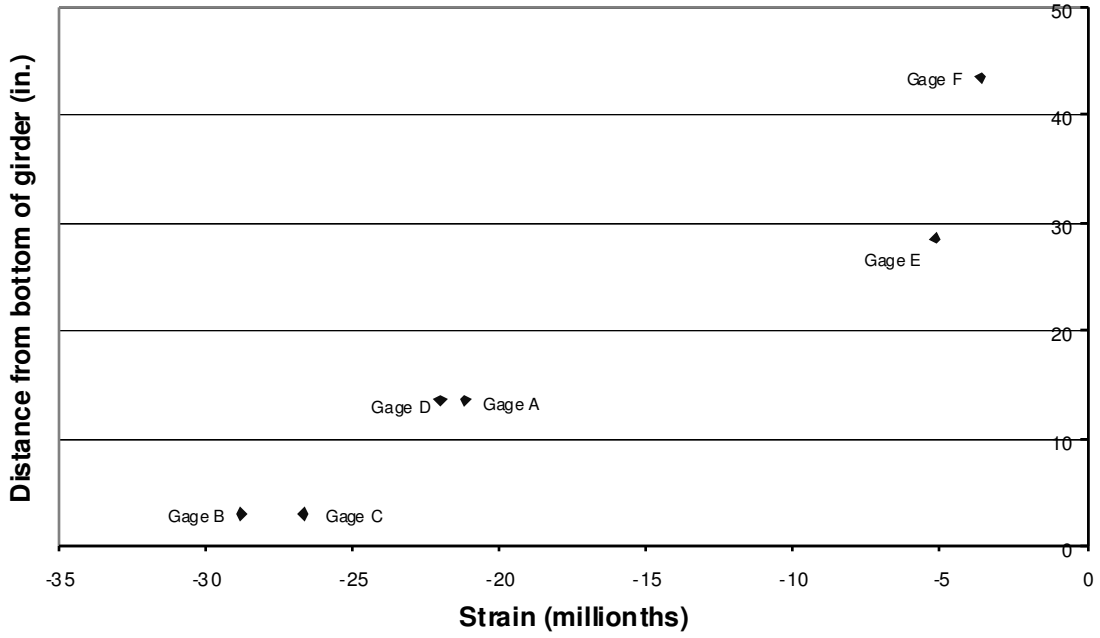


**Figure D-265:** C9 Span 10 Girder 8 Cross Section 1

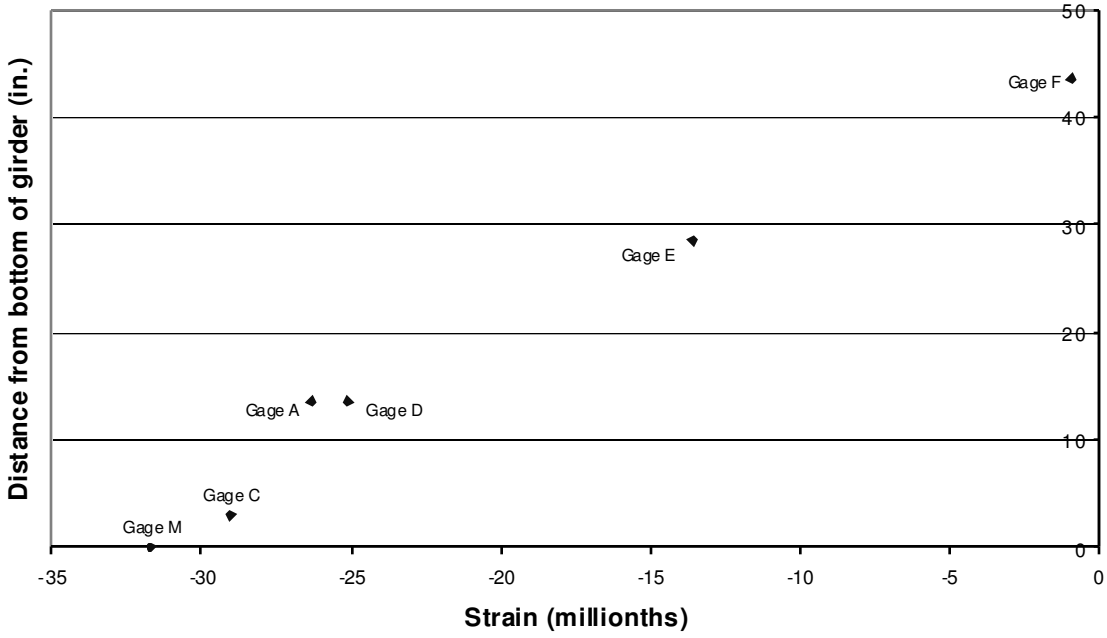


**Figure D-266:** C9 Span 10 Girder 8 Cross Section 2

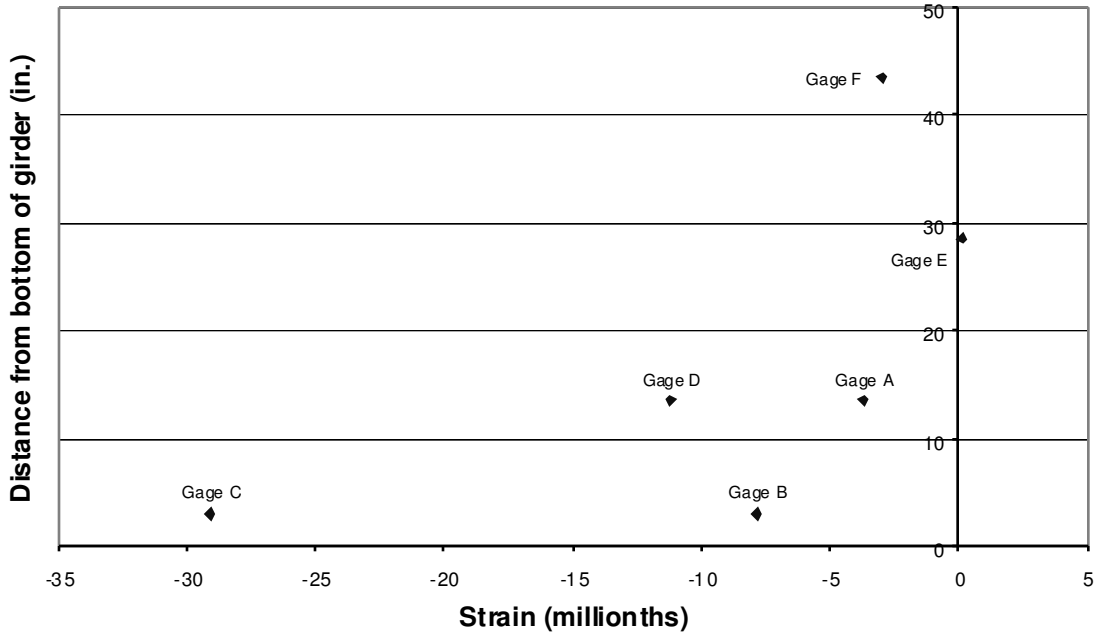


**Figure D-267:** C9 Span 11 Girder 7 Cross Section 1

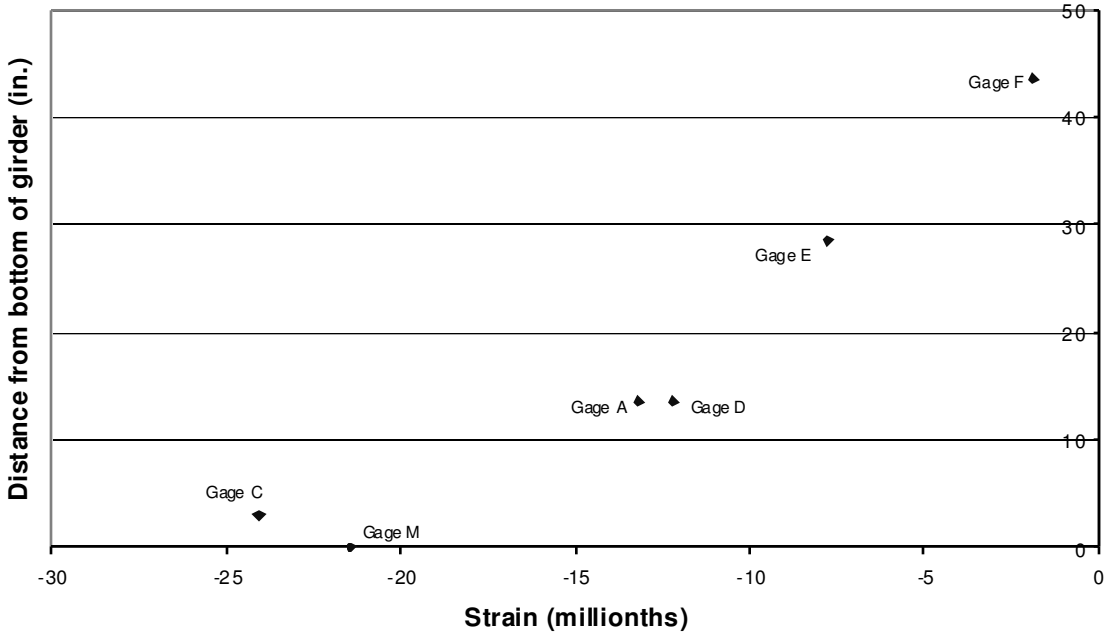


**Figure D-268:** C9 Span 11 Girder 7 Cross Section 2

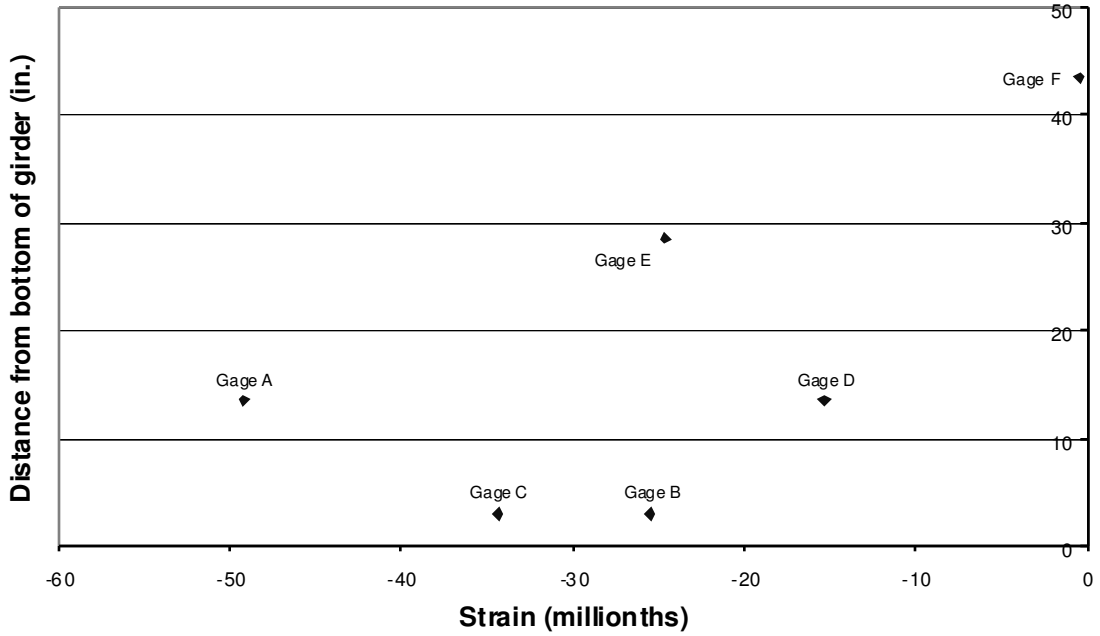


**Figure D-269:** C9 Span 11 Girder 8 Cross Section 1

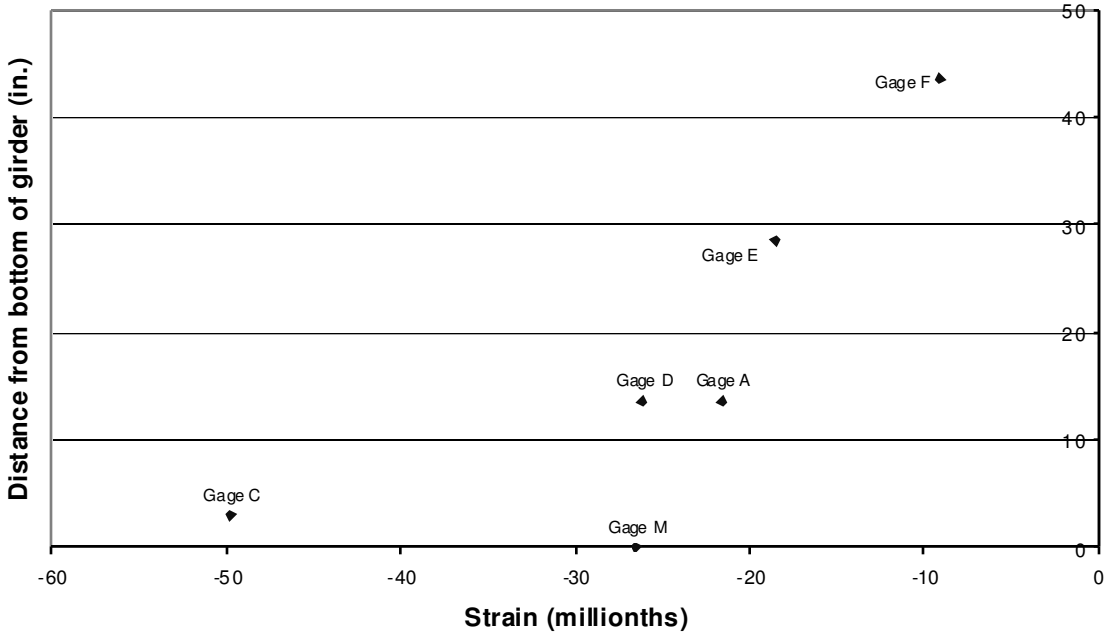


**Figure D-270:** C9 Span 11 Girder 8 Cross Section 2